Metal Complexes of *Bis*- and *Tris*-Dioxolenes and Related Ligands

Jonathan James Loughrey

Submitted in accordance with the requirements for the degree of
Doctor of Philosophy

The University of Leeds
School of Chemistry

November 2013

The candidate confirms that the work submitted is his/her own, except where work which has formed part of jointly-authored publications has been included. The contribution of the candidate and the other authors to this work has been explicitly indicated below. The candidate confirms that appropriate credit has been given within the thesis where reference has been made to the work of others. The reference for the jointly authored paper is stated below:

J. J. Loughrey, C. A. Kilner, M. J. Hardie, M. A. Halcrow, *Supramol. Chem.* **2012,** *24,* 2-13.

Acknowledgements

The research for chapters 3 and 4 has been carried out by a team which has included Nathan Patmore (University of Sheffield), Stephen Sproules (University of Glasgow) and Eric McInnes (University of Manchester). My own contributions, fully and explicitly indicated in the thesis, have been in the synthesis and analysis of all complexes and compounds, along with running the specialist measurements in collaboration with those mentioned above. The other members of the group and their contributions have been as follows: useful academic discussions and their grateful aid in interpreting the results obtained.

First and foremost I would like to thank my supervisors, Professors Malcolm Halcrow and Michaele Hardie, it truly has been a pleasure to work for you both. All of your help with interpreting results and your never-ending suggestions have helped more than I'm sure you can both imagine. Thank you for sending me away to exotic places; to conferences, courses and Diamond, hopefully I haven't made the past 3 years too painful!

A huge thank you to all the technical staff at the University of Leeds; Ian Blakeley, Tanya Marinko-Covell, Simon Barrett and Colin Kilner, I'm extremely grateful for all the hours you've put into helping me along the way.

Working in office 1.25 and 1.29 has been a delight, I owe a lot to past and present Halcrow and McGowan group members; Amedeo, Laurence, Tom, Rufeida, Raf, Grant, Chris, Andrew, Ben, Steph, Rianne, Andrea and Aida and and all the past MChems. Thanks for the Secret Santa's, Christmas parties, cake days, drinks and all the general banter inbetween. A massive thanks to Tia (your strong South African accent always cheered us up), Flora, Vikki, Mike, Jordan, Heba and I certainly can't forget to thank Marc Little for his help from the beginning and right through to the end. I owe a massive thanks to Charlotte for your kind use of the glove-box and the endless number of lifts I've cadged off you in the past three years but I certainly couldn't have achieved this without the help of my two best friends, Ben and James, thank you both for carrying me this far!

I can't forget my friends in The Netherlands; Pim, Carï, Jan and Wendy. Thankfully you didn't put me off science and I know that without all of your help I wouldn't have even got the opportunity to do a Ph.D.

I would like to thank my family (Loughreys, Newbegins and Jensen) I hope you've witnessed the transition in me from student to scientist. Last, but by no-means least however, I would like to thank my wife Chantel, to whom I dedicate this thesis to. All your love and support has helped in making the writing of this thesis as painless as possible, I hope I've made you proud.

Abstract

This thesis concerns the synthesis and analysis of poly-dioxolene complexes and their related ligands, for the purposes of generating complexes of mixed valence. Work was firstly performed using the *tris*-dioxolene cavitand species, cyclotricatechylene (ctc), due to its structural rigidity and non-conjugation of the dioxolene rings. A preliminary investigation into the ability of cyclotricatechylene to support electron transfer was performed by addition of selected electron acceptor molecules to solutions of ctc. Two novel donor : acceptor complexes were isolated although displayed a lack of formal electron transfer between the two molecules, and is presented in chapter 2. Ctc was then substituted at the upper-rim to form a number of complexes of general formula $[\{(L)M\}_3(\mu_3\text{-ctc})]$. It was found that in each synthesised, with the exception of where M = Cu(II) and L = ^{t}Bu$_2$Bipy, the dioxolene rings could be independently oxidised as shown by electrochemical analysis and two were capable of supporting mixed valence upon electrochemical oxidation where M = Pt(II) and L = dppb and ^{t}Bu$_2$Bipy. These were characterised fully and displayed Robin/Day class II or III character as determined by UV/vis/NIR spectroeletrochemistry, and is presented in chapter 3. Due to challenges faced during the synthesis and analysis of complexes containing the ctc core, a simpler system was investigated containing two dioxolene rings based upon the 2,3,6,7-tetrahydroxy-9,10-dimethyl-9,10-dihydro-9,10-ethanoanthracene (H_4thea) unit. Three diplatinum(II) complexes were synthesised of general formula $[\{(L)Pt\}_2(\mu_2\text{-thea})]$ where L = dppb, dppe and ^{t}Bu$_2$Bipy which again showed two one-electron redox processes corresponding to the reversible oxidation and reduction of each dioxolene ring. These complexes were chemically oxidised where it was found that the two halves of each were strongly coupled, near the Robin/Day class II/III border by UV/vis/NIR and EPR spectroscopy, and is presented in chapter 4. Finally, attempts were made to synthesise the analogous thiolated ligands to ctc and H_4thea, although challenges faced during their synthesis resulted in this remaining incomplete. The progress made towards these compounds is presented in chapter 5.

Table of Contents

Chapter 2

Chapter 3

Chapter 4

List of Abbreviations

Å	Angstrom, 1×10^{-10} m
A	Coupling constant (EPR)
approx.	Approximately
B	Magnetic Field
bdt	Benzene-1,2-dithiol
bipy	2,2'-bipyridine
Biscat	3,3',4,4'-tetrahydroxybiphenyl
bpm	2,2'-bipyrimidine
bpyz	2,2'-bipyrazine
br.	Broad singlet
^{13}C	Carbon (NMR)
$^{13}C\{^{1}H\}$	Proton-decoupled Carbon (NMR)
°C	Degrees Celcius
cat	Catechol
Cl_4SQ	Tetrachloro-1,2-benzosemiquinone
cm^{-1}	Wavenumbers
COD	Cyclooctadiene
CT	Charge Transfer
cth	*dl*-5,7,7,12,14-hexamethyl-1,4,8,11-tetraazacyclotetradecane
ctc	Cyclotricatechylene
ctg	Cyclotriguaiacylene
ctp	Cyclotrithiophenolene
ctv	Cyclotriveratrylene
CV	Cyclic Voltammetry

D	Zero-field splitting
dafl	4,5-diazafluoren-9-one
dba	dibenzylidineacetone
DBCat	3,5-di-*tert*-butylcatechol
DBSQ	3,5-di-*tert*-butylsemiquinone
DBQ	3,5-di-*tert*-butylquinone
dde	1-diphenylphosphino-2-dimethylaminoethane
ddq	2,3-dichloro-5,6-dicyano-1,4-benzoquinone
DHBA	3,4-dihydroxybenzaldehyde
diox	Dioxolene
dmac	N,N'-Dimethylacetamide
dmf	Dimethylformamide
dmso	Dimethylsulfoxide
dpa	dipyridylamine
dppb	1,2-*bis*(diphenylphosphinobenzene)
dppe	1,2-*bis*(diphenylphosphinoethane)
DPV	Differential Pulse Voltammetry
ε	Molar absorptivity
ES	Electrospray
et al	*et alii* (and others)
[$FeCp_2$]	Ferrocene
G	Gauss
G_{af}	Antiferromagnetic stabilisation free energy
G_{com}	Free energy of comproportionation
G_{elec}	Free energy of electrostatic repulsion between charged sites

G_{ind}	Inductive free energy
G_{ip}	Free energy of ion pairing
G_{stat}	Statistical Distribution of free energy between states
H_{AB}	Electronic coupling
H_2bispicen	*N*,*N*'-*bis*(2-pyridylmethyl)-1,3-propanediamine
H_2bispictn	*N*,*N*-*bis*(2-pyridylmethyl)-1,3-propanediamine
H_2cat	1,2-dihydroxybenzene
H_2O	Water
H_4acetA	5,5′-(buta-1,3-diyne-1,4-diyl)bis(3-*tert*-butylcatechol
H_4acetB	5,5′-(2,5-dimethoxy-1,4-phenylene)bis(ethyne-2,1-diyl)bis(3-*tert*-butyl-catechol)
H_4acetC	5,5′-(4,4′-(buta-1,3-diyne-1,4-diyl)bis(2,5-dimethoxy-4,1-phenylene))bis(ethyne-2,1-diyl)bis(3-*tert*-butyl-catechol)
H_4spiro	3,3,3',3'-tetramethyl-5,6,5',6'-tetrahydroxy-1,1'-spiro-bis(indane)
HOMO	Highest occupied molecular orbital
hs	High spin
Hz	Hertz
J	Coupling constant (NMR)
K_{con}	Comproportionation Constant
$^{31}P\{^1H\}$	Proton-decoupled Phosphorus (NMR)
^{i}Pr	Isopropyl-
ITO	Indium-Tin Oxide
IVCT	Intervalence Charge Transfer
L	Ligand
$L_{1\text{-}R}$	Derivatives of 2,5-hydroxy-1,4-benzoquinone

LMCT	Ligand-Metal Charge Transfer
ls	low spin
LUMO	Lowest occupied molecular orbital
m	Medium
M	Molar
μ_{eff}	Effective magnetic moment
MeOH	Methanol
MeCN	Acetonitrile
m_I	Secondary nuclear spin quantum number
MMCT	Metal-Metal Charge Transfer
MOF	Metal Organic Framework
m_s	Secondary electron spin quantum number
MS	Mass spectrum
NIR	Near Infrared
ν_{max}	Maximum absorption
NMR	Nuclear Magnetic Resonance
I	Nuclear spin
o	*ortho-*
OTf	Triflate ($CF_3SO_3^-$)
p	*para-*
Ph	Phenyl-
phen	1,10-phenanthroline
phenSQ	9,10-phenanthrene-semiquinone
ppm	parts per million

PTP	2-[5-2(2-pyridyl)-1,2,4,-triazol-3-yl]
q	quinone
Q_2ethene	4,4'-(ethane-1,2-diylidine)bis(2-hydroxy-3,6-di-*tert*-butyl-cyclohexa-2,5-dienone
R	Gas constant
s	strong
S	Electron spin
sq	Semiquinone
T	Temperature
$^{t}Bu_2$Bipy	4,4'-di-*tert*-butyl-2,2'-bipyridine
tcne	Tetracycanoethylene
tert	Tertiary
TD-DFT	Time dependent density functional theory
THF	Tetrahydrofuran
thio-ctc	Thiocyclotricatechylene
thio-ctg	cyclotrithioguaiacylene
tmeda	N,N`,N``,N```-tetramethylethylenediamine
tpa	*Tris*-2-pyridylmethylamine
$Tp^{Cum,Me}$	Hydrotris(3-methyl-5-cumenylpyrazolyl)borate
triphos	*Tris*(diphenylphosphanomethyl)ethane
triscat	hexahydroxtriphenylene
TTF	Tetrathiafulvalene
V	Volts
vs	versus
w	Weak

Chapter 1
Introduction

1.1 Overview

This thesis is concerned with the preparation and characterisation of novel, multinuclear complexes of *bis*- and *tris*- dioxolenes and related ligands. The ligands and complexes discussed were prepared to provide further insight into the redox capabilities of molecules containing multinuclear redox-active centres, and have been investigated accordingly using techniques known to the field. All of the results in this thesis are reproducible using the described conditions and reagents.

This chapter contains a brief summary of the concepts and background discussed within this thesis, beginning with an introduction to mixed valency and redox active ligands before moving onto discuss the family of 1,2-dioxolenes and their fascinating redox chemistry. The aim of this chapter is to provide the reader a measure of relevance to the work presented in this thesis and how it relates to that previously conducted in the field.

1.2 Introduction to Mixed Valency

In recent years there has been a considerable surge in attention towards molecular-scale systems capable of exhibiting intramolecular electron transfer processes (IET) induced by application of an external stimulus.[1] One of the main driving forces behind this interest is in the development of a system which displays a reversible change in electronic distribution within its molecular framework. If successful, this could open the possibility for their use as molecular-sized information storage devices. Complexes of mixed valency are excellent candidates for this purpose as they contain a minimum of two redox-active sites in different oxidation states, linked by a bridge which may facilitate electron transfer between the two.[2] It is important here to clarify what is meant by mixed valence species and how they differ from ‘standard’ donor-acceptor species, despite both containing two redox active centres one of which acts as ‘donor’ and one as ‘acceptor’. This difference is somewhat easier to explain by analogy to organic mixed valence and donor : acceptor species. Both systems can undergo electron or charge transfer (defined as partial electron transfer between the two species), by optical excitation of an electron into a charge transfer band. The key difference that separates the two species however, is that organic mixed valence species always contain an open electron shell ground state, and the valent electron may be transferred from one redox-active centre to another (often by optical excitation), as illustrated in **Scheme 1.1**,[3] resulting in an altered charge distribution.

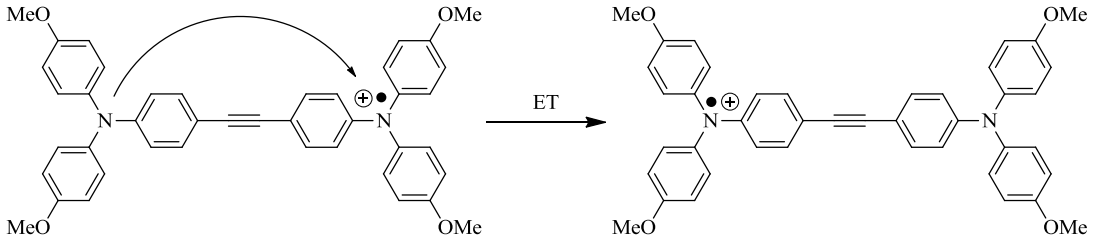

Scheme 1.1. Example of mixed valency in a purely organic system prepared by Lambert *et al.*[3b]

Unfortunately, this relatively simplistic view of mixed valency becomes invalid with the introduction of metal atoms. A general definition based upon whether or not an unpaired electron is present fails to account for higher states of spin multiplicity, as is common in metal-containing complexes. Because of this, inorganic mixed valence complexes are often defined based upon the *formal* oxidation state of the redox-active metal atoms as investigations based upon heterometallic complexes, containing low-spin Fe^{II}-Co^{III} for example, may be closed-shell.[4] Perhaps the most recognised (but not the earliest) system of inorganic mixed valency was performed by Creutz *et al.* in their investigative work on bridged dinuclear ruthenium complexes of the general formula $[\{(NH_3)_5Ru\}L\{Ru(NH_3)_5\}]^{5+}$.[5] This work led to the familiarly known 'Creutz-Taube Ion', prepared by the oxidation of a previously prepared pyrazine-bridged dinuclear ruthenium complex using one equivalent of silver tetrafluoroborate, yielding a species containing two chemically equivalent $Ru^{2.5+}$ centres due to delocalisation of the valent electron throughout the whole framework.[6] Creutz *et al.*[5] were not the only researchers in the mixed valence scene in the early 1970s. Only a couple of years after the publication of the 'Creutz-Taube' ion, Cowan *et al.* presented the synthesis and analysis of a series of organometallic mixed valence complexes containing ferrocene moieties directly linked by their cyclopentadienyl (Cp) rings.[7] A series of these complexes were prepared, using various counteranions, by the one-electron oxidation of biferrocene using benzoquinone. What was found indicated that the valent electron was localised on one iron centre although the barrier to electron transfer was low and could be excited optically.[8] This was apparent despite the iron centres being significantly closer (approximately 3.8 Å for *cis*-coplanar, 5.1 Å for *trans*-coplanar) compared to the ruthenium centres in the Creutz-Taube ion (separated by approximately 6.8 Å). It wasn't until 1990, with work conducted by Riemers *et al.*,[9] who showed that the valent electron of the 'Creutz-Taube' ion could instead be localised on one ruthenium site, by increasing the distance between ruthenium centres by replacement of the central pyrazine with a vinylogue (n = 0-2), as shown in **Figure 1.1.** This key question of electron localisation (or delocalisation) in mixed valence species is therefore very important to

address as given certain circumstances, the valent electron may adopt a state of delocalisation, localisation or an intermediate. This will be explored in the next section.

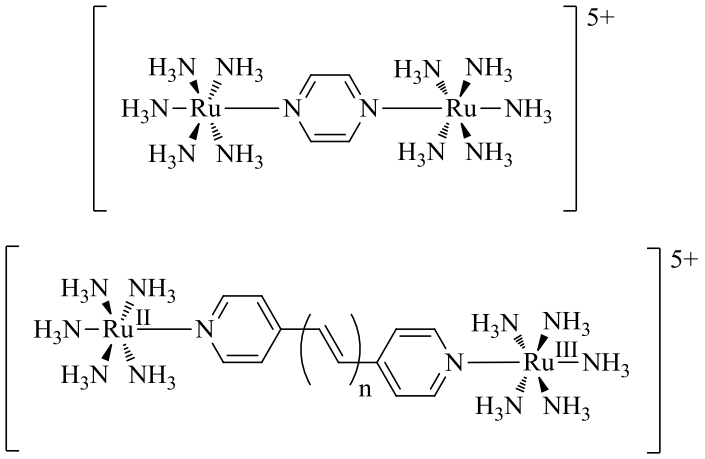

Figure 1.1. (Top) Original Creutz-Taube ion $[\{(NH_3)_5Ru\}L\{Ru(NH_3)_5\}]^{5+}$ prepared by Creutz *et al.*[5] (Bottom) Vinologue of Creutz-Taube Ion prepared by Riemers *et al*.[9]

1.3 Classification of Mixed Valence

In 1967, Melvin B. Robin and Peter Day published a detailed study into mixed valency encompassing almost the entire periodic table.[10] Within this survey, they put forward the notion that the properties of complexes could be classified by their structures (molecular or single-crystal determinations). Their theory was that if a metal, M, can appear in two different oxidation states (A and B) and occupies two sites in the crystal (Y and Z) then the extent of electronic mixing between the two, simplified by $M_Y{}^A M_Z{}^B$ and $M_Y{}^B M_Z{}^A$, would be reflected in how easily discernible the two sites are. They grouped the difference between sites into three 'classes'. If the two sites are obviously very different, the valence will be trapped on one site and unable to interconvert therefore this was scenario was attributed to be 'class I', as the sites do not interact with one another (which in practice manifests as a situation where the interaction between sites is too small to measure). If the two sites are completely indistinguishable and the valence is spread across the two due to strong interaction, this would be 'class III'. If sites M_Y and M_Z can be distinguished however, but are still similar due to weak interaction, then an intermediate 'class II' would be applicable.[11] While these classes are today widely accepted, once the Marcus classical electron transfer theories were applied to the theories of Robin *et al.* to describe the processes of electron transfer between the two redox active centres, a unified Marcus-Hush theory of the electron transfer processes between the sites was born. Their work resulted in the commonly accepted two state model of mixed valency, best described by the treatment

of the redox active centres as diabatic (non-interacting, class I) or adiabatic (interacting, class II and III) free energy harmonic profiles across a reaction coordinate.

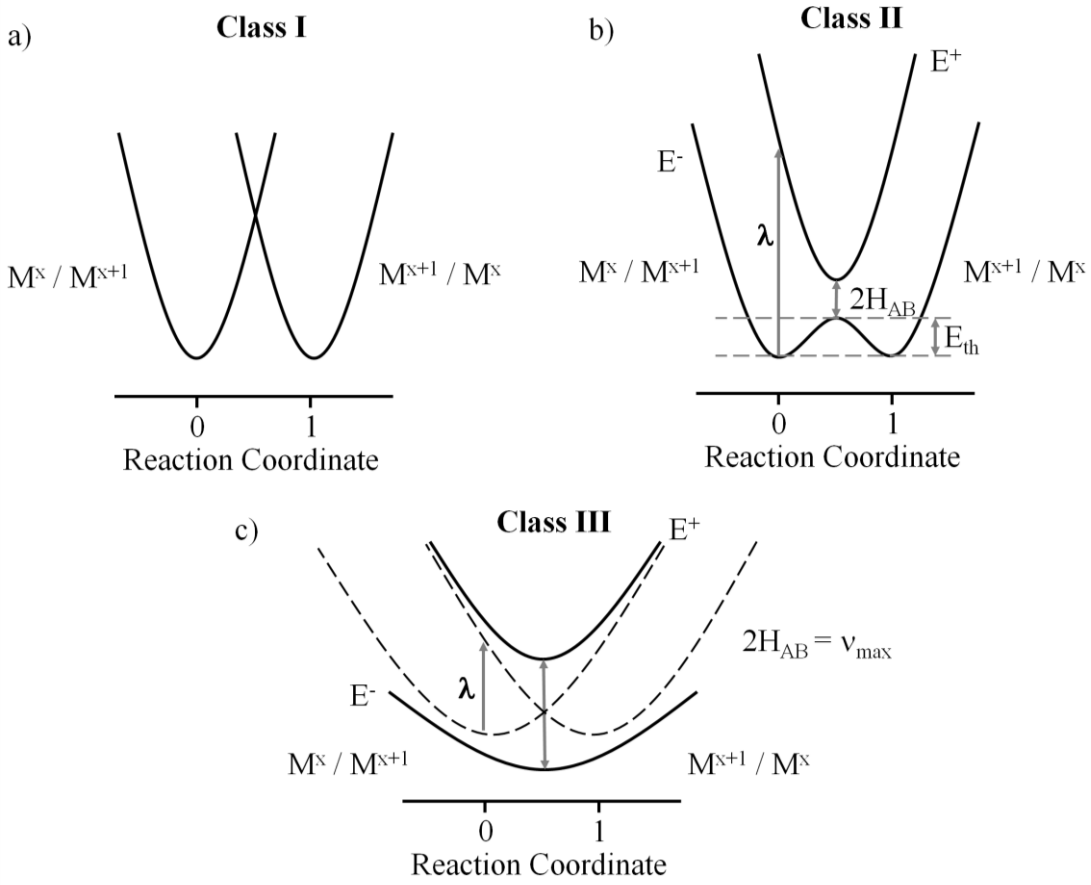

Figure 1.2. Marcus-Hush potential energy surfaces for electron transfer in symmetric mixed-valence complexes in terms of reorganization energy, λ; electronic coupling, H_{AB} and the thermal barrier to electron transfer, E_{th}. (**a**) Robin / Day class I. (**b**) Robin / Day Class II. (**c**) Robin / Day class III.

Extension of the theory to include electronic interaction between redox centres resulted the three classes of mixed valence being described in terms of reorganisation energy (λ), electron coupling (H_{AB}) and thermal energy barrier (E_{th}) as opposed to only electron delocalisation, as summarised in **Figure 1.2**. For the purposes of this section, only symmetric transitions ($\Delta G^o = 0$) will be discussed between two states, reactant (initial, reaction coordinate = 0) and product (final, reaction coordinate = 1). As is perhaps expected, complexes of class I shown in **Figure 1.2(a)** where the valence is localised show no interaction between redox centres (i.e. diabatic states). These can therefore be classed as isolated centres, resulting in no optical or thermal transitions resultant of a lack of electronic coupling $H_{AB} = 0$ between the two. In class II complexes, shown in **Figure 1.2(b)**, there is electronic coupling and the diabatic free energy surfaces are split into two adiabatic surfaces

to reflect this, of which the ground state surface (E^-) exhibits a double potential well and the valence is generally localised on one redox-site. **Figure 1.2(b)** depicts an instance only true of complexes exhibiting degenerate ground states, as the discussion of complexes with non-degenerate ground states is beyond the scope of this survey. In the case highlighted, the additional valence can be optically induced as seen by a metal-to-metal (MMCT) or inter-valence charge transfer (IVCT) transitions in their electronic spectra by absorption of energy equalling λ, the Marcus reorganisation parameter. This is built up from the two Franck-Codon factors; the inner electron sphere reorganisation energy (λ_v) due to the changes in the bond angles and lengths at the redox centre upon change in oxidation state, and the outer-sphere solvent reorganisation energy (λ_o). Because of the outer-sphere solvent reorganisational energy, the IVCT is expected to show high solvent dependence.[12] The electronic transition may also be thermally induced (E_{th}) according to the Boltzmann distribution k_BT, due to the low activation barrier between potential wells. In class II mixed-valence complexes, the electronic coupling energy, H_{AB}, is a measure of the interaction between donor and acceptor states and is typified by a small value between zero and half the Marcus reorganisation parameter, $0 < H_{AB} < \lambda/2$. It should be noted here that as the coupling between redox-active sites increases, the energy required to thermally induce a transition decreases as the process becomes more favoured. The final case is that of Robin-Day class III behaviour, as shown in **Figure 1.2(c),** where the adiabatic state has only one energy minimum, and the charge is delocalised across both redox-active centres. This case is defined by large electronic coupling energy between redox-active centres, approaching covalency, equal-to or greater than half of the Marcus reorganisation parameter; $H_{AB} \geq \lambda/2$, which increases with the increasing strength of the electronic interaction. Because of a lack of charge transfer in Class III complexes, hence no net dipole moment change, the absorption profile of the IVCT band observed shows no solvent dependence and involves transitions between delocalised orbitals of the complex.

1.4 Standard Characterisation of Mixed Valency

1.4.1 Electronic Interaction Energy

As mentioned above, the appearance of intervalence charge transfer (IVCT) absorption bands are often recognised as solid evidence for the presence of a mixed valence species. Arising from the intramolecular electronic transition between electron rich, low valent site to electron poor, high valent site. These transitions may be in the visible region (e.g. Prussian Blue) or in the NIR region (e.g. 6,370 cm^{-1} for the Creutz-Taube ion). The interest in the IVCT band, although not straightforward, arises from the strength of electronic interaction between mixed valence sites. In a classical model, the bandwidth at half height

($\Delta\nu_{½}$) is related to the energy maximum of the process by the Hush equation (**equation 1.1**).[13]

$$\Delta\nu_{½} = [2310\ \{E_{max}\}]^{½} \quad \textbf{(Equation 1.1)}$$

The electronic coupling energy, $H_{AB,}$ of a symmetric band may therefore be represented by **equation 1.2** where ε_{max} = molar absorption coefficient, ν_{max} = absorption maximum, R = distance between mixed valence sites for a class II situation. For a fully delocalised class III complex, $H_{AB} = \nu_{max} / 2$.[14]

$$H_{AB} = \{[2.05 \times 10^{-2}(\varepsilon_{max}\ \nu_{max}\ \nu_{½})^{½}] / R\} \quad \textbf{(Equation 1.2)}$$

1.4.2 Comproportionation Constant

The comproportionation constant K_{com} is related to the degree of electronic interaction between mixed valence states. Calculated from the separation of two-step redox processes obtained by electrochemical analysis (cyclic voltammetry, differential pulse voltammetry or polography), K_{com} may be calculated by **equation 1.4** where E_1 and E_2 correspond to the potentials of the first and second redox processes and n corresponds to the number of electrons transferred in each process.[15]

$$K_{com} = 10^{\Delta E/59mV} \text{ at } 298\ K \quad \textbf{(Equation 1.3)}$$

$$\Delta E = E_2 - E_1\ ;\ RT \ln K_{com} = n\ F\ \Delta E \quad \textbf{(Equation 1.4)}$$

As the difference between E_1 and E_2 decreases, the peaks become less separated until they appear as one single process. This is represented in the value of K_{com} where as a general indication;[16]

Class I $K_{con} < 10^2$

Class II $10^2 < K_{con} < 10^6$

Class III $K_{con} > 10^6$

For instance, where there is no interaction between redox centres(class I) K_{com} adopts a small value due to virtually no differentiation between E_1 and E_2, resulting in a small ΔE. Where electronic communication is large, K_{com} is large due to an increased ΔE separation. For example, the Creutz-Taube ion displays a separation of 0.39 V between successive Ru^{II} / Ru^{III} couples therefore a large K_{com} of 3×10^6.[16]

K_{com} is dependent on the free energy of comproportionation, ΔG_{com}, which is comprised of multiple components, as shown in **equation 1.5**. Where; ΔG_{stat} = the statistical distribution

between states, ΔG_{elec} = electrostatic repulsion of the charged sites, ΔG_{ind} = inductive factor related to the competitive coordination of groups ancillary to the redox active centre, ΔG_{res} = the resonance exchange, ΔG_{af} = the antiferromagnetic stabilisation and ΔG_{ip} = ion pairing effect dependent on charges within the complex.[17] In instances where K_{con} is small, further considerations may be required owing to the presence of neighbouring redox states, which could also be concentration dependent.[18]

$$\Delta G_{com} = \Delta G_{stat} + \Delta G_{elec} + \Delta G_{ind} + \Delta G_{res} + \Delta G_{af} + \Delta G_{ip} \quad \textbf{(Equation 1.5)}$$

Since having unified the observed properties of mixed valence systems,[11] interest in the development of mixed valence systems has increased enormously. The majority of research into mixed valency has been performed on the synthesis and analysis of homo- and heterometallic complexes[19] or metallocenes[20] due to their ease of oxidation, relative stability and kinetic inertness. The generation of organic mixed-valence systems is also a rapidly growing field and present the advantage of fine-tuning spectral characteristics in a very precise manner due to the flexibility of organic synthesis,[21], [22] which may be used for either the synthesis of novel purely-organic mixed valence species, or by coordination to a metal centre as a ligand.

1.5 Introduction to Redox Active 'Non-Innocent' Ligand Systems

As changes in oxidation state of a transition metal or any other element are very often central themes in chemistry, chemists have found ways of using these changes to describe specific spectroscopic and magnetic phenomena, or indeed chemical reactivity. In the vast majority of cases, describing the oxidation state of a given species may be straightforward (ferrocene, for example) although as was recognised by Jørgensen in 1966,[23] there may be instances where this may be unclear. In an attempt to avoid any confusion, Jørgensen classified ligands as redox 'innocent' and 'non-innocent', depending on whether or not the ligand permitted "the oxidation states of the central atoms to be defined".[23] This classification of 'non-innocence' has since been (generally) adopted to describe ligands involved in the differing of the experimental oxidation state of a central atom from its formal oxidation state, as pre-determined by an accepted set of rules. The simplest case to highlight this point is that of nitric oxide (NO). Nitric oxide is well known as an important biological molecule, partly due to its unique redox behaviour and ground state radical character which may bind metals either as NO^+ as in metmyoglobin (Fe^{II}-NO^+),[24] or NO^- as in reduced vitamin B_{12} (Co^{III}-NO^-).[25] These examples not only highlighted the fascinating redox-active characteristics of NO ions, but also its biological importance therefore winning it the 'molecule of the year' prize in 1992.[26] Alongside NO, there are a number of other

interesting non-innocent ligands which have also been studied. These range from simple 'non-innocent' diatomics, dioxygen ($O_2/O_2^{\bullet-}/O_2^{2-}$) and cyano- ligands to polycyano acceptor-substituted olefins (e.g. tetracyanoethylene (tcne), tetracyanoquinodimethane (tcnq)), α-diimines (e.g. 1,4-diazabutadiene), *o*-quinonediamines, α-diketo compounds, α-dithiolates and 1,2-dioxlenes. Biological research has also yielded flavins, large heterocyclic π-systems (tetrapyrroles and corroles) and phenolates[27] whilst organometallic chemistry has given non-innocent ligands, comprised entirely of carbon-carbon bonds, which may undergo structural changes once oxidised or reduced.[28] Of these systems, the earliest and most heavily studied are α-dithiolenes which began with the preparation and characterisation of planar complexes containing platinum, palladium and nickel some 50 years ago.[29] The interest in these planar complexes stemmed from the three possible resonance structures the complexes may adopt, either as mono- *bis*- or *tris*-dithiolene species, as illustrated **Scheme 1.2**, for example.[30]

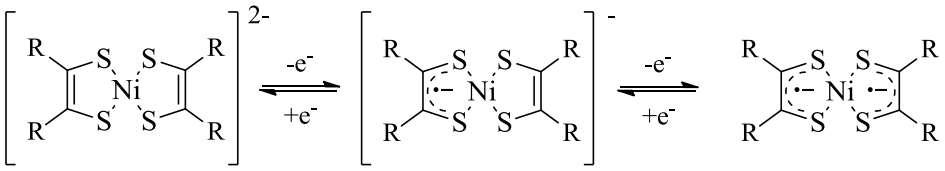

Scheme 1.2. Redox isomers of square-planar *bis*-dithiolene complexes, e.g. R = -Ph.[29a]

Complexes of this type have therefore been actively pursued ever since, with the majority of interest in their curious magnetic and spectroscopic characteristics due to extensive orbital mixing between metal and dithiolene. Extensive studies have therefore been undertaken to determine the correct bonding mode and oxidation state of the ligand or metal. By simple extension, benzene-1,2-dithiol (bdt) has also been investigated for similar reasons owing to the fascinating redox series it may exhibit, as depicted in **Scheme 1.3** below.

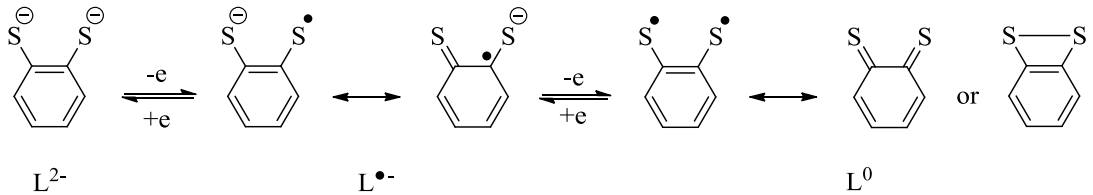

Scheme 1.3. One electron redox processes exhibited by benzene-1,2-dithiol (bdt).

As with the α-dithiolene family, complexes incorporating $[bdt]^{n-}$ have also been investigated for their curious magnetic and spectroscopic characteristics in either mononuclear or multinuclear complexes.[30-31]

1.6 Background to Dioxolene Chemistry

In an analogy to dithiolene chemistry, the term 'dioxolene' was coined by Bach *et al.* to provide a direct comparison to complexes of the extensively studied benzene-1,2-dithiol family.[32] Perhaps the most studied and well known member of the dioxolene family is catechol (H_2cat, 1,2-dihydroxybenzene) which can chelate metal atoms in three different modes as; dianionic catechol (cat^{2-}), monoanionic semiquinone ($sq^{\bullet-}$) or neutral quinone (q^0), related by one electron redox processes as illustrated in **Scheme 1.4.**

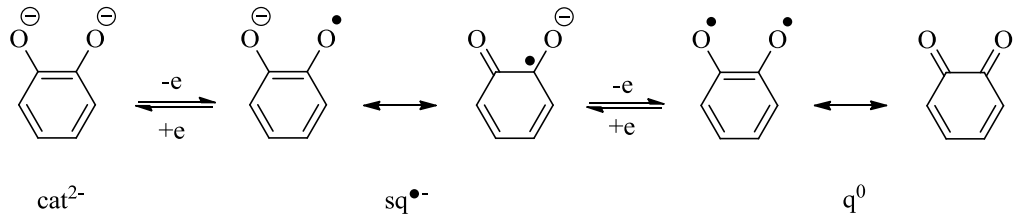

Scheme 1.4. Ligand-based redox activity of the dioxolene family; cat^{2-} = catechol, $sq^{\bullet-}$ = semiquinone, q = quinone.

Consequent of this redox-activity, ligands of the dioxolene family may be 'non-innocent' when coordinated to a metal centre as ligands, despite the fact that the low covalent character between metal and dioxolene results in well defined charge distributions.[33] Their charge distribution is actually so well defined that, unlike α-dithiolenes, the oxidation state of the ligand or metal can normally be unambiguously assigned on the basis of their magnetic and spectroscopic features, particularly as semiquinones are paramagnetic.[34] This is illustrated excellently in one-electron reduced complexes of vanadium, where $[V(bipy)_3]$ and $[V(S_2C_2Ph_2)_3]$ display delocalised structures (as shown by large couplings to ^{51}V in their EPR spectra), whilst the isoelectronic $[V(sq)_2]$ displays very small metal hyperfine coupling, indicating the valent electron is localised on the semiquinone ligand.[35] This being said, interest in the field grew relatively slowly with only sporadic reports of complexes prior to 1975 which relied mainly on characterisation via elemental analysis. There was only one reported structural characterisation on the analysis of a dinuclear oxo-bridged dianionic complex, $[Mo_2O_5(o\text{-}O_2C_6H_4)_2]^{2-}$, containing two highly distorted octahedral molybdenum(IV) centres bound to two catecholate rings.[36]

Since 1975 however, interest in the field has increased significantly and the structural characterisation of dioxolene complexes experienced significant growth, mainly due to advancements in characterisation techniques (e.g. single crystal X-ray diffraction). As a result, complexes containing all three possible oxidation states (cat, sq, q) have now been reported.[37] Much of the progress in the field has been related to biological applications,[27] particularly their affinity for iron as in mimetics of entreobactin, the iron sequestering

siderophore which is used to selectively bind and solubilise and ferric iron with an extremely high formation constant (10^{49}) due the affinity of iron(III) for hard O-donors.[38] Iron dioxolene complexes have also been investigated for their dioxolene oxidation reactions, as in catechol dioxygenase enzymes which add O_2 across the ring C-C catechol substrates. The addition may be either across the bridge C-C of both catechol C-O, yielding muconic acid product, as in intradiol dioxygenases, or exo- to this bond producing an α-hydroxymuconic semialdehyde as in the mechanism of extradiol hydroxygenase enzymes.[39]

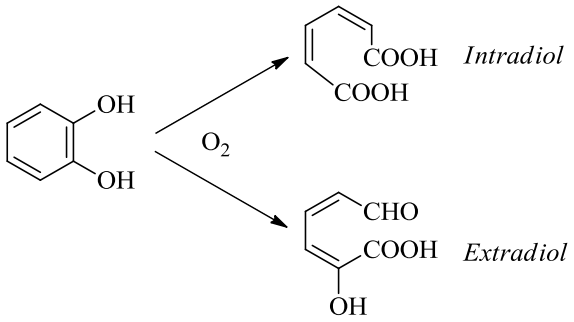

Scheme 1.5. Enzymatic oxidation of catechol by either intra- or extradiol dioxygenase activity.

The electron-rich nature of dioxolenes has also led to their importance in catalysis, where ligand-based-redox activity is important for their use as 'electron reservoirs'.[40] For example, investigations into the reduction of water using bridged ruthenium complexes[41] or in the oxidation of alcohols to aldehydes using a rhenium(V) dioxolene complex.[42] Dioxolenes have also been investigated extensively for uses as biomimetic functional materials, which have many potential applications in pharmaceuticals.[43]

1.7 Complexes of Mononuclear Dioxolene Ligands

Complexes containing mononuclear dioxolene moieties are unsurprisingly the best studied systems and have displayed fascinating insights into the pro-radical nature of dioxolene moieties and their bonding profiles. A study conducted in 1986 by Lever *et al.*[44] typified their fascinating bonding in the investigation of $[(bipy)_2Ru^{II}(cat)]$ (bipy = 2,2'-bipyridine, cat = catecholate). The complex was shown to undergo two one electron oxidation processes yielding the species $[\{(bipy)_2Ru\}^{II}(sq^{\bullet})]^{+}$ and $[\{(bipy)_2Ru\}^{II}(q)]^{2+}$ (sq = semiqinone, q = quinone), as shown by infrared, UV-vis/NIR spectroscopy and theoretical calculations. Subsequent chemical oxidation of $[\{(bipy)_2Ru\}^{II}(cat)]$ to $[\{(bipy)_2Ru\}^{II}(sq^{\bullet})]ClO_4$ in 1,2-dichloroethane at room temperature showed an isotropic EPR spectrum centred at g = 2.003 with broad linewidth (30 G). Lowering the temperature to 77 K failed to extract any hyperfine structure, although it was noticed that analysis in polar solvents such as acetonitrile or dimethylformamide showed an axial spectrum with $g_{\perp}$ = 1.985 and $g_{\parallel}$ =

2.067 (DMF) and reduced $g_{\perp}$ / $g_{\parallel}$ separation resembling that of Ru(III) species, e.g. $[(NH_3)_4Ru(cat)]^+$.[45] The axial symmetry therefore showed that the delocalised electron is partially localised on the metal and the ground state contains some Ru(III) contribution. In a similar vein, single crystal X-ray analysis on the structure displayed internal C=C dioxolene and Ru-O bond lengths consistent with a semiquinone oxidation state, although the dioxolene C-O distances were inconclusive and implied both catecholate and semiquinone character. It was therefore concluded that while the two oxidations are primarily ligand centred, there is clearly strong mixing of the ruthenium and dioxolene frontier molecular orbitals, evident by the intense ($\varepsilon = 10^4$ $M^{-1}cm^{-1}$) MLCT character of both HOMO-LUMO transitions in $[\{(bipy)_2Ru\}^{II}(sq^{\bullet})]^+$ and $[\{(bipy)_2Ru\}^{II}(q)]^{2+}$. Following this investigation, Pierpont *et al.*[46] investigated the osmium analogue $[\{(bipy)_2Os\}^{II}(cat)]$, which also showed two reversible one electron oxidation processes corresponding to the cat/ sq and sq / q oxidation couples. In this instance though, the EPR spectrum (77 K, dichloromethane / acetonitrile glass) of the one-electron oxidised product was rhombic in symmetry (g_1 = 2.448, g_2 = 1.71, g_3 unobserved at their experimental field) resembling that of a characteristic low-spin d^5 osmium(III) in a distorted octahedral geometry.[47] Bond length analysis of the complex from single crystal X-ray diffraction confirmed this observation, giving the structure as $[\{(bipy)_2Os\}^{III}(cat)]^+$. The difference between these complexes was therefore attributed to the greater ease of oxidation of third-row transition metals (osmium) compared to those of the second row.[48] The differences between osmium and ruthenium was further compounded by the fact that the osmium analogue of the Creutz-Taube ion appeared 19 years after the original report, proving they have significantly different redox chemistry.[49] Subsequent investigations into ruthenium dioxolene systems have also shown that by modification of the dioxolene and/or ancillary ligand may cause either more-ligand or metal centred spin, resulting in situations where the interaction between metal and ligand is essentially a resonance model of $Ru^{II}(sq^{\bullet-}) \leftrightarrow Ru^{III}(cat^{2-})$, as shown in calculations based on model complexes.[50]

These investigations demonstrate the interest in transition-metal dioxolene chemistry well as they highlighted that the electron 'holes' generated by oxidation could be localised on either the metal or ligand, and that their subsequent characterisation is relatively straightforward due to characteristic structural, magnetic and spectroscopic attributes. This makes dioxolene complexes attractive to study because if the reversible changes in electron transfer or oxidation state could be controlled by application of an external stimulus, e.g. temperature, they could hold potential applications as molecular switches or memory storage devices, depending on the mechanism of transition.[1, 51] Of interest for this purpose are complexes containing more than one dioxolene centre, either by coordination to the same metal atom or

linked by an organic spacer. If present in different oxidation states, these dioxolene centres may communicate electronically, leading to intense near infrared (NIR) absorption spectra which have been postulated to be useful in electrochromic applications requiring electronic switching, the conversion of solar energy[52] or optoelectronic communication devices.

1.7.1 Platinum and Palladium Dioxolene Complexes

Despite the interest in complexes of the dioxolene series, there are relatively few platinum and palladium complexes known. Early studies of catechol or semiquinone complexes of formula $[(PPh_3)_2M(Cl_4cat)]$ (M = Pd or Pt) were formed by the oxidative addition of Cl_4Q (Cl_4Q = tetrachlorobenzoquinone) to phosphine complexes of Pd^0 or Pt^0.[53] Subsequent chemical or electrochemical oxidation was performed to give the semiquinone complexes, $[(PPh_3)_2M(Cl_4SQ)]$ (Cl_4SQ = tetrachlorosemiquinone) which were characterised by EPR where both displayed isotropic spectra with $g \approx 2.00$ indicating localisation of the radical onto the semiquinone ligand. Other ancillary ligands have been used (e.g. COD = cyclooctadiene)[54] although the majority of palladium and platinum monoclulear dioxolene complexes synthesised to date contain nitrogen-donor ancillary ligands, which are often very darkly coloured due to intense LMCT or LLCT optical transitions. The majority of those reported have therefore been investigated for their photophysical properties.[52] Amongst the first series of complexes synthesised containing chelating diimine nitrogen donors; bipy, phen or dpa (phen = 1,10-phenanthroline and dpa = dipyridylamine) which were investigated for their use as photosensitisers for $^1O_2$ formation.[55]

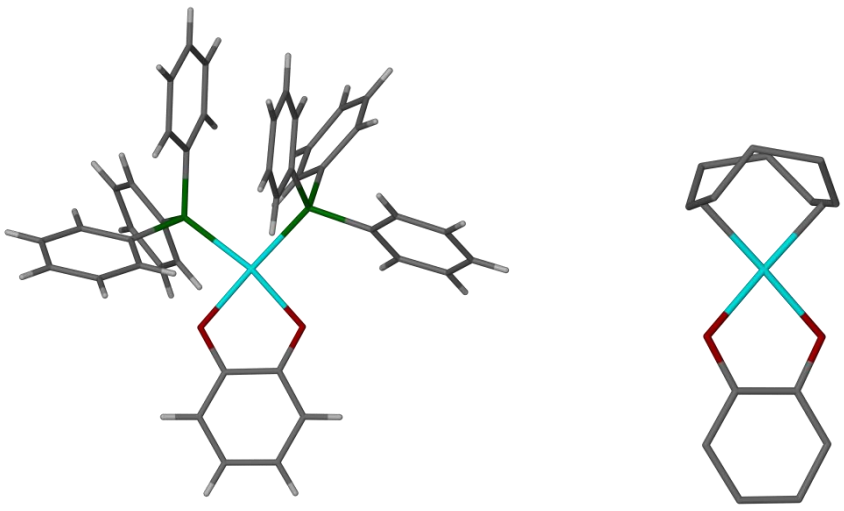

Figure 1.3. (Left) Single crystal structure of $[\{(PPh)_3\}_2Pt(cat)]$ prepared by Lesley *et al.*[56]. (Right) Single crystal structure of [(cod)Pt(cat)] prepared by Don *et al.*[54] Colour code; Pt, cyan; P, green; O, red; C, grey; H, white.

Platinum(II) diimine complexes have since been investigated extensively by Weinstein *et al.* or their potential in harnessing solar energy.[52] Variation of the diimine ancillary ligand (of

which the majority are 2,2`-bipyridine substituted in the 4,4` positions) resulted in tuneable electronic character of the complex. Spectroelectrochemical and cyclic voltammetric analysis of these complexes showed that the lowest electronic transition is primarily ligand-to-ligand (LL'CT) in character with the HOMO dioxolene-localised and LUMO diimine-localised.[57] Bis(semiquinone) complexes of palladium and platinum have also been prepared by the reaction of zero-valent precursors [(dba)Pd] and [(dba)Pt] (dba = dibenzylidineacetone) with two equivalents of DBQ (DBQ = 3,5-di-*tert*-butylbenzoquinone), yielding the square planar species $[(DBSQ)_2M]$ (M = Pd^{II} or Pt^{II}) (DBSQ = 3,5-di-*tert*-butylsemiquinone).[58] Interestingly, the ^1H NMR spectra of both complexes were sharp indicating strong antiferromagnetic coupling between the semiquinone radicals. The authors also noted how at lower temperatures the *tert*-butyl substituient in the 5- position of complex $[(DBSQ)_2Pd]$ showed a temperature dependent shift between 213 and 323 K, indicating a weaker (sq-sq) interaction compared to the platinum analogue.

1.8 Switchable Mononuclear Dioxolene Complexes

The feature of charge localisation in dioxolene complexes is now a well established field with plenty of examples displaying mixed valency for all three coordination modes (cat / sq / q). What was not anticipated during this research though was that the energy levels between metal dπ and dioxolene π* could be close enough to interact (as seen in $[\{(bipy)_2Ru\}^{II}(cat)]$) or exhibit intramolecular electron transfer resulting in altered charge distributions under equilibrium conditions, as depicted in **Scheme 1.6**. This alteration may be temperature, pressure or light induced yielding the potential for reversible changes in charge distribution and geometric transition without migration of groups or atoms.[59] Complexes of this type have been termed 'valence tautomers' and are of particular interest as they provide fascinating insights into intramolecular electron transfer processes alongside exhibiting structural, optical and magnetic changes therefore lending themselves to potential switchable applications. An added curiosity of complexes which undergo valence tautomeric changes is that changes in the bond lengths within the dioxolene ring(s)[37a] or between metal and ligand once oxidised may lead to cooperative changes within the lattice.

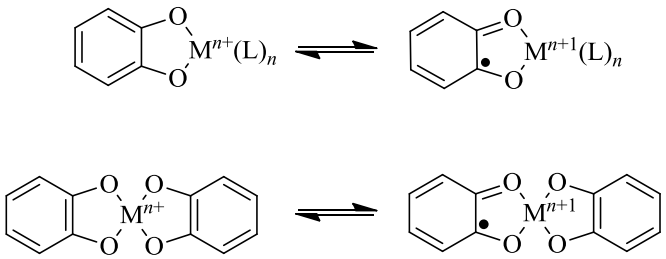

Scheme 1.6. Schematic of the altered charge seen in two types of valence tautomeric complexes.

The first reported observations of complexes exhibiting mixed valency were performed over thirty years ago, in the investigation of [(3,5-DBCat)(3,5-DBSQ)Co^{III}(bipy)] (3,5-DBCat = 3,5-di-*tertiary*-butylcatechol).[60]

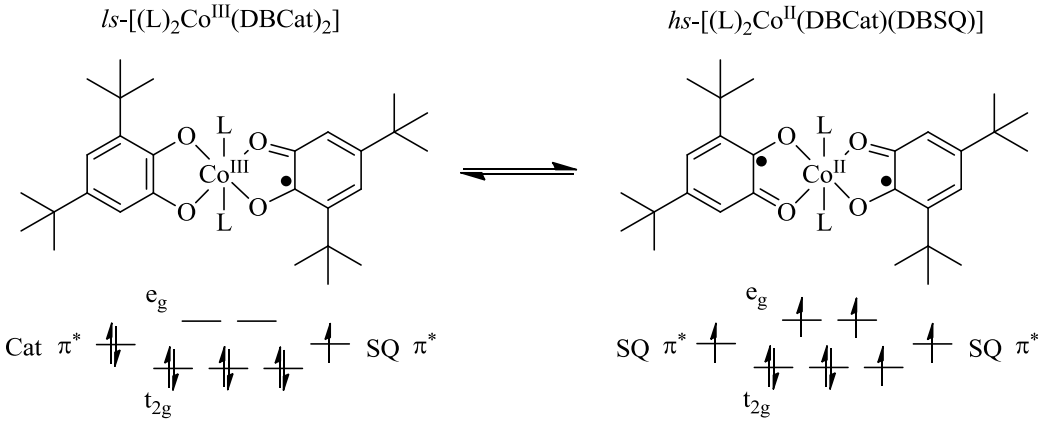

Scheme 1.7. Schematic representation of the valence tautomeric behaviour of a cobalt complex containing two dioxolene ligands, L = bipy, for example.[60]

It was found that complexes in the solid state differed significantly to complexes in the solution phase. In the solid state, the complex was crystallographically determined to be [(3,5-DBCat)(3,5-DBSQ)Co^{III}(bipy)], with *ls*-Co(III) (*ls* = low spin) metal centre and one semiquinone ligand. At room temperature, this gave a magnetic susceptibility measurement expected of a $S = ½$ complex, again indicating a diamagnetic *ls*-Co(III) metal centre whilst EPR analysis on powder samples of the complex supported this with organic based radical ($g = 2.00$) with weak hyperfine coupling to one ^{59}Co ($I = 7/2$) centre (approximately 30 G) and slight anisotropy. Once in solution, variable temperature EPR showed that above -40 °C the signal began to decrease, and at temperatures above 65 °C only baseline was observed with a paramagnetically shifted NMR spectrum characteristic of Co(II). [60-61] This behaviour indicated intramolecular electron transfer from DBCat to cobalt(III) yielding the species [$(3,5\text{-DBSQ})_2Co^{II}$(bipy)]. The transition could also be monitored by UV-vis, as shown in **Figure 1.4**, where a dichloromethane solution of [(3,5-DBCat)(3,5-

DBSQ)Co^{III}(bipy)] was warmed from 278 K to 303 K. Spectral changes associated with the transition of [(3,5-DBCat)(3,5-DBSQ)Co^{III}(bipy)] ⇌ [(3,5-DBSQ)$_2Co^{II}$(bipy)] were noted by the decrease in cat → cobalt LMCT close to 600 nm whilst a temperature-dependent increase in cobalt → sq band close to 750 nm was observed, also seen in the complex [(3,5-DBSQ)$_2$Co]$_4$.[62] Unfortunately there was no mention of the presence or changes in the IVCT band expected of [(3,5-DBCat)(3,5-DBSQ)Co^{III}(bipy)] during the transition.

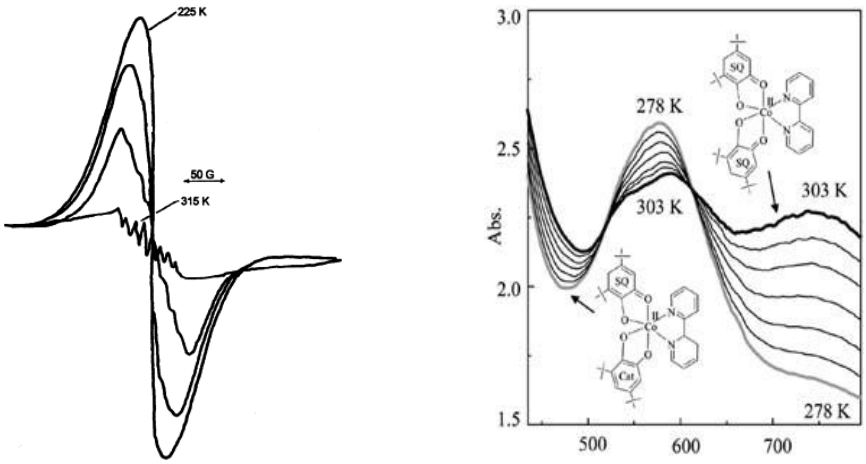

Figure 1.4. (Left) Variable temperature EPR and (Right) UV/vis spectral changes upon warming [(3,5-DBCat)(3,5-DBSQ)Co^{III}(bipy)], as observed by Buchanan *et al.*[60]

Following on from this investigation, analogous valence tautomers of [(bipy)Co^{II}(DBSQ)$_2$] were synthesised by replacing the bipyridine ligand with 1,10-phenanthroline (phen), 2,2'-bipyrimidine (bpym) or 2,2'-bipyrazine (bpyz).[61] It was found that solution measurements were typically solvent dependent and the transition shifted to a higher temperature on increasing solvent polarity. Extraction of thermodynamic parameters from the magnetic spectra indicated that both the entropic and enthalpic changes were large and positive due to the population of antibonding e_g orbital from the Co(III)-*ls* to Co(II)-*hs* transition.[63] The change in enthalpy was found to be due to a weakening of the Co-O and Co-N bonds, leading to an increase in conformational flexibility contributing to a positive entropic factor. This led to the understanding that the T_c (transition temperature) of valence tautomers is a factor dependent on ΔH^o and ΔS^o.[63] It was also found that alteration of the nitrogen-containing ancillary group affected T_c, whereby electron donating groups on the backbone increased T_c whilst electron withdrawing groups decreased T_c, resulting in the complexes [(NO_2phen)Co^{II}(DBSQ)(DBCat)] and [(dafl)Co^{II}(DBSQ)(DBCat)] (NO_2phen = 5-nitro-1,10-phenanthroline and dafl = 4,5-diazafluoren-9-one) which are essentially 'locked' as Co(II), therefore permitting their crystallographic structural determinations.[64] Further experiments were also conducted on different metal ions where it was found that spin transitions were not always necessary in the valence isomerism. This was particularly

obvious with manganese complexes which remained in their high-spin form throughout the process; $[(3,5\text{-DBCat})_2Mn^{IV}(py)_2] \rightleftharpoons [(3,5\text{-DTBSQ})_2Mn^{II}(py)_2]$ (py = pyridine) in toluene at room temperature.[65] Analogous mixed valence iron(III) complexes; have also been prepared, for example [(bipy)Fe(3,5-DBSQ)(3,5-DBCat)], [(phen)Fe(DBSQ)(DBCat)], from the reduction of their corresponding $[Fe(DBSQ)_3]$ complexes, although both failed to show any valence tautomerisation, understood to be due to the instability of the $[Fe(SQ)_3]$ species.[66] Despite this, there has been one report to-date where evidence of an iron(III) valence tautomer has been presented in the complex $[(bispicen)Fe^{III}(Cl_4Cat)(Cl_4SQ)]$ (bispicen = *N*,*N*'-bis(2-pyridylmethyl)-1,3-propanediamine, Cl_4Cat = tetrachlorocatecholate, Cl_4SQ = tetrachlorosemiquinone).[67] A temperature-dependent reduction in the intensity of IVCT transition close to 1925 nm between catechol and semiquinone was observed, as shown in **Figure 1.5 (top)**. **Figure 1.5 (bottom)** shows the valence tautomeric manganese complex dimer, $[(H_2bispictn)[Mn_2^{III}(Cl_4Cat)_4(DMF)_2]$ (**H_2**bispictn = *N*,*N*-bis(2-pyridylmethyl)-1,3-propanediamine) which also displays a decrease in this IVCT band although no change in the EPR was noted.

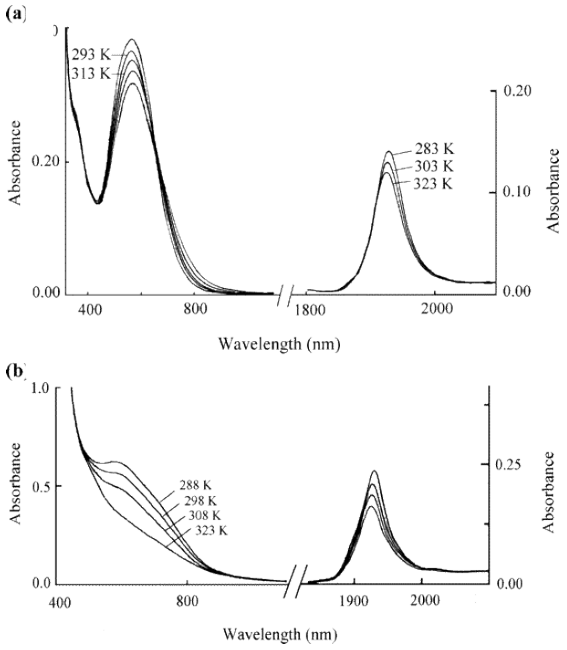

Figure 1.5. Temperature dependent changes in the UV/vis-NIR spectra of (top) $[(bispicen)Fe^{III}(Cl_4Cat)(Cl_4SQ)]$ and (bottom) $[(H_2bispictn)[Mn_2^{III}(Cl_4Cat)_4(DMF)_2]$ prepared by Shaikh *et al.*[67]

1.9 Mononuclear Copper Dioxolene Complexes

Dioxolene-containing complexes of copper have also been investigated extensively, and appears to be a growing field. In the mononuclear dioxolene complex, [(L-L)Cu(diox)] (L-L = any dinuclear ligand), it was found that where L-L was that of a 'hard' nitrogen donor,

2,2'-bipyridine for example, the dioxolene ligand was of the full catecholate (2-) oxidation state with paramagnetic copper(II) metal atom, e.g. [(bipy)Cu^{II}(DBCat)]. By substitution of the dinucleating bipyridine to a 'soft' phosphine however, PPh_3 (PPh_3 = triphenylphosphine) for example, it was found that electron transfer between dioxolene and copper had occurred, to give the complex corresponding semiquinonate complex, [$(PPh_3)_2Cu^{I}$($DBSQ^{\bullet}$)] with g value close to 2.00 and coupling to ^{63}Cu, ^{65}Cu and ^{31}P.[68] The electron transfer process; $Cu^{II}[cat^{2-}] \leftrightarrow Cu^{I}[sq^{\bullet-}]$ has since been realised a number of times, and shown to be in thermal equilibria as redox isomers. One of the earliest examples of their thermal equilibria was illustrated in an amine oxidase enzyme for the oxidation of amines to aldehydes which was shown to proceed via a two-electron reduction of O_2 to H_2O_2, catalysed by an oxygen-activating $Cu^{I}[sq^{\bullet-}]$ site.[69] The behaviour observed by Dooley *et al*.[69a] was particularly amenable to follow by EPR owing to the large differences in *g*-value between organic radical (close to 2.00) and paramagnetic copper(II) (close to 2.12). This was integral in determining the mechanism and temperature dependence of the process, which stabilises the $Cu^{II}[cat^{2-}]$ form at low temperatures and $Cu^{I}[sq^{\bullet-}]$ above 295 K. Addition of cyanide to the sample was also shown to stabilise the copper(I) form at low temperatures, due to the prevention of back electron transfer whilst more detailed enzymatic studies have shown that the $Cu^{I}[sq^{\bullet-}]$ is a viable intermediate in the process.[70] Complexes of this type are therefore particularly amenable to study due to the large structural and chemical differences between copper(I) and copper(II), which may be followed based upon their magnetic properties.[71] In addition to the displaying of thermal equilibria, the effect of the ancillary ligand to the copper has also been investigated in complexes of general formula [(L)Cu^{n+}($diox^{n-}$)].[72] It has been found that use of strong π-accepting ligands, such as PR_3, AsR_3, CO, CNR, alkenes or alkynes stabilises the $Cu^{I}[sq^{\bullet-}]$, whilst use of a non π-accepting ligand, such as tmeda (tmeda = N,N`,N``,N```-tetramethylethylenediamine) favours the $Cu^{II}[cat^{2-}]$ isomer.[73] Kaim *et al.* have investigated this preference of copper to adopt a specific oxidation state in the synthesis of a $Cu^{I}[sq^{\bullet-}]$ complex with thioether ancillary ligand, mmb (mmb = 1-methyl-2-(organothiomethyl)-1H-benzimidazole). The ligand mmb was chosen in their investigation as it coordinates as bidentate N,S- chelate ligand,[74] and is a good biological mimetic which can form a 5-membered metal chelate ring and mimicking histidine (imidazole-imine nitrogen) and methionine (saturated thioether).[75] EPR analysis (X-band, THF or toluene solution) of the synthesised complex [(mmb)Cu^{n+}(diox)]$^{n+}$ (diox = DBCat or DBSQ) showed the [(mmb)Cu^{II}(DBCat)] form is dominant at low temperature. Once warmed to above 250 K the copper(II) starts to be replaced by an isotropic signal at g = 2.005 which dominates above 350 K, corresponding to the [(mmb)Cu^{I}(DBSQ)] form, similar to that observed by Dooley *et al*.[69a] and implying temperature dependent isomerism. The process was found to be reversible, unless heated for prolonged periods above 360 K.[75]

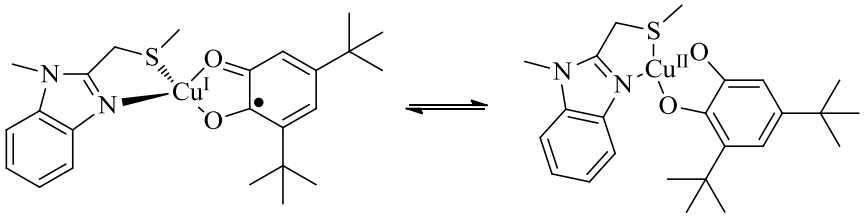

[(mmb)Cu^{I}(DBSQ)] [(mmb)Cu^{II}(DBCat)]

Scheme 1.8. Temperature dependent valence tautomeric transitions exhibited by [(mmb)Cu^{II}(DBCat)] as shown by Kaim *et al.*[75]

Extension of the investigation into use of other ancillary ligands containing N...S coordination to the copper (e.g. mtq, 8-methylthioquinolene) or N...P coordination (e.g dde, 1-diphenylphosphino-2-dimethylaminoethane) have also been shown to support this redox isomerism over similar temperature ranges.[76] In both investigations it was found that the $Cu^{II}[cat^{2-}]$ form was again dominant at low temperatures and $Cu^{I}[sq^{\bullet-}]$ at higher temperatures. A series of selenoether ligands analogous to mmb have also been prepared, although their redox chemistry as ancillary ligands to copper-dioxolene complexes has not been reported.[77]

1.10 Complexes of the [M(dioxolene)$_3$] Series

Some of the earliest examples containing multiple dioxolene ligands were synthesised using chromium, molybdenum and tungsten metal centres which could be prepared relatively easily by the reaction of appropriate metal carbonyl [$M(CO)_6$] with the parent quinone.[78] This was shown in the synthesis of complexes [$Cr^{III}(Cl_4SQ)_3$] (Cl_4SQ = tetrachloro-1,2-benzosemiquinone) and [$Cr^{III}(phenSQ)_3$] (phenSQ = 9,10-phenanthrene-semiquinonequinone) which were both octahedral and monomeric.[79] Studies on both complexes showed that they were indeed paramagnetic due to the $S = {}^{3}/_{2}$ Cr^{III} centre, although this paramagnetism decreased upon cooling due to the antiferromagnetic coupling between S = ½ semiquinone ligands and Cr^{III} metal centre.[80] Electrochemical analysis of the complexes showed that in both, each dioxolene ring could be sequentially oxidised and reduced, as shown in **Figure 1.6**, resulting in a three-stage redox process corresponding to the reduction and oxidation of each semiquinone ring to their corresponding catecholate (note the reversed scale of the voltammogram).[81]

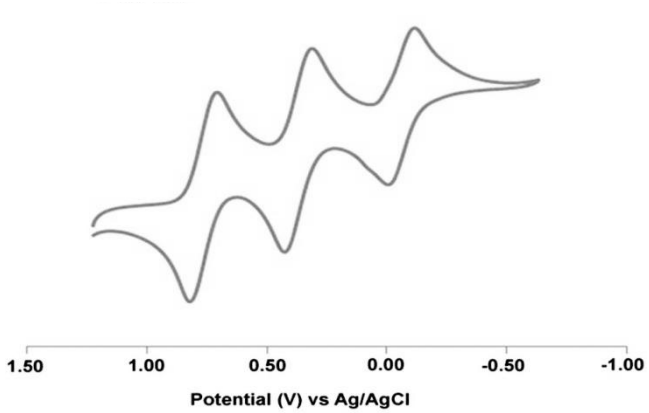

Figure 1.6. Cyclic voltammogram of $[Cr^{III}(Cl_4SQ)_3]$ (Cl_4SQ = tetrachloro-1,2-benzosemiquinone) as prepared by Pierpont *et al.*[79] Figure reproduced from reference [82].

An interesting feature to note regarding the voltammogram reported, is the significant positive shift of approximately 1 V when compared to the analogous complex $[Cr^{III}(DBSQ)_3]$ which has been attributed to the effect of the chlorine atoms on the ligand.[82] The redox series of $[Cr^{III}(Cl_4SQ)_3]$ has been extensively investigated by Kitagawa *et al.*[83] [84] where it was found that one or two electron reduction of $[Cr^{III}(Cl_4SQ)_3]$ yielded complexes of $[Cr^{III}(Cl_4SQ)_2(Cl_4cat)]^-$ and $[Cr^{III}(Cl_4SQ)(Cl_4cat)_2]^{2-}$, the latter crystallising as a discrete complex whilst the former crystallised with $[Cr^{III}(Cl_4SQ)_3]$.[84a] [84b] The process of reduction from $Cl_4SQ \rightarrow Cl_4Cat$ could be followed by magnetic measurements as the sequential spin-decoupling between chromium(III) and semiquinone ligands. Unfortunately analysis of the structures failed to indicate which ligands were of a different oxidation state. Despite this, for each species broad and intense IVCT transitions were observed at 5,560 cm^{-1} for $[Cr^{III}(Cl_4SQ)(Cl_4cat)_2]^{2-}$ which is shifted to higher energy for $[Cr^{III}(Cl_4SQ)_2(Cl_4cat)]^-$ and $[Cr^{III}(Cl_4SQ)_2(Cl_4cat)]^-$. $[Cr^{III}(Cl_4SQ)_3]$ with absorptions at 4, 550 and 4,590 cm^{-1} respectively. Analysis of the bandshapes of these absorptions indicated that these were of class II mixed valency[85] with large electronic coupling (H_{AB}), three times larger than that of the similar cobalt complexes,[86] indicating strong coupling through the chromium(III) atom. The analogous complex, $K_3[Cr^{III}(cat)_3]$ as shown in **Figure 1.7**, has also been synthesised and crystallographically characterised which also indicated the charge is localised on the ligand.[87]

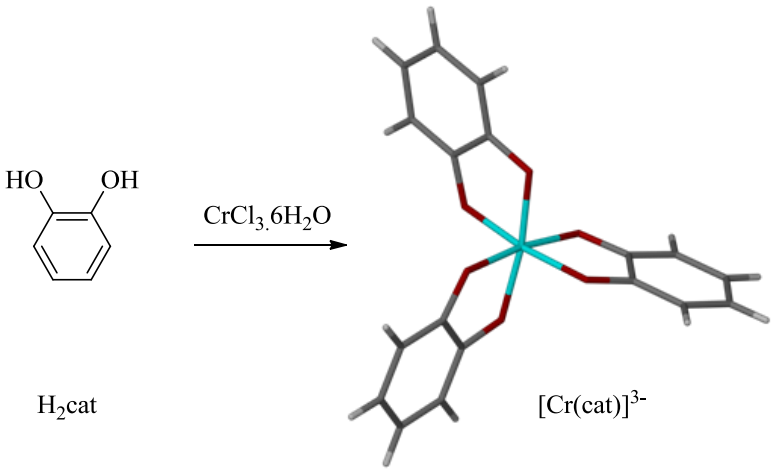

Figure 1.7. Synthesis and crystal structure of $K_3[Cr^{III}(cat)_3]$ by Raymond *et al*.[87] The potassium counter-anions are omitted for clarity. Colour code : Cr, cyan; C, grey; H, white; O, red.

Similar studies have been performed on the analogous complexes of molybdenum and tungsten although these complexes are more complicated as both are dimeric, linked by two catecholate ligands giving the general formula $[M_2(Cl_4cat)_6]$. Structural characterisation of the complexes agreed well with the assignments and, as with the complex $[Cr^{III}(Cl_4SQ)_3]$, all redox processes are ligand centered. Changing the dioxolene ligand to phenQ (phenQ = 1,10-phenanthroline quinone) however yielded the Mo^V mixed ligand complex $[Mo^V(phenSQ)(phencat)_2]$ as synthesised by the reaction of $[Mo(CO)_6]$ and phenanthrolinequinone.[78b] The high oxidation state of the molybdenum atom was not immediately obvious, although later studies found some evidence within coupling of the valent semiquinone electron coupling to molybdenum.[88]

As the coordination chemistry of the dioxolene series has developed, it has become obvious that when more than one dioxolene centre is present, coordinated to the same metal atom or more unusually separated by an organic spacer, these may display the potential for electron transfer if present in different oxidation state. The resultant electron transfer may belong to one of the three mixed valence classes (class I, II or III), described by Robin and Day,[10] depending on whether the dioxolene centres are distinguishable or not.

Of interest are bistable materials which hold the potential for interconversion between two distinct states which hold potential for simple molecular logic gates.[89] Increasing the number of redox active states yields further applications, particulary if interconversion between three states is accessible by different stimuli (e.g. heat, pressure, light).[90] This

could give rise to more complicated logic processes such as write–lock–read–unlock–erase cycles provided the interaction between redox-active centres is small but non-zero.[89]

1.11 Redox Activity of *Bis*-Dioxolene Complexes

1.11.1 Complexes of 2,5-hydroxy-1,4-benzoquinone

Combining several dioxolene units into one ligand is a convenient way of increasing the number of accessible redox states within a complex. Perhaps the best studied example of bridged dioxolenes are in derivatives of ligand 2,5-hydroxy-1,4-benzoquinone ($L_{1\text{-}R)}$, which can bind two metal atoms as shown in **Figure 1.8**.

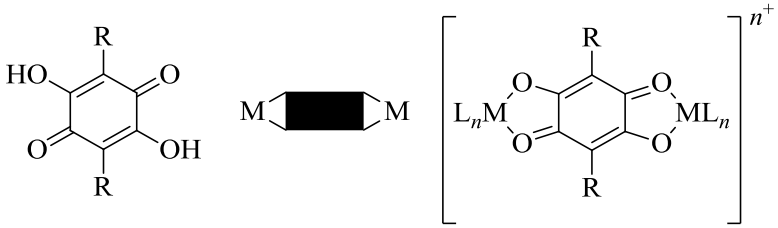

$\mathbf{L_{1\text{-}R}}$
R = H, Cl, Br, I, NO_2,
Me, ^{i}Pr, ^{t}Bu, Ph

$[\{ML_n\}(\mathbf{L_{1\text{-}R}})\{ML_n\}]^{n+}$
R = H, Cl, Br, I, NO_2,
Me, ^{i}Pr, ^{t}Bu, Ph

Figure 1.8. (Left) General structure of 2,5-hydroxy-1,4-benzoquinone derivatives. (Centre) Schematic representation of μ_2-$L_{1\text{-}R}$. (Right) general structure of $[\{MLn\}(L_{1\text{-}R})\{MLn\}]^{n+}$.

Technically a tetraoxalene, this ligand is of interest due to the accessible redox forms of $(L_{1\text{-}R})^{n-}$ where n = 0, 1, 2, 3 or 4, and $(L_{1\text{-}R})^{3-}$ / $(L_{1\text{-}R})^{-}$ are paramagnetic, with the most studied examples taking the general form $[\{ML_n\}(\mathbf{L_{1\text{-}R}})\{ML_n\}]^{n+}$ where M = Cr, Fe or Co and L_n is a bi- or tetradentate 'capping' ligand.[91] Complexes of this type were initially investigated for the purposes of generating a mixed valence species based upon the metal ions, for instance $[\{(tpa)Co^{II}\}(L_{\mathbf{1\text{-}Cl}}^{2-})\{tpa)Co^{III}\}]^{3+} \leftrightarrow [\{(tpa)Co^{III}\}(L_{\mathbf{1\text{-}Cl}}^{2-})\{tpa)Co^{II}\}]^{3+}$ (tpa = *tris*(2-pyridylmethyl)amine), which was expected to show one Co^{II} (S = $^{3}/_{2}$) site prepared from the one-electron oxidation of $[\{(tpa)Co^{II}\}(L_{\mathbf{1\text{-}Cl}}^{2-})\{ tpa)Co^{II}\}]^{2+}$ which displayed four, reversible one electron processes corresponding to the processes; ; $[cat / cat]^{4-} \leftrightarrow [sq / cat]^{3-} \leftrightarrow [sq / sq]^{2-} \leftrightarrow [q / sq]^{-} \leftrightarrow [q / q]^{0}$ at accessible potentials.[92] Once oxidised, the magnetic behaviour noticed instead was that of a S = ½ system, with g = 2.0027. This was certainly not what could be expected of *hs*-Co^{II}, where typically $g \approx 4.3$,[93] but instead that of an organic radical. Based upon this observation, and a temperature independent effective magnetic moment [$\mu_{eff}(T)$] equal to 1.75 μ_B, indicated the presence of one spin per molecule as this was significantly smaller than the expected $\mu_{eff}(T)$ = 5.68 μ_B for a S = $^{3}/_{2}$ system.[91]

Consequently, the system was assigned as the complex [{(tpa)Co^{III}}($L_{1\text{-}Cl}^{3\bullet-}$){tpa)$Co^{III}$}]$^{3+}$.[92] The crystal structure of the resultant complex was also obtained and is displayed in **Figure 1.9**, where analysis of internal and Co-O / Co-N bond lengths supported this assignment.

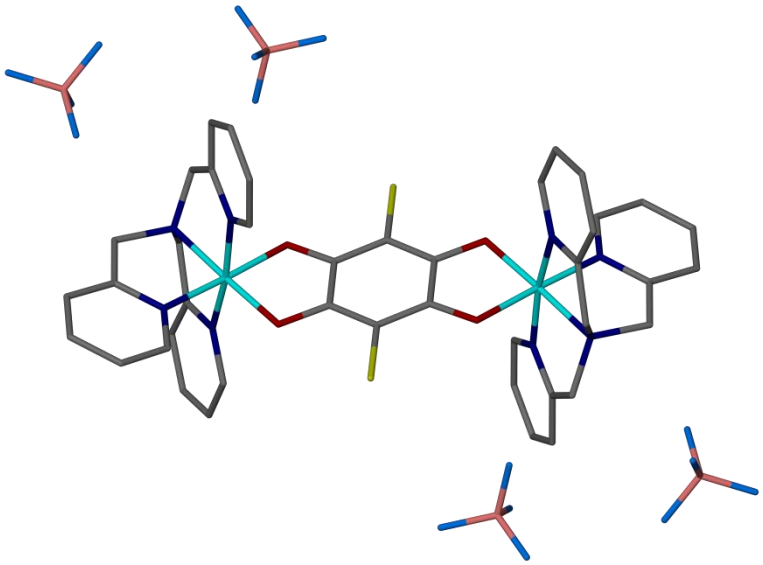

Figure 1.9. Structure of complex [{(tpa)Co^{III}}($L_{1\text{-}Cl}^{3\bullet-}$){tpa)$Co^{III}$}][$BF_4$]$_3$ prepared by Min *et al.*[92]. Colour code; C, grey; N, dark blue; O, red; B, Pink; F, sky blue; Co, cyan; Cl, yellow.

An interesting study on the analogous complex, [{(bipy)Ru^{II}}($L_{1\text{-}H}^{2-}$){Ru^{II}(bipy)}]$^{2+}$ (bipy = 2,2'-bipyridine) by Ward[19b] showed the HOMO is delocalised extensively across the entire complex, with major contributions from the d_{xz} of each ruthenium(II) atom (20% each) and 60% from the π-orbitals of the bridging $L_{1\text{-}H}^{2-}$ ligand. The LUMO, on the other hand, was again primarily located on the $L_{1\text{-}H}^{2-}$ ligand π*-orbital (94%), with small metal d_{xz} contribution (3% each).[19b] As a result, this ligand has generated a lot of interest in redox-induced electron transfer (RIET) complexes, where it has been found that in addition to a one electron process, a consequential second electron process also occurs i.e. a reduction following an oxidation or oxidation following a reduction. Other examples of complexes displaying this curious feat have been reported, involving the oxidation of [{(cth)Fe^{II}}($L_{1\text{-}H}^{2-}$){Fe^{II}(cth)}]$^{2+}$ (cth = *dl*-5,7,7,12,14-hexamethyl-1,4,8,11-tetraazacyclotetradecane, **Figure 1.10**). This complex was assumed to undergo the same, double-oxidation / mono-reduction between [{(cth)Fe^{II}}($L_{1\text{-}H}^{2-}$){Fe^{II}(cth)}]$^{2+}$ ↔ [{(cth)Fe^{III}}($L_{1\text{-}H}^{3\bullet-}$){$Fe^{III}$(cth)}]$^{3+}$ after one-electron oxidation by silver perchlorate according to its IR and ^{57}Fe Mössbauer spectra. In addition, a large μ_{eff} = 9.1 μ_B, which increases with decreasing temperature (resultant of two spins > ½ antiferromagnetically coupling to one S = ½ state) indicated the absence of Fe(II), due to a $S = {}^{9}/_{2}$ ground state.[94] In the same study, Dei *et al.* also reported the analogous chromium analogue [{(cth)Cr^{II}}($L_{1\text{-}H}^{2-}$){Cr^{II}(cth)}]$^{2+}$, which undergoes the same RIET process upon oxidation, yielding [{(cth)Cr^{III}}($L_{1\text{-}H}^{3\bullet-}$){$Cr^{III}$(cth)}]$^{3+}$. An interesting

observation of this complex was that the coupling between $L_{1\text{-}H}^{3\bullet-}$ radical and Cr(III) was smaller than in complexes containing semiquinato-ligands[95] indicating a greater propensity for delocalisation in the $L_{1\text{-}H}^{3\bullet-}$ ligand.[94]

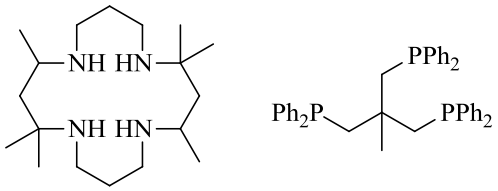

cth triphos

Figure 1.10. (Left) Schematic structure of *dl*-5,7,7,12,14-hexamethyl-1,4,8,11-tetraazacyclotetradecane (cth). (Right) Schematic structure of 1,1,1-*tris*(diphenylphosphanomethyl)ethane (triphos).

Mixed valence species of complexes containing the central ligand $[\mathbf{L_{1\text{-}R}}]^{4-}$ (R = H, Cl, Br, I, NO_2, Me, ^{i}Pr and Ph) have been demonstrated for complexes containing cobalt with the triphos (1,1,1-*tris*(diphenylphosphanomethyl)ethane, **Figure 1.10**) ancillary ligand.[96] Cobalt complexes containing this triphos ancillary ligand were chosen to be investigated as it was shown by Bianchini *et al.*[97] that the electron delocalisation in complexes of $[(triphos)Co^{III}(cat)]^+$ is very small resulting in a relatively pure Co^{III}-cat oxidation state, as proven by their diamagnetic nature. As a result, the complexes synthesised containing triphos were shown to contain *ls*-$(triphos)Co^{III}$ (*ls* = low spin) bridged by $[L_{1\text{-}R}]^{4-}$ as the complex $[\{(triphos)Co^{III}\}(L_{\mathbf{1\text{-}R}}^{\mathbf{4-}})\{Co^{III}(triphos)\}]^{2+}$.[96] The complexes were analysed electrochemically which interestingly showed two, one-electron reductions separated by over 1 V, corresponding to one electron redox processes of Co(III) ↔ Co(II) on either side of the molecule whilst analysis by UV-vis/NIR absorption spectroscopy showed the presence of one very intense IVCT absorption in the NIR region at 1185 nm ($\varepsilon = 44 \times 10^4$ $M^{-1}cm^{-1}$) at 295 K. Once cooled to 100 K, this band shifted slightly (150 cm^{-1}) and almost doubled in intensity ($\varepsilon = 80 \times 10^4$ $M^{-1}cm^{-1}$), with a significant reduction in band width. The band also showed some solvatochromism, where polar solvents exhibited a blue-shift to the transition whilst non-polar solvents demonstrated a red-shift. The authors attributed this to an increased stabilisation of the ground state by polar solvents with respect to the excited state, a feature also seen in charge-transfer bands of the mononuclear complex $[(triphos)Co^{III}(cat)]^+$. Variable temperature EPR analysis of the electrochemically singly reduced complex, $[\{(triphos)Co^{n+}\}(L_{\mathbf{1\text{-}R}}^{\mathbf{4-}})\{Co^{n+}(triphos)\}]^+$ was performed in order to determine the local environment of the valent electron. At 295 K, the spectrum showed a very broad isotropic signal centred at g = 2.11 whilst measurements at 100 K (dichloromethane, frozen glass) generated a complex spectrum again centred at g = 2.11

with hyperfine coupling to ^{57}Co (I = $^{7}/_{2}$) of A_x = 40, A_y = 40 and A_z = 34 G. This could not be simulated by assuming coupling to one metal centre only, therefore implying the valent electron couples to both metal ions, and is not localised on the bridging ligand.[98] DFT analysis of the complex showed the LUMO is predominately (68%) on the two cobalt centres, with small ligand contributions whilst the HOMO is the inverse and lies predominately on the ligand (70%) with the remaining as metal character (30%). This observation was confirmed by analysis and reduction of the analogous mononuclear complex. As a result, the EPR and intense and narrow IVCT transition indicated that the valent electron is class III in character across both cobalt centres.

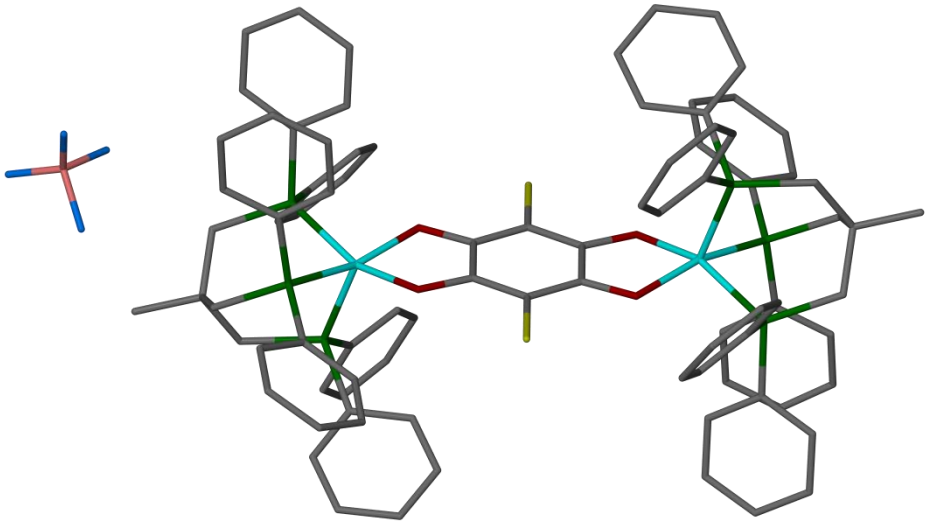

Figure 1.11. One-electron reduced complex [{(triphos)Co}($L_{1\text{-}R}^{4-}$){Co(triphos)}][BF_4] prepared by Heinze *et al*.[96] Colour code: Co, cyan; Cl, yellow; P, green; F, sky blue; B, pink; C, grey; O, red.

1.11.2 Complexes of biscat

When two dioxolene rings are bonded via an organic linker, as in 3,3',4,4'-tetrahydroxybiphenyl (biscat) for example, this may result in a potentially reversible 5-membered redox-chain; $[cat/cat]^{4-} \leftrightarrow [sq/cat]^{3-} \leftrightarrow [sq/sq]^{2-} \leftrightarrow [q/sq]^{-} \leftrightarrow [q/q]^{0}$, of which the $[sq/cat]^{3-}$ and $[q/sq]^{-}$ will be paramagnetic (S = $^{1}/_{2}$) and of mixed valence.

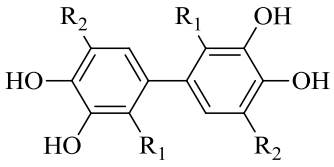

biscat ; $R_1 = R_2 = H$
^{t}Bu$_2$biscat ; $R_1 = {}^t$Bu, $R_2 = H$
^{t}Bu$_2$Me$_2$biscat ; $R_1 = {}^t$Bu, R_2 = Me

Figure 1.12. Schematic structures of biscat derivatives.

The redox chemistry of biscat (R_1 = R_2 H) has been investigated extensively by Ward *et al.*[48] in complexes containing ruthenium(II) and osmium(II), owing to their rich and stable electrochemistry permitting the study of a large number of redox states. Electrochemical analysis of complexes [{(bipy)Ru^{II}}$_2$(cat-cat)] and [{(bipy)Os^{III}}$_2$(cat-cat)]$^{2+}$ (cat-cat used here to denote the presence of both dioxolene rings in [biscat]$^{n-}$ are of the catecholate oxidation state) showed the presence of four separate redox processes for each. For [{(bipy)Ru^{II}}$_2$(cat-cat)], these corresponded as four ligand centred oxidations; [cat / cat]$^{4-}$ ↔ [sq / cat]$^{3-}$ ↔ [sq / sq]$^{2-}$ ↔ [q / sq]$^{-}$ ↔ [q / q]^{0}. For [{(bipy)Os^{III}}$_2$(cat-cat)]$^{2+}$ however, the four redox processes were attributed to two ligand-centred; [cat / cat]$^{4-}$ ↔ [sq / cat]$^{3-}$ ↔ [sq / sq]$^{2-}$ and two metal-centred redox processes Os^{III} ↔ Os^{II}, which were reduced in separation, as shown in **Figure 1.13**.[99] This had the implication that the complexes in their tetra-cationic forms were best described as [{(bipy)Ru^{II}}$_2$(q-q)]$^{4+}$ and [{(bipy)Os^{III}}$_2$(sq-sq)]$^{4+}$, reflecting the ease of oxidation of osmium compared to ruthenium. Interestingly also, the *bis*-semiquinonate complex [{(bipy)Ru^{II}}$_2$(sq-sq)]$^{2+}$ was isolated under aerobic conditions, and surprisingly showed the pairing of electrons across the bridge yielding a diamagnetic, extensively delocalised structure with very intense Ru(II)→(sq-sq) MLCT at lower energy compared to the mononuclear [{(bipy)Ru^{II}}(sq)]$^{+}$ complex ($\varepsilon = 10^4$ $M^{-1}cm^{-1}$).[99-100]

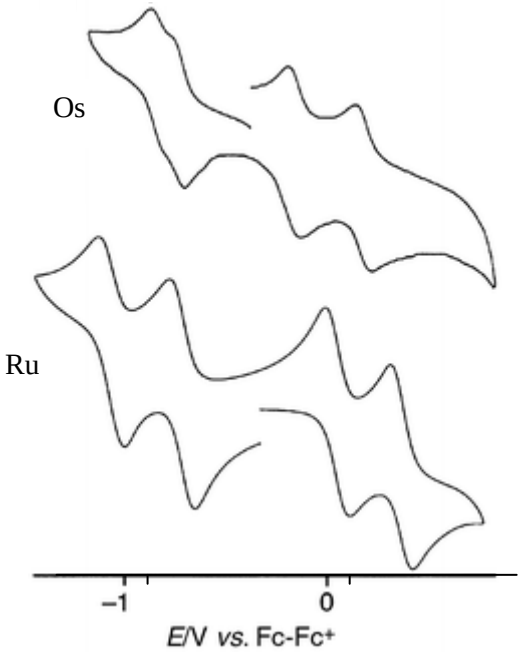

Figure 1.13. Cyclic voltammograms of (top) [{(bipy)Os^{III}}$_2$(biscat)]$^{2+}$ and (bottom) [{(bipy)Ru^{II}}$_2$(biscat)] in MeCN reported by Bartharam *et al.*[99]

Weinstein *et al.*[101] have used the same ligand in an investigation into its mixed valence characteristics using platinum(II)diimine termini yielding complexes [{(N-N)Pt}$_2$(cat-cat)] including a comparison to their mononuclear homologues [(N-N)Pt(DBCat)]. Again, reversible one-electron redox processes for the [cat / cat]$^{4-}$ ↔ [sq / cat]$^{3-}$ ↔ [sq / sq]$^{2-}$ redox

processes were noted, in similar positions and separation (ΔE = 340 mV) to complexes [{(bipy)Ru^{II}}$_2$(cat-cat)] and [{(bipy)Os^{III}}$_2$(cat-cat)]$^{2+}$, indicating similar electronic communication between dioxolene rings.[99] Electrochemical one-electron oxidation of the complex to give [{(N-N)Pt}$_2$(biscat)]$^+$ was performed to characterise the mixed valence species generated. What was found indicated a primarily ligand-centred HOMO with the growth of an intense and narrow new band in the near-infrared region, assignable as an IVCT transition from catechol→semiquinone (π- π*) of the entire ligand. The corresponding narrowness and intensity of the transition indicated it was Robin-Day class III in character. X-band EPR analysis confirmed this assignment, as the isotropic spectrum obtained was close to free electron value (indicating an organic-based radical) at g = 2.0005 showing no extractable hyperfine coupling between radical and platinum as shown in **Figure 1.14 (top).** One-electron reduction of the complex on the other hand displayed a rhombic spectrum with clear coupling to one ^{195}Pt nucleus, as shown in **Figure 1.14 (bottom)**, indicating the valent electron is localised on a bipyridine ligand at one terminus of the molecule.

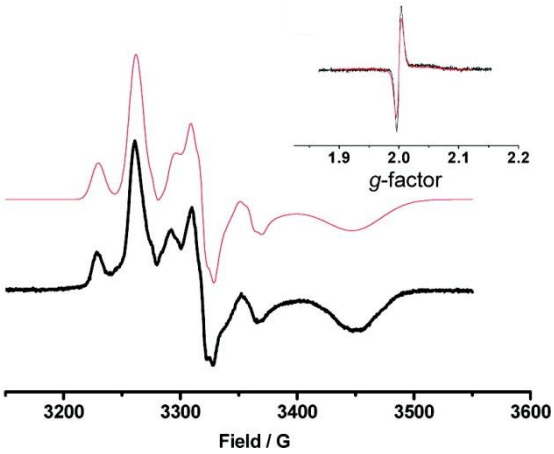

Figure 1.14. X-band EPR spectra recorded at 77 K in CH_2Cl_2. (Top) Spectrum of [{(^{t}Bu$_2$Bipy)Pt}$_2$(biscat)]$^+$ recorded after electrochemical oxidation. (Bottom) Spectrum of [{(^{t}Bu$_2$Bipt)Pt}$_2$(biscat)]$^-$ recorded at 77 K after electrochemical reduction. Red lines are the simulated spectra, black lines are the experimental spectra.

These observations were unlike the previously reported analysis of a similar mononuclear-platinum semiquinoate radical complex [(dpphen)Pt(DBSQ)] (dpphen = 4,7-diphenyl-9,10-phenanthroline, DBSQ = 3,5-di-*tert*-butyl-semiquinone), as seen in **Figure 1.15**.[57] This investigation instead showed the presence of significant localisation onto the platinum in both the reduced [(dpphen)Pt(DBCat)]$^-$ and oxidised [(dpphen)Pt(DBSQ)]$^+$ forms. An interesting observation in this study was the presence of coupling between radical and ^{195}Pt in the radical cation, this was attributed to the partial delocalisation of the SOMO into the platinum (calculated to have overall 7% contribution) despite the presence of the MLCT

absorption matching that of a valence localised Ni^{II}(DBSQ) complex, at approximately 21,400 cm^{-1}.[57]

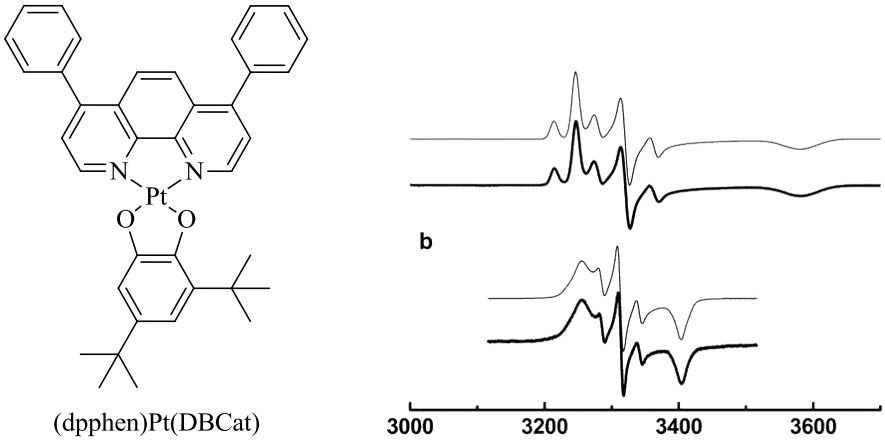

(dpphen)Pt(DBCat)

Figure 1.15. (Left) Schematic structure of [(dpphen)Pt(DBCat)]. (Top right) X-Band EPR spectrum of electrochemically reduced $[(dpphen)Pt(DBCat)]^-$ recorded at 77 K. (Bottom right) X-Band EPR spectrum of electrochemically reduced $[(dpphen)Pt(DBCat)]^+$ recorded at 77 K. Grey lines are the simulated spectra, black lines are the experimental spectra.

The observation of the electron localised on one terminus of the molecule was investigated by DFT calculations which showed the HOMO is localised on the bridging ligand whilst the LUMO is localised primarily on the bipyridine with some platinum character. DFT analysis also calculated that in the ground state the structure is not planar, with an angle of approximately 32° between the planes of the dioxolene rings as has been seen in similar biphenyl units. Once oxidised however, this angle is reduced to 19°, as in the calculated excited state and one-electron oxidised forms. The barrier to rotation between the rings was also calculated, and was shown to decrease from 1.75 kT for the singlet state to 0.4 kT for the oxidised radical cation, implying almost free rotation about the central C-C bond at room temperature and likely facilitating electron delocalisation throughout the $[biscat]^{n-}$ ligand, resulting in class III character. This observation was shared by Ward *et al.,* who observed the pairing of electrons at this central bridge as described above.[99] It would therefore appear that the electron delocalisation is sensitive to the dihedral angle between dioxolene rings. In order to investigate this relationship, constrained complexes where R_1 = ^{t}Bu and R = Me, were synthesised where the unreduced compound, 4,4′-bis(3-methyl-6-tert-butyl-1,2-benzoquinone) displayed near orthogonal rings (83°). Complexation of $[Tl(Me)_2(3,6\text{-}DBSQ)]$ and 4,4′-bis(3-methyl-6-tert-butyl-1,2-benzoquinone) in THF yielded the polymeric species $\{[Tl(Me)_2(THF)(t\text{Bu}_2\text{Me}_2\text{biscat})]_2\}_n$ shown crystallographically, as in **Figure 1.16**.[102]

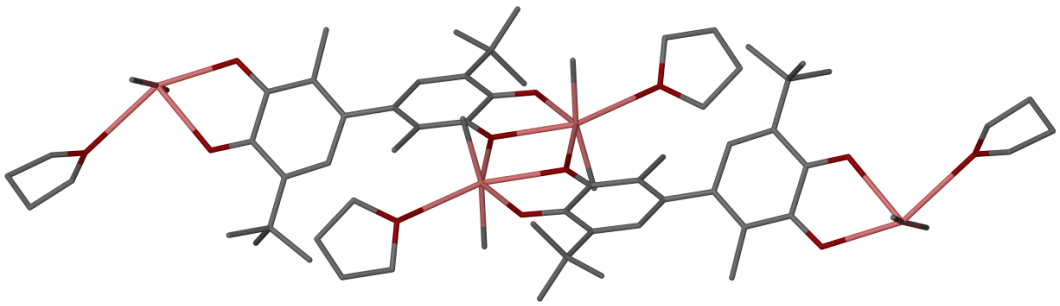

Figure 1.16. Two subunits of polymeric species $\{[Tl(Me)_2(THF)(^tBu_2\text{-}Me_2biscat)]_2\}_n$ prepared by Abakumov *et al.*[102] Colour code: Tl, pink; O, red; C, grey.

Analysis of this complex showed that upon complexation, the angle between least squares-planes of the two dioxolene rings reduces significantly to 51.5° although the C-C bond length between rings is distinctly longer than that expected of double bond character. The structure therefore appeared as two distinct semiquinone rings. EPR analysis however showed the complex was diamagnetic, indicating strong coupling between the radical centres likely through the highly distorted bridging carbon. Subsequent oxidation of the complex by addition of one equivalent of ($^tBu_2$-biscat) (q-q) to give the mono-radical (sq-q), yielded the spectrum displayed in **Figure 1.17**, centred at g = 2.0039 consisting of two well separated resonances arising from coupling between the two $^{203,205}Tl$ (I = ½) nuclei. Unfortunately though, this spectrum was attributed to the transfer of one $TlMe_2^+$ to the reduced $^tBu_2$-biscat (sq-q) resulting in two molecules of $[Tl(Me)(THF)(^tBu_2Me_2biscat)]_2$ (sq-q) due to the lack of a resonance originating from the unsubstitited monoradical ligand in the spectrum.[102]

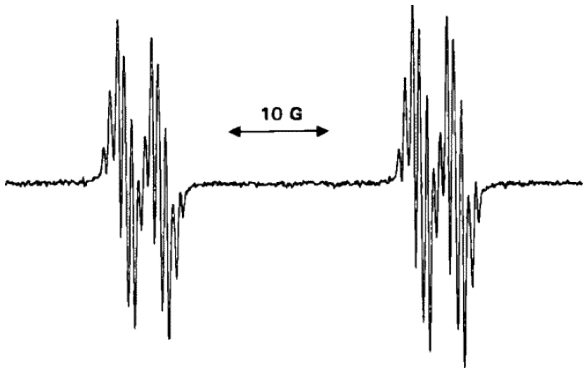

Figure 1.17. X-band EPR for $[Tl(Me)(THF)(^tBu_2\text{-}biscat)]_2$ (sq-q) prepared by Abakumov *et al.*[102]

The same ligand, $[^tBu_2Me_2biscat]^{n-}$ was again investigated by Abakumov and Pierpont *et al.* in the synthesis of complexes containing Copper with bipy or PPh_3 ancillary ligands.[103] Attempted synthesis of $[\{(bipy)Cu\}_2(^tBu_2Me_2biscat)]$ resulted only in the mono-metallic complex $[(bipy)Cu^{II}(cat\text{-}q)]$. Single crystal analysis and showed the $\{(bipy)Cu^{II}\}$ moiety was bound at the catecholate terminus with dihedral angle between the (cat-q) rings equal to

49.5°. EPR analysis showed a spectrum consistent with the copper(II) oxidation state, apparent with an axial spectrum with $g_{\parallel} = 2.198$, $g_{\perp} = 2.049$ and coupling to $^{63,65}Cu$ and ^{14}N. Dissolution of the complex in air free toluene and in the presence of PPh_3 permitted the formation of the complex $[(PPh_3)_2Cu^{I}(sq\text{-}q)]$, as shown by a shift in EPR signal to $g_{iso} = 2.00$ with coupling to $^{63,65}Cu$ and ^{31}P. A more recent investigation was made using the same ligand by Poddel'sky *et al.* in complexes containing (trimethyl)- and (triethyl)antimony(V).[104] In both cases, the (cat-cat) complexes were synthesised first, and the complex $[\{(Et)_3Sb\}_2(cat\text{-}cat)]$ characterised crystallographically with torsion angle between rings equal 75°. Attempted chemical oxidation of the same complex by addition of ferrocenium tetrafluoroborate ($[FeCp_2]BF_4$) caused loss of one $\{(Et)_3Sb\}^{2+}$ group and formation of the complex $[\{(Et)_3Sb\}(cat\text{-}sq)][(Et)_3SbF]$. EPR analysis of this complex displayed an isotropic spectrum with $g = 2.003$ with hyperfine coupling to both hydrogen nuclei in the 5- position of the dioxolene rings implying the radical electron is delocalised throughout the complete complex.

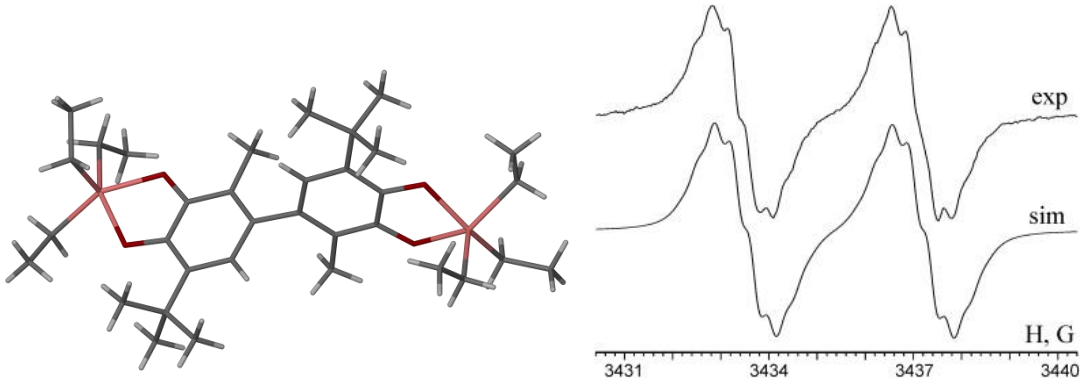

Figure 1.18. (Left) Single crystal X-ray structure of $[\{(Et)_3Sb\}_2(^{t}Bu_2Me_2biscat)]$ (cat-cat). Colour code: Sb, pink; C, grey; H, white; O, red. (Right) X-band EPR (toluene 295 K) of $[\{(Et)_3Sb\}(cat\text{-}sq)][(Et)_3SbF]$.

The core unit ($^{t}Bu_2$-biscat) was also studied by Dei *et al.* for the preparation of dinuclear chromium(III) and cobalt(III) (sq-cat) complexes containing the ancillary ligand cth.[105] The complexes synthesised were $[\{Co^{III}_2(cth)\}_2(cat\text{-}cat)][PF_6]$ and $[\{Cr^{III}_2(cth)\}_2(cat\text{-}cat)][PF_6]$, and both displayed two sequential redox processes between $-0.47 \leq E_{½} \leq +0.12$, corresponding to the one-electron cat ↔ sq processes of each dioxolene ring. Oxidation of these complexes by addition of one equivalent of $[FeCp_2]PF_6$ yielded the mono-oxidised, mixed valence complexes $[\{Co^{III}_2(cth)\}_2(cat\text{-}sq)][PF_6]_2$ and $[\{Cr^{III}_2(cth)\}_2(cat\text{-}sq)][PF_6]$. Characterisation by UV/vis-NIR showed both complexes had similar absorptions, indicating the internal ligand π and π* levels contribute strongly to the spectrum. Bands in the near-IR region could be assigned as an IVCT transition at 7,200 cm^{-1}, shifting to lower energy on increasing donor ability of the solvent (6950 cm^{-1} in dimethylsulfoxide). EPR analysis of the complexes similarly confirmed the presence of two radical complexes, although displayed

significant delocalisation. Complex $[\{Co^{III}_2(cth)\}_2(cat\text{-}sq)][PF_6]_2$ displayed a 17 line spectrum, centred at g = 2.00 attributed to the coupling of the valent electron with two equivalent Co^{III} nuclei and two equivalent ^1H nuclei of the bridging ligand. Analysis of $[\{Cr^{III}_2(cth)\}_2(cat\text{-}sq)][PF_6]$ displayed a similar story, consistent with that of an isolated sextet ground state, resultant of the antiferromagnetic coupling of the two chromium ions with the valent ligand electron. Due to this delocalisation, the two complexes could be appropriately described as class III mixed-valence species which was supported by DFT analysis of the complexes which showed the HOMO extends across the whole bridging ligands, with some unspecified metal character.

1.11.3 Modified Units of the H_4biscat Core

Due to the extensive delocalisation in mixed-valence complexes containing the $[biscat]^{n-}$ core unit, it seems intuitive that modification of the tether between the redox-active centres would have the effect of reducing the electron delocalisation, thereby promoting class II or class I character. Simple introduction of a phenylene spacer inbetween the dioxolene rings was therefore attempted,[106] and the complex $[\{(bipy)_2Ru\}_2(p\text{-}Phcat_2)]$ (R = H, *p*-Ph = 3,3",4,4"-tetrahydroxy-*p*-terphenyl) synthesised in the same manner as $[\{(bipy)_2Ru\}_2(biscat)]$.

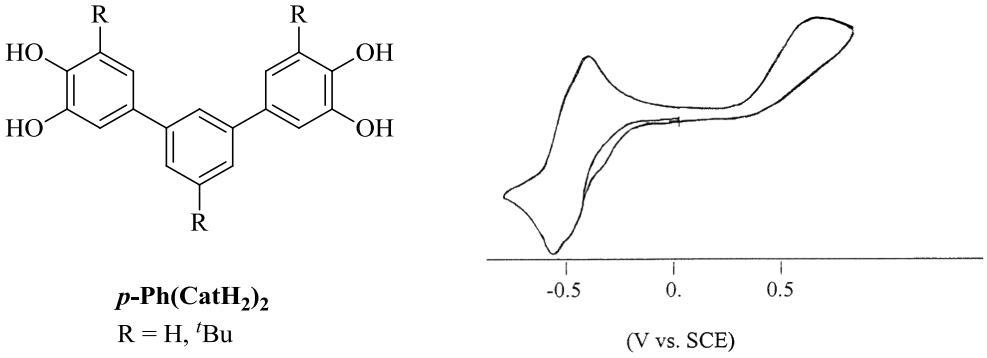

***p*-Ph(CatH$_2$)$_2$**
R = H, ^{t}Bu

Figure 1.19. (Left) Schematic of the chemical structure of compounds of the *p*-Ph$(H_2cat)_2$ core unit. (Right) Cyclic voltammogram of [{(cth)Ni}(sq-sq){Ni(cth)}] investigated by Caneschi *et al.*[107].

Unfortunately, electrochemical analysis of $[\{(bipy)_2Ru\}_2(p\text{-}Phcat_2)]$ displayed only two poorly separated and broad redox processes, corresponding to the concomitant oxidation and reduction of both dioxolene rings. This is resultant of the reduced electronic interaction between halves of the complex, meaning that the only the fully reduced cat-cat and fully oxidised q-q states are accessible. Complexes of the *tert*-butyl analogue displayed similar behaviour, whereby electrochemical distinction between the two dioxolene rings in $[\{(L)_nM\}(cat\text{-}sq)\{M(L)_n\}]$ (L_nM = (cth)Cr^{III} and (cth)Ni^{II}) was very difficult due to the same

reasons, resulting in significant quantities of the *bis*-catechol and *bis*-semiquinone species rather than the mixed valence complex [{(L)$_n$M}(cat-sq){M(L)$_n$}] (**Figure 1.19**).[107] In the same investigation, analysis of the complexes [{(L)$_n$M}(sq-sq){M(L)$_n$}] were interestingly found to exist as the diradical species, indicating the radicals are ferromagnetically coupled with smaller coupling than expected (J = 30 – 35 cm^{-1}). The authors took this to mean that the angle between dioxolene planes again plays a part in the extent of coupling, and provided that no significant structural changes occur upon reduction of the compound to form the mixed valence species (cat-sq), class II character could potentially be attainable. To date, this ligand has been investigated for the purposes of synthesising a [{(phen)Co^{n+}}μ-(cat-sq)•CH_2Cl_2]$_\infty$ polymeric valence tautomeric complex, where each cobalt atom is six-coordinate.[108] It was found that at low temperatures, a gradual temperature-dependent transition to *hs-ls* of [{(phen)Co^{III}}-μ-(cat-sq){Co^{III}(phen)]$_\infty$ ⇄ [{(phen)Co^{II}}-μ-(sq-sq){Co^{II}(phen)]$_\infty$ with thermal hysteresis of approximately 12 K despite at 310 K the transition was incomplete. This observation displayed the class II nature of the ligand however, as was postulated above.

More recently, the complex was investigated for the purposes of inducing a valence tautomeric transition by irradiation at 658 nm, into a partial LMCT band,[86] at 9 K.[109] The process was found to be reversible and reaching a plateau after one hour (corresponding to 10% of the sample) as shown by the decrease in intensity of the EPR g = 2 transition due to the [{(phen)Co^{III}}-μ-(cat-sq){Co^{III}(phen)]$_\infty$ species. No growth of alternative EPR transitions were noted, although as mentioned above Co^{II}(SQ) species are EPR silent, likely due to unfavourable electronic relaxation times.[110] The subsequent relaxation back to the ground state is thermally induced, as shown in experiments plotting the relaxation as a function of time at four different temperatures (9, 20, 30 and 40 K) exhibiting a first-order exponential decay. The decay was found to be significantly slower (10^5 s at 9 K) compared to mononuclear systems e.g. [(Phen)Co(DBCat)(DBSQ)] (10^4 s at 5 K), which was attributed to the small one-dimensional cooperativity exhibited between photoinduced centres. To date no further work has been conducted on this ligand.

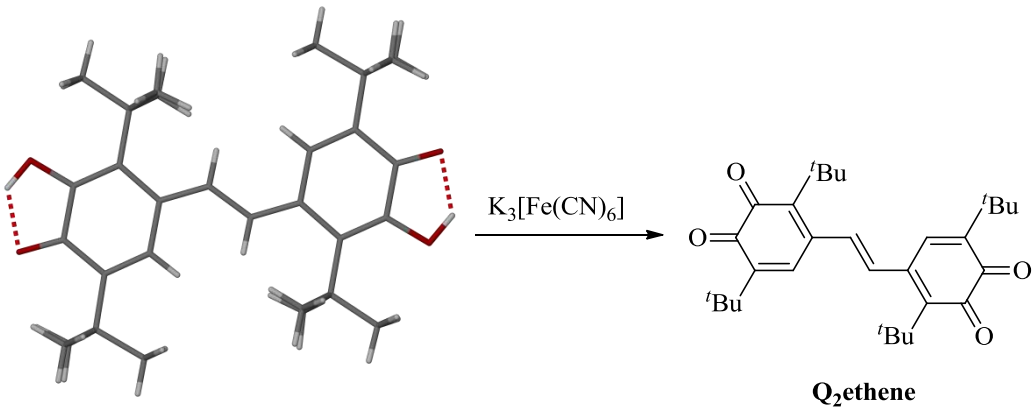

Q_2ethene

Scheme 1.9. Preparation of ligand Q_2ethene from the oxidation of 4,4′-(ethane-1,2-diylidene)bis(2-hydroxy-3,6-di-*tert*-butyl-cyclohexa-2,5-dienone).[111] Colour code: O, red; C, grey; H, white. The dashed red line inbetween hydrogen and oxygen denotes a intramolecular hydrogen bond.

Variation of the spacer between redox-active centres has also been investigated. A study by Poddel'sky *et al.* synthesised the ethylene-bridged quinone, 4,4'-(ethene-1,2-diyl)bis(3,6-di-tert-butyl-o-benzoquinone) (Q_2ethene) prepared from the two-electron oxidation of 4,4′-(ethane-1,2-diylidene)bis(2-hydroxy-3,6-di-*tert*-butyl-cyclohexa-2,5-dienone), as show in **Scheme 1.9**.[111] One electron reduction of Q_2ethene by reaction with potassium in THF, yielded the mixed valence monoanionic radical species [q / sq]$^-$. EPR analysis of the compound displayed a six line spectrum at g = 2.004 corresponding to the radical electron interacting with three hydrogen nuclei, one ring proton and two methylene protons two of which were identical with A^H = 3.6 G, 1.95 G. Preparation of complexes containing triphenyltin(IV) and triphenylantiminony(V) was also performed, although both were determined to be diamagnetic.

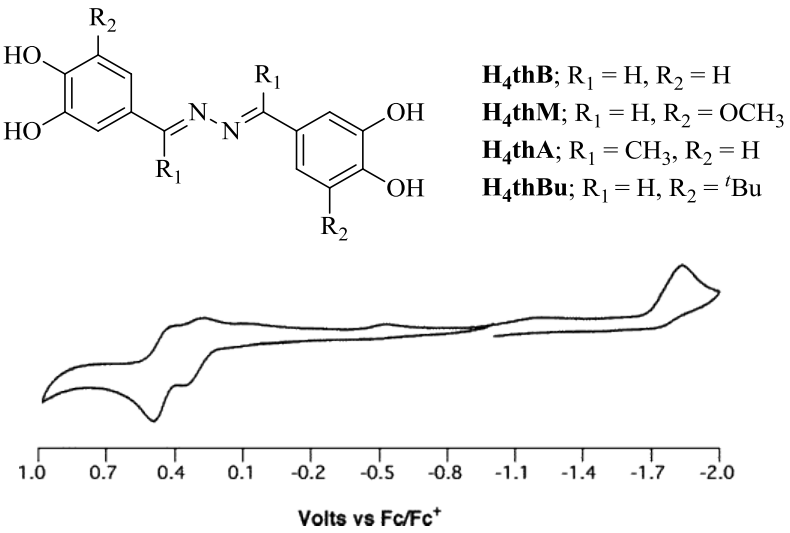

Figure 1.20. (Top) Schematic representation of 3,3′,4,4′-tetrahydroxybenzaldazine derivatives and (bottom) cyclic voltammogram of complex $[\{(bipy)_2Co^{III}\}_2(thM^{4-})]^{2+}$ investigated by Suenaga *et al.*[112]

Complexes of planar 3,3′,4,4′-tetrahydroxybenzaldazine (H_4thB) and its derivatives (H_4thM and H_4thA), which place the metal atoms approximately 16 Å apart, have also been investigated.[112] Each ligand may undergo four electron oxidation processes as above between cat / cat ⇄ cat / sq ⇄ sq / sq ⇄ q/sq ⇄ q / q, although an added curiosity was the *bis*-sq electron delocalisation at the hydrazone bridge, resulting in a spin singlet complex. This delocalisation, and subsequent coupling was again investigated in $\{(bipy)_2Co\}^{n+}$ complexes for the purposes of developing a valence tautomeric complex. Electrochemical analysis of complex $[\{(bipy)_2Co^{III}\}_2(thM^{4-})]^{2+}$ displayed two quasi-reversible oxidations corresponding to the one electron oxidations of the central ligand between cat / cat ⇄ cat / sq ⇄ sq / sq at +0.3 and +0.7 V (*vs* ferrocene), as shown in **Figure 1.20**. Oxidation of the complex with one equivalent of $AgPF_6$ to form the cat-sq ligand failed to show any evidence of ligand-based mixed valency whilst further oxidation using two equivalents of $AgBF_4$ resulted in decomposition of the complex, yielding the monomeric species $[\{(bipy)_2Co^{III}\}(DHBA^{2-})][BF_4]$ (DHBA = 3,4-dihydroxybenzaldehyde). A second investigation at later date by the same authors,[112b] in complexes $[\{(bipy)_2Co^{III}\}_2(thBu^{4-})]^{2+}$ and $[\{(dpa)_2Co^{III}\}_2(thBu^{4-})]^{2+}$ (dpa = 2,2'-dipyridylamine) again showed two reversible electron ligand based oxidations, separated by approximately 0.16 V, corresponding to the same processes as above and $[\{(dpa)_2Co^{III}\}_2(thBu^{4-})]^{2+}$ appeared easier to oxidise. This being said, oxidation of $[\{(bipy)_2Co^{III}\}_2(thBu^{4-})]^{2+}$ using one or two equivalents of Ag^+ offered no spectral changes. Oxidation of $[\{(dpa)_2Co^{III}\}_2(thBu^{4-})]^{2+}$ on the other hand, displayed a growth of an absorbance at 543 nm corresponding to the Co(III)→sq MLCT although failed to offer any paramagnetic shifts in the NMR between 293 and 303 K

implying the formation of *hs*-Co^{II} was precluded. The authors attributed this lack of paramagnetic shift upon dual oxidation to the antiferromagnetic coupling of the two radicals across the hydrazone bridge. They concluded upon these observations, the redox properties of the central cobalt metal atom are strongly dependent on the metal-bound ancillary ligands.

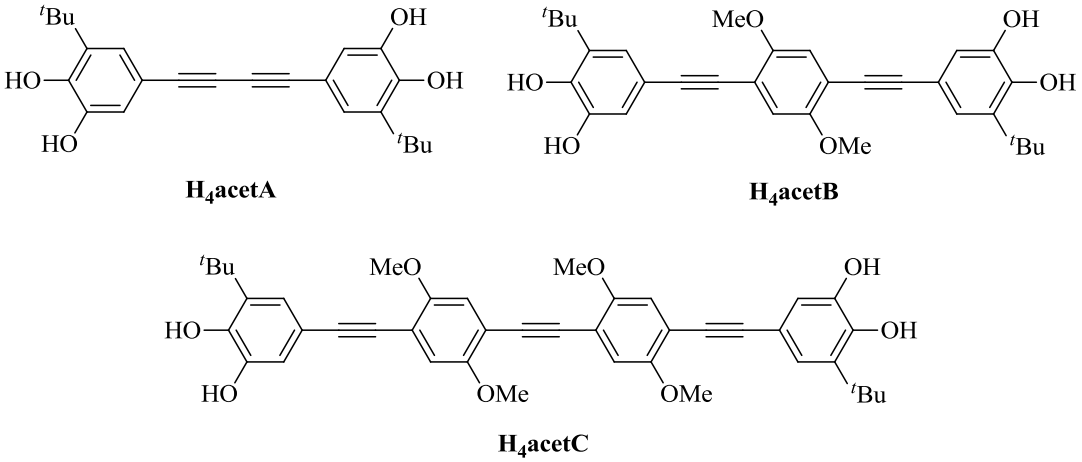

Figure 1.21. Three acetylene-linked ligands H_4acetA, H_4acetB and H_4acetC investigated by Suenga *et al.*[113]

The effect of introducing larger spacers between the dioxolene rings has also been investigated by Suenga *et al.*, for the purposes of determining the long-range coupling between dioxolene rings.[113] Again substituted using $\{(bipy)_2Co^{III}\}$ moieties, electrochemical analysis of (5,5′-(buta-1,3-diyne-1,4-diyl)bis(3-*tert*-butylcatechol) (H_4acetA) displayed two ligand-centred, reversible oxidations at 0.12 and 0.28 V (*vs* ferrocene) whilst 5,5′-(2,5-dimethoxy-1,4-phenylene)bis(ethyne-2,1-diyl)bis(3-*tert*-butyl-catechol) (H_4acetB) and 5,5′-(4,4′-(buta-1,3-diyne-1,4-diyl)bis(2,5-dimethoxy-4,1-phenylene))bis(ethyne-2,1-diyl)bis(3-*tert*-butyl-catechol) (H_4acetC) displayed broad redox processes over the same region, as seen in $[\{(bipy)_2Ru\}_2(m\text{-Ph})]$ by Ward *et al.*,[106] presumably due to a lack of electronic communication between the two redox-active centres. One electron oxidation of $[\{(bipy)Co^{III}\}_2(acetA)]^{2+}$ by addition of $AgPF_6$ to form the mixed valence (cat-sq) complex, again displayed growth of the Co(III)→sq MLCT absorbance at lower energy than in $[\{(dpa)_2Co^{III}\}_2(thBu^{3-})]^{3+}$ (613 nm). Oxidation with a second equivalent of $AgPF_6$, caused the radical electrons to again delocalise to the centre of the molecule, forming a stable tetracation and cunnalene bond. Evidence for this was shown by a broadened alkyne IR band at 2123 cm^{-1} and lack of a paramagnetic shift in the ^1H NMR. In contrast, there were no reported spectral changes upon oxidation of $[\{(bipy)Co^{III}\}_2(acetB)]^{2+}$ and $[\{(bipy)Co^{III}\}_2(acetC)]^{2+}$. Unfortunately, no discussion on the mixed valence characteristics of these complexes was offered, although based upon the

propensity for the two radical electrons in complexes of (sq-sq) and the planarity of the ligands, it appears most likely that these would again be of class III character.

1.11.4 Influence of the Bridge on Electron Delocalisation

The influence of the bridge on the coupling between semiquinone radicals has been investigated extensively by Shultz *et al.*[114] Their studies have focussed on isostructural *bis*-dioxolene ligands, with varying bridge moieties, and their semiquinone-quinone mixed-valence compounds prepared by the reduction of their corresponding *bis*-quinones.[114a] Their studies focussed on the synthesis of zinc(II) complexes, capped with the bulky ancillary ligand hydrotris(3-methyl-5-cumenylpyrazolyl)borate ($Tp^{Cum,Me}$), which limits the conformational degrees of freedom and attenuates intermolecular forces in the solid state.[115]

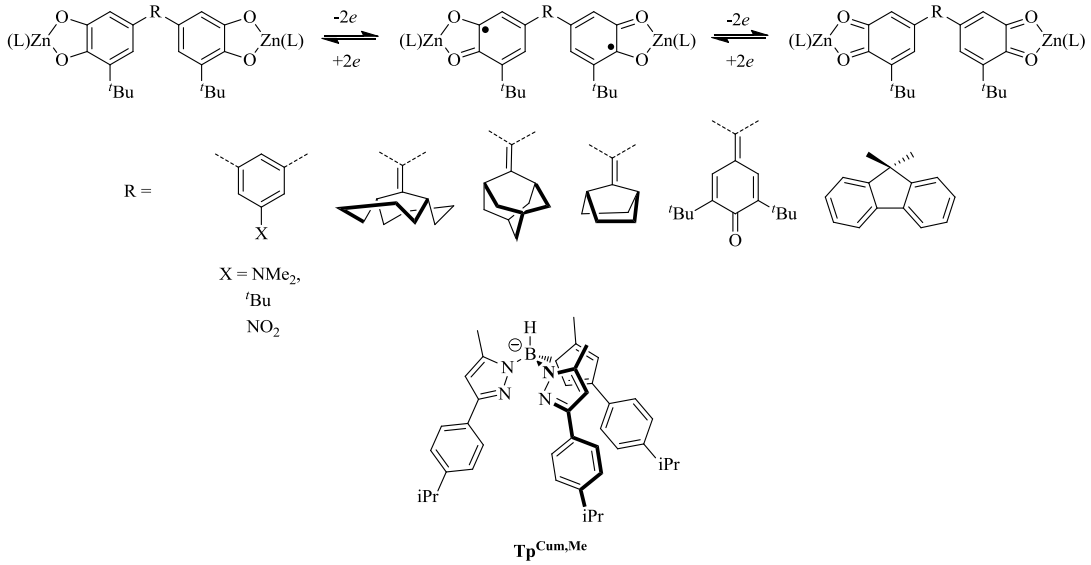

Scheme 1.10. Schematic of the *bis*-semiquinone ligands and complexes investigated by Shultz *et al*.[114]

Electrochemical analysis of the *bis*-quinone ligands showed the redox process (q-q) / (sq-q) were well separated in each ligand by 0.20 – 0.25 V with high comproportionation constants (K_{com}). High K_{com} and good separation are known to be good indications of stable mixed valence species, as redox splitting is proportional to the delocalisation in mixed valence species.[16] An interesting trend in the complexes was noted whereby the extent of electronic delocalisation strength was determined by the strength of ferromagnetic coupling between semiquinone radicals, which itself was determined by the torsion angle between dioxolene rings. It was found that as ring torsion between dioxolenes increases (extracted from crystallographic structures of the complexes) ferromagnetic coupling of the radicals

decreases due to a lack of conjugation between rings. The extent of radical electron coupling was extracted from the zero-field splitting parameters (D and E) of frozen solution X-band EPR spectra of the complexes, which have previously been shown to be direct measures of semiquinone ring torsions.[116] The study showed that larger D-values corresponded to greater redox separations and larger K_{com} values. As a result, increasing the size of the coupling unit modulated the extent of radical coupling in *bis*-semiqunione species by disrupting conjugation between the spin containing-units. This was either by van der Waal's repulsion between radicals and bridgehead hydrogens or inferring steric clashes, therefore preventing coplanarity of the ligand. The electron delocalisation in mixed valence species of these complexes was found to correlate with the strength of ferromagnetic exchange between rings, therefore is directly affected by the modulation in ring torsion. It could therefore be expected that where large torsion angles exist, class I or class II mixed valency could be expected whilst when close to coplanarity, class III would be most likely.

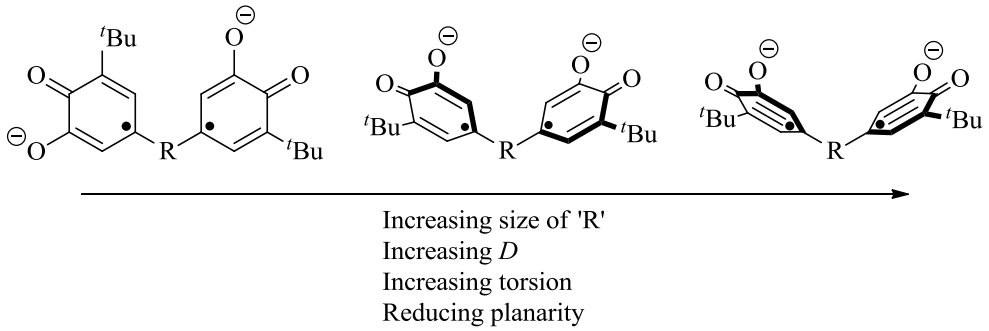

Scheme 1.11. Observations of effect of bulky bridging substituients between semiquinone rings by Shultz *et al*.[114a, 114c]

1.11.5 Complexes of H_4spiro

From the investigations containing complexes of the H_4biscat core and its derivatives, extensive delocalisation and strong radical electron coupling seemed to be the underlying theme, strongly associated with not only the distance between dioxolene centres, but also the nature of spacer inbetween and the extent of planarity. Introduction of a saturated carbon bridge was therefore another method of separating the dioxolene rings, whilst keeping them relatively close in space. A ligand which has been investigated for this purpose is *bis*-dioxolene 3,3,3',3'-tetramethyl-5,6,5',6'-tetrahydroxy-1,1'-spiro-bis(indane) (H_4spiro), as shown in **Figure 1.22**.

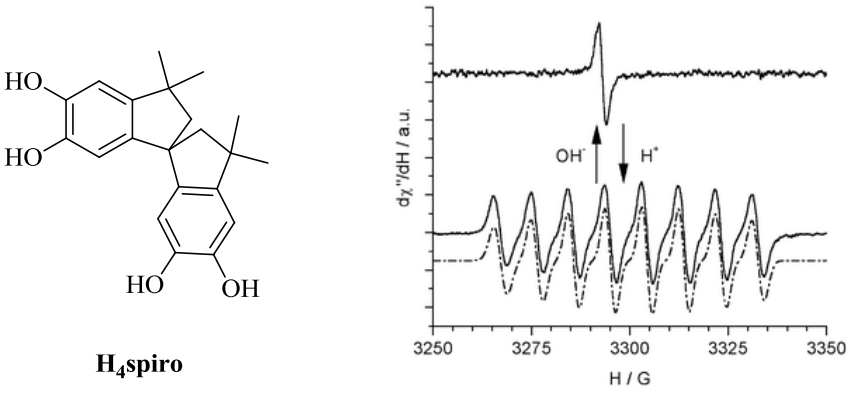

Figure 1.22. (Left) Schematic structure of H_4spiro. (Right) EPR spectrum of $[H_2spiro]^{2-}$ (sq-sq) reported by Dei *et al.*[117]

As with the *bis*-dioxolenes described above, the dioxolene rings can be oxidised independently whilst the spiroconjugation may permit electronic communication between the two.[118] Firstly, an investigation into the redox activity of the ligand was undertaken by Dei *et al.* where it was found that two electron oxidation of the ligand under acidic conditions (using cerium(IV)nitrate) gave the mixed valence species ($catH_2$-q), where the catecholato- form was stabilised by its interactions with the acidic protons.[117] Delocalisation of the additional charge could not take place throughout the molecule due to the nature of the ligand, therefore effectively 'trapping' the electron, and surprisingly permitting separation of the compound by column chromatography. Dissolution of the isolated compound under basic conditions gave an instant colour change and spectrum consistent with the (sq-sq) compound, whilst addition of acid again regenerated the original spectrum. Definitive proof for the generation of the (sq-sq) state came from EPR which displayed a signal at g = 2.00 with hyperfine to the two *ortho* protons of the rings indicating spin delocalisation into the dioxolene ring. Importantly for later studies, the two semiquinone radicals did not appear to interact, even at low temperatures, although the ^1H hyperfine was lost. The synthesis of monometallic complexes $[(cth)Co^{III}(sq\text{-}catH_2)][PF_6]_2$ and $[(cth)Cr^{III}(sq\text{-}catH_2)][PF_6]_2$ were reported in the same investigation where it was found that the complexes strongly resembled their corresponding mononuclear semiquinonate complexes. EPR analysis of $[(cth)Co^{III}(sq\text{-}cat)][PF_6]_2$ showed a typical pattern arising from the interaction of the semiquinone radical with coordinated Co^{III} (g = 2.001, A^{Co} = 9.35 G) which vanished upon addition of a stoichiometric amount of NMe_4OH by replacement with an isotropic signal at g =2.00 as shown in **Figure 1.22**. The hyperfine coupling could be regenerated by addition of perchloric acid corresponding to a change in oxidation number of the coordinated dioxolene upon deprotonation, therefore suggesting class I behaviour of the complex with no coupling between dioxolenes according to the equilibrium $[(cth)Co(sq\text{-}catH_2)] \rightleftarrows [(cth)Co(cat\text{-}sq)] + 2H^+$. This observation was confirmed by UV/vis whereby the

reversible disappearance of a strong Co(IIII)→sq MLCT transition at 19,000 cm^{-1} upon addition of NMe_4OH was noted along with similar behaviour for the Cr(III) derivative. Analysis of the magnetic properties of the complexes confirmed this pH-dependent charge distribution where the $[(cth)Cr^{III}(sq\text{-}catH_2)][PF_6]_2$ displays strong antiferromagnetic coupling between Cr(III) ($S = {}^3/_2$) and the semiquinone ($S = ½$) resulting in a triplet ground state whilst deprotonation of the opposing catechol changes this resulting in two weakly interacting paramagnetic centres. With this in mind, Dei *et al.*[119] synthesised a heteronuclear complex again using $\{(cth)Co^{III}\}$ and $\{(cth)Cr^{III}\}$ in order to investigate the potential for isomers $[\{(cth)Co^{III}\}(cat\text{-}sq)\{(cth)Cr^{III}\}]$ and $[\{(cth)Co^{III}\}(sq\text{-}cat)\{(cth)Cr^{III}\}]$ which could potentially coexist in solution and be determined based upon their magnetic moments. Complex $[\{(cth)Co^{III}\}(cat\text{-}sq)\{(cth)Cr^{III}\}]$ would be expected to exhibit a triplet ground state with χT = 1 emu mol^{-1} K^{-1} whilst for $[\{(cth)Co^{III}\}(sq\text{-}cat)\{(cth)Cr^{III}\}]$, χT would be expected to equal 2.25 emu mol^{-1} K^{-1} where the spins are uncorrelated. Successful synthesis of the complexes was achieved, even permitting their purification by column chromatography, where its magnetic properties and electronic spectra were intermediate of the two charge distributions. Variable temperature magnetic susceptibility measurements unfortunately showed no changes on decreasing the temperature therefore indicating a lack of equilibrium between isomers, indicating class I nature of the ligand.

Valence tautomeric character was again witnessed of the core $[spiro]^{3-}$ unit in the synthesis of 1D polymers $[(phen)Co(spiro)]_\infty \bullet 3H_2O$ and $[(bipy)Co(spiro)]_\infty \bullet 3H_2O$.[120] Both complexes were shown to contain $[spiro]^{3-}$ in the mixed valence (cat-sq) form, with the Co^{III} atom acting as a bridge. Thermally-induced valence tautomerism was attainable above 250 K, where the *hs*-Co^{II} atoms are all coordinated by one semiquinone and one catecholate ligand, as shown below.

$$[ls\text{-}Co^{III}/2(cat\text{-}cat)ls\text{-}Co^{III}/2]_\infty \rightleftarrows [hs\text{-}Co^{II}/2(sq\text{-}cat)ls\text{-}Co^{III}/2]_\infty$$

This was attributed as the most stable state owing to the instability of $Co^{III}(sq)_2$ complexes. As a result, the mechanism of forming the final species proceeds via the valance tautomeric transition of $[hs\text{-}Co^{II}/2\text{-}(sq–sq)\text{-}hs\text{-}Co^{II}/2]_\infty$ and decays *via* electron transfer between coordinated catechol and the metal centre, then back-electron transfer to form $[hs\text{-}Co^{II}/2(sq\text{-}cat)ls\text{-}Co^{III}/2]_\infty$. This mechanism was deemed the most acceptable due to the lack of electronic communication between the two dioxolene rings of the $[spiro]^{n-}$ ligand.

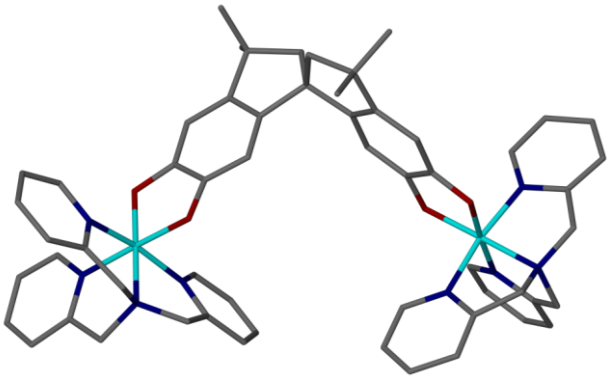

Figure 1.23. Crystal structure of $[\{(tpa)Co^{III}\}_2(cat\text{-}cat)]^{2+}$ prepared by Alley *et al.*[114] Hydrogen atoms and PF_6 counter-anions have been omitted for clarity. Colour code; Co, cyan; N, blue; O, red; C, grey.

As seen previously, variation of the ancillary ligand can be used to tune the electronic character of the complex. This approach was attempted very recently by Boskovic *et al.*[121] in the synthesis of valence tautomeric $\{(Me_ntpa)Co^{III}\}$ (n = 0-3) complexes of $[spiro]^{n-}$. Electrochemical analysis of all complexes displayed two ligand-centred redox processes separated by approximately 0.15 V indicating the accessibility of the (cat-sq) and (sq-sq) forms of the complexes once coordinated. It was found that when n = 0 or 1, the temperature independent redox isomer $Co^{III}(cat\text{-}cat)Co^{III}$ is prevalent in both solution and solid state whilst where n = 3, the $Co^{II}(sq\text{-}sq)Co^{II}$ isomer is dominant. Their study permitted the single crystal characterisation of $[\{(tpa)Co^{III}\}_2(cat\text{-}cat)]^{2+}$, $[\{(tpa)Co^{III}\}_2(sq\text{-}sq)]^{4+}$ and $[\{(Me_3tpa)Co\}_2(cat\text{-}cat)]^{2+}$ as shown in **Figure 1.23**. Where n = 2 however, the room temperature UV-vis spectra indicated the existence of the $Co^{II}(sq\text{-}sq)Co^{II}$ redox isomer by identification of absorptions arising from the internal transitions of the semiquinone ligands and the presence of Co(II)→sq MLCT bands which are consistent with the mononuclear complex $[(Me_2tpa)Co^{II}(DBSQ)]$. In the solid state however, IR, X-ray absorption spectra and magnetic susceptibility data suggests the presence of a Co^{II}/Co^{III} catecholate/semiquinonate mixture. Variable temperature magnetic susceptibility measurements were consequently undertaken where a rare two-step temperature dependent valence tautomeric transition was observed corresponding to the $Co^{III}(cat\text{-}cat)Co^{III}$ ⇄ $Co^{II}(sq\text{-}cat)Co^{III}$ ⇄ $Co^{II}(sq\text{-}sq)Co^{II}$ equilibrium in solution and the solid state. Each half of the complex switches independently, resulting in this two-step transition. Interestingly, it was also the Me_2tpa ancillary ligand in studies of mononuclear complexes which displayed a valence tautomeric transition in the 2-300 K range. In addition to the temperature-dependent transition, $[\{(Me_3tpa)Co^{III}\}_2(cat\text{-}cat)]^{2+}$ also displays sensitivity to low temperature irradiation with light, and possibly 'soft' X-rays from the Co K-edge XAFS.

The rich redox chemistry of the metal centres and [sprio]$^{n-}$ ligand permitted the isolation of two additional redox isomers; Co^{III}(sq-cat)Co^{III} and Co^{III}(sq-sq)Co^{III} as a part of their investigation. Frozen solution EPR of the complex Co^{III}(sq-sq)Co^{III} (**Figure 1.24)** showed a half field transition (Δm_s = 1), visible up to approximately 50 K with moderate antiferromagnetic coupling between semiquinone radicals, calculated to be equal to 8 cm^{-1}. Upon warming, the coupling was lost whilst the main spectrum tightened to give an eight line spectrum due to coupling to one cobalt centre. The extent of electron delocalisation in the mixed valence species Co^{III}(sq-cat)Co^{III} was also investigated by variable temperature EPR. Interestingly, it was found that at room temperature the valent electron is delocalised across both halves of the [spiro]$^{3-}$ ligand via the spyrocyclic carbon. This exchange was evident by the 15 line spectrum obtained by coupling to two equivalent ^{59}Co (I = $^{7}/_{2}$) with g = 2.0018. The exchange can be slowed by lowering the temperature to 220 K, where an 8 line spectrum was recorded (**Figure 1.24**). The authors attributed this effect to the existence of two non-instantaneously equivalent Co atoms even at room temperature, and the electron delocalisation is likely activated by a specific vibronic mode of the ligand at a specific temperature, which was calculated as 242 K, implying class II character of the [spiro]$^{3-}$ ligand.

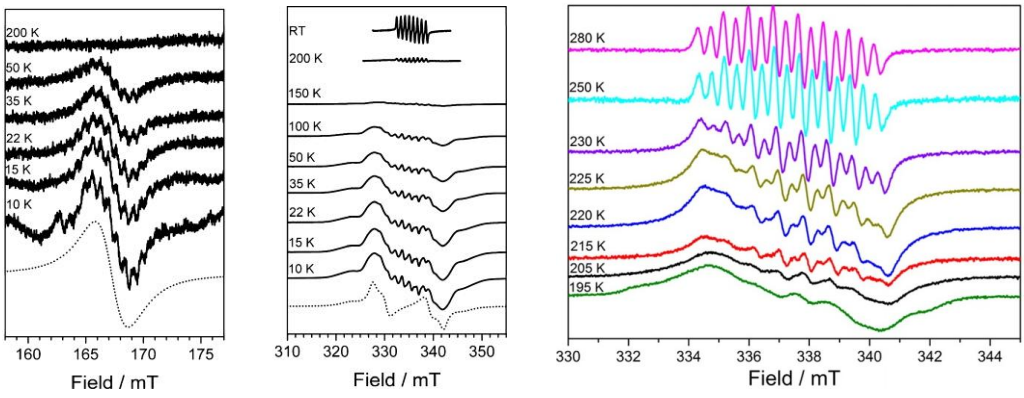

Figure 1.24. Variable temperature X-band EPR studies (left) Co^{III}(sq-sq)Co^{III} complex of [spiro]$^{2-}$ and (right) mixed valence complex Co^{III}(sq-cat)Co^{III} of [spiro]$^{3-}$ investigated by Alley *et al.*[155]

1.12 Redox Activity of *Tris* Dioxolene Complexes

As mentioned above, introduction of an additional dioxolene moiety increases the complexity of the system even further, in giving rise to the potential for write−lock−read−unlock−erase cycles provided the interaction between redox-active centres is small but non-zero.[89] Despite this paradigm, to the detailed redox chemistry of only two

tris-dioxolene ligands has been investigated, for; hexahydroxtriphenylene and 1,3,5-trimethylenebenzene, by Ward *et al.*[122] and Dei *et al.*[123] respectively.

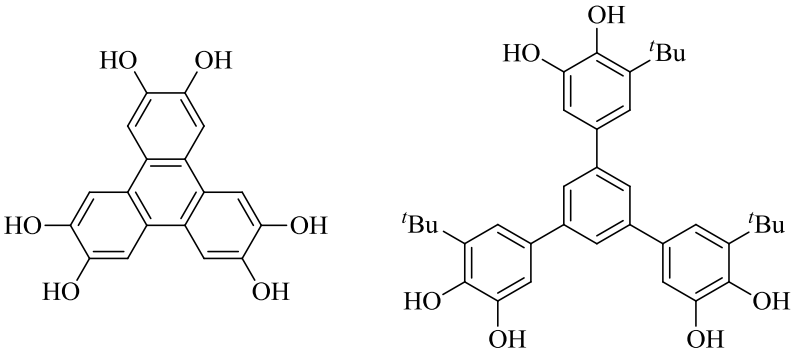

H_6triscat **H_6Phcat$_3$**

Figure 1.25. Schematic representation of previously studied *tris*-dioxolene ligands H_6triscat and H_6Phcat$_3$.[122-123]

1.12.1 Investigations of 'triscat'

Most recently investigated for the purposes of synthesising a porous coordination polymer,[124] the triscat framework was first substituted with $\{(bipy)_2Ru^{II}\}$ moieties for the purposes of synthesising the μ_3- complex $[\{(bipy)_2Ru^{II}\}_3(triscat)]^{3+}$ by Ward *et al.*[122] Analysis of the complex showed that as synthesised, each dioxolene was in the semiquinone oxidation state, although as in the case of biscat, two of the radical electrons couple to form double-bond *para* to the dioxolene. This therefore gives the monoradical product of $[\{(bipy)_2Ru^{II}\}_3(triscat)]^{3+}$, proven by frozen solution EPR at 77 K which displayed an isotropic peak at $g = 2.01$ with no evidence for $\Delta m_s = 2$ or 3 transitions. Electrochemical analysis displayed six redox processes between -1.0 and +0.7 V *vs* $[FeCp_2]$ / $[FeCp_2]^+$ separated by 0.2-0.3 V. These corresponded to the sequential cat / sq / q processes for each dioxolene ring whilst the large separations suggested strong electronic communication between dioxolenes. Spectroelectrochemical analysis of $[\{(bipy)_2Ru^{II}\}_3(triscat)]^{3+}$ at 243 K permitted the study of oxidation states (sq/sq/sq), (sq/sq/q), (sq/q/q) and (q/q/q) where clean conversions for all three oxidations were observed implying a stable complex whilst re-reduction regenerated the initial complex. Analysis of the two mixed valence species (sq/sq/q) and (sq/q/q) displayed intense and broad transitions at 9,230 cm^{-1} (74×10^3 $M^{-1}cm^{-1}$) and 11,000 cm^{-1} (32×10^3 $M^{-1}cm^{-1}$) implying the radical electron was delocalised, although no Robin/Day class was indicated. During the investigation however, it was noted that reduction of the sq/cat couples caused precipitation of the complex due to insolubility.

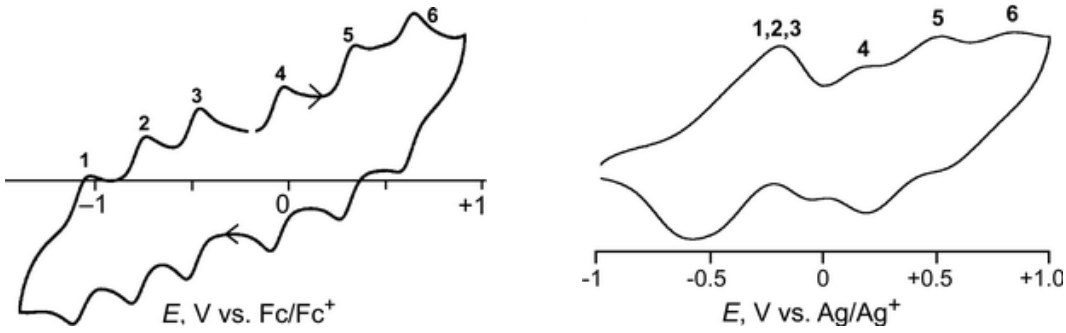

Figure 1.26. (Left) Solution phase cyclic voltammogram of $[\{(^{t}Bu_2Bipy)_2Ru\}_3(triscat)]$. (Right) Solid phase cyclic voltammogram of $[\{(^{t}Bu_2Bipy)_2Ru\}_3(triscat)]$ deposited on ITO glass, both investigated by Ward *et al.*[125].

As a result, this investigation provided the preliminary work for a more detailed investigation into an analogous system where the unsubstituted bipy ancillary ligands were swapped for $^{t}Bu_2Bipy$ for solubility purposes.[125] The renewed investigation displayed similar observations to their prior investigation with the (sq/sq/sq) state again first isolated, with mono-radical character as previously seen. Cyclic voltammetric analysis again displayed six redox processes, corresponding to the sequential redox process of each dioxolene ring as shown in **Figure 1.26**. Increased solubility of the complex permitted spectroelectrochemical analysis on all oxidation states of the complex which displayed an intense NIR transition close to 4,350 cm^{-1} for the mixed valence (sq/sq/cat) state, assignable as the intraligand IVCT which was backed up by detailed TD-DFT (time dependent density functional theory) calculations. Unfortunately, however there was again no identification of the mixed valence classification. Despite this, the solid state electrochemical behaviour of the complex was analysed where poorer peak separation was observed compared to in solution. Despite this, $[\{(^{t}Bu_2Bipy)_2Ru^{II}\}_3(triscat)][PF_6]_3$ was deposited onto ITO (indium tin oxide) conductive glass and it was found that the complex could be switched rapidly between the (sq/sq/sq) and (cat/cat/cat) states, taking advantage of a strong transition close to 9,100 cm^{-1} which disappears in the (cat/cat/cat) state. The resulting film was found to be able to be switched reversibly for approximately 4300 cycles over 24 hours with 17% loss in optical density.

1.12.2 Investigation of H_6Phcat_3

With the view to investigate the ferromagnetic radical coupling between semiquinone rings, complexes of H_6Phcat_3 containing $\{(cth)Ni^{II}\}$ and $\{(Tp^{Cum,Me})Mn^{II}\}$ moieties were prepared.[123] The complexes $[\{(cth)Ni^{II}\}_3(Phcat)]$ and $[\{(Tp^{Cum,Me})Mn^{II}\}_3(Phcat)]$ were both shown to be synthesised as the *tris*-semiquinone derivatives, owing to the similaraties noted between the electronic spectra of the mononuclear complex $[(cth)Ni^{II}(DBSQ)]PF_6$. Both

complexes displayed strong absorptions in the region 24,100-26,300 cm^{-1}, assignable to an internal semiquinone transition.[107,126] Cyclic voltammetric analysis of $[\{(cth)Ni^{II}\}_3(PhSQ)]^{3+}$, displayed three reversible redox processes between $-1.08 \leq E_{½} \leq -0.86$ (*vs* $FeCp_2$ / $FeCp_2^+$) corresponding to the sequential reduction/oxidation of the semiquinone rings. Unfortunately, due to the poor spacing of the redox processes a value for K_{com} was calculated to be 33 indicating very little communication between the dioxolene rings. Consequent of this, it would be impossible to generate the mixed valence species (cat/cat/sq) or (cat/sq/sq) without significant contamination of the other redox isomers. This implies that the energies of the frontier orbitals are the same. Despite this, the extent of radical coupling within the complexes was determined by analysis of their magnetic properties. In $[\{(Tp^{Cum,Me})Mn^{II}\}_3(PhSQ)]$, it was found that the semiquinone radicals are strongly antiferromagnetically coupled to the Mn^{II} ($S = {}^5/_2$) ions, giving rise to three $S = 2$ centres ($S = 6$ ground state). This was confirmed by fitting a model assuming antiferromagnetic coupling between manganese(II) and radical (J_1), and ferromagnetic coupling between semiquinones (J_2). The parameters which gave the best fit were found to be $g = 2.00$, $J_1 > 350$ cm^{-1} and $J_2 = -40$ cm^{-1}, which matched well with the experimental χT *vs* T. The same process was performed with the complex $[\{(cth)Ni^{II}\}_3(PhSQ)]^{3+}$ which showed strong ferromagnetic coupling between nickel(II) and semiquinone and again ferromagnetic coupling between semiquinone radicals. The best fit parameters for this complex were $g = 2.14$, $J_1 = -173$ cm^{-1} and $J_2 = -26.5$ cm^{-1} with $S = {}^9/_2$ ground state. The relatively high g value is expected for a ferromagnetically coupled Ni^{II}(sq) complex.[126] In addition, the differences in ferromagnetic coupling between semiquinone radicals (J_2) were attributed to the variation in the dihedral angle between the semiquinone rings, due to the diamagnetic ligand employed. As seen above, the $Tp^{Cum,Me}$ ligand is larger and bukier than cth and therefore might cause the ring to lie closer to planarity, resulting in more facile electron delocalisation.[114a] To date, no further work has been conducted on the ligand H_6Phcat_3.

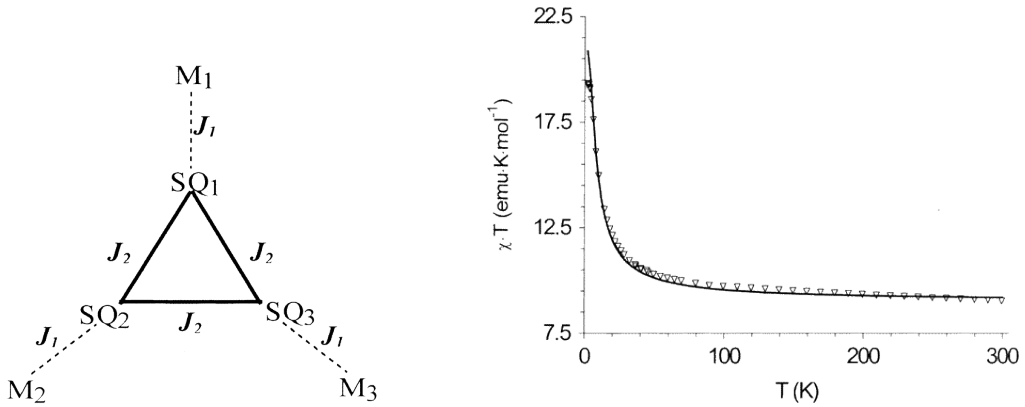

Figure 1.27. (Left) Schematic of the semiquinone coupling model for [{($Tp^{Cum,Me}$)Mn^{II}}$_3$(PhSQ)]. (Right) χT vs T curve for the complex [{($Tp^{Cum,Me}$)Mn^{II}}$_3$(PhSQ)]. (empty triangles). The continuous line is the result of the best fit obtained with the model. Adapted from reference.[123]

Even though mixed valency was not achieved in the complexes of H_6Phcat$_3$, it seems likely that electron delocalisation throughout the ligand would be facile due to the similarities the ligand shares with certain *bis*-dioxolene ligands outlined above. For instance, *m*-Ph(H_2cat)$_2$ which was shown to display very poor separation between redox processes of the two dioxolene rings, likely due to relatively large torsion angles between rings. It therefore seems to be that the field of *tris*-dioxolene ligand systems is underfed, particularly where conjugation between rings is discouraged by introduction of a spacer, or coupling group between dioxolenes. A fascinating ligand which could hold potential for this purpose is a member of the cyclotriveratrylene family.

1.13 An Introduction to the Chemistry of Cyclotriveratrylene

Related to the family of calix[*n*]arenes, cyclotriveratrylene (ctv) is a cyclic molecular host easily prepared by the condensation of veratrole, in the presence of an acid catalyst (e.g. phosphoric acid).[127] Most commonly found in its crown conformation, ctv contains an electron-rich shallow molecular cavity (although has been shown to exist in a saddle conformation when rapidly quenched from a melt[128]) capable of supporting non-covalently bound guest molecules, e.g. cationic metal complexes (e.g. [(arene)FeCp]$^+$ complexes),[129] *o*-carborane[130] or fullerenes.[131] In addition to displaying host : guest capabilities, cyclotriveratrylene-type molecules have been used extensively as a scaffold for the formation of extended arm complexes, by substitution at the upper-rim of either C_3 symmetric cyclotricatechylene (ctc) or cyclotriguaiacylene (ctg) used for a variety of reasons including the assembly of supramolecular assemblies[132] and anion recognition.[133]

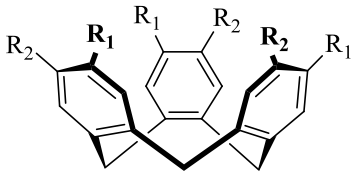

ctv ; $R_1 = R_2 = OMe$

ctc ; $R_1 = R_2 = OH$

ctg ; $R_1 = OMe$, $R_2 = OH$

ctp ; $R_1 = H$, $R_2 = SH$

thio-ctg ; $R_1 = OMe$, $R_2 = SH$

Figure 1.28. Selected molecules of the cyclotriveratrylene family.

Recently, novel analogous thiolated molecules of ctg have been synthesised and used in the synthesis of novel capsules. These include cyclotrithiophenolene (ctp) which has been used for the synthesis of a novel S-cryptophane-0.0.0 for investigations into methane and nitrogen binding and cyclotrithioguaiacylene (thio-ctg).[134] Very recently, an analogue of thio-ctg was reported by the Hardie group, where one -SH is replaced by -OMe at the upper rim. Once oxidised, the compound dimerises by disulfide bond formation resulting in an offset capsule.[135]

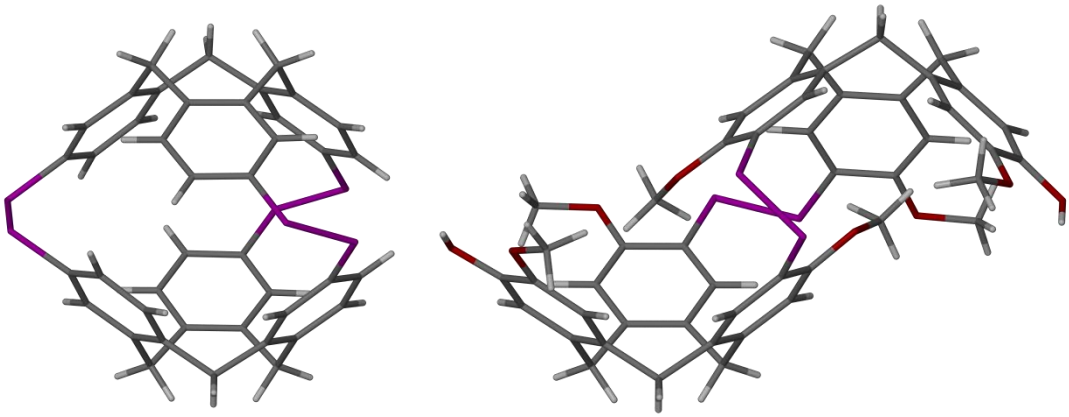

Figure 1.29. Two novel structures of thiolated members of the cyclotriveratrylene family, prepared in the Hardie group. (Left) novel S-cryptophane-0.0.0 formed by the intermolecular dimerisation of two ctp formula units[134a] and (right) offset capsule formed by the dimerisation of two formula units of thio-ctg analogue.[135] Colour code; S, purple; O, red; C, grey; H, white.

1.13.1 Chemistry of Cyclotricatechylene

Easily prepared by the demethylation of cyclotriveratrylene using boron tribromide, the *tris*-dioxolene species cyclotricatechylene (ctc) is rigid and retains the characteristic 'bowl' feature of ctv. Due to the positioning of the dioxolene rings and retention of the methylene bridge, the structural characteristics of ctc result in a non-planar structure, unlike previously reported *tris*-dioxolene systems. The majority of studies involving ctc have been concerned

with the formation of novel capsules and extended supramolecular structures, of which only a small number exist. Robson *et al.*[136] have demonstrated the host : guest properties of deprotonated $[ctc]^{2-}$ which forms 'clam-like' assemblies encapsulating cationic guest molecules resultant of hydrogen bonding interactions between the phenoxyl- groups at the upper rim. Dependent on the size of the guest, a closed or 'open clam' capsule was formed where rubidium(I) and caesium(I) preferred the enclosed aromatic environment of the bowl whilst alkyl cations NMe_4^+ and NEt_4^+ were 'open clam'.

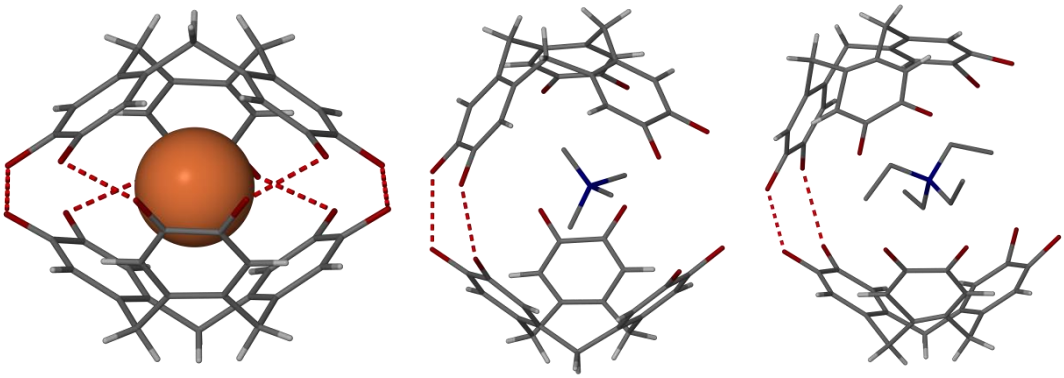

Figure 1.30. Three capsules prepared by Robson *et al.* (Left) 'Closed clam' capsule $Rb^+.(ctc)^-.(ctc)^{2-}]^{2-}$. (Centre) 'Open clam' $[(NMe_4)^+.(ctc)_2^{2-}]^-$, $(NMe_4)^+$ is shown as the guest. (Right) 'Open clam' $[(NEt_4)^+.(ctc)_2^{2-}]^-$, $(NEt_4)^+$ is shown as the guest. Colour code: Rb, orange; O, red; N, blue; C, grey; H, white.

The use of $[ctc]^{6-}$ as a scaffold in larger supramolecular structures has also been accomplished in the synthesis of a symmetric 'diamond-like' $[M_6(ctc)_4]^{12-}$ (M = Cu, Mn, VO and Co) cage complexes.[137] More recently though, the $[ctc]^{n-}$ core unit has been used in the synthesis of large propeller-shaped hydrogen-bonded capsules, containing 2,2'-bipyrdine, 4,4'bipyridine, pyrazine or1,10-pehnanthroline.[138] The synthesised capsules were probed for guest binding where planar molecules such as pyrene or naphthalene could be encapsulated with little reorganisation.

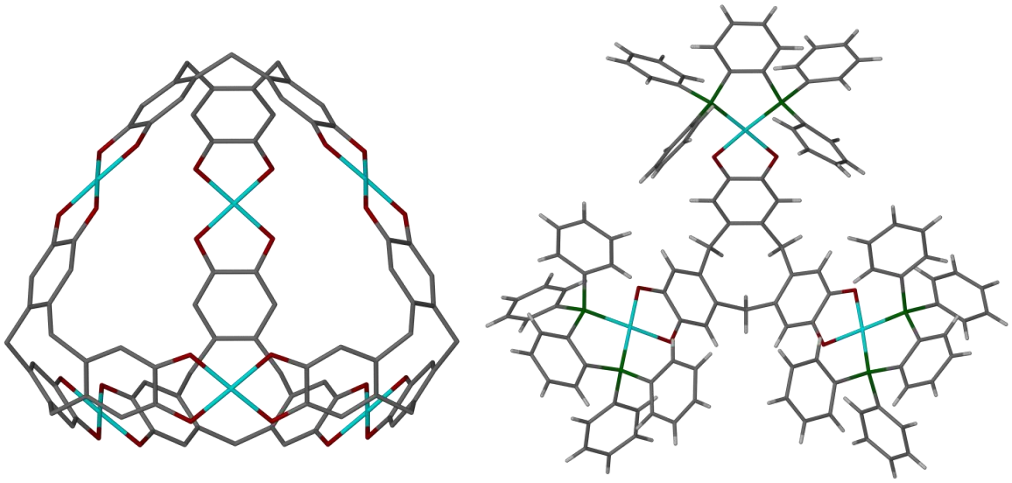

Figure 1.31. Structures synthesised of the core $[ctc]^{6-}$ unit. (Left) Symmetric 'diamond-like' $[Cu_6(\mu_3\text{-ctc})_4]^{12-}$ cage complex prepared by Robson *et al.*[137]. (Right) Extended rim $[\{(dppb)Pt\}_3(\mu_3\text{-ctc})]$ prepared by Bohle *et al.*[139]

Unfortunately, these investigations provided no further insights into the redox chemistry of $[ctc]^{n-}$. There has been only one prior report for this purpose which was communicated fifteen years ago by Bohle *et al.* in the synthesis of two complexes with general formula $[\{(L)Pt\}_3(\mu_3\text{-ctc})]$ where L is a chelating bidentate diphosphine; diphenylphosphinobenzene (dppb) or diphenylphosphinoferrocene (dppf).[139] Their short investigation detailed the ability of both complexes to show three very distinct low-potential oxidations between $+0.04 \leq E_{½} \leq +0.49$ V *vs* SHE corresponding to the sequential oxidation of each dioxolene ring between (cat/sq). In both complexes, one further irreversible process close to +1.00 V was also noted corresponding to the (sq/q) oxidation and concomitant decomposition of the complexes. Calculated separation between each (cat/sq) redox process was calculated to be between 0.20 - 0.25 V indicating moderate communication between dioxolene rings, although no further investigation into their radical complexes was provided. The trinuclear nature of $[ctc]^{n-}$ therefore makes it an ideal candidate for investigations into synthesising *tris*-dioxolene complexes of mixed valency. [140]

1.14 Project Aims

The aims of this project are divided into three distinct regions of research. The first is concerned with the investigation into the organic donor : acceptor capabilities of cyclotriveratrylene and the redox active non-innocent *tris*-dioxolene ligand, cyclotricatechylene. The second is concerned with the synthesis and analysis of novel multinuclear dioxlene complexes of mixed-valency and the third with the synthesis of novel multinuclear thiolated ligands.

1.14.1 Organic Donor : Acceptor Complexes

The electron rich nature of dioxolene and veratrole moieties makes them excellent candidates for forming donor : acceptor complexes or charge-transfer salts. When combined with the 3-dimensional nature of cyclotriveratrylene and cyclotricatechylene, these molecules present themselves as excellent models to study for the purposes of forming such complexes or salts, by the addition of suitable oxidant or electron-accepting molecule. An investigation into the charge transfer capabilities of cyclotricatechylene and cyclotriveratrylene along with a selection of novel clathrate structures isolated during the investigation is presented in chapter two.

1.14.2 Multinuclear Complexes of Mixed Valency

As currently the field of mixed valence complexes containing *tris*-dioxolene species is underfed, the non-conjugated dioxolene rings and rigid structure of cyclotricatechylene presents a fantastic opportunity for further investigations into its rich redox chemistry as illustrated by Bohle *et al*. To open up this molecule to studies on mixed valency, an aim is to successfully prepare novel μ_3-ctc complexes and oxidise each ring sequentially to determine the extent of radical electron delocalisation within the structure. A detailed investigation into the redox capabilities of complexes of cyclotricatechylene is presented in chapter 3.

As has been seen above, the study of *bis*-dioxolene complexes for the purposes of generating a species of mixed valency is still a growing field. The effect of the conjugation between rings appears to be a determining factor in the Robin / Day class of mixed valency. An interesting investigation would be in the study of an analogous, rigid and non-conjugated system to cyclotricatechylene. The investigation conducted into mixed valence complexes of a rigid *bis*-dioxolene ligand is presented in chapter 4.

1.14.3 Novel Multinuclear Dithiolene Ligands

As the study of dithiolene complexes may be more complicated than the study of their analogous dioxolene systems, due to extensive orbital mixing between metal and ligand, the

synthesis of novel thiolated homologues of cyclotricatechylene and the rigid *bis*-dioxolene ligand studied in chapter 4 would be attempted. Chapter 5 details these synthetic attempts.

1.15 References

[1] a) P. Gütlich, Y. Garcia, T. Woike, *Coord. Chem. Rev.* **2001**, *219–221*, 839-879; b) A. Hauser, *Coord. Chem. Rev.* **1991**, *111*, 275-290; c) O. Kahn, J. P. Launay, *Chemtronics* **1988**, *3*, 140-151.

[2] N. Sutin, *Acc. Chem. Res.* **1982**, *15*, 275-282.

[3] a) C. Lambert, G. Nöll, *Angew. Chem., Int. Ed.* **1998**, *37*, 2107; b) C. Lambert, G. Nöll, *Angew. Chem.* **1998**, *110*, 2239-2242.

[4] P. V. Bernhardt, M. Martinez, *Inorg. Chem.* **1999**, *38*, 424-425.

[5] C. Creutz, H. Taube, *J. Amer. Chem. Soc.* **1969**, *91*, 3988-3989.

[6] a) J. K. Beattie, N. S. Hush, P. R. Taylor, *Inorg. Chem.* **1976**, *15*, 992-993; b) N. S. Hush, A. Edgar, J. K. Beattie, *Chemical Phys. Lett.* **1980**, *69*, 128-133; c) S. B. Piepho, *J. Am. Chem. Soc.* **1990**, *112*, 4197-4206.

[7] a) D. O. Cowan, F. Kaufman, *J. Am. Chem. Soc.* **1970**, *92*, 219-220; b) D. O. Cowan, R. L. Collins, F. Kaufman, *Journal Phys. Chem.* **1971**, *75*, 2025-2030.

[8] D. O. Cowan, C. LeVanda, J. Park, F. Kaufman, *Acc. Chem. Res.* **1973**, *6*, 1-7.

[9] J. R. Reimers, N. S. Hush, *Inorg. Chem.* **1990**, *29*, 3686-3697.

[10] M. B. Robin, P. Day, *Advan. Inorg. Chem. Radiochem.* **1967**, *10*, 247-422.

[11] P. Day, N. S. Hush, R. J. H. Clark, *Philos. Trans. R. Soc., A* **2008**, *366*, 5-14.

[12] B. S. Brunschwig, C. Creutz, N. Sutin, *Chem. Soc. Rev.* **2002**, *31*, 168.

[13] N. S. Hush, *Prog. Inorg. Chem.* **1967**, *8*, 391-444.

[14] N. S. Hush, *Coord. Chem. Rev.* **1985**, *64*, 135-157.

[15] D. M. D'Alessandro, F. R. Keene, *Dalton Trans.* **2004**, 3950-3954.

[16] M. D. Ward, *Chem. Soc. Rev.* **1995**, *24*, 121.

[17] R. J. Crutchley, in *Advances in Inorganic Chemistry, Vol. Volume 41* (Ed.: A. G. Sykes), Academic Press, **1994**, pp. 273-325.

[18] S. Berger, A. Klein, W. Kaim, J. Fiedler, *Inorg. Chem.* **1998**, *37*, 5664-5671.

[19] a) R. Ziessel, M. Hissler, A. El-ghayoury, A. Harriman, *Coord. Chem. Rev.* **1998**, *178-180*, 1251-1298; b) M. D. Ward, *Chem. Ind.* **1996**, 568-573; c) M. N. Paddon-Row, *Acc. Chem. Res.* **1994**, *27*, 18-25; d) M. R. Wasielewski, *Chem. Rev.* **1992**, *92*, 435-461; e) J.-P. Launay, *Chem. Soc. Rev.* **2001**, *30*, 386-397.

[20] a) T. M. Figueira-Duarte, V. Lloveras, J. Vidal-Gancedo, A. Gegout, B. Delavaux-Nicot, R. Welter, J. Veciana, C. Rovira, J.-F. Nierengarten, *Chem. Commun.* **2007**, 4345-4347; b) S. Barlow, D. O'Hare, *Chem. Rev.* **1997**, *97*, 637-669.

[21] a) A. Heckmann, C. Lambert, *Angew. Chem. Int. Ed.* **2012**, *51*, 326-392; b) J. Hankache, O. S. Wenger, *Chem. Rev.* **2011**, *111*, 5138-5178.

[22] C. P. Kubiak, *Inorg. Chem.* **2013**, *52*, 5663-5676.

[23] C. K. Jørgensen, *Coord. Chem. Rev.* **1966**, *1*, 164-178.

[24] L. E. Laverman, A. Wanat, J. Oszajca, G. Stochel, P. C. Ford, R. van Eldik, *J. Am. Chem. Soc.* **2000**, *123*, 285-293.

[25] a) M. Wolak, A. Zahl, T. Schneppensieper, G. Stochel, R. van Eldik, *J. Am. Chem. Soc.* **2001**, *123*, 9780-9791; b) J. A. McCleverty, *Chem. Rev.* **2004**, *104*, 403-418.

[26] E. Culotta, D. E. Koshland, Jr., *Science* **1992**, *258*, 1862-1865.

[27] W. Kaim, B. Schwederski, *Coord. Chem. Rev.* **2010**, *254*, 1580-1588.

[28] a) J. Maurer, M. Linseis, B. Sarkar, B. Schwederski, M. Niemeyer, W. Kaim, S. Záliš, C. Anson, M. Zabel, R. F. Winter, *J. Am. Chem. Soc.* **2008**, *130*, 259; b) M. Linseis, R. F. Winter, B. Sarkar, W. Kaim, S. Záliš, *Organometallics* **2008**, *27*, 3321; cY. Hoshino, S. Higuchi, J. Fiedler, C. Y. Su, A. Knödler, B. Schwederski, B. Sarkar, H. Hartmann, W. Kaim, *Angew. Chem.* **2003**, *115*, 698; dC. Olivier, K. Costuas, S. Choua, V. Maurel, P. Turek, J. Y. Saillard, D. Touchard, S. Rigaut, *J. Am. Chem. Soc.* **2010**, *132*, 5638.

[29] a) G. N. Schrauzer, V. Mayweg, *J. Am. Chem. Soc.* **1962**, *84*, 3221-3221; b) A. Davison, N. Edelstein, R. H. Holm, A. H. Maki, *J. Am. Chem. Soc.* **1963**, *85*, 2029-2030; c) A. Davison, N. Edelstein, R. H. Holm, A. H. Maki, *Inorg. Chem.* **1963**, *2*, 1227-1232; d) H. B. Gray, R. Williams, I. Bernal, E. Billig, *J. Am. Chem. Soc.* **1962**, *84*, 3596-3597; e) E. Billig, R. Williams, I. Bernal, J. H. Waters, H. B. Gray, *Inorg. Chem.* **1964**, *3*, 663-666; f) J. A. McCleverty, *Prog. Inorg. Chem.*, **1968**, 49-221.

[30] R. Eisenberg, H. B. Gray, *Inorg. Chem.* **2011**, *50*, 9741-9751.

[31] R. Sakamoto, S. Tsukada, H. Nishihara, *Dalton Trans.* **2012**, *41*, 10123-10135.

[32] J. A. Ladd, M. M. Olmstead, A. L. Balch, *Inorg. Chem.* **1984**, *23*, 2318-2323.

[33] C. G. Pierpont, C. W. Lange, *Prog. Inorg. Chem.* **1993**, *41*, 331.

[34] W. P. Griffith, *Transition Met. Chem.* **1993**, *18*, 250-256.

[35] M. E. Cass, N. R. Gordon, C. G. Pierpont, *Inorg. Chem.* **1986**, *25*, 3962.

[36] L. O. Atovmyan, V. V. Tkachev, T. G. Shishova, *Dokl. Akad. Nauk SSSR* **1972**, *205*, 609-610.

[37] a) O. Carugo, C. B. Castellani, K. Djinovic, M. Rizzi, *J. Chem. Soc., Dalton Trans.* **1992**, 837-841; b) C. G. Pierpont, R. M. Buchanan, *Coord. Chem. Rev.* **1981**, *38*, 45-87.

[38] L. D. Loomis, K. N. Raymond, *Inorg. Chem.* **1991**, *30*, 906-911.

[39] M. Costas, M. P. Mehn, M. P. Jensen, L. Que, *Chem. Rev.* **2004**, *104*, 939-986.

[40] O. R. Luca, R. H. Crabtree, *Chem. Soc. Rev.* **2013**, *42*, 1440-1459.

[41] a) J. J. Concepcion, J. W. Jurss, M. K. Brennaman, P. G. Hoertz, A. O. v. T. Patrocinio, N. Y. Murakami Iha, J. L. Templeton, T. J. Meyer, *Acc. Chem. Res.* **2009**, *42*, 1954-1965; b) J. L. Boyer, J. Rochford, M.-K. Tsai, J. T. Muckerman, E. Fujita, *Coord. Chem. Rev.* **2010**, *254*, 309-330.

[42] C. A. Lippert, K. Riener, J. D. Soper, *Eur. J. Inorg. Chem.* **2012**, *2012*, 554-561.

[43] J. Sedó, J. Saiz-Poseu, F. Busqué, D. Ruiz-Molina, *Adv. Mater.* **2013**, *25*, 653-701.

[44] M. Haga, E. S. Dodsworth, A. B. P. Lever, *Inorg. Chem.* **1986**, *25*, 447-453.

[45] R. B. Salmonsen, A. Abelleira, M. J. Clarke, S. D. Pell, *Inorg. Chem.* **1984**, *23*, 385-387.

[46] M. Haga, K. Isobe, S. R. Boone, C. G. Pierpont, *Inorg. Chem.* **1990**, *29*, 3795-3799.

[47] G. K. Lahiri, S. Bhattacharya, B. K. Ghosh, A. Chakravorty, *Inorg. Chem.* **1987**, *26*, 4324-4331.

[48] M. D. Ward, J. A. McCleverty, *J. Chem. Soc., Dalton Trans.* **2002**, 275-288.

[49] P. A. Lay, R. H. Magnuson, H. Taube, *Inorg. Chem.* **1988**, *27*, 2364-2371.

[50] C. Remenyi, M. Kaupp, *J. Am. Chem. Soc.* **2005**, *127*, 11399-11413.

[51] a) P. Gütlich, A. Hauser, H. Spiering, *Angew. Chem., Int. Ed. Engl.* **1994**, *33*, 2024; b) A. Aviram, *Int. J. Quantum Chem.* **1992**, *42*, 1615.

[52] S. Archer, J. A. Weinstein, *Coord. Chem. Rev.* **2012**, *256*, 2530-2561.

[53] A. L. Balch, *J. Am. Chem. Soc.* **1973**, *95*, 2723.

[54] M.-J. Don, K. Yang, S. Bott, M. Richmond, *J. Chem. Crystallogr.* **1996**, *26*, 335-340.

[55] a) K. H. Puthraya, T. S. Srivastava, *Polyhedron* **1985**, *4*, 1579-1584; b) S. S. Kamath, V. Uma, T. S. Srivastava, *Inorg. Chim. Acta.* **1989**, *161*, 49-56; c) L. Kumar, K. H. Puthraya, T. S. Srivastava, *Inorg. Chim. Acta.* **1984**, *86*, 173-178.

[56] M. J. G. Lesley, W. Clegg, T. B. Marder, N. C. Norman, A. G. Orpen, A. J. Scott, J. Starbuck, *Acta Cryst. Sect. C* **1999**, *55*, 1272-1275.

[57] J. A. Weinstein, M. T. Tierney, E. S. Davies, K. Base, A. A. Robeiro, M. W. Grinstaff, *Inorg. Chem.* **2006**, *45*, 4544-4555.

[58] G. A. Fox, C. G. Pierpont, *Inorg. Chem.* **1992**, *31*, 3718.

[59] O. Sato, J. Tao, Y.-Z. Zhang, *Angew. Chem., Int. Ed.* **2007**, *46*, 2152-2187.

[60] R. M. Buchanan, C. G. Pierpont, *J. Am. Chem. Soc.* **1980**, *102*, 4951-4957.

[61] D. M. Adams, A. Dei, A. L. Rheingold, D. N. Hendrickson, *J. Am. Chem. Soc.* **1993**, *115*, 8221-8229.

[62] R. M. Buchanan, C. G. Pierpont, *Inorg. Chem.* **1979**, *18*, 3439.

[63] C. G. Pierpont, O.-S. Jung, *Inorg. Chem.* **1995**, *34*, 4281-4283.

[64] O.-S. Jung, C. G. Pierpont, *J. Am. Chem. Soc.* **1994**, *116*, 2229-2230.

[65] M. W. Lynch, D. N. Hendrickson, B. J. Fitzgerald, C. G. Pierpont, *J. Am. Chem. Soc.* **1984**, *106*, 2041.

[66] C. G. Pierpont, *Coord. Chem. Rev.* **2001**, *216–217*, 95.

[67] N. Shaikh, S. Goswami, A. Panja, X.-Y. Wang, S. Gao, R. J. Butcher, P. Banerjee, *Inorg. Chem.* **2004**, *43*, 5908-5918.

[68] G. A. Razuvaev, V. K. Cherkasov, G. A. Abakumov, *J. Organomet. Chem.* **1978**, *160*, 361-371.

[69] a) D. M. Dooley, M. A. McGuirl, D. E. Brown, P. N. Turowski, W. McIntire, P. F. Knowles, *Nature* **1991**, *349*, 262; b) C. M. Wilmot, *Biochem. Soc. Trans.* **2003**, *31*, 493; c) C. Anthony, *Arch. Biochem. Biophys.* **2004**, *428*, 2.

[70] a) J. Stubbe, W. A. van der Donk, *Chemical Reviews* **1998**, *98*, 2661-2662; b) D. M. Dooley, D. E. Brown, *JBIC* **1996**, *1*, 205-209; c) M. A. McGuirl, D. E. Brown, D. M. Dooley, *JBIC* **1997**, *2*, 336-342.

[71] W. Kaim, J. Rall, *Angew. Chem. Int. Ed.* **1996**, *35*, 43-60.

[72] J. Rall, W. Kaim, *J. Chem. Soc., Faraday Trans.* **1994**, *90*, 2905-2908.

[73] a) R. M. Buchanan, C. Wilson-Blumenberg, C. Trapp, S. K. Larsen, D. L. Greene, C. G. Pierpont, *Inorg. Chem.* **1986**, *25*, 3070-3076; b) J. Kaizer, Z. Zsigmond, I. Ganszky, G. Speier, M. Giorgi, M. Réglier, *Inorg. Chem.* **2007**, *46*, 4660-4666.

[74] M. Albrecht, K. Hübler, T. Scheiring, W. Kaim, *Inorg. Chim. Acta.* **1999**, *287*, 204-208.

[75] J. Rall, M. Wanner, M. Albrecht, F. M. Hornung, W. Kaim, *Chem. A Eur. J.* **1999**, *5*, 2802-2809.

[76] a) S. Ye, B. Sarkar, M. Niemeyer, W. Kaim, *E. J. Inorg. Chem.* **2005**, *2005*, 4735-4738; b) W. Kaim, M. Wanner, A. Knödler, S. Záliš, *Inorg. Chim. Acta.* **2002**, *337*, 163-172.

[77] M. Leboschka, M. Sieger, B. Sarkar, J. Heck, M. Niemeyer, D. Bubrin, F. Lissner, T. Schleid, S. Záliš, C.-Y. Su, W. Kaim, *Zeitschrift für anorganische und allgemeine Chemie* **2009**, *635*, 2177-2184.

[78] aC. G. Pierpont, H. H. Downs, T. G. Rukavina, *J. Am. Chem. Soc.* **1974**, *96*, 5573-5574; bC. G. Pierpont, H. H. Downs, *J. Am. Chem. Soc.* **1975**, *97*, 2123-2127.

[79] C. G. Pierpont, H. H. Downs, *J. Am. Chem. Soc.* **1976**, *98*, 4834-4838.

[80] a) R. M. Buchanan, H. H. Downs, W. B. Shorthill, C. G. Pierpont, S. L. Kessel, D. N. Hendrickson, *J. Am. Chem. Soc.* **1978**, *100*, 4318; b) R. M. Buchanan, S. L. Kessel, H. H. Downs, C. G. Pierpont, D. N. Hendrickson, *J. Am. Chem. Soc.* **1978**, *100*, 7894.

[81] S. R. Sofen, D. C. Ware, S. R. Cooper, K. N. Raymond, *Inorg. Chem.* **1979**, *18*, 234-239.

[82] C. G. Pierpont, *Inorg. Chem.* **2011**, *50*, 9766-9772.

[83] H.-C. Chang, H. Miyasaka, S. Kitagawa, *Inorg. Chem.* **2000**, *40*, 146-156.

[84] a) H.-C. Chang, T. Ishii, M. Kondo, S. Kitagawa, *J. Chem. Soc., Dalton Trans.* **1999**, 2467-2476; bH.-C. Chang, S. Kitagawa, *Angew. Chem. Int. Ed.* **2002**, *41*, 130-133.

[85] S. Kitagawa, H. C. Chang, Y. Fukuda, *Inorganic Chromotropism. Basic Concepts and Applications of Colored Materials*, Springer, **2007**.

[86] D. M. Adams, D. N. Hendrickson, *J. Am. Chem. Soc.* **1996**, *118*, 11515-11528.

[87] K. N. Raymond, S. S. Isied, L. D. Brown, F. R. Fronczek, J. H. Nibert, *J. Am. Chem. Soc.* **1976**, *98*, 1767.

[88] C. G. Pierpont, *Coord. Chem. Rev.* **2001**, *219–221*, 415.

[89] V. Balzani, M. Venturi, A. Credi in *Molecular Devices and Machines*, Wiley-VCH, **2003**.

[90] C. Simão, M. Mas-Torrent, J. Casado-Montenegro, F. Otón, J. Veciana, C. Rovira, *J. Am. Chem. Soc.* **2011**, *133*, 13256-13259.

[91] J. S. Miller, K. S. Min, *Angew. Chem. Int. Ed.* **2009**, *48*, 262-272.

[92] K. S. Min, A. G. DiPasquale, J. A. Golen, A. L. Rheingold, J. S. Miller, *J. Am. Chem. Soc.* **2007**, *129*, 2360-2368.

[93] A. Sokolowski, B. Adam, T. Weyhermüller, A. Kikuchi, K. Hildenbrand, R. Schnepf, P. Hildebrandt, E. Bill, K. Wieghardt, *Inorg. Chem.* **1997**, *36*, 3702.

[94] A. Dei, D. Gatteschi, L. Pardi, U. Russo, *Inorg. Chem.* **1991**, *30*, 2589.

[95] C. Benelli, A. Dei, D. Gatteschi, H. U. Guedel, L. Pardi, *Inorg. Chem.* **1989**, *28*, 3089-3091.

[96] K. Heinze, G. Huttner, L. Zsolnai, A. Jacobi, P. Schober, *Chem. Eur. J.* **1997**, *3*, 732-743.

[97] C. Bianchini, D. Masi, C. Mealli, A. Meli, G. Martini, F. Laschi, P. Zanello, *Inorg. Chem.* **1987**, *26*, 3683-3693.

[98] K. Heinze, G. Huttner, O. Walter, *Eur. J. of Inorg. Chem.* **1999**, *1999*, 593-600.

[99] A. M. Barthram, Z. R. Reeves, J. C. Jeffery, M. D. Ward, *J. Chem. Soc., Dalton Trans.* **2000**, 3162-3169.

[100] L. F. Joulié, E. Schatz, M. D. Ward, F. Weber, L. J. Yellowlees, *J. Chem. Soc., Dalton Trans.* **1994**, 799.

[101] J. Best, I. V. Sazanovich, H. Adams, R. D. Bennett, E. S. Davies, A. J. H. M. Meijer, M. Towrie, S. A. Tikhomirov, O. V. Bouganov, M. D. Ward, J. A. Weinstein, *Inorg. Chem.* **2010**, *49*, 10041-10056.

[102] G. A. Abakumov, V. K. Cherkasov, V. I. Nevodchikov, V. A. Kuropatov, B. C. Noll, C. G. Pierpont, *Inorg. Chem.* **1998**, *37*, 6117.

[103] G. A. Abakumov, V. K. Cherkasov, V. I. Nevodchikov, V. A. Kuropatov, G. T. Yee, C. G. Pierpont, *Inorg. Chem.* **2001**, *40*, 2434-2436.

[104] A. I. Poddel'sky, N. V. Somov, N. O. Druzhkov, V. K. Cherkasov, G. A. Abakumov, *J. Organomet. Chem.* **2011**, *696*, 517-522.

[105] A. Bencini, C. A. Daul, A. Dei, F. Mariotti, H. Lee, D. A. Shultz, L. Sorace, *Inorg. Chem.* **2001**, *40*, 1582.

[106] L. F. Joulie, E. Schatz, M. D. Ward, F. Weber, L. J. Yellowlees, *J. Chem. Soc., Dalton Trans.* **1994**, 799-804.

[107] A. Caneschi, A. Dei, H. Lee, D. A. Shultz, L. Sorace, *Inorg. Chem.* **2001**, *40*, 408.

[108] S. H. Bodnar, A. Caneschi, A. Dei, D. A. Shultz, L. Sorace, *Chem. Commun.* **2001**, 2150-2151.

[109] A. Beni, A. Dei, D. A. Shultz, L. Sorace, *Chem. Phys. Lett.* **2006**, *428*, 400-404.

[110] A. Caneschi, A. Dei, D. Gatteschi, V. Tangoulis, *Inorg. Chem.* **2002**, *41*, 3508-3512.

[111] A. I. Poddel'sky, A. V. Piskunov, N. O. Druzhkov, G. K. Fukin, V. K. Cherkasov, G. A. Abakumov, *Zeitschrift für anorganische und allgemeine Chemie* **2009**, *635*, 2563-2571.

[112] a) Y. Suenaga, C. G. Pierpont, *Inorg. Chem.* **2005**, *44*, 6183-6191; b) Y. Suenaga, Y. Umehata, Y. Hirano, T. Minematsu, C. G. Pierpont, *Inorg. Chim. Acta.* **2008**, *361*, 2941-2949.

[113] Y. Suenaga, Y. Hirano, Y. Umehata, T. Minematsu, *Inorg. Chim. Acta.* **2011**, *365*, 505-512.

[114] a) D. A. Shultz, R. M. Fico, n. Jr, R. K. Kumar, K. E. Vostrikova, J. W. Kampf, P. D. Boyle, *J. Am. Chem. Soc.* **2003**, *125*, 11761; b) D. A. Shultz, A. K. Boal, H. Lee, G. T. Farmer, *J. Org. Chem* **1998**, *63*, 9462; cJ. C. Sloop, D. A. Shultz, T. Coote, B. Shepler, U. Sullivan, J. W. Kampf, P. D. Boyle, *J. Phys. Org Chem.* **2012**, *25*, 314-321.

[115] D. A. Shultz, S. H. Bodnar, H. Lee, J. W. Kampf, C. D. Incarvito, A. L. Rheingold, *J. Am. Chem. Soc.* **2002**, *124*, 10054-10061.

[116] a) R. Jain, M. B. Sponsler, F. D. Coms, D. A. Dougherty, *J. Am. Chem. Soc.* **1988**, *110*, 1356-1366; b) A. Rajca, S. Utamapanya, J. Xu, *J. Am. Chem. Soc.* **1991**, *113*, 9235-9241.

[117] A. Dei, L. Sorace, *Dalton Trans.* **2003**, 3382.

[118] a) H. E. Simmons, T. Fukunaga, *J. Am. Chem. Soc.* **1967**, *89*, 5208-5215; b) N. L. Frank, R. Clérac, J.-P. Sutter, N. Daro, O. Kahn, C. Coulon, M. T. Green, S. Golhen, L. Ouahab, *J. Am. Chem. Soc.* **2000**, *122*, 2053-2061; c) H. Dürr, R. Gleiter, *Angew. Chem. Int. Ed.* **1978**, *17*, 559-569.

[119] A. Dei, D. Gatteschi, C. Sangregorio, L. Sorace, *Acc. Chem. Res.* **2004**, *37*, 827-835.

[120] M. Affronte, A. Beni, A. Dei, L. Sorace, *Dalton Trans.* **2007**, 5253-5259.

[121] a) K. G. Alley, G. Poneti, J. B. Aitken, R. K. Hocking, B. Moubaraki, K. S. Murray, B. F. Abrahams, H. H. Harris, L. Sorace, C. Boskovic, *Inorg. Chem.* **2012**, *51*, 3944-3946; b) K. G. Alley, G. Poneti, P. S. D. Robinson, A. Nafady, B. Moubaraki, J. B. Aitken, S. C. Drew, C. Ritchie, B. F. Abrahams, R. K. Hocking, K. S. Murray, A. M. Bond, H. H. Harris, L. Sorace, C. Boskovic, *J. Am. Chem. Soc.* **2013**, *135*, 8304-8323.

[122] A. M. Barthram, R. L. Cleary, R. Kowallick, M. D. Ward, *Chem. Commun.* **1998**, 2695.

[123] A. Caneschi, A. Dei, C. P. Mussari, D. A. Shultz, L. Sorace, K. E. Vostrikova, *Inorg. Chem.* **2002**, *41*, 1086-1092.

[124] M. Hmadeh, Z. Lu, Z. Liu, F. Gandara, H. Furukawa, S. Wan, V. Agustyn, R. Chang, L. Liao, F. Zhou, E. Perre, V. Ozolins, X. Duan, B. Dunn, Y. Yamamto, O. Terasaki, O. M. Yaghi, *Chem. Mater.* **2012**, *24*, 3511-3513.

[125] C. S. Grange, A. J. H. M. Meijer, M. D. Ward, *Dalton Trans.* **2010**, *39*, 200-211.

[126] C. Benelli, A. Dei, D. Gatteschi, L. Pardi, *Inorg. Chem.* **1988**, *27*, 2831-2836.

[127] J. L. Scott, D. R. MacFarlane, C. L. Raston, C. M. Teoh, *Green Chem.* **2000**, *2*, 123-126.

[128] H. Zimmermann, P. Tolstoy, H.-H. Limbach, R. Poupko, Z. Luz, *J. Phys. Chem. B* **2004**, *108*, 18772-18778.

[129] K. T. Holman, J. L. Atwood, J. W. Steed, *Angew. Chem. Int. Ed.* **1997**, *36*, 1736-1738.

[130] M. J. Hardie, C. L. Raston, *Chem. Commun.* **1999**, 1153-1163.

[131] a) H. Matsubara, S.-y. Oguri, K. Asano, K. Yamamoto, *Chem. Lett.* **1999**, *28*, 431-432; b) A. M. Bond, W. Miao, C. L. Raston, T. J. Ness, M. J. Barnes, J. L. Atwood, *J. Phys. Chem. B* **2001**, *105*, 1687-1695.

[132] T. K. Ronson, J. Fisher, L. P. Harding, M. J. Hardie, *Angew. Chem. Int. Ed.* **2007**, *46*, 9086-9088.

[133] J. A. Gawenis, K. T. Holman, J. L. Atwood, S. S. Jurisson, *Inorg. Chem.* **2002**, *41*, 6028-6031.

[134] a) M. A. Little, J. Donkin, J. Fisher, M. A. Halcrow, J. Loder, M. J. Hardie, *Angew. Chem., Int. Ed.* **2012**, *51*, 764-766, S764/761-S764/722; b) J. Sanseverino, J.-C. Chambron, E. Aubert, E. Espinosa, *J. Org. Chem.* **2011**, *76*, 1914-1917.

[135] M. A. Little, M. A. Halcrow, M. J. Hardie, *Chem. Commun.* **2013**, *49*, 1512-1514.

[136] B. F. Abrahams, N. J. FitzGerald, T. A. Hudson, R. Robson, T. Waters, *Angew. Chem., Int. Ed.* **2009**, *48*, 3129.

[137] B. F. Abrahams, B. A. Boughton, N. J. FitzGerald, J. L. Holmes, R. Robson, *Chem. Commun.* **2011**, *47*, 7404.

[138] P. Satha, G. Illa, C. S. Purohit, *Cryst. Growth Des.* **2013**, *13*, 2636-2641.

[139] D. Scott Bohle, D. Stasko, *Chem. Commun.* **1998**, 567-569.

[140] D. Hendrickson, C. Pierpont, in *Spin Crossover in Transition Metal Compounds II, Vol. 234*, Springer Berlin Heidelberg, **2004**, pp. 63-95.

Chapter 2

Novel Crystalline Cavitand Clathrates, Including Three Cyclotriveratrylene and Cyclotricatechylene Donor-Acceptor Complexes[1]

2.1 Introduction

The π-electron rich nature of catechol species makes them very good electron donor species in classical inorganic complexations whereby a metal ion (most commonly with ancillary ligand) acts as an electron accepting species. These reactions have been shown to not only be fascinating yet optoelectronically important also. If we consider the catechol species to be nothing more than an electron donor however, it appears plausible that use of an organic electron accepting species instead of a metal ion may also be investigated, in the hope that they also offer interesting catecholato complex donor : acceptor charge transfer species. Complexes of this orientation would directly fall within the subject bracket of 'organic electronics' whereby the majority of structures known to date involve organic donors with low dimensionality, such as tetrathiafulvalene (TTF) derivatives due to their extensive π-conjugation.[2] *Para*-cyclophanes have been considered in the past as a method to increase the dimensionality of these organic charge-transfer species, with a very recent example utilising the ubiquitous organic electron acceptor species tetracyanoethylene (tcne) (**Figure 2.1**) with [3,3]paracyclophane in a 1 : 1 stoichiometry.[3] Paracyclophanes have displayed a particularly interesting trait in their ability to mediate strong transannular π-electron interactions via the stacking of two rings ontop of each other.

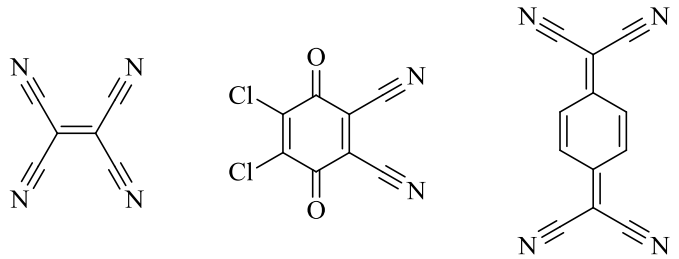

Figure 2.1. Shematic representations of tetracyanoethylene (tcne), 2,3-dichloro-5,6-dicyanobenzoquinone (ddq) and tetracycanoquinodimethane (tcnq).

Tetracycanoethylene has been utilised on many occasions for the synthesis of electronic materials, based upon organic and inorganic frameworks. In addition, tcne is a particular amenable compound for the study of charge transfer states due to its versatility in displaying characteristic structural features through bond lengths and IR absorption data which have been extensively tabulated.[4] Low lying π^* orbitals of the cyano groups teamed with

conjugation about the central carbon-carbon double bond make the system very electrophilic and may act as a one-electron oxidant towards groups such as alkenes, ketones, alcohols and thiols.[4] Consequently, tcne has proven to be a very valuable molecule in the synthetic chemist's toolbox. As many of the reactions tcne participates in involve the formation of a charge transfer complex, further uses of tcne have been found and a vast array of materials has been synthesised with research concentrating on electronic and magnetic properties. The first reported formation of a charge transfer complex involving tcne was by Merrifield and Philips[5] in 1958. Since their report, a plethora of contributions to a variety of aspects within research of the molecule has been achieved, leading to many more examples of charge-transfer materials containing tcne as an electron acceptor, many with material applications in mind. For example, molecule-based magnets are a relatively new class of materials, with new examples surfacing regularly in a variety of forms including hybrid organic-inorganic thin film magnets[6] and *x*-dimensional coordination polymers[7] to name two of an ever-growing field. These materials tend to grow very large block-based materials with qualities approaching those required for real-life applications.

The redox-rich chemistry of catecholato compounds makes them attractive for the formation of a charge transfer complex upon addition of a one-electron oxidant. In these species, a fraction of electronic charge may be transferred between the two species resulting in excited electronic state of the acceptor and best characterised as an electronic resonance between non-bonded and dative state.[8] The ability of the catechol subunit to display a charge-transfer association between catechol or phenol subunits has been investigated in the past, although their structures have not been determined.[9-12]

Work performed by Frey *et al*.[9] has been instrumental in determining the actual charge-transfer mechanism between tcne and donors containing C-O bonds, by a variety of dichloromethane solution-phase measurements. It was found that the association constants of charge transfer bands was increased by introduction of better electron-donating groups (i.e. Me < Et < ^{i}Pr < ^{t}Bu) for acyclic alkyl substituents, whilst increasing ring size offered greater association constants for cyclic alkyl substituents placed on the phenolic or aryl ether moiety. More recent work performed by Reddy *et al*.[12] again involved the formation of charge-transfer species between a phenolic donor species. Their investigation involved the use of other electron-accepting species, such as 2,3-dichloro-5,6-dicyanobenzoquinone (ddq) (**Figure 2.1**) *p*-benzoquinone and *p*-chloranil, was invoked. Solid state and solution phase analysis delivered results whereby darkly-coloured charge-transfer complexes were obtained and displayed an interesting conclusion whereby naphthalene derivatives displayed stronger charge-transfer interactions between acceptor species than dihydroxy or trihydroxy

benzyl derivatives whilst it was also concluded that the position of the hydroxyl moiety on the aryl ring had little effect on the electron donating ability of the donor.

One further electron accepting molecule of particular interest for the formation of charge-transfer complexes is that of tetracyanoquinodimethane (**Figure 2.1**) (tcnq), again commonly used in a manner of reactions as in the case of tcne.[13] Structures involving tcnq have been mainly concerned with crystallisations with other planar molecules such as TFF[14] and its derivatives.[15] A limited number of tcnq plus phenol charge transfer salts have also been reported along with their crystalline structures.[16-17] Work performed by Lagrenée[17] involved the formation of a charge-transfer complex between tcnq and 2-[5-2(2-pyridyl)-1,2,4,-triazol-3-yl] (PTP), where it was found that molecules of tcnq and PTP displayed a motif whereby the molecules pack ontop of one another in order to mediate π…π contacts, the same packing motif as has been seen previously in structures containing tcnq.[18]

Cyclotriveratrylene (ctv, **2.1**) is a very important cavitand host in supramolecular chemistry, both individually,[19,20] and as a scaffold for derivatives with extended cavities, organic capsules (cryptophanes)[21] and metal-organic capsules and other architectures.[20] In the crystalline state ctv readily forms in-cavity complexes with fullerenes and some other globular molecules, but usually forms exclusion clathrates with solvents or other small molecules.[19,20] Extended cavitands and capsules containing the ctv (**2.1**) core however, have a much more varied inclusion chemistry, complexing a range of small organic molecules and even gases.[20,21] The *tris*-catechol analogue cyclotricatechylene (ctc, **2.2**) is obtained via simple demethylation of **2.1**,[22] but has been little studied. There are four previously published clathrate materials of ctc with organic solvents, which have varying stoichiometries.[22-24] Three adopt a similar crystal packing motif in which the ctc molecules and solvent associate into alternating 'up' and 'down' hydrogen bonded bilayers within the ctc cavities. The connectivity of the ctc nodes in the hydrogen bonding topology of the bilayers varies between the structures, however, depending on the number of solvent molecules present and their hydrogen bonding character. The exception to this generalisation is ctc•$[dmf]_2$•$[H_2O]_2$, which forms an alternative lattice type containing sheets of dmf solvent encapsulated by an "up" and a "down" monolayer of hydrogen bonded ctc molecules.[25] As well as taking part in the hydrogen bond network, one equivalent of solvent is always included in the ctc host cavity in these structures. This implies that ctc may be a stronger host for small molecules in the solid state than ctv, whose clathrate crystals rarely contain in-cavity solvent. A small number of metal complexes of ctc have also been reported, some of which also contain included solvent.[26, 27]

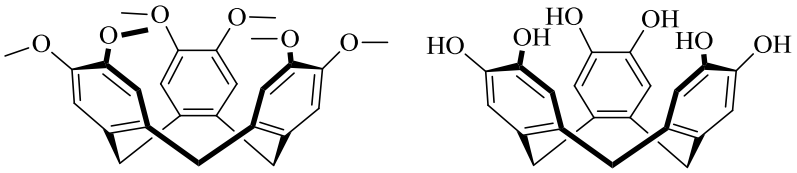

2.1 **2.2**

Figure 2.2. Cyclotriveratrylene (ctv, **2.1**) and Cyclotricatechylene (ctc, **2.2**).

The aim of this work was therefore to investigate the ability of **2.1** and **2.2** to form charge transfer materials by addition of an electron-acceptor molecule such as tcne, ddq or tcnq. The formation of a charge transfer complex was particulary of interest for **2.2** as this would highlight its ability to support oxidation of the dioxolene moieties to form a stable oxidised radical compound which could potentially have interesting EPR and electronic absorption spectra.

2.2 Results and Discussion

Addition of various charge acceptor species to solutions of ctv and ctc, in a number of different solvents yielded intense colours of green, blue, yellow, orange and red depending on the species involved. These intense colour changes undoubtedly announced the presence of donor : acceptor complexes and in two cases, for tcne and tcnq, yielded large blue and green crystals respectively. Certain solvents displayed an inability to retain the donor : acceptor complexes however, and bleached over the course of two days which was particularly prevalent when dissolved in methanol or ethanol. This was understood to be due to the hydrolysis of tcne, ddq or tcnq into cyanoethanolate compounds and hydrogencyanide where undried solvents were used, as displayed below for tcne as an example.[4, 28-29]

$$\text{tcne} + H_2O \rightarrow [C_2CN_3O]^- + HCN + H^+$$

2.2.1 Donor : Acceptor Complex of $[ctc]_2.[tcne].[THF]_6$ (2.3)

Large blue crystals of the charge-transfer complex $[ctc]_2.[tcne].[THF]_6$ (**2.3**) showed that the asymmetric unit contained two complete molecules of cyclotricatechylene hydrogen bonded to two separate half-molecules of tcne and three molecules of THF. Consequent of the hydrogen-bonding interactions between the cyclotricatechylene and tcne half-molecules, the extended network within the crystal packs to form a puckered 2D sheet where the cyclotricatechylene molecules are 3-connected and tcne molecules 4-connected (**Figure 2.3**).

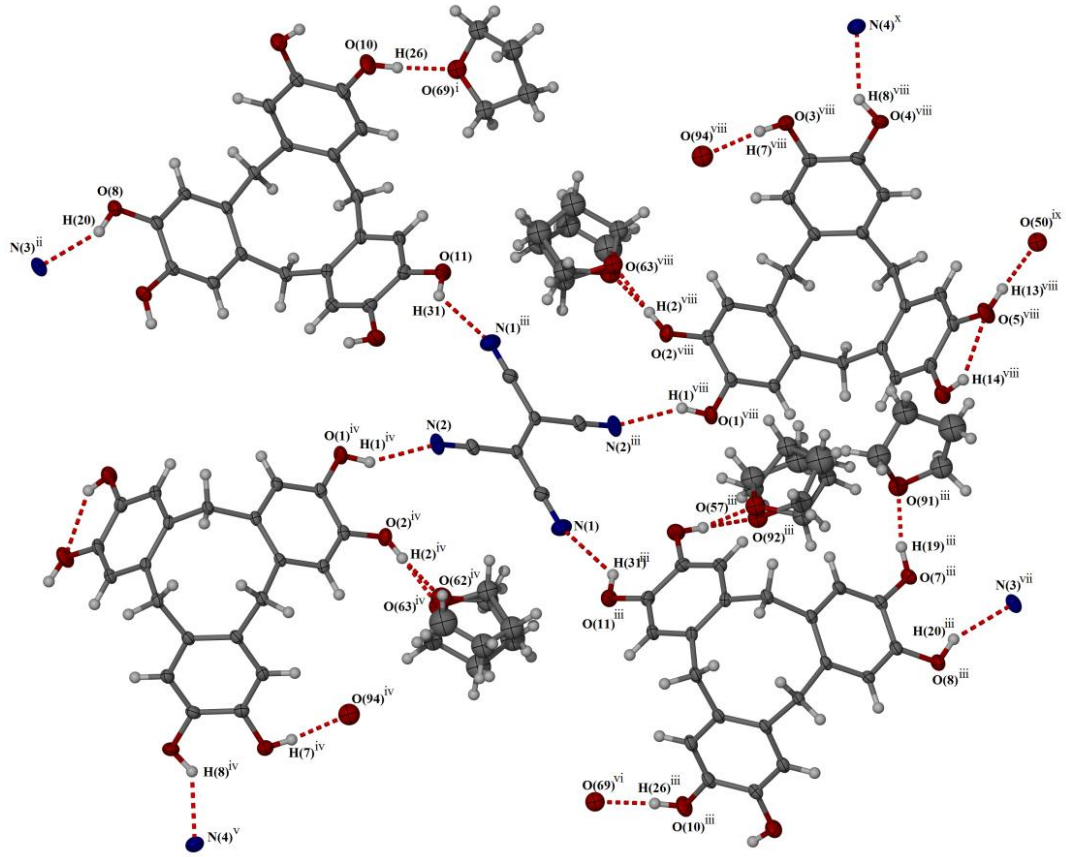

Figure 2.3. Hydrogen bonding of the 4-connected tcne molecule in **2.3**. Displacement ellipsoids are set at 50% probability. Colour code: O, red; N, blue; C, grey; H, white.

The formation of an exclusion complex between cyclotricatechylene and tcne gives rise to the existence of strong hydrogen bonding interactions between the molecules whereby each tcne molecule is sandwiched between two phenylene groups of two different cyclotricatechylene molecule (**Figure 2.4**).

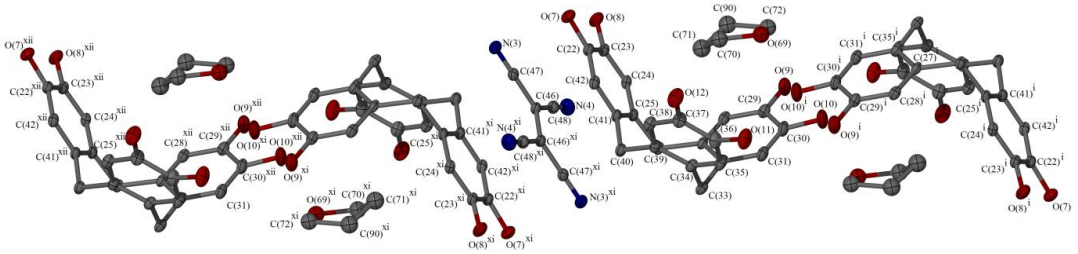

Figure 2.4. View of one tcne molecule sandwiched between two ctc molecules in **2.3.** Hydrogen atoms have been omitted for clarity and displacement ellipsoids are set to 50%. Colour code: O, red; N, blue; C, grey.

This orientation is a common motif in crystalline tcne/aryl complexes where these π…π interactions within the motif demonstrate approximate co-planarity within the groups with similar separations and dihedral angles (**Table 2.1**), linking the hydrogen-bonded network into a three dimensional lattice. Central alkene bond lengths of the two tcne molecules within the lattice exist display values of 1.380(4) and 1.382(4) Å, which are closer to the values expected for the monoanion radical $[tcne]^{\bullet-}$ of 1.385(6) – 1.413(5) Å as opposed to that of the neutral $TCNE^0$ state, equal to 1.344(3) – 1.355(2) Å.[4] Inspection of the cyclotricatechylene catechyl moieties associated with the tcne molecule did imply a catechol (2-) oxidation state due to their protonation, therefore indicating formal electron transfer from cyclotricatechylene to tcne did not occur thus retaining the $tcne^0$ state.[30] Despite the lack of a formal electron transfer between the species, the short distance between tcne molecule and cyclotricatechylene phenyl groups certainly suggests a strong π…π interaction, and when teamed with an increased C=C bond length, certainly suggests strong donor : acceptor complexation.

Table 2.1 Dihedral angles, interplanar spacing and horizontal offsets between ctc phenylene ring and tcne molecule in **2.3**.

	Dihedral Angle (°)	Interplanar Spacing (Å)	Horizontal Offset
[C(1)-C(4)-C(20)-C(21)]…[C(43)-N(2), $C(43)^{iii}$-$N(2)^{iii}$]	2.21(6)	3.109(5)	0.21
[C(22)-C(25)-C(41)-(C42)]…[C(48)-N(4), $C(48)^{xi}$-$N(4)^{xi}$]	1.85(6)	3.099(5)	0.16

Also contained within the asymmetric unit are six THF molecules, two of which occupy the cavities of each cyclotricatechylene molecule whilst the remaining four occupy a solvent channel passing between the two cyclotricatechylene molecules and running throughout the crystal structure (**Figure 2.5**). The THF molecules occupying the cyclotricatechylene

cavities are oriented such that their ring planes lie approximately co-parallel with one phenylene group of each cyclotricatechylene molecule (**Figure 2.6**) although there appears to be no evidence to suggest hydrogen bonding or CH…π interactions occur between the phenylene and THF molecules however.

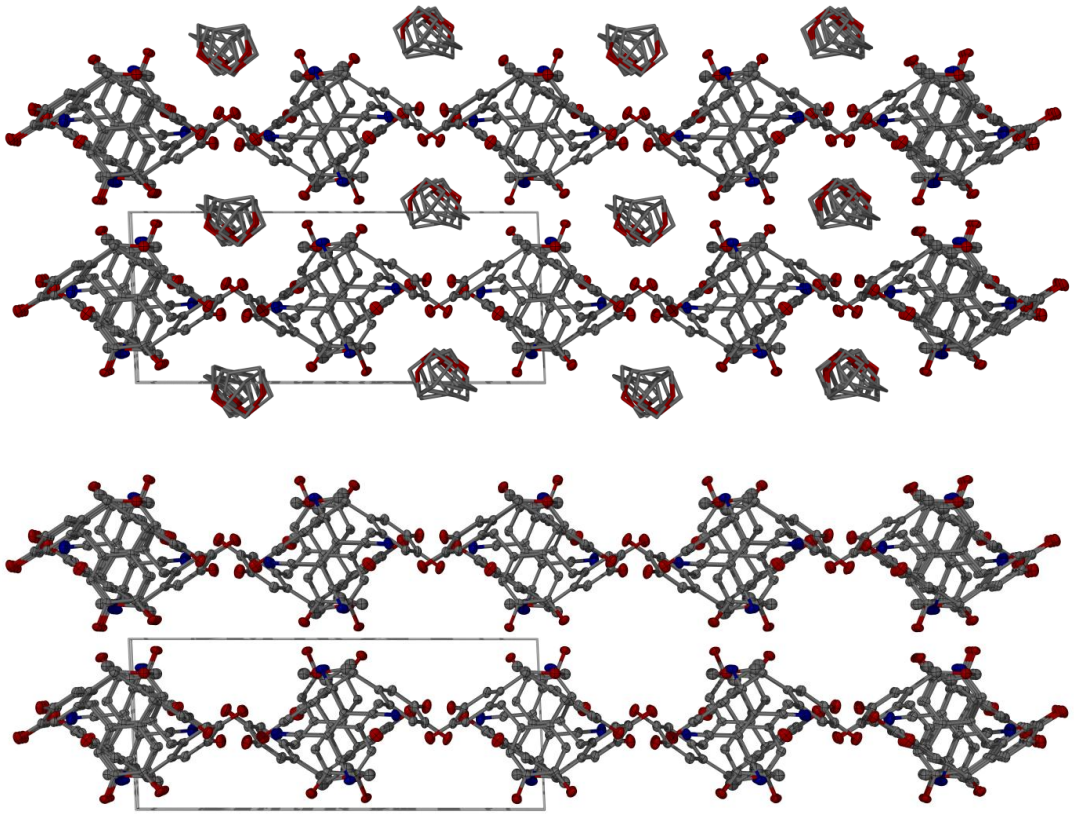

Figure 2.5. View of **2.3** along unit cell *b* axis showing (top) occupied THF solvent channels and (bottom) unoccupied solvent channels. Hydrogen atoms have been omitted for clarity and displacement ellipsoids set at 50% probability level. Colour code: O, red; N, blue; C, grey.

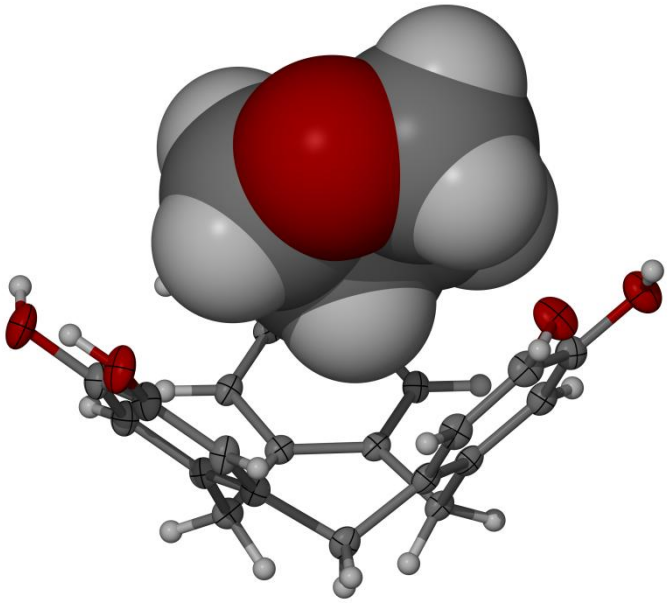

Figure 2.6. Space filling diagram of encapsulated THF guest molecule in host molecule of ctc for structure **2.3**. Displacement ellipsoids for the ctc molecule are set at 50% probability. Colour code: O, red; N, blue; C, grey; H, white.

Table 2.2. Definitions of symmetry codes used in the discussion for crystal structure **2.3**.

(i)	1-*x*, 1-*y*, 1-*z*	(vii)	*x*+1, 1+*y*, *z*-1
(ii)	2-*x*, -*y*, 1-*z*	(viii)	*x*-1, *y*, *z*
(iii)	1-*x*, 1-*y*, -*z*	(ix)	-*x*, 2-*y*, -*z*
(iv)	2-*x*, 1-*y*, -*z*	(x)	-*x*, 1-*y*, 1-*z*
(v)	1+*x*, *y*, *z*-1	(xi)	1-*x*, -*y*, 1-*z*
(vi)	*x*, *y*, *z*-1	(xii)	*x*, *y*-1, *z*

The infrared spectrum of **2.3** showed vibrations expected of a donor : acceptor complex containing tcne. Vibrations at 2249 and 2220 cm^{-1} are typical ν_{CN} stretches alongside another vibration, albeit weakened due to strong hydrogen-bonding between the two species, present at 2238 cm^{-1} again due to the C≡N stretch.[31] The presence of these vibrations certainly confounds the presence of a weakened C≡N bond whereby two native ν_{CN} stretches of $tcne^0$ occur at 2262, 2228 and 2214 cm^{-1}. These shifts are due to the characteristics of the donor : acceptor association whereby configurationally some electron density is transferred from cyclotricatechylene to tcne π^* orbital. Unfortunately probing the ν_{CC} mode of $tcne^0$ is inaccessible by IR due to selection rule requirements.[4]

Powder EPR spectra of the donor : acceptor complex were recorded at 150 K displaying a spectrum with *g* values close to 2.00 (1.998 and 1.993) (**Figure 2.7**). These are very similar to that of the tcne radical anion and free electron *g* values of 2.00.[12, 32] The presence of two, very sharp resonances confirms the presence of two half-molecules of tcne, with one signal originating from each.

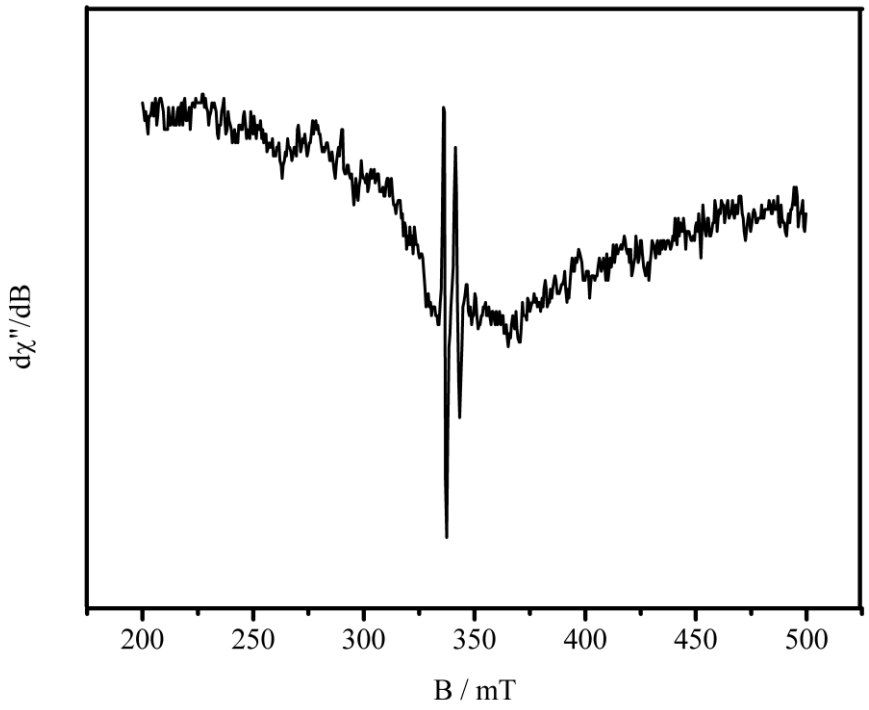

Figure 2.7. X-band powder EPR spectrum of **2.3** recorded at 150 K.

Elemental analysis of complex **2.3** indicated that the crystals retained the majority of crystallised solvent whereby three were removed under vacuum, most likely those present within the solvent channel whilst there is also evidence to suggest absorption of atmospheric water. Electrospray mass spectrometry provided some evidence for the presence of a donor : acceptor complex whereby the negative ion scan yielded a peak at *m/z* 495.1 which may assigned as $[(ctc)(tcne)+H]^-$. The positive ion scan however yielded peaks belonging only to sodium complexes of cyclotricatechylene indicating that tcne is not present in any positive state (i.e. $[tcne]^+$), thereby confirming the mode of cyclotricatechylene as a donor and TCNE as acceptor within their association.

UV/vis optical spectra were recorded of the donor : acceptor complex THF feed solutions where the ν_{max} found at 15,300 cm^{-1} is very close to that previously reported for a donor between dialkylcatechol and tcne.[33]

2.2.2 Donor : Acceptor Complex of $[ctc]_2.[tcnq].[THF]_4$ (2.4)

Large green crystals of the charge transfer complex **2.4** showed that the asymmetric unit contains one complete cyclotricatechylene molecule associated to one half of a tcnq molecule along with two THF molecules, one of which was heavily disordered. The disordered THF molecule within the structure was successfully modelled isotropically over two separate sites with occupancies 0.59 : 0.41 about the common oxygen atom with refined restraints C-O = C-C = 1.44(2) Å. All carbon-bound hydrogen atoms were refined in calculated positions using a riding model whilst all hydroxyl hydrogens, except that bound to O(15), were found within the fourier map and refined with the restraint O-H = 0.90(2). The remaining hydroxyl hydrogen bound to O(15) was refined in a calculated position using a riding model with the restraint O-H = 0.90(2) as no suitable peak was found within the fourier map. Slight disorder about the hydroxyl hydrogens of O(6) and O(13) was noted during the refinement process, understood to be due to the effects of hydrogen bonding thus was modelled with arbitrary site occupancies of 50% each. The thermal ellipsoid of catechyl O(4) was similarly noted to be large, although within appreciable limits, and deemed so for the exact same reasons. Oxygens O(37) and O(38) of the THF molecule contained within the cavity of cyclotricatechylene were modelled as two separate parts as residual electron density peaks were significantly large when considered as one part. The residual electron peak of +1.5 e $Å^{-3}$ is most likely due to further disorder within the twice modelled THF molecule, attempts were made to determine whether another THF molecule was present with the view of modelling, however this proved fruitless.

The position of the tcnq molecule within the crystal is similar to that as demonstrated in the donor : acceptor complex **2.3** whereby the tcnq acceptor molecule holds a crystallographic inversion centre and is placed between two cyclotricatechylene catechyl rings (**Figure 2.8**).

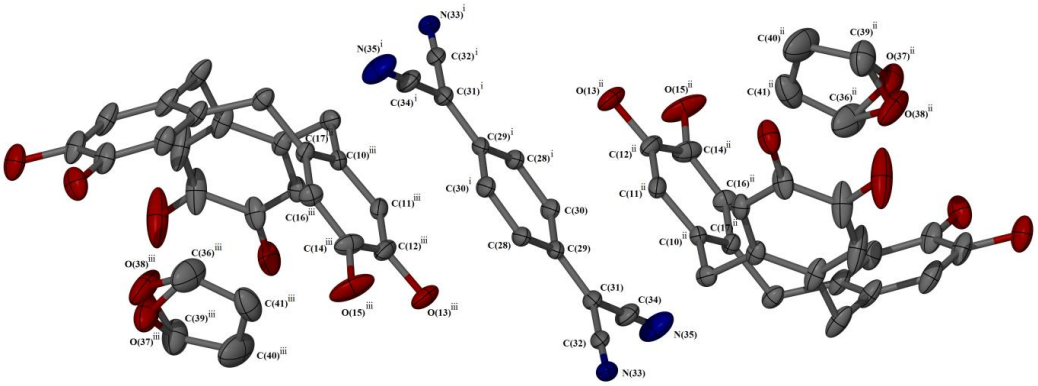

Figure 2.8. View of one tcnq molecule sandwiched between two ctc molecules plus two guest THF molecules in **2.4.** Hydrogen atoms have been omitted for clarity. Displacement ellipsoids are set at 50% probability level. Colour code: O, red; N, blue; C, grey.

Disorder present within the hydroxyl hydrogens complicates the crystalline hydrogen bonding network slightly whereby the hydrogen-bonding interaction between hydroxyl groups of neighbouring molecules (i.e. O(6)-H(6A)…O(6)) which requires the hydroxyl group to be mildly disordered to allow this association (**Figure 2.9**).

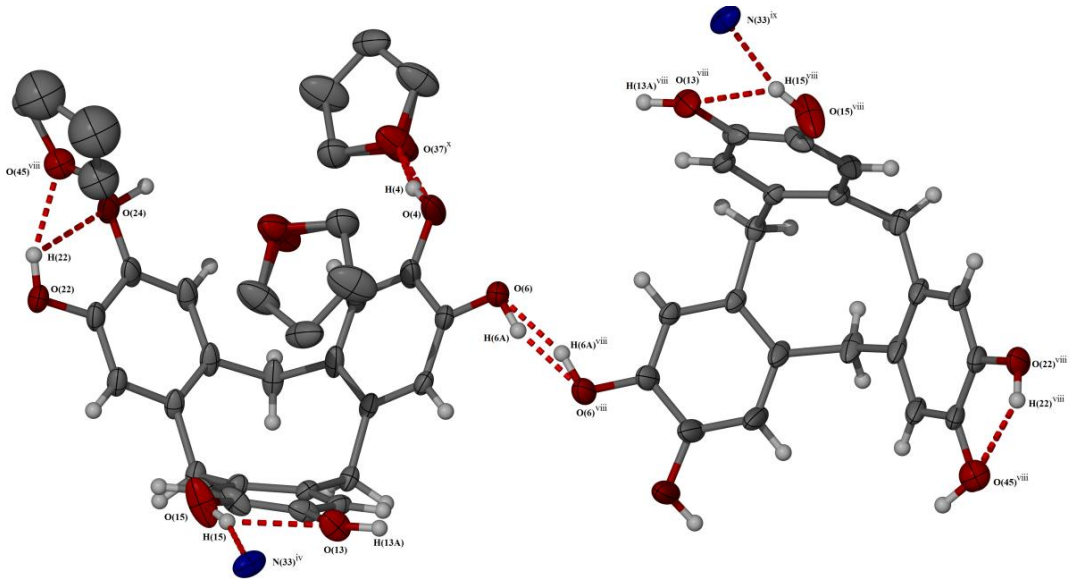

Figure 2.9. Hydrogen bonding interactions between ctc molecules in **2.4.** Hydrogen atoms have been omitted from solvent molecules for clarity. Displacement ellipsoids are set at 50% probability level. The dashed red line indicates hydrogen bonding interactions within the lattice. Colour code: O, red; N, blue; C, grey; H, white.

The two cyclotricatechylene molecules are arranged in a staggered fashion permitting each quinoid C=C bond to overlay with one catechyl ring with interplanar distances of 3.238(14) Å, thereby mediating π…π between the molecules. Furthermore, two of the four cyano groups belonging to the tcnq molecules, C(32)≡N(33) and the symmetry equivalent group,

accept one full hydrogen bond each between the donor group H(15)-O(15) linking the molecules into chain (**Figure 2.10**).

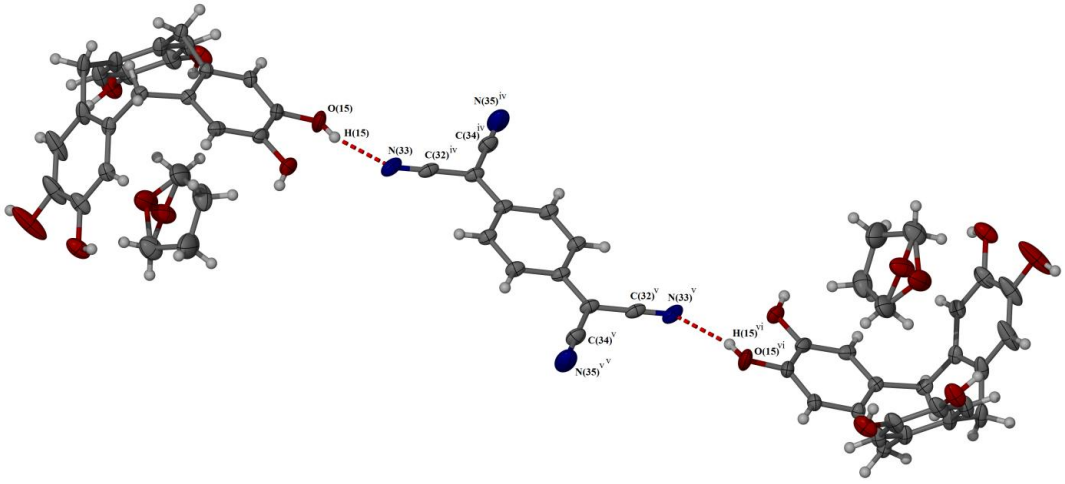

Figure 2.10. Hydrogen bonding between tcnq and two ctc molecules within **2.4.** Displacement ellipsoids are set at 50% probability level. Colour code: O, red; N, blue; C, grey; H, white. The dashed red line indicates hydrogen bonding interactions within the lattice.

Consequent of these interactions there is firm evidence for the existence of a donor : acceptor association between the two species, however, inspection of internal geometries of the tcnq molecule are consistent with that of tcnq in a neutral state whereby the quinodal C=C = 1.386(3) and average internal C-C = 1.452(2).[15] Furthermore, the C=C of the catechyl rings involved in the association are identical to those in the donor : acceptor complex **2.3** indicating formal electron transfer has not occurred thereby retaining the $tcnq^0$ and ctc^0 states.

The infrared spectrum of the complex **2.4** shows one ν_{CN} vibration expected of a donor : acceptor complex containing tcnqat 2219 cm^{-1}.[18] The position of the vibration is less than that of native tcnq due to the added electron density placed across this bond into the vacant π^* conduction band of tcnq.

As in the case of **2.3**, elemental analysis of **2.4** implied that it retained the majority of its crystallised solvent on drying and again displayed some replacement of THF with atmospheric water. The THF molecule lost under vacuum most likely originated from those contained within the solvent channel of the crystal, particularly evident when viewed along the crystallographic *c*-axis (**Figure 2.11**).

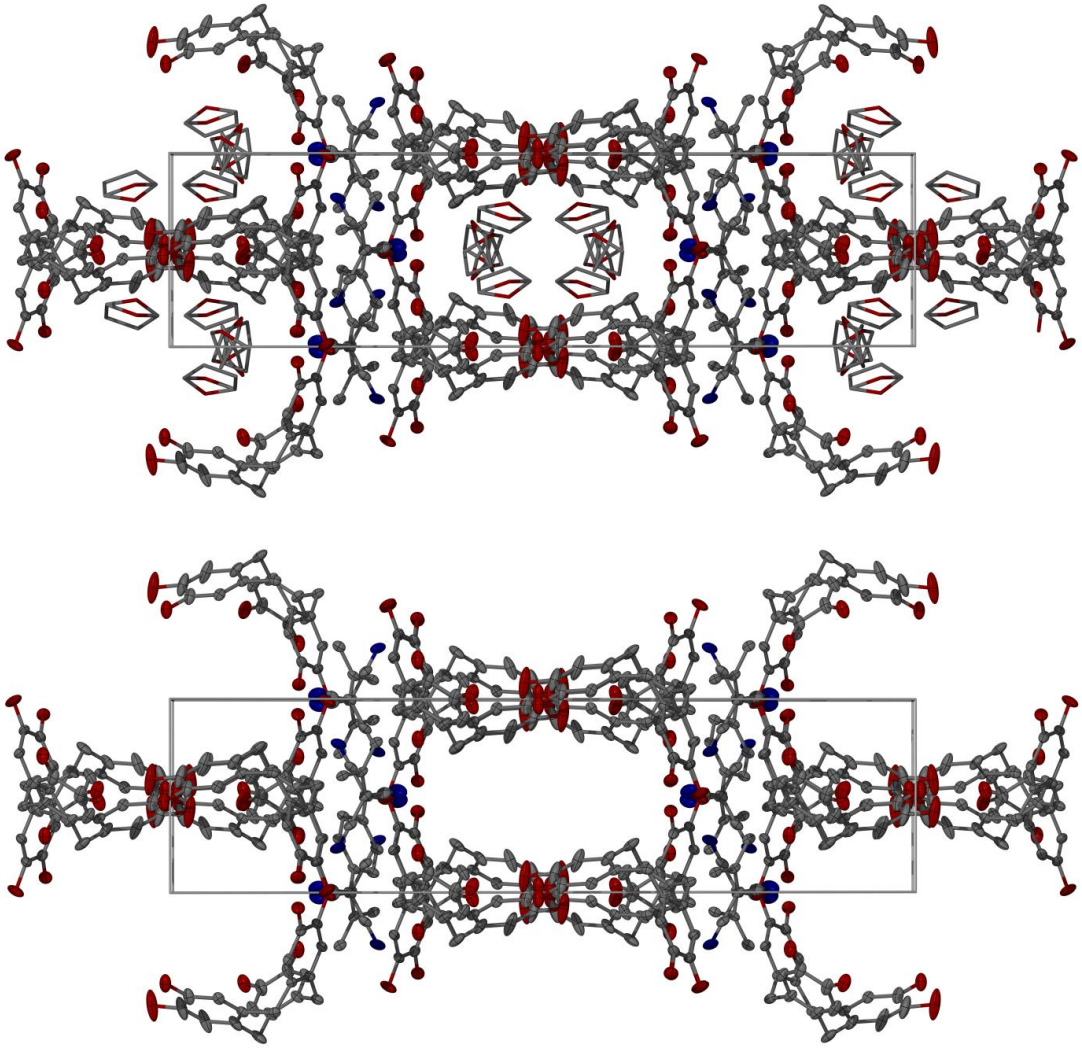

Figure 2.11. View along the unit cell *c* axis of **2.4** depicting, top) occupied solvent channels and b) unoccupied solvent channels. Hydrogen atoms have been omitted for clarity and displacement ellipsoids set at 50% probability. Colour code: O, red; N, blue; C, grey.

Analysis by electrospray mass spectrometry was again performed although failed to provide direct evidence for the presence of a donor : acceptor complex. As with the complex **2.4**, the positive ion scan contained only cyclotricatechylene sodium complexes whilst the negative ion scan yielded peaks belonging only to hydrolysis products of tcnq and the monoanion $[tcnq]^-$. The presence of the monoanion $[tcnq]^-$ in the negative ion scan and only cyclotricatechylene complexes in the positive scan, may again be used as evidence to support the understanding of cyclotricatechylene as donor and tcnq as acceptor, although in this instance is subjective.

Table 2.3 Definitions of symmetry codes used in the discussion for crystal structure **2.4.**

(i)	1/2-*x*, 3/2-*y*, -*z*	(vi)	½-*x*, -*y*-3/2, 1-*z*
(ii)	1/2-*x*, 1/2+*y*, 1/2+*z*	(vii)	*x*, -*y*, *z*-1/2
(iii)	*x*, 1-*y*, *z*-1/2	(viii)	-*x*, *y*, *z*-1/2
(iv)	½-*x*, *y*-3/2, ½-*z*	(ix)	*x*-1/2, *y*-3/2, *z*
(v)	*x*, -*y*, ½+*z*	(x)	-*x*, 1-*y*, -*z*

2.2.3 Clathrate Crystal Structure of [ctc].[dmso]$_5$ (2.5)

Very large and stable, orange/yellow crystals of the solvated clathrate **2.5** showed the asymmetric unit contained one complete molecule of ctc and five complete dimethylsulfoxide molecules, one of which was found to be disordered over two sites. This disordered dmso molecule was modelled without restraints over two sites with occupancies 0.68 : 0.32 utilising a common wholly occupied oxygen atom and one wholly occupied (disordered) methyl group. ctc hydroxyl hydrogen atoms were located in the fourier map and subjected to the restraint O-H = 0.90(2) whilst all carbon-bound hydrogen atoms were placed in calculated positions and refined using a riding model as in *HFIX* in *SHELXL* with common U_{iso} thermal parameter. All non-hydrogen atoms were refined anisotropically including those displaying some solvent disorder as this was found to improve the model slightly without providing significantly large U_{ij}s. The high residual electron density peak of +2.0 *e* Å^{-3} likely represents further disorder present within the already twice modelled dmso structure.

The crystalline structure of **2.5** is a pseudopolymorph of a 1 : 1 ctc : dmso clathrate structure previously published by Chakrabarti *et al.*[22] which was crystallised in the monoclinic space group P 2_1 / *n* as opposed to our structure which crystallised in the triclinic space group P $\bar{1}$. Molecules of ctc within our structure crystallise in a 'parallel piped' manner associating with strong hydrogen-bonding in the topology 4^4 to form chains running parallel to the unit cell *a* axis.

All bonds and angles within the ctc molecule are within the expected ranges when compared to literature values[23] i.e. C-C (phenyl) = 1.3995(2) – 1.425(2) Å, C (sp^3)-C (Ar) = 1.534(2) – 1.542(2) Å, C (Ar)-O = 1.377(2) – 1.389(2)Å However, an exact threefold molecular axis is lacking due to the direction in which the hydroxyl hydrogens point, particularly H(22) which is rotated approximately 166 ° in the opposite direction to all others *vis-a-vis* the catechyl ring. All remaining hydroxyl hydrogen atoms point in one common direction although the degree by which they are rotated (again with respect to the plane of their catechyl rings) varies between the values 1° H(2)-O(2) and 21° H(11)-O(11). Of these

hydroxyl hydrogen atoms, only H(2) and H(13) may participate in intramolecular hydrogen bonding and because of this, the degree by which they are rotated is less than those which may not. These values compared to those reported by Chawla *et al.* (excluding H(22)) are rather conservative however, due to the increased number of dmso molecules thereby increasing the number of available hydrogen-bonding associations.

The intermolecular hydrogen bonding network within the structure is rather extensive, and is again similar to that reported by Chawla *et al.* whereby monolayers of ctc sheets are associated via a pattern of hydrogen bonds mediated through dmso molecules and catechyl hydroxyl groups. Molecules of ctc within these monolayers are related by a symmetry translation whilst the monolayers themselves are related by a crystallographic inversion about the centre of the unit cell (**Figure 2.12**). This association results in the formation of channels running throughout the crystal parallel to the crystallographic (100) plane and are restricted to travel in one direction only due to the large separation of neighbouring ctc molecules by additionally bonded dmso molecules.

The formation of the unidirectional chains and channels may be understood by considering a simple unit cell containing two ctc molecules and ten dmso molecules. When visualised along the unit cell *c* axis, this appears as a dimer although it is important to stress there is no direct association between the two ctc molecules.

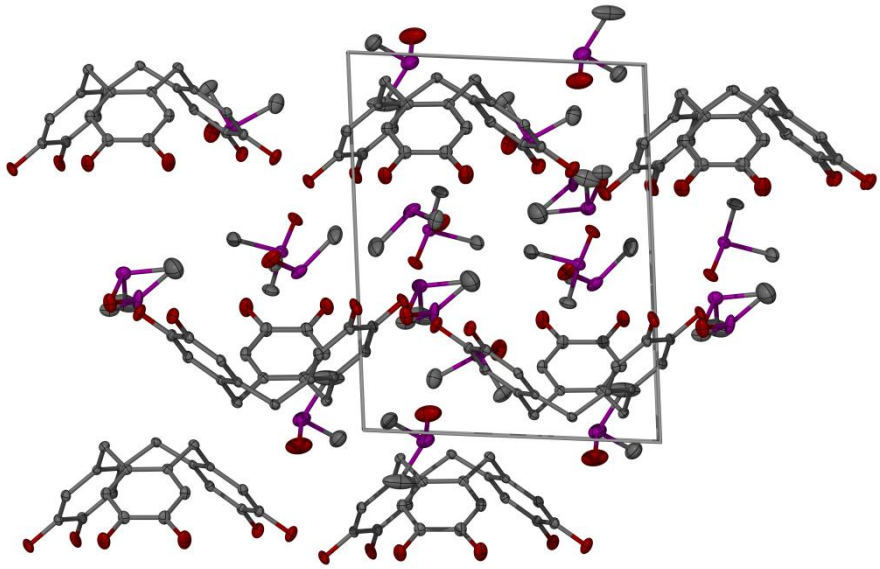

Figure 2.12. View of **2.5** along the unit cell *c* axis. Hydrogen atoms have been omitted for clarity and displacement ellipsoids set at 50% probability. Colour code: S, purple; O, red; C, grey.

Both ctc molecules within the unit cell are related by a crystallographic inversion centre and may be considered in the same manner. Each CTC molecule is connected to two others

along the unit cell axis *a* via the association O(11)-H(11)…O(20)^{i} (**Figure 2.13**). Two further hydrogen bonded associations per molecule extend in the same direction although are mediated through the common oxygen atom of the doubly disordered DMSO solvent molecule in the manner O(22)-H(22)…O(48)^{ii}…H(4)O(4)^{i}. It is these associations which act to extend the monolayered ctc chain along the unit cell *a* axis.

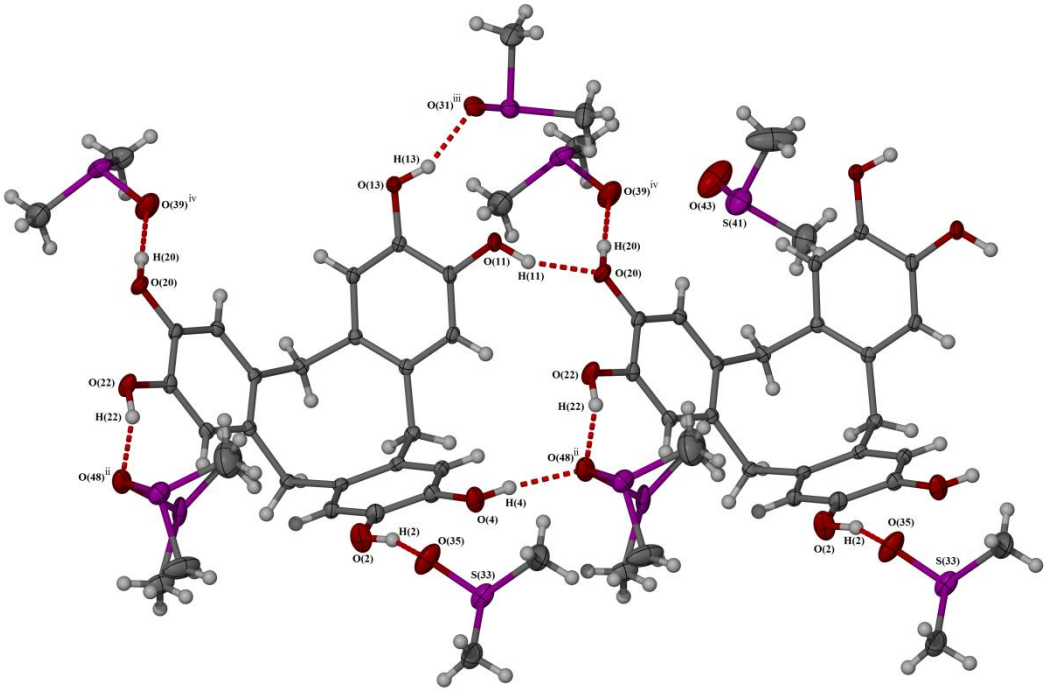

Figure 2.13. Diagram to show the hydrogen bonding motif between two ctc molecules and neighbouring dmso solvent molecules within a monolayer of **2.5.** Colour code: S, purple; O, red; C, grey. The dashed red line illustrates hydrogen bonding within the lattice.

Each ctc unit is further associated to three other dmso molecules. One molecule of dmso from the asymmetric unit is encapsulated within the cavity of oppositely facing ctc molecule, through O(13)-H(13)…O(31)^{iii} hydrogen-bonding interaction and O(11)…S(29)^{iii} sulphur-oxygen nonbonded interaction. These interactions hold the polar end of the molecule pointing out of the ctc cavity allowing the molecule to orientate itself such that one methyl group points directly into the cavity, maximising contact between the hydrophobic core. The distance between methyl group and base of one phenylene ring equals 2.830 – 2.852 Å, which is within distance to form C(28)-H(28B)…π contacts between host and guest (**Figure 2.14**).

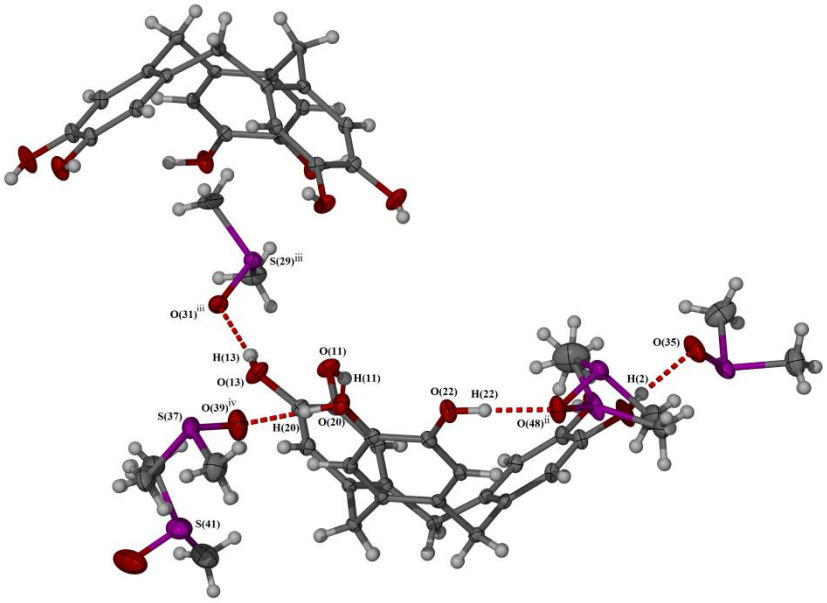

Figure 2.14. Hydrogen bonding motif between two opposite 'face-to-face' monolayers of ctc molecules holding a guest molecule of dmso within the cavity of host ctc in **2.5**. Displacement ellipsoids are set at 50% probability. Colour code: S, purple; O, red; C, grey. The dashed red line illustrates hydrogen bonding within the lattice.

Throughout the formation of the chain hydrophobic pockets form at the walls of the ctc molecules populated by two molecules of crystallographically ordered dmso resides. Placed on either side of the ctc molecule, these dmso molecules are held in place via hydrogen bonding interactions between O(2)-H(2)…O(35) and O(20)-H(20)…O(39)^{iv} and what appears to be a weak, long hydrogen bond between O(20)-H(20)…S(37)^{iv}. The oxygen atoms of the two dmso molecules point inwards towards the walls of the ctc molecule in order to mediate these interactions, thereby permitting the two methyl groups of the dmso molecules to point towards the hydrophobic cavity formed between one layer of the ctc chains (**Figure 2.15** and **Figure 2.16**). It is consequence of this association that the hydroxyl hydrogen H(20) is turned 166 ° This orientation is mirrored by the doubly-disordered molecule of dmso whereby the hydrogen-bonded oxygen atom O(48)^{ii} is held in place inbetween two ctc molecules, therefore permitting the two methyl groups to point in towards this hydrophobic channel. One final molecule of crystallographically ordered dmso is also contained within this hydrophobic channel, which although appears too far away from any other molecule to form distinct intermolecular interactions, is within Van der Waals contact distance of the rear of two ctc molecules, therefore suggesting some weak C-H…π character to their interaction.

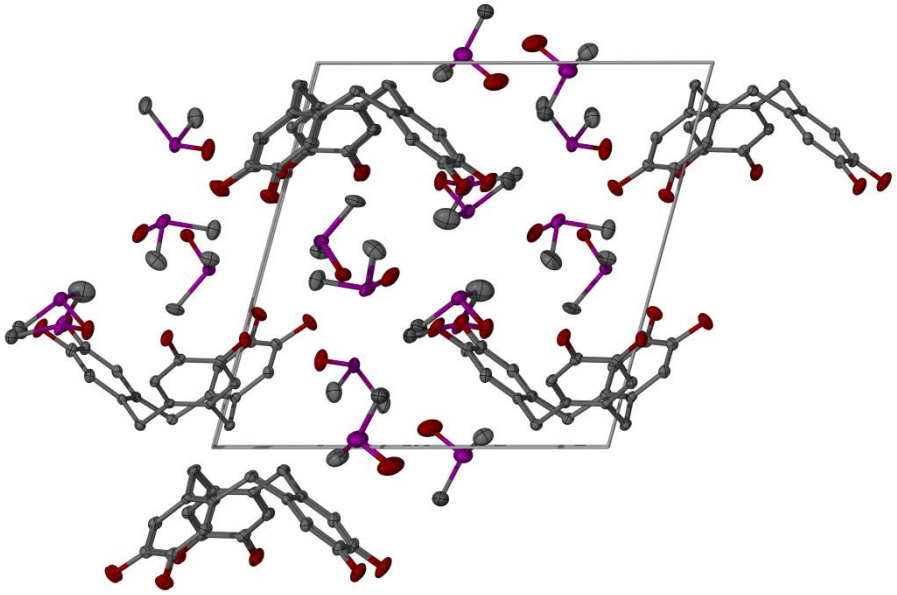

Figure 2.15. View along the unit cell *a* axis of complex **2.5.** Colour code: S, purple; O, red; C, grey.

The structure observed is similar to that reported by Chakrabarti *et al.*[22] however due to the large spacings between ctc molecules in our structure, there are only two direct ctc interactions per molecule as compared to Chakrabarti's work whereby there either five or seven of such interactions depending on the molecule considered. This interaction therefore extends the hydrogen-bonding network out along the unit cell axes *bc* as opposed to only the axis *a* described in our work. The reason behind the one-dimensional chains prepared in this work stems from the high separation achieved by an addition of more hydrogen-bonded dmso molecules compared to Chakrabarti's 1 : 1 dmso solvate, which sit in sheets between ctc molecules related by translation within one monolayer and their crystallographically inverted counterparts within the unit cell.

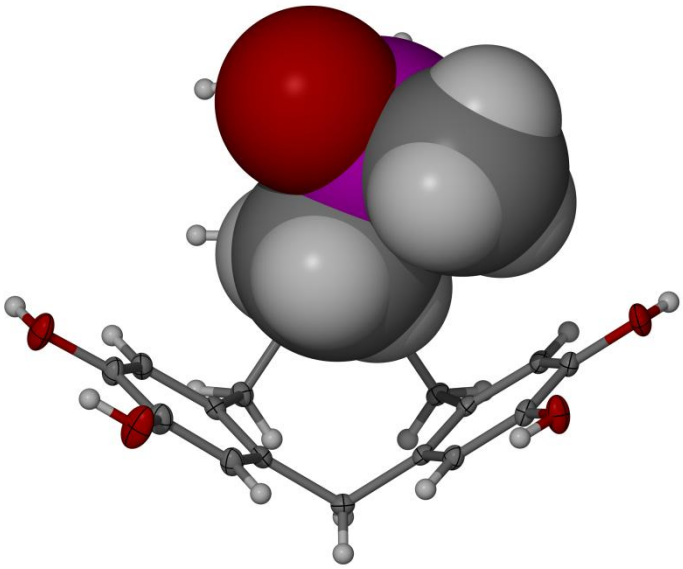

Figure 2.16. Spacefilling diagram of one guest dmso molecule held within the cavity of a host ctc molecule in **2.5**. Spacefilling spheres are set as one Van der Waals radius and displacement ellipsoids set at 50% probability. Colour code: S, purple; O, red; C, grey; H, white.

Table 2.4. Definitions of symmetry codes used in the discussion of complex **2.5.**

(i)	1-*x*, *y*, *z*
(ii)	1-*x*, 1-*y*, 1-*z*
(iii)	2-*x*, 1-*y*, -*z*
(iv)	1-*x*, 1-*y*, -*z*

2.2.4 Clathrate Crystal Structure of [ctc]•[dmac]$_3$ (2.6)

Orange crystals of the solvated cyclotricatechylene clathrate structure **2.6** showed the asymmetric unit contained one complete molecule of cyclotricatechylene and three molecules of dmac, one of which showed disorder about the carbonyl carbon and amide nitrogen atoms thus was modelled as two separate molecules without restraints and occupancy ratios [0.78 : 0.22]. All carbon-bound hydrogen atoms were placed in calculated positions and refined using a riding model as in *HFIX* through *SHELXL*. Catechyl hydroxyl hydrogens however were located in the fourier map and restrained to O-H = 0.90(2) and refined using a common U_{iso} thermal parameter whilst all non-hydrogen atoms were refined anisotropically, except those contained within the disordered dmac molecule.

The ctc molecules within the structure adopt a hydrogen bonded network, mediated through solvent dmac molecules with the simple connectivity 4^4. Each ctc molecule is associated to four others utilising connections via solvent molecules forming a network parallel to the

plane (101), thus forming a monolayer structure. Molecules of ctc within these monolayers formed via this connectivity are related to one another by a symmetry translation whilst adjacent monolayers themselves are related by a crystallographic C_2 axis. This relationship gives rise to an alternate hydrogen-bonded *bis*-monolayer structure, similar to that reported by Steed *et al.*[25] in the clathrate structure [ctc].[dmf]$_2$.[H_2O]$_2$ where crystallographically ordered solvent molecules of dmf are contained within the cavity of two 'face-to-face' ctc molecules. This relationship is again repeated in our dmac-containing clathrate where one dmac molecule is contained within the cavity of one ctc molecule with solvent amide oxygen atom, O(36), pointing out of the cavity in order to allow an association to an oppositely facing ctc molecule, offset by one half of a ctc molecule along the unit cell *a* axis, via hydroxyl H(15)-O(15). The one *N*-methyl group of the dmac guest molecule contained within the ctc host is orientated such that it is in Van der Waals contact with the phenylene base, thereby maximising contact with the hydrophobic core of the host ctc molecule. However, there is a lack of evidence for the existence of short C-H…O or C-H…π contacts between catechylene ring and dmac molecule. Despite this, the arrangement is repeated in an 'up-down' manner parallel to the (101) plane due to the C_2 axis by which molecules of cyclotricatechylene within a layer are arranged (**Figure 2.17**).

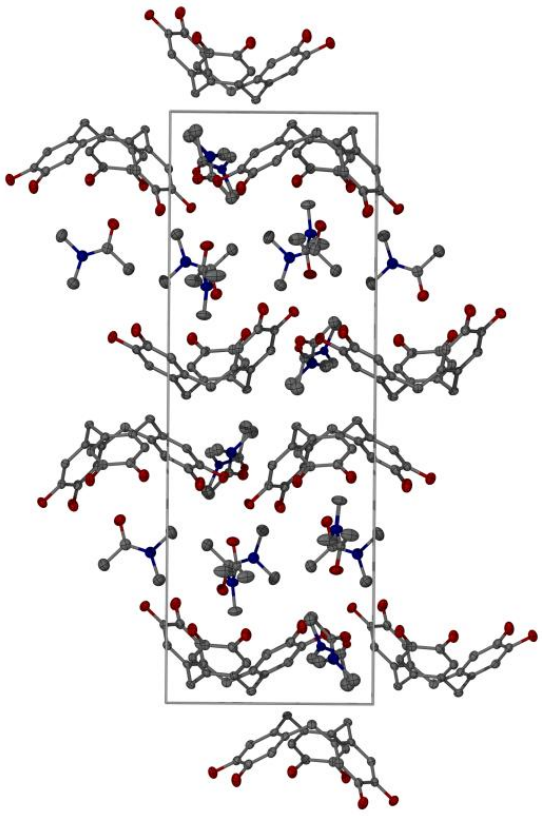

Figure 2.17. View along unit cell *a* axis of **2.5**. Hydrogen atoms are omitted for clarity and displacement ellipsoids are set at 50% probability. Colour code: N, blue; O, red; C, grey.

The two remaining dmac molecules are both external to the ctc cavities, as in the structure reported by Steed *et al.*,[25] where the remaining crystallographically ordered molecule holds an important connectivity between the walls of two ctc molecules parallel to the (100) plane only. This association O(13)-H(13)…O(30)…H(24)^{i}-O(24)^{i} holds the dmac molecule in place and orientates it such that the methyl groups occupy a small hydrophobic space inbetween the 'face-to face' ctc molecules within the monolayers, as shown when space-filling effects are considered (**Figure 2.18**).

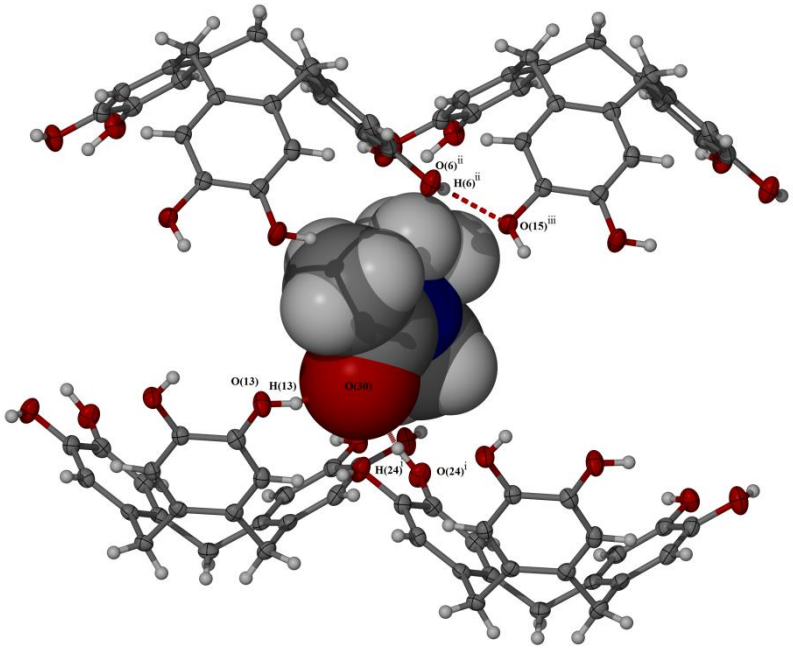

Figure 2.18. Spacefilling diagram of dmac solvent molecule held within the hydrophobic cavity between ctc monolayers in **2.6**. Space filling spheres are set at one Van der Waals radius and displacement ellipsoids set at 50%. Colour code: N, blue; O, red; C, grey. The dashed red line illustrates hydrogen bonding within the lattice.

The one final dmac molecule within the structure is disordered over two positions, however it is importantly placed to mediate a connection between two cyclotricatechylene molecules along the unit cell axis *c* between O(22)-H(22)…O(42)/O(48)…H(4)O(4) where O(42) and O(48) belong to the doubly disordered solvent molecule. This association mediated between the two ctc molecules is repeated on each layer of ctc molecules within the *bis*-monolayer structure, thus extending the network parallel to the (001) plane only. Interestingly also, in a manner similar to that of the structure reported by Steed *et al.*,[25] these dmac molecules orientate themselves such that one *N*-methyl group points directly into the hydrophobic channel created inbetween the 'back-to-back' ctc molecules where no hydrogen-bonding interactions exist. This creates a smooth hydrophobic channel inbetween the hydrogen-bonded layers approximately 3.54(2) Å wide (**Figure 2.19**).

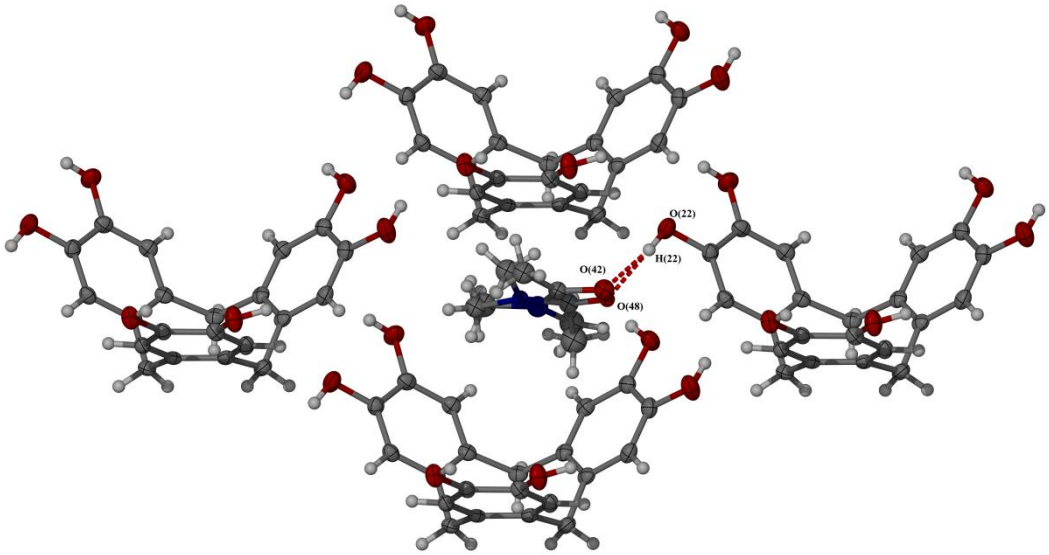

Figure 2.19. Diagram showing the small hydrophobic pocket formed within one monolayer of ctc in **2.6.** Colour code: N, blue; O, red; C, grey. The dashed red line illustrates hydrogen bonding within the lattice

This layered packing arrangement is highly similar to those found in calix[4]arenesulfonates[34] whereby alternate hydrophilic and hydrophobic layers are also present. Their reported structure again displays a *bis*-monolayer structure similar to ours whereby a hydrophilic layer is formed containing water and counter-ions held in place by 'face-to-face' sulfonate residues separated from a hydrophobic layer containing π-stacked phenylene groups.

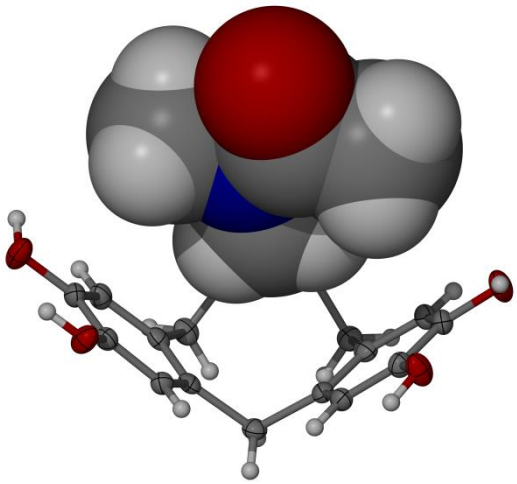

Figure 2.20. Space filling diagram of ctc host plus dmac guest in complex **2.6.** Colour code: N, blue; O, red; C, grey.

Table 2.5. Definitions of symmetry codes used in the discussion of complex **2.6.**

(i)	1+*x*, *y*, *z*
(ii)	1/2+*x*, 1/2-*y*, 1/2+*z*
(iii)	1/2+*x*, 1/2-*y*, *z*-1/2

2.2.5 Clathrate Crystal Structure of [ctc]•[THF]$_{3.5}$•[H_2O]$_{0.5}$ (2.7)

Large yellow crystals of the solvated cyclotricatechylene clathrate structure [ctc].[THF]$_{3.5}$.[H_2O]$_{0.5}$ (**2.7**) showed that the asymmetric unit contained one complete molecule of cyclotricatechylene, two complete molecules of THF and one region of solvent disorder at the inversion centre 0, ½, 0 modelled as two one-quarterly occupied THF sites and one half-molecule of water. These molecules of THF were subjected to the refined restraints C-C = C-O = 1.45(2) Å and 1,3-C…C = 1,3-C…O = 2.37(2) Å. As the distance of O(43) (belonging to the half-molecule of water) is within distance to permit hydrogen-bonding between itself and the molecule of cyclotricatechylene, it is inferred that one side of the inversion centre is populated with disordered THF whilst the other is with water, with a random distribution throughout the crystal. One further region of solvent disorder at the position 1, ¾, ½ was also modelled as three equally occupied THF molecules although as C_5 rings only due to their position within the solvent channels running along the unit cell *c*-axis leading to poorly defined electron density making it impossible to define oxygen from carbon atoms. For the molecule of cyclotricatechylene, two wholly occupied and two ¼ occupied molecules of THF hydrogen atoms were placed in calculated positions and refined using a riding model using *HFIX* within *SHELXL*. The triply disordered THF C_5 ring and partial water site were not assigned any hydrogen atoms for the final model although were used for density calculations. All non-hydrogen atoms except those at disordered solvent sites were refined anisotropically.

The crystalline structure of **2.7** is of particular interest for the reason that it forms a hydrogen bonding network between ctc molecules in an undulating along the *b* direction of the unit cell as a S-shaped sheet with hydrogen bond topology $3^3 4^2$. This mode of association is contrary to that of previously described cyclotricatechylene clathrate structures whereby planar hydrogen bonding networks are preferred.[24-25]

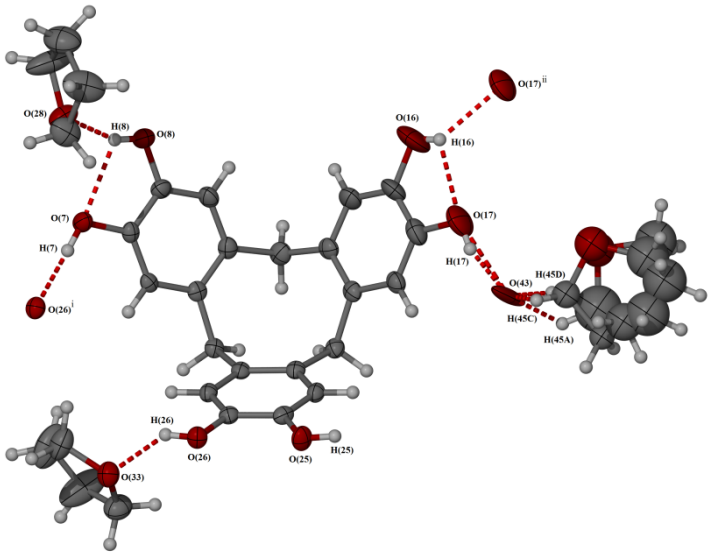

Figure 2.21. Hydrogen bonding associations of one ctc molecule of complex **2.7.** Displacement ellipsoids are set at 50% probability. Colour code: O, red; C, grey. The dashed red line illustrates hydrogen bonding within the lattice.

THF molecules contained within the cavities of the cyclotricatechylene molecules importantly participate in the hydrogen bonding network whereby they associate with the hydroxyl hydrogen of a neighbouring cyclotricatechylene group, thereby extending the network in the unit cell *c* direction. This THF molecule contained within the cavity of the cyclotricatechylene molecule again orientates itself such that it lies coplanar with one of the catechyl rings in order to maximise π…π interactions whilst also manages to orientate itself such that this hydrogen-bonding is possible in the same manner as in donor acceptor complexes **2.3** and **2.4**. Further hydrogen bonding interactions come from the water molecule O(43) to H(17)-O(17) of the local cyclotricatechylene molecule, however this does not influence the network topology. One further ordered THF molecule, contained outside of the cyclotricatechylene cavities, hydrogen bonds to the rear of the cyclotricatechylene group via hydroxyl hydrogen in the manner O(33)…H(26)-O(26). The remaining disordered THF molecules do not take part in hydrogen bonding to the cyclotricatechylene molecules, however interestingly occupy voids created throughout the crystal from construction of the undulating cyclotricatechylene sheets. These voids traverse the crystal in the (001) direction measuring approximately 15.5 x 7.5 Å and are lined by the ordered THF molecules (**Figure 2.22**). It is in this void that the THF C_5 rings reside, therefore are unsurprisingly disordered. There is also the presence of one further, smaller void measuring 7.7 x 6.1 Å, positioned inbetween the undulating cyclotricatechylene sheets, related by translation along the direction (010). It is in this void that the crystallised water molecule and doubly disordered THF molecule reside (**Figure 2.23**).

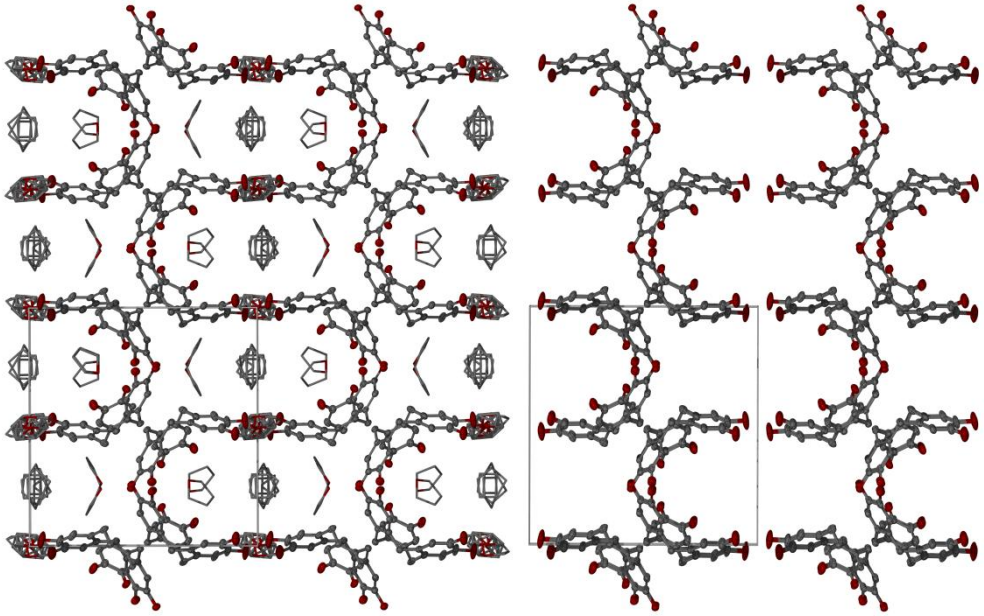

Figure 2.22. View parallel to the crystal (001) plane of **4.7** left) with solvent occupying the channels and right) without solvent occupying the channels. Hydrogen atoms have been omitted for clarity and displacement ellipsoids set at 50% probability level. Colour code: O, red; C, grey.

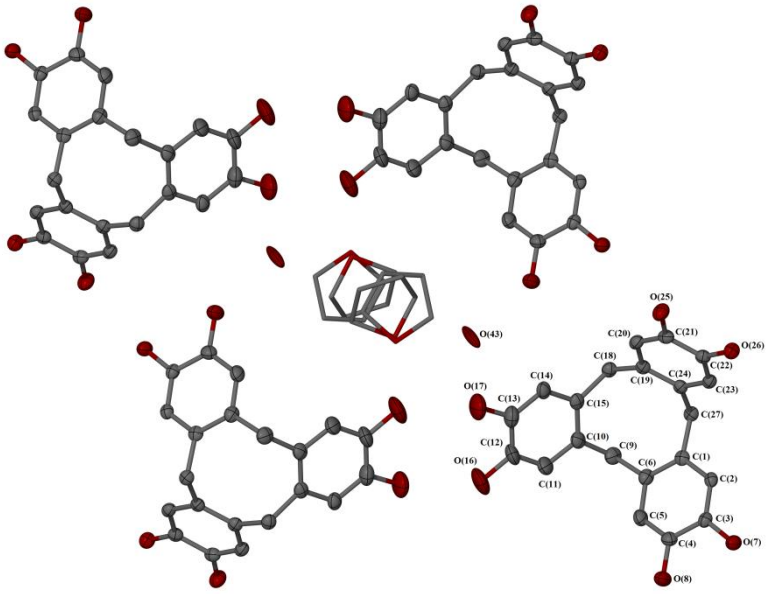

Figure 2.23. Diagram showing the presence of the smaller solvent cavity (containing disordered THF and water) between ctc molecules in structure **4.7**. Probability ellipsoids are set at 50%. Colour code: O, red; C, grey.

Table 2.6 Definitions of symmetry codes used in the discussion of complex **2.7.**

(i)	*x*, 3/2-*y*, 1/2+*z*
(ii)	-*x*, 1-*y*, 1-*z*

2.2.6 Donor : Acceptor Complex of $[ctv]_2$•$[tcne]_3$ (2.8)

Following on from the successful preparation of **2.3** and **2.4**, similar reactions were attempted utilising cyclotriveratrylene (**2.1**), in similar solvent systems however due to the greater hydrophobicity of **2.1** (due to the incorporation of methyl-ether functional groups at the upper rim of the molecule as opposed to hydroxyl functionalities as in **2.2**), less polar solvents were used, such as chloroform, dichloromethane and toluene. While these low-polarity solvents delivered immediate colour changes where a donor : acceptor state was almost certainly formed, these were not possible to isolate. Using THF as a reaction solvent again permitted the formation of a deep-blue crystalline sample of $[ctv]_2.[tcne]_3$ (**2.8**) which was isolated using slow-diffusion methods (THF / pentane).

Very small blue needles of the charge-transfer complex **2.8** showed that the asymmetric unit contained two crystallographically independent complete molecules of ctv and three complete molecules of tcne, crystallized in the orthorhombic space group $Pc2_1b$. Unlike **2.3**, there appears to be no hydrogen-bonding contacts between the ctv and tcne molecules, with interactions between the two molecules due only to π…π electron overlap and Van der Waals contacts. There is also complete absence of solvent molecules within the structure, again unlike **2.3** which contains six THF molecules within the pores of the lattice and one contained as a guest in the hydrophobic core of ctc. Structure **2.8** however displays a motif often seen in ctv-derived chemistry where one ctv arm occupies the hydrophobic core of another as a guest. This has been seen numerous times, including instances where the upper-rim of the ctv molecule has been functionalised (**Figure 2.24**).[20]

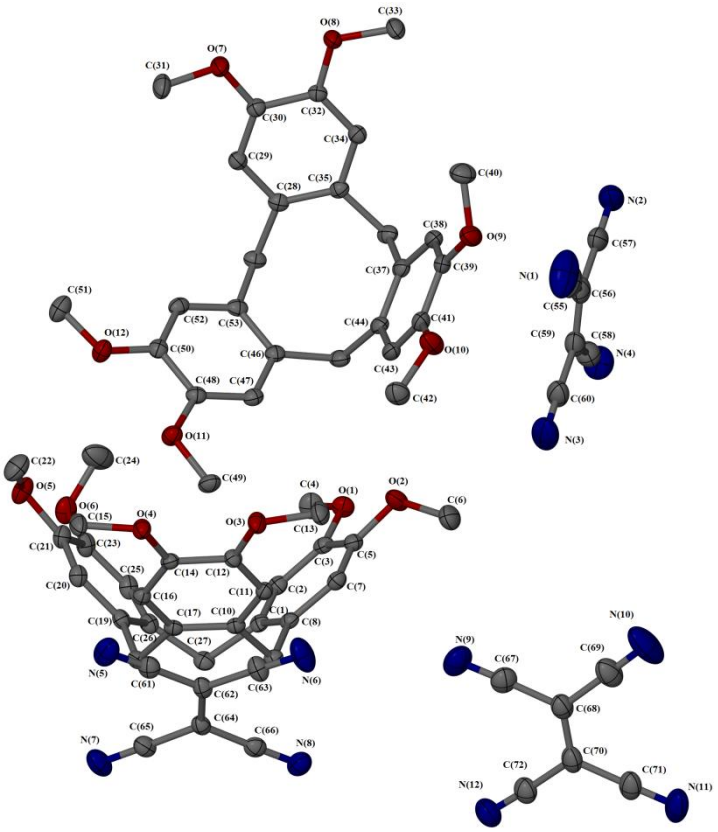

Figure 2.24 Asymmetric unit of structure **2.8** containing two crystallographically independent molecules of ctv and three crystallographically independent molecules of tcne. Hydrogen atoms omitted for clarity. Atoms are displayed as thermal ellipsoids at 50% probability. Colour code: N, blue; O, red; C, grey.

2.8 includes two different interactions between tcne and ctv. Arene ring [C(10)-C(17)] and tcne molecule [N(5)-C(61)-C(68)-N(8)] and ring [C(28)-C(35)]^{i} and tcne molecule [N(9)-C(67)-C(72)-N(12)] both display π…π orbital overlap, as shown by **Figure 2.25** with interplanar separations between molecules of 3.161 Å and 3.199 Å respectively. This orientation is a common motif in crystalline tcne / aryl complexes where these π…π interactions within the motif demonstrate approximate co planarity within the groups with similar separations.[35] Central alkene bond lengths of the two tcne molecules within the lattice exist within values expected of the neutral tcne^{0} molecule, with values of 1.357(2) and 1.347(2) Å respectively.[4] This is unsurprising as an aryl-ether would be expected to be highly difficult to oxidise under ambient conditions. Despite the lack of a formal electron transfer between the species, the short distance between tcne molecule and cyclotriveratrylene phenyl groups certainly suggests a strong π…π interaction therefore implies strong donor : acceptor complexation.

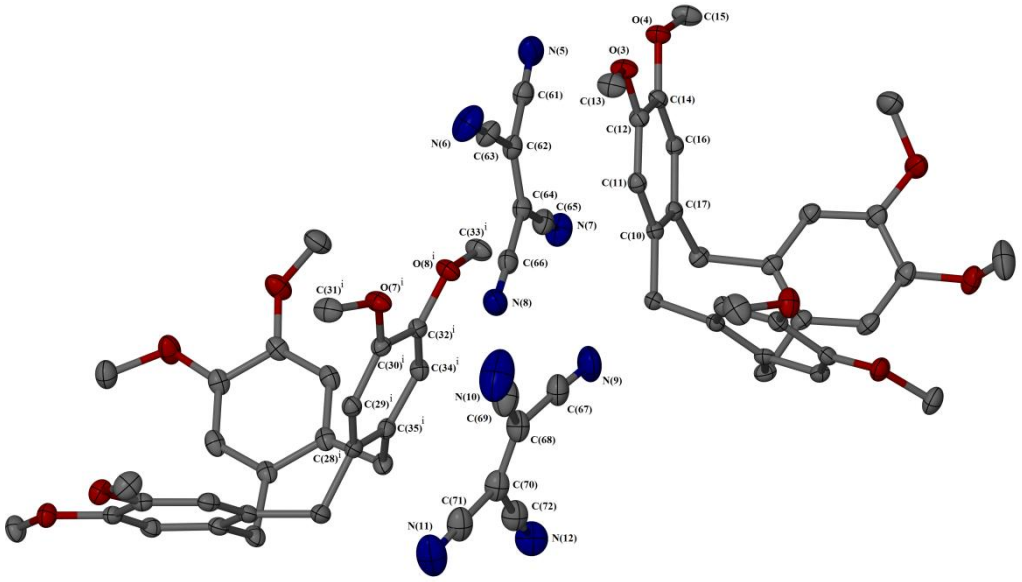

Figure 2.25 Structure **2.8** showing π orbital overlap between two ctv arene rings and tcne molecules with approximate co planarity. Atoms are displayed as thermal ellipsoids at 50% probability, hydrogen atoms omitted for clarity. Colour code: N, blue; O, red; C, grey.

Tcne also forms another association between two ctv molecules in the form of an exclusion complex as depicted in **Figure 2.26** whereby tcne molecule [N(1)-C(55)-C(60)-N(4)]-is sandwiched between two *ortho*-methyl ether functions of cyclotriveratrylene aryl rings [C(37)-C(44)] and [C(19)-C(26)]^{ii}. Again arising from π…π orbital overlap, however in this instance electron density from the aryl-ether linkage overlaps with the tcne molecule as opposed to the aryl ring exclusively. Interplanar separations between the two groups were significantly smaller than the arene / tcne molecule overlap with separation between generated centroids of 2.942 Å for ring [C(37)-C(44)] and 2.769 Å for ring [C(19)-C(26)]^{ii}. These small separations with respect to those observed for the tcne / arene rings are indicative of a very strong donor : acceptor species. Interestingly, this strong attraction is not mirrored in the lengthening of any bonds where all bond lengths within the two arene rings and ether-linkages are not statistically different to a neutral-state cyclotriveratrylene molecule.[36] Similarly, this lack of formal electron transfer is also mirrored in the internal tcne C=C whereby the bond length of 1.332(3) Å is again within tolerance for assignment to the tcne^0 neutral state.[4]

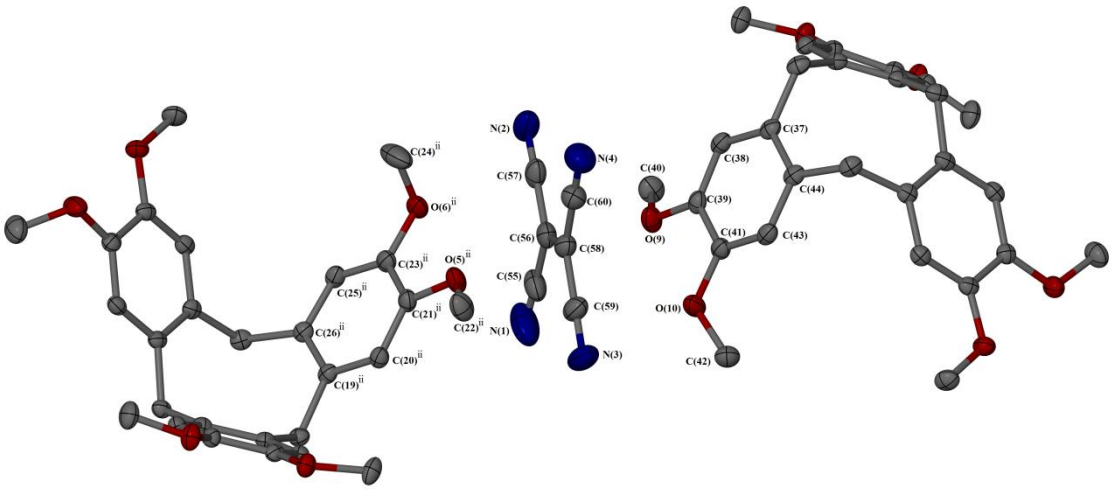

Figure 2.26 Structure **2.8** showing overlap between two ctv aryl-methyl ether linkages and one sandwiched tcne molecule. Atoms are displayed as thermal ellipsoids at 50% probability, hydrogen atoms omitted for clarity. Colour code: N, blue; O, red; C, grey.

Alongside the associations between ctv and tcne, each tcne molecule throughout the structure associates with at least one other tcne molecule as shown in **Figure 2.27** whereby C(68) and C(62) share short contacts (<Van der Waals radii) with tcne terminal nitrogen atoms $N(2)^{i}$ and $N(4)^{ii}$ which are sandwiched between two ctv aryl-methyl ether linkages.

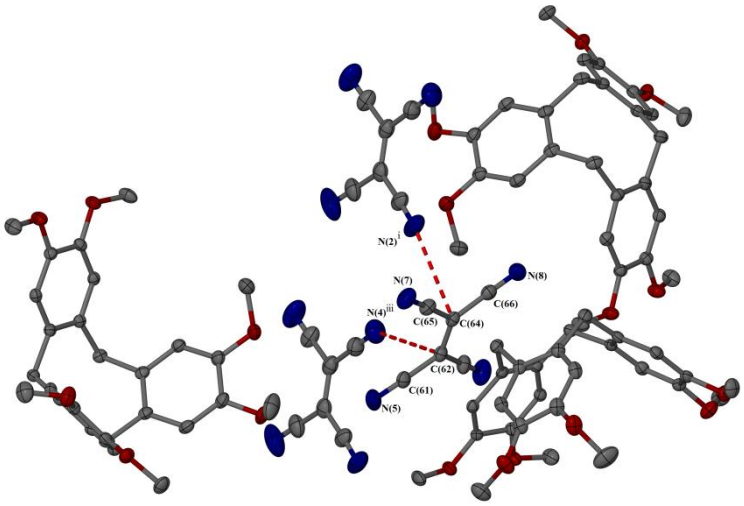

Figure 2.27 Connectivity of tcne throughout **2.8**. Atoms are displayed as thermal ellipsoids at 50% probability, hydrogen atoms omitted for clarity. Colour code: N, blue; O, red; C, grey.

The connectivity between tcne molecules is continued further from this sandwiched tcne molecule via N(3) of the same molecule associating with C(70) of the adjacent arene π-stacked tcne molecule (**Figure 2.28**). These associations are shown in a simplified form in **Figure 2.29**.

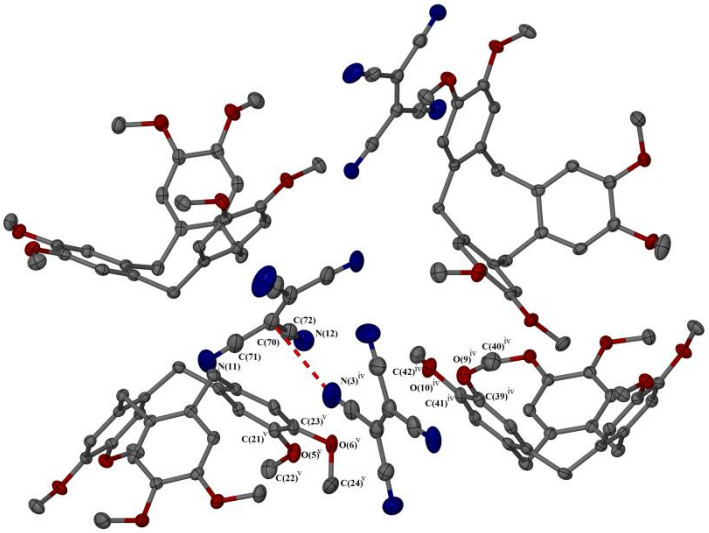

Figure 2.28 Connectivity of tcne throughout **2.8**. Atoms are displayed as thermal ellipsoids at 50% probability, hydrogen atoms omitted for clarity. Colour code: N, blue; O, red; C, grey.

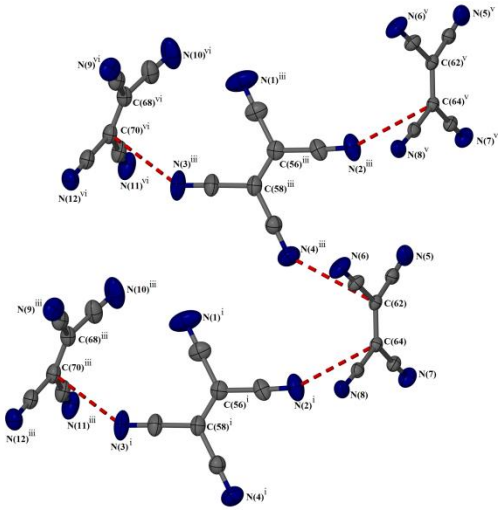

Figure 2.29 Simplified tcne *N*-mediated associations in structure **2.8.** Atoms are displayed as thermal ellipsoids at 50% probability. Colour code: N, blue; C, grey.

The tcne-mediated associations give rise to a continuous arrangement along the unit cell axis *a* whereby tcne molecules form sheets between the ctv molecules, which themselves reside in distinct columns due to one arm of the ctv upper-rim pointing towards the hydrophobic core of another ctv molecule (*cf* C(4) and C(49)) as shown in **Figure 2.30**.

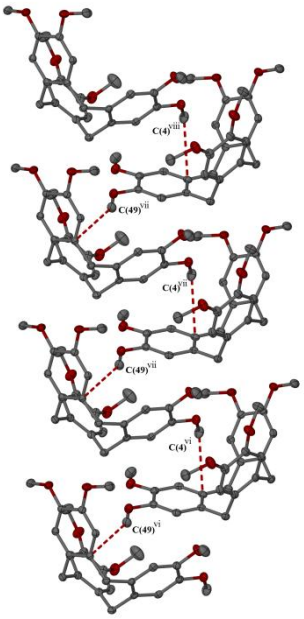

Figure 2.30 Columnar structure of ctv molecules traversing along unit cell direction *a* due to methyl groups of the CTV upper rim pointing towards the hydrophobic core of another ctv molecule in structure **2.8**. Atoms are displayed as thermal ellipsoids at 50% probability, hydrogen atoms omitted for clarity. Colour code: O, red; C, grey.

The directional associations give rise to the combined structure shown in **Figure 2.31** whereby ctv molecules are stacked on top of one another in a columnar fashion, separated by tcne molecules, between which a donor : acceptor state is formed. The infrared spectrum of **2.8** also displays vibrations expected of a donor : acceptor complex containing tcne. As with **2.3,** vibrations at 2247 and 2219 cm^{-1} are typical ν_{CN} stretches.[31] The presence of these vibrations again confounds the presence of a donor : acceptor association.

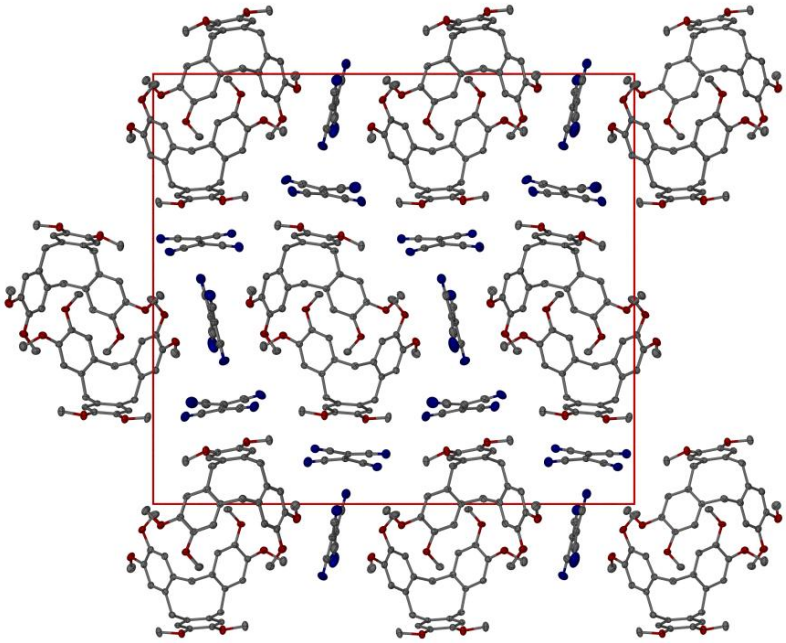

Figure 2.31 View down unit cell axis *a* of structure **2.8** depicting the separation of ctv and tcne molecules into distinct layers. Atoms are displayed as thermal ellipsoids at 50% probability, hydrogen atoms omitted for clarity. Colour code: N, blue; O, red; C, grey.

Table 2.7 Definitions of symmetry codes used in the discussion for crystal structure **2.8**.

(i)	*x*-1, *y*-½, ½-*z*
(ii)	–*x*, *y*-½, ½-*z*
(iii)	*x*, *y*-½, ½-*z*
(iv)	*x*-1,*y*,*z*
(v)	–*x*-1, *y*, *z*-½
(vi)	1+x, *y*-½, ½-*z*
(vii)	1+*x*, *y*, *z*
(viii)	2+*x*, *y*, *z*
(ix)	3+*x*, *y*, *z*

2.3 Conclusions

Donor : acceptor complexes **2.3**, **2.4** and **2.8** are the first crystallised and characterised examples of an organic cavitand molecule acting as a donor and complexing with a cycloalkane acceptor. [37-40] Furthermore, complexes **2.3** and **2.4** represent the first recorded structures of tcne or tcnq with a catechol whilst the first of tcne with any derivative of a

phenol.[9-12], as a limited number of phenol-tcnq adducts have been previously reported.[16-17] Interestingly, the crystallised structures of **2.3** and **2.4** are consistent with a reported adduct of resorcinarene and tcne which was as here identified as an exclusion complex through semi-empirical calculations.[38] The presence of tcne and tcnq crystallised in their neutral state, opposed to their radical anionic states, is an example of particular rarity alongside this is the first documented ability of $tcne^0$ acting as a classical hydrogen-bond acceptor to accept more than two hydrogen bonds. Evidence of a tangible degree of charge transfer between ctc and tcne/tcnq has also been provided by infrared and UV/vis spectra, whereby complexes **2.6** and **2.7** strongly resemble complexes with poly-hydroxybenzenes[12] or catechols[9-12] themselves, although it appears the transfer is short of formal ionisation between molecules despite EPR measurements of **2.6** displaying two peaks with *g* values close to those of the tcne monoanion radical.[4]

The reported clathrate structures of ctc follow the majority of observations made in the literature that every ctc containing structures encapsulate solvent molecules within the host cavity.[22-26] For instance, the structures of clathrates **2.3** and **2.4** are consistent with an investigation into ctc clathrate stoichiometries.[41] These observations are in direct contrast to structures containing ctv derivatives which prefer to associate through π...π intercavity interactions forming a 'handshake motif' in preference to the encapsulation of guest solvent molecules with the exception of dmf, as seen in the structure of **2.7**.[20],[41-42] It is interesting to note here that there is a distinct lack of direct hydrogen bonding occurring between ctc host and encapsulated guest molecule. The guest molecule is only held in place inside the cavity by weak Van der Waals, hydrophobic and C-H...π interactions. This therefore suggests the preference for solvent molecules to occupy the ctc cavity is due to the self-associative nature of crystalline ctc, thereby leaving the molecular cavities open for guest encapsulation.

2.4 References

[1] J. J. Loughrey, C. A. Kilner, M. J. Hardie and M. A. Halcrow, *Supramol. Chem.* **2012,** *24,* 1-13.

[2] L. Wang, H. Cho, S.-H. Lee, C. Lee, K.-U. Jeongand M.-H. Lee, *J. Mater. Chem.* **2011,** *21,* 60-64.

[3] M. Shibahara, M. Watanabe, C. Yuan, K. Goto and T. Shinmyozu, *Tetrahedron Lett.* **2011,** *52,* 3371-3375.

[4] J. S. Miller, *Angew. Chem. Int. Ed. Engl.,* **2006,** *45,* 2508-2525.

[5] R. E. Merrifield and W. D. Philips, *J. Am. Chem. Soc.* **1958,** *80,* 2778-2782.

[6] P. Bhatt and S. M. Yusuf, *AIP. Conf. Proc.* **2011,** *1349*, 615-616.

[7] a) K. R. Dunbar and R. A. Heintz, *Prog. Inorg. Chem.* **1997,** *45*, 283-391; b) N. Ishii, Y. Okamura, S. Chiba, T. Nogami and T. Ishida, *J. Am. Chem. Soc.*, **2008,** *130*, 24-25.

[8] R. S. Mulliken, *J. Phys. Chem.* **1952,** 56, *7*, 801-822.

[9] J. E. Frey, T. Aiello, D. N. Beaman, S. D. Combs, S. -L. Fu and J. J. Puckett, *J. Org. Chem.* **1994,** *59*, 1817-1830.

[10] R. Beukers and A. Szent-Gyorgyi, *Recl. Trav. Chim. Pays-Bas* **1962,** *81*, 255-268.

[11] S. Spange, K. Maenz and D. Stadermann, *Liebigs Annal.* **1992,** 1033-1037.

[12] A. R. Reddy, N. V. KrishnaMurthy and B. Bhudevi, *Spectrochim. Acta A* **2006,** *63*, 700-708.

[13] L. R. Melby, R. J. Harder, W. R. Hertler, W. Mahler, R.E. Benson and W. E. Mochel, *J. Am. Chem. Soc.* **1962,** *84*, 3374.

[14] R. J. Kistenmacher, T. E. Philips and D. O. Cowan, *Acta. Crystallogr., Sect. B* **1974,** *30*, 763-768.

[15] A. J. Moore, M. R. Bryce, A. S. Batsanov, J. N. Heaton, C. W. Lehmann, J. A. K. Howard, N. Robertson, A. E. Underhill and I. F. Perepichka, *J. Mater. Chem.* **1998,** *8*, 1541-1550.

[16] T. Inabe, K. Okaniwa, H. Okamoto, T. Mitani, Y. Maruyama and S. Takeda, *Mol. Cryst. Liq. Cryst. Sci. Tech. Sect. A* **1992,** *216*, 229-234.

[17] F. Bentiss, M. Lagrenee, O. Mentre, J. P. Wignacourt, H. H. Vezin and E. M. Holt, *J. Mol. Struct.* **2002,** *607*, 31-41.

[18] W. Kaim and M. Moscherosch, *Coord. Chem. Rev.* **1994,** *129*, 157-193.

[19] a) A. Collet, *Tetrahedron* **1987**, *43*, 5725–5759; b) M. J. Hardie, P. J. Nichols and C. L. Raston, *Adv. Supramol. Chem.* **2002**, *8*, 1–41.

[20] M. J. Hardie, *Chem. Soc. Rev.* **2010**, *39*, 516–527.

[21] T. Brotin and J.-P. Dutasta, *Chem. Rev.* **2009**, *109*, 88–130.

[22] A. Chakrabarti, H. M. Chawla, G. Hundal and N. Pant, *Tetrahedron* **2005**, *61*, 12323–12329.

[23] J. A. Hyatt, E. N. Duesler, D. Y. Curtin and I. C. Paul, *J. Org. Chem.* **1980**, *45*, 5074–5079.

[24] C. J. Sumby and M. J. Hardie, *Acta Cryst. Sect. E* **2007**, *63*, o1537–o1539.

[25] J. W. Steed; H. Zhang and J. L Atwood, *Supramol. Chem.* **1996**, *7*, 37–45.

[26] D. S. Bohle and D. Stasko, *Chem. Commun.* **1998**, 567–568.

[27] a) B. F. Abrahams, N. J FitzGerald, T. A. Hudson, R. Robson and T. Waters, *Angew. Chem. Int. Ed.* **2009**, *48*, 3129–3132; b) B. F. Abrahams, N. J. FitzGerald and R. Robson, R. *Angew. Chem. Int. Ed.* **2010**, *49*, 2896–2899; c) B. F. Abrahams, B. A. Boughton, N. J. FitzGerald, J. L. Holmes and R. Robson, *Chem. Commun.* **2011**, *47*, 7404–7406.

[28] O. Pietraszkiewicz, M. Kozbial and M. Pietraszkiewicz, *Adv. Mater. Opt. Electron.*, **1998,** *8*, 277-284.

[29] A. Chehak, A. Chyla, M. Radomska and R. Radomski, *Mol. Cryst. Liq. Cryst.* **1985,** *120,* 327-331.

[30] O. Carugo, C. B. Castellani, K. Djinović and M. Rizzi, *J. Chem. Soc. Dalton Trans.* **1992,** 837-841.

[31] S. Pons, S. B. Khoo, A. Bewick, M. Datta, J. J. Smith, A. S. Hinman and G. Zachmann, *J. Phys. Chem.* **1984,** 88, 3575-3578.

[32] S. E. Bell, J. S. Field, R. J. Haines, M. Moescherosch, W. Matheis and W. Kaim, *Inorg. Chem.* **1992,** *31*, 3269-3276.

[33] J. E. Frey, T. Aiello, D. N. Beaman, S. D. Combs, S. –L. Fu and J. J. Puckett, *J. Org. Chem.* **1994,** *59*, 1817-1830.

[34] J. L. Atwood, G. W. Orr, N. C. Means, F. Hamada, H. Zhang, S. G. Bott and K. D. Robinson, *Inorg. Chem.* **1992,** *31*, 603-606.

[35] a) K. R. Dunbar and R. A. Heintz, *Progress in Inorganic Chemistry*, **1997,** *45*, 283-391. b) N. Ishii, Y. Okamura, S. Chiba, T. Nogami and T. Ishida, *J. Am. Chem. Soc.*, **2008,** *130,* 24-25.

[36] M.R.Caira, A.Jacobs and L.R.Nassimbeni, *Supramol. Chem*. **2004**, *16*, 337-342

[37] A. Ikeda, T. Nagasaki, K. Araki and S. Shinkai, *Tetrahedron* **1992,** *48*, 1059-1070.

[38] M. Urbaniak and W. Iwanek, *Tetrahedron* **1999,** *55,* 14459-14466.

[39] O. Pietraszkiewicz, *Adv. Mater. Opt. Electron*. **1998,** *8,* 277-284.

[40] T. Ogoshi, K. Kitajima, K. Umeda, S. Hiramitsu, S. Kanai, S. Fujinami, T. Yamagishi and Y. Nakamoto, *Tetrahedron* **2009,** *65,* 10644-10649.

[41] C. Carruthers, T. K. Ronson, C. J. Sumby, A. Westcott, L. P. Harding, T. J. Prior, P. Rizkallah and M. J. Hardie, *Chem. Eur. J.* **2008,** *14,* 10286-10296.

[42] a) M. Caira, A. Jacobs and L. R. Nassimbeni, *Supramol. Chem.,* **2004**, *16,* 337-342. b) M. J. Hardie and C. L. Raston, *Cryst. Growth Des.,* **2001,** *1,* 53-58. c) S. T. Mough and K. T. Holman, *Chem. Commun.,* **2008,** 1407-1409. d) C. J. Sumby, K. C. Gordon, T. J. Walsh and M. J. Hardie, *Chem. Eur. J.,* **2008,** *14,* 4415-4425.

Chapter 3

Novel Metallated Structures of Cyclotricatechylene

3.1 Introduction

The redox chemistry of metal/dioxolene complexes has long been known and owing to their unique redox chemistry and characteristic spectroscopy, complexes of this type have generated a significant amount of interest. As was explored in chapter 1, metal/dioxolene complexes display a fascinating ability to undergo one electron oxidation/reduction processes between the three oxidation states catecholate ('cat'), semiquinone ('sq') and quinone ('q') as displayed in **Scheme 1.4**. A particular interest in complexes of this type is in the ease of charge transfer between metal and dioxolene, often giving rise to very intense visible and near-infrared (NIR) absorptions which have been postulated to be useful in solar energy applications.[1]

Complexes which incorporate multiple dioxolene centres, whether dinuclear or polynuclear, introduce the possibility for further complicating the potential redox processes whereby electron transfer may occur between multiple metal and/or ligand sites. There have been a number of multinuclear dioxolene ligands previously investigated with the most studied being derivatives of 2,5-hydroxy-1,4-benzoquinone ($\mathbf{L_{1\text{-}R}}$) where generally, two metal centres bind to one ligand, as shown in **Figure 1.8**. Complexes of this type have been investigated for their potential in redox induced electron transfer (RIET) processes,[2] with the best characterised being that of $[\{(tpa)Co\}^{III}[\mathbf{L_{1\text{-}Cl}}^{3-}]\{Co(tpa)\}^{III}]^{3+}$ (tpa = *tris*(2-pyridylmethyl)amine) prepared from the one-electron oxidation of $[\{(tpa)Co^{II}\}[\mathbf{L_{1\text{-}Cl}}^{2-}]\{Co^{II}(tpa)\}](BF_4)_2$ as explored in chapter 1.[3]

Whilst complexes of this type have been shown to be able to undergo electron transfer, introduction of a spacer inbetween the multiple dioxolene sites may yield the potential for ligand based mixed-valency.[4] A number of such complexes incorporating multiple dioxolene centres have been investigated in the past with those bearing *bis*-dioxolenes the most abundant.[5] More unusual are complexes which contain more than two dioxolene centres, for example; 1,3,5-*tris*(3-*tert*-butyl-4,5,-dihydroxy-phenyl)benzene (H_6Phcat_3),[6] H_6triscat[7] and cyclotricatechylene (ctc, **2.2**).

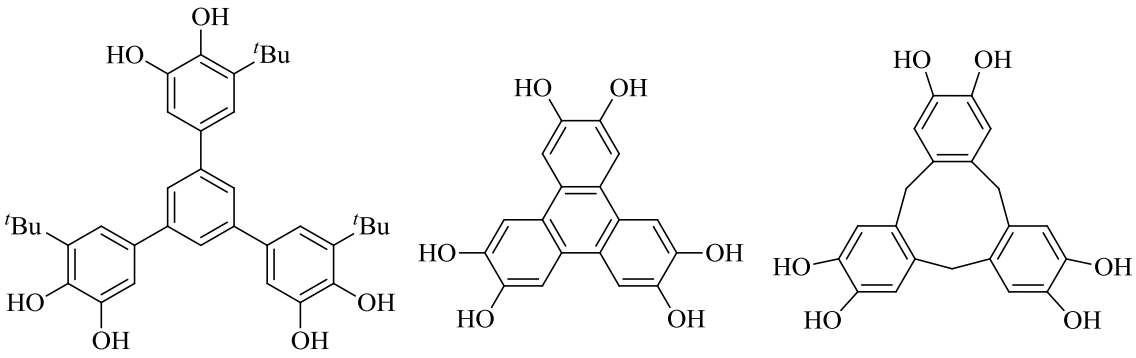

H_6Phcat_3 $H_6triscat$ H_6ctc, **2.2**

Figure 3.1. Schematic representation of *tris*-dioxolene species, (H_6Phcat_3),[6] $H_6triscat$[7] and cyclotricatechylene (ctc, **2.2**).

There have been a number of published examples of complexes containing the $[ctc]^{6-}$ core unit, for instance its use as a component in supramolecular capsules,[8] a $[Cu_6L_4]^{12-}$ metal-organic cage complex.[9] There has been only one investigation where it's complex chemistry was investigated, however, when substituted at the upper rim with $[(dppf)Pt]^{2+}$ (dppf = diphenylphosphinoferrocene) (**3.1**) or $[(dppb)Pt]^{2+}$ (dppb = diphenylphosphinobenzene) (**3.2**) ancillary ligands, as reported by Bohle *et al.*[10]

Our interest in ctc stems from the cyclic voltammetric analysis of complexes **3.1** and **3.2**, which showed the $[ctc]^{6-}$ core unit is capable of supporting reversible, sequential oxidation of each dioxolene ring independently between catecholate and semiquinone oxidation states. Despite there being no further discussion on the redox capabilities of these complexes to date, it is clear that the three catechol rings may be oxidised independently to novel semiquinato- centres at very accessible potential to afford the mono-, di- and tri-radical species $[\mathbf{2.2}]^{5-}$, $[\mathbf{2.2}]^{4-}$ and $[\mathbf{2.2}]^{3-}$ as in **Scheme 3.1.**

.

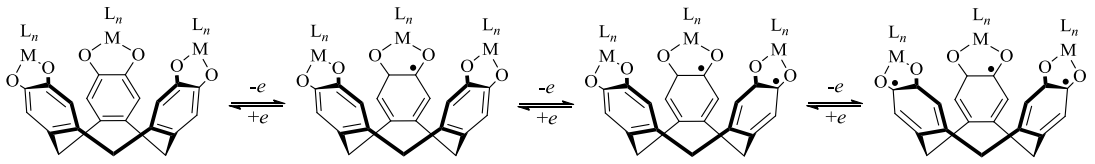

$[(ML_n)_3(\mathbf{2.2})^{6-}]$ $[(ML_n)_3(\mathbf{2.2})^{5-}]^{+}$ $[(ML_n)_3(\mathbf{2.2})^{4-}]^{2+}$ $[(ML_n)_3(\mathbf{2.2})^{3-}]^{3+}$

cat / cat / cat cat / cat / sq cat / sq / sq sq / sq / sq

Scheme 3.1. Ligand-based redox processes previously reported by Bohle *et al.*[10] where L = dppf (diphenylphosphinoferrocene) or dppb (diphenylphosphinobenzene).

This chapter is concerned with the preparation of novel, extended structures of the bowl-shaped *tris*-catechol cavitand cyclotricatechylene (ctc). As has been seen in Chapter 2, ctc

may be easily and cleanly prepared from the demethylation of cyclotriveratrylene (ctv) using boron tribromide. The C_3 symmetry of the molecule was retained in all complexes, whereby all substitutions on the upper rim were identical. Proton NMR was a key method of analysing whether this symmetry was retained, with signals observed only for each of the C_3 symmetric subunits. Due to this symmetry and rigidity of the core $[ctc]^{6-}$ unit, protons of the methylene bridge reside in different chemical environments, CH_{endo} and CH_{exo}, pointing inside and outside of the bowl respectively (**Figure 3.2**). The chemical shifts of these protons differ by approximately 1 ppm, and they couple to each other with $^2J_{HH}$ values of approximately 13-14 Hz resulting in two very characteristic doublets in the ^{1}H NMR spectrum. These doublets may therefore be used as a handle to determine whether or not the desired complex has been synthesised, and ctc has retained its characteristic C_3 symmetry.

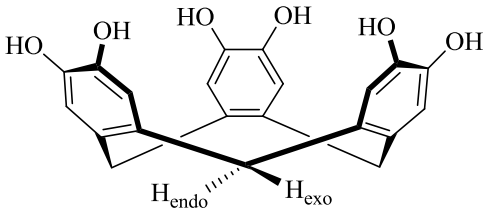

Figure 3.2. Schematic structure of cyclotricatechylene. The methylene bridge between dioxolene rings has been extended to emphasise the positioning of the characteristic CH_{endo} and CH_{exo} protons.

3.2 Results and Discussion

3.2.1 Synthesis of Novel Cyclotricatechylene Complexes

In order to provide a detailed investigation into the redox capabilities of complexes containing the core $[ctc]^{6-}$ unit, the synthesis of complexes containing palladium(II) metal centres were first attempted owing to their short reaction times and the rigid square-planar geometry of palladium(II). The reaction conditions followed by Bohle and Stasko in their original work,[10] potassium carbonate/methanol mixture as a base and deoxygenated dimethylacetamide as solvent (**Scheme 3.3**), were utilised and the first reactions performed used unsubstituted 2,2'-bipyridine as an ancillary ligand. It quickly became apparent however that by use of this ligand, product purification was hampered by severe insolubility of the product. It was therefore decided to modify the approach towards complexes incorporating bipyridyl ancillary ligands with additional substituents in the 4,4'- position. Attempted complexes included those bearing methyl-, methoxy- and *tertiary*-butyl groups in order to discourage potential π-π interactions in the solid state therefore leading to increased solubility. With complexes bearing methyl- and methoxy- substituents, this alteration

imparted some solubility to the complexes although could not solve the issue completely as evident by the presence of some palladium-dichloride precursors in the ^{1}H NMR spectrum. Incorporation of *tertiary*-butyl substituients however, yielded a significantly more soluble product which permitted purification by recrystallisation from deoxygenated dichloromethane / acetone yielding complex [{(^{t}Bu$_2$Bipy)Pd}$_3$(ctc)] **(3.3)** as a deep purple solid.

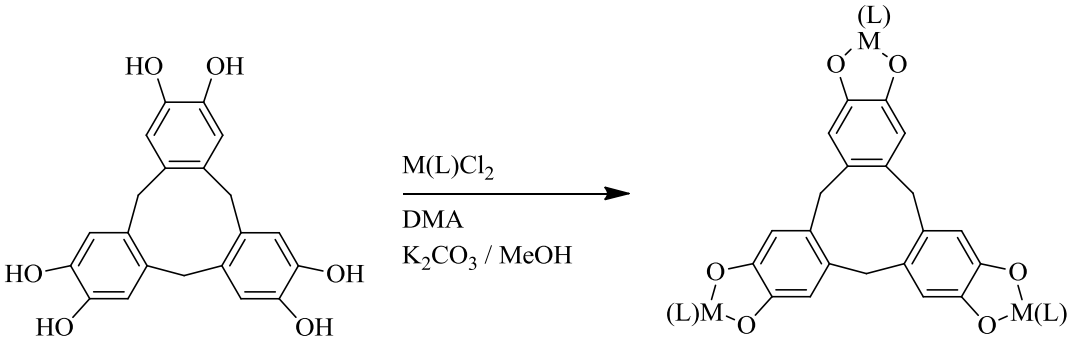

H_6ctc, **2.2**

[{(L)M}$_3$(ctc)]

M = Pd ; L = ^{t}Bu$_2$Bipy, **3.3**
M = Pt ; L = dppb, **3.2**
L = dppe, **3.4**
L = ^{t}Bu$_2$Bipy, **3.5**
M = Cu ; L = ^{t}Bu$_2$Bipy, **3.6**

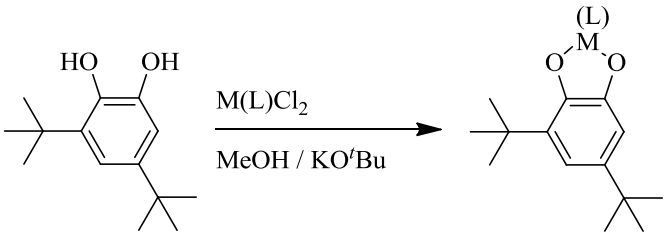

DBCat

[{(L)M}(DBCat)]

M = Pt ; L = dppe, **3.7**
L = ^{t}Bu$_2$Bipy, **3.8**

Scheme 3.2. Reaction scheme for the synthesis of [μ_3-ctc]$^{6-}$ complexes **3.3** – **3.6** and [DBCat]$^{2-}$ (DBCat = 3,5-di-*tert*-butyl catechol) complexes **3.7 - 3.8** discussed in this work.

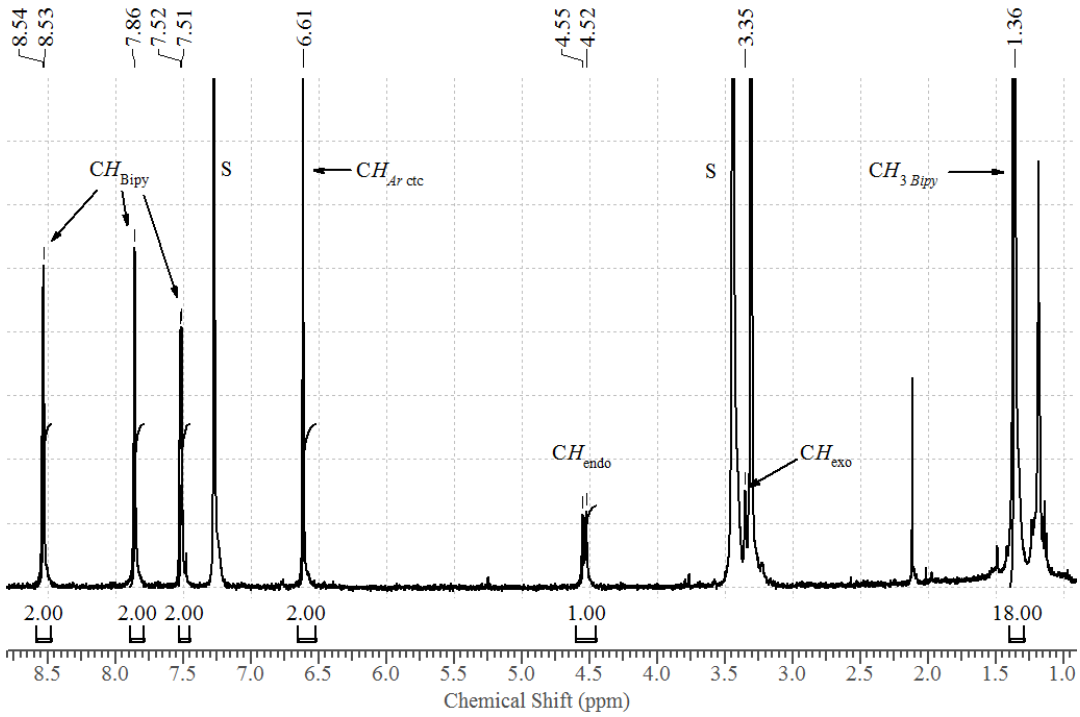

Figure 3.3. Interpreted ^{1}H NMR (500 MHz, 5 : 1, $CDCl_3$: MeOD) spectrum of [{(^{t}Bu$_2$Bipy)Pd}$_3$(ctc)] (**3.3**) showing μ_3-substitution of $[ctc]^{6-}$. Solvent (S) signals at δ = 7.27 and 3.44 ppm belong to C*H*Cl$_3$ and C*H*$_3$OH respectively.

As shown by ^{1}H NMR (5 : 1, $CDCl_3$: MeOD) in **Figure 3.3**, the complex [{(^{t}Bu$_2$Bipy)Pd}$_3$(ctc)] was synthesised cleanly, showing one set of resonances with matching integrations for one third of the molecule only, indicating the complex retained its C_3-symmetry. Additionally, the presence of the characteristic CH_{endo} doublet being clearly visible at 4.54 ppm (CH_{exo} is partially hidden by the water and methanol resonances) indicated the rigidity of the molecule had not been compromised, nor its shape significantly perturbed by substitution at the upper rim. The $^{2}J_{HH}$ value of CH_{endo} equals 13 Hz, therefore confirming this assignment. High resolution mass spectrometry (ES+) also confirmed the tri-substituted structure of **3.3** as shown in **Figure 3.4**, where a dicationic cluster at *m*/*z* = 1485.3651 corresponding to the ionisation of two intact molecules of **3.3.** The spectrum additionally showed the fragmentation of **3.3** whereby peaks associated with the di- and mono-substituted $[ctc]^{6-}$ unit at 1112.2802 and 743.1864 corresponding to the fragments $\{[\{(^{t}Bu_2Bipy)Pd\}_2(ctc)].[H]\}^{+}$ and $\{[\{(^{t}Bu_2Bipy)Pd\}(ctc)]_2.H_2O\}^{2+}$ respectively. Fragmentation of complex **3.3** was relatively high, presumably due to the labile nature of palladium.

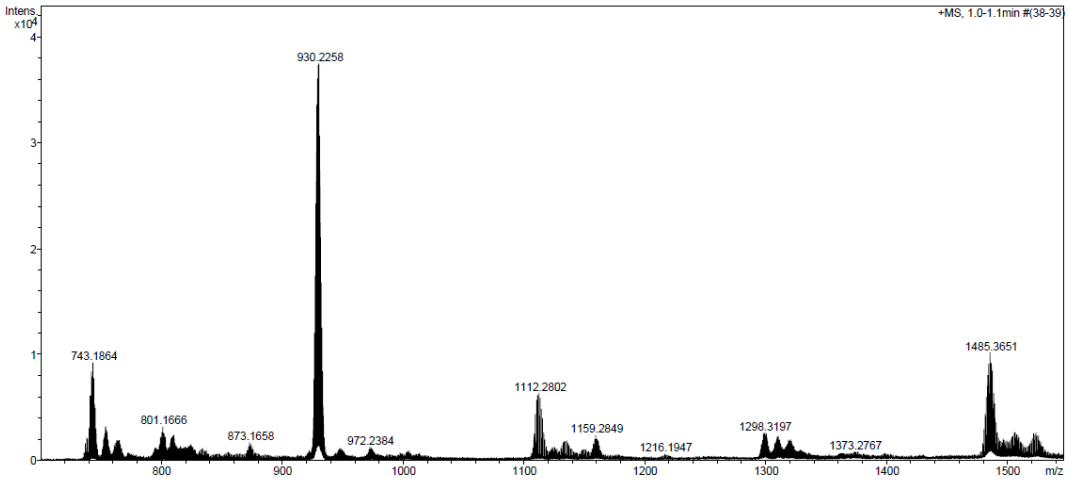

Figure 3.4. Mass spectrum ES(+) of [{(^{t}Bu$_2$Bipy)Pd}$_3$(ctc)] (**3.3**).

Owing to the success found in the synthesis of complex **3.3**, the investigation was extended to include diphosphine analogues using diphenylphosphinobenzene (*c.f.* **3.2)** and diphenylphosphinoethane (dppe, *c.f.* **3.4**) ancillary ligands. All attempts at purifying these complexes failed however, owing to their significant air sensitivity in solution, assumed to be due to the lability of palladium(II), which often bleached the deep green solutions and precipitated as the [(dppb)PdCl$_2$] or [(dppe)PdCl$_2$] precursors in chlorinated solvents. This was particularly prevalent at room temperature. Consequent of the challenges faced in the synthesis of these molecules, the investigation was extended to use platinum(II) as a central metal atom as this had previously offered the desired complexes **3.1** and **3.2**, using the same conditions as outlined above.[10]

As with the investigation of complexes incorporating palladium(II) centres, the first complex cleanly synthesised was that of [{(^{t}Bu$_2$Bipy)Pt}$_3$(ctc)] (**3.5**). The stability of the complex compared to **3.3** was immediately obvious as purification was achievable by either recrystallisation from deoxygenated dichloromethane / acetone or column chromatography (silica, 2.5% methanol in dichloromethane). Similarly as with **3.3**, the ^{1}H NMR of complex **3.5** displayed resonances matching one third of the molecule only as can be seen in **Figure 3.5**.

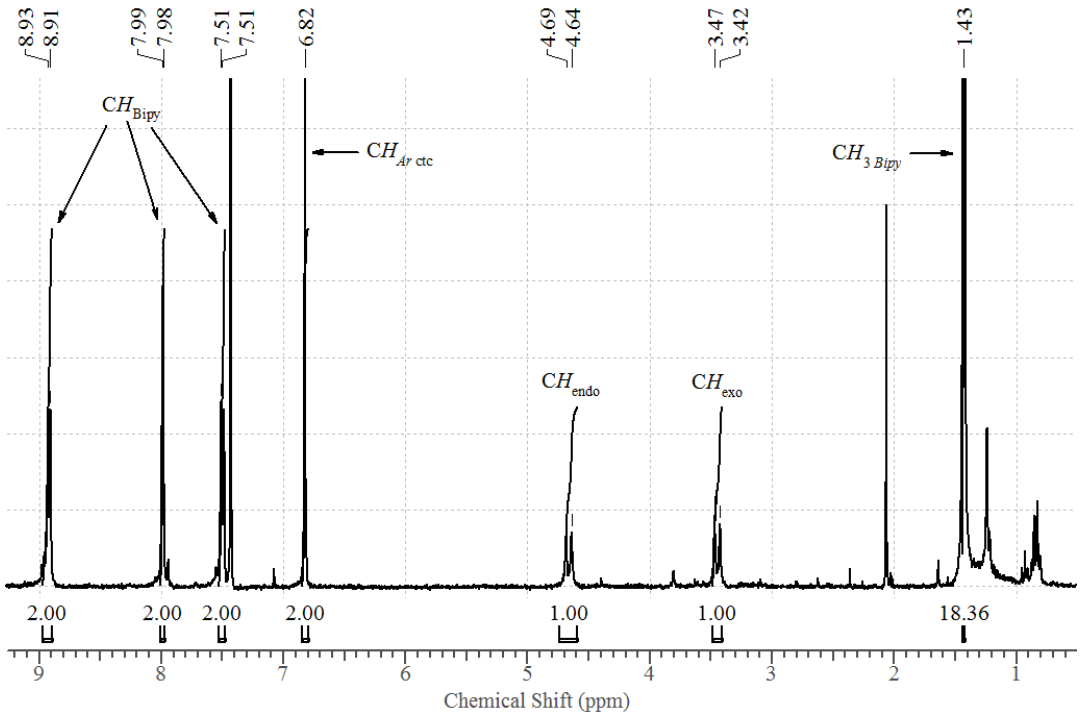

Figure 3.5. Interpreted ^{1}H NMR (500 MHz, 5 : 1, $CDCl_3$: CD_3OD) spectrum of complex **3.5**, [{($^{t}Bu_2$Bipy)Pt}$_3$(ctc)] showing μ_3-substitution of $[ctc]^{6-}$.

NMR analysis (^{1}H and ^{31}P) of complexes **3.2** and **3.4** proved to be a lot more difficult than for **3.5**, due to their significant solution-phase air sensitivity. Complex **3.2** appeared to be more stable than **3.4,** allowing for representative NMR spectra to be recorded matching those previously published in the mixed solvent $CDCl_3$; CD_3OD (5 : 1), as shown in **Figure 3.6**.[10] Again, the ^{1}H NMR confirmed tri-substitution, with the characteristic ditopic CH_{endo} and one half of the CH_{exo} resonances visible at δ = 4.51 and 3.22 ppm respectively.

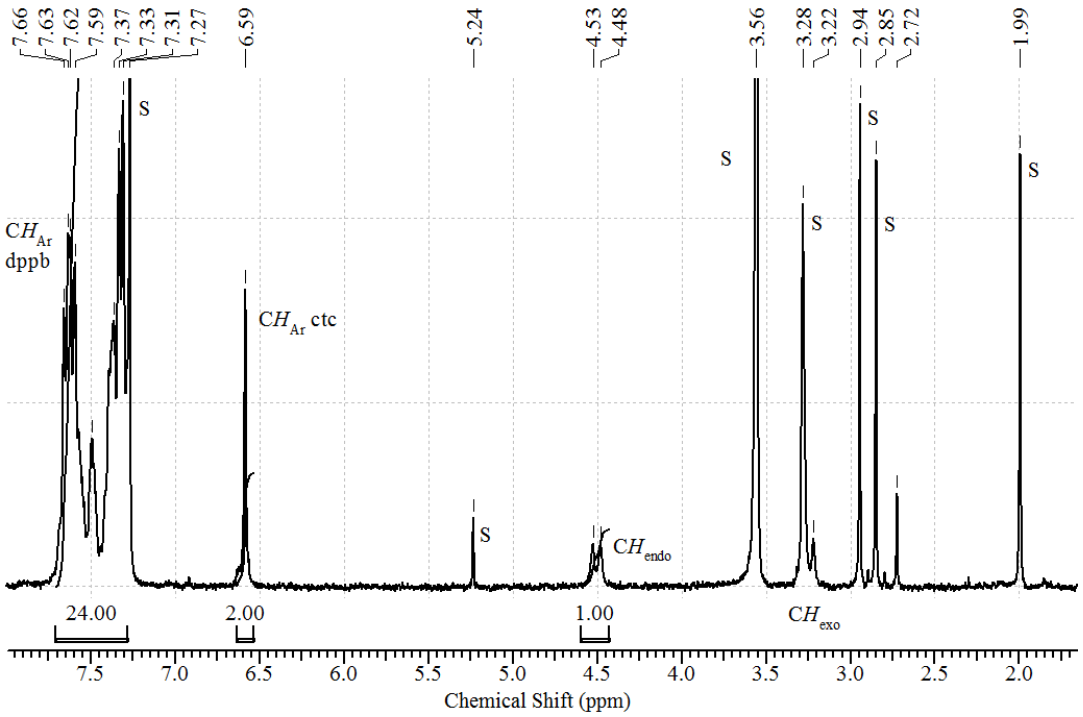

Figure 3.6. Interpreted ^{1}H NMR (500 MHz, 5 :1 $CDCl_3$: CD_3OD) spectrum of complex **3.2**, [{(dppb)Pt}$_3$(ctc)] indicating μ_3-substitution of $[ctc]^{6-}$. S = solvent resonance.

3.4 on the other hand, proved itself to be poorly soluble in all conventional deuterated solvents, and significantly oxygen sensitive resulting in decomposition throughout the lifetime of longer experiments (>128 scans) evident by a colour change to deep green and precipitation of an insoluble white precipitate in wet, oxygenated chlorinated solvents. Use of dried, anoxic solvents appeared to stem this precipitation for the most part although colour changes associated with oxidation were still noticed. Some spectra were recorded in dried d_6-dmso (dmso = dimethylsulfoxide), although poor solubility of the complex was again evident, resulting in the noisy spectra seen in **Figure 3.7**. This is shown over a reduced range due to the high intensity of the solvent signal (dimethylsulfoxide) compared to the sample resonances.

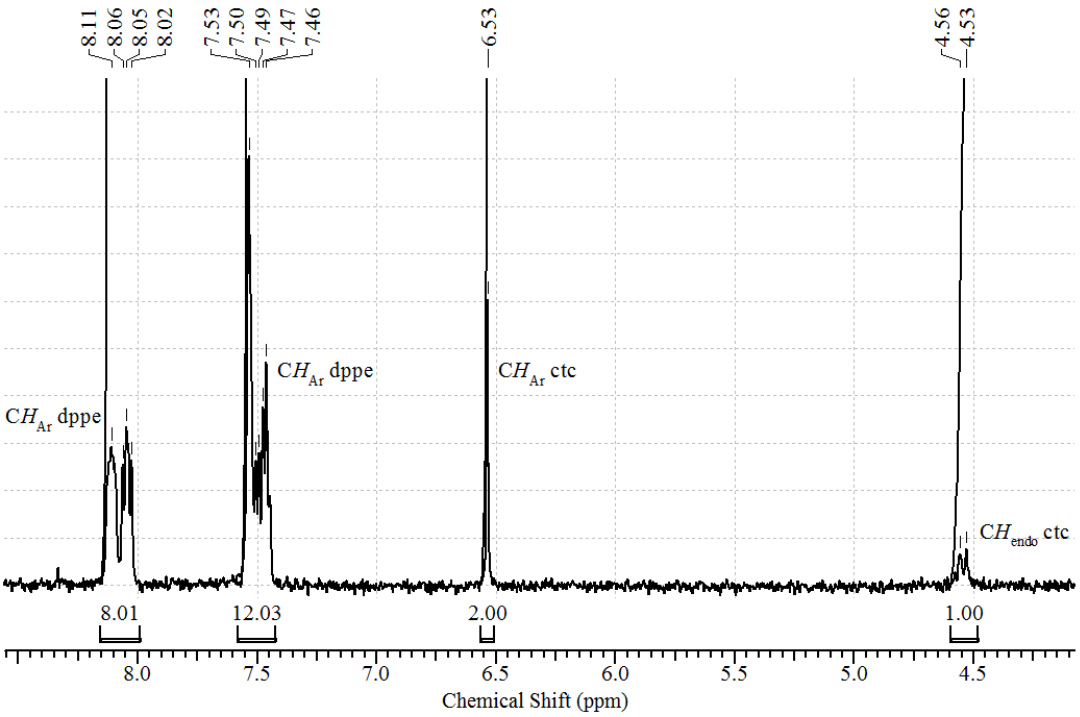

Figure 3.7. Interpreted ^{1}H NMR (500 MHz, DMSO-d_6) spectrum of complex **3.4**, [{(dppe)Pt $_3$(ctc)] indicating μ_3-substitution of $[ctc]^{6-}$.

The spectrum compared well to that recorded of complex **3.2**, where both displayed matching integrals to one third of each molecule, and the characteristic CH_{endo} doublet of the methylene bridge clearly observable above the baseline. As both spectra of **3.2** and **3.4** were recorded in different solvents comparison of their chemical shifts is inappropriate.

This poor solubility also translated into a weak ^{31}P{^{1}H} NMR spectrum which although clearly showed the presence of a symmetric diphosphine with δ = 30.8 ppm, in the same environment as **3.2** (δ = 31.2 ppm).[10] The presence of one peak was important in confirming the C_3 symmetry of the product whilst the spectrum also (weakly) displayed the presence of platinum satellites, arising from the coupling of ^{31}P to one ^{195}Pt (I = ½) nucleus. The coupling constant for this was calculated to be $J_{P\text{-}Pt}$ = 3344 Hz, comparable to that reported for **3.2** ($J_{P\text{-}Pt}$ = 3492 Hz).[10]

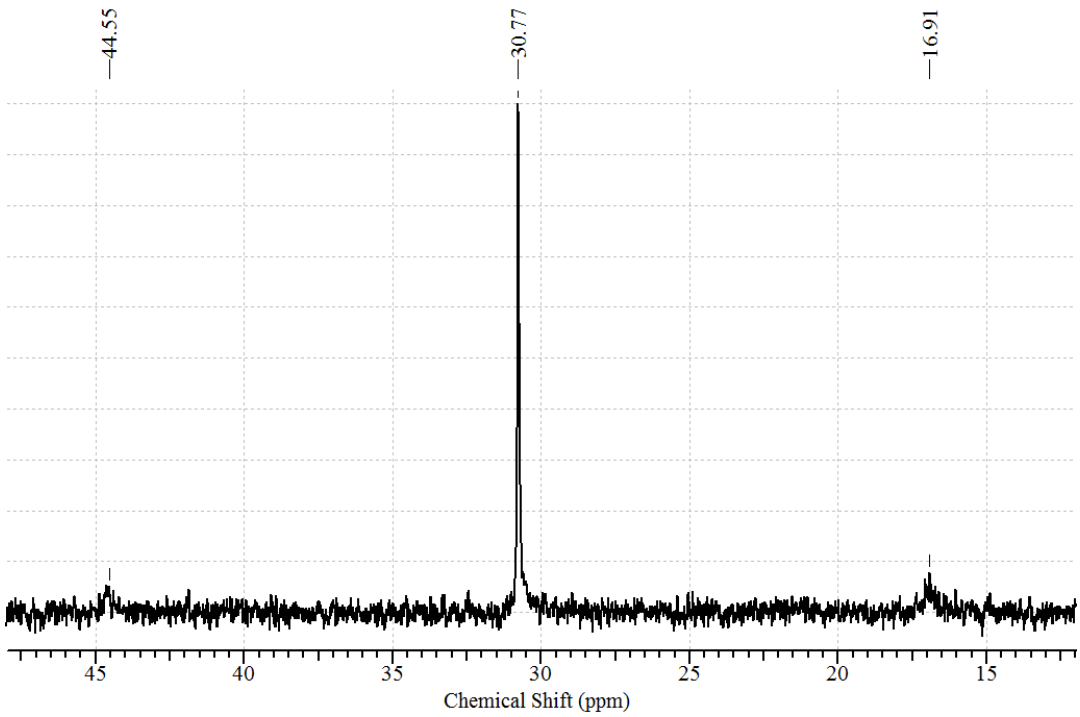

Figure 3.8. $^{31}P\{^{1}H\}$ NMR (121 MHz, DMSO-d_6) of complex **3.4** showing evidence for ^{31}P-^{195}Pt coupling.

After analysis, these samples were left open to the air for several hours and the spectra re-taken. It was found that by doing so, peaks in the proton NMR spectra in similar positions to those discussed above were observed but were significantly broadened, as in displayed in **Figure 3.9** whilst all phosphorus-platinum coupling was lost in the $^{31}P\{^{1}H\}$ NMR spectrum (although the central peak at δ = 30.8 ppm remained). This paramagnetic broadening was assumed to be due to the aerial oxidation of the complex, although it did not appear to have dissociated owing to the lack of additional peaks within the spectrum. It should be noted that a colour change to pale green was also noted, without precipitation. The oxidation of these complexes will be discussed further into the chapter. Unfortunately, no $^{13}C\{^{1}H\}$ spectra could be recorded for any cyclotricatechylene complex to the poor solubility of the complexes and their obvious decomposition over the course of long experiments. Numerous attempts were made, although at no point could a representative spectrum be obtained.

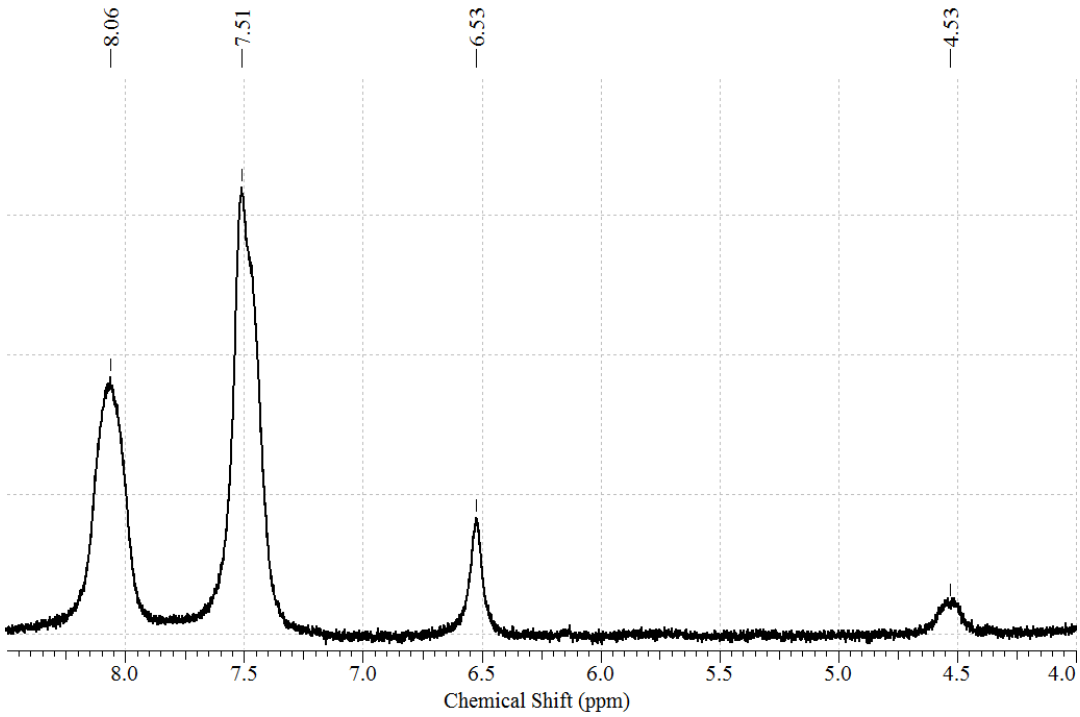

Figure 3.9. Paramagnetically broadened ^{1}H NMR (500 MHz, DMSO-d_6) spectrum of complex **3.4**, [{(dppe)Pt$_3$(ctc)] indicating oxidation upon exposure to air.

Mass spectrometry (ES+) was again useful for the characterisation of complexes **3.2, 3.4** and **3.5**. In all cases, the spectra were complicated due to inclusion of sodium or potassium cations (sodium from sodium formate calibrant and potassium originating from the potassium carbonate base used in the reactions) or solvent molecules which could potentially be within the 'bowl' of the molecule, as seen in chapter 2. Despite this, all spectra also obtained showed strong cationic peaks associated with the intact molecules [**3.2**]$^{n+}$, [**3.4**]$^{n+}$ and [**3.5**]$^{n+}$ (n = 1,2,3), as displayed in **Figure 3.10** whilst surprisingly, fragmentation was relatively low.

Synthesis of copper(II) complexes of [ctc]$^{6-}$ was also attempted using bipyridyl and diphosphine ancillary ligands although this was complicated owing to the redox isomerism often shown by copper-dioxolene complexes.[11] Attempted synthesis of complexes bearing diphosphine ancillary ligands (dppb, dppe), using the same reaction route as complexes **3.2 - 3.5**, yielded extremely air-sensitive solutions presumably due to the formation of ctc Cu^{I}[sq$^{\bullet}$]$^{-}$ species.[12] Attention was therefore turned to use of bipyridyl ancillary ligands where it was again found that use of unsubstituted 2,2'-bipyridine or 1,10-phenanthroline yielded only insoluble powders, while ^{t}Bu$_2$Bipy gave a much more soluble product therefore permitting the synthesis of **3.6**. Owing to the paramagnetic nature of the **3.6**, NMR analysis was precluded and mass spectrometry ES(+) displayed complicated spectra due to ligand scrambling and copper dissociation. Characterisation by elemental analysis showed the

complex could be assigned with a formula containing crystallisation solvent, which is not uncommon for complexes containing the cyclotricatechylene core unit.[9, 13]

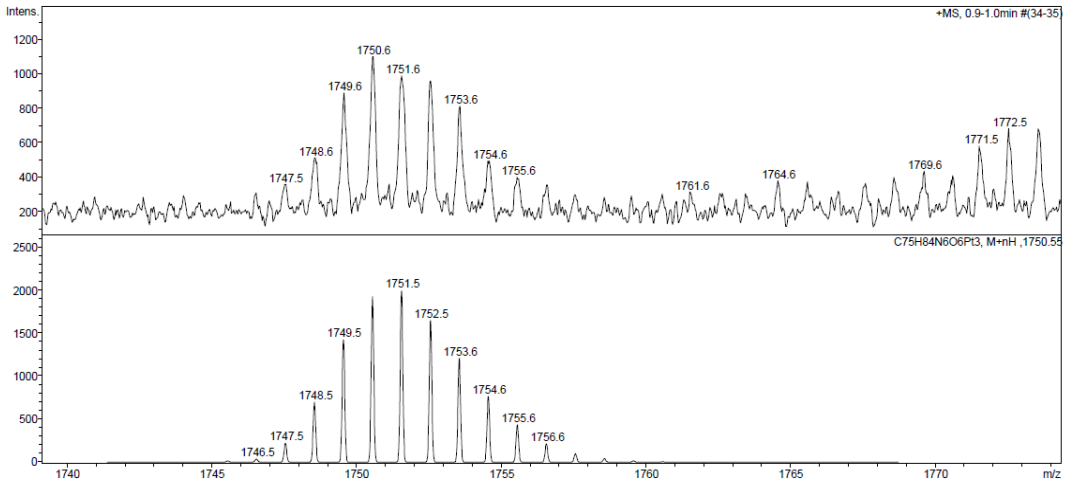

Figure 3.10. (Top) ES(MS+) Spectrum of molecular ion **[3.5]**$^{+}$ [{(^{t}Bu$_2$Bipy)Pt}$_3$(ctc)]$^{+}$ from a dimethylsulfoxide feed solution. (Bottom) Predicted spectrum for molecular ion **[3.5]**$^{+}$ [{(^{t}Bu$_2$Bipy)Pt}$_3$(ctc)]$^{+}$.

Infrared analysis of all complexes was also an informative technique, with each complex displaying IR active ν(CO) vibrations often used to characterise catecholate complexes close to 1270 cm^{-1}. Infrared analysis was particularly informative for complex **3.6**, as it is paramagnetic NMR analysis was exempt, which displayed a strong ν(CO) bands at1251 cm^{-1} and between 1489 - 1410 cm^{-1} corresponding to the internal ν(CC) associated with coordination to Cu(II).[14] In addition, the presence of bands at 1024 cm^{-1} and 551cm^{-1}correspond to ν(CuN) and ν(CuO) respectively.[14]

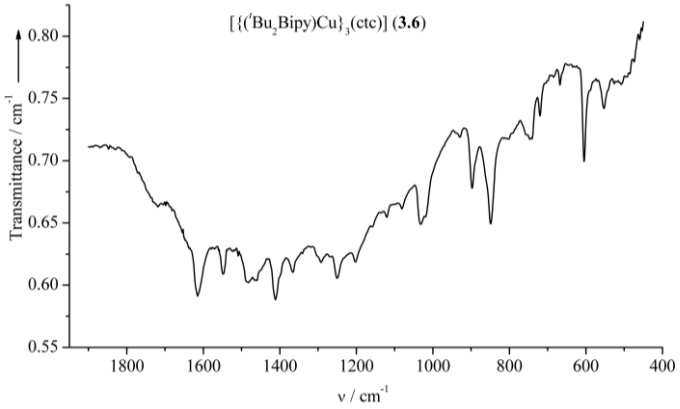

Figure 3.11. IR spectrum (solid state) of [{(^{t}Bu$_2$Bipy)Cu}$_3$(ctc)] **(3.6).**

In addition to the cyclotricatechylene complexes described above, two analogous mononuclear complexes [(dppe)Pt(DBCat)] (**3.7**) and [(^{t}Bu$_2$Bipy)Pt(DBCat)] (**3.8**) were

synthesised for comparative purposes. Their synthesis was straightforward, by the reaction of DBCat / potassium *tert*-butoxide mixture with appropriate metal-dichloride precursor in methanol, under an inert atmosphere. The NMR (^{1}H, $^{31}P\{^{1}H\}$) and mass spectroscopic showed good agreement with that previously described in the literature.[15]

3.2.1 Single crystal X-ray Structure Determinations of [{(dppe)Pt}$_3$(ctc)] (3.4)

A mixture of two solvates of compound **3.4** were grown from dimethylacetamide (dma) / methanol and characterised using synchrotron radiation at Diamond Light Source (beamline I19). Both solvates, **3.4**•$2H_2O$•1.3dma•0.5MeOH and **3.4**•$2H_2O$•8dma are described separately below.

Structure refinement and analysis of [{(dppe)Pt}$_3$(ctc)]•$2H_2O$•1.3dma•0.5MeOH

The first solvate **3.4**•$2H_2O$•1.3dma•0.5MeOH crystallised as yellow needles and was solved and refined in the monoclinic space group $P2_1$ showing the expected μ_3- substitution at the $[ctc]^{6-}$ upper-rim and retention of the characteristic 'bowl' as can be seen in **Figure 3.12**.

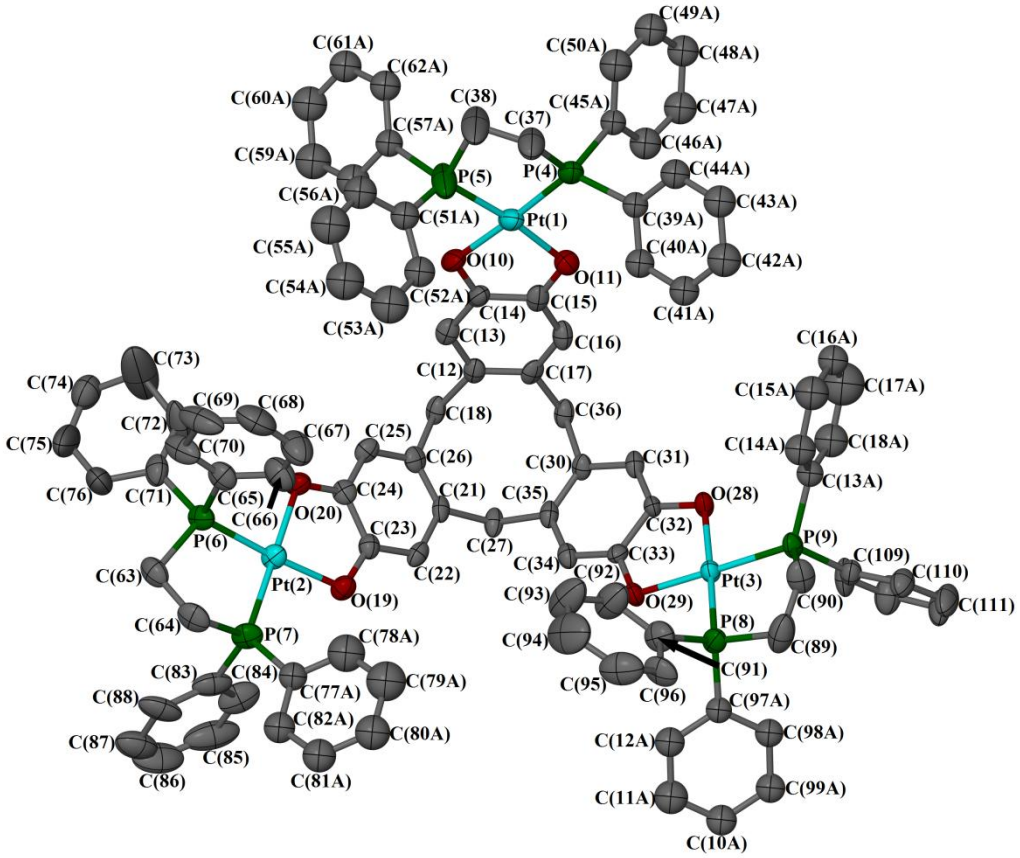

Figure 3.12. View directly into the characteristic bowl of complex **3.4** in [{(dppe)Pt}$_3$(ctc)]•2H$_2$O•1.3dma•0.5MeOH**.** Displacement ellipsoids are set at 50% probability and solvent molecules and hydrogen atoms are omitted for clarity. Colour code: Pt, cyan; P, green; O, red; C, grey.

The asymmetric unit of **3.4**•2H$_2$O•1.3dma•0.5MeOH was shown to contain one full complex formula unit on a general crystallographic position, one methanol molecule with occupancy 0.50 and two dimethylacetamide molecules, one with occupancy 0.50 and another with occupancy of 0.80 which was incompletely determined within the model due to its disorder over two positions (with occupancies of 0.3 and 0.5) within the ctc 'bowl' as shown in **Figure 3.13**. This disordered dimethylacetamide molecule exhibited large thermal isotropic displacement parameters, indicating there may be further unresolved disorder within the molecule which unfortunately could not be modelled. There were also four Fourier peaks which were not bonded to any other atom which refined well as water molecules with occupancies of 0.55, 0.38, 0.50 and 0.61. Of these, the water molecule centred on O(133) with occupancy 0.5 shares its position in the model with dimethylacetamide molecule centred on N(130), close to the upper rim of the molecule between P(5) and P(6). There was obvious disorder on seven of the twelve dppe phenyl rings, which were refined as rigid hexagons with occupancies varying between 0.37 and 0.63 with the exception of two rings,

C(71) > C(76) and C(91) > C(96), which deviated from planarity therefore indicating disorder. This could not be modelled however, therefore exhibit large thermal anisotropic displacement parameters.

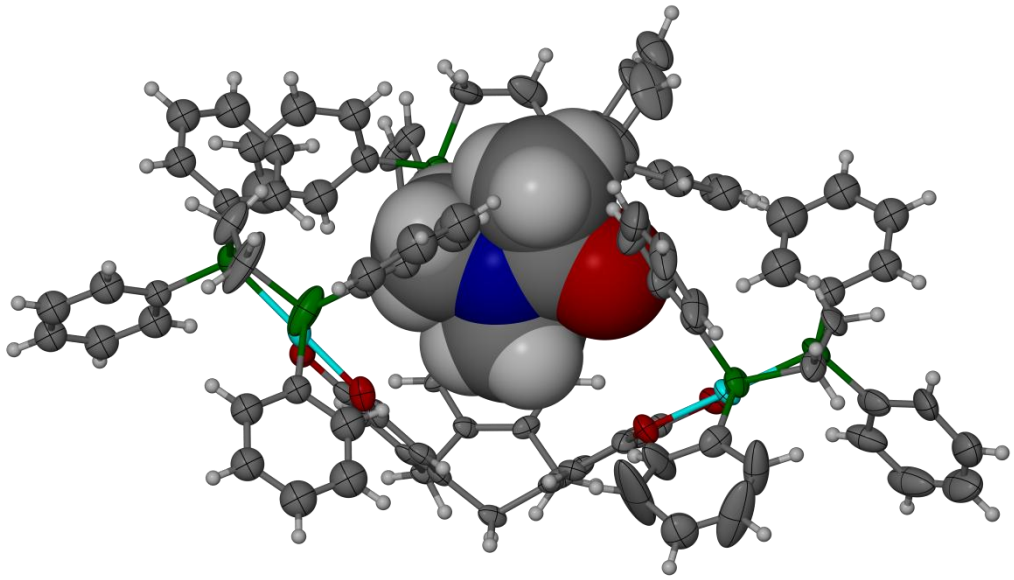

Figure 3.13. Side-on view of complex **3.4** in $[\{(dppe)Pt\}_3(ctc)]\bullet 2H_2O\bullet 1.3dma\bullet 0.5MeOH$ highlighting the guest molecule of dimethylacetamide within the ctc 'bowl'. Displacement ellipsoids of all non-hydrogen atoms of complex **3.4** are set at 50% probability whilst the molecule of dimethylacetamide centred on N(118) is shown as space-filling. Colour code: Pt, cyan; P, green; O, red; N, blue; C, grey; H, white.

A *SQUEEZE*[16] analysis of the model indicated the presence of two further dimethylacetamide molecules within the lattice, although they could not be located within the Fourier map presumably due to disorder. All fully occupied atoms were refined anisotropically, and all hydrogen atoms placed in calculated positions and refined using a riding model. The hydrogen atoms on all water molecules could not be found in the Fourier map or placed in a calculated position therefore were omitted from the model, although were taken account of in F_{000} and density calculations. The highest residual Fourier peak of 1.62 $e.Å^{-3}$ was found in a small pocket approximately 3.3 Å outside of the complex upper rim, close to two other residual peaks of 1.18 and 1.10 $e.Å^{-3}$ which are likely due to further disordered solvent molecules which could not be determined. The deepest hole within the Fourier map was -1.56 $e.Å^{-3}$.

As with the previously reported complex of **3.2**,[10] the cavity is approximately 9.5 Å with rim diameter of 6.8 Å and distance between platinum atoms of 9.9 Å. Similarly, the dihedral angle between the dioxolene rings is 71.2(5) ^{o}, which are close and within experimental error to the average value of 71.9 ^{o} for complex **3.2**.

Structure refinement of [{(dppe)Pt}$_3$(ctc)]•H_2O•8dma

The structure of solvate **3.4**•H_2O•8dma was originally solved in the triclinic space group P$\bar{1}$ then transformed up to the hexagonal space group P63/m using the *ADDSYM* routine of *PLATON*.[17] The molecule again showed tri-substitution at the $[ctc]^{6-}$ upper rim with retention of the ctc 'bowl' and crystallographic C_3 symmetry (**Figure 3.14**), although it was disordered over the crystallographic mirror plane *x*, *y*, ¼ as shown in **Figure 3.15**. All atoms in the complex were refined with half-occupancies to account for this molecule disorder.

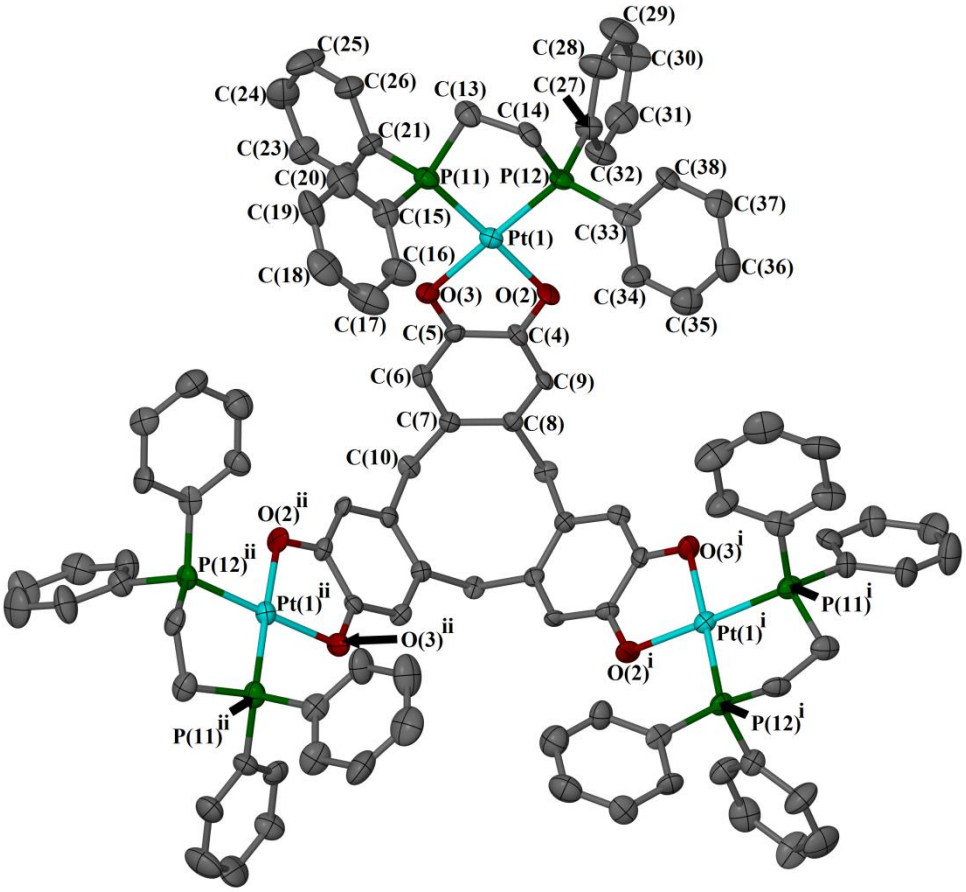

Figure 3.14. View directly into the characteristic bowl of complex **3.4** in **3.4**•H_2O•8dma**.** Displacement ellipsoids are set at 50% probability and solvent molecules and hydrogen atoms are omitted for clarity. Symmetry codes; (i) = 1-*y*, 1+(*x*-*y*), *z*; (ii) = -*x*+*y*, 1-*x*, *z*. Colour code: Pt, cyan; P, green; O, red; C, grey.

The asymmetric unit was shown to contain one third of a complex (excluding the full molecule disorder shown below) across the C_3 axis $^1/_3$, $^2/_3$, *z*, two half-occupied dimethylacetamide molecules and one Fourier peak which refined reasonably as one half of a water molecule in the ctc 'bowl'. The hydrogen atoms of this water molecule could not be

found in the Fourier map or placed in calculated positions therefore were omitted. For the purposes of F_{000} and density calculations however, these were included. The four unique phenyl moieties of the dppe fragment were all refined as a rigid hexagons, and could be assigned to each $\{Pt(dppe)\}^{2+}$ fragment within the full molecule disorder. No further restraints were required, and all non-hydrogen atoms were refined anisotropically whilst hydrogen atoms (except those belonging to the water molecule) were placed in calculated positions and refined using a riding model. The highest residual Fourier peak within the model was 1.4 $e.Å^{-3}$, found close to the dimethylacetamide molecule centred on C(46) which may be due to some disorder within the dimethylacetamide molecule which was not modelled, whilst the deepest Fourier hole was -1.3 $e.Å^{-3}$.

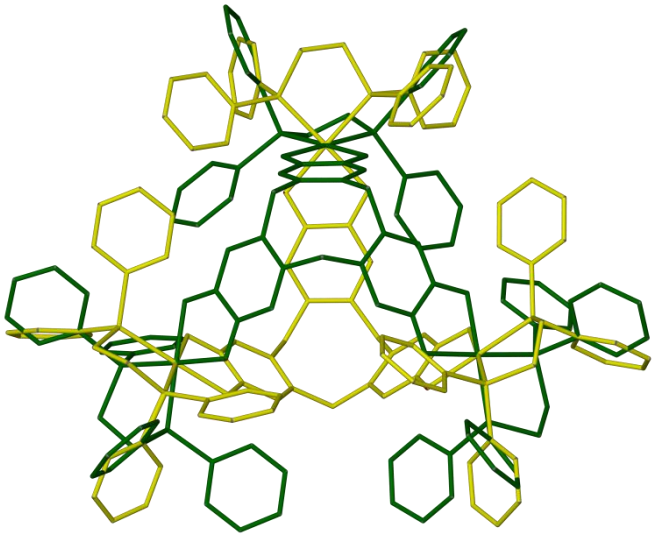

Figure 3.15. View of **3.4**•H_2O•8dma full molecule disorder across a crystallographic mirror plane with the two molecules coloured differently. All atoms have arbitrary radii and hydrogen atoms are omitted for clarity.

Visually, both structures closely resemble that of the previously described structure of **3.2** (as shown in **Figure 3.16)**, although a more detailed analysis to determine apparent signs of dioxolene oxidation is by analysis of internal bond lengths of each dioxolene ring.[10, 18] Generally, useful parameters which are extracted from the structural analysis are focussed on the aryl C-O bond lengths which may show characteristic bond lengths of approximately 1.23 Å for *o*-benzoquinones, 1.29 Å for *o*-semiquinonates and 1.35 Å for catecholates.[19] This generalised view however may not take into account bond length alterations due to coordination, chelation, bridging or stereochemical effects on the metal centre (such as Jahn-Teller distortion). Therefore, use of more detailed metric parameters must be considered which may include the alteration of long and short bonds within the dioxolene aromatic ring in *o*-benzoquinones, but not catecholate molecules. Use of parameter Δ, as

defined by equations **3.1** and **3.2** below, may therefore be used to calculate the oxidation state of the ligand by correlation of all eight bond lengths within the dioxolene moiety.[18]

$\Delta_i = -2(d_i - d_{\mathbf{III}i}) / (d_{\mathbf{I}i} - d_{\mathbf{III}i})$ (**Equation 3.1**)

$\Delta = (\Sigma w_i \Delta_i) / (\Sigma w_i)$ (**Equation 3.2**)

$w_i = d_i / [\sigma(d_{\mathbf{I}i}) + \sigma(d_{\mathbf{III}i}) + \sigma(d_i)]$ (**Equation 3.3**)

Where, d_i is the experimental *i*th bond length, and $d_{\mathbf{I}i}$ and $d_{\mathbf{III}i}$ are the corresponding *i*th bond lengths for pure uncomplexed 1,2-dihydroxybenzene (catechol)[20] (**I**) and *o*-benzoquinone[21] (**III**) extracted from literature and w_i is a weighting value based upon the standard uncertainty (σ) of each bond length.[22] The value of Δ may take a value between 0.0 for a neutral ligand isostructural with uncomplexed *o*-benzoquinone, or -2.0 for dianionic ligand isostructural with 1,2-dihydroxybenzene (catechol).[20]

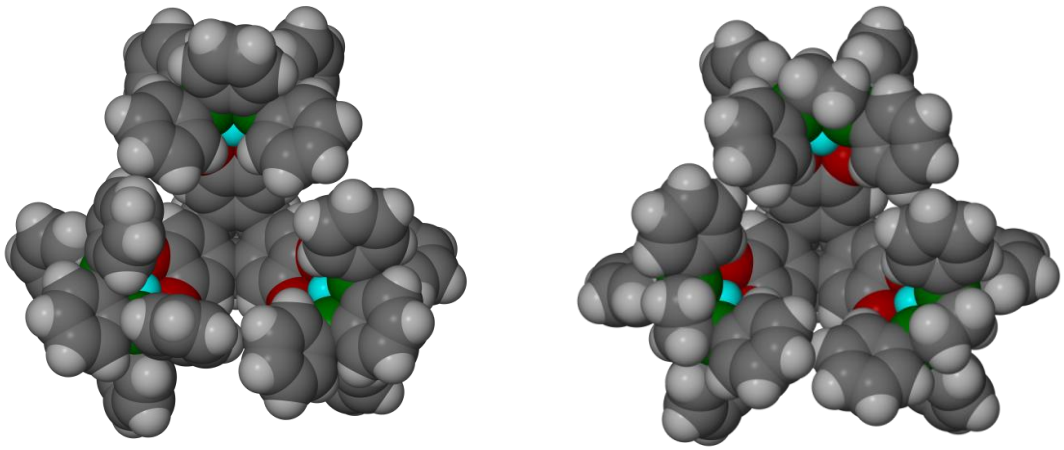

Figure 3.16. (Left) Space filling view of **3.2.**[10] (Right) Space filling view of **3.4** from **3.4**•H_2O•8dma. Colour code: Pt, cyan; P, green; O, red; C, grey; H, white.

Taking the eight bond bond lengths for each dioxolene ring, and using **equations 3.1-3.3,** the parameter Δ may be calculated for each ring where it was found that none offer signs of any oxidation. The large value of Δ= -2.5 calculated for ring C(21) > C(26) of structure **3.4**•2H_2O•1.3dma•0.5MeOH, is likely due to the high standard uncertainties associated with all bond lengths in the ring and as a result artificially increase the value.

Table 3.1. Selected metric parameters extracted from the two crystallographic structures of **3.4.**

	Pt–O [Å]	Pt–P [Å]	Δ	θ [°]
3.4•2H_2O•1.3dma•0.5MeOH	2.025(7) - 2.060(7)	2.208(2) - 2.223(3)	-2.2(4) ≥ Δ ≥ -1.9(4)	103.8(8)–117.1(5)
3.4•H_2O•8dma[a]	2.049(14) - 2.041(13)	2.234(6) - 2.219(5)	-1.8(2)	108.8(4)

[a] This structure contains only one unique dioxolene ring.

Table 3.2. Selected bond distances and angles for solvomorphs **3.4**•2H_2O•1.3dma•0.5MeOH and **3.4**•H_2O•8dma [Å, °].

3.4•2H_2O•1.3dma•0.5MeOH		**3.4**•H_2O•8dma	
Pt(1)-O(10) / O(11) [Å]	2.025(7) / 2.060(7)	Pt(1)-O(2) / O(3)	2.049(14) / 2.041(13)
Pt(1)-P(4) / P(5) [Å]	2.223(3) / 2.208(3)	Pt(1)-P(11) / P(12)	2.234(6) / 2.219(5)
O(10)-C(14) / O(11)-C(15)	1.330(11) / 1.364(12)	O(2)-C(4) O(3)-C(5)	1.31(2) / 1.32(2)
Pt(2)-O(19) / O(20)	2.044(6) / 2.025(7)		
Pt(2)-P(6) / P(7)	2.215(3) / 2.220(3)		
O(19)-C(23) / O(20)-C(24)	1.360(12) / 1.366(11)		
Pt(3)-O(28) / O(29)	2.039(6) / 2.052(5)		
Pt(3)-P(8) P(9)	2.218(3) / 2.208(2)		
O(28)-C(32) / O(29)-C(33)	1.366(9) / 1.359(10)		
O(10)-Pt(1)-O(11)	82.3(3)	O(3)-Pt(1)-O(2)	83.1(5)
P(5)-Pt(1)-P(4)	85.61(11)	P(12)-Pt(1)-P(11)	86.1(2)
O(10)-Pt(1)-P(5)	91.44(19)	O(2)-Pt(1)-P(12)	95.7(4)
O(11)-Pt(1)-P(4)	100.7(2)	O(3)-Pt(1)-P(11)	95.2(4)
O(10)-Pt(1)-P(4)	177.02(18)	O(2)-Pt(1)-P(11)	178.2(4)
O(11)-Pt(1)-P(5)	173.3(2)	O(3)-Pt(1)-P(12)	178.8(4)
O(20)-Pt(2)-O(19)	83.1(3)		
P(6)-Pt(2)-P(7)	85.53(10)		
O(19)-Pt(2)-P(7)	97.7(2)		
O(20)-Pt(2)-P(6)	93.70(19)		
O(19)-Pt(2)-P(6)	176.4(2)		
O(20)-Pt(2)-P(7)	179.1(2)		
O(28)-Pt(3)-O(29)	84.1(2)		
P(9)-Pt(3)-P(8)	85.41(10)		
O(28)-Pt(3)-P(9)	94.59(17)		
O(29)-Pt(3)-P(8)	95.98(19)		
O(28)-Pt(3)-P(8)	176.43(19)		
O(29)-Pt(3)-P(9)	178.55(19)		

3.2.3 Electrochemical analysis of complexes

Analysis of complexes **3.2 - 3.6** by cyclic voltammetry and differential pulse voltammetry in CH_2Cl_2/0.1 M $^nBu_4NPF_6$ at 298 K showed, in the majority of cases, the presence of at least three oxidation processes between $-0.35 \leq E_{½} \leq +0.10$ V (*vs.* Fc/Fc^+), as displayed in **Figure 3.17-Figure 3.21**. These processes may be attributed to the sequential oxidations of $[ctc]^{6-/5-/4-/3-}$ (cat/cat/cat ; sq/cat/cat ; sq/sq/cat ; sq/sq/sq), as illustrated in **Scheme 3.1**.

The three oxidation processes displayed by complex **3.2** acted to confirm the observations first reported by Bohle and Statsko,[10] whereby their original investigation showed three chemically reversible oxidations between $-0.3 \leq E_{½} \leq +0.1$ V *vs* $[FeCp_2]$ / $[FeCp_2]^+$. Perhaps unsurprisingly, the three oxidations of **3.4** are similar to those of **3.2**, although it displays an additional process centred at +0.23 V which is not displayed by **3.2**. The position of this oxidation, its intensity in the DPV compared to the previous three peaks and the peak shape leads to the assumption that this may be due to one or more daughter products arising from the partial decomposition of $[\mathbf{3.2}^{\bullet\bullet}]^{2+}$. Oxidation of **3.5** were shown by CV and DPV (**Figure 3.18**, **Figure 3.20**) to resemble that of **3.2**, with the presence of four oxidation processes also. Of these, the first and second oxidations appear at more positive potentials (-0.17 and -0.05 V for (**3.5**) as opposed to -0.35 and -0.17 V for (**3.2**)) whilst the third and fourth are in almost identical positions with significantly reduced peak intensities compared to the first two. Again, the fourth oxidation is understood to be a daughter product from the decomposition of $[\mathbf{3.5}^{\bullet\bullet}]^{2+}$ at the electrode surface. The redox profile of **3.3** was also investigated, and appeared to resemble that of **3.5** with the presence of at least four closely separated oxidations, which were all shifted to more positive potentials. The first process of the sequence appeared to offer some reversibility whilst upon further oxidation, all reversibility was lost assumed to be due to decomposition.

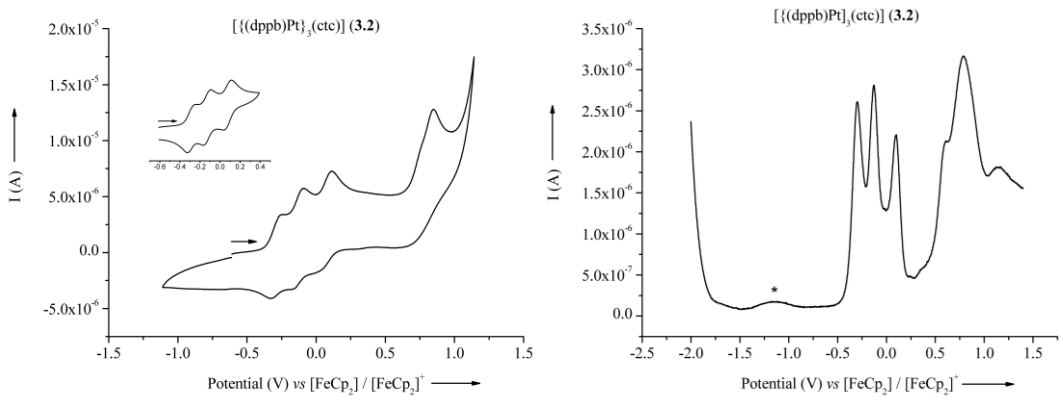

Figure 3.17. (Left) Cyclic voltammogram (CV) of [{(dppb)Pt}$_3$(ctc)] (**3.2)** in CH_2Cl_2/0.1 M nBu$_4$NPF$_6$ at 298 K. Insert shows a CV scan of the first three oxidations, highlighting some chemical reversibility. (Right) Differential pulse voltammogram (DPV) of [{(dppb)Pt}$_3$(ctc)] (**3.2)** in CH_2Cl_2/0.1 M nBu$_4$NPF$_6$ at 298 K The starred feature is likely a weak decomposition product.

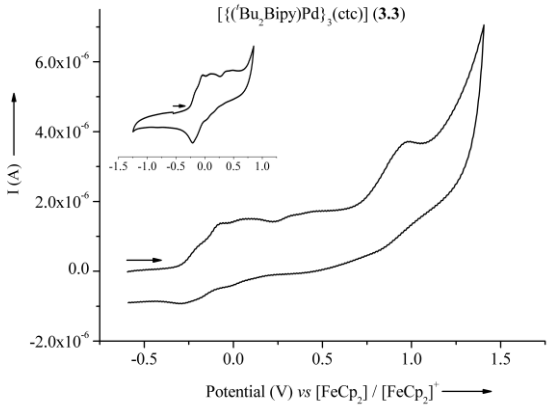

Figure 3.18. Cyclic voltammogram (CV) of [{(^{t}Bu$_2$Bipy)Pd}$_3$(ctc)] (**3.3**) in CH_2Cl_2/0.1 M ^{n}Bu$_4$NPF$_6$ at 298 K (0.1 V/s). Insert shows a CV scan of the first four oxidations, highlighting some chemical reversibility.

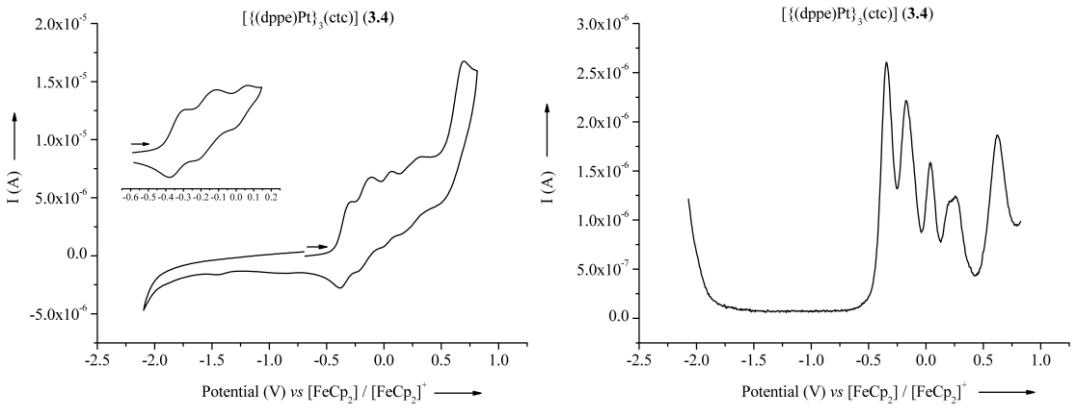

Figure 3.19. (Left) Cyclic voltammogram (CV) of [{(dppe)Pt}$_3$(ctc)] (**3.4)** in CH_2Cl_2/0.1 M nBu$_4$NPF$_6$ at 298 K. Insert shows a CV scan of the first three oxidations, highlighting some chemical reversibility. (Right) Differential pulse voltammogram (DPV) of [{(dppe)Pt}$_3$(ctc)] (**3.4)** in CH_2Cl_2/0.1 M nBu$_4$NPF$_6$ at 298 K

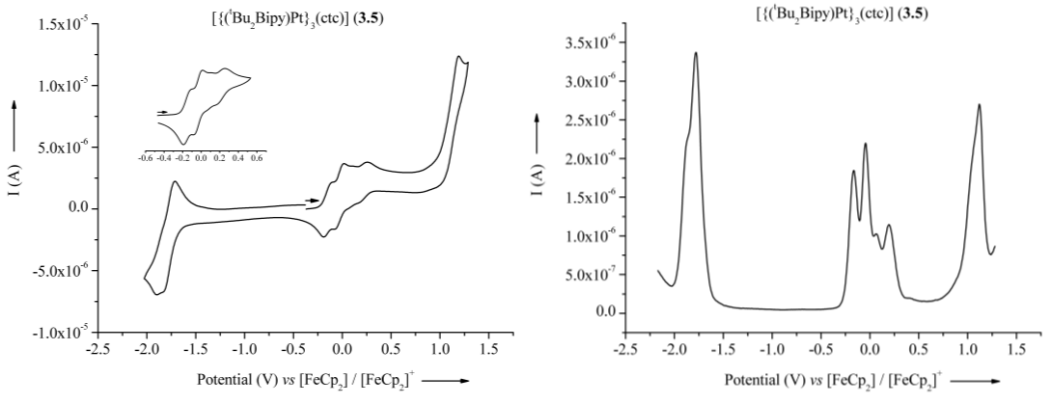

Figure 3.20. (Left) Cyclic voltammogram (CV) of [{(^{t}Bu$_2$Bipy)Pt}$_3$(ctc)] (**3.5**) in CH_2Cl_2/0.1 M nBu$_4$NPF$_6$ at 298 K. Insert shows a CV scan of the first four oxidations, highlighting some chemical reversibility. (Right) Differential pulse voltammogram (DPV) of [{(^{t}Bu$_2$Bipy)Pt}$_3$(ctc)] (**3.5)** in CH_2Cl_2/0.1 M nBu$_4$NPF$_6$ at 298 K .

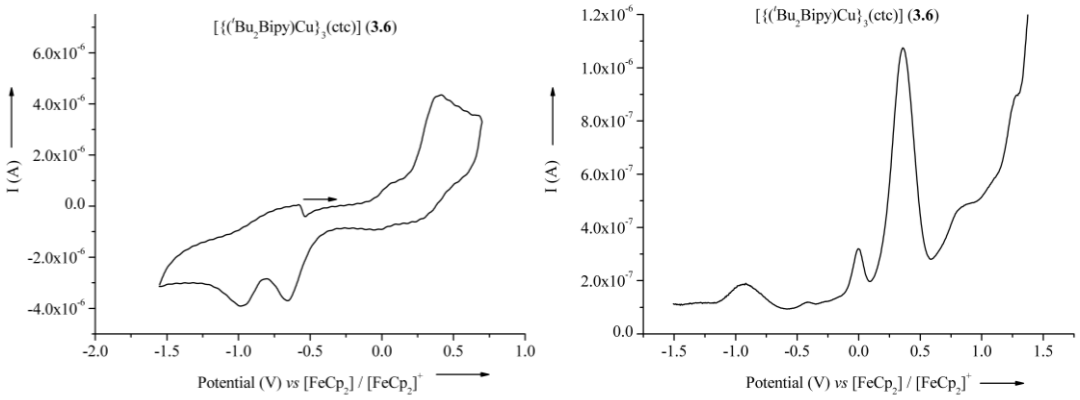

Figure 3.21. (Left) Cyclic voltammogram (CV) of [{(^{t}Bu$_2$Bipy)Cu}$_3$(ctc)] **(3.6)** in CH_2Cl_2/0.1 M nBu$_4$NPF$_6$ at 298 K (0.1 V/s). (Right) Differentail pulse voltammogram (DPV) of [{(^{t}Bu$_2$Bipy)Cu}$_3$(ctc)] **(3.6)** in CH_2Cl_2/0.1 M nBu$_4$NPF$_6$ at 298 K.

Peak-to-peak and $E_{½}$ separations for the first three oxidation processes in complexes **3.2** and **3.4** (ΔE_p and $\Delta E_{½}$ = 0.18 – 0.22 V) are larger than for **3.5** (ΔE_p and $\Delta E_{½}$ = 0.12 V), indicating there is some moderate-to-weak communication between the dioxolene rings in each complex. Similar separations for the oxidative processes of $[thea]^{4-}$ (see chapter 4) and $[spiro]^{4-}$, which are both separated by methylene spacers, equal 0.25 V and 0.15 V respectively.[5]

Complexes **3.2-3.5** also display a series of irreversible oxidation processes between +0.6 - 1.1 V corresponding to the oxidation processes $[ctc]^{3-/2-/-/0}$ (sq/sq/sq ; q/sq/sq ; q/q/sq ; q/q/q). For complex **3.2** this is clearly split into at least two processes with separations of 0.16 V whilst complexes **3.4** and **3.5** this process appears as one process (despite **3.5** displaying a slight shoulder, this is not discernible). Complex **3.5** also displays a chemically reversible, three electron reduction process centred at -1.8 V which is split into at least two components in the DPV, corresponding to the reduction of the ^{t}Bu$_2$Bipy ancillary ligands. Unfortunately, these could not be determined in complex **3.3**.

Cyclic and differential pulse voltammetric analysis of complex **3.6** over the same region displayed one small redox process at E_P = 0.06 V *vs* $[FeCp_2]$ / $[FeCp_2]^+$ and one large irreversible oxidation at 0.40 V. The position of these processes indicate they are associated with oxidation of $[ctc]^{6-}$ and concomitant release of the Cu(II) metal ion. These two peaks is also visible in the DPV at 0 and +0.36 V respectively, with the latter displaying large intensity therefore indicating a multi-electron redox process. As a result of this oxidation, the irreversible peak at -0.66 V corresponds to the reduction of free solvated Cu(II) to metallic copper on the electrode surface.[23] It is key to note that this peak does not appear if the scan is run in the opposite direction or in the DPV. The identity of the following peak at

-0.97 V is unclear, although does appear if the scan is conducted in the opposite direction therefore is associated with intact **3.6** and is in a similar position to the reduction of complexed Cu(II) as seen in complexes containing [(phen)Cu(DBCat)].[24] As a result, this peak is associated with the reduction of complexed Cu(II) → Cu(I) in $[\{(^{t}Bu_2Bipy)Cu\}(ctc)]^{n-}$, and is irreversible likely due to a structural rearrangement associated with the process.[25] This peak is also visible in the same position in the DPV, although severely broadened.

Table 3.3. Cyclic voltammetric (CV) data for complexes **3.2 – 3.6** recorded in dichloromethane / 0.1 M NBu_4PF_6 at 298 K. Potentials (V) are referenced against an internal $[FeCp_2]$ / $[FeCp_2]^+$ standard, and were measured at a scan rate of 0.1 Vs^{-1}.

	$E_{½}$ $[^{t}Bu_2Bipy]^{-/0}$	$E_{½}$ $[ctc]^{n-}$ cat / sq			$E_{½}$ $[ctc]^{n-}$ sq/q (irr.)
$[\{(dppb)Pt\}_3(ctc)]$ (**3.2**)[a]	–	-0.29	-0.09	+0.07	+0.69
$[\{(^{t}Bu_2Bipy)Pd\}_3(ctc)]$ (**3.3**)	–	-0.11	0.13	0.44	+0.96
$[\{(dppe)Pt\}_3(ctc)]$ (**3.4**)	–	-0.35	-0.17	+0.03, +0.29	+0.85
$[\{(^{t}Bu_2Bipy)Pt\}_3(ctc)]$ (**3.5**)	–1.79	-0.16	-0.04	+0.07, +0.22	+1.19[b, c]
$[\{(^{t}Bu_2Bipy)Cu\}_3(ctc)]$ (**3.6**)	–	0.40[c]			

[a]Literature cat / sq $E_{½}$ = +0.04, +0.24, +0.49 V *vs* NHE.[10] [b] Partly chemically reversible. [c] $[ctc]^{3-/2-}$, $[ctc]^{2-/-}$ and $[ctc]^{-/0}$ half-potentials are indistinguishable. [c] Decomposition.

Table 3.4. Differential Pulse Voltammetric (DPV) data for complexes **3.2 – 3.6** recorded in dichloromethane / 0.1 M NBu_4PF_6 at 298 K.. Potentials (V) are referenced against an internal $[FeCp_2]$ / $[FeCp_2]^+$ standard, and were measured at a scan rate of 0.1 Vs^{-1}.

	E_p $[^{t}Bu_2Bipy]^{-/0}$	E_p $[ctc]^{n-}$ cat / sq			E_p $[ctc]^{n-}$ sq/q (irr.)
$[\{(dppb)Pt\}_3(ctc)]$ (**3.2**)	–	0.30	0.12	+0.10	+0.62
$[\{(dppe)Pt\}_3(ctc)]$ (**3.4**)	–	-0.35	-0.17	+0.04, +0.23	+0.61(sh), +0.79
$[\{(^{t}Bu_2bipy)Pt\}_3(ctc)]$ (**3.5**)	–1.86 (sh), -1.78	-0.17	-0.05	+0.07, +0.20	+1.12
$[\{(^{t}Bu_2bipy)Cu\}_3(ctc)]$ (**3.6**)		0.36[a]			

(sh) = Shoulder. [a] Decomposition.

In addition to the electrochemical analysis of complexes **3.2** – **3.6**, electrochemical analysis of compound cyclotricatechylene itself (**2.5)** was also performed as unsubstituted catechol (H_2cat) is a well-known redox-active unit.[26] At neutral pH, compound **2.5** displayed two irreversible waves shown by cyclic voltammetry at E_{pa} = 0.34 and E_{pb} = 0.45 V (*vs* $[FeCp_2]$ /

$[FeCp_2]^+$) along with a large number of peaks at negative potentials, presumably due to daughter products arising from decomposition. DPV analysis of the solution across the same region showed the presence of one large peak at E_{pa} = 0.25 V (*vs* $[FeCp_2]$ / $[FeCp_2]^+$) and a shoulder at 0.37 V (*vs* $[FeCp_2]$ / $[FeCp_2]^+$). The asymmetry of the peak again indicates its irreversibility, confirming what was shown by cyclic voltammetry. These two peaks were identified as rapid, two electron oxidation processes of each catechol ring to their corresponding *o*-quinones, all occurring at the same time. Their irreversibility is shared by H_2cat, although their position is shifted significantly more negative compared to H_2cat which displays one irreversible wave at +1.21 V (*vs* Ag / AgCl in acetonitrile / $^nBu_4NBF_4$).[27] This large shift is likely due to the instability of the complex once oxidised, resulting in rapid oxidation of the remaining catechol ring(s) whilst the accumulation of positive charge on the whole molecule likely forces its dissociation, resulting in an irreversible process. In addition to these cathodic processes, the presence of a large irreversible reduction at -2.32 V is likely due to the reduction of free protons in solution[24] whilst reduction peaks between -0.39 and -1.35 V are due to daughter products arising from decomposition.

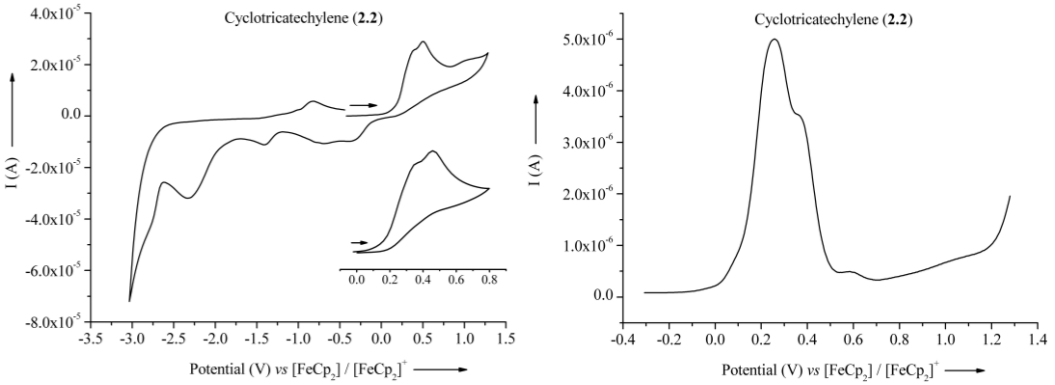

Figure 3.22. (Left) Cyclic voltammogram (CV) of cyclotricatechylene **(2.2)** in DMF/0.1 M nBu$_4$NPF$_6$ at 298 K (0.1 V/s). (Right) Differentail pulse voltammogram (DPV) of cyclotricatechylene **(2.2)** in DMF/0.1 M nBu$_4$NPF$_6$ at 298 K (0.1 V/s)

Addition of a non-nucleophilic base, to the solution in order to clear the protons lost from **2.2** once oxidised, and hopefully simplify the oxidative processes, was also attempted. Oxidation over the same region in the presence of 2,6-lutidine resulted in a more complex spectrum. Analysis by cyclic voltammetry again showed the oxidations were irreversible, but displayed an increased number of processes compared to the analysis without 2,6-lutidine. The number of oxidation processes increased from two to five, with the first three between $0 \leq E_p \leq +0.23$ V (*vs* $[FeCp_2]$ / $[FeCp_2]^+$) assumed to be due to the oxidation of each catecholate ring to their corresponding semiquinones in quick succession. These processes are followed immediately after by further oxidations, the first at +0.38 V, likely

the corresponding semiquinone → quinone oxidation which is again irreversible, followed by their decomposition and +0.59 V. Analysis over the same region by differential pulse voltammetry shows these processes much more clearly; the first three evident between -0.04 ≤ E_p ≤ +0.17 V (*vs* Ferrocene), again corresponding to the cat → sq oxidation of each ring which are all overlapping. The sequential decrease in intensity of each succeeding peak indicates their decomposition at the electrode surface. These are followed immediately by one large peak, at +0.31 V, close to that seen in the cyclic voltammogram, again corresponding to the sq → q oxidation. It is interesting to note the symmetry of this peak which indicates a reversible process. This is followed by an asymmetric peak at +0.52 V, likely due to decomposition as seen in the cyclic voltammogram. It is key to note here the significant shift in potential of these oxidations, compared to the instance where no base is present. This pH dependent shift has also been seen in the electrochemical analysis of other catechols and has been attributed to the removal of protons which may help stabilise the oxidised species *via* coordination to one or two of the dioxolene oxygens.[24, 28]

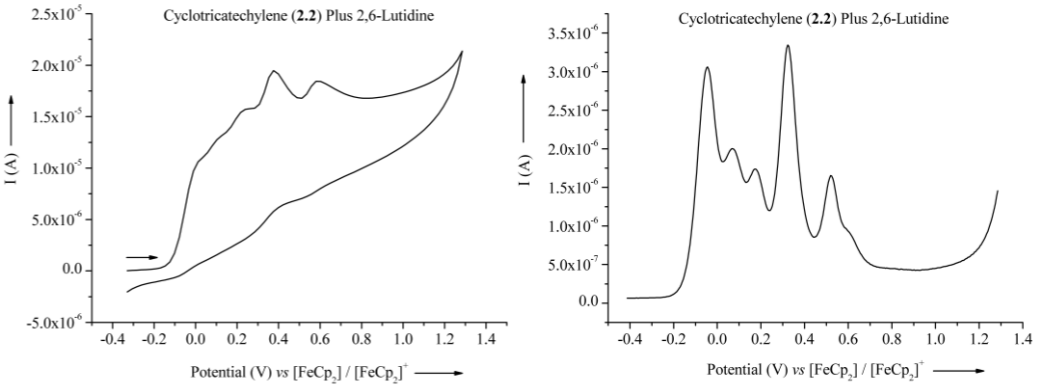

Figure 3.23. (Left) Cyclic voltammogram (CV) of cyclotricatechylene **(2.2**) plus 2,6-lutidine in DMF/0.1 M $^{n}Bu_4NPF_6$ at 298 K (0.1 V/s). (Right) Differential pulse voltammogram (DPV) of cyclotricatechylene **(2.2**) plus 12 equivalents of 2,6-lutidine in DMF/0.1 M nBu$_4$NPF$_6$ at 298 K (0.1 V/s).

Table 3.5. Cyclic voltammetric (CV) data for ctc (**2.2**) with and without 2,6-lutidine, recorded in DMF / 0.1 M NBu_4PF_6 at 298 K. Potentials (V) are referenced against an internal $[FeCp_2]$ / $[FeCp_2]^+$ standard, and were measured at a scan rate of 0.1 Vs^{-1}

	E_p $[ctc]^{n-}$ cat / sq (irr.)			E_p $[ctc]^{n-}$ sq/q (irr.)
ctc (**2.2**)	-+0.40[b]			+0.50
ctc (**2.2**)[a]	+0.01	+0.12	+0.23	+0.38, +0.59[b]

[a] Sample plus 2,6-lutidene. [b] Decomposition.

Table 3.6. Differential pulse voltammetric (DPV) data for ctc (**2.2**) with and without 2,6-lutidine, recorded in DMF / 0.1 M NBu_4PF_6 at 298 K. Potentials (V) are referenced against an internal $[FeCp_2]$ / $[FeCp_2]^+$ standard, and were measured at a scan rate of 0.1 Vs^{-1}

	E_p $[ctc]^{n-}$ cat / sq (irr.)			E_p $[ctc]^{n-}$ sq/q (irr.)
ctc (**2.2**)	-+0.25[b]			+0.37(sh)
ctc (**2.2**)[a]	-0.04	+0.07	+0.18	+0.32, +0.52, +0.60(sh)[b]

[a] Sample plus 2,6-lutidene. [b] Decomposition.

3.2.4 Electronic Absorbance Spectra of Complexes

As complexes **3.2 – 3.5** displayed a capability to be oxidised sequentially, the first thought was to monitor these optically by UV/vis-NIR oxidative titrations by adding appropriate aliquots of oxidant ferrocenium hexafluorophosphate ($[FeCp_2]PF_6$). This process was first attempted using complex **3.3**, however immediate precipitation and bleaching of the solution precluded any further analysis, th reaction was therefore instead attempted with **3.4**.

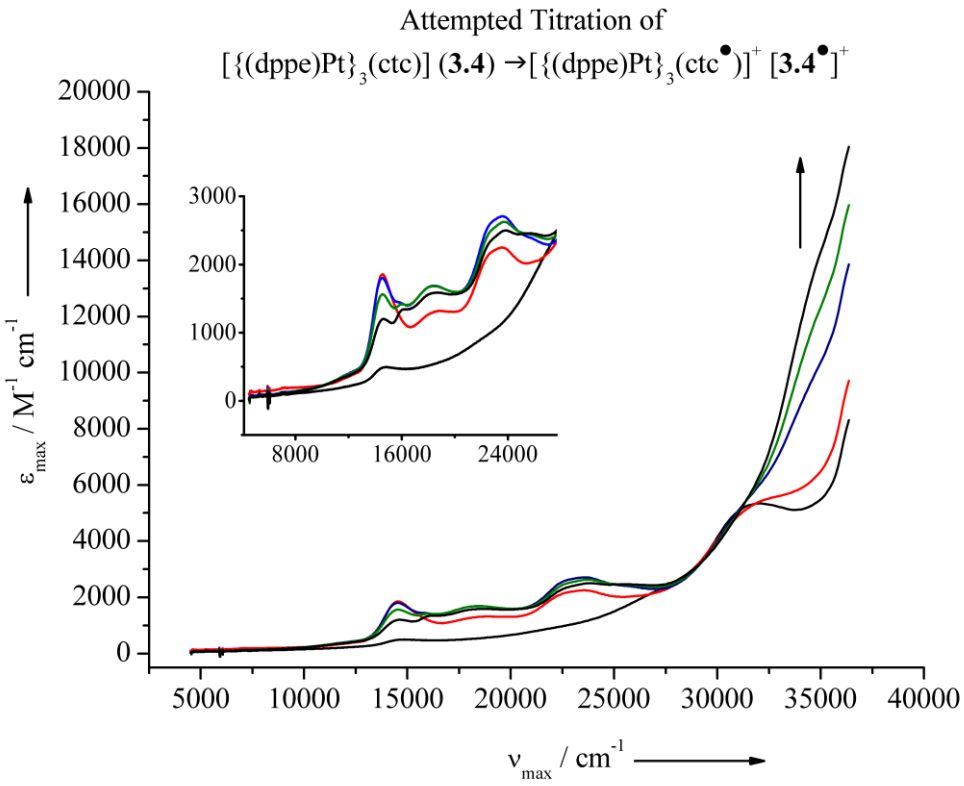

Figure 3.24. Attempted oxidative titration of [{(dppe)Pt]$_3$(ctc)] (**3.4**) → [{(dppe)Pt]$_3$(ctc$^{\bullet}$)]$^+$ **[3.4$^{\bullet}$]**$^+$ by addition of [FeCp$_2$]PF$_6$. Insert shows a close-up of the region 7,000 – 27,000 cm^{-1} highlighting decomposition of the complex upon oxidation. Colour code: Black, 0 and 1.0 equivalents of oxidant; Red, 0.25 equivalents of oxidant ; Blue, 0.50 equivalents of oxidant ; Green, 0.75 equivalents of oxidant.

As can be seen in **Figure 3.24** above, after the addition of 0.25 equivalents of [FeCp$_2$]PF$_6$ the temperature and air sensitivity of oxidised products quickly became apparent where rapid bleaching and non-isobesticity of the obtained spectra were obvious indicating decomposition of the initial complex after the addition of 0.25 equivalents of [FeCp$_2$]PF$_6$ (red line). Whilst detailed analysis of the spectra is inappropriate due to the decomposition, a minor increase in baseline after addition of 0.25 equivalents of oxidant at approximately 7,100 cm^{-1} was noted, although rapidly quenched upon addition of further oxidant (see **Figure 3.24** insert).

UV-vis analysis of complexes **3.6** and **3.3** was also performed across the region 12,500 to 42,000 cm^{-1}, and are both displayed in **Figure 3.25**. Complex **3.3** displayed one large absorbance across this region at ν_{max} = 32,500 cm which can be assigned to the electron rich catechol → bipy LLCT,[29] the low energy absorption at approximately 18,000 cm^{-1} may be assigned as a Pd(dπ) → bipy(π*) backbonding whilst the shoulder at 39,000 cm^{-1} is likely a bipyridine intraligand π → π* transition.[30] The electronic spectrum recorded of **3.6** is

similar to previously reported copper-catecholate complexes, with two intense absorptions at approximately 40,000 and 33,500 cm^{-1} corresponding to two intraligand absorptions of the bipyridine unit.[31] Intraligand absorptions of the catechol units are expected in this region also although it is likely that they are dwarfed by those from the bipyridine ligand.[32] In addition to these absorptions, there is also a very broad absorbance centred at approximately 26,000 cm^{-1}. Owing to the extinction coefficient associated with the absorbance (6, 600 $M^{-1}cm^{-1}$), and its relatively high energy it is unlikely to be a symmetry forbidden d-d transition therefore is understood to be due to a charge transfer from ctc cat → bipy LL'CT.[31] The broadness of the absorbance between 12, 600 and 23,000 cm^{-1} does not exclude the presence of a d-d transition within the complex, which generally appear between 14,000 and 20,000 cm^{-1} with extinction coefficients of 10^2 $M^{-1}cm^{-1}$, although further investigations would have to performed to confirm this assignment.

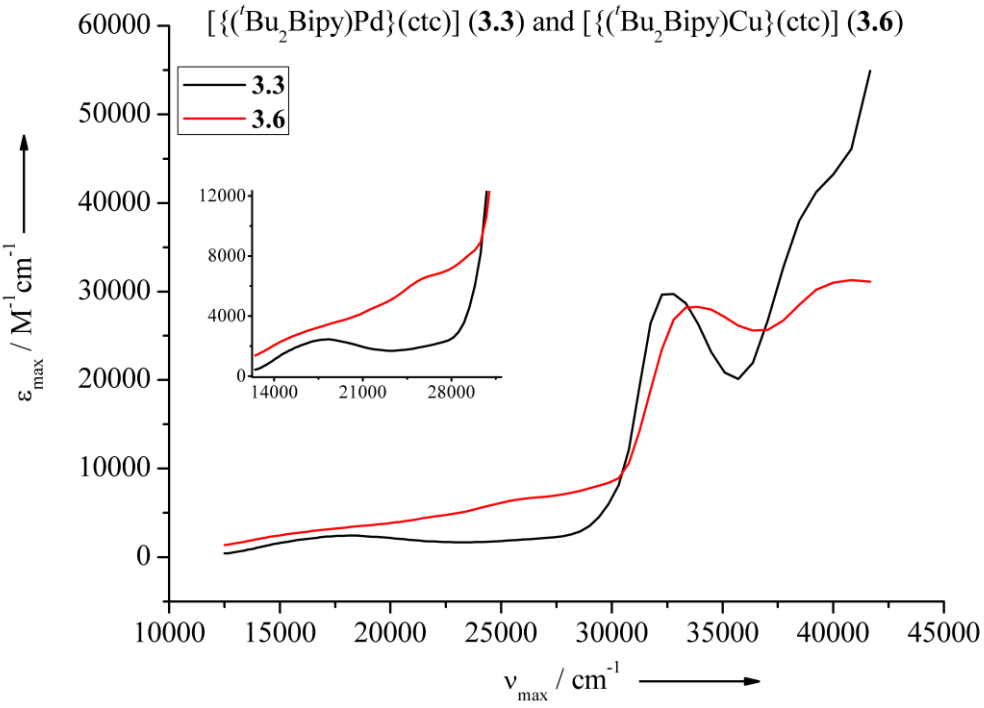

Figure 3.25. UV-vis electronic absorbance spectra of [{(^{t}Bu$_2$Bipy)Pd}$_3$(ctc)] (**3.3**, black line) and [{(^{t}Bu$_2$Bipy)Cu}$_3$(ctc)] (**3.6**, red line).

For comparative purposes, and to aid spectral characterisation, oxidative titrations of mononuclear complexes **3.7 (Figure 3.26)** and **3.8 (Figure 3.27)** were also performed, again using $[FeCp_2]PF_6$ at 295 K in dichloromethane and both proceeded isobestically, and to full completion as shown by the closeness of lines towards the end of each titration. As the oxidation of **3.8** has been previously described,[15b] it will not be discussed but will be used

as an aid to describe the spectral differences in **3.7**. Of the spectral differences noticed for **3.7** upon oxidation, the major change was at approximately 24,000 cm^{-1} with the growth of a new band. The position of this band is similar to previously reported platinum-semiquinone complexes, and it is present in $[\mathbf{3.8}]^+$ therefore indicates it is a Pt(dπ) → sq MLCT. In addition, the growth of low intensity band at approximately 14,300 cm^{-1} is also shared with $[\mathbf{3.8}]^+$ and has also been attributed to the Pt(dσ) → sq MLCT. Decay of absorptions at 28,800 cm^{-1} and growth of absorbance at 32,000 cm^{-1} upon oxidation are absent in the spectrum of **3.8** therefore impling that they are due to the presence of the diphosphine ancillary ligand. As a result, these could be attributed to interligand charge transfer absorptions. The first, as the decrease of absorbance at 28,000 cm^{-1} is likely a LL'CT between electron rich cat → diphosphine whilst growth of new absorbance at 32,000 cm^{-1} could potentially be the opposite sq → diphosphine LL'CT.

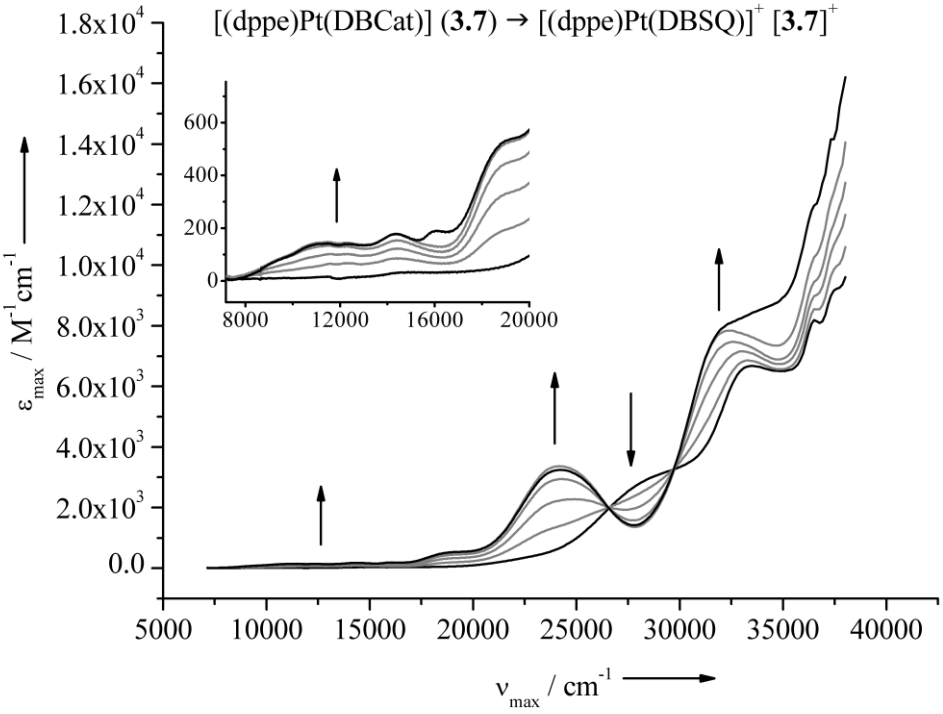

Figure 3.26. Oxidative titration of [(dppe)Pt(DBCat)] **(3.7).** Pure **3.7** and $[\mathbf{3.7}]^+$ are shown in black and intermediate spectra re shown in grey. Insert shows a close-up of band at approximately 12,000 cm^{-1}.

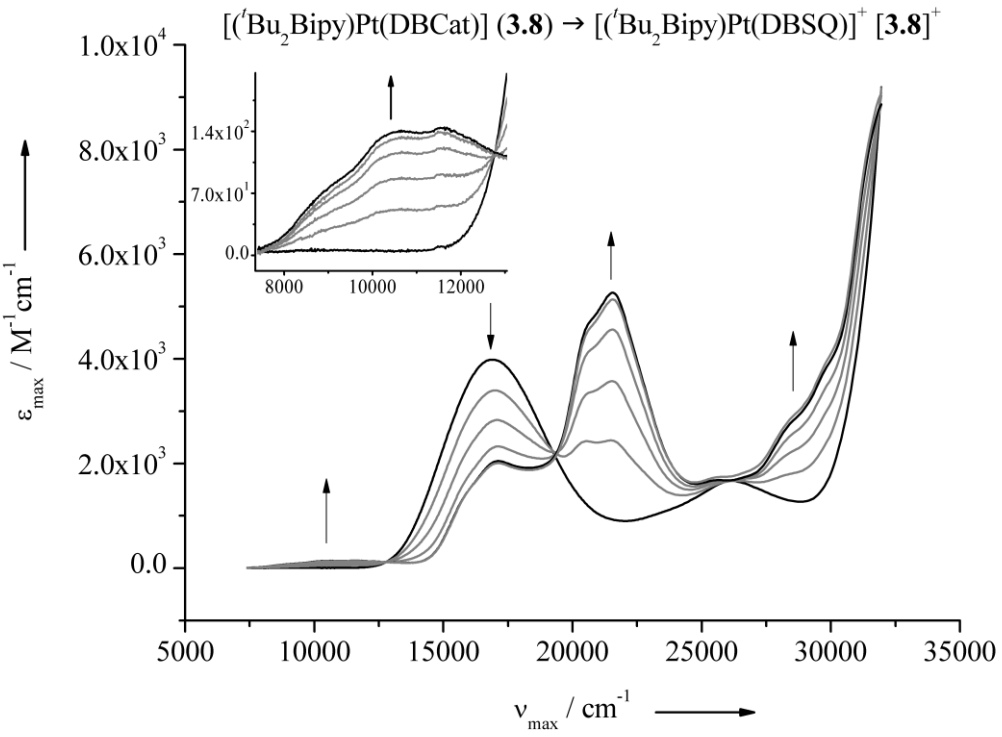

Figure 3.27. Oxidative titration of [(^{t}Bu$_2$Bipy)Pt(DBCat)] **(3.8).** Pure **3.8** and [**3.8**$^{\bullet}$]$^+$ are shown in black and intermediate spectra re shown in grey**.** Insert shows a close-up of the band at approximately 10,000 cm^{-1}.

3.2.5 Spectroelectrochemical analysis of complexes

Due to the non-isobesticity noted in the chemical oxidations using ferrocenium hexafluorophosphate at 298 K, it was decided to analyse the complexes spectroelectrochemically at 253 K in deoxygenated CH_2Cl_2/0.1 M ^{n}Bu$_4$NPF$_6$ in an optically transparent electrode (OTTLE) cell. Unfortunately, complex **3.4** was shown to be too insoluble at the low temperature required to acquire accurate spectroscopic data without decomposition, therefore its spectroelectrochemical analysis was omitted. Due to the small potential separation in both complexes **3.2** and **3.5**, difficulties were encountered in poising the potential at a position to oxidise each species individually although there were sufficient differences between the different oxidised species to permit their individual analysis.

Oxidation of complex **3.2** to **[3.2$^{\bullet}$]$^+$**, as shown in **Figure 3.28**, led to the growth of a very broad NIR absorption at 7,900 cm^{-1} which may be assigned as an intervalence charge transfer (IVCT) arising from the change in oxidation state of one dioxolene ring, whilst peaks between 14,400 and 15,700 also show an increase in intensity, and may be assigned as Pt → sq metal-to-ligand charge transfers (MLCT). The dppb intraligand absorbance at

32,200 cm^{-1} shows no significant change in intensity, but shifts to a higher energy by 200 cm^{-1}, putting it closer to that found in the dichloride precursor [(dppb)$PtCl_2$] at 32,700 cm^{-1}.[33] Further oxidation of **[3.2$^{\bullet}$]$^{+}$** to **[3.2$^{\bullet\bullet}$]$^{2+}$** results in an increase in extinction coefficient for both IVCT and LL'CT, with a significant IVCT red-shift of 800 cm^{-1} to 7,100 cm^{-1}. The attempted oxidation of **[3.2$^{\bullet\bullet}$]$^{2+}$** to **[3.2$^{\bullet\bullet\bullet}$]$^{3+}$** was nearly isobestic and resulted in the decrease in intensity of the IVCT as expected and decrease in intensity of the dppb intraligand absorption at 32,400 cm^{-1}. Attempted re-reduction of **[3.2$^{\bullet\bullet\bullet}$]$^{3+}$** to **[3.2$^{\bullet\bullet}$]$^{2+}$** or **[3.2$^{\bullet}$]$^{+}$**, by cycling the potential back to -0.4 V *vs* ferrocene displayed some regeneration of the IVCT transition indicating reassembly of the radical species at the electrode surface which is supported by the chemical reversibility of the **[3.2$^{\bullet\bullet\bullet}$]$^{3+}$ / [3.2$^{\bullet\bullet}$]$^{2+}$** and **[3.2$^{\bullet\bullet}$]$^{2+}$ / [3.2$^{\bullet}$]$^{+}$** couples.

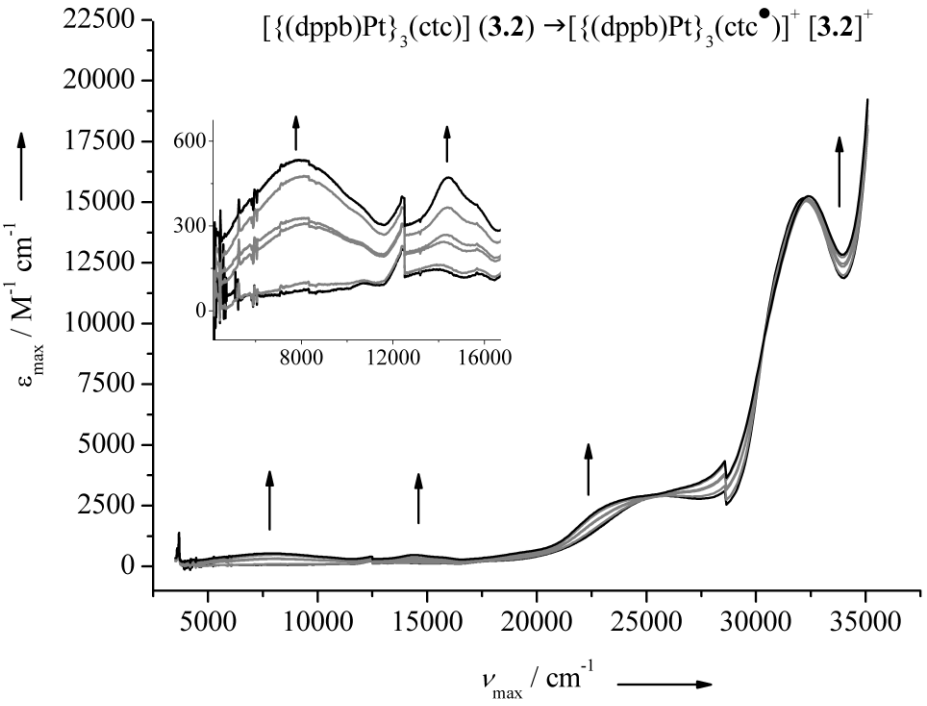

Figure 3.28. UV-vis/NIR spectroelectrochemical data at 253 K in CH_2Cl_2 / 0.1 $^{n}Bu_4NPF_6$ for the oxidation of [{(dppb)Pt}$_3$(ctc)] [**3.2**] → [{(dppb)Pt}$_3$(ctc$^{\bullet}$)]$^{+}$ [**3.2$^{\bullet}$**]$^{+}$. The spectra of pure **3.2** and cation [**3.2$^{\bullet}$**]$^{+}$ are shown in black, whilst intermediate spectra are shown in grey.

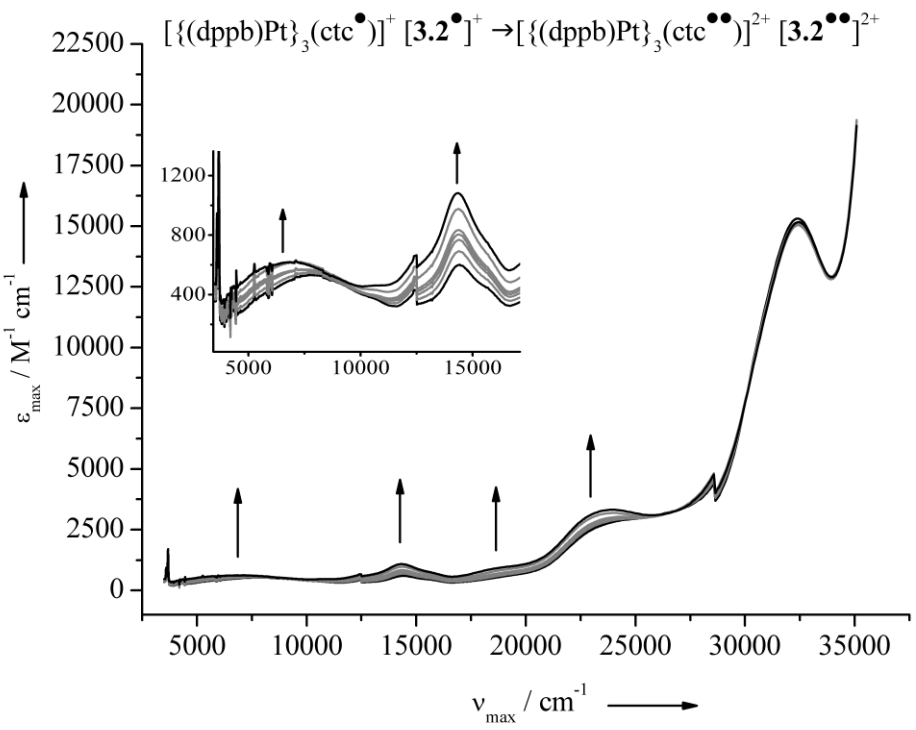

Figure 3.29. UV-vis/NIR spectroelectrochemical data at 253 K in CH_2Cl_2 / 0.1 $^nBu_4NPF_6$ for the oxidation of $[\{(dppb)Pt\}_3(ctc^{\bullet})]^+$ $[\mathbf{3.2}^{\bullet}]^+ \rightarrow [\{(dppb)Pt\}_3(ctc^{\bullet\bullet})]^{2+}$ $[\mathbf{3.2}^{\bullet\bullet}]^{2+}$. The spectra of pure cation $[\mathbf{3.2}^{\bullet}]^+$ and di-cation $[\mathbf{3.2}^{\bullet\bullet}]^{2+}$ are shown in black, whilst intermediate spectra are shown in grey.

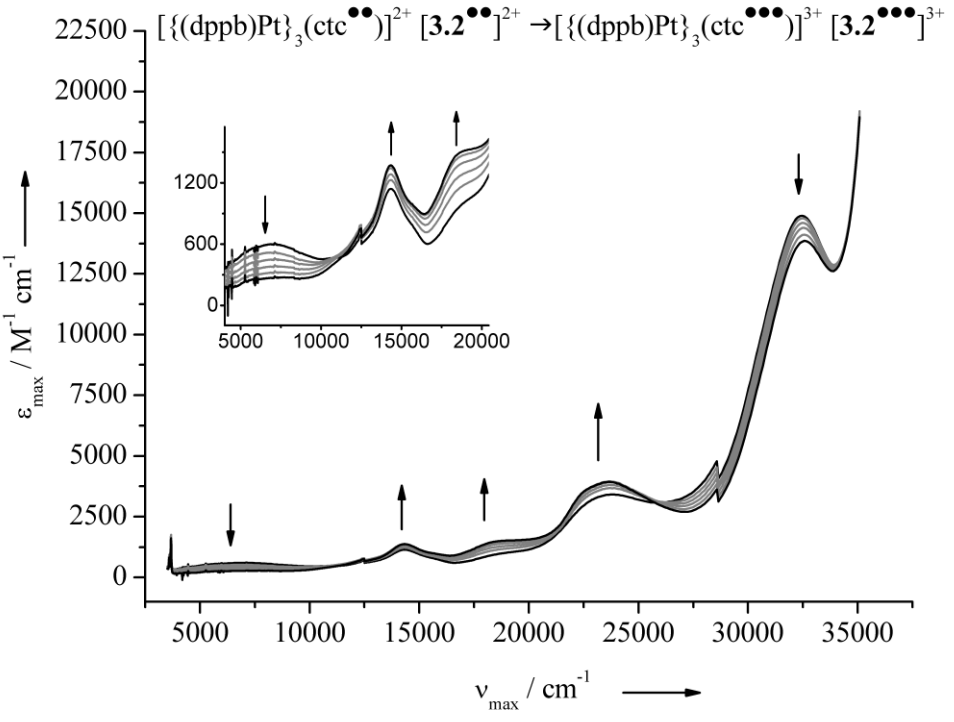

Figure 3.30. UV-vis/NIR spectroelectrochemical data at 253 K in CH_2Cl_2 / 0.1 $^nBu_4NPF_6$ for the oxidation of $[\{(dppb)Pt\}_3(ctc^{\bullet\bullet})]^+$ $[\mathbf{3.2^{\bullet\bullet}}]^{2+}$ → $[\{(dppb)Pt\}_3(ctc^{\bullet\bullet})]^{2+}$ $[\mathbf{3.2^{\bullet\bullet\bullet}}]^{3+}$. The spectra of pure di-cation $[\mathbf{3.2^{\bullet\bullet}}]^+$ and tri-cation $[\mathbf{3.2^{\bullet\bullet\bullet}}]^{3+}$ are shown in black, whilst intermediate spectra are shown in grey.

Oxidation of **3.5** to $\mathbf{[3.5^{\bullet}]^+}$ again results in the growth of an IVCT absorption, although at a lower energy (6,200 cm^{-1}) compared to that observed in $\mathbf{[3.2^{\bullet}]^+}$. The intensity of the cat → bipy LLCT absorption at 17,500 cm^{-1} does not increase greatly during the course of the oxidation, although it does experience a small blue-shift of approximately 500 cm^{-1} to 18,000 cm^{-1}.[15a] A new peak close to 21,000 cm^{-1} was seen to grow in during the course of the oxidation, and is assignable as a Pt($d\pi$)→sq MLCT[34] whilst a peak at approximately 27,000 cm^{-1}, which blue-shifts slightly upon oxidation, is present in the (^{t}Bu$_2$Bipy)$PtCl_2$ precursor therefore assignable to the Pt→bipy MLCT.[15a] Further oxidation of $\mathbf{[3.5^{\bullet}]^+}$ to $\mathbf{[3.5^{\bullet\bullet}]^{2+}}$, displayed a significant increase in IVCT ε_{max} of 3,300 $M^{-1}cm^{-1}$ and as with the oxidation of $\mathbf{[3.2^{\bullet}]^+ \rightarrow [3.2^{\bullet\bullet}]^{2+}}$, the absorption experienced an almost identical red-shift of 800 cm^{-1} from 6, 200 cm^{-1} to 5,400 cm^{-1}. Again, small increases in the cat → bipy LLCT peak at 18,000 cm^{-1} were noted whilst the two flanking peaks at 21, 000 and 14,000 cm^{-1} also experience increases in intensity. The introduction of a weak absorption at 11,000 cm^{-1} was also observed, corresponding to a Pt($d\sigma$)→sq MLCT absorption.[34] As with the oxidation of $[\mathbf{3.2^{\bullet\bullet}}]^{2+}$ to $[\mathbf{3.2^{\bullet\bullet\bullet}}]^{3+}$, the oxidation of $\mathbf{[3.5^{\bullet\bullet}]^{2+} \rightarrow [3.5^{\bullet\bullet\bullet}]^{3+}}$, again proceeded non-isobestically with bleaching of the spectra and decay of IVCT again likely due to the

decomposition of **3.5**. As with **3.2**, re-reduction of **[3.5$^{\bullet\bullet\bullet}$]$^{3+}$** resulted in the re-introduction of IVCT absorption at 5,200 cm^{-1} which is within experimental error of the position of the band at 5,400 cm^{-1} for **[3.5$^{\bullet\bullet}$]$^{2+}$**. This indicates that, as with complex **3.2**, **3.5** may be reassembled from its respective constituents at the electrode surface which is in agreement with what is observed in the cyclic-voltammetric analysis of **3.5** whereby the **[3.5$^{\bullet}$]$^{+}$** ⇆ **[3.5$^{\bullet\bullet}$]$^{2+}$** couple is clearly reversible despite the decomposition of **3.5** on the electrode face (**Figure 3.20**).

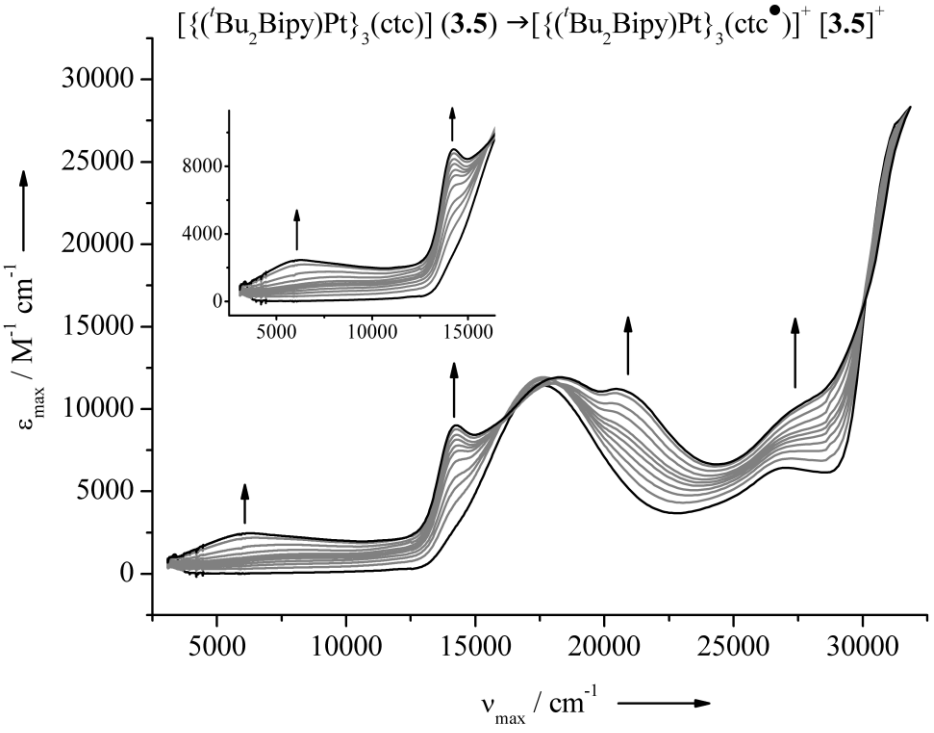

Figure 3.31. UV-vis/NIR spectroelectrochemical data at 253 K in CH_2Cl_2 / 0.1 $^{n}Bu_4NPF_6$ for the oxidation of [{(^{t}Bu$_2$Bipy)Pt}$_3$(ctc)] (**3.5**) → [{(^{t}Bu$_2$Bipy)Pt}$_3$(ctc$^{\bullet}$)]$^{+}$ [**3.5**$^{\bullet}$]$^{+}$. The spectra of pure 3.5 and mono-cation [3.5$^{\bullet}$]$^{+}$ are shown in black, whilst intermediate spectra are shown in grey.

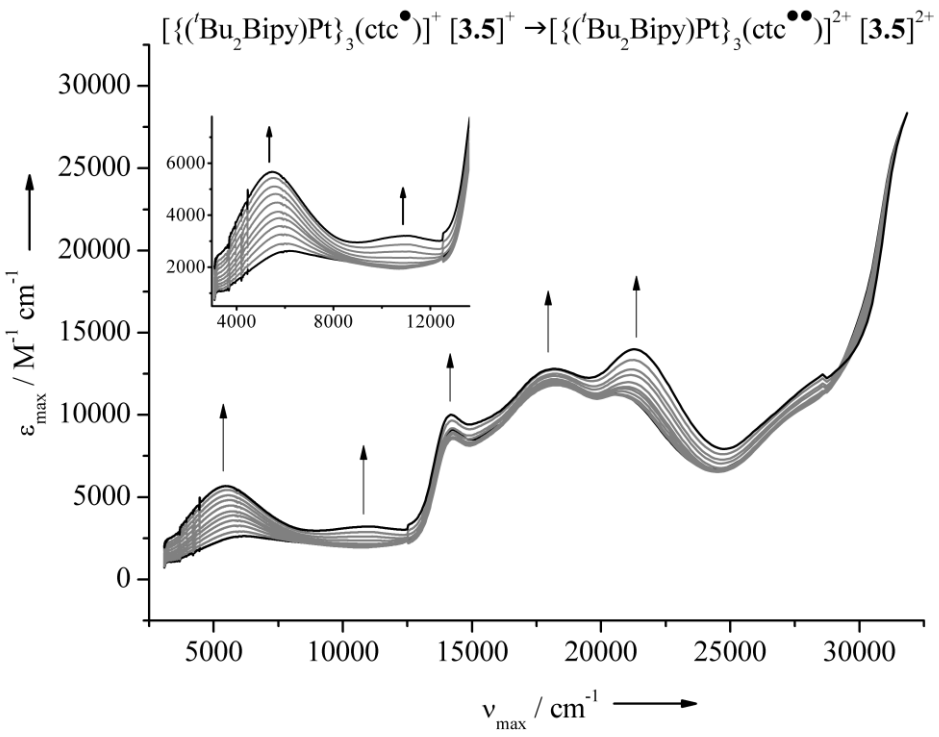

Figure 3.32. UV-vis/NIR spectroelectrochemical data at 253 K in CH_2Cl_2 / 0.1 $^nBu_4NPF_6$ for the oxidation of $[\{(^tBu_2Bipy)Pt\}_3(ctc^{\bullet})]^+$ $[\mathbf{3.5}^{\bullet}]^+ \rightarrow [\{(^tBu_2Bipy)Pt\}_3(ctc^{\bullet\bullet})]^{2+}$ $[\mathbf{3.5}^{\bullet\bullet}]^{2+}$. The spectra of pure mono-cation $[\mathbf{3.5}^{\bullet}]^+$ and di-cation $[\mathbf{3.5}^{\bullet\bullet}]^{2+}$ are shown in black, whilst intermediate spectra are shown in grey.

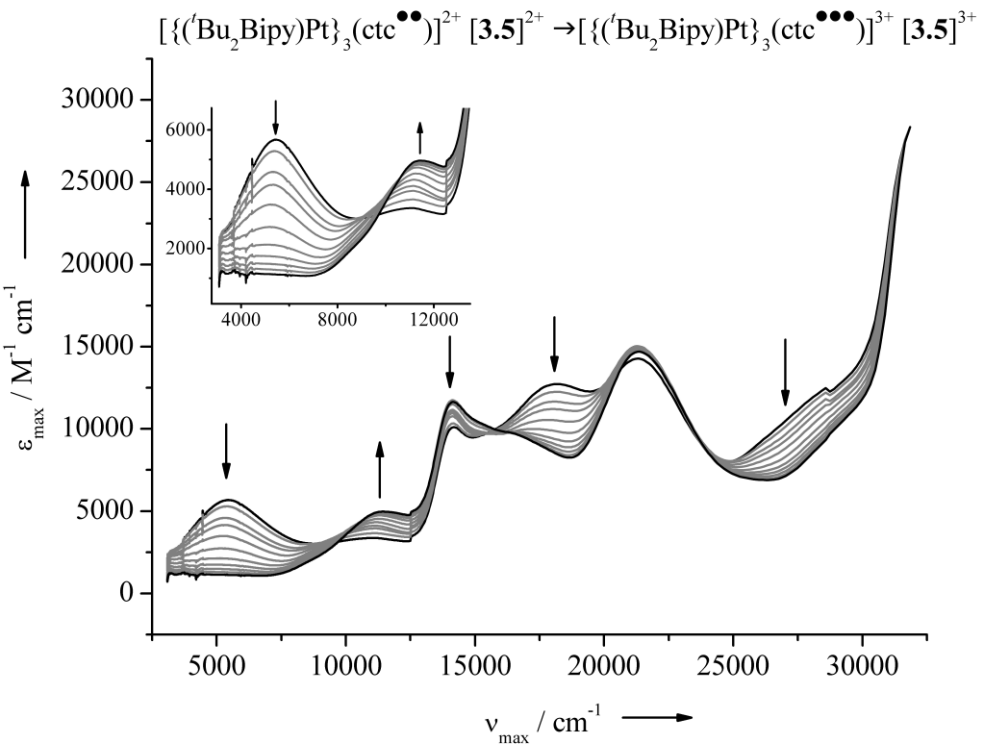

Figure 3.33. UV-vis/NIR spectroelectrochemical data at 253 K in CH_2Cl_2 / 0.1 $^nBu_4NPF_6$ for the oxidation of $[\{(^tBu_2Bipy)Pt\}_3(ctc^{\bullet\bullet})]^+$ $[\mathbf{3.5^{\bullet\bullet}}]^{2+}$ → $[\{(^tBu_2Bipy)Pt\}_3(ctc^{\bullet\bullet})]^{2+}$ $[\mathbf{3.5^{\bullet\bullet\bullet}}]^{3+}$. The spectra of pure di-cation $[\mathbf{3.5^{\bullet\bullet}}]^+$ and tri-cation $[\mathbf{3.5^{\bullet\bullet\bullet}}]^{3+}$ are shown in black, whilst intermediate spectra are shown in grey.

A characteristic manner of analysing IVCT transitions is to measure their width at half-height ($\Delta\nu_{1/2}$), which may give an insight into the degree of valent electron delocalisation throughout the molecule.[35] Larger $\Delta\nu_{1/2}$ values indicate that the IVCT transition is broad, therefore approaching the Robin/Day class II formalism whilst narrow IVCT transitions with smaller $\Delta\nu_{1/2}$ values indicate the process is approaching Robin/Day class III behaviour.[36] The the positions of IVCT energy diffebandsrences between complexes $\mathbf{[3.2^{\bullet}]^+}$ / $\mathbf{[3.2^{\bullet\bullet}]^{2+}}$ and $\mathbf{[3.5^{\bullet}]^+}$ / $\mathbf{[3.5^{\bullet\bullet}]^{2+}}$ virtually identical (within experimental error) although differ within their lineshape and intensities, with the IVCT absorption of $\mathbf{[3.5^{\bullet}]^+}$ and $\mathbf{[3.5^{\bullet\bullet}]^{2+}}$ being between 5 and 10 times more intense that those of both $\mathbf{[3.2^{\bullet}]^+}$ and $\mathbf{[3.2^{\bullet\bullet}]^{2+}}$. Analysis of $\Delta\nu_{1/2}$ of the transitions for $\mathbf{[3.2^{\bullet}]^+}$ and $\mathbf{[3.2^{\bullet\bullet}]^{2+}}$ is complicated because of the overlapping high-wavelength shoulder but can be estimated by **Equation 3.1**, which may predict values for a system exhibiting class II mixed-valency at a specific energy (E).[35] These are calculated as 4,270 cm^{-1} (E = 7,900 cm^{-1}) and 4,050 cm^{-1} (E = 7,100 cm^{-1}) for $\mathbf{[3.2^{\bullet}]^+}$ and $\mathbf{[3.2^{\bullet\bullet}]^{2+}}$ respectively. By inspection of the spectra, these values are clearly conservative indicating an extremely broad transition, tending towards the class III formalism.

$$\Delta\nu_{1/2} = (2310E)^{1/2} \qquad \textbf{(Equation 3.1)}$$

Analysis of the IVCT bands of [**3.5**$^{\bullet}$**]**$^{+}$ and [**3.5**$^{\bullet\bullet}$**]**$^{2+}$ yielded experimental $\Delta\nu_{1/2}$ values of 4950 and 3550 cm^{-1} for [**3.5**$^{\bullet}$**]**$^{+}$ and [**3.5**$^{\bullet\bullet}$**]**$^{2+}$ respectively. As with **[3.2**$^{\bullet}$**]**$^{+}$ and [**3.2**$^{\bullet\bullet}$**]**$^{2+}$, the $\Delta\nu_{1/2}$ of the transitions at their respective energies may be calculated giving values of 3,800 cm^{-1} (E = 6,200 cm^{-1}) for **[3.5**$^{\bullet}$**]**$^{+}$ and 3,500 cm^{-1} (E = 5,400 cm^{-1}) for **[3.5**$^{\bullet\bullet}$**]**$^{2+}$. Based on these values, and those calculated for **[3.2**$^{\bullet}$**]**$^{+}$ and [**3.2**$^{\bullet\bullet}$**]**$^{2+}$, it appears that at 253 K species **[3.5**$^{\bullet\bullet}$**]**$^{2+}$ is weakly class II delocalised whilst **[3.2**$^{\bullet}$**]**$^{+}$, [**3.2**$^{\bullet\bullet}$**]**$^{2+}$ and **[3.5**$^{\bullet}$**]**$^{+}$ tend towards full class III delocalisation about the [ctc]$^{n-}$ core unit. Based upon this observation, and assuming pure class III behaviour of the valency, the electron coupling energy (H_{AB}) of **[3.5**$^{\bullet}$**]**$^{+}$ may be calculated using **Equation 3.2**. This was not performed for complexes **[3.2**$^{\bullet}$**]**$^{+}$ and [**3.2**$^{\bullet\bullet}$**]**$^{2+}$ as no experimental $\Delta\nu_{1/2}$ values could be extracted from the spectra.

$$H_{ab} = \tfrac{1}{2}\,\Delta\nu_{1/2} \qquad \textbf{(Equation 3.2)}$$

The electron coupling energy for **[3.5**$^{\bullet}$**]**$^{+}$ was therefore calculated to be 2475 cm^{-1}, indicating very strong through-space coupling of the radical electrons, comparable to that found for the through-space coupling (4.8 Å) between stacked planes of the tetraaryl-*p*-phenylenediamine oligomer (H_{ab} = 2350 cm^{-1}) upon one electron oxidation.[37]

Table 3.7. Spectroelectrochemical UV/vis/NIR data for the different redox states of **3.2** and **3.5** in deoxygenated dichloromethane at 253 K (0.1 M $^{n}Bu_4NPF_6$) and UV/vis NIR data for **3.4** in dichloromethane at 298 K.

	Colour of solution	ν_{max} [10^3 cm^{-1}] (ε_{max} [10^3 $M^{-1}cm^{-1}$])
[{(dppb)Pt}$_3$(ctc)] (**3.2**)	Orange	32.2 (15.2), 30.6 (10.8), 26.3 (2.8). 17.6 (sh), 15.7 (0.1), 13.9 (0.1)
[{(dppb)Pt}$_3$(ctc$^{\bullet}$)] ([**3.2**$^{\bullet}$]$^{+}$)	Green	32.4 (15.3), 24.7 (sh), 15.6 (sh), 14.4 (0.5), 7.9 (0.5)
[{(dppb)Pt}$_3$(ctc$^{\bullet\bullet}$)] ([**3.2**$^{\bullet\bullet}$]$^{2+}$)	Green	32.4 (15.2), 23.5 (3.3), 18.6 (sh), 15.7 (sh), 14.3 (1.1), 7.1 (0.7)
[{(dppb)Pt}$_3$(ctc$^{\bullet\bullet\bullet}$)] ([**3.2**$^{\bullet\bullet\bullet}$]$^{3+}$)	Green	32.6 (13.9), 23.6 (3.9), 22.5 (sh), 14.3 (1.4), 10.6 (sh)
[{(^{t}Bu$_2$Bipy)Pd}$_3$(ctc)] (**3.3**)	Purple	39.0 (sh), 32.4 (30.0), 17.7 (2.5)
[{(dppe)Pt}$_3$(ctc)] (**3.4**)	Yellow	32.8 (5.4), 26.9 (sh), 14.6 (0.5)
[{(^{t}Bu$_2$Bipy)Pt}$_3$(ctc)] (**3.5**)	Blue	31.2 (27.1), 27.2 (6.4), 17.6 (11.6), 14.1 (sh)
[{(^{t}Bu$_2$Bipy)Pt}$_3$(ctc$^{\bullet}$)] ([**3.5**$^{\bullet}$]$^{+}$)	Purple	27.2 (sh), 20.8 (11.1), 18.1 (11.9), 14.2 (9.0), 6.2 (2.4)
[{(^{t}Bu$_2$Bipy)Pt}$_3$(ctc$^{\bullet\bullet}$)] ([**3.5**$^{\bullet\bullet}$]$^{2+}$)	Purple	27.4 (sh), 21.1 (14.0), 18.2 (12.8), 14.2 (10.0), 11.0 (3.2), 5.4 (5.7)
[{(^{t}Bu$_2$Bipy)Pt}$_3$(ctc$^{\bullet\bullet\bullet}$)] ([**3.5**$^{\bullet\bullet\bullet}$]$^{3+}$)	Purple	21.3 (14.7), 16.3 (sh), 14.1 (11.7), 11.4 (5.0)
[{(^{t}Bu$_2$Bipy)Cu}$_3$(ctc)] (**3.6**)	Green	39.9 (30.8), 33.3 (28.5), 25.8 (6.5)
[(dppe)Pt(DBSQ)] (**3.7**)	Yellow	37.5 (9.1), 36.5 (8.2), 33.2 (6.6), 28.2 (2.8)
[(dppe)Pt(DBSQ)] [**3.7**$^{\bullet}$]$^{+}$	Bleached	32.0 (8.0), 24.0 (sh), 18.7 (0.5), 16.0 (0.2), 14.3 (0.2), 12.3 (0.1)
[(^{t}Bu$_2$Bipy)Pt(DBCat)] (**3.8**)	Blue	26.0 (1.7), 16.8 (4.0)
[(^{t}Bu$_2$Bipy)Pt(DBSQ$^{\bullet}$)]$^{+}$ ([**3.8**$^{\bullet}$]$^{+}$)	Bleached	29.7 (sh), 28.5 (sh), 21.6 (5.3), 20.5 (sh), 17.0 (2.0), 16.0 (sh), 10.4 (0.1)

(sh) = shoulder

3.2.6 EPR Analysis of Chemically Oxidised Species

In collaboration with Dr. Stephen Sproules and Professor Eric McInnes of the University of Manchester, electron paramagnetic resonance (EPR) spectroscopy was used to investigate the local environment of the valent electron in the mono-oxidised species of complexes **3.4-3.5** and **3.7-3.8**. Samples were prepared by the addition of one equivalent of $[FeCp_2]PF_6$ in deoxygenated dichloromethane at 195 K. The dark solutions were found to be very air and temperature sensitive with rapid decomposition and precipitation of the chlorinated platinum(II) precursors if warmed to room temperature. X-band EPR analysis of freshly generated radical complexes at 150 K clearly showed the presence of a ligand-centred radical (S = ½), with g close to 2.00. Spectra of diphosphine complex $[\mathbf{3.4}^{\bullet}]^+$ displayed axial symmetry with clear hyperfine to ^{195}Pt whilst $[\mathbf{3.5}^{\bullet}]^+$ displayed rhombic symmetry, again with clear coupling to ^{195}Pt. Freshly prepared solutions of the mono-dioxolene species $[\mathbf{3.}7^{\bullet}]^+$ and $[\mathbf{3.8}^{\bullet}]^+$ were also analysed for comparative purposes.

The spectrum obtained for $[\mathbf{3.7}^{\bullet}]^+$ displayed axial symmetry with extracted parameters g_1 = g_2 = 2.006 and g_3 = 1.987 assuming the superposition of two axially symmetric spectra arising from the interaction of the valent electron with one platinum nucleus of standard isotopic contribution (I = ½, 33.8% and I = 0, 66.2%). Visually, the spectrum of $[\mathbf{3.7}^{\bullet}]^+$ compared well to $[\mathbf{3.4}^{\bullet}]^+$, where both displayed axial symmetry whilst in both cases the observed g-values are close to 2.00, with small downfield shift of 0.02-0.03 in $[\mathbf{3.4}^{\bullet}]^+$. Hyperfine coupling to ^{195}Pt was not obvious in the spectrum, although some could be extracted from the lineshapes of the g_1, g_2 and g_3 components, where A_1 = A_2 = 20.5 and A_3 = 4.7 x 10^{-4} cm^{-1}, which are almost identical to those of $[\mathbf{3.4}^{\bullet}]^+$ indicating the valent electron in both complexes interact almost identically with the platinum nuclei. Interestingly, no superhyperfine coupling to ^{31}P (I = ½, 100%) could be extracted from either spectra implying the ancillary ligand dppe does not hold any discernible electronic contribution in the HOMO whilst the observed ^{195}Pt hyperfine couplings are small, implying a small contribution of the platinum metal to the HOMO. As a result, it certainly appears in $[\mathbf{3.4}^{\bullet}]^+$ and $[\mathbf{3.7}^{\bullet}]^+$, the radical is predominately localised on the dioxolene with little metal character.

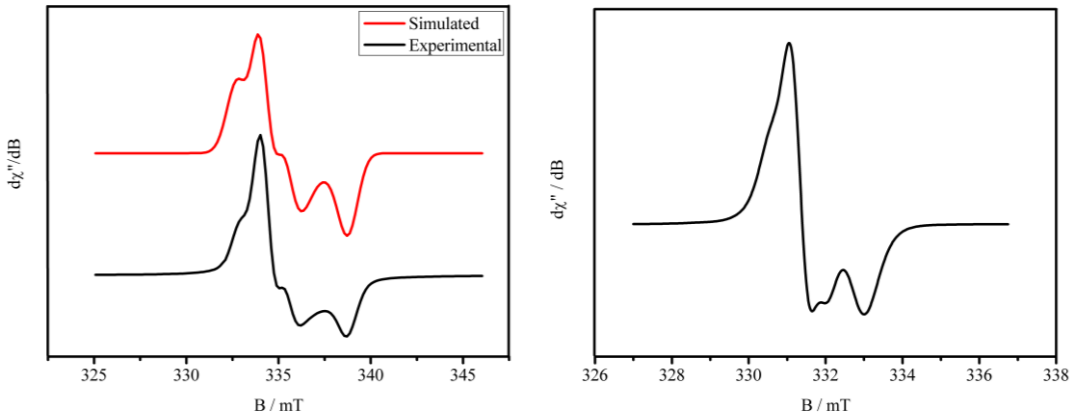

Figure 3.34. X-band EPR spectra recorded in 10:1 CH_2Cl_2/THF at 150 K. (Left) Simulated and experimental spectra of [**3.4**$^{\bullet}$]$^{+}$. (Right) Experimental spectrum of [**3.7**$^{\bullet}$]$^{+}$. Colour code; Simulated, red; Experimental, black.

The spectrum obtained for [**3.8**$^{\bullet}$]$^{+}$ was similar to that previously described,[15a] in displaying rhombic symmetry. This could be simulated reasonably again assuming interaction with one platinum nucleus of standard isotopic contribution, using g_1 = 2.036, g_2 = 2.008 and g_3 = 1.9613 and A_1 = 16.8, A_2 = 42.0 and A_3 = 14.9 x 10^{-4} cm^{-1} compared to g_1 = 2.034, g_2 = 2.005 and g_3 = 1.954 and A_1 = 32, A_2 = 51 and A_3 = 16 x 10^{-4} cm^{-1} of [**3.8**$^{\bullet}$]$^{+}$.[15a] Average *g*-values (g_{av} = $^{1}/_{3}\{g_1+g_2+g_3\}$) for both structures were shown to be very similar, (2.002 and 1.998) indicating the conditions used in this study have not perturbed the complex significantly. Both spectra also displayed hyperfine contributions in all directions with the smallest, A_3, corresponding to the out-of-plane contribution A_{zz}.[15a] The hyperfine values for A_1 and A_2 in this study were smaller than those found by Weinstein *et al.* indicating, a slightly weaker interaction between ^{195}Pt and radical under these conditions. Complex [**3.5**$^{\bullet}$]$^{+}$ displayed a visually similar spectrum to [**3.8**$^{\bullet}$]$^{+}$, which could again be simulated by assuming coupling to one platinum nucleus only. Parameters extracted again showed *g* values in the range of 2.00; g_1 = 2.065, g_2 = 2.033 and g_3 = 1.982. A downfield shift in g_{av} was again apparent, equal to 2.027 compared to 2.002 and 1.998, although is still in the region previously reported of complexes of this type.[15a] Hyperfine coupling to one ^{195}Pt was observed in for g_1 and g_2 (A_1 = 32.7 and A_2 = 40.1 x 10^{-4} cm^{-1}) whilst the broadness of g_3 meant that none could be observed directly, but the lineshape appeared to fit better upon inclusion of some metal hyperfine contribution (A_3 =23.3 x 10^{-4} cm^{-1}). Interestingly, the average hyperfine (A_{av} = $^{1}/_{3}\{A_1+A_2+A_3\}$) value for [**3.5**$^{\bullet}$]$^{+}$ (A_{av} = 32.0 x 10^{-4} cm^{-1}) was almost identical to that of the previously reported complex of [**3.8**$^{\bullet}$]$^{+}$ (A_{av} = 33.0 x 10^{-4} cm^{-1}) implying the valent electron is localised on one dioxolene ring on the EPR timescale, as in

[**3.4**$^{\bullet}$]$^{+}$. This observation is in direct contrast to complexes of containing [biscat$^{\bullet}$]$^{3-}$ which are delocalised across the full molecule, under similar conditions.[38]

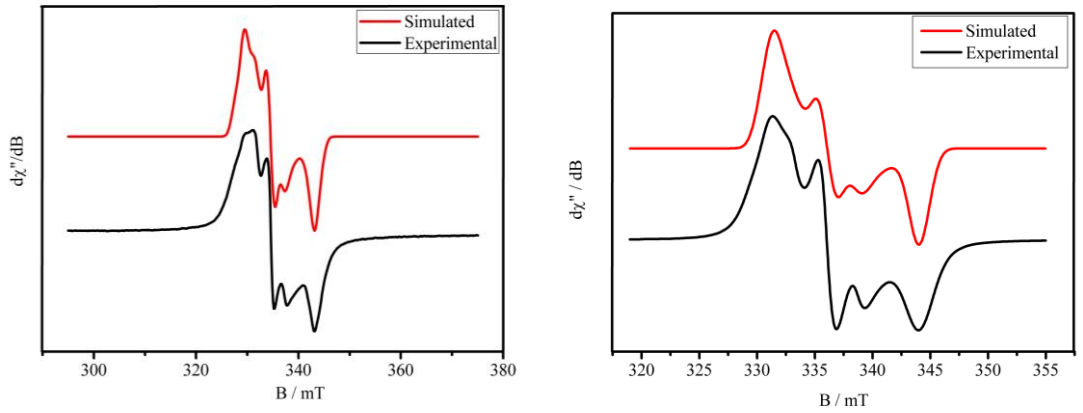

Figure 3.35. X-band EPR spectra recorded in 10:1 CH_2Cl_2/THF at 150 K. (Left) Simulated and experimental spectra of [**3.5**$^{\bullet}$]$^{+}$. (Right) Simulated and experimental spectra of [**3.8**$^{\bullet}$]$^{+}$. Colour code; Simulated, red; Experimental, black.

Upon warming to 230 K, chilled fluid solution spectra were recorded where the symmetry of all were reduced to isotropic and the *g* values collapsed to approximately 2.00. In the cases of [**3.4**$^{\bullet}$]$^{+}$ and [**3.5**$^{\bullet}$]$^{+}$, observable hyperfine was lost while the oxidised mononuclear complexes displayed hyperfine coupling to platinum, which was much larger in the $^{t}Bu_2$Bipy analogue [**3.8**$^{\bullet}$]$^{+}$ than in the diphosphine [**3.7**$^{\bullet}$]$^{+}$. Complex [**3.7**$^{\bullet}$]$^{+}$ also displayed superhyperfine coupling to ^{31}P, equal to 2.8 × 10^{-4} cm^{-1}, as shown in **Figure 3.36**.

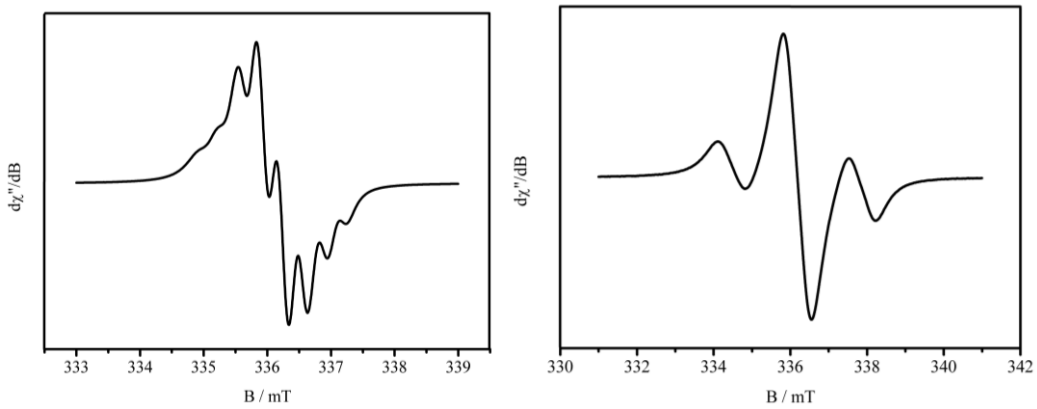

Figure 3.36. Chilled fluid solution X-band EPR spectra recorded in 10:1 CH_2Cl_2/THF at 230 K. (Left) Experimental spectrum of [**3.7**$^{\bullet}$]$^{+}$. (Right) Experimental spectrum of [**3.8**$^{\bullet}$]$^{+}$.

Table 3.8. Extracted EPR spectroscopic parameters for [**3.4**$^{\bullet}$]$^{+}$-[**3.8**$^{\bullet}$]$^{+}$ in 10:1 CH_2Cl_2 : THF solution. Hyperfine couplings are to one ^{195}Pt nucleus, and are in 10^{-4} cm^{-1}.

	230 K $g_{iso}(A_{iso})$	150 K g_1 (A_1)	g_2 (A_2)	g_3 (A_3)
[**3.4**$^{\bullet}$]$^{+}$	2.002[a]	2.035 (21)	2.035 (21)	2.008 (4.7)
[**3.5**$^{\bullet}$]$^{+}$	2.003[a]	2.065 (32.7)	2.033 (40.1)	1.982 (23.3)
[**3.7**$^{\bullet}$]$^{+}$	2.001 (7.5)[b]	2.007 (20.5)	2.007 (20.5)	1.987 (4.7)
[**3.8**$^{\bullet}$]$^{+}$	2.003 (32.7)	2.036 (16.8)	2.007 (42.0)	1.961 (14.9)

[a] No extractable hyperfine. [b] Additional superhyperfine to ^{31}P equal to 2.8×10^{-4} may be extracted from this spectrum.

Frozen solution (CH_2Cl_2, 150 K) X-band EPR analysis on complex **3.6** showed a typical axial spectrum ($g_{\parallel} > g_{\perp} > 2.0023$) of square-planar Cu(II) ($I = {}^3/_2$) with dx^2-y^2 ground state where $g_{\parallel} = 2.29$, $g_{\perp} = 2.08$ ($g_{av} = 2.15$; calculated from $2(g_{\perp}) + g_{\parallel} / 3$) and $A_{\parallel} = 14.5 \times 10^{-4}$ cm^{-1}. The high value of $g_{\parallel}$ and low $A_{\parallel}$ indicate that the geometry of each copper is strongly distorted from planarity,[39] although $g_{\parallel}$ is in the range of those expected of CuO_2N_2 complexes[40] and is less than 2.30, indicating covalent character of the metal-ligand bonds.[41] The extracted g values here compare favourably to a previously reported example of a distorted square pyramidal CuO_2N_2 complex Unfortunately no hyperfine coupling to the nitrogen atoms of ^{t}Bu$_2$Bipy could be seen, as in previously reported {(Bipy)Cu}$^{2+}$ dioxolene complexes,[25] although the broadness of the central line means that hyperfine is likely hidden underneath. Closer inspection of the spectrum showed the presence of the forbidden half-field resonance, observed at the $\Delta m_s = 2$ resonance line ($g = 4.16$). Often this is undetected due to its low intensity, although indicates the dipolar through-space coupling of two copper atoms which must be separated by more than 5 Å, therefore preventing the coupling of two copper atoms by water or hydroxide atoms.[42] This is consistent with the proposed trinuclear structure of **3.6**.

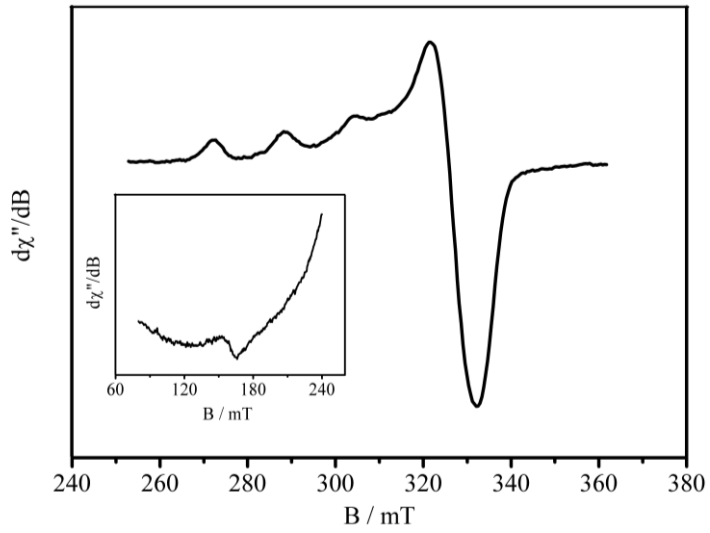

Figure 3.37. X-band EPR spectrum of **3.6** recorded in CH_2Cl_2 at 150 K. Insert shows the presence of a half-field signal $\Delta m_s = 2$.

3.2.7. DFT Calculation of [{(bipy)Pt}$_3$(ctc)]

Initial density functional (DF) calculations were performed on the neutral (ctc) owing to the success in calculating the frontier orbitals and molecular geometries (*c.f.* previously published structures),[43] the computational procedures were extended to include a representative complex of the $[ctc]^{6-}$ framework. As the computational procedures for large complexes containing multiple heavy atoms, the model complex used in the computational procedures was [{(bipy)Pt}$_2$(thea)] where bipy = 2,2'-bipyridine (analogous to [{(^{t}Bu$_2$Bipy)Pt}$_2$(ctc)] without *tertiary*-butyl substituents for computational simplicity). DFT calculations were performed using Gaussian *03*[44] calculation software package with B3LYP functional method and SDD basis set (Dresden / Stuttgart pseudopotential on platinum and D95 basis set on all other atoms).[45] No solvent effects were included in the calculation and the complex was treated as a singlet (486 electrons, 819 basis functions). The computational procedure was as follows, first geometry optimisation was performed on the complete complex, where the central $[ctc^{6-}]$ unit originated from the crystal structure of neutral complex **3.4** from the structure of **3.4**•H_2O•8dma and {(bipy)Pt} moieties appended manually. On the basis of this optimised structure shown in **Figure 3.38**, the frontier orbitals were calculated.

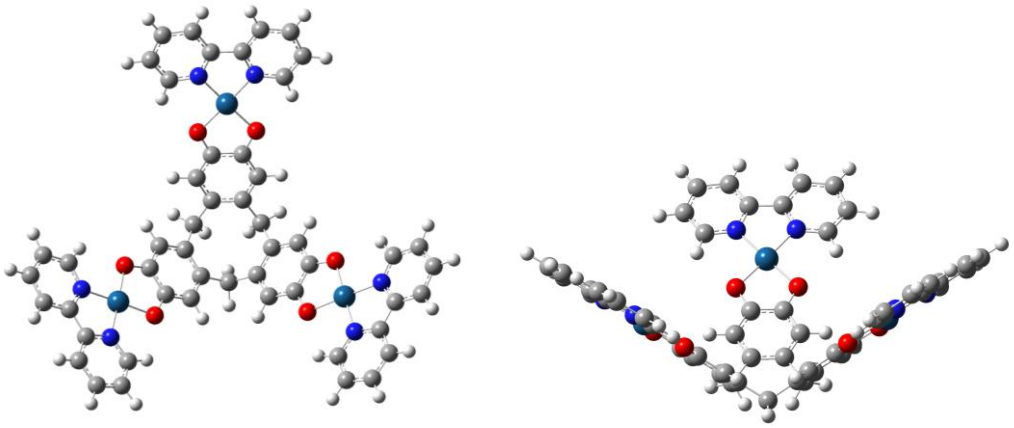

Figure 3.38. Two views of geometry optimised structure [{(bipy)Pt}$_3$(ctc)].

Importantly, the geometry optimisation of [{(bipy)Pt}$_3$(ctc)] acted to retain the familiar bowl structure of [ctc]$^{6-}$ although it deviates from C_3 symmetry slightly. The calculated structure also opened the structure up, as seen by an decrease in dihedral angle between least-squares planes of the dioxolene groups as an average value of 116° compared with *c.a.* 108° for synthetic complexes **3.2** and **3.4.**[10] A consequence of this geometric flattening was that the average distance between the triangle of platinum centres increased from approximately 9.8-9.9 Å, again in **3.2** and **3.4**, to an average distance of 10.4 Å.[10] Other metric parameters extracted from the structure compare well with previously reported structures, with no significant deviations in bond lengths and angles, as can be seen in **Table 3.9.**

Table 3.9. Selected parameters extracted from the geometry optimised structure of [{(bipy)Pt}$_3$(ctc)].

	Pt−N [Å]	N–Pt–N [Å]	Pt−O [Å]	O–Pt–O [°]	O–Pt–N [°]	θ [°]
[{(bipy)Pt}$_3$(ctc)]	2.007	80.13 - 80.14	2.008	83.83	98.00 - 98.03	116.50 - 115.72
3.4•H_2O•8dma	-	-	2.049(14) - 2.041(13)	83.1(5)	-	108.8(4)

The molecular orbitals calculated from the optimised structure of [{(bipy)Pt}$_3$(ctc)] are displayed as an energy diagram in **Figure 3.39** and showed the two highest occupied energy levels are a degenerate (E = -3.91844 eV) pair localised on the [ctc]$^{6-}$ ligand with very minor contributions from the [(bipy)Pt]$^{2+}$ moieties. The energy levels are antibonding between the dioxolene rings separated by a nodal plane which is rotated by 90° between the two orbitals. The HOMO-2 (E = -4.13613 eV) on the other hand, is a symmetric combination of the

HOMO pair with bonding character between all three dioxolene rings. The energy gap (ΔE) between this HOMO pair and HOMO-2 equals approximately 0.22 eV, which may be taken as a measure of the coupling between dioxolene rings, and is smaller than the corresponding gap between HOMO and HOMO-1 of calculated complex [{(Bipy)Pt}$_2$(thea)] (to be explored in chapter 4) which equals approximately 0.30 eV. This reduced energy gap helps to explain the very small separation between cat / sq oxidations as seen in the electrochemical analysis of complexes **3.2**, **3.4**-**3.5**.

Table 3.10. Selected molecular orbital energies of the geometry optimised structure [{(bipy)Pt}$_3$(ctc)].

	LUMO+1	LUMO	HOMO	HOMO-1
Energy [eV]	-2.53066	-2.55787	-3.91844	-4.13613

The HOMO / LUMO gap is 1.36 eV and in direct contrast to the HOMO energy levels, all three LUMO energy levels are extremely close in energy and are all centred on the bipy ancillary ligand with very small contributions from the platinum and oxygen atoms of the core $[ctc]^{6-}$ unit. Within the LUMO, all bipy fragments are in phase with one-another whilst the analogous degenerate LUMO+1 displays one node 90° between the dioxolene rings. It is interesting to note here that the degenerate HOMO of this complex implies that the radical cation should be Jahn-Teller active, which complicates the discussion somewhat. Although, it could help potentially help to explain why the separation (ΔE) between the first and second oxidations in **3.2** and **3.5** are slightly reduced (0.18 V) compared to the second and third (0.21-0.22 V) although further investigations would need to be undertaken to determine this.

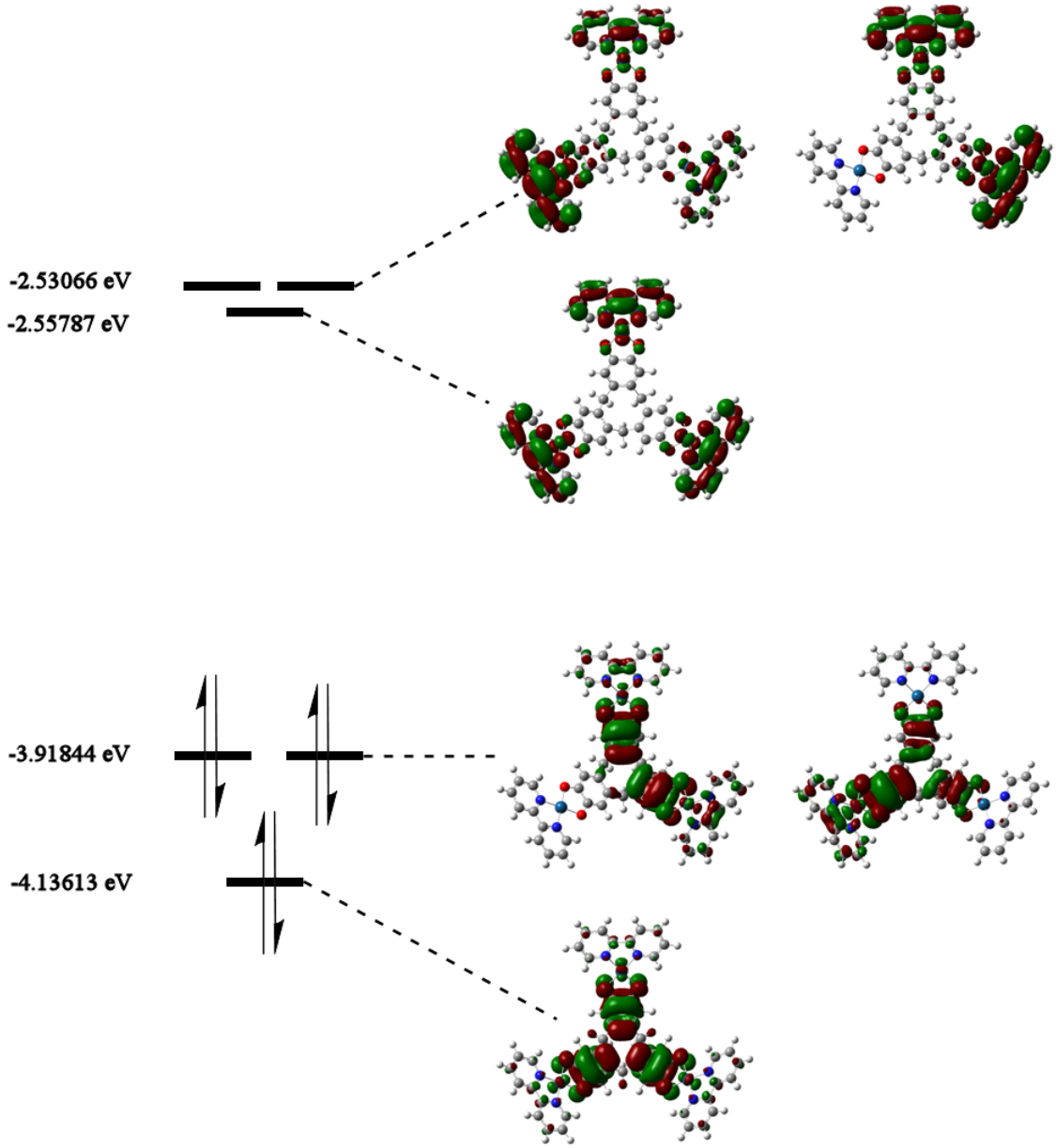

Figure 3.39. Energy diagram of the molecular orbitals of the geometry optimised, calculated structure of [{(bipy)Pt}$_3$(ctc)].

3.3 Conclusions

The synthesis of four novel complexes containing the core $[ctc]^{n-}$ unit has been presented along with their detailed structural and electronic characterisation. Analysis of the three μ_3-ctc platinum(II) complexes bearing different ancillary ligands showed chemically reversible oxidations separated by approximately 0.25 V, corresponding to the stepwise oxidations between cat and sq levels of each dioxolene ring. Electrochemical analysis of complexes containing palladium(II) and copper(II) were more complicated, presumably due to dissociation of the metal. Oxidation of complexes **3.2-3.5** was also attempted, although due to a combination of solution-phase sensitivity and temperature dependent solubility of the complexes, spectroelectrochemical analysis was only permitted for two complexes; **3.2** and **3.5**. The results obtained for their mixed valence species demonstrated IVCT transitions within the ctc ligand, which showed $\mathbf{[3.5^{\cdot\cdot}]^{2+}}$ is weakly class II delocalised whilst $\mathbf{[3.2^{\cdot}]^{+}}$, $[\mathbf{3.2^{\cdot\cdot}}]^{2+}$ and $\mathbf{[3.5^{\cdot}]^{+}}$ tend towards full class III delocalisation despite the non-conjugation of the dioxolene rings.[36] The electron coupling energy (H_{AB}) at the class III limit was calculated for $[\mathbf{3.5^{\cdot}}]^{+}$ as 2475 cm^{-1} showing strong through-space coupling of the mixed valence sites, comparable to that found between stacked molecules of an oxidised tetraaryl-*p*-phenylenediamine oligomer.[37] DFT analysis of a model complex, $[\{(bipy)Pt\}_3(ctc)]$ confirmed the ligand-based nature of the radicals by showing the HOMO is a degenerate pair of antibonding orbitals localised on the ctc ligand. Frozen solution EPR analysis of oxidised complexes $[\mathbf{3.4^{\cdot}}]^{+}$ and $[\mathbf{3.5^{\bullet}}]^{+}$ displayed spectra consistent with their analogous mononuclear species with coupling to one platinum nucleus, indicating the radical electron is localised on the timescale of the measurement at 150 K. DFT analysis of $[\{(bipy)Pt\}_3(ctc)]$ also showed the LUMO is a degenerate pair of antibonding orbitals, localised on the bipyridine ancillary ligands. Future experiments on **3.5** could therefore be directed towards the reduction of this complex in order to determine the localisation or delocalisation of the radical electron. Analysis of **3.6** displayed a typical axial spectrum expected of copper(II) with *g* values in the range expected of complexes containing the CuO_2N_2 coordination sphere. The presence of a spin forbidden half-field shift ($\Delta m_s = 2$) was also noted, indicating the close spatial arrangement of at least two copper nuclei.

3.4 References

[1] S. Archer, J. A. Weinstein, *Coord. Chem. Rev.* **2012**, *256*, 2530-2561.

[2] J. S. Miller, K. S. Min, *Angew. Chem. Int. Ed.* **2009**, *48*, 262-272.

[3] K. S. Min, A. G. DiPasquale, J. A. Golen, A. L. Rheingold, J. S. Miller, *J. Am. Chem. Soc.* **2007**, *129*, 2360-2368.

[4] a) A. Heckmann, C. Lambert, *Angew. Chem. Int. Ed.* **2012**, *51*, 326-392; b) A. Dei, D. Gatteschi, C. Sangregorio, L. Sorace, *Acc. Chem. Res.* **2004**, *37*, 827-835; c) J. Hankache, O. S. Wenger, *Chem. Rev.* **2011**, *111*, 5138-5178.

[5] K. G. Alley, G. Poneti, P. S. D. Robinson, A. Nafady, B. Moubaraki, J. B. Aitken, S. C. Drew, C. Ritchie, B. F. Abrahams, R. K. Hocking, K. S. Murray, A. M. Bond, H. H. Harris, L. Sorace, C. Boskovic, *J. Am. Chem. Soc.* **2013**, *135*, 8304-8323.

[6] A. Caneschi, A. Dei, C. P. Mussari, D. A. Shultz, L. Sorace, K. E. Vostrikova, *Inorg. Chem.* **2002**, *41*, 1086-1092.

[7] C. S. Grange, A. J. H. M. Meijer, M. D. Ward, *Dalton Trans.* **2010**, *39*, 200-211.

[8] P. Satha, G. Illa, C. S. Purohit, *Crystal Growth & Design* **2013**, *13*, 2636-2641.

[9] a) B. F. Abrahams, B. A. Boughton, N. J. FitzGerald, J. L. Holmes, R. Robson, *Chem. Commun.* **2011**, *47*, 7404; b) B. F. Abrahams, N. J. FitzGerald, R. Robson, *Inorg. Chem.* **2010**, *49*, 5953-5956; c) B. F. Abrahams, N. J. FitzGerald, T. A. Hudson, R. Robson, T. Waters, *Angew. Chem., Int. Ed.* **2009**, *48*, 3129.

[10] D. Scott Bohle, D. Stasko, *Chem. Commun.* **1998**, 567-569.

[11] W. Kaim, M. Wanner, A. Knödler, S. Záliš, *Inorg. Chim. Acta* **2002**, *337*, 163-172.

[12] G. A. Razuvaev, V. K. Cherkasov, G. A. Abakumov, *J. Organometallic Chem.* **1978**, *160*, 361-371.

[13] J. A. Hyatt, E. N. Duesler, D. Y. Curtin, I. C. Paul, *J. Org. Chem.* **1980**, *45*, 5074.

[14] N. V. Loginova, A. T. Gres, G. I. Polozov, T. V. Koval'chuk, N. P. Osipovich, R. A. Zheldakova, Y. V. Faletrov, I. S. Strakha, I. I. Azarko, *Polyhedron* **2013**, *57*, 39-46.

[15] a) N. M. Shavaleev, E. S. Davies, H. Adams, J. Best, J. A. Weinstein, *Inorg. Chem.* **2008**, *47*, 1532-1547; b) J. Best, I. V. Sazanovich, H. Adams, R. D. Bennett, E. S. Davies, A. J. H. M. Meijer, M. Towrie, S. A. Tikhomirov, O. V. Bouganov, M. D. Ward, J. A. Weinstein, *Inorg. Chem.* **2010**, *49*, 10041-10056.

[16] A. L. Spek, *J. Appl. Crystallogr.* **2003**, *36*, 7.

[17] A. Spek, *Acta Cryst. Sect. D* **2009**, *65*, 148-155.

[18] O. Carugo, C. B. Castellani, K. Djinovic, M. Rizzi, *J. Chem. Soc., Dalton Trans.* **1992**, 837-841.

[19] a) C. G. Pierpont, R. M. Buchanan, *Coord. Chem. Rev.* **1981**, *38*, 45-87; b) S. Bhattacharya, S. R. Boone, G. A. Fox, C. G. Pierpont, *J. Am. Chem. Soc.* **1990**, *112*, 1088-1096.

[20] H. Wunderlich, D. Mootz, *Acta Cryst. Sect. B* **1971**, *27*, 1684-1686.

[21] A. L. Macdonald, J. Trotter, *J. Chem. Soc., Perkin Transactions 2* **1973**, 476-480.

[22] O. Carugo, K. Djinovic, M. Rizzi, C. B. Castellani, *J. Chem. Soc., Dalton Trans.* **1991**, 1255-1258.

[23] S. Harmalker, S. E. Jones, D. T. Sawyer, *Inorg. Chem.* **1983**, *22*, 2790-2794.

[24] E. Gojon, J.-M. Latour, S. J. Greaves, D. C. Povey, V. Ramdas, G. W. Smith, *J. Chem. Soc., Dalton Trans.* **1990**, 2043-2051.

[25] S. Deepalatha, P. S. Rao, R. Venkatesan, *Spectrochim. Acta Part A* **2006**, *64*, 178-187.

[26] M. D. Stallings, M. M. Morrison, D. T. Sawyer, *Inorg. Chem.* **1981**, *20*, 2655-2660.

[27] K. J. Winstanley, A. M. Sayer, D. K. Smith, *Org. Biomol. Chem.* **2006**, *4*, 1760-1767.

[28] W. Si, W. Lei, Y. Zhang, M. Xia, F. Wang, Q. Hao, *Electrochim. Acta* **2012**, *85*, 295-301.

[29] P. Ghosh, A. Begum, D. Herebian, E. Bothe, K. Hildenbrand, T. Weyhermüller, K. Wieghardt, *Angew. Chem. Int. Ed.* **2003**, *42*, 563-567.

[30] V. Anbalagan, T. S. Srivastava, *Polyhedron* **1994**, *13*, 291-299.

[31] R. Benedix, A. Vogler, *Inorg. Chim. Acta* **1993**, *204*, 189-193.

[32] D. G. Brown, W. J. Hughes, G. Knerr, *Inorg. Chim. Acta* **1980**, *46*, 123-126.

[33] W. Levason, C. A. McAuliffe, *Inorg. Chim. Acta* **1976**, *16*, 167-172.

[34] F. Hartl, A. Vlcek, *Inorg. Chem.* **1996**, *35*, 1257.

[35] K. D. Demadis, C. M. Hartshorn, T. J. Meyer, *Chem. Rev.* **2001**, *101*, 2655-2685.

[36] M. B. Robin, P. Day, *Advan. Inorg. Chem. Radiochem.* **1967**, *10*, 247-422.

[37] X. Z. Yan, J. Pawlas, T. Goodson, J. F. Hartwig, *J. Am. Chem. Soc.* **2005**, *127*, 9105.

[38] L. F. Joulie, E. Schatz, M. D. Ward, F. Weber, L. J. Yellowlees, *J. Chem. Soc., Dalton Trans.* **1994**, 799-804.

[39] a) U. Sakaguchi, A. W. Addison, *J. Chem. Soc., Dalton Trans.* **1979**, 600-608; b) C. Rajarajeswari, R. Loganathan, M. Palaniandavar, E. Suresh, A. Riyasdeen, M. A. Akbarsha, *Dalton Trans.* **2013**, *42*, 8347-8363.

[40] M. Vaidyanathan, R. Viswanathan, M. Palaniandavar, T. Balasubramanian, P. Prabhaharan, P. Muthiah, *Inorg. Chem.* **1998**, *37*, 6418-6427.

[41] D. Kivelson, R. Neiman, *J. Chem Phys.* **1961**, *35*, 149-155.

[42] F. G. Mutti, G. Zoppellaro, M. Gullotti, L. Santagostini, R. Pagliarin, K. K. Andersson, L. Casella, *Eur. J. Inorg. Chem.* **2009**, *2009*, 554-566.

[43] J. J. Loughrey, C. A. Kilner, M. J. Hardie, M. A. Halcrow, *Supramol. Chem.* **2011**, *24*, 2-13.

[44] M. J. Frisch, G. W. T, H. B. Schlegel, G. E. Scuseria, M. A. Robb, J. R. Cheeseman, J. A. Montgomery, T. Vreven, K. N. Kudin, J. C. Burant, J. M. Millam, S. S. Iyengar, J. Tomasi, V. Barone, B. Mennucci, M. Cossi, G. Scalmani, N. Rega, G. A. Petersson, H. Nakatsuji, M. Hada, M. Ehara, K. Toyota, R. Fukuda, J. Hasegawa, M. Ishida, T. Nakajima, Y. Honda, O. Kitao, H. Nakai, M. Klene, X. Li, J. E. Knox, H. P. Hratchian, J. B. Cross, V. Bakken, C. Adamo, J. Jaramillo, R. Gomperts, R. E. Stratmann, O. Yazyev, A. J. Austin, R. Cammi, C. Pomelli, J. W. Ochterski, P. Y. Ayala, K. Morokuma, G. A. Voth, P. Salvador, J. J. Dannenberg, V. G. Zakrzewski, S. Dapprich, A. D. Daniels, M. C. Strain, O. Farkas, D. K. Malick, A. D. Rabuck, K. Raghavachari, J. B. Foresman, J. V. Ortiz, Q. Cui, A. G. Baboul, S. Clifford, J. Cioslowski, B. B. Stefanov, G. Liu, A. Liashenko, P. Piskorz, I. Komaromi, R. L. Martin, D. J. Fox, T. Keith, M. A. Al-Laham, C. Y. Peng, A. Nanayakkara, M. Challacombe, P. M. W. Gill, B. Johnson, W. Chen, M. W. Wong, C. Gonzalez, J. A. Pople, *Gaussian 03*, **2004**.

[45] T. H. Dunning Jr., P. J. Hay, 'Modern Theoretical Chemistry' *Vol. 3*, Plenum,, New York, 1977.

Chapter 4

Novel Mixed-Valence Species of a *Bis*-dioxolene Ligand

4.1 Introduction

This chapter is concerned with the synthesis and characterisation of novel complexes of the 2,3,6,7-tetrahydroxy-9,10-dimethyl-9,10-dihydro-9,10-ethanoanthracene framework. These complexes were investigated for the purposes of generating a mixed valence-radical species with intermediate character of radical localisation and delocalisation. Our initial interest in complexes containing a *bis*-dioxolene core unit stemmed from the very obvious oxygen-sensitivity of complexes explored in chapter 3, especially their radical semiquinone-cations. An alternative strategy to keep the system comparative, yet hopefully increase the stability of the oxidised species, the dimensionality of the complexes was reduced from μ_3- to μ_2-.

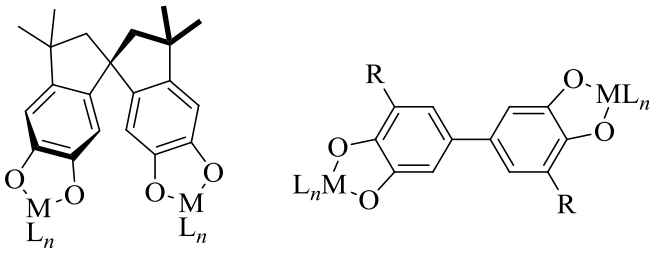

[{ML$_n$}$_2$(**spiro**)]

R = H or ^{t}Bu
[{ML*n*}$_2$(***bis*cat**)]

Figure 4.1. Two previously described mixed valence complexes containing the [spiro]$^{n-}$ and [biscat]$^{n-}$ core ligand units.

Various *bis*-dioxolene ligands, e.g [spiro]$^{n-}$ and [biscat]$^{n,-}$ have been previously shown to be capable of supporting mixed valence species of Robin/Day class II and class III character respectively, the aims of this chapter were to investigate the ligand-based mixed valency of *bis*-dioxolene complexes which hold the potential to be intermediate of these two, i.e. class II behaviour. A suitable ligand for this purpose was chosen to be 2,3,6,7-tetrahydroxy-9,10-dihydro-anthracene, due to its methylene spacers in order to maintain structurally comparative to cyclotricatechylene. To provide this, the initial target molecule was 2,3,6,7-tetramethoxy-9,10-dihydroanthracene (**4.1**) which could be subsequently demethylated to give 2,3,6,7-tetramethoxy-9,10-dihydroanthracene (**4.2**). The synthesis and characterisation of both compounds have been reported previously,[1] however their redox chemistry and complexes have not been investigated.

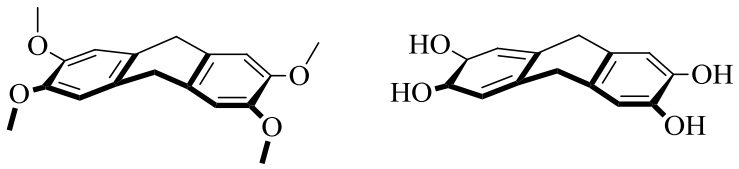

4.1 **4.2**

Figure 4.2. Initial target compounds for this study; 2,3,6,7-tetramethoxy-9,10-dihydroanthracene (**4.1**) and 2,3,6,7-tetramethoxy-9,10-dihydroanthracene (**4.2**).

As prior investigations of radical semiquinone species have shown extensive electron delocalisation into the 3- and 4- positions of dioxolene rings, the majority of previously investigated complexes incorporating dioxolene moieties include some form of protection in this position. It was therefore hoped in this case that use of a complex which contains some steric protection in these positions would enable clean synthesis and analysis without the challenges of aerial oxidation that were particularly apparent in complexes containing the core $[ctc]^{n-}$ unit. Retention of the spacer inbetween dioxolene rings, as in cyclotricatechylene, was envisaged to keep the two dioxolene rings close in space, hopefully permitting electronic communication between redox-active centres although prevent formal conjugation of the two rings. This would hopefully give rise to the independent redox processes as illustrated in **Scheme 4.1**.

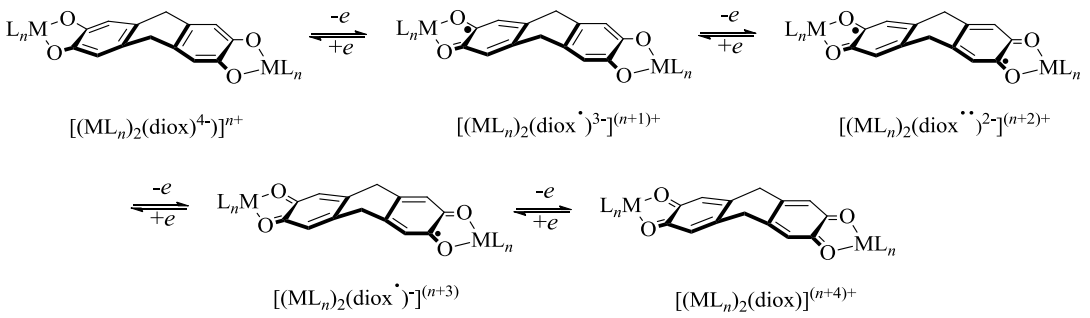

Scheme 4.1. Potential redox processes of interest to this study in complexes containing a *bis*-dioxolene ligand**.**

4.2 Results and Discussion

4.2.1 Ligand synthesis

The first route investigated to **4.1** was that reported by Kohn *et al.*,[1b] using the rapid ionisation of *N*-(3,4-dimethoxybenzyl)sulfamide (**4.3**) in trifluoroacetic acid. This route was particularly attractive due to the simple and high yielding steps involved, with the first step giving **4.3** from the reaction of 3,4-dimethoxybenzylamine and sulfamide as seen below, which proceeded in very high yield (89%).

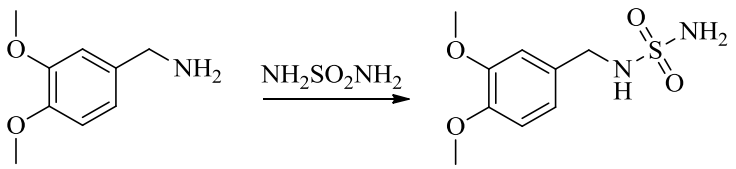

4.3

Scheme 4.2. Reaction scheme for the synthesis of *N*-(3,4-dimethoxybenzyl)sulfamide (**4.3**).

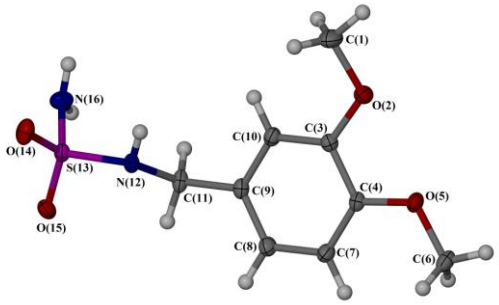

Figure 4.3. Structure of *N*-(3,4-dimethoxybenzyl)sulfamide (**4.3**). Atoms are displayed as thermal ellipsoids at 50% probability. Colour code: S, purple; O, red; N, blue; C, grey; H, white.

Crystals of **4.3** were grown by slow evaporation of a methanol / *n*-hexane solution and crystallised in the monoclinic spacegroup $P2_1/n$. The asymmetric unit contained one full molecule of **4.3** and confirmed the connectivity as shown by ^{1}H NMR while mass spectrometry (ES+) confirmed the expected mass of the product. The structure showed that throughout the lattice, each molecule of **3.2** is 3-connected via hydrogen bonding between; O(2)….H(2F) 2.166(2) Å and H(1D)…O(4) 2.166(4) Å, as shown in **Figure 4.4**, resulting in an alternate orientation of the molecules throughout the layers as viewed along (010) (**Figure 4.5**).

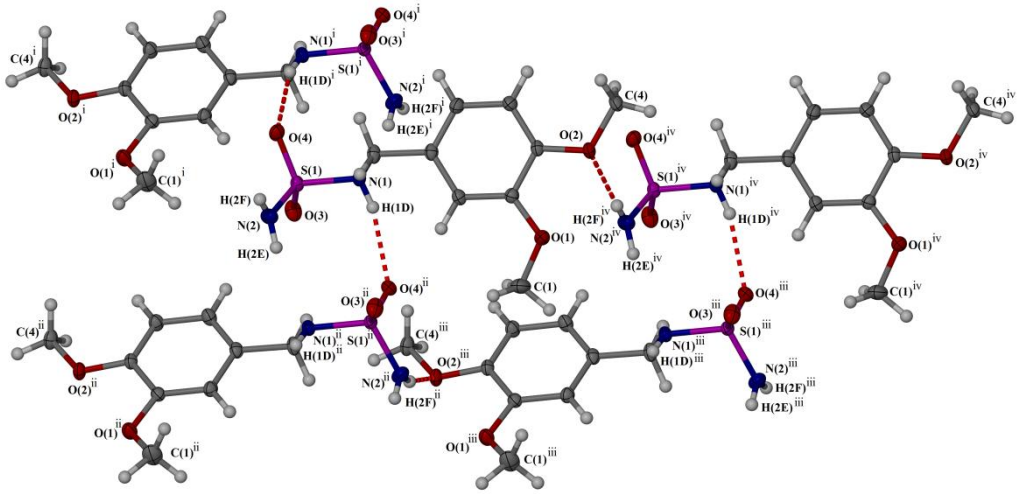

Figure 4.4. View of **4.3** depicting the hydrogen bonding 3-connectivity of each molecule. Atoms are displayed as thermal ellipsoids at 50% probability. (i) $^{3}/_{2}$-*x*, *y*-½. ½-*z*, (ii) $^{3}/_{2}$-*x*, ½+*y*. ½-*z*, (iii) $^{5}/_{2}$-*x*, ½+*y*. ½-*z*, (iv) 1+*x*, *y*, *z*. Colour code: S, purple; O, red; N, blue; C, grey; H, white.

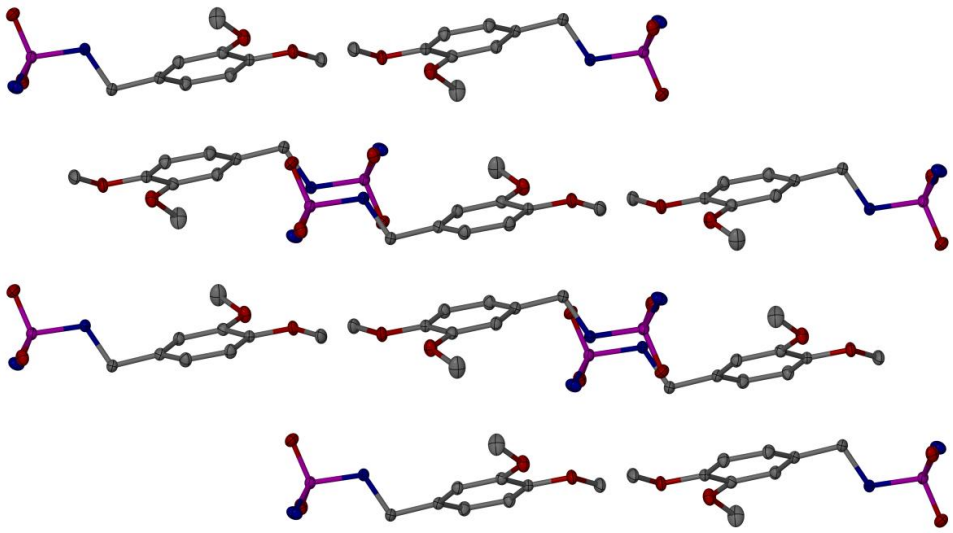

Figure 4.5. View along unit cell *b* axis showing an alternate arrangement of molecules of **4.3** throughout layers. Atoms are displayed as thermal ellipsoids at 50% probability, hydrogen atoms omitted for clarity. Colour code: S, purple; O, red; N, blue; C, grey.

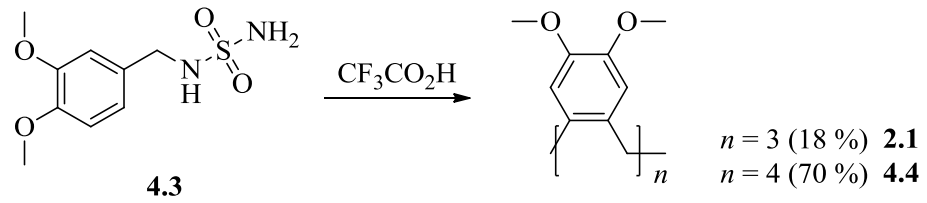

4.3

Scheme 4.3. Attempted cyclisation of **4.3** under conditions described by Kohn *et al.*[1b]

The trifluoroacetic acid-catalysed reaction of **4.3** was performed with the view to providing **4.1** *via* acid-catalysed intermolecular dimerisation of two *N*-(3,4-dimethoxybenzyl)sulfamide molecules (**4.3**). Unfortunately however, the reaction provided only cyclotriveratrylene (**2.1**) and cyclotetraveratrylene (cttv, **4.4**) after a particularly challenging separation (silica, 2% acetone in chloroform). Compound **4.4** was characterised by mass spectrometry (ES+), elemental analysis and NMR spectroscopy however due to the empirical similarity of ctv to the desired compound, these techniques were unable to distinguish the two compounds. The ^{1}H NMR spectrum recorded of **4.4** was broad and failed to indicate the presence of either **4.1** or **4.4** as both molecules may display slow room temperature conversions on the NMR experiment timescale. This results in a series of broad peaks for the different proton environments as **4.4** may adopt one of four 'sofa' conformations whilst **4.1** may interconvert due to the lack of rigidity within the methylene spacers.[2] It should be noted here that conducting the experiment at a higher temperature may sharpen the peaks giving rapid conversion of the molecule on the NMR timescale and one set of averaged signals however this would not have offered a definitive identity of the product simply due to integration ratios being identical for the two species. Similarly, freezing out the interconversions at 233 K may also be performed, showing a spectrum consistent with a C_{2h} 'sofa' conformation. Resultant of this uncertainty, a definitive solution to the identity of **4.4** was given by the single crystal X-ray analysis of the product whereby it was found to contain only cttv with one disordered molecule of dichloromethane (**Figure 4.6**) as a solvomorph of the previously reported solvate [cttv.C_6H_6].[3]

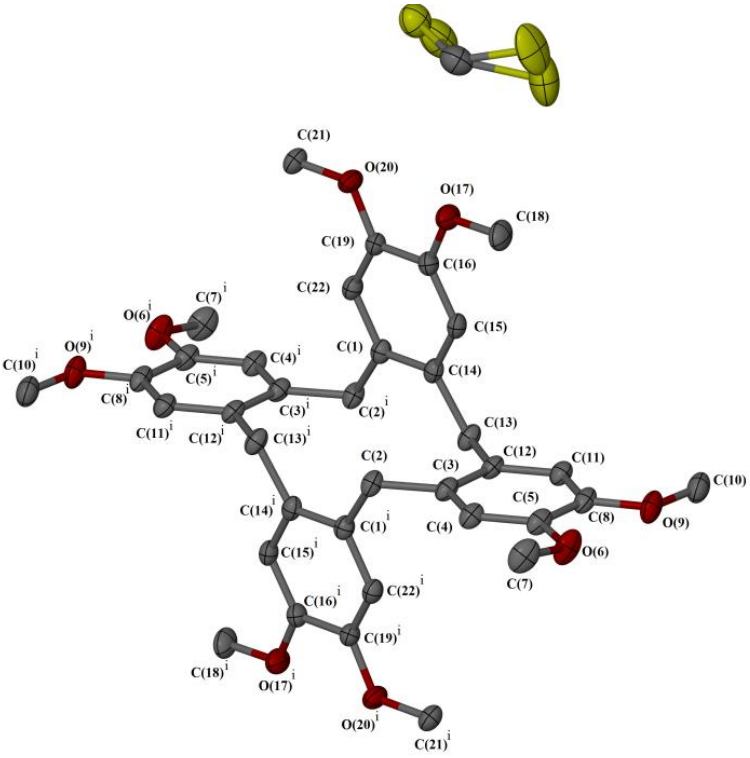

Figure 4.6. Chair conformation of **4.4** with one disordered molecule of dichloromethane. Atoms are displayed as thermal ellipsoids at 50% probability, hydrogen atoms omitted for clarity. (i) 1-*x*, 1-*y*, 1-*z*. Colour code: Cl, yellow; O, red; C, grey.

As previously reported, cttv adopts its characteristic chair conformation, with half the molecule related to the other half by a crystallographic inversion.[4] This structure packs into an array whereby all molecules orient with methyl groups pointing towards small hydrophobic cavities within the structure. Similarly, owing to the chair conformation of **3.3**, the molecules may stack back-to-back with one another, with molecules of dichloromethane occupying the remaining cavities within the lattice, as shown in **Figure 4.7**.

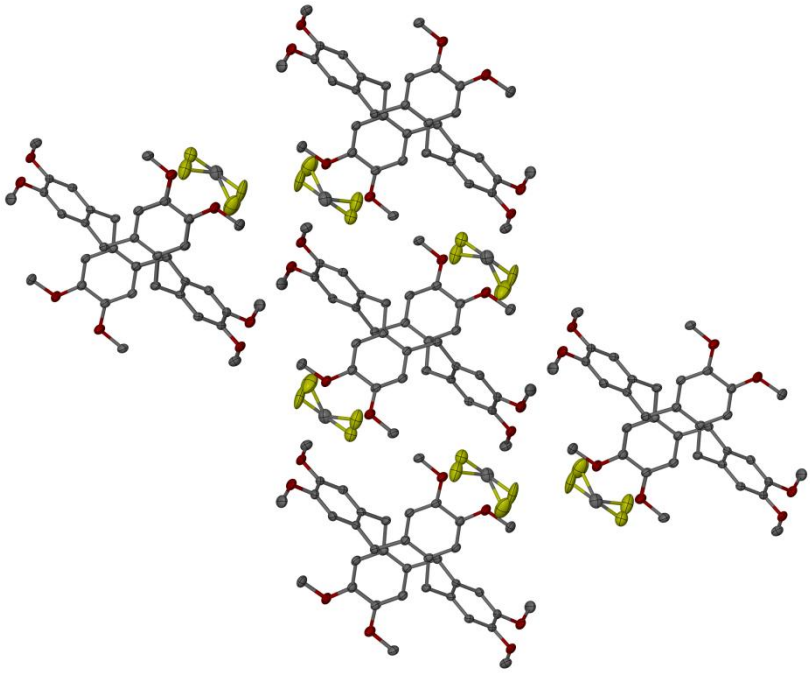

Figure 4.7. Packing view of **4.4** along unit cell axis *b*. Atoms are displayed as thermal ellipsoids at 50% probability, hydrogen atoms omitted for clarity**.** Colour code: Cl, yellow; O, red; C, grey.

Although advantageous as an alternative route towards cyclotetraveratrylene and potentially higher order cyclotriveratrylene analogues, an alternative synthetic route towards **4.1** was devised as it was clear a new reaction route was required. Utilising a number of reactions previously reported,[1a, 5] **Scheme 4.4** was devised starting from the condensation of readily-available veratrole with paraldehyde in sulfuric acid to give 2,3,6,7-tetramethoxy-9,10-dimethylanthracene (**4.5**) in a moderate yield (63%). Oxidation of the two methyl groups in the 9,10- positions of the central anthracene ring using sodium dichromate in refluxing acetic acid yielded 2,3,6,7-tetramethoxy-9,10-dioneanthracene (**4.6**) in high yield without the requirement of any purification.

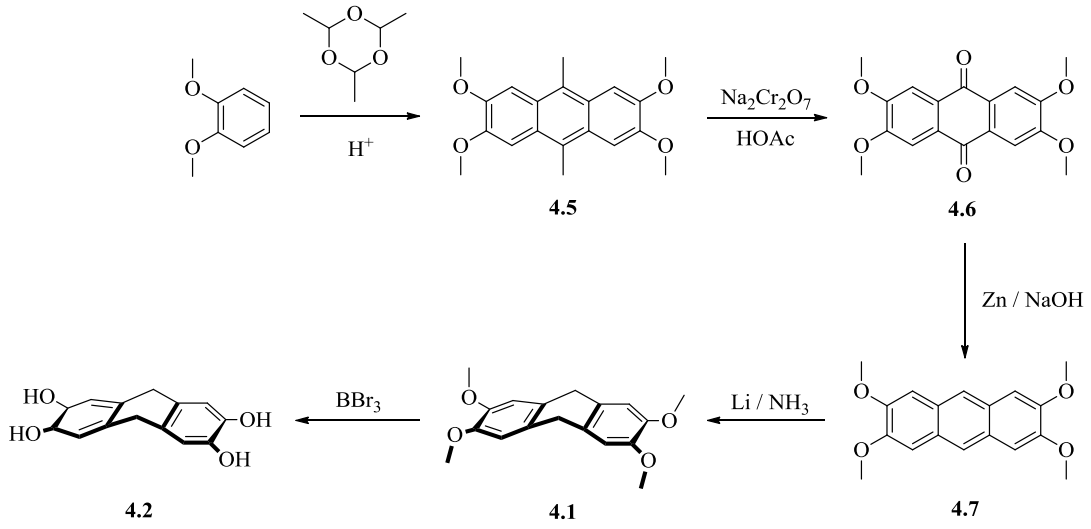

Scheme 4.4. Revised reaction scheme towards target compound **4.2.**

It was hoped that dual ketone reduction of the 9,10-dione using zinc/sodium hydroxide would have directly yielded **4.1**, however the reaction gave only 2,3,6,7-tetramethoxyanthracene in moderate yield after recrystallisation from toluene, confirmed by mass spectrometry (ES+), NMR and elemental analysis. Interestingly also, once purified, the material turns slowly from colourless to yellow in dichloromethane solution, this is assumed to be oxidative decomposition back to the ketone precursor. Reduction of the central anthracene ring to **4.1** was achieved by Birch reduction[6] (lithium / refluxing ammonia) at -78 ^{o}C, although the product was isolated only in low yield (22%).

Spectral identification of **4.1** was performed using ^{1}H NMR, with resonaces at δ = 6.63, 3.86 and 3.23 ppm corresponding to the CH_{Ar}, CH_3 and CH_2 protons respectively. Key evidence also came from the ^{13}C{^{1}H} NMR which displayed all expected resonances, including that of the methylene bridge *C*H$_2$ at δ = 57.2 ppm, which can be positively identified in the DEPT-135 spectrum. It was found however that **4.1** oxidises rapidly back to **4.7** resulting in poor-looking spectra. This sensitivity precluded any further work using **4.1**, including demethylation as the significant air sensitivity would likely be heightened upon conversion to the tetrahydroxy- analogue. Consequent of this discovery, and as the synthetic route towards **4.1** was found to be synthetically nontrivial, an alternative *bis*-dioxolene ligand was found in the form of 2,3,6,7-tetramethoxy-9,10-dimethyl-9,10-dihydro-ethanoanthracene (**4.8**) which may be synthesised very simply in one step by simple acid-catalysed reaction of veratrole and acetonyl acetone.[7] Demethylation of **4.8** using boron tribromide in dry conditions yielded 2,3,6,7-tetrahydroxy-9,10-dimethyl-9,10-dihydro-ethanoanthracene (H$_4$thea, **4.9**) in excellent yield (91%).

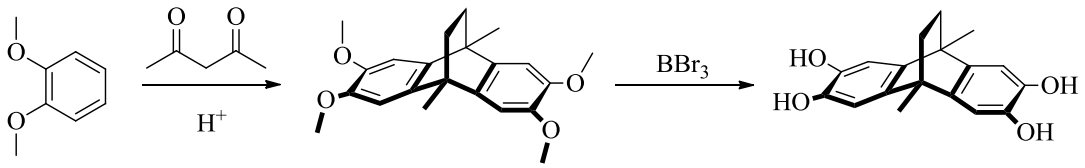

4.8 **4.9**

Scheme 4.5. Reaction scheme of alternative ligand 2,3,6,7-tetrahydroxy-9,10-dimethyl-9,10-dihydro-ethanoanthracene (H_4thea, **4.9**) via 2,3,6,7-tetramethoxy-9,10-dimethyl-9,10-dihydro-ethanoanthracene (**4.8**).

Ligand **4.9** was chosen as an alternative to **4.2** as it retained a saturated carbon spacer between the two dioxolene rings in order to prevent their formal conjugation whilst the addition of ethano-bridge added structural rigidity resulting in a compound which does not show interconversion on the NMR timescale, as shown below in **Figure 4.8**.

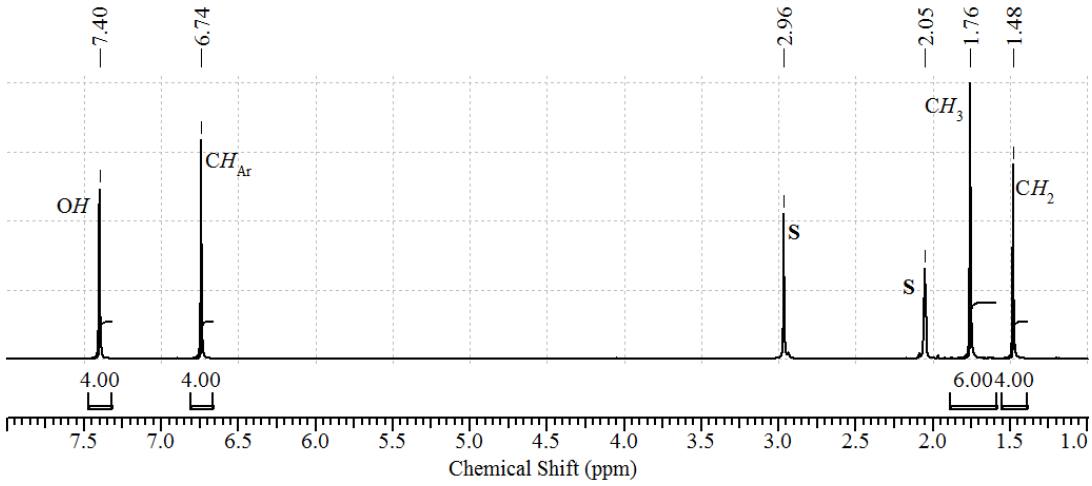

Figure 4.8. Interpreted ^{1}H NMR (300 MHz, acetone-d_6) spectrum of ligand **4.9**. The two solvent (S) signals; 2.96 ppm = water, 2.05 ppm = acetone.

4.2.2 Synthesis of novel $[thea]^{4-}$ Complexes

To date, compound **4.8** has previously been investigated as a comparison to the oxidation of hexamethoxytriptycene where voltammetric analysis showed two sequential oxidations of each veratrole ring. Subsequent oxidation by addition of one equivalent of nitrosonium hexachloroantimonate showed the growth of an IVCT absorption at 6,410 cm^{-1} (1560 nm) in the NIR region. Unfortunately no further characterisation was performed on the oxidised species.[8]

The $[thea]^{4-}$ unit used in this work has also been used previously as a component in a $[Na_{12}\{[Mn(H_20)]_{12}(thea^{4-})_{12}]$ metallacycle[3,] and $[(C_8H_{16}N)_8\{(UO_2)(O_2)\}_4(thea^{4-})_4].(H_2O)_{22}$

cage complex,[9] however during the investigations, the redox chemistry of $[thea]^{4-}$ ligand was not discussed.

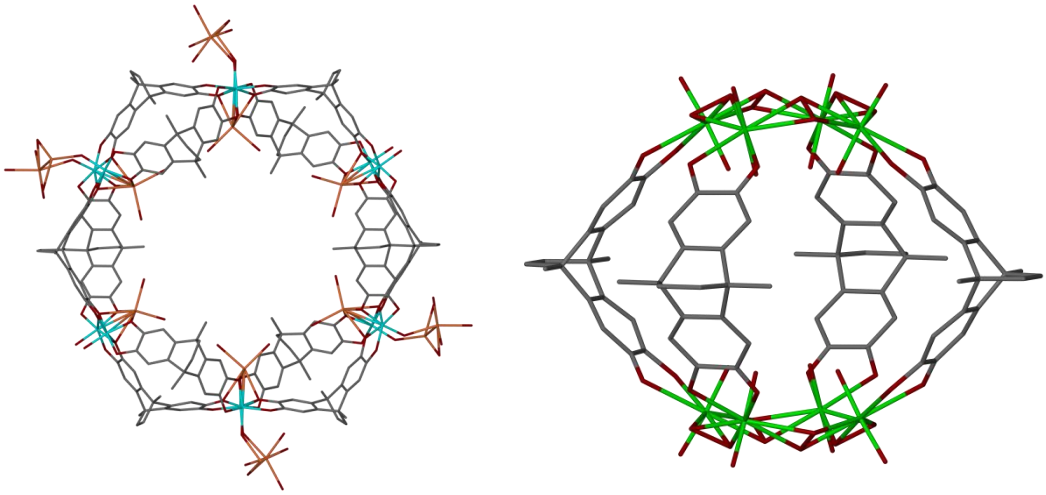

Figure 4.9. Two previously published structures containing the $[thea]^{4-}$ core unit. (Left) $[Na_{12}\{[Mn(H_2O)]_{12}(thea^{4-})_{12}]$ metallacycle.[10] (Right) $[(C_8H_{16}N)_8\{(UO_2)(O_2)\}_4(thea^{4-})_4].(H_2O)_{22}$ cage complex.[9] All hydrogen atoms and counterions are omitted and atoms are shown with arbitrary radii.

A series of novel complexes containing the $[thea]^{n-}$ core unit, were prepared by reaction of a *bis*- protected metal dichloride precursor with $[H_4thea]$ in the presence of suitable base. Ancillary ligands used were the same as those in chapter 3, diphenylphosphinobenzene (dppb), diphenylphosphinoethane (dppe) and di-*tert*-buytl-bipyridine ($^tBu_2Bipy$). For the synthesis of complexes $[\{(dppe)Pt\}_2(thea)]$ (**4.11**) (and $[\{(^tBu_2Bipy)Pt\}_2(thea)]$ (**4.12**), potassium *tert*-butoxide in methanol was used as this appeared to offer the best conversion to the desired product. For $[\{Pt(dppb)\}_2(thea)]$ (**4.10**) however, a mixture of potassium carbonate and methanol in deoxygenated dimethylacteamide gave the best conversion due to poor solubility of the $[(dppb)PtCl_2]$ precursor.

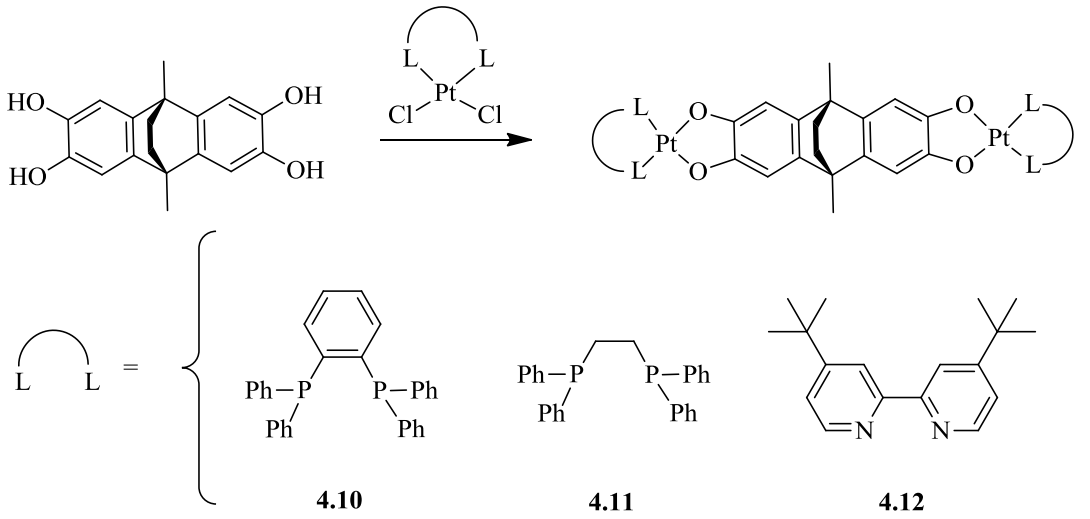

Scheme 4.6. Schematic outline of the synthesis of complexes [{(dppb)Pt}$_2$(thea)] (**4.10**), [{(dppe)Pt}$_2$(thea)] (**4.11**) and [{(^{t}Bu$_2$Bipy)Pt}$_2$(thea)] (**4.12**) discussed in this work.

The products obtained were found to show solution-phase oxygen sensitivity, with those containing diphosphine ancillary ligands affected significantly more compared to the *tert*-butyl bipyridine analogue. This was evident by bleaching and precipitation after prolonged exposure to air when in solution, particularly apparent in oxygenated chlorinated solvents where decomposition to dichloride containing precursors was prevalent presumably due to the small acid content in the solvent. This solution-phase oxygen-sensitivity impacted on the post-synthetic purification techniques resulting in complexes **4.10** and **4.11** being suitable only for recrystallisation from deoxygenated dichloromethane / acetone whilst **4.12** was able to be purified by column chromatography (silica, 1% methanol in dichloromethane).

^{1}H NMR was a key tool in the analysis of neutral complexes **4.10**, **4.11** and **4.12**. Owing to the C_2 symmetry of the μ_2-thea^{4-} products formed, symmetric spectra were again recorded showing one set of resonances and integrations to match one half of each complex. The ^{1}H NMR of **4.11** can be seen in **figure 4.10**, as an example. In the ^{1}H NMR spectrum, resonances from the core [thea]$^{4-}$ are clearly visible at 1.88 and 6.90 ppm corresponding to the methyl protons of in the 9,10- position of the central ethanoanthracene ring and aromatic hydrogen resonances respectively. The peak from resonances originating from the protons of the dihydroxyethano bridge are hidden underneath the water peak at 1.64 ppm. Aromatic resonances arising from the phenylene groups of the {(dppe)Pt}$^{2+}$ moiety are visible as multiplets at 7.39 and 8.08 ppm whilst the characteristic broadened doublet arising from the methylene protons of the dppe backbone is visible at 2.34 ppm with $^2J_{HH}$ = 17 Hz.

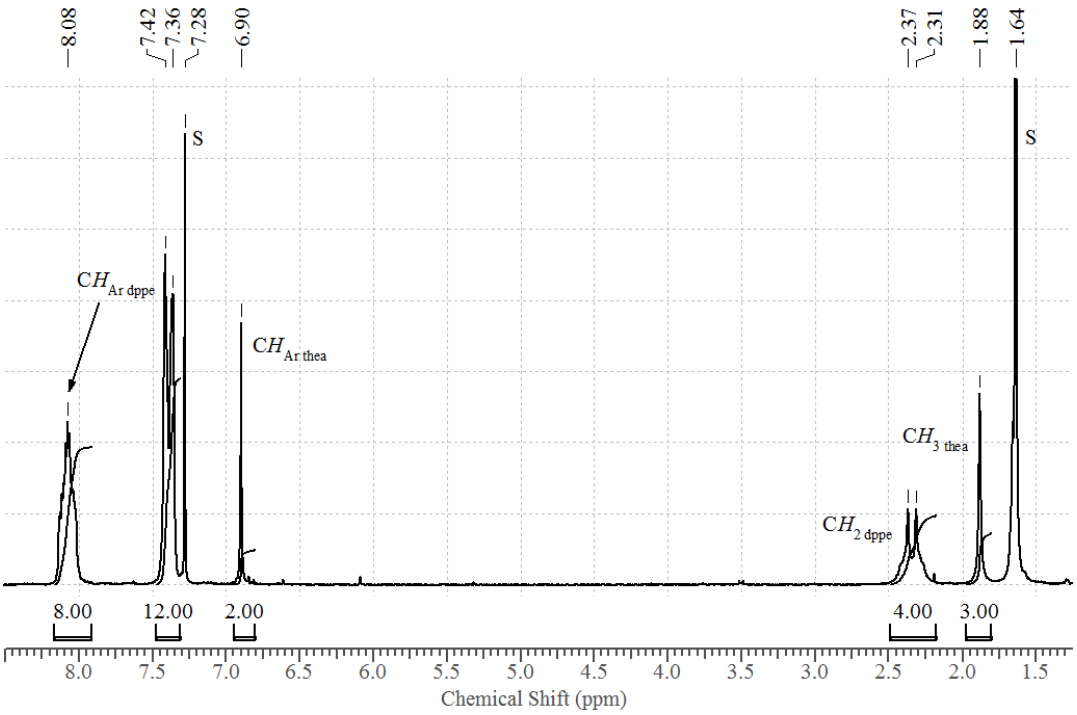

Figure 4.10. Interpreted ^{1}H NMR (300 MHz, 5 :1 $CDCl_3$: MeOD) spectrum of **4.11**. Solvent (s) signals at δ = 7.28 and 1.64 ppm belong to $CHCl_3$ and H_2O respectively.

As complexes **4.10** and **4.11** both contained phosphorus nuclei, these could also be probed by $^{31}P\{^{1}H\}$ NMR which displayed a chemical shift close to δ = 29.8, close to that expected of a symmetric diphosphine bound to a platinum catecholate.[11] In addition to the central phosphorus peak, the spectrum also showed satellites arising from coupling to one ^{195}Pt (I = ½) nucleus. The $J_{P\text{-}Pt}$ value arising from this coupling was calculated as 3406 Hz, again within that expected of a complex containing a symmetric platinum(II) diphosphine.[11-12]

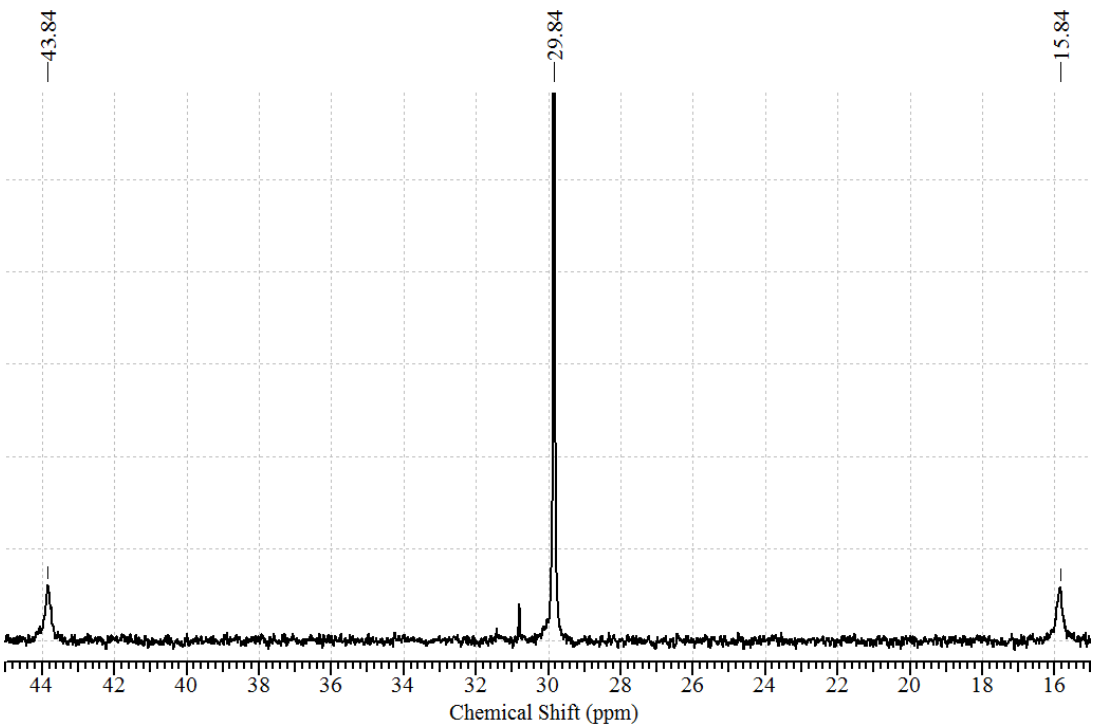

Figure 4.11. $^{31}P\{^{1}H\}$ NMR (121 MHz, 5 :1 $CDCl_3$: MeOD) of **4.11** showing additional Platinum satellites.

Infrared spectroscopic analysis of complexes containing dioxolene moieties can be very informative with the presence of specific peaks assignable to each dioxolene oxidation state. Each of the neutral complexes, **4.10 - 4.12**, display strong characteristic bands between 1230-1290 cm^{-1} assignable to the catceholate ν(CO) whilst weaker bands at 1200 and 1340 cm^{-1} are assignable to the skeletal ring vibrations ν(CC) and ν(CO) which are virtually independent of the ancillary ligand. Other characteristic bands are evident between 1420 and 1490 cm^{-1} which are also commonly used to identify catecholate internal ν(CC) whilst for **4.12**, evidence for the coordination of a bipyridine moiety is seen at 1550 $cm^{-1,}$ corresponding to the bipy ν(CC) whilst the band at approximately 1620 cm^{-1} corresponds to the internal ν(CN).

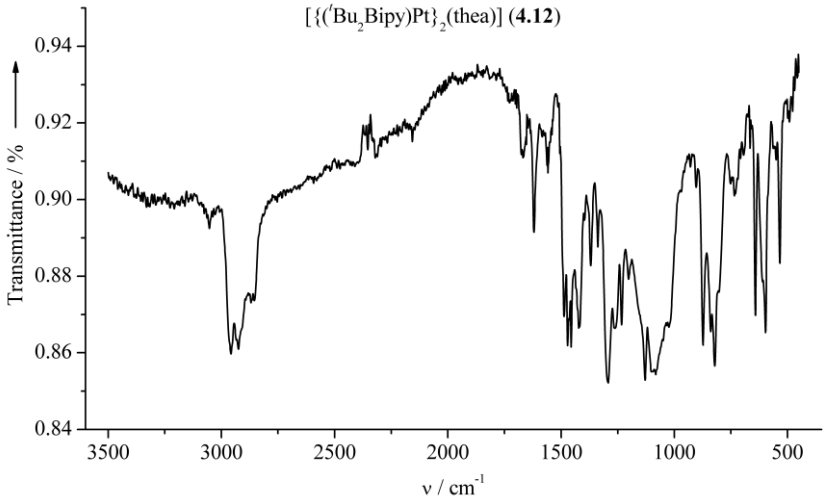

Figure 4.12. IR (solid state) spectrum of **4.12**.

Mass spectrometry (ES+) was again useful for the characterisation of complexes **4.10** - **4.12** where each case the spectra clearly displayed the intact complexes, $[\mathbf{4.10}]^{n+}$, $[\mathbf{4.11}]^{n+}$ and $[\mathbf{4.12}]^{n+}$ (n = 1,2) as major components. In addition, strong cationic peaks were associated with the formation of sodium adducts (from use of a sodium formate calibrant) and exogenous dimethylsulfoxide molecules. Evidence for daughter products arising from fragmentation was seen in all complexes as the loss of one $\{(L)Pt\}^{2+}$ unit (L = dppb, dppe or $^{t}Bu_2Bipy$), whilst the formula associated with each structure was confirmed by microanalysis.

4.2.3 Single-crystal X-ray Structural Characterisation of Neutral Complexes

Single crystals of complexes **4.10** and **4.11** were grown by slow diffusion of pentane into a dichloromethane solution of **4.10** or **4.11**, under a nitrogen atmosphere. Details of their structure refinements, analysis and determination of parameter Δ, are given below.

Structure Refinement of $[\{Pt(dppb)\}_2(thea)]\bullet C_5H_{12}\bullet(4\text{-}x)CH_2Cl_2$ ($\mathbf{1}\bullet C_5H_{12}\bullet(4\text{-}x)CH_2Cl_2$ (4.10)

The single crystal X-ray structure of **4.10** was solved and refined in the monoclinic space group $P2_1/c$, despite the closeness of angle β to 90°. Attempts to identify a unique orthorhombic space group from the dataset using *XPREP*[13] and *NEWSYMM*[14] were unsuccessful however, likely consequent of the pseudosymmetry present due to disorder of the complex as described below.

As shown in **Figure 4.13** and **Figure 4.14**, The crystal structure acted to confirm the μ_2-coordination mode of the central $[thea]^{n-}$ ligand, and confirm the retention of the dihydroxy-ethano bridge as seen by ^1H NMR.

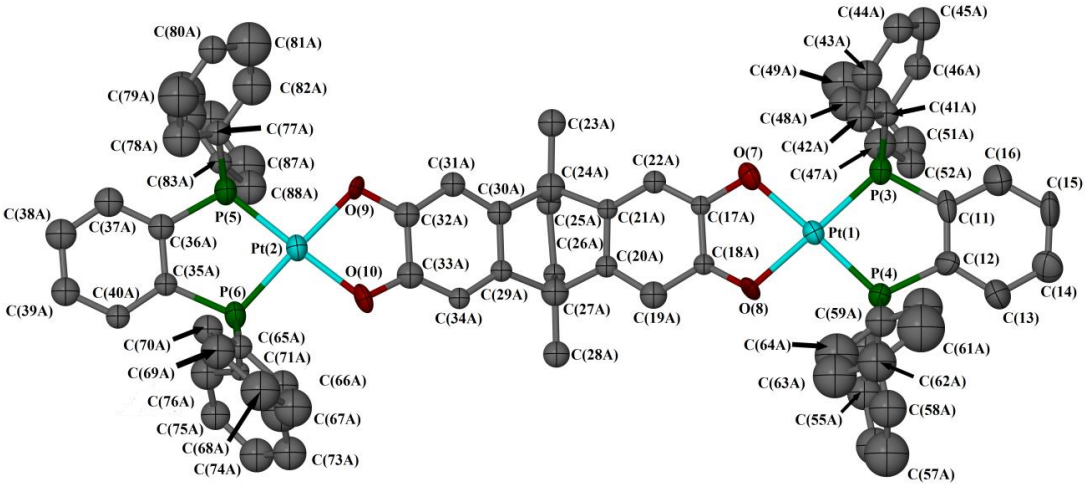

Figure 4.13. View and atom numbering scheme of disorder site 'A' of complex $[\{(dppb)Pt)\}_2(thea)]$ in **4.10**•$x$$C_5H_{12}$•(4-$x$)$CH_2Cl_2$. Displacement ellipsoids are set at 50% probability and only one orientation of disordered phenylene rings has been included. All hydrogen atoms have been removed for clarity**.** Colour code: Pt, cyan; P, green; O, red; C, grey.

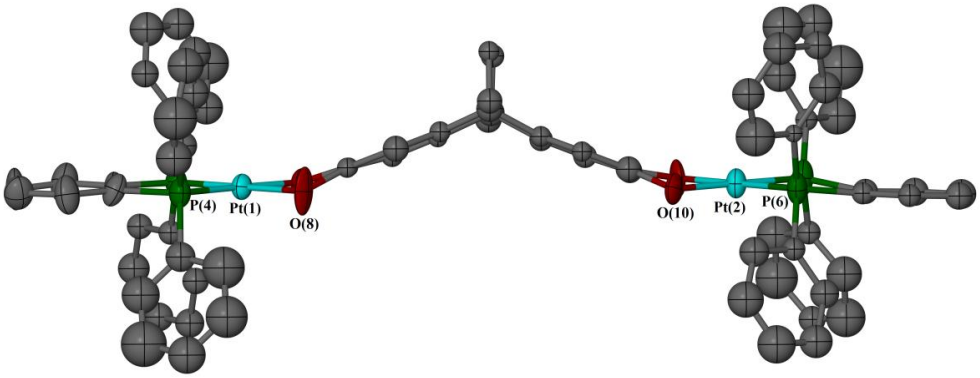

Figure 4.14. Side-on view and partial atom numbering of disorder site 'A' of complex [{(dppb)Pt)}$_2$(thea)] in **4.10**•*x*C_5H_{12}•(4-*x*)CH_2Cl_2. Displacement ellipsoids are set at 50% probability and only one orientation of disordered phenylene rings has been included. All hydrogen atoms have been removed for clarity. Colour code: Pt, cyan; P, green; O, red; C, grey.

The asymmetric unit of **4.10** was shown to contain one complex, disordered over two sites spanning a non-crystallographic mirror plane. Of this whole complex disorder, both platinum atoms, all phosphorus atoms and phenylene ring C(11) > C(16) lie on this presumed mirror plane and were modelled as fully occupied whilst all other atoms were disordered over two sites and modelled with occupancies of one half and labelled as 'A' and 'B'. The two halves of the $[thea]^{4-}$ unit appeared to refine reasonably without restraints, whilst all other phenyl and phenylene rings C(35A) > C(40A) and C(35B) > C(40B) were modelled as rigid hexagons with half occupancies.

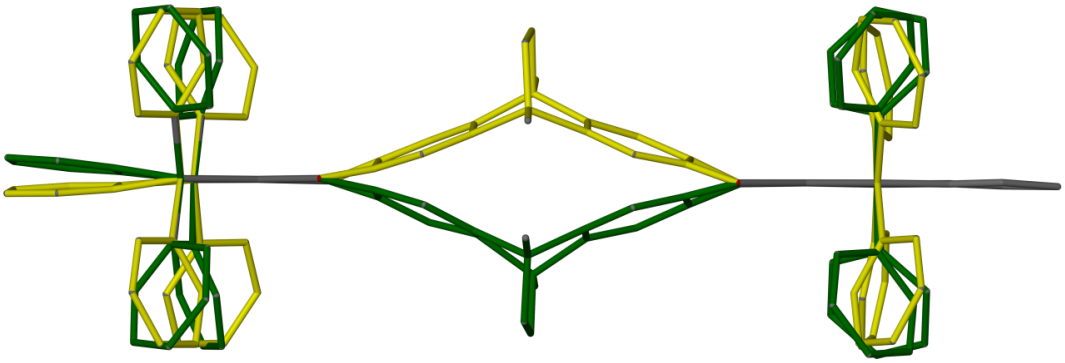

Figure 4.15. Side-on view of full molecule disorder of [{(dppb)Pt}$_2$(thea)] (**4.10**) across a non-crystallographic mirror plane. The 'A' orientation of show in yellow whilst the 'B' orientation is shown in green. All atoms have arbitrary radii and full occupied atoms are shown in grey for comparison.

There were two reasonably defined regions of solvent obvious in the structure, both of which were occupied by pentane molecules. Due to a number of high isotropic thermal parameters (U_{iso}) for both of these molecules, it is likely that they be modelled further into at least two completely disordered molecules, however this could not be achieved. Instead, both molecules were refined with occupancies lower than 1, as 0.30 for C(89)...C(93) and 0.50 for C(94)...C(98). Both of these pentane molecules reside in channels, running along parallel to the unit cell direction *a*, with approximate sizes of 7.7 x 5.0 Å and 7.1 x 4.0 Å due to the disorder present in the molecules which define the pore 'walls'. It was evident that these pores contained further disordered molecules, which unfortunately could not be modelled, therefore a *SQUEEZE*[14] analysis of a model containing only the complex molecule was performed which showed a total void space of 2077 Å^3, or 24% of the unit cell volume. It is likely that this is a conservative estimate however, as the model will always show both types of 'A' and 'B' orientations of **4.10**. These voids were shown to contain 680 electrons per unit cell, equating to 170 per asymmetric unit. This could be calculated to be either four complete molecules of pentane, four complete molecules of dichloromethane or a combination as both contain 42 electrons. As only pentane was positively identified in the Fourier map however, the formula unit and density calculations were performed using the complex formula and 4 molecules of pentane.

A packing diagram of the structure **4.10**•*x*C_5H_{12}•(4-*x*)CH_2Cl_2 showed that these pentane molecules reside in channels parallel to the crystallographic (100) plane, as shown in **Figure 4.16**.

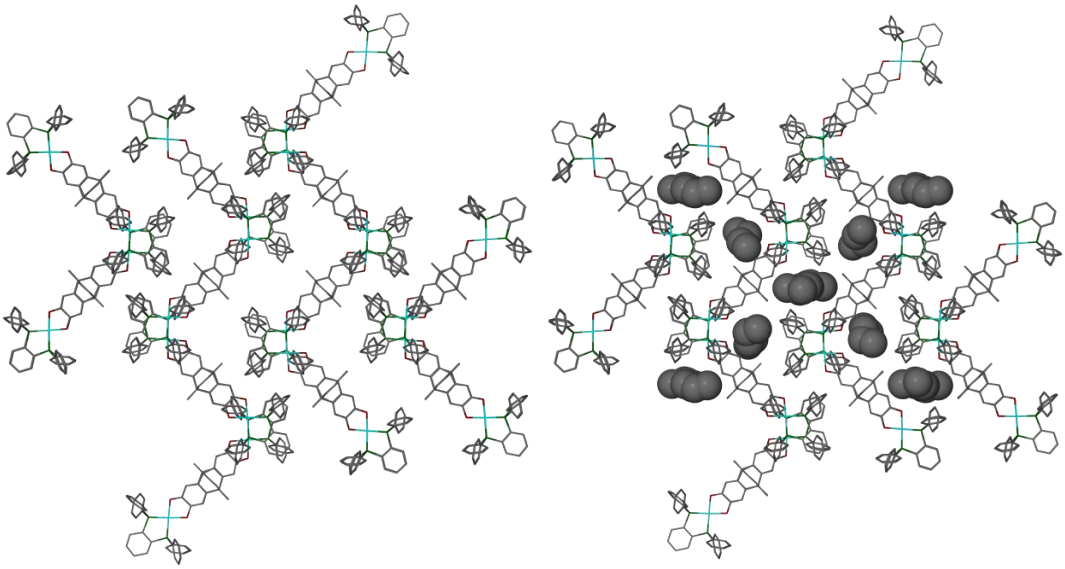

Figure 4.16. Packing diagrams of **4.10**•*x*C_5H_{12}•(4-*x*)CH_2Cl_2 viewed parallel to the crystallographic plane (100) showing (left) empty solvent channels and (right) filled solvent channels. Pentane molecules are shown as space-filling to highlight the position of the solvent channels whilst all complex molecules are shown with atoms of arbitrary radii. Colour code: Pt, cyan; P, green; O, red; C, grey.

For the final model, the original dataset was used and the one remaining Fourier peak left unassigned within the solvent channel was modelled as a half-occupied carbon-atom. The highest remaining Fourier peaks were found in the vicinity of disordered pentane molecule C(94)...C(98), likely due to the presence of another orientation within the structure which was not modelled, close to the platinum atoms and on the ethenyl groups of the 9,10-dihydroxy-9,10-ethanoanthracene backbone. Finally, all fully occupied non-hydrogen atoms were refined anisotropically and all hydrogen atoms placed in calculated positions and refined using a 'riding model'.

Table 4.1. Selected bond distances and angles for the two formula units of structure **4.10**•*x*C_5H_{12}•(4-*x*)CH_2Cl_2.

4.10•*x*C_5H_{12}•(4-*x*)CH_2Cl_2	
Pt(1)-P(3) / P(4) [Å]	2.210(5) / 2.211(4)
Pt(1)-O(7) / O(8) [Å]	2.2019(14) / 2.046(12)
Pt(2)-P(5) / P(6) [Å]	2.2089(6) /2.2101(5)
Pt(2)-O(9)/ O(10) [°]	2.0327(12) / 2.0356(14)
P(3)-Pt(1)-P(4) [°]	87.50(14)
O(7)-Pt(1)-P(3) [°]	94.8(3)
O(8)-Pt(1)-P(4) [°]	93.6(4)
O(7)-Pt(1)-P(4) [°]	177.6(3)
O(8)-Pt(1)-P(3) [°]	178.9(4)
O(8)-Pt(1)-O(7) [°]	84.1(5)
P(5)-Pt(2)-P(6) [°]	87.3(2)
O(9)-Pt(2)-P(5) [°]	91.5(3)
O(10)-Pt(2)-P(6) [°]	93.6(4)
O(10)-Pt(2)-P(5) [°]	178.9(4)
O(9)-Pt(2)-P(6) [°]	177.6(3)
O(10)-Pt(2)-O(9) [°]	84.0(5)
O(10)-Pt(2)-P(5) [°]	178.9(4)
C(20a)-C(27a)-C(29a) [°]	115.2(18)
C(30a)-C(24a)-C(21a) [°]	109.(3)
C(20b)-C(27b)-C(29b) [°]	92.8(18)
C(21b)-C(24b)-C(30b) [°]	107.(3)

Structure Refinement and Analysis of [{Pt(dppe)}$_2$(thea)]•0.67H_2O•2.07CH_2Cl_2 (4.11)

The single crystal X-ray structure of **4.11**•0.67H_2O•2.07CH_2Cl_2 was solved and refined in the orthorhombic space group $P2_12_12_1$. The asymmetric unit was shown to contain three complex units, ten dichloromethane molecules (nine of these are only partially occupied) and two remaining peaks in the Fourier map which refined as fully occupied water molecules.

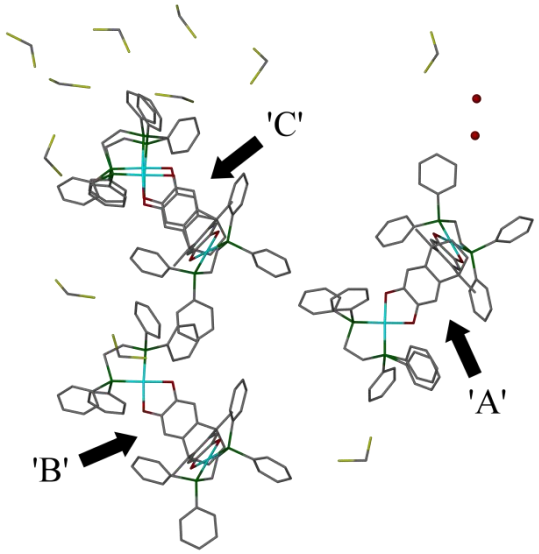

Figure 4.17. View of asymmetric unit of **4.11**•0.67H_2O.2.07CH_2Cl_2 along unit cell axis *a* showing the three complex units of **4.11** named 'A', 'B' and 'C' and the spatial positions of dichloromethane and water solvent molecules. All hydrogen atoms have been omitted for clarity and specific molecule disorder has been retained as this is referred to in the text. Colour code: Pt, cyan; Cl, yellow; P, green; O, red; C, grey.

The obtained structure confirmed the bent μ_2- coordination mode of the $[thea]^{4-}$ core unit, as can be seen in **Figure 4.18** below.

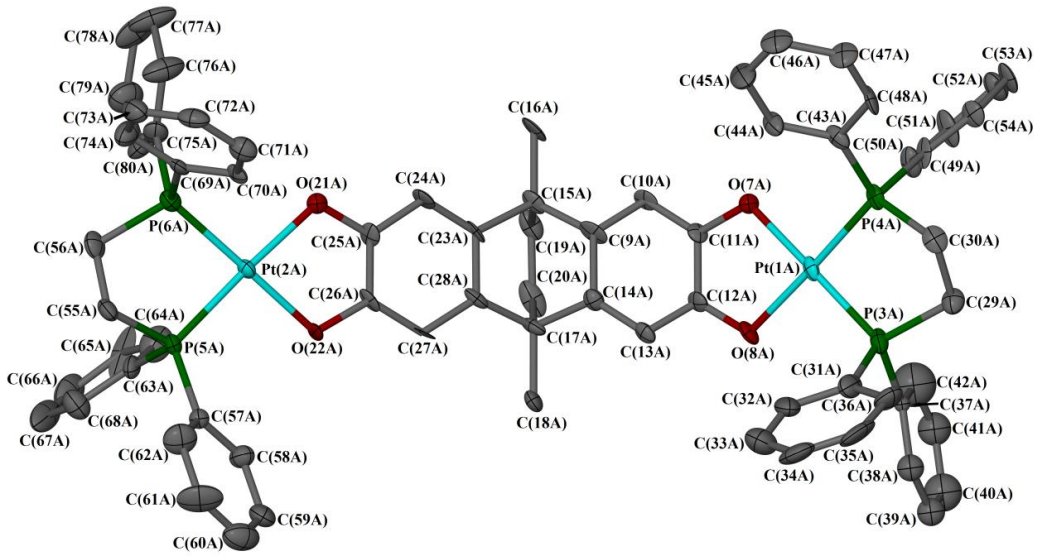

Figure 4.18. View and atom numbering scheme of $[\{(dppe)Pt\}_2(thea)]$ complex 'A' in **4.11**•$0.67H_2O.2.07CH_2Cl_2$. Only one orientation of disordered phenylene ring C(37A)...C(42A) is shown and displacement ellipsoids are set at 50% probability. All hydrogen atoms have been removed for clarity. Colour code: Pt, cyan; P, green; O, red; C, grey.

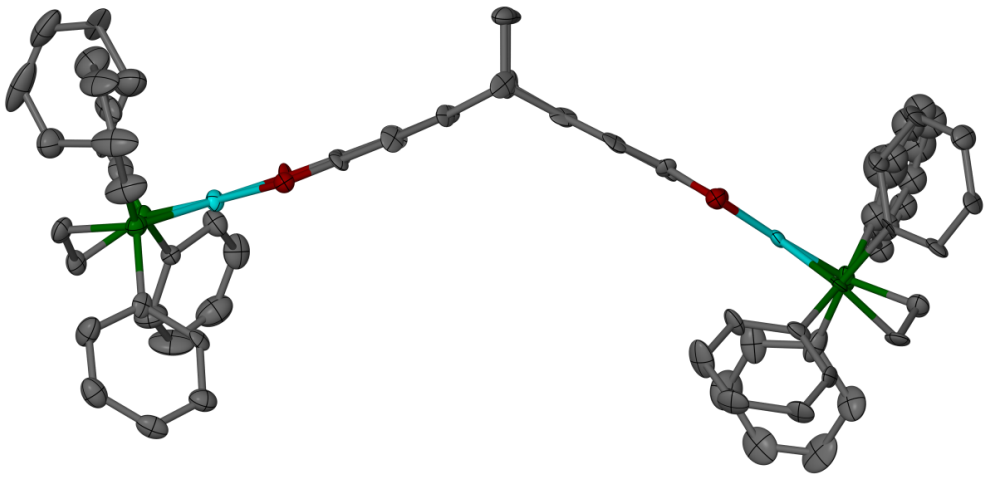

Figure 4.19. Second view of $[\{(dppe)Pt\}_2(thea)]$ complex 'A' in **4.11**•$0.67H_2O.2.07CH_2Cl_2$. Only one orientation of disordered phenylene ring C(37A)...C(42A) is shown and displacement ellipsoids are set at 50% probability. All hydrogen atoms have been removed for clarity. Colour code: Pt, cyan; P, green; O, red; C, grey.

Disorder present in complex 'C' on fragment [(dppe)Pt($O_2C_6H_2$], centred on Pt(2C) was successfully refined over two sites with occupancy ratios of 0.62 : 0.38. Two of the four phenyl groups of the disordered dppe moiety were able to be refined over two sites with the same occupancy ratio whilst the remaining two were refined as fully occupied and shared over the two fragments. Of these two phenyl groups, ring C(75C) > C(80C) could likely be modelled over another site, however the additional orientation could not be defined in the Fourier map. An additional phenyl ring belonging to complex 'A', C(36C) > C(40C) was also refined over two positions and along with all other disordered rings, refined as rigid hexagons. Other restraints applied within the refinement included distance restraints of P-C = 1.85(2) Å and C-C = 1.52(2) Å to the disordered fragment [(dppe)Pt($O_2C_6H_2$] of complex 'C' and C-Cl = 1.78(2) Å and Cl...Cl = 2.90(2) Å to two partially occupied dichloromethane molecules centred on C(81) and C(121).

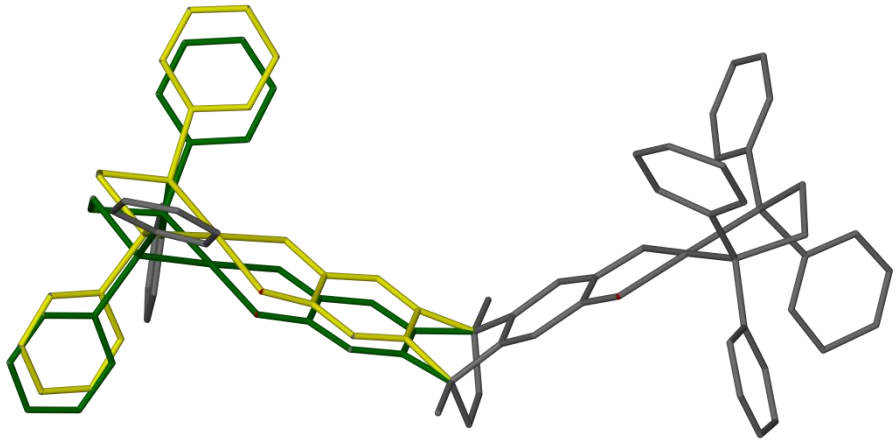

Figure 4.20. View of disordered fragment [(dppe)Pt($O_2C_6H_2$], centred on Pt(2C) present in complex 'C' of **4.11**•$0.67H_2O.2.07CH_2Cl_2$. All atoms have arbitrary radii and hydrogen atoms are omitted for clarity.

The majority of non-hydrogen atoms (including partial Pt and Cl atoms with occupancies greater than 0.4), were refined anisotropically with the exception of disordered fragment [(dppe)Pt($O_2C_6H_2$] of complex 'C' and three other C and O atoms which refined continually as non-positive definite. All hydrogen atoms were placed in calculated positions and refined using a riding model. Residual Fourier peaks within the structure numbered greater than 30, with values between 2.5-8.1 *e*. $Å^3$, and are almost all less than 1 Å from one of six platinum atoms within the model. Furthermore, the deepest Fourier hole of -21 *e*. $Å^3$ is 0.8 Å away from Pt(1A).

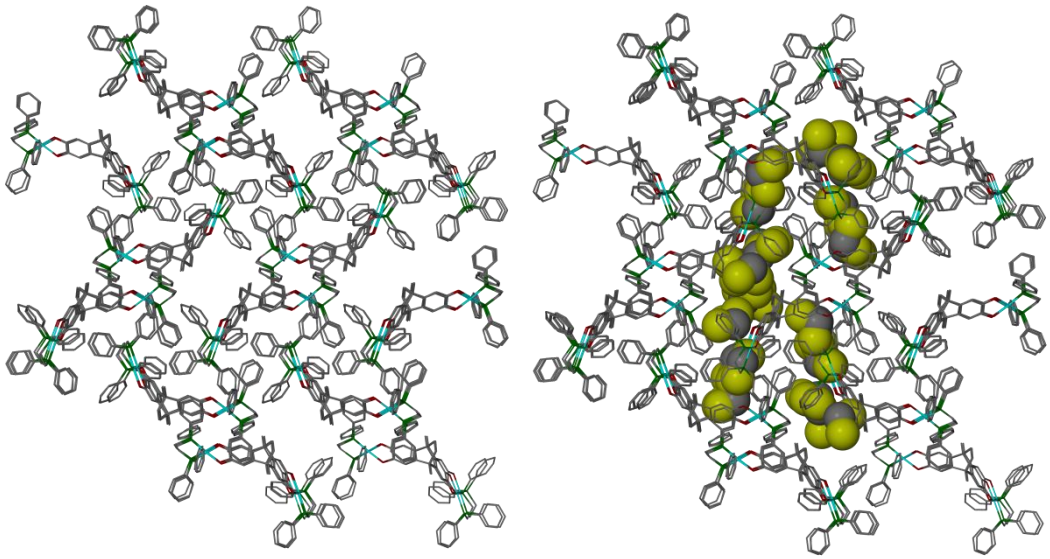

Figure 4.21. Packing diagrams of **4.11**•0.67H_2O.2.07CH_2Cl_2 showing (left) empty solvent channels and (right) filled solvent channels. Dichloromethane molecules are shown as space-filling to highlight the position of the solvent channels whilst all molecules of 4.11 are shown with atoms of arbitrary radii. Colour code: Pt, cyan; Cl, yellow; P, green; O, red; C, grey.

The water molecules and the majority of dichloromethane molecules within the model reside in crystallographic channels along the unit cell *c* axis, parallel to [0 0 1], as shown in **Figure 4.21**.

Table 4.2. Selected bond lengths and angles extracted from the structure **4.11**•0.67H_2O•2.07CH_2Cl_2 for the three different molecules 'A', 'B' and 'C'.

4.11•0.67H_2O•2.07CH_2Cl_2			
	A	B	C
Pt(1)-P(3) / P(4) [Å]	2.202(4) / 2.227(3)	2.236(4) / 2.228(5)	2.222(4) / 2.216(3)
Pt(1)-O(7) / O(8) [Å]	2.026(8) / 2.048(8)	2.040(10) / 2.006(13)	2.037(10) / 2.034(9)
Pt(2)-P(5) / P(6) [Å]	2.225(3) / 2.220(4)	2.223(4) / 2.205(4)	2.216(6) / 2.222(10)
			2.195(6) / 2.225(10)
Pt(2)-O(21) / O(22) [°]	2.042(9) / 2.032(9)	2.045(9) / 2.049(9)	2.071(15) / 2.05(2)
			2.039(14) / 2.04(2)
P(3)-Pt(1)-P(4) [°]	85.93(13)	85.73(17)	85.96(13)
P(3)-Pt(1)-O(7) [°]	177.7(3)	179.2(3)	179.2(3)
P(3)-Pt(1)-O(8) [°]	95.5(3)	96.8(3)	98.1(3)
P(4)-Pt(1)-O(7) [°]	95.6(3)	94.1(3)	93.3(3)
P(4)-Pt(1)-O(8) [°]	177.4(3)	177.5(3)	175.3(3)
O(7)-Pt(1)-O(8) [°]	83.0(4)	83.4(4)	82.7(4)
P(5)-Pt(2)-P(6) [°]	85.60(4)	86.21(15)	85.8(2) / 87.3(4)
P(5)-Pt(2)-O(21) [°]	176.3(3)	178.6(4)	178.0(5) / 177.9(6)
P(5)-Pt(2)-O(22) [°]	93.9(2)	96.5(3)	97.4(4) / 95.3(6)
P(6)-Pt(2)-O(21) [°]	97.8(3)	93.9(3)	93.4(4) / 94.8(6)
P(6)-Pt(2)−O(22) [°]	179.3(3)	176.1(3)	176.0(4) / 175.6(7)
O(21)-Pt(2)-O(22) [°]	82.7(3)	83.4(4)	83.5(5) / 82.6(7)
C(9)-C(15)-C(23) [°]	108.5(11)	107.3(12)	107.9(11) / 102.4(13)
C(14)-C(17)-C(28) [°]	107.6(10)	109.7(12)	113.0(14) / 100.0(15)

4.2.4 Electrochemical Analysis of Complexes

Cyclic and differential pulse voltammetry of complexes **4.10-4.12** were recorded in dichloromethane / 0.1 M $^{n}Bu_4NPF_6$ at 298 K and are displayed in **Figure 4.22**-**Figure 4.24**. All spectra showed two clear reversible, low-potential oxidations at -0.37±0.02 and -0.11±0.02 V *vs* $[FeCp_2]$ / $[FeCp_2]^+$. These processes were assigned as belonging to the ligand-centred $[thea]^{4-} \leftrightarrow [thea^{\bullet}]^{3-} \leftrightarrow [thea^{\bullet\bullet}]^{2-}$ (cat/cat ↔ cat/sq ↔ sq/sq) redox series. The processes for all complexes were well separated (ΔE) of approximately 250 mV which is intermediate between those observed for complexes of spiro^{4-} (ΔE = 0.14-0.17 V) and biscat (ΔE = 0.32-0.5 V) although are similar to that of **4.8** (ΔE = 0.28 V).[8] The following $[thea^{\bullet\bullet}]^{2-} \leftrightarrow [thea^{\bullet}]^{-} \leftrightarrow [thea]^{0}$ (sq/sq ↔ sq/q ↔ q/q) oxidations occurred at approximately +0.75 V *vs* $[FeCp_2]$ / $[FeCp_2]^+$ however were significantly less well separated ($\Delta E \leq 110$ mV) and were only partially reversible at room temperature. **Table 4.3** and **Table 4.4**

summarise the half-potentials ($E_{1/2}$) and peak potentials (E_p) extracted from the voltammograms.

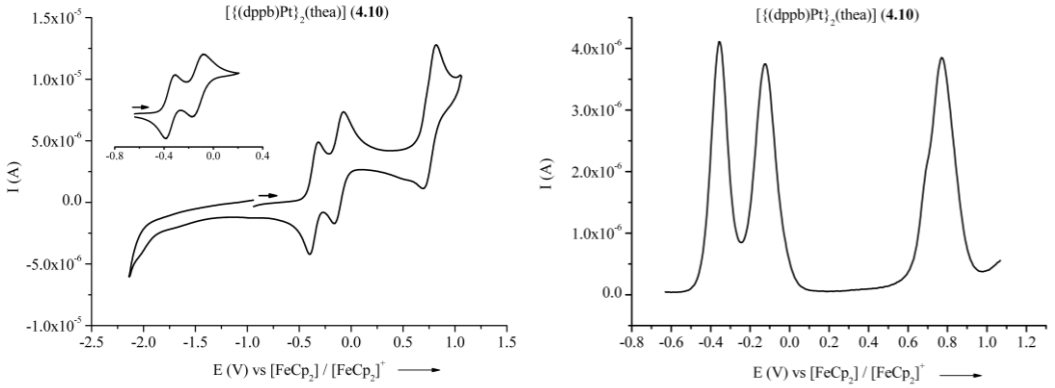

Figure 4.22. (Left) Cyclic voltammogram (CV) of [{(dppb)Pt}$_2$(thea)] (**4.10**) in CH_2Cl_2/0.1 M $^nBu_4NPF_6$ at 298 K. Insert shows a CV scan of the first two oxidations, highlighting their chemical reversibility. (Right) Differential pulse voltammogram (DPV) of [{(dppb)Pt}$_2$(thea)] (**4.10**) in CH_2Cl_2/0.1 M nBu$_4$NPF$_6$ at 298 K.

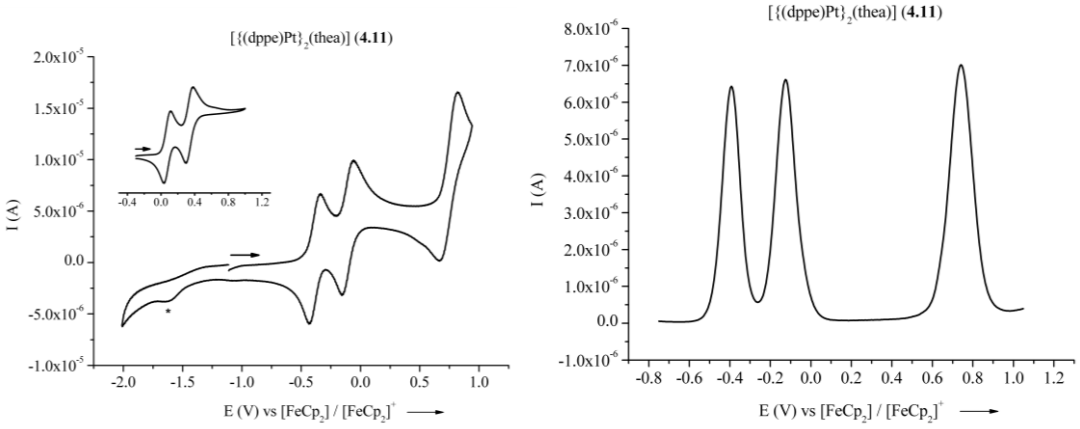

Figure 4.23. (Left) Cyclic voltammogram (CV) of [{(dppe)Pt}$_2$(thea)] (**4.11)** in CH_2Cl_2/0.1 M nBu$_4$NPF$_6$ at 298 K. The starred feature is a weak decomposition product perhaps associated with the high oxidation potential associated with the partly reversible sq/q couples. Insert shows a CV scan of the first two oxidations, highlighting their chemical reversibility. (Right) Differential pulse voltammogram (DPV) of [{(dppe)Pt}$_2$(thea)] (**4.11)** in CH_2Cl_2/0.1 M nBu$_4$NPF$_6$ at 298 K.

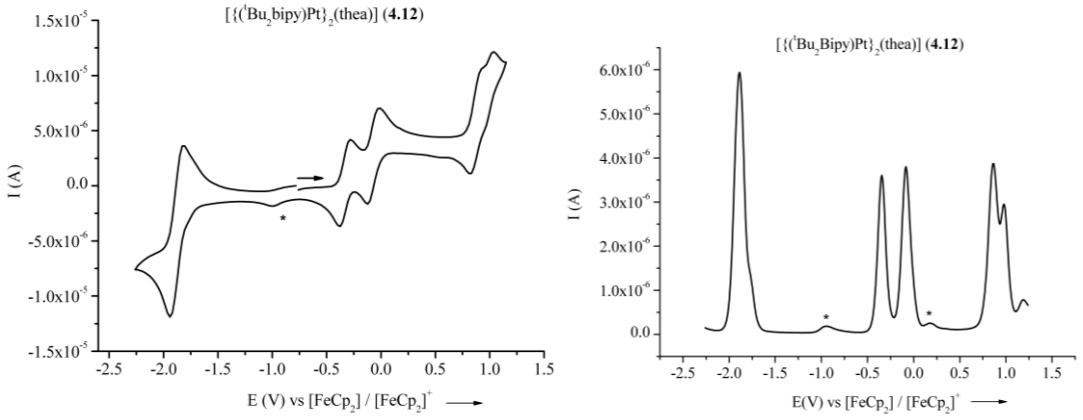

Figure 4.24. (Left) Cyclic voltammogram (CV) of [{(^{t}Bu$_2$Bipy)Pt}$_2$(thea)] (**4.12)** in CH_2Cl_2/0.1 M nBu$_4$NPF$_6$ at 298 K. The starred feature is understood to be a weak decomposition product. (Right) Differential pulse voltammogram (DPV) of [{(^{t}Bu$_2$Bipy)Pt}$_2$(thea)] (**4.12)** in CH_2Cl_2/0.1 M ^{n}Bu$_4$NPF$_6$ at 298 K. The two starred features are understood to be weak decomposition products.

Table 4.3. Cyclic voltammetric (CV) data for complexes **4.10** – **4.12** recorded in dichloromethane / 0.1 M NBu$_4$PF$_6$ at 298 K. Potentials (V) are referenced against an internal [FeCp$_2$] / [FeCp$_2$]$^+$ standard, and were measured at a scan rate of 0.1 Vs^{-1}.

	$E_{½}$ [bipy]$^{-/0}$	$E_{½}$ [thea]$^{4-/3-}$	$E_{½}$ [thea]$^{3-/2-}$	$E_{½}$ [thea]$^{2-/-}$	$E_{½}$ [thea]$^{-/0}$
[{Pt(dppb)}$_2$(thea)] (**4.10**)	–	–0.36	–0.13	0.77[a,b]	0.77[a,b]
[{Pt(dppe)}$_2$(thea)] (**4.11**)	–	–0.39	–0.12	0.74[a,b]	0.74[a,b]
[{Pt(^{t}Bu$_2$Bipy)}$_2$(thea)] (**4.12**)	–1.89	–0.35	–0.09	0.87[a]	0.98[a]

[a] Partly chemically reversible. [b] [thea]$^{2-/-}$ and [thea]$^{-/0}$ half-potentials are indistinguishable.

Table 4.4. Differential Pulse Voltammetric (DPV) data for complexes **4.10** – **4.12** recorded in dichloromethane / 0.1 M NBu_4PF_6 at 298 K. Potentials (V) are referenced against an internal $[FeCp_2]$ / $[FeCp_2]^+$ standard, and were measured at a scan rate of 0.1 Vs^{-1}.

	E_p $[bipy]^{-/0}$	E_p $[thea]^{4-/3-}$	E_p $[thea]^{3-/2-}$	E_p $[thea]^{2-/-}$	E_p $[thea]^{-/0}$
[{(dppb)Pt}$_2$(thea)] (**4.10**)	–	–0.36	–0.13	0.72 (sh)[a]	0.77
[{(dppe)Pt}$_2$(thea)] (**4.11**)	–	–0.39	–0.12	0.74[b]	0.74[b]
[{(^{t}Bu$_2$Bipy)Pt}2(thea)] (**4.12**)	–1.89	–0.35	–0.09	0.87	0.98

[a] (sh) = shoulder. [b] $[thea]^{2-/-}$ and $[thea]^{-/0}$ peak potentials are indistinguishable.

Due to the accessible potentials of the oxidation processes $[thea]^{4-} \leftrightarrow [thea^{\bullet}]^{3-} \leftrightarrow [thea^{\bullet\bullet}]^{2-}$ (cat/cat ↔ cat/sq ↔ sq/sq) of **4.10**, **4.11** and **4.12**, as shown by cyclic and differential pulse voltammetry, it was possible to generate oxidised products $[\mathbf{4.10}]^+$, $[\mathbf{4.10}]^{2+}$, $[\mathbf{4.11}]^+$, $[\mathbf{4.11}]^{2+}$ and $[\mathbf{4.12}]^+$ by treatment of neutral precursors with 1 or 2 equivalents of ferrocenium hexafluorophosphate ($[FeCp]PF_6$). These were analysed by UV-vis/NIR and electron paramagnetic resonance (EPR) spectroscopies. It was found that solutions of $[\mathbf{4.10}]^+$, $[\mathbf{4.10}]^{2+}$, $[\mathbf{4.11}]^+$ and $[\mathbf{4.11}]^{2+}$ were stable for days at 298 K under an inert atmosphere therefore allowing them to be isolated as solids and complexes $[\mathbf{4.10}]^+PF_6$ and $[\mathbf{4.11}]^+PF_6$ to be obtained in single crystalline form however, $[\mathbf{4.12}]^+$ decomposed slowly under these conditions. Results from the analysis of these oxidised species are presented below.

4.2.5 UV-vis/NIR $[FeCp_2]PF_6$ Titrations

Oxidative titrations of neutral complexes **4.10**, **4.11** and **4.12** were monitored by UV-vis/NIR performed in nitrogen-degassed dichloromethane at 298 K using Ferrocenium hexafluorophosphate $[FeCp_2]PF_6$ owing to the negative potentials of the first and second oxidations *versus* ferrocene as seen above. Oxidation of **4.10** and **4.11** gave deep green solutions of $[\mathbf{4.10}]^+$, $[\mathbf{4.10}]^{2+}$, $[\mathbf{4.11}]^+$, $[\mathbf{4.11}]^{2+}$ whilst oxidation of **4.12** yielded a dark purple solution of $[\mathbf{4.12}]^+$.

Oxidations of **4.10** and **4.11** proceeded isobestically, therefore showing their stability to high oxidation states, showing the ingrowth of a new IVCT transition at approximately 5,500 cm^{-1}. The presence of at least one other high wavelength shoulder to this transition was also noted, at approximately 7,700 cm^{-1}, along with a small increase in intensity of the

dioxolene → ancillary L (dppb or dppe) LL'CT near 14,500 cm^{-1}. Interestingly, the intensity of the IVCT bands of [**4.11**]$^{+}$ and [**4.11**]$^{2+}$ are significantly greater than [**4.10**]$^{+}$ and [**4.10**]$^{2+}$. A very strong IVCT transition at 5,200 cm^{-1} for the oxidation of **4.12** to [**4.12**]$^{+}$ was also noted, reaching ε_{max} = 6.3 × 10^{3} M^{-1} cm^{-1}, twice the intensity of [**4.11**]$^{+}$. Despite this, the titration was unfortunately not isobestic therefore indicating the slow decomposition of [**4.12**]$^{+}$ at 298 K. Interestingly also, it can be seen in **Figure 4.27** that under these conditions, there is a small percentage of [**4.12**]$^{+}$ present before the addition of any oxidant, evident by the presence of the IVCT at 5,200 cm^{-1}. This is assumed to be due to partial aerial oxidation whilst in the solution phase although did not seem to affect purification of the complex by column chromatography.

A characteristic method of analysing IVCT transitions is to measure the width and half-height ($\Delta\nu_{1/2}$), this gives an insight into the degree of valent electron delocalisation throughout the molecule.[15] Larger $\Delta\nu_{1/2}$ values indicate that the IVCT transition is broad, therefore approaching the Robin/Day class II formalism whilst narrow IVCT transitions with smaller $\Delta\nu_{1/2}$ values indicate the process is approaching Robin/Day class III behaviour. Taking into account the high wavelength shoulder, the experimental value for [**4.10**]$^{+}$ $^{+}$and [**4.11•**]$^{+}$ taken from **Figure 4.25** and **Figure 4.26**, this could be estimated as $\Delta\nu_{1/2}$ = 2300 ± 50 cm^{-1} using **Equation 3.1**. This experimental value is actually smaller than that predicted using eq. 1 for [**4.10**]$^{+}$ and [**4.11**]$^{+}$ which gives $\Delta\nu_{1/2}$ = 3550 cm^{-1} for a class II mixed valence system with IVCT λ_{max} = 1810 nm (E = 5525 cm^{-1}).

The discrepancy between predicted and experimental values here indicates that the two halves of the [thea$^{\bullet}$]$^{3-}$ framework are strongly coupled, and are approaching class III in character at 298 K. Therefore, from $\Delta\nu_{1/2}$ it is possible to calculate the electron coupling energy (H_{AB}) in the class III limit using **Equation 3.2**, yielding H_{AB} = 1150 cm^{-1}.

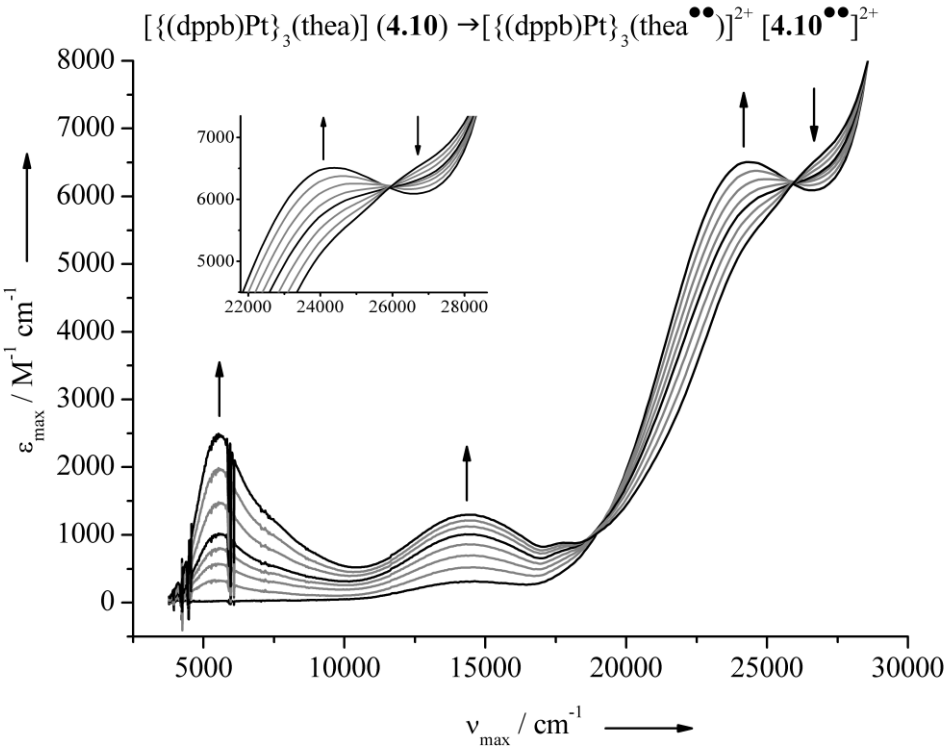

Figure 4.25. Oxidative titration of **4.10** to [**4.10**]$^{+}$ and [**4.10**]$^{2+}$ using one or two equivalents of $[FeCp_2]PF_6$. The spectra of **4.10**, [**4.10**]$^{+}$ and [**4.10**]$^{2+}$ are shown as black lines whilst intermediate oxidations are shown in grey. The high-energy isobestic point is shown as an insert.

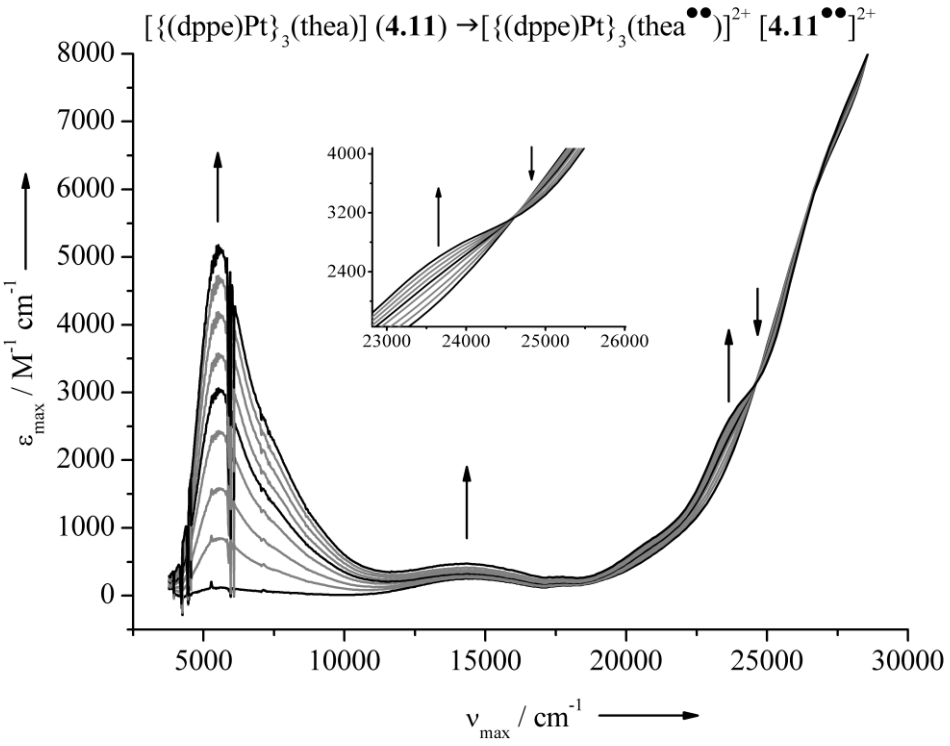

Figure 4.26. Oxidative titration of **4.11** to [**4.11**$^{\bullet}$]$^{+}$ and [**4.11**$^{\bullet\bullet}$]$^{2+}$ using one or two equivalents of $[FeCp_2]PF_6$. The spectra of **4.11**, [**4.11**$^{\bullet}$]$^{+}$ and [**4.11**$^{\bullet\bullet}$]$^{2+}$ are shown as black lines whilst intermediate oxidations are shown in grey. The high-energy isobestic point is shown as an insert.

The same process for the oxidation of **4.12** to [**4.12**]$^{+}$ may be adopted, although taken as tentative as the oxidation was not isobestic, by estimating $\Delta\nu_{1/2}$ = 2850 ± 50 cm^{-1} experimentally again due to the presence of a high wavelength shoulder. Using **Equation 3.1**, $\Delta\nu_{1/2}$ for a class II mixed valence system with IVCT ν_{max} = 5,200 cm^{-1}, may be estimated as $\Delta\nu_{1/2}$ = 3470 cm^{-1}. This is again significantly larger than experimentally observed therefore indicating the two halves of the [thea$^{\bullet}$]$^{3-}$ are strongly coupled and are approaching class III formalism. Consequently, as with [**4.3**]$^{+}$ and [**4.4**]$^{+}$, the electron coupling energy H_{AB}, may again be calculated using **Equation 3.2** giving H_{AB} = 1425 cm^{-1}. It is interesting here to note that the electron coupling energy for [**4.5**]$^{+}$ is larger than those for [**4.3**]$^{+}$ and [**4.4**]$^{+}$ indicating stronger coupling between the two [thea$^{\bullet}$]$^{3-}$ halves. Whilst it is not immediately apparent why this may be the case, it could be postulated that the actual electronic characteristics of the ancillary ligands, diphosphines *versus* bipyridine, may play a part due to the better π-accepting nature of bipyridine compared to the strongly σ-donating diphosphine family. The extent and strength of coupling between the two dioxolene rings of

[thea$^{\bullet}$]$^{3-}$ framework with different ancillary ligands will be explored later in the chapter using EPR spectroscopy.

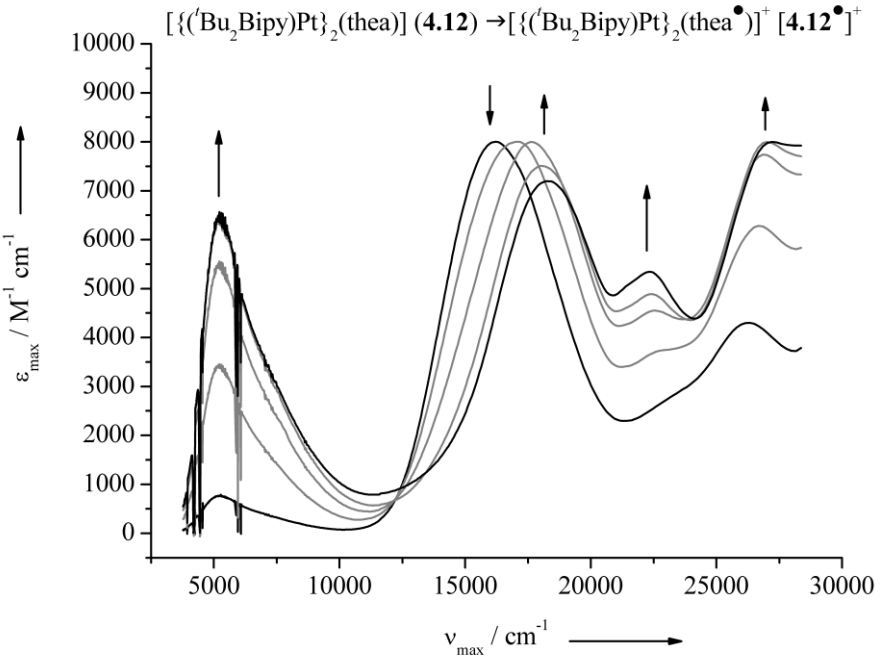

Figure 4.27. Addition of one equivalent of $[FeCp_2]PF_6$ to **4.12**. The spectra of pure **4.12** and [**4.12**$^{\bullet}$]$^{+}$: $[FeCp_2]PF_6$ (1 :1) are shown as black lines whilst intermediate oxidations are shown in grey.

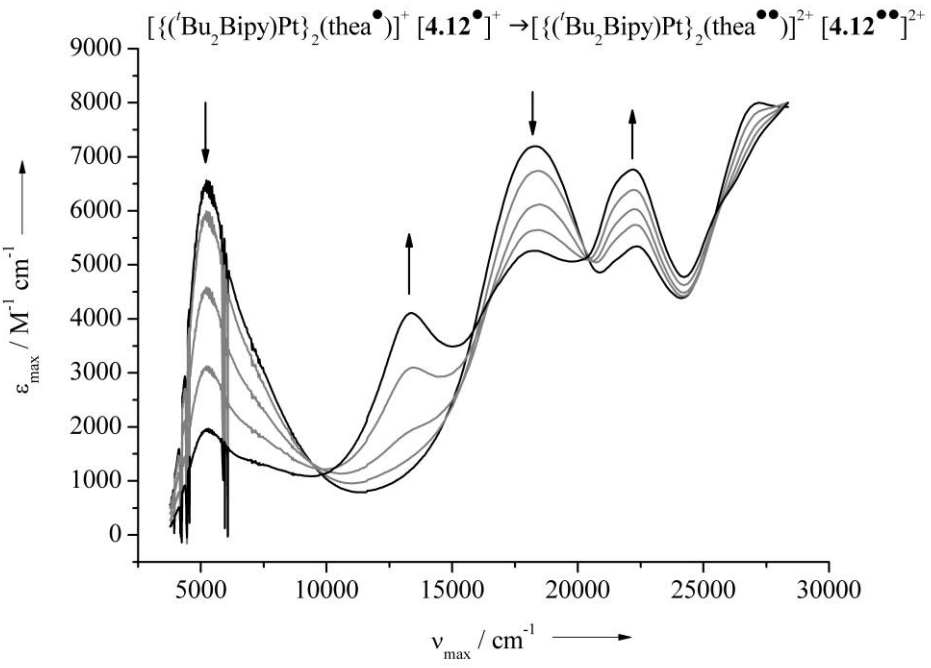

Figure 4.28. Addition of a second equivalent of $[FeCp_2]PF_6$ to **4.12**. $[\mathbf{4.12^{\bullet}}]^+$: $[FeCp_2]PF_6$ (1:1) to $[\mathbf{4.12^{\bullet\bullet}}]^+$: $[FeCp_2]PF_6$ (1 :2) are shown as black lines whilst intermediate oxidations are shown in grey.

Table 4.5. UV/vis/NIR data for the different redox states of **4.10**-**4.12** in CH_2Cl_2 at 296 K. Data are shown in **Figures 4.25-4.28.**

	Solution Colour	ν_{max}, 10^3 cm^{-1} (ε_{max}, 10^3 $M^{-1}cm^{-1}$])
[{Pt(dppb)}$_2$(thea)] (**4.10**)	Orange	24.3 (6.5), 14.6 (0.3)
[{Pt(dppb)}$_2$(thea$^{\bullet}$)] ([**4.10$^{\bullet}$**]$^+$)	Green	25.3 (sh), 18.2 (sh), 14.3 (1.0), 6.8 (sh), 5.5 (1.0)
[{Pt(dppb)}$_2$(thea$^{\bullet\bullet}$)] ([**4.10$^{\bullet\bullet}$**]$^{2+}$)	Green	25.3 (sh), 18.2 (sh), 14.3 (1.3), 6.8 (sh), 5.5 (2.5)
[{Pt(dppe)}$_2$(thea)] (**4.11**)	Yellow	14.3 (0.3)
[{Pt(dppe)}$_2$(thea$^{\bullet}$)] ([**4.11$^{\bullet}$**]$^+$)	Green	24.6 (sh), 21.1 (sh), 14.3 (0.3), 6.8 (sh), 5.5 (3.1)
[{Pt(dppe)}$_2$(thea$^{\bullet\bullet}$)] ([**4.11$^{\bullet\bullet}$**]$^{2+}$)	Green	24.7 (sh), 21.1 (sh), 14.3 (0.5), 6.8 (sh), 5.5 (5.1)
[{Pt(^{t}Bu$_2$Bipy)}$_2$(thea)] (**4.12**)	Blue	26.5 (4.3), 16.3 (8.0).
[{Pt(^{t}Bu$_2$Bipy)}$_2$(thea$^{\bullet}$)] ([**4.12$^{\bullet}$**]$^+$)	Purple	27.3 (8.0), 22.5 (5.3), 18.4 (7.2), 6.7 (sh), 5.2 (6.3)[a]

[a] Formation of $[\mathbf{4.12^{\bullet}}]^+$ from **4.12** was not isosbestic, so these data are only approximate.

4.2.6 UV-vis/NIR Spectroelectrochemistry

Owing to the success of chemical oxidative titrations outlined above, in collaboration with Dr. Nathan Patmore at The University of Sheffield, UV-vis/NIR spectroelectrochemical data for the oxidation processes of **4.10** were recorded in 0.1 M $^{n}Bu_4NPF_6$ in dichloromethane at 253 K. The spectra recorded for each oxidation process are displayed below.

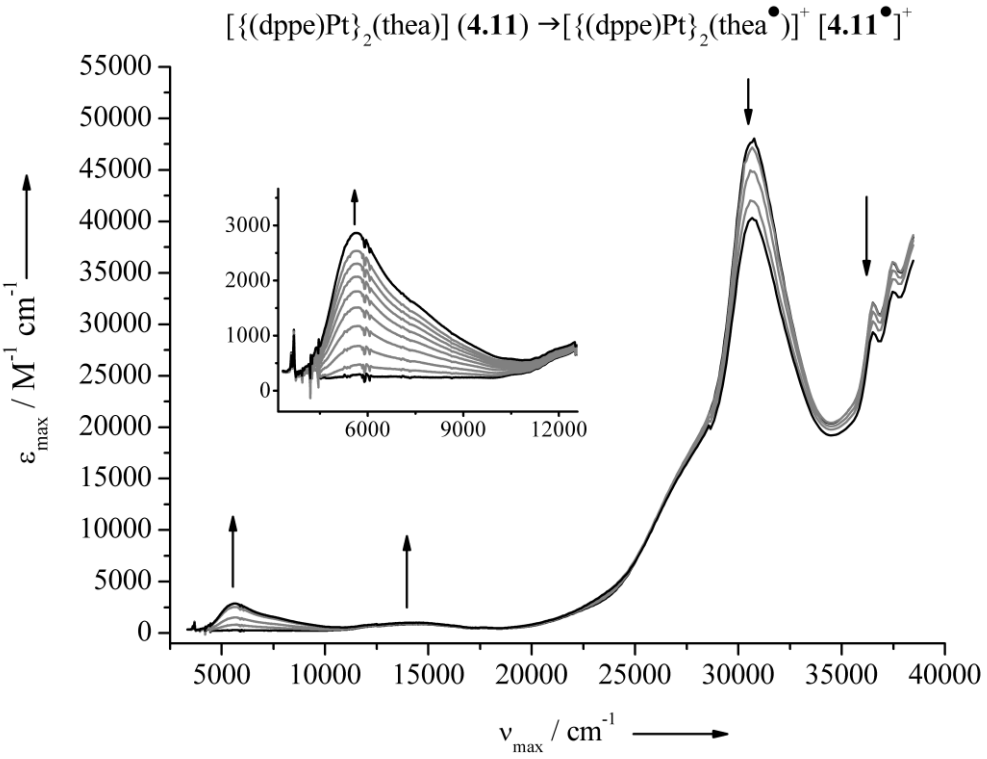

Figure 4.29. UV-vis/NIR spectroelectrochemical data at 253 K in CH_2Cl_2 / 0.1 $^{n}Bu_4NPF_6$ for the oxidation of [{(dppe)Pt}$_2$(thea)] (4.11) → [{(dppe)Pt}$_2$(thea$^{\bullet}$)]$^+$ [**4.11**$^{\bullet}$]$^+$. The spectra of **4.11** and [**4.11**$^{\bullet}$]$^+$ are shown in black, whilst intermediate spectra are shown in grey. Insert shows a close up of IVCT band at 5,500 cm^{-1}. The discontinuities observed near 12,400 and 28, 700 cm^{-1} are artefacts from the grating changes in the spectrometer.

Oxidation of **4.11** to [**4.11**$^{\bullet}$]$^+$ again resulted in the growth of a very intense IVCT transition with ν_{max} of 5,500 cm^{-1}. The oxidation also resulted in the increase in intensity of the band at 30,800 cm^{-1}, assumed to be sq→dppe LL'CT in character, due to its presence in the homologous mononuclear complex **3.7** at approximately 32,000 cm^{-1}.[11] This process matched the first chemical oxidation of **4.11** well, whereby both processes displayed an IVCT transition in similar positions, intensity and bandwidth. Both complexes spectra similarly display a growth in intensity of the band close to 14,000 cm^{-1} and both display an isobestic point close to 25,000 cm^{-1}.

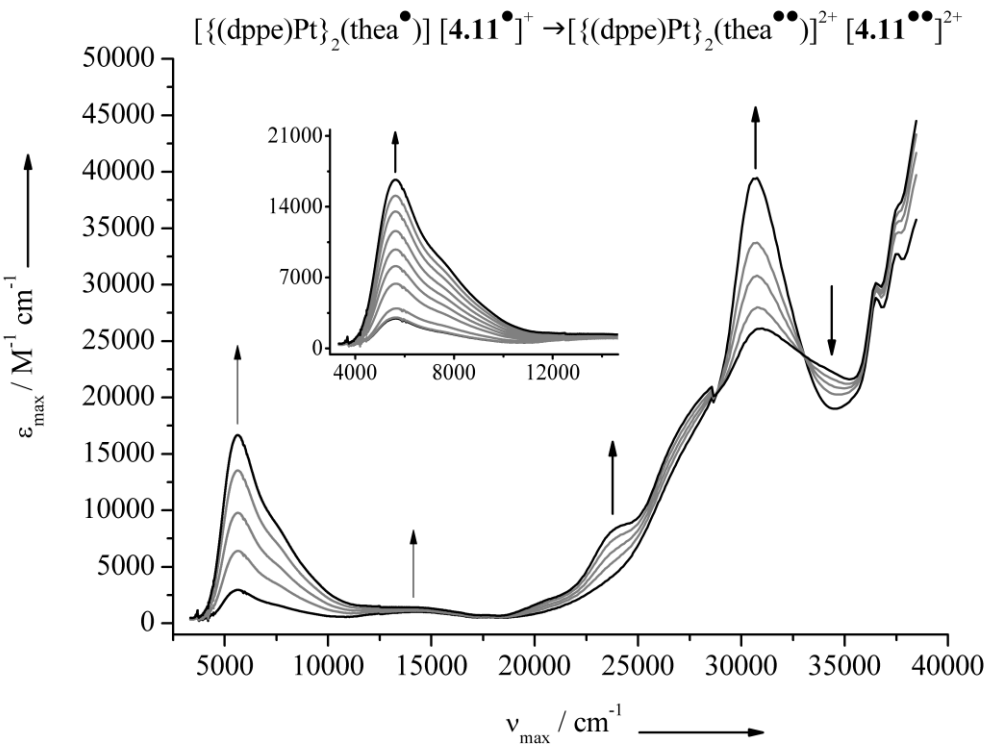

Figure 4.30. UV-vis/NIR spectroelectrochemical data at 253 K in CH_2Cl_2 / 0.1 $^nBu_4NPF_6$ for the oxidation of $[\{(dppe)Pt\}_2(thea^{\bullet})]^+$ $[\mathbf{4.11}^{\bullet}]^+ \rightarrow [\{(dppe)Pt\}_2(thea^{\bullet\bullet})]^{2+}$ $[\mathbf{4.11}^{\bullet\bullet}]^{2+}$ The spectra of $[\mathbf{4.11}^{\bullet}]^+$and $[\mathbf{4.11}^{\bullet\bullet}]^{2+}$ are shown in black, whilst intermediate spectra are shown in grey. Insert shows a close up of IVCT band at ν_{max} = 5,500 cm^{-1}. The discontinuities observed near 12,400 and 28, 700 cm^{-1} are artefacts from the grating changes in the spectrometer.

The second electrochemical and chemical oxidations of **4.11** again displayed similar positions in the IVCT band (approximately 5,500 cm^{-1}). Despite this, both differed significantly in the intensity of the band where the spectrum of electrochemically oxidised $[\mathbf{4.11}^{\bullet\bullet}]^{2+}$, this was shown to be over three times more intense than that of the chemically oxidised complex (16.6 and 5.1 × 10^3 $M^{-1}cm^{-1}$ respectively). The band close to 14,000 cm^{-1} was also significantly more intense, and again almost three times more intense (1.4 and 0.5 × 10^3 $M^{-1}cm^{-1}$ respectively). This result implied the second chemical oxidation of **4.11** did not proceed to completion, likely due to the closeness of the second oxidation of **4.11** to the oxidation potential of the $[FeCp_2]$/ $[FeCp_2]^+$ couple ($E_{½}$ = 0.12 V *vs* $[FeCp_2]$ / $[FeCp_2]^+$). As a result, no further work was conducted on the chemically double-oxidised complex $[\mathbf{4.11}^{\bullet\bullet}]^{2+}$.

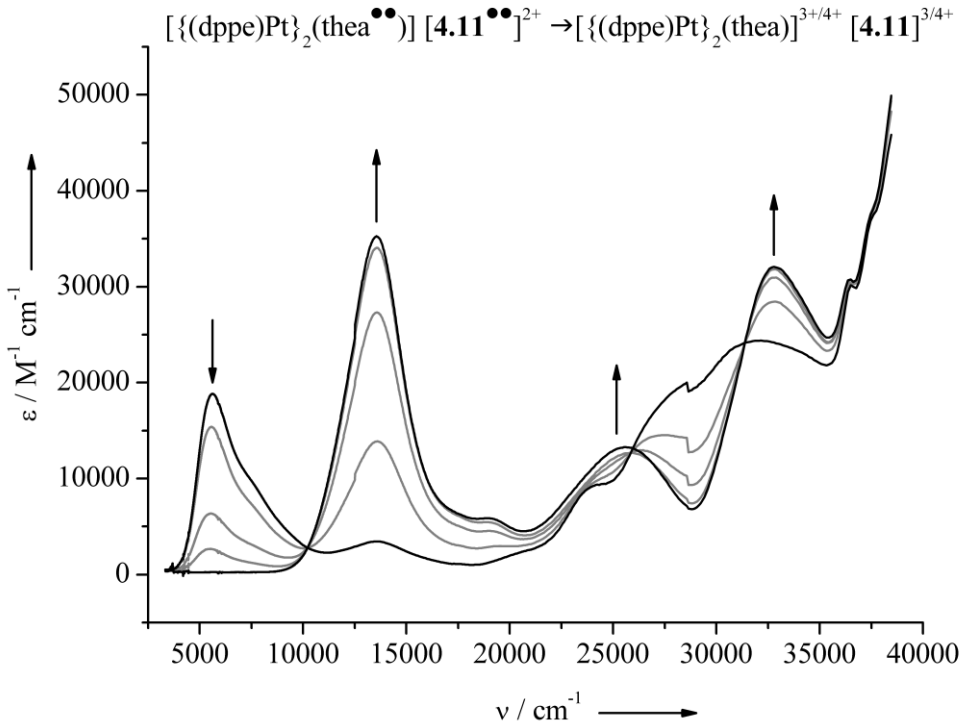

Figure 4.31. UV-vis/NIR spectroelectrochemical data at 253 K in CH_2Cl_2 / 0.1 $^nBu_4NPF_6$ for the oxidation of $[\{(dppe)Pt\}_2(thea^{\bullet\bullet})]^{2+}$ $[\mathbf{4.11}^{\bullet\bullet}]^{2+}$ → $[\{(dppe)Pt\}_2(thea)]^{3+/4+}$ $[\mathbf{4.11}]^{3+/4+}$ The spectra of pure $[\mathbf{4.11}^{\bullet\bullet}]^{+}$ and $[\mathbf{4.11}]^{3+/4+}$ are shown in black, whilst intermediate spectra are shown in grey. The discontinuities observed near 12,400 and 28, 700 cm^{-1} are artefacts from the grating changes in the spectrometer.

As the higher oxidation states of the complex were accessible using the spectroelectrochemical technique, the third and fourth oxidations corresponding to the two sq/q oxidation processes of complex **4.11** were also monitored, as shown in and appeared to display two isobestic points close to 31,000 and 10,000 cm^{-1}. Further oxidation of $\mathbf{[4.11}^{\bullet\bullet}\mathbf{]}^{2+}$ to $\mathbf{[4.11]}^{3+}$ and $\mathbf{[4.11]}^{4+}$ resulted in the decay of the IVCT absorption at 5,600 cm^{-1} and growth of a very intense absorption close to 35,000 cm^{-1}, assignable as a Pt(dπ) → q MLCT, as seen at 13,300 cm^{-1} in the quinone complex $[\{(Bipy)_2Ru\}biscat]$ (q-q).[16]

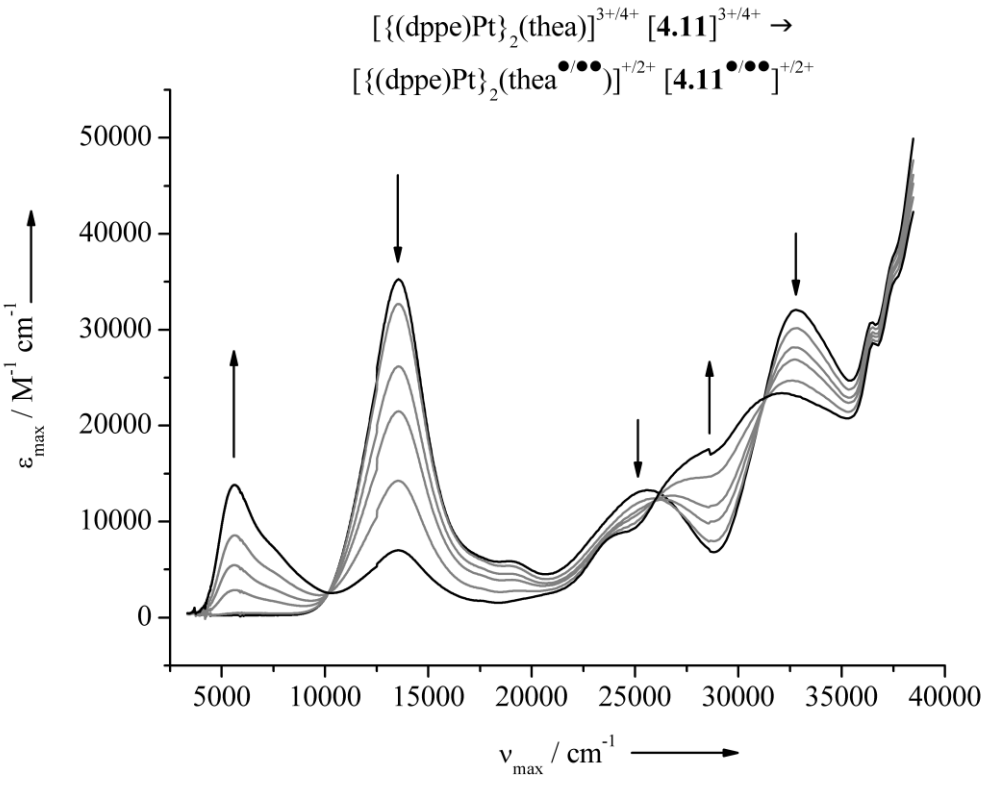

Figure 4.32. UV-vis/NIR spectroelectrochemical data at 253 K in CH_2Cl_2 / 0.1 $^nBu_4NPF_6$ for the re-reduction of $[\{(dppe)Pt\}_2(thea)]^{4+}$ $[\mathbf{4.11}]^{4+} \rightarrow [\{(dppe)Pt\}_2(thea^{\bullet/\bullet\bullet})]^{+/2+}$ $[\mathbf{4.11}^{\bullet/\bullet\bullet}]^{+/2+}$ The spectra of $[\mathbf{4.11}]^{4+}$ and $[\mathbf{4.11}^{\bullet/\bullet\bullet}]^{+/2+}$ are shown in black, whilst intermediate spectra are shown in grey. The discontinuities observed near 12,400 and 28,700 cm^{-1} are artefacts from the grating changes in the spectrometer.

Re-reduction of $[\mathbf{4.11}]^{3+/4+}$ to $[\mathbf{4.11}^{\bullet\bullet}]^{2+}$ or $[\mathbf{4.11}]^{3+}$ by cycling the potential back to -0.40 V resulted in the re-growth of IVCT absorption in the same position as previously observed along with the re-growth of absorptions at 30,800 cm^{-1} tentatively assigned as the sq → dppe LL'CT, as seen in complex **3.7** and decay of the Pt(dπ) → q MLCT at 13,500 cm^{-1}.

Table 4.6. Spectroelectrochemical UV/vis/NIR data for the different redox states of **4.11** in CH_2Cl_2 at 253 K.

	Solution Colour	ν_{max} 10^3 cm^{-1} (ε_{max} 10^3 $M^{-1}cm^{-1}$)
[{Pt(dppe)$_2$(thea)] (**4.11**)	Yellow	37.5 (36.2), 36.4 (32.14), 30.8 (47.9) 25.0 (sh), 14.1 (0.8)
[{Pt(dppe)}$_2$(thea$^{\bullet}$)]$^+$ ([**4.11$^{\bullet}$**]$^+$)	Green	37.5 (33.2), 36.5 (29.2), 30.7 (40.4), 25.0 (sh), 21.1 (sh), 14.1 (0.8), 7.4 (sh), 5.5 (2.9)
[{Pt(dppe)}$_2$(thea$^{\bullet\bullet}$)]$^{2+}$ ([**4.11$^{\bullet\bullet}$**]$^{2+}$)	Green	37.5 (36.9), 36.4 (30.1), 30.8 (25.9), 24.1 (8.7), 14.3 (1.4), 7.4 (sh), 5.5 (16.6).
[{Pt(dppe)}$_2$(thea)]$^{4+}$ ([**4.11**]$^{4+}$	Brown	32.8 (32.4), 25.6 (13.3), 19.0 (5.9), 13.5 (35.5)

(sh) = shoulder

4.2.7 EPR Analysis of Chemically Oxidised Species

Electron paramagnetic resonance (EPR) spectroscopy was used as a tool to evaluate the local environment of the valent electron in oxidised species **[4.10$^{\bullet}$]$^+$**, **[4.11$^{\bullet}$]$^+$**, and **[4.12$^{\bullet}$]$^+$**. Oxidised species were generated by careful addition of either one equivalent of $[FeCp_2]PF_6$ in deoxygenated dichloromethane at -78^{o}C. Continuous wave (CW) EPR spectra of all oxidised species were recorded in-house (X-band, 9.4 GHz) and in collaboration with Dr. Stephen Sproules and Professor Eric McInnes at The University of Manchester EPSRC EPR service (S-band, 3.9 GHz and X-band 9.4 GHz)

Analysis of chemically generated radical species [**4.10**]$^+$ and [**4.11**]$^+$ between 210 and 290 K displayed spectra which were very similar with isotropic line near g_e, indicating an organic-based radical. Whilst the hyperfine coupling on both spectra was not clearly resolved, by assuming a small coupling (4.9 – 4.7 x 10^{-4} cm^{-1}) to two ^{195}Pt (I = ½, natural abundance = 33%) this could be extracted based upon the S-band lineshape. The spectrum of the chemically generated radical of [**4.12$^{\bullet}$**]$^+$ over the same temperature range was visually different to those of [**4.10$^{\bullet}$**]$^+$ and [**4.11$^{\bullet}$**]$^+$, in containing five lines according to the clear coupling of the electron to two ^{195}Pt nuclei. Hyperfine coupling extracted from the spectra was equal to 13.5 × 10^{-4} cm^{-1}, approximately 2.5 times larger than for [**4.10$^{\bullet}$**]$^+$ and [**4.11$^{\bullet}$**]$^+$ indicating enhanced electron delocalisation onto both ^{195}Pt centres. By cooling the samples close to 100 K, the spectra of all three monocationic species change to become slightly rhombic with coupling to one ^{195}Pt nuclei approximately 4 times larger than between 210 – 290 K for [**4.10$^{\bullet}$**]$^+$-[**4.12$^{\bullet}$**]$^+$. This change in symmetry of the spectra upon cooling to 100 K indicates that the exchange between dioxolene groups may therefore be frozen out on the EPR timescale,[17] while the enhanced hyperfine coupling to ^{195}Pt for [**4.12$^{\bullet}$**]$^+$, is likely due

to the strong π-accepting nature of the $^{t}Bu_2Bipy$ ancillary ligand compared to the strong σ-donating nature of diphosphines dppb and dppe.

Table 4.7 Simulated EPR spectroscopic parameters for [**4.10**]$^+$-[**4.12**]$^+$ in 10:1 CH_2Cl_2 : THF solution. Hyperfine couplings are to ^{195}Pt, and are in 10^{-4} cm^{-1}.

	210 K		100 K			
	g ($A^{[a]}$)	$A\{^{31}P\}$	g_1 ($A_1^{[b]}$)	g_2 ($A_2^{[b]}$)	g_3 ($A_3^{[b]}$)	$A\{^{31}P\}$
[**4.10**]$^+$	2.0011 (4.9)	1.0	2.0045 (20)	2.0031 (19)	1.9844 (–10)	2.5
[**4.11**]$^+$	2.0012 (4.7)	1.5	2.0055 (19.5)	2.0032 (19)	1.9833 (–10)	2.5
[**4.12**]$^+$	2.0019 (13.5)	-	2.0292 (48)	1.9872 (48)	1.9796 (40)	

[a] Coupling to two ^{195}Pt nuclei. [b] Coupling to one ^{195}Pt nucleus.

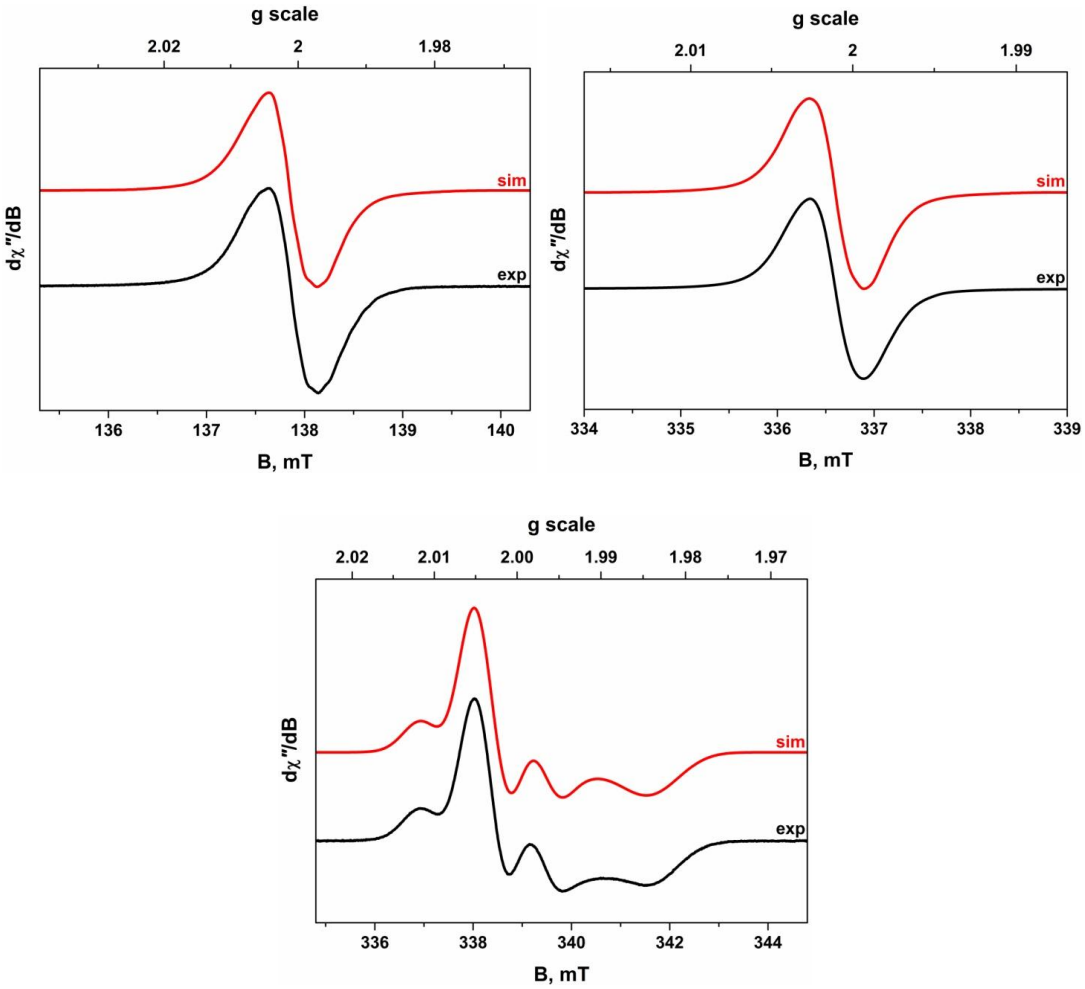

Figure 4.33. EPR spectra of $[\{(dppb)Pt\}_2(cat\text{-}sq^{\bullet})]^+$ $[\mathbf{4.10}^{\bullet}]^+$ recorded in 10:1 CH_2Cl_2/THF. (Top left) S-band spectrum recorded at 210 K. (Top right) X-band spectrum recorded at 230 K. (Bottom) X-band EPR spectrum recorded at 100 K. Colour code; simulated, red; experimental, black.

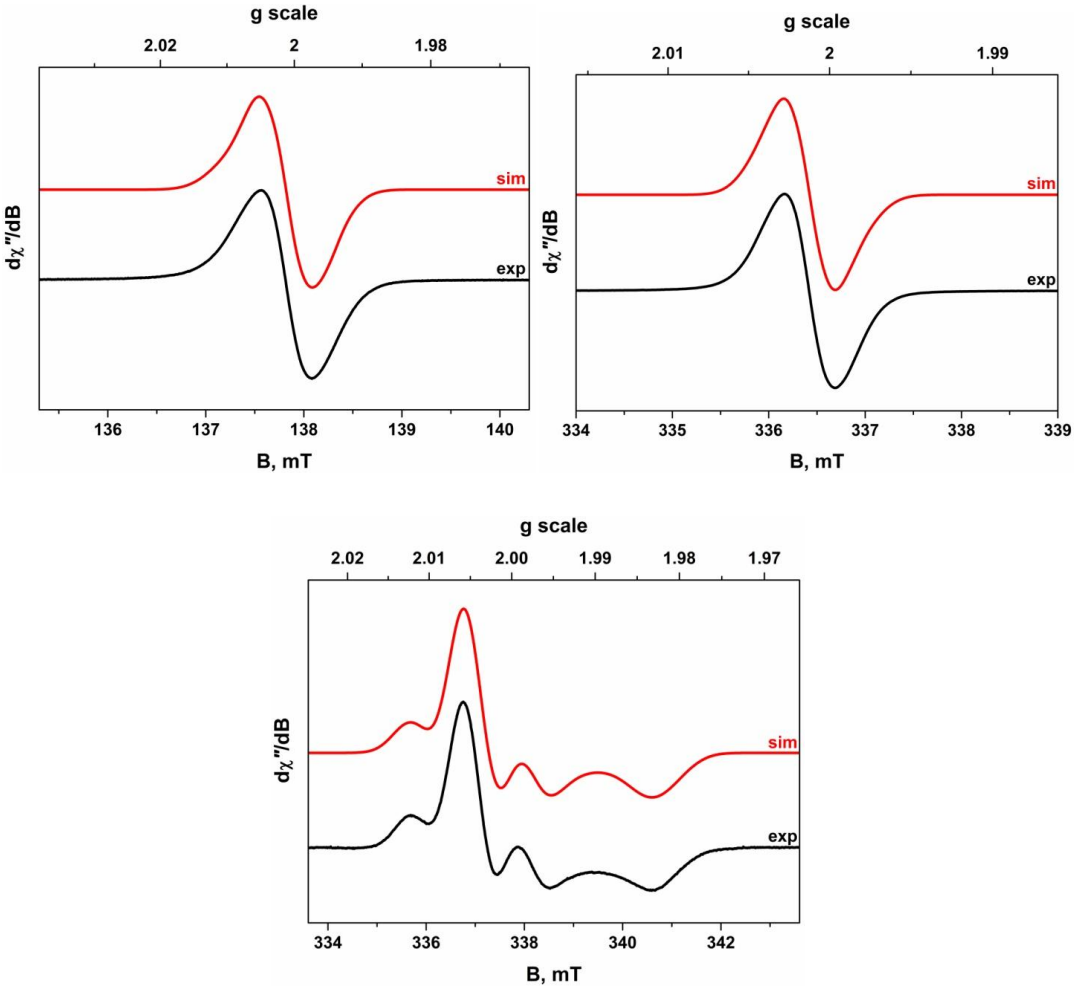

Figure 4.34. EPR spectra of $[\{(dppe)Pt\}_2(cat\text{-}sq^{\bullet})]^+$ [**4.11**$^{\bullet}$]$^+$ recorded in 10:1 CH_2Cl_2/THF. (Left) S-band EPR spectrum recorded at 210 K. (Right) X-band EPR spectrum recorded at 230 K. (Bottom) X-band spectrum recorded at 100 K. Colour code; simulated, red; experimental, black.

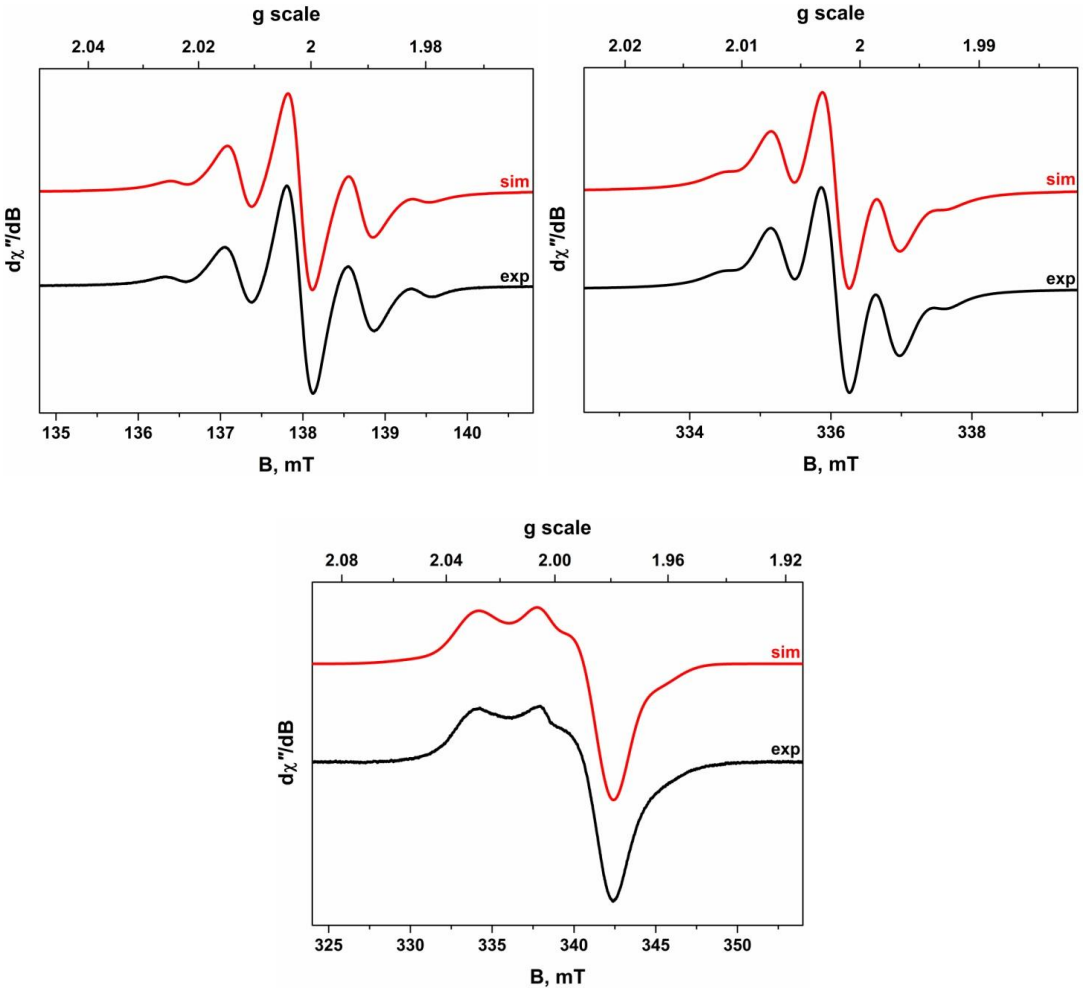

Figure 4.35. EPR spectra of $[\{(^{t}Bu_2Bipy)Pt\}_2(cat\text{-}sq^{\bullet})]^{+}$ $[\mathbf{4.12^{\bullet}}]^{+}$ recorded in 10:1 CH_2Cl_2/THF. (Top left) S-band spectrum recorded at 210 K. (Top right) X-band spectrum recorded at 230 K .(Bottom) X-band spectrum recorded at 80 K. Colour code; simulated, red; experimental, black.

4.2.8 Single-crystal X-ray Structural Characterisation of Neutral Complexes

Attempted Structure Refinement of $[\{(dppb)Pt\}_2(thea)]PF_6 \bullet xC_4H_{10}O \bullet (5\text{-}x)CH_2Cl_2$ ($[\mathbf{4.10}]PF_6 \bullet xC_4H_{10}O \bullet (5\text{-}x)CH_2Cl_2$)

Single crystals of $[\mathbf{4.10}]PF_6$ to were grown by slow diffusion of deoxygenated diethyl ether into a dichloromethane solution of $[\mathbf{4.10}]PF_6$ inside a glovebox. Attempts were made to collect the data firstly in-house and then at Diamond Light Source (beamline I19) using synchrotron radiation, although only a low-resolution dataset was achievable ($2\theta_{max} = 45^{o}$). Despite this, the dataset could be solved to clearly show the presence of oxidised species $[\mathbf{4.10}]PF_6$, although the presence of extensive solvent disorder in the crystal further limits the preciseness by which the model can be analysed. As a result, the dataset was used only to examine connectivity as full analysis of bond lengths and angles is inappropriate.

The structure was solved in the orthorhombic space-group *Pnma*, and the asymmetric unit was shown to contain two half-molecules of complex **[4.10]PF_6** spanning the crystallographic mirror plane *x*, ¾, *z*. Of the two PF_6^- anions associated with each complex, one resides on the mirror plane *x*, ¾, *z* also and the other on inversion centre 1, 1, ½. Whilst the structure was unsuitable for detailed bond length and angle analysis, the structure importantly showed the retained μ_2- connectivity of central $[thea^{\bullet}]^{3-}$ ligand upon oxidation, as can be seen in **Figure 4.37**.

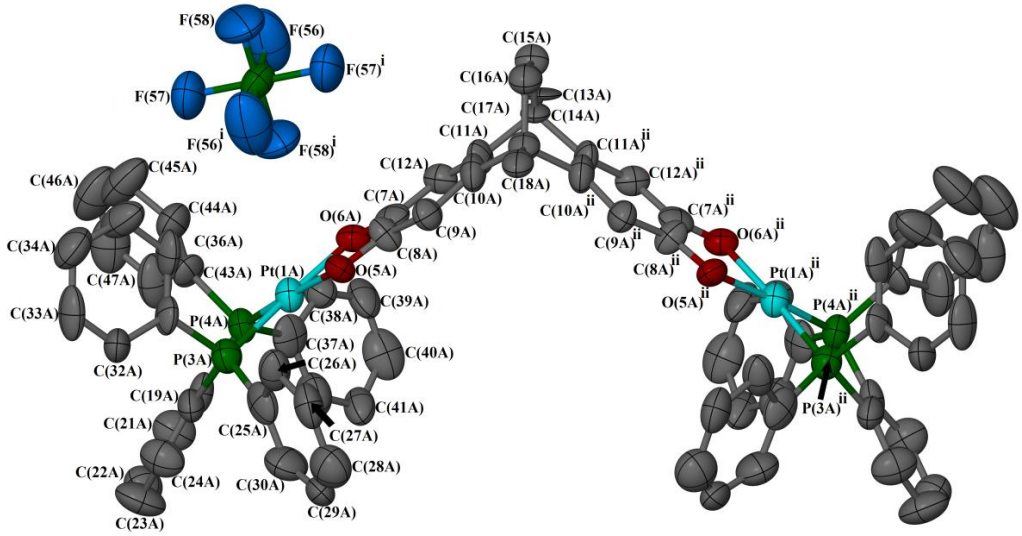

Figure 4.36. View and atom numbering scheme of one formula unit as complex 'A' in [**4.10**]PF_6•*x*$C_4H_{10}O$•(5-*x*)CH_2Cl_2. Displacement ellipsoids are set at 50% probability and hydrogen atoms are omitted for clarity. Symmetry codes: (i) 2-*x*, 2-*y*, 1-*z*; (ii) *x*, $^3/_2$-*y*, 1-*z*. Colour code: Pt, cyan; P, green; O, red; F, blue; C, grey.

When packing, the complexes assemble to form a small 'capsule-type' structure spanning a crystallographic mirror plane, where Pt(1B) and Pt(2B) and P(49) lie on a crystallographic mirror plane and P(46) lies on inversion centre.

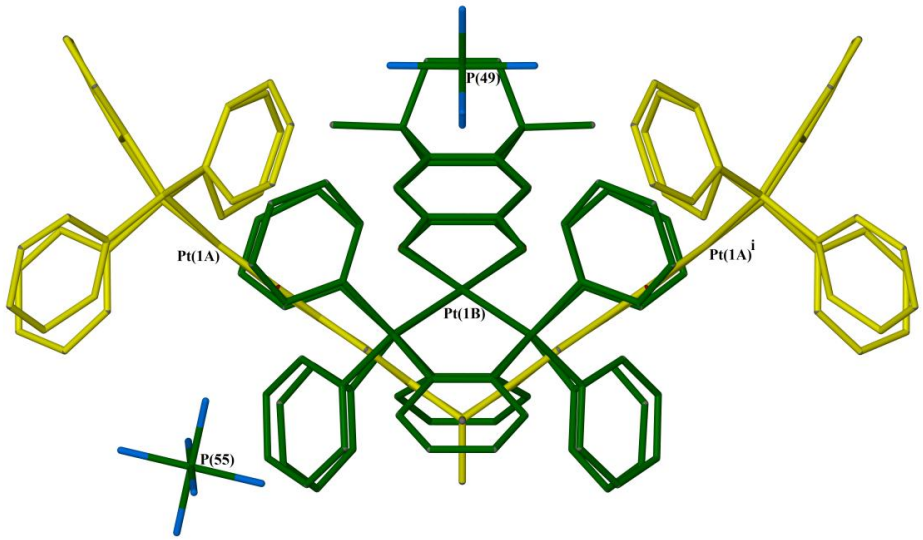

Figure 4.37. View of two unique formula units of [**4.10**]PF_6 in [**4.10**]PF_6•*x*$C_4H_{10}O$•(5-*x*)CH_2Cl_2. Pt(2B) is hidden directly behind Pt(1B) and the two complex molecules are coloured differently to highlight their packing arrangements Symmetry code: (i) *x*, $^3/_2$-*y*, *z*.

Between the two complex molecules, the closest interactions appear to be CH...π interactions between hydrogen atoms of the CH_3 groups of dihydroxyethano- bridge and phenyl rings of the dppb moieties. In addition to these apparent CH...π interactions, there appear to be some evidence of CH...anion interactions between H(40B) and H(33B) of dppb phenyl rings and F(56) of the PF_6^- anion centred on P(55). Similarly, the same type of interactions are apparent between H(47B), H(48B) again of dppb phenyl rings and F(57), F(58) of the PF_6^- anion centred on P(49). However due to the low precision of the dataset, this cannot be determined exactly. When viewed throughout the lattice, this packing arrangement forms exclusion complexes with the PF_6^- anions packed into pockets inbetween each association of the two **[4.10]**$^+$ molecules, best viewed parallel to the crystallographic plane (001) as in **Figure 4.38**.

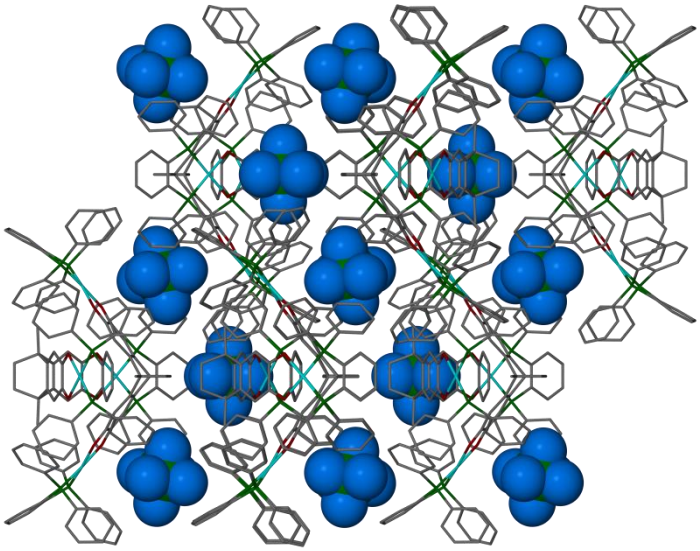

Figure 4.38. Packing diagram of [4.10]PF_6•*x*$C_4H_{10}O$•(5-*x*)CH_2Cl_2 viewed along crystallographic plane (001). Molecules of complex $[4.10]^+$ are shown with arbitrary radii whilst PF_6^- anion molecules are shown as their Van Der Waals radii to highlight their position in the lattice. All hydrogen atoms have been omitted for clarity. Colour code: Pt, cyan; P, green; O, red; F, blue; C, grey.

A *SQUEEZE*[14] analysis of the model identified a large void volume of 4235 $Å^3$, equalling approximately 25% of the unit cell volume, which contained 1585 electrons or simply 198 electrons per [**4.10**]PF_6 formula unit. This could therefore be calculated to be equal to 4.7 molar equivalents of dichloromethane (42 electrons each), diethyl ether (42 electrons each) or a mixture of the two solvents. For the purposes of calculated density (D_{calc}) and F_{000} calculations, 4.7 mole equivalents of dichloromethane were added to the formula. When viewed along crystallographic plane (010), as shown in **Figure 4.39** a potential void within the lattice may be seen between complexes associated as in **Figure 4.37**. Due to the large void space within the structure and low precision of the obtained dataset, the dataset which had been '*SQUEEZE*'d' was used in the final stages of least-squares refinement. All non-hydrogen atoms were refined anisotropically whilst all hydrogen atoms were placed in calculated positions and refined using a riding model. There was some clear disorder in the model, particularly obvious with the large displacement ellipsoids on F(56) of the PF_6^- anion, all attempts to resolve this disorder in the model were unsuccessful however likely consequent of the low precision of the acquired dataset. The highest residual peak in the Fourier map was 2.93 *e*.$Å^{-3}$ approximately 1.8 Å from Pt(2B) whilst another high peak of 2.33 *e*.$Å^{-3}$ was also found approximately 1.95 Å from the centre of dioxolene ring C(11B) > $C(11B)^i$ {(i) = *x*, 3/2-*y*, *z*}, although this could not be modelled. Other high Fourier peaks

close to 2 $e.Å^{-3}$ are all found close to platinum atoms Pt(1A) and Pt(1B) whilst the deepest Fourier hole of -2.61 $e.Å^{-3}$ is also found close to Pt(2B).

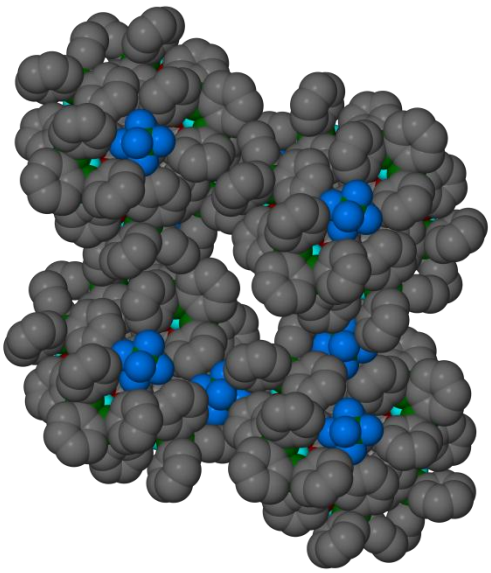

Figure 4.39. Packing diagram of [**4.10**]PF_6•$x$$C_4H_{10}O$•(5-$x$)$CH_2Cl_2$ viewed along crystallographic plane (010). All molecules are displayed as Van Der Waals radii to highlight the potential solvent void at the centre of the figure. Hydrogen atoms are omitted for clarity. Colour code: Pt, cyan; P, green; O, red; F, blue; C, grey.

Structure Refinement and Analysis of [{(dppe)Pt}$_2$(thea)]PF_6•2.4CH_2Cl_2 ([4.11]PF_6•2.4CH_2Cl_2)

As with the structure of [**4.10**]PF_6•$x$$C_4H_{10}O$•(5-$x$)$CH_2Cl_2$ described above, a solvate of oxidised species [**4.11**]$^+$ was grown in deoxygenated dichloromethane / pentane inside a glovebox and collected at Diamond Light source (beamline I19). The structure was solved and refined in the tetragonal space group *P*4/*nnc* and the asymmetric unit shown to contain half a complex molecule across the C_2 axis ¾, ¼, *z*, one quarter of a PF_6^- counteranion on C_4 axis ¼, ¼, *z* and a further two more PF_6^- counteranions; one of which with occupancy of 0.10 centred on P(45) at C_2 site *x*, ¼, ¾ and 3 atoms of another centred on P(49) which lies on C_2 axis *x, y,* ¾ with occupancy 0.15 but displays significant disorder therefore could only be partly modelled. The model also displays disordered dichloromethane solvent molecules; one fully occupied molecule disordered about mirror plane *y, x,* ½-*z*, another fully occupied molecule disordered about mirror plane *y, x,* ½-*z* and a molecule in a general position with occupancy of 0.4 which is disordered about two positions. All crystallographically ordered

non-hydrogen atoms were refined anisotropically, including half occupied Cl atoms, whilst all hydrogen atoms were placed in calculated positions and refined using a riding model. The highest remaining Fourier peak was +3.06 *e*.Å^{-3}, 0.6 Å from P(49). Unfortunately this could not be assigned and is therefore assumed to be due to the significant disorder within the counter anion.

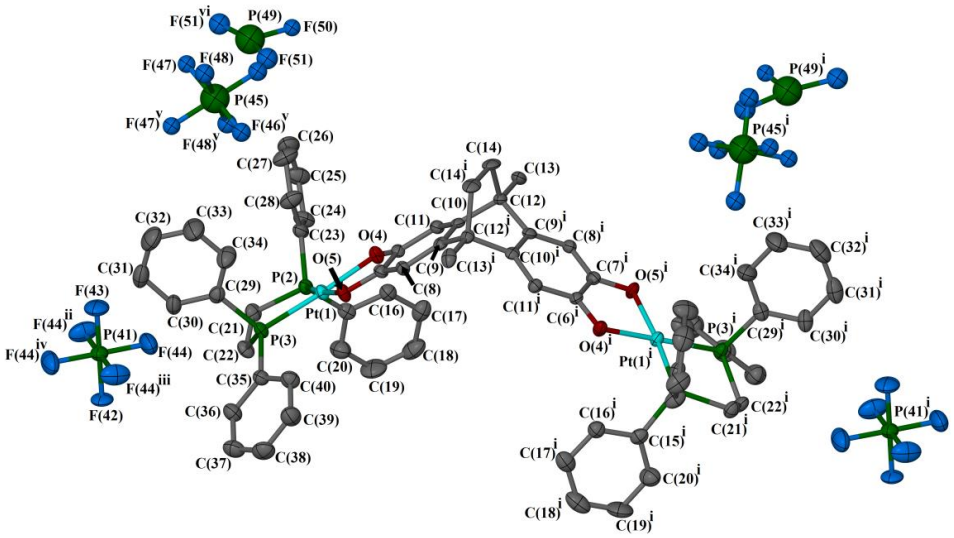

Figure 4.40. View and atom numbering scheme of [{(dppe)Pt)}$_2$(thea)]PF_6 in [**4.11**]PF_6•2.2CH_2Cl_2. Displacement ellipsoids are set at 50% probability. All hydrogen atoms, symmetry codes on Flourine atoms bonded to P(41)^i, P(45)^i and P(49)^i and solvent molecules have been removed for clarity. Symmetry codes : (i) $^3/_2$-*x*, ½-*y*, *z*; (ii) 1+*y*, ½-*x*, *z*; (iii) ½-*y*, *x*-1, *z*; (iv) $^3/_2$-*x*, -*y*-½, *z*; (v) $^3/_2$-*x*, *y*, ½-*z*; (vi) 1+*y*, *x*-1, ½-*z*. Colour code: Pt, cyan; P, green; O, red; F, blue; C, grey.

The association of two formula units of **[4.11]PF_6** again appears to be driven by CH...π interactions between H(8) of dioxolene ring C(6) > C(11) and C(16) of dppe phenyl ring C(11) > C(16) which are separated by 2.819(2) Å. This association again provides an exclusion complex whereby the PF_6^- anions and dichloromethane solvent molecules mentioned above pack into disordered sheets running parallel to (001), as can be seen in **Figure 4.42.** These sheets traverse the lattice inbetween two complex units of **[4.11]PF_6** which associate together to form a 'capsule-type' structure, as with two formula units of the structure [**4.10**]PF_6•*x*$C_4H_{10}O$•(5-*x*)CH_2Cl_2, as can be viewed in **Figure 4.41.**

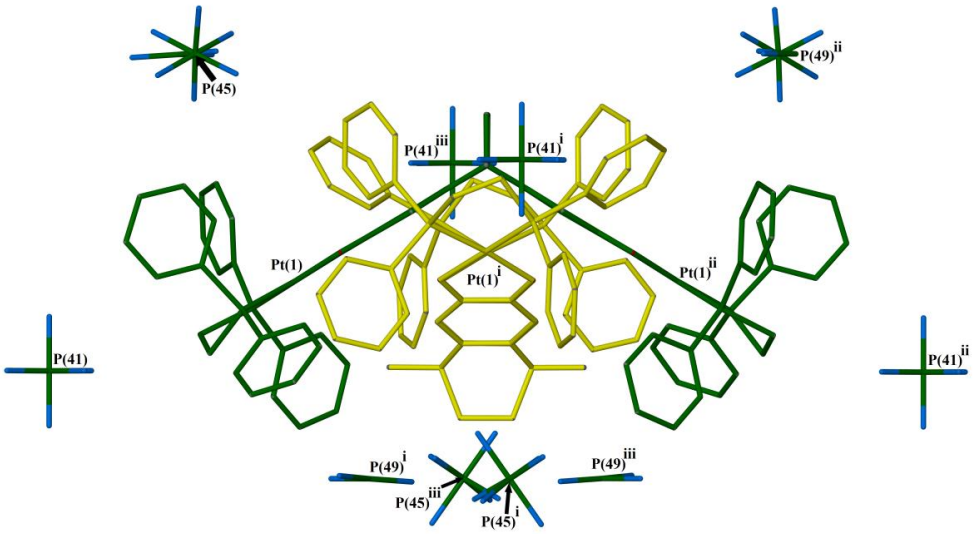

Figure 4.41. View of two formula units [**4.11**]PF_6. All atoms have arbitrary radii and hydrogen atoms are omitted for clarity. The two complex molecules are coloured differently to highlight their packing arrangements. Symmetry codes: (i) ½+*y*, 1-*x*, 1-*z*; (ii) $^3/_2$-*x*, ½-*y*, *z*; (iii) 1-*y*, *x*-$^1/_2$, 1-*z*.

Within the structure, these disordered anions and solvent molecules pack to form sheets inbetween each layer of [**4.11**]$^+$ molecules as shown below in **Figure 4.42**.

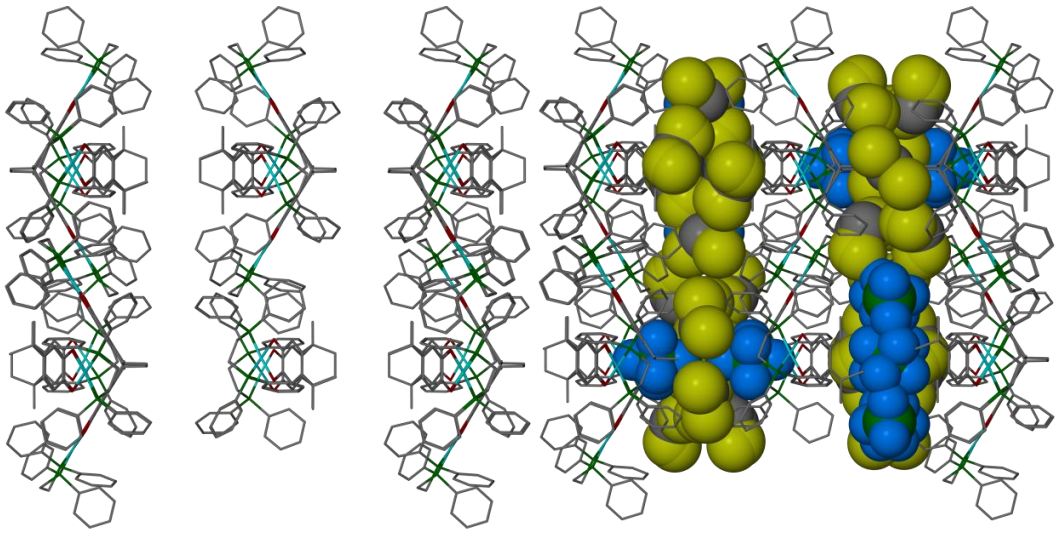

Figure 4.42. Two packing diagrams of [**4.11**]PF_6•2.2CH_2Cl_2 viewed parallel to the crystallographic plane (100). (Left) Solvent molecules and PF_6^- anion molecules omitted. (Right) solvent molecules and PF_6^- anion molecules shown with Van der Waals radii to highlight their positions in the lattice. All other atoms have arbitrary radii and hydrogen atoms omitted for clarity. Colour code: Pt, cyan; Cl, yellow; P, green; O, red; F, blue; C, grey.

Table 4.8. Selected bond lengths and angles extracted from structure [**4.11**]PF_6•2.2CH_2Cl_2 for complex [**4.11**]PF_6.

	[**4.11**]PF_6•2.2CH_2Cl_2
Pt(1)-P(2)/P(3) [Å]	2.2103(18)/ 2.2200(17)
Pt(1)-O(4)/O(5) [Å]	2.042(5)/ 2.057(5)
P(2)-Pt(1)-P(3) [°]	85.77(7)
O(4)-Pt(1)-O(5) [°]	81.75(18)
O(4)-Pt(1)-P(2) [°]	91.59(14)
O(4)-Pt(1)-P(3) [°]	176.38(15)
O(5)-Pt(1)-P(2) [°]	173.34(14)
O(5)-Pt(1)-P(3) [°]	100.88(14)

4.2.8.3 Comparison of Neutral and Cationic Crystal Structures

As described above, the two oxidised structures, **[4.10]PF_6** and **[4.11]PF_6** firstly served the purpose of confirming that upon oxidation of **4.10** and **4.11** with one equivalent of [$FeCp_2$]PF_6, generation of a radical cation onto the [thea] core unit did not cause loss of the either the $\{Pt(dppb)\}^{2+}$ or $\{Pt(dppe)\}^{2+}$ substituents mode nor did either lose their dihydroxyethano- bridges. This was a potential cause for concern as during the course of this investigation, some limited mass-spectral (ES+) evidence was obtained for the loss of the bridge upon in-situ oxidation of complex **4.12** by addition of one equivalent of TCNE (TCNE = tetracyanoethane), yielding a μ_2-substituted compound of core unit 2,3,6,7-tetrahydroxy-9,10-dimethylanthracene. However, to provide a detailed study into this effect, all attempts to cleanly synthesise the planar complex on a larger scale failed due to the almost unwettable nature of the precursor ligand. As a result, this study was not pursued. Retention of the dihydroxyethano- bridges in the complexes resulted in all of the complexes appearing visually very similar, although it was noticed that upon oxidation, both structures **[4.10]PF_6** and **[4.11]PF_6** appeared to 'pinch', i.e. the dihedral angle between least squares planes of each dioxolene ring reduced significantly. For complex **[4.11]PF_6**, this translated into a reduction of approximately 13.5° whilst for **[4.10]PF_6**, this appeared to be much larger and closer to 30°, although the low resolution of the dataset again precluded any meaningful conclusions. In order to illustrate this observation, the complexes are presented in side-on views to emphasise the conformational changes in **Figure 4.43** and **Figure 4.44**. This reduction acted to bring the *ipso*-carbon atoms of the dioxolene rings approximately 0.1 Å closer in space, the reason behind this reduction was suspected to be due to the frontier molecular orbitals therefore investigations on a model complex were performed.

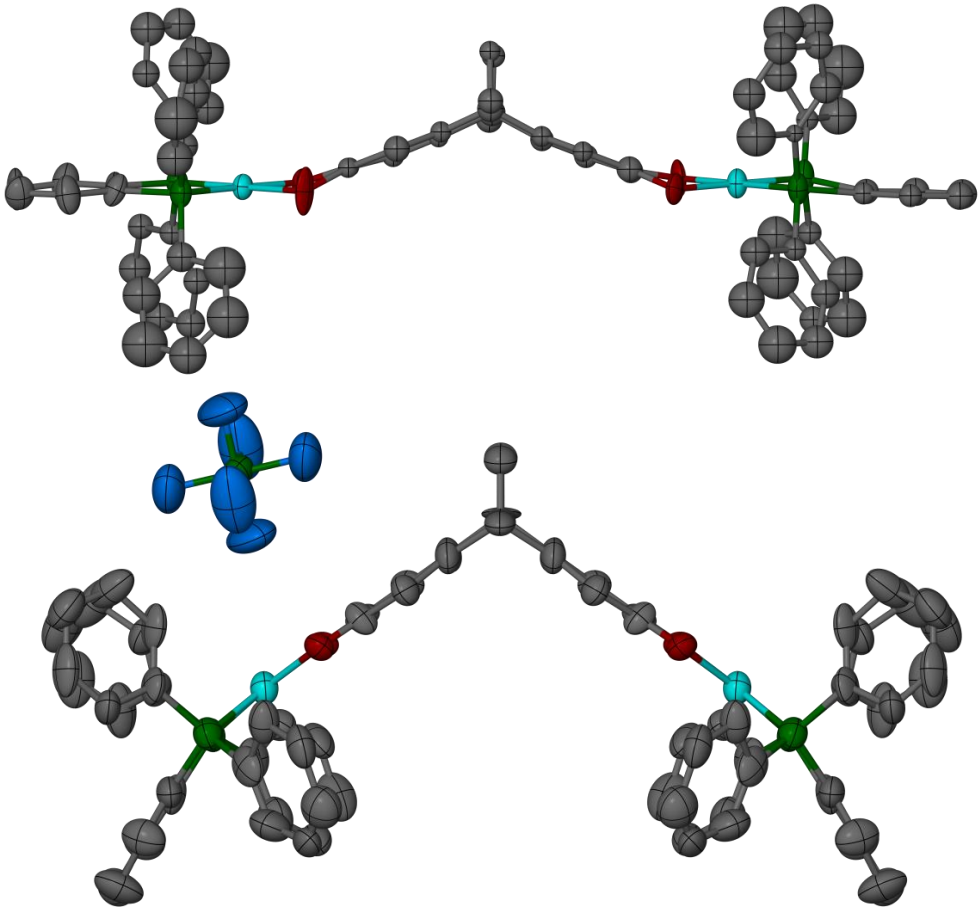

Figure 4.43. (Top) Side-on view of molecule disorder site 'A' in the structure of complex **4.10**. (Bottom) Side on view of 'complex A' in the structure of complex [**4.10**]PF_6. The two views have been oriented in this manner to emphasise the decrease in angle between *ipso*-carbons of the dioxolene rings upon oxidation. All symmetry codes and hydrogen atoms have been omitted for clarity. Colour code: Pt, cyan; P, green; O, red; F, blue; C, grey.

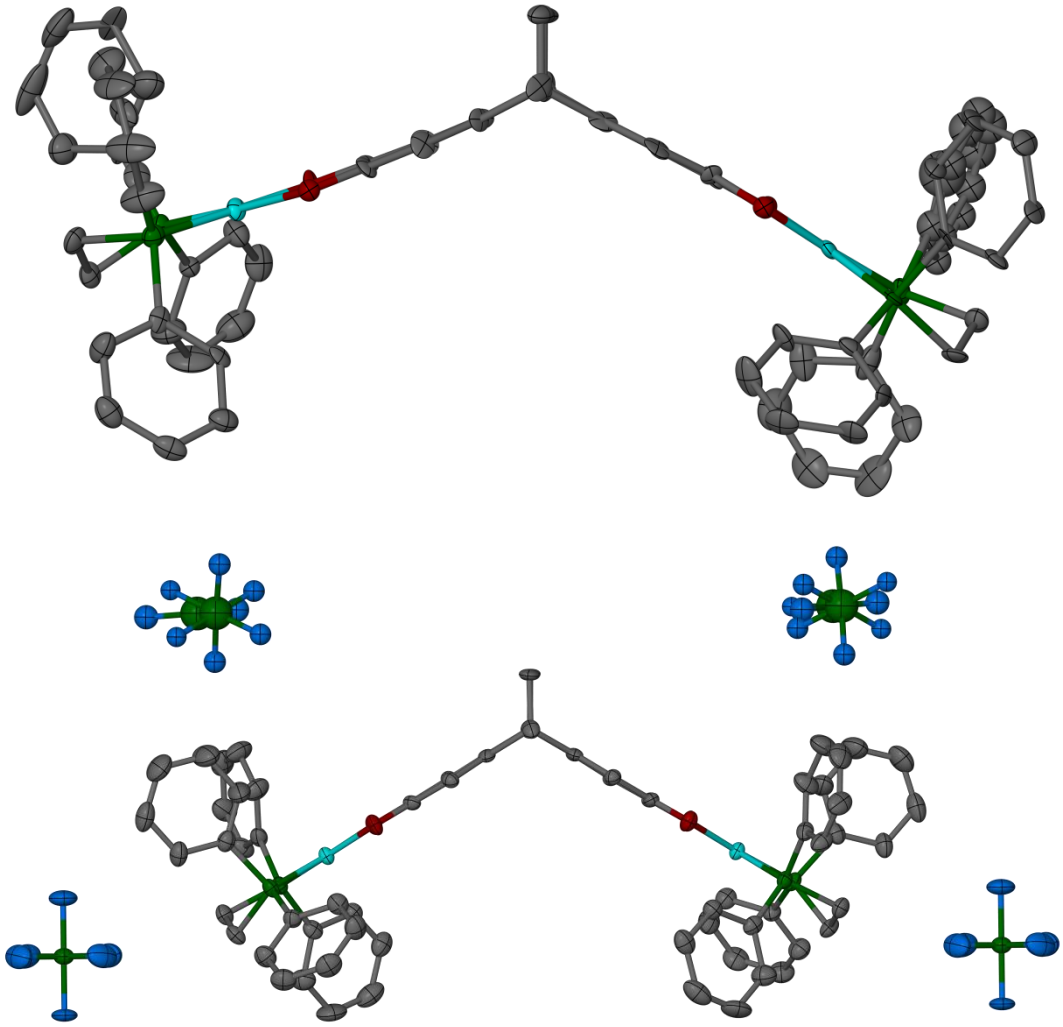

Figure 4.44. (Top) Side-on view of molecule 'A' in complex **4.11**. (Bottom) Side on view of one formula unit of [**4.11**]PF_6 in complex. The two views have been oriented in this manner to highlight the decrease in angle between *ipso*-carbons of the dioxolene rings upon oxidation. All symmetry codes and hydrogen atoms have been omitted for clarity. Colour code: Pt, cyan; P, green; O, red; F, blue; C, grey.

As seen in chapter 3, useful parameters may be extracted from the crystal structures of dioxolene complexes by their comparison to *o*-semiquinonates and catecholates.[18] Use of Carugo's parameter Δ, as defined by equations **3.1** and **3.2**, may therefore be used to calculate the oxidation state of the ligand by correlation of all eight bond lengths within the dioxolene moiety and their comparison to uncomplexed *o*-benzoquinone,[19] and 1,2-dihydroxybenzene (catechol).[20]

These calculated values for are **4.10** and **4.11** and **[4.11]PF_6** are summarised in **Table 4.9**. As described above, the low resolution dataset for oxidised complex **[4.10]PF_6** again precluded this analysis. It was found that in every instance for neutral molecules **4.10** and **4.11,** the oxidation state of each dioxolene ring was calculated to be within error of the full catecholate (2-) oxidation state.

Oxidised compounds [**4.10**]PF_6 [**4.11**]PF_6 crystallised with C_2 symmetry, implying that the two dioxolene groups in each are equivalent. Analysis of internal bond lengths and angles within the obtained structure showed no significant changes in the Pt-O or Pt-P bond length when compared to those extracted from the structure of **4.11**•$0.67H_2O$•$2.07CH_2Cl_2$. By the same method presented above, parameters from the internal bond lengths of the equivalent dioxolene rings may be extracted to calculate the valence bond-sum parameter Δ,[15] as detailed in **Table 4.9**. The value of -1.57(15) obtained is within error of the expected value of -1.5, therefore confirming that the complex has been 1-electron oxidised and each dioxolene ring is of oxidation state -1.5 with the valent electron delocalised between the two.

Table 4.9. Selected bond lengths and metric parameters for the calculation of Δ.

		Pt-O [Å]	Pt-P	Δ	θ [°]
4.10		1.98(2)-2.05(2)	2.201(3)-2.207(3)	$-1.7(3) \geq \Delta \geq -1.9(2)$ [a]	140.8(5)-141.1(5)[a]
4.11	Molecule A	2.026(8)- 2.048(8)	2.202(4)-2.227(3)	-1.77(15), -2.1(2)	130.8(5)
	Molecule B	2.006(13)-2.049(9)	2.205(4)-2.236(4)	-1.86(14), -2.1(2)	131.1(6)
	Molecule C	2.034(9)-2.071(15)	2.195(6)-2.222(4)	-1.90(15)[b]	129.8(9) - 131.5(6)[a]
[4.11]PF_6•$2.2CH_2Cl_2$		2.042(4)-2.060(4)	2.2101(14)-2.2197(14)	-1.57(15)[c]	117.14(11)

[a] Due to the full-molecule disorder present, a range of values is given here. [b] Due to restraints applied in the structure, θ for the disordered dioxolene centred on Pt(2C) was not determined. [c] There is only one unique dioxolene centre in the structure.

4.2.9 Solid State Infrared Analysis of the Oxidised Species

As complexes [**4.10**$^{\bullet}$]$^{+}$, [**4.10**$^{\bullet\bullet}$]$^{2+}$, [**4.11**$^{\bullet}$]$^{+}$ and [**4.11**$^{\bullet\bullet}$]$^{2+}$ were isolated and appeared stable at room temperature, they were analysed by IR spectroscopy. The spectra observed for the second oxidation products ([**4.10**$^{\bullet\bullet}$]$^{2+}$ and [**4.11**$^{\bullet\bullet}$]$^{2+}$) are included to indicate the trend observed upon oxidation, and should be taken as tentatively due to incomplete oxidation.

Addition of one equivalent of ferrocenium caused the decay of a strong band close to 1290 cm^{-1} corresponding to ν(C-O), and peaks in the region 1420 – 1490 cm^{-1} shift to higher energy by approximately 30 cm^{-1} corresponding to the ν(CC) of the dioxolene rings, indicating a change in internal structure. Both complexes also display growth of a weak band close to 1370 cm^{-1}, which has been assigned as ν(C=O) by *ab initio* DFT calculations on the complex $[(tpa)Co(DBSQ)]^{2+}$ by Andrea *et al.*.[21] The growth of characteristic ν(P-F) close 840 cm^{-1} was also apparent, therefore positively identifying it's integration into the structure. Addition of one further equivalent of $[FeCp_2]PF_6$ caused this ν(P-F) to grow significantly in intensity alongside increased changes in the region 1420 – 1490 cm^{-1} whilst the ν(C=O) close to 1370 cm^{-1} grows significantly in intensity with additional semiquinone character of the ligand. As the majority of changes observed between spectra upon oxidation are associated with the $[thea]^{n-}$ ligand, it would appear that the HOMO is predominately localised on this ligand. This will be explored in the next section.

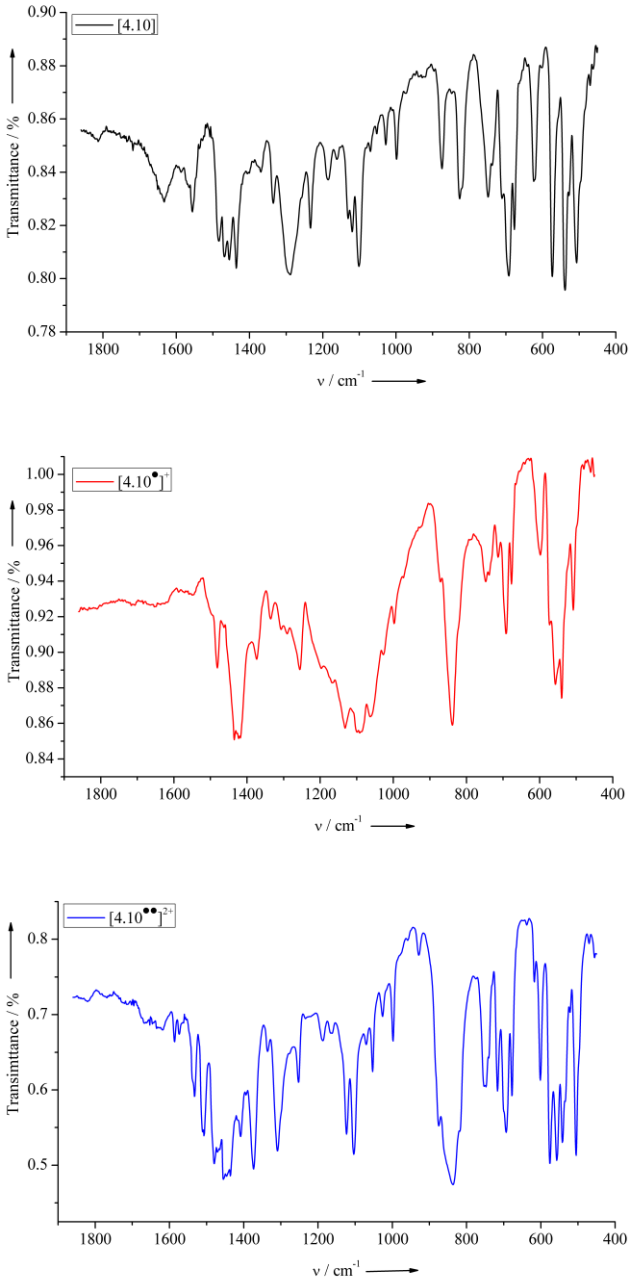

Figure 4.45. IR (solid state) spectral changes of isolated **4.10** upon oxidation with sequential stoichiometric amounts of $[FeCp_2]PF_6$ oxidant. Colour code; **4.10**, black; $[\mathbf{4.10}^{\bullet}]^{+}$, red; $[\mathbf{4.10}^{\bullet\bullet}]^{2+}$, blue**.**

4.2.10 DFT Analysis of [{(Bipy)Pt}$_2$(thea)]

In order to elucidate the frontier orbitals involved with the structural changes and strong coupling within the oxidised complexes **[4.10]**$^+$, **[4.10]**$^{2+}$, **[4.11]**$^+$, **[4.11]**$^{2+}$, **[4.12]**$^+$ and **[4.12]**$^{2+}$ gas-phase DF computational analysis of a representative complex [{(bipy)Pt}$_2$thea] (analogous to [{(^{t}Bu$_2$Bipy)Pt}$_2$thea] without ^{t}Bu substituents for computational simplicity) was performed, using the central [thea]$^{4-}$ fragment from molecule A of structure **4.11**•0.67H_2O.2.07CH_2Cl_2.

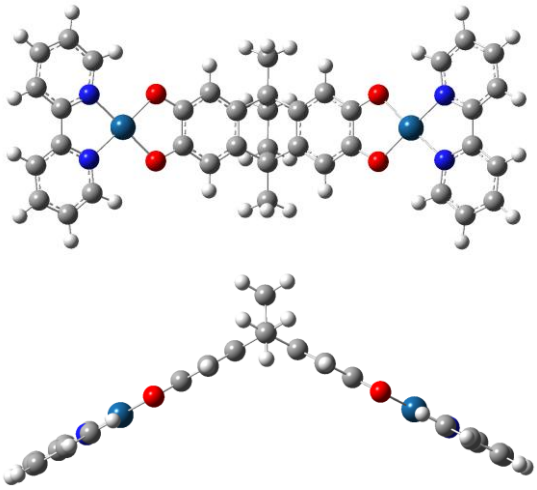

Figure 4.46. Two views of optimised [{(bpy)Pt}$_2$(thea)] structure from DFT calculations (B3LYP, SDD; {D95 basis set on C, H, N} {Dresden / Stuttgart pseudopotential on Pt}).Colour code: C, grey; H, white; N, blue, O, red; Pt, light blue.

DFT calculations were performed using Gaussian03W calculation software package with B3LYP functional method and SDD basis set (Dresden / Stuttgart pseudopotential on platinum and D95 basis set on all other atoms).[22] No solvent effects were included in the calculation and the complex was treated as a singlet (354 electrons, 598 basis functions) The computational procedure was as follows, first geometry optimisation was performed on the complete complex, where the central [thea^{4-}] unit originated from the crystal structure of neutral complex [({dppe)$_2$Pt}(thea)] and {(bpy)Pt} moieties appended. On the basis of this optimised structure, the frontier orbitals were calculated and are displayed below.

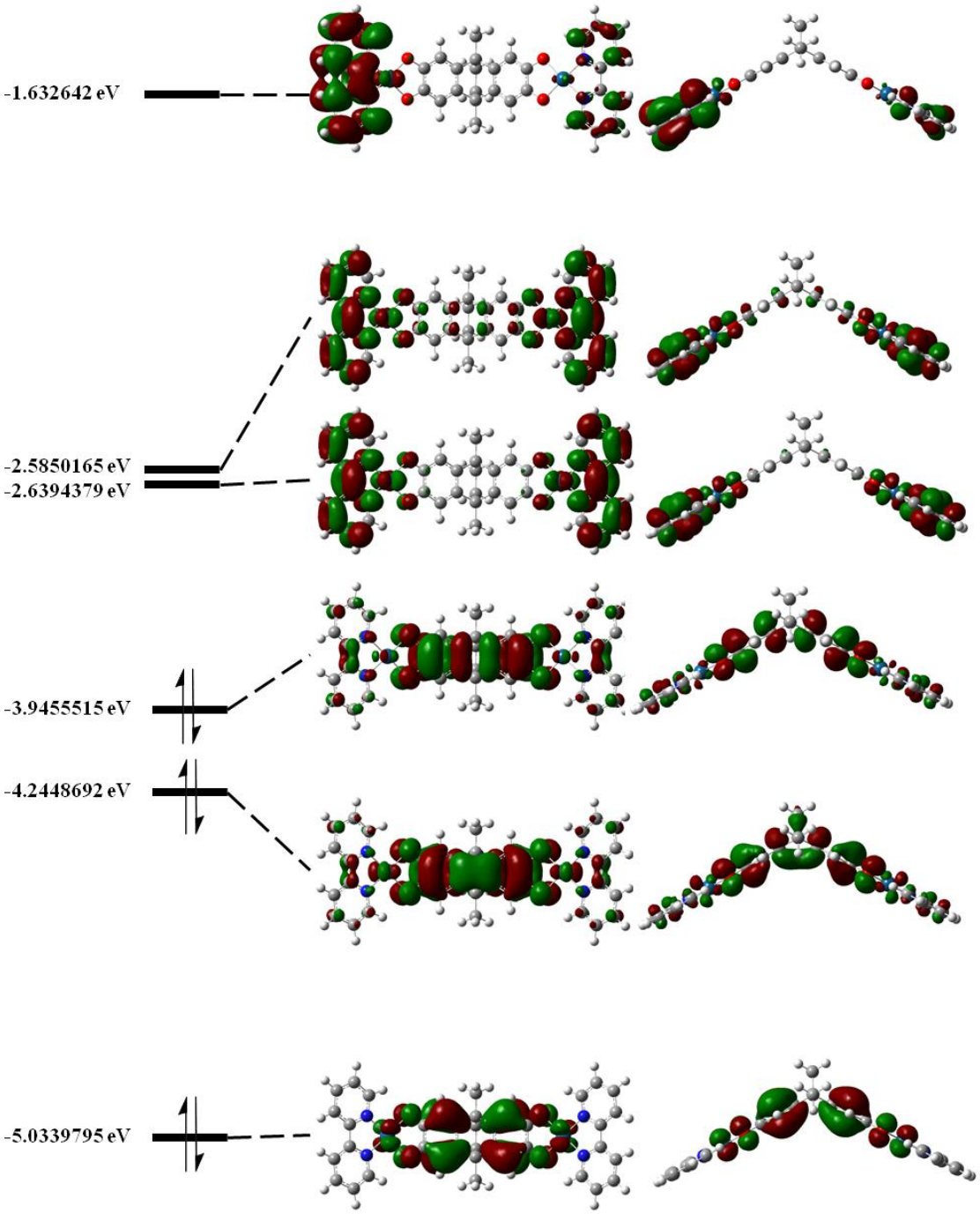

Figure 4.47. Calculated frontier molecular orbital energy diagram of optimised [{(bipy)Pt}$_2$(thea)] structure from DFT calculations (B3LYP, SDD; {D95 basis set on C, H, N} {Dresden / Stuttgart pseudopotential on Pt}).

Importantly the geometry optimisation retained the characteristic bent structure of the central $[thea]^{4-}$ ligand, although with the small increase in the angle between the least squares plane of the opposing dioxolene rings to 56.16^o from a starting angle of 49.2(5)^o causing a reduction of approximately 0.25 Å between the two platinum atoms. This

indicating that there is some calculated conformational flexibility within the structure, which was indeed seen experimentally.

Table 4.10. Comparison of the minimised molecular geometry of calculated structure[{Pt(bipy)}$_2$(thea)], with crystallographic determined structural parameters of relevant complexes, **4.10**•*x*C_5H_{12}•(4–*x*)CH_2Cl_2, **4.11**•0.67H_2O•2.07CH_2Cl_2 and [Pt(bipy)(DBCat)][11] (H_2DBcat = 3,5-di-*tert*butylcatechol). θ is defined as the dihedral angle between the least squares planes of the thea^{4-} dioxolene rings.

[Å], [°]	[{(bipy)Pt}$_2$(thea)]	**4.10**•*x*C_5H_{12} •(4–*x*)CH_2Cl_2	**4.11**•0.67H_2O •2.07CH_2Cl_2	[Pt(bipy)(DBCat)][11]
Pt-N	2.007-2.008		–	1.978(1), 1.992(1)
N-Pt-N	80.13 – 80.14		–	80.38(6)
Pt-O	2.006-2.008	1.98(2)-2.05(2)[a]	2.006(13)–2.048(8)[b]	1.982(1), 1.984(1)
O-Pt-O	83.7	82.1(7)-83.5(8)[a]	82.7(3)–83.5(5)[b]	84.24(5)
cis-N-Pt-O	98.0-98.1	–	–	96.61(5), 98.76(5)
trans-N-Pt-O	178.2-178.3	–	–	174.42(5), 176.99(5)
Pt...Pt	11.555	12.3748(8)	11.788(2) – 11.812(2)[b]	–
θ	123.8	140.8(5)–141.1(5)[a]	129.8(9)–131.5(6)[b]	–

[a] Range of values consequent of the full molecule disorder present in the structure. [b] These ranges were extracted from all three unique molecules in the asymmetric unit without considering the disorder present centred on Pt(2C).

Analysis of the frontier molecular orbitals displayed the highest occupied molecular orbitals (HOMO, HOMO-1, HOMO-2) are localised on [thea]$^{4-}$ core unit, with very small contribution from the two [(bipy)Pt]$^{2+}$ moieties. The HOMO is clearly antibonding across the ligand whilst HOMO-1 displays a small region of bonding character between *ipso*-carbons of the dioxolene rings. The small energy gap (Δ*E*) between HOMO and HOMO-1

of only 0.30 eV may explain the reason as to why such strong through-space coupling is observed once the $[thea]^{4-}$ ligand is oxidised, as the population in the antibonding HOMO is decreased. In contrast, the three unoccupied orbitals (LUMO, LUMO+1, LUMO+2) are all localised on the two $\{(bipy)Pt\}^{2+}$ fragments with some contributions from the Pt atoms and $[thea]^{4-}$ O donors. The LUMO and LUMO+1 of these three levels display a very small energy gap of 0.05 eV, which may explain the two overlapping bipyridyl reductive waves in the CV and DPV measurements of **4.12.** The HOMO-LUMO gap was calculated to be 1.31 eV.

Table 4.11. Electron orbital energies of optimised $[\{(bipy)Pt\}_2(thea)]$ structure from DFT calculations (B3LYP, SDD; {D95 basis set on C, H, N} {Dresden / Stuttgart pseudopotential on Pt}).

	LUMO+2	LUMO+1	LUMO	HOMO	HOMO-1	HOMO-2
Energy [eV]	-1.63264	-2.58502	-2.63944	-3.94555	-4.24487	-5.03398

4.3 Conclusions

Three novel platinum(II) *bis*-dioxolene complexes containing the central $[thea]^{4-}$ ligand and diphosphine (dppb [**4.10**], dppe [**4.11**]) and bipyridyl ($^{t}Bu_2Bipy$ [**4.12**]) ancillary ligands have been prepared and analysed in detail. Analysis of the neutral complexes **4.10**-**4.12** showed successful complexation of both dioxolene rings and their non-conjugation, by retention of the central bicyclo[2.2.2]octyl spacer. Electrochemical analysis of the complexes displayed two reversible one-electron redox processes of each dioxolene ring of the central $[thea]^{n-}$ ligand. This permitted clean, ligand-centered one-electron oxidation of each complex by the addition of a stoichiometric amount of ferrocenium hexafluorophosphate. Analysis by UV/vis-NIR showed the oxidation was ligand centered, with the growth of an intense intervalence charge transfer (IVCT) in the near-infrared region of the electronic spectrum in each case. Analysis of the transition displayed that in all oxidised species, the two halves of the complex are strongly coupled and are approaching Robin-Day class III at 298 K. Addition of one further equivalent of $[FeCp_2]PF_6$ caused further growth in this transition for **4.10** and **4.11**, although non-isobestic decomposition of **4.12**. Spectroelectrochemical analysis of **4.11** displayed sequential, clean one-electron electrochemical oxidations where the IVCT band of $[\mathbf{4.11^{\bullet\bullet}}]^{2+}$ was significantly more intense than observed for when chemically oxidised. This was attributed to the closeness of the second oxidation potential of the complexes to that of ferrocene, which therefore requires the use of a stronger oxidising agent to investigate the di-cationic species in detail. Spectroelectrochemical analysis of higher oxidation states of complex $[\mathbf{4.11}]^{n-}$ (n = 3,4)

showed the complex is very stable, and would permit the detailed analysis of these high oxidation states without decomposition. EPR analysis of the complexes showed the oxidised radical is ligand centred and could be frozen out on the EPR timescale at temperatures less than 100 K. Crystallographic characterisation of [**4.10**]$\mathbf{PF_6}$ and [**4.11**]$\mathbf{PF_6}$ showed both experience a structural change once oxidised, by a decreased dihedral angle between dioxolene rings. DFT analysis on a model complex, [{(bipy)Pt}$_2$thea)], showed that this is likely due to a decrease in population of the antibonding HOMO. Further work on the complexes should be directed towards the characterisation of the doubly-oxidised species, and to determine whether or not the valent electrons are coupled, as in complexes of *biscat*, or not.[16, 23]

4.4 References

[1] a) P. W. Rabideau, *J. Org. Chem.* **1971,** *36*, 2723-2724; b) C. H. Lee, H. Kohn, *J. Org. Chem.* **1990,** *55*, 6098-6104.

[2] G. M. Martinez, O. P. Arroyo, O. F. Lara, P. G. Espinosa, O. S. Hernandez, U. M. I. Chavez, M. Salmon, R. Cruz-Almanza, *Tetrahedron* **1997,** *53*, 17633-17642.

[3] M. Martinez, F. L. Ochoa, R. Cruz-Almanza, R. A. Toscano, *J. Chem. Crystallogr.* **1996,** *26*, 451-456.

[4] L. J. Barbour, J. W. Steed, J. L. Atwood, *J. Chem. Soc., Perkin Trans. 2* **1995,** 857-860.

[5] T. S. Balaban, A. Eichhoefer, M. J. Krische, J.-M. Lehn, *Helv. Chim. Acta* **2006,** *89*, 333-351.

[6] a) A. J. Birch, *J. Chem. Soc. Res.* **1944,** 430-436; b) A. J. Birch, *J. Chem. Soc. Res.* **1945,** 809-813; c) A. J. Birch, *J. Chem. Soc. Res.* **1946,** 593-597; d) A. J. Birch, *J. Chem. Soc. Res.* **1947,** 102-105; e) A. J. Birch, *J. Chem. Soc. Res.* **1947,** 1642-1648; f) A. J. Birch, S. M. Mukherji, *J. Chem. Soc. Res.* **1949,** 2531-2536.

[7] I. M. Davidson, O. C. Musgrave, *J. Chem. Soc.* **1963,** 3154-3155.

[8] V. J. Chebny, T. S. Navale, R. Shukla, S. V. Lindeman, R. Rathore, *Org. Lett.* **2009,** *11*, 2253-2256.

[9] P. Thuéry, B. Masci, *J. Supramol. Chem.* **2003,** *15*, 95-99.

[10] B. F. Abrahams, N. J. FitzGerald, R. Robson, *Inorg. Chem.* **2010,** *49*, 5953-5956.

[11] J. Best, I. V. Sazanovich, H. Adams, R. D. Bennett, E. S. Davies, A. J. H. M. Meijer, M. Towrie, S. A. Tikhomirov, O. V. Bouganov, M. D. Ward, J. A. Weinstein, *Inorg. Chem.* **2010**, *49*, 10041-10056.

[12] D. Scott Bohle, D. Stasko, *Chem. Commun.* 1998, 567-569.

[13] Bruker (2004). APEX2, SAINT-Plus, XPREP and SADABS. Bruker AXS Inc., Madison, Wisconsin, USA.

[14] A. Spek, *Acta Cryst. Sect. D* **2009,** *65*, 148-155.

[15] K. D. Demadis, C. M. Hartshorn, T. J. Meyer, *Chem. Rev.* **2001,** *101*, 2655-2685.

[16] L. F. Joulie, E. Schatz, M. D. Ward, F. Weber, L. J. Yellowlees, *J. Chem. Soc. Dalton Trans.* **1994,** 799-804.

[17] K. G. Alley, G. Poneti, P. S. D. Robinson, A. Nafady, B. Moubaraki, J. B. Aitken, S. C. Drew, C. Ritchie, B. F. Abrahams, R. K. Hocking, K. S. Murray, A. M. Bond, H. H. Harris, L. Sorace, C. Boskovic, *J. Am. Chem. Soc.* **2013,** *135*, 8304-8323.

[18] a) C. G. Pierpont, R. M. Buchanan, *Coord. Chem. Rev.* 1981, *38*, 45-87; b) S. Bhattacharya, S. R. Boone, G. A. Fox, C. G. Pierpont, *J. Am. Chem. Soc.* **1990,** *112*, 1088-1096.

[19] A. L. Macdonald, J. Trotter, *J. Chem. Soc. Perkin Trans. 2* **1973,** 476-480.

[20] a) O. Carugo, C. B. Castellani, K. Djinovic, M. Rizzi, *J. Chem. Soc., Dalton Trans.* **1992,** 837-841; b) H. Wunderlich, D. Mootz, *Acta Cryst., Sect. B* **1971,** *27*, 1684-1686.

[21] T. T. Patricia, M. V. Sandra, L. Manuela, L. Andrea, F. Paolo, D. Andrea, R. Roberto, *Phys. Chem. Chem. Phys.* **2012,** *14*, 1038-1047.

[22] T. H. Dunning Jr., P. J. Hay in *Modern Theoretical Chemistry*. *Vol. 3*, Plenum,, New York, **1977**.

[23] A. M. Barthram, Z. R. Reeves, J. C. Jeffery, M. D. Ward, *J. Chem. Soc., Dalton Trans.* **2000,** 3162-3169.

Chapter 5

Attempted Synthesis of Novel, Multinuclear Thiolated Ligands

5.1 Introduction

Metallodithiolenes are a series of well-known, redox-active compounds capable of oxidising readily to their dithiosemiquinoate and dithioquinone forms.[1] The ability to demonstrate reversible sequential one-electron steps makes these excellent centres to study with fascinating electrochemical, photochemical and magnetic properties. Complexes incorporating dithiolene moieties have been utilised in mimics of numerous enzyme active sites[2] and magnetic or conductive materials.[3] Platinum/diimine/dithiolene ternary complexes display strong MMLL'CT absorptions ($\varepsilon = 10^4\ M^{-1}cm^{-1}$) in the visible or near-IR region,[4] opening the possibility for tuning their use as sensitisers in dye-sensitised solar cells,[5] hydrogen evolution systems[6] or optoelectronic communication purposes.

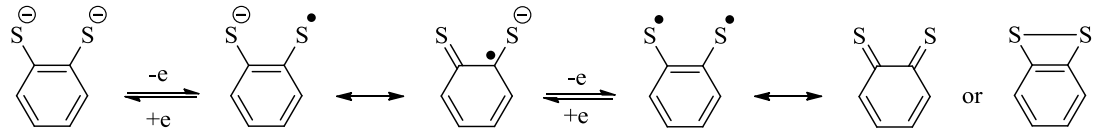

L^{2-} $L^{\cdot -}$ L^{0}

Scheme 5.1. Schematic representation of the reversible one electron redox processes displayed by $[bdt]^{n-}$ (bdt = 1,2-benzenedithiol).

Further interest arises when complexes contain multiple dithiol ligands,[7].[8] particularly when present in different oxidation levels, therefore opening the possibility of communication between metal centres *via* the same mixed valence pathways as discussed in chapter 1. Changes in overall complex oxidation state has been shown to manifest in two ways; reduction of the overall complex has been shown to reside mainly on the metal centre or ancillary ligand(s)[9] whilst oxidation gives an electron residing predominantly on the ligand, yielding intriguing magnetic and optical properties.[10]

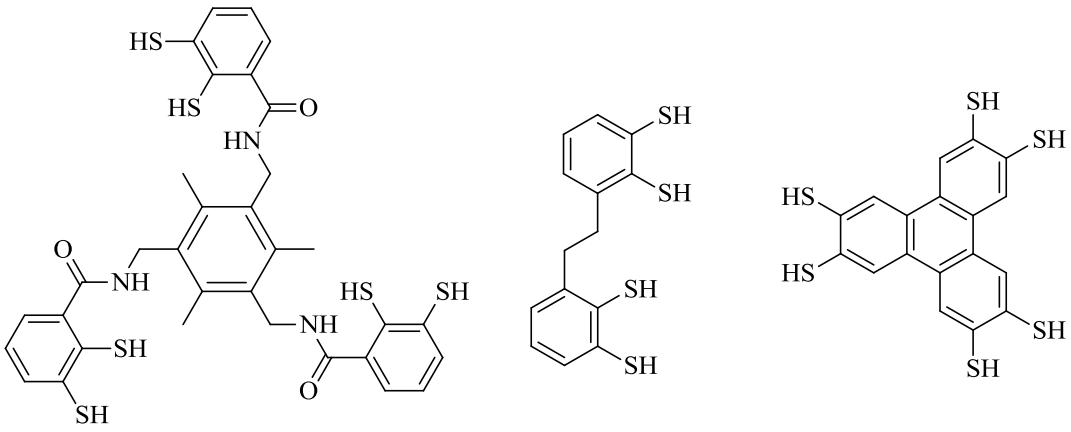

$L_{5\text{-}1}$ $L_{5\text{-}2}$ $L_{5\text{-}3}$

Figure 5.1. Examples of previously synthesised multinuclear thiolated ligands. $L_{5\text{-}1}$ and $L_{5\text{-}2}$ have previously been prepared by Kreickmann et al,[7] **$L_{5\text{-}3}$** has been previously studied by Nishihara *et al.*[8]

The aim of this investigation was therefore to synthesise two novel poly-thiol homologues to ctc (**2.2**) and H_4thea (**4.9**), as shown in **Figure 5.2**, with the view to generate similar radical complexes by oxidation, to those presented in chapters 3 and 4. The synthesis of thiocyclotricatechylene (thio-ctc) has been attempted previously by Dr. Little but was unfortunately unsuccessful, this will be discussed later into the chapter.[11]

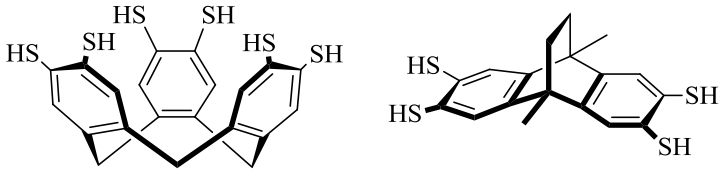

thio-ctc **thio-thea**

Figure 5.2. Schematic representations of the two thiolated molecules; (thio-ctc and thio-thea) targeted during this study.

5.1.1 Newman-Kwart Rearrangement

The synthesis of aromatic thiols can be an extremely involved synthetically, most often using odorous thiolates (e.g. NaSMe) via an aromatic substitution reaction using halogenated phenyl derivatives. There exists an alternative reaction however, whereby the migration of $O_{Ar} \rightarrow S_{Ar}$ may be induced in aryl thiocarbamates using high temperatures. This migration is often referred to as the Newman-Kwart rearrangement (NKR)[12] and has seen extensive use in a variety of reactions[13] including the synthesis of macrocyclic disulfides,[14] helicenes[15] and a redox-active molecular switch.[16]

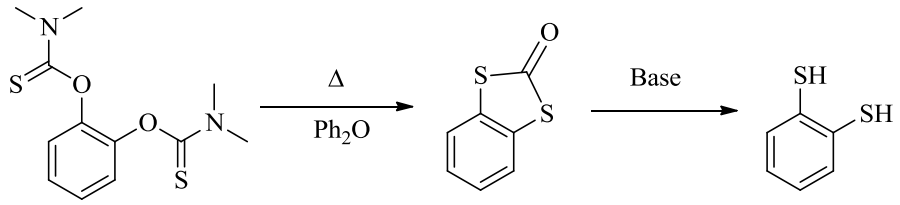

Scheme 5.2. Schematic representation of the Newman-Kwart Rearrangement (NKR) in 1,2-phenylene *bis*(dimethylcarbamothioate) to benzene-1,2-dithiol (bdt).

The rearrangement is seen as energetically favourable due to the formation of a C=O bond from a C=S bond and is understood to proceed via an intramolecular aromatic nucleophilic substitution reaction and a resonance stabilised 4-membered transition state, as displayed in **Scheme 5.3**.[17]

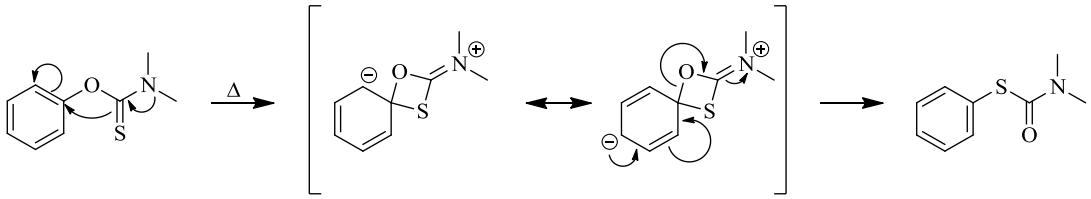

Scheme 5.3. Accepted mechanism of the Newman-Kwart Rearrangement.[17]

This reaction was found to be useful in chemistry of the cyclotriveratrylene family, with the successful synthesis of two novel thiolated compounds; thiocyclotriphenolene (thio-ctp) and thiocyclotriguaiacylene (thio-ctg).[18] Both were synthesised *via* the Newman-Kwart rearrangement and could be used in the synthesis of novel capsules, as illustrated in chapter 1.[18a, 19]

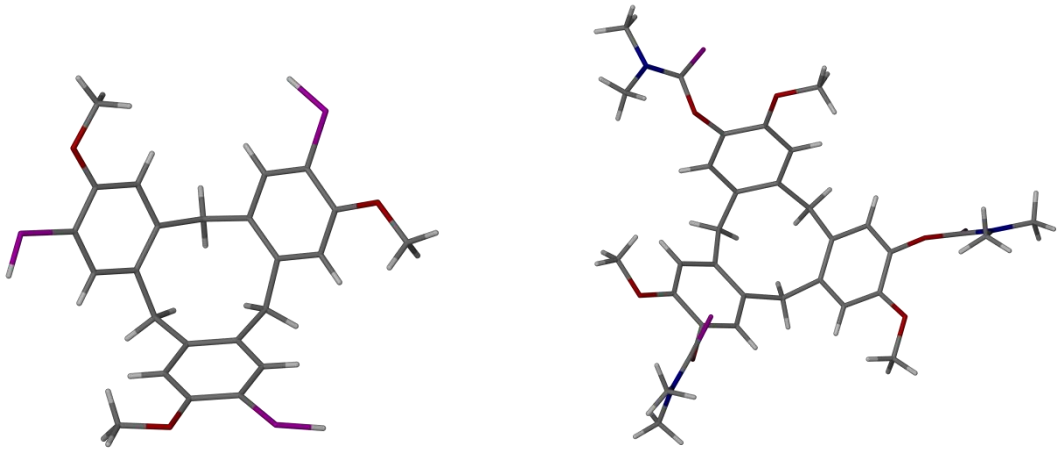

Figure 5.3. (Left) Structure of thio-ctg, prepared *via* the Newman-Kwart rearrangement of (right) *tris*-(dimethylthiocarbamoyl)cyclotriguaiacylene.[18a] Colour code: S, purple; O, red; N, blue; C, grey; H, white.

5.1.2 Previously Attempted Synthesis of Thiocyclotricatechylene

Work conducted by Dr. Marc Little during his Ph.D came tantalisingly close to yielding the target molecule thio-ctc. Although, various challenges faced in the deprotection of the final products unfortunately led to the target molecule remaining unsynthesised.

A number of reaction routes were attempted during the project, beginning with the synthesis of dimethyl-thiocarbamic acid *O*-(3,7,8,12,13-pentakis-dimethylthiocarbamoyloxy-10,15-dihydro-5*H*-tribenzo[*a*,*d*,*g*]cyclononen-2-yl) ester, from the substitution of cyclotricatechylene using dimethylthiocarbamoyl chloride in the presence of caesium chloride, in deoxygenated NMP (NMP = *N*-Methyl-2-pyrrolidone). It was anticipated that this product could be rearranged via a heat-induced Newman-Kwart reaction, again in deoxygenated NMP, yielding the analogous *S*-(3,7,8,12,13-pentakis-dimethylthiocarbamoylthio-10,15-dihydro-5*H*-tribenzo[*a*,*d*,*g*]cyclononen-2-yl) ester. At high temperatures (>250 °C) however, the precursor decomposed. Lower temperatures (*c.a.*180 °C) were consequently investigated although failed to offer the desired compound, even with long reaction times (>72 hours). This was assumed to be due to the instability of the precursor at elevated temperatures. As a consequence, simple cleavage of the protecting group using base (e.g. NaOH) to give thio-ctc was not available.

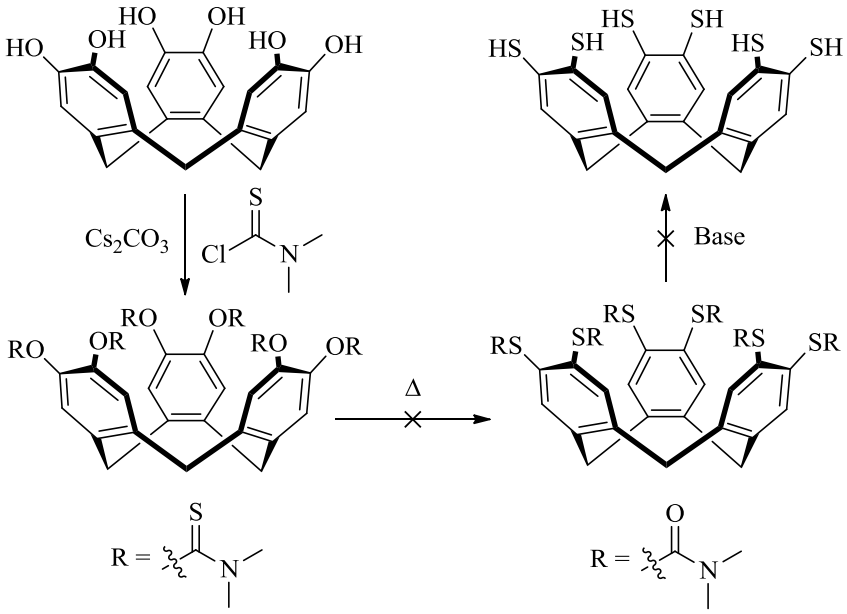

Scheme 5.4. Initial attempted reaction route towards thio-ctc by Dr. Little.

In light of this, a revised reaction route was devised. Proceeding *via* the acid-catalysed cyclisation of alkyl- or phenyl-substituted 3,4-dithiobenzyl alcohol to give the desired thiolated-cyclotriveratrylene analogue, which could then be deprotected using literature conditions to give thio-ctc. The reaction appeared to proceed well, despite a relatively low-yielding Newman-Kwart rearrangement (step 3), up until deprotection where both methyl- and ethyl- protecting groups could not be removed using a mixture of sodium in hexamethylphosphoramide or mCPBA (mCPBA = *meta*-chloroperoxybenzoic acid) to selectively oxidise each thiol. Synthesis of the analogous benzyl-thiocyclotriveratrylene was then attempted, as benzyl groups are routinely used as protecting groups for thiol moieties. Unfortunately the cyclisation step was very poor resulting in an unworkable yield. The revised attempted reaction route is summarised in **Scheme 5.5** below.

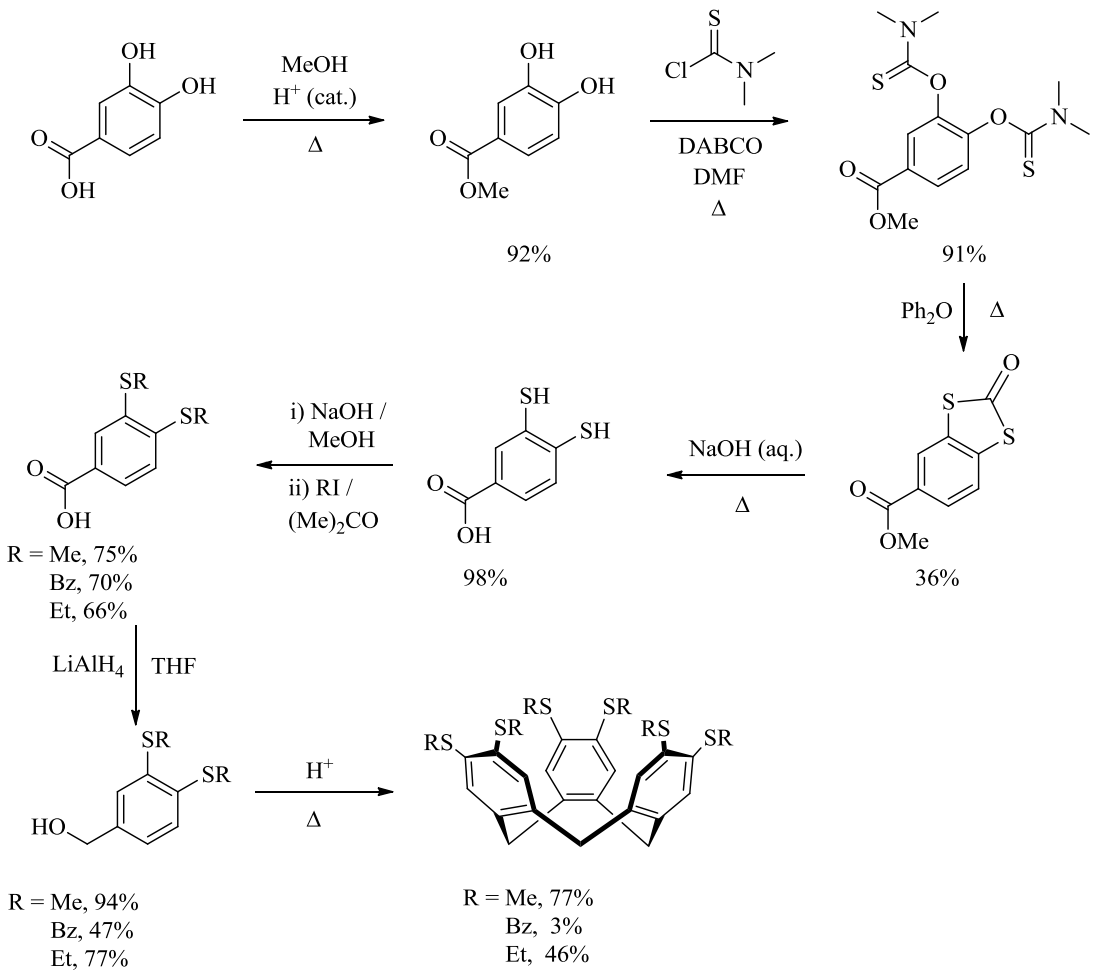

Scheme 5.5. Revised reaction scheme towards thio-ctc employed by Dr. Little.

5.2 Results and Discussion

5.2.1 Reattempted Synthesis of Thiocyclotricatechylene

The conclusion drawn from the reaction routes attempted by Dr. Little was that the key step towards the synthesis of thio-ctc was in the choice of a suitable thiol-protecting group, which could be selectively cleaved under conditions avoiding destruction of the molecule. In the investigation though, cyclisation was not attempted without the presence of this protecting group (i.e. use of 3,4-dithiobenzyl alcohol) therefore this was looked at first. Following the reaction scheme outlined in **Scheme 5.6**, which is for the most part identical to that outlined in **Scheme 5.5**, the synthesis of all compounds leading up to 3,4-dithiobenzoic acid (**5.1**) were achieved in good yields, comparable to those outlined above and reported in the literature.[20] Surprisingly though, the synthesis of 2-oxo-1,3-benzodithiole-5-carboxylate (**5.3**) via Newman-Kwart rearrangement at 240 ^{o}C in diphenyl ether proceeded in yields better than previously reported.[20b] This was attributed to a

slightly increased reaction time of 1 hour compared to 40 minutes used by Mahendran *et al.* although less than the 3 hours used by Dr. Little, but the reason for this is unclear. Cleavage of the dithiocarbonyl protecting group of **5.3** was achieved by hydrolysis using sodium hydroxide in degassed water, followed by an acid work-up to give 3,4-dithiobenzoate (**5.4**) in excellent yield (98%). This was reduced by lithium aluminium hydride in dry THF to give 3,4-dithiobenzyl alcohol (**5.5**) as an air-sensitive yellow oil, shown to be slightly impure by ^{1}H NMR. Attempts were made to purify the product by extraction into hot hexane but the air-sensitivity of the product quickly became apparent at elevated temperatures, obvious by the precipitation of an insoluble yellow powder assumed to be an oligomeric species. Cyclisation of **5.5** to thio-ctc in formic acid at 70 ^{o}C was therefore attempted without full purification. After workup, analysis by ^{1}H NMR showed only a complex spectrum, with no peaks to indicate the presence of thio-ctc. Analysis by mass spectrometry (ES+) on the other hand showed the presence of peaks assignable to the coupling of two units of **5.5** but no peaks assignable to thio-ctc or any other species of higher order. All attempts to extract this mono-coupled product failed as the sample could not be extracted or purified on silica or alumina. Increased reaction times, higher temperatures and the use of the lewis acid scandium(III)triflate as a catalyst (1 mol%) were also attempted to increase conversion,[21] although these approaches offered no advancement on the homo-coupled product.

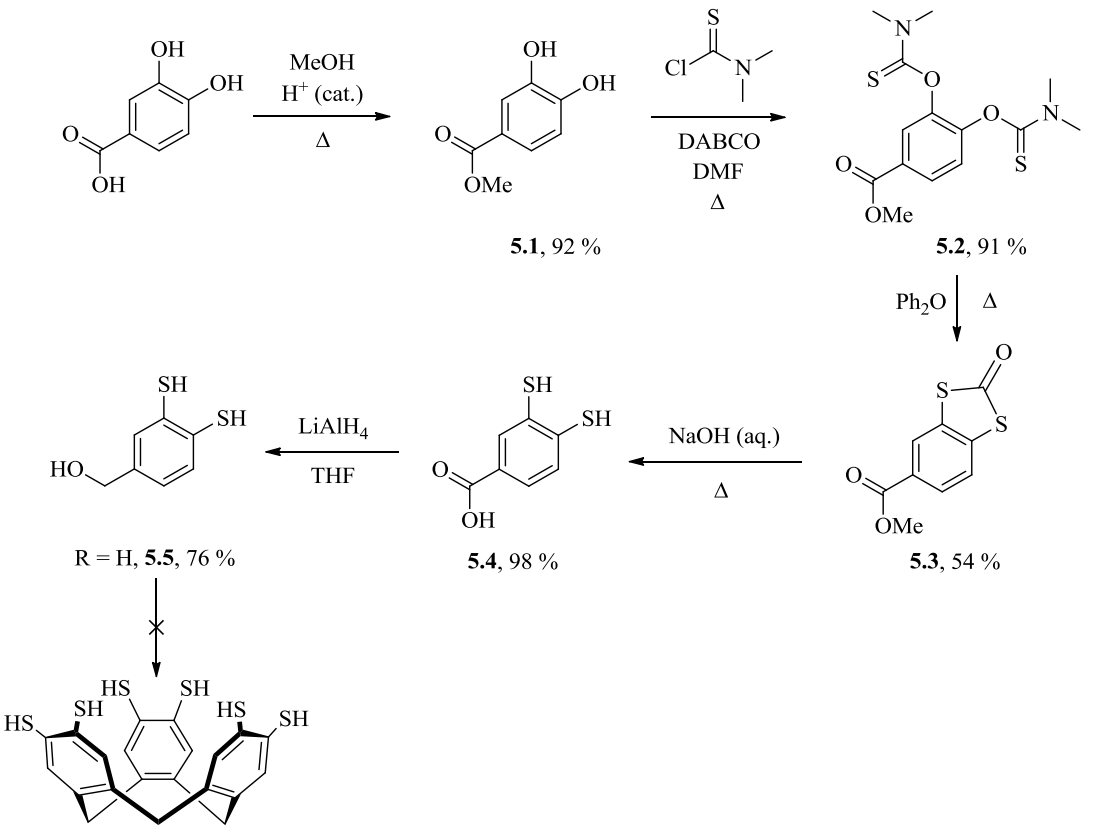

Scheme 5.6. Reaction scheme for the attempted synthesis of thio-ctc via 3,4-dithiobenzyl alcohol (**5.5**).

In light of these observations, it therefore appeared that cyclisation of pre-protected thiobenzyl alcohol species was the best manner by which to proceed. It was therefore decided to simply continue from where the initial investigation left off, with an attempt to increase the synthesised yield of benzyl-thiocyclotriveratrylene using more forcing conditions for the cyclisation of 3,4-benzylthiobenzyl alcohol (**5.6**). Following the reaction scheme shown below (**Scheme 5.7)**, **5.6** was prepared by the reaction of the sodium salt of **5.4** with 2.2 equivalents of benzyl bromide in acetone, and was synthesised in moderate yield (70%). Reduction of **5.6** using lithium aluminium hydride in anhydrous THF yielded a crude mixture. Compound **5.7** could be extracted by column chromatography (silica, 5% methanol in dichloromethane) again in moderate yield (64%) and as a low melting point solid. Renewed attempts at cyclising **5.7** failed however, and it was found that use of formic acid could not improve on the original yield of isolated product (≤3%). Use of more forcing conditions, perchloric acid (10%) in methanol for instance, gave only a complex mixture while use of $Sc(OTf)_3$ in acetonitrile[21] at 60 °C failed to offer any conversion. It is likely that the –M effect of the thiobenzyl substituent *para* to the primary alcohol has an effect on the yields obtained in these reactions, considering the mechanism of cyclisation. As a result, further attempts of cyclising **5.7** were precluded.

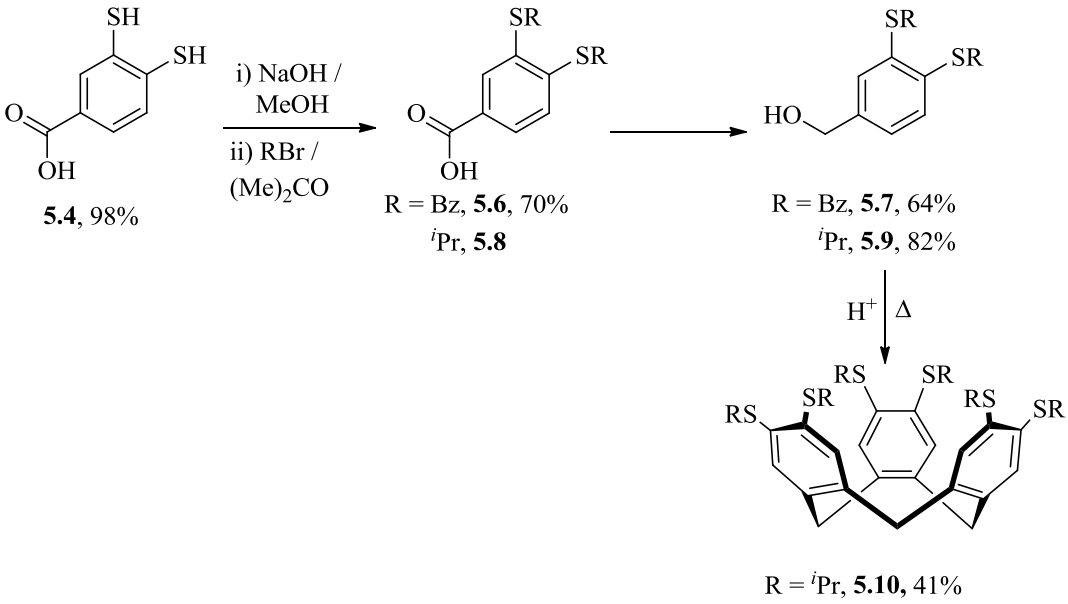

Scheme 5.7. Synthetic route towards hexaisopropylthio-ctc (**5.10**).

Attention was then turned to other protecting groups with a positive donating (+I) effect. It was noted that a number of reactions involving the synthesis of compounds incorporating 1,2-dithiobenzene moieties proceeded via the nucleophilic aromatic substitution of 3,4-dichlorobenzyl- or 3,4-dibromobenzyl- derivatives with sodium isopropylthioate.[22] Following successful synthesis of the diisopropylthiobenzyl- compound, the isopropyl protecting groups could then be cleaved by reduction without destruction of the compounds. As a satisfactory route had already been devised towards the synthesis of 3,4-dithiobenzoic acid (**5.4**), simple reaction with 2-iodopropane after deprotonation using sodium hydroxide gave a mixture of the mono-substituted product and **5.8** in the approximate ratio 20 : 80 (determined by ^{1}H NMR). Attempts to purify the product were unsuccessful, therefore the mixture was reduced using lithium aluminium hydride in anhydrous THF and purified by column chromatography (silica, $CHCl_3$) yielding **5.9** as a low-melting point solid. Subsequent cyclisation of **5.9** was then performed by heating in formic acid under an inert atmosphere at 70 °C for 48 hours, after which extraction of the product could be achieved either by column chromatography (CH_2Cl_2→2.5% MeOH in CH_2Cl_2) or trituation in diethyl ether / methanol yielding **5.10** as a white microcrystalline solid. The ^{1}H NMR (300 MHz, $CDCl_3$) of **5.10**, as shown in **Figure 5.4**, confirmed it's characteristic bowl-structure and C_3 symmetry due to the presence of ditopic proton resonances CH_{endo} and CH_{exo} at δ = 4.73 and 3.66 ppm respectively, with J_{HH} coupling equal to 13.6 Hz and integrations to match their respective environments (3H each). In addition, the presence of one CH_{Ar} resonance and clear CH(CH_3)$_2$ septet with J_{HH} = 6.7 Hz, characteristic of *iso*-propyl substituients, indicated a symmetric product.

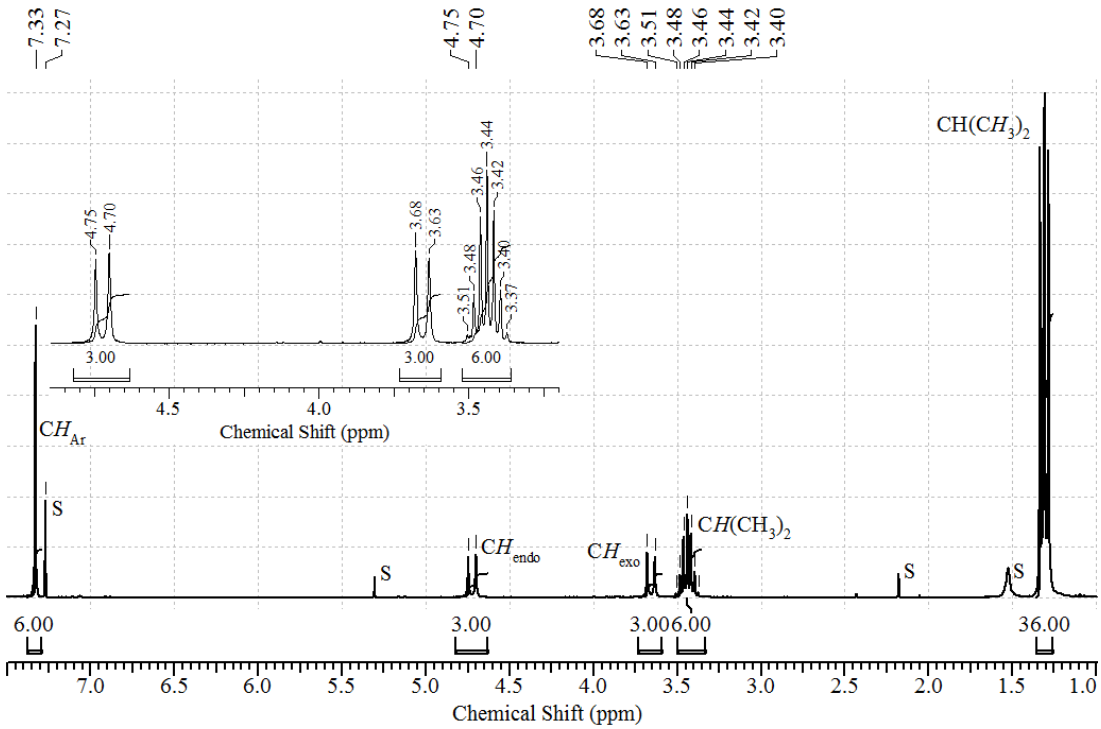

Figure 5.4. Interpreted ^{1}H NMR (300 MHz, $CDCl_3$) of **5.10.** Insert shows a close-up of region δ = 3.20-4.90 ppm to highlight the position of ditopic protons and isopropyl septet. Solvent (S) peaks at δ = 7.27, 5.30, 2.10 and 1.56 ppm correspond to C*H*Cl_3, CH_2Cl_2, (CH_3)CO and H_2O respectively.

Crystals suitable for single-crystal X-ray diffraction were grown via the slow evaporation of a chloroform / hexane solvent mixture. The structure crystallised in the triclinic space group $P\bar{1}$ and the assymmetric unit contained one full molecule of **5.10.** During the refinement, two carbon atoms, C(32) and C(33), could not be refined anisotropically therefore were kept as isotropic. All other non-hydrogen atoms were refined anisotropically and all hydrogen atoms placed in calculated positions and refined using a 'riding model'. The highest remaining electron peak was 0.78 *e*.A^{-3}, found 0.9 Å from S(33) whilst a *SQUEEZE*[23] analysis showed the structure contained no accessible solvent voids.

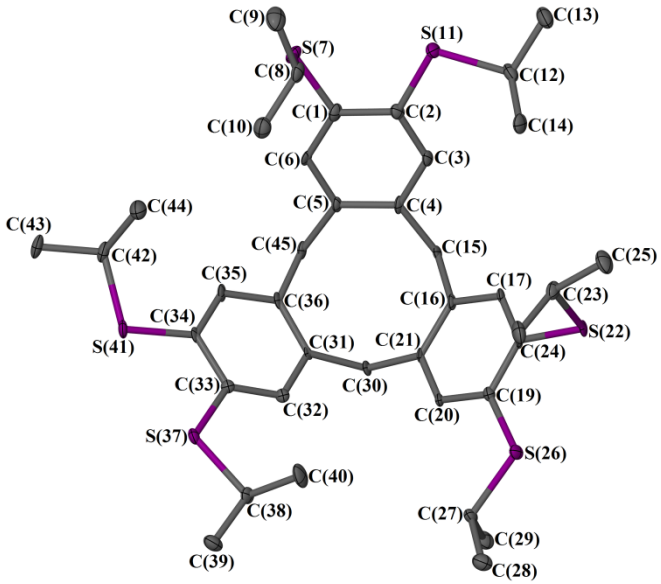

Figure 5.5. View and atom numbering scheme of **5.10**. Thermal displacement ellipsoids are set at 50% and all hydrogen atoms have been removed for clarity. Within the figure, C(18) is hidden behind C(24). Colour code: S, purple; C, grey.

As expected, the structure obtained confirmed the C_3 symmetry of **5.10** and retention of the characteristic hydrophobic bowl of CTV-based molecules. Interestingly the cavity of **5.10** appears to be shallower than that of CTV. This was apparent by an increase in angle between least squares planes of each isopropyl-thiol ring to approximately 117°, compared to an average value of approximately 111° in CTV.[24] This increase translates into an increased distance of approximately 1.1 Å between O,O or S,S moieties at the upper rim. Unfortunately, there is no analogous isopropyl-substituted structure to compare these parameters to, although this effect is likely due to increased steric bulk at the upper rim as opposed to anything else. A side-on view of molecule **5.10** is shown in **Figure 5.6**.

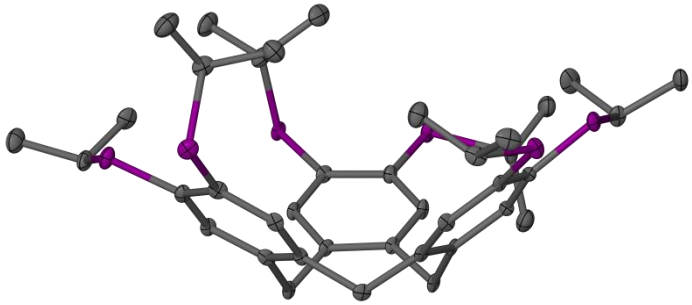

Figure 5.6. Side-on view of **5.10.** Thermal displacement ellipsoids are set at 50% and all hydrogen atoms have been removed for clarity. Colour code: S, purple; C, grey.

Within the lattice, the molecules pack 'back-to-back' into alternate sheets along the plane [001] as shown in **Figure 5.7**.

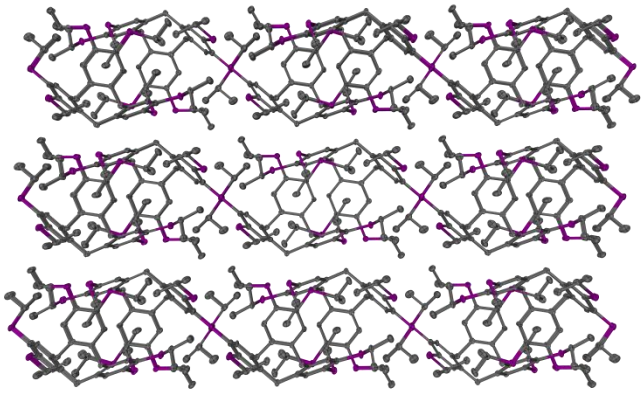

Figure 5.7. View perpendicular to plane [001] in structure **5.10**. Colour code: S, purple; C, grey.

Within these layers, the methyl group centred on C(23) of one isopropyl arm points into the cavity of an adjacent molecule as seen in **Figure 5.8**, forming an intermolecular host : guest association commonly seen by molecules of the CTV core unit.[25] All other methyl groups of the isopropyl arms point towards hydrophobic cavities within the lattice.

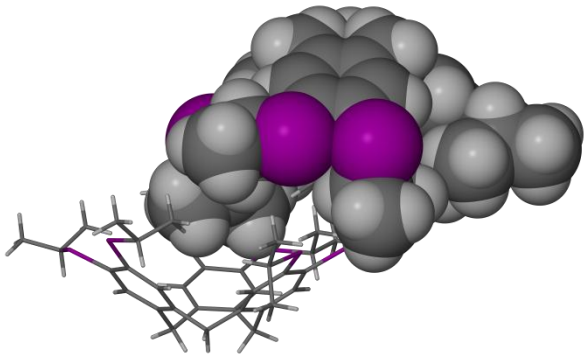

Figure 5.8. Intermolecular host : guest association shown between two molecules of **5.10** in the solid state. The top formula unit is shown according to its Van Der Waal's radii whilst the bottom molecule is shown with arbitrary radii. Colour code: S, purple; C, grey; H, white.

Table 5.1. Selected bond distances and angle between least squares planes (θ) of di(isopropyl)thiobenzene rings, extracted from the crystal structure of **5.11.**

	C_{Ar}-S [Å]	θ
5.10	1.769(3) – 1.826(3)	116.18(10) – 118.48(11)

Unfortunately, despite its clean and moderate yielding synthesis, the deprotection of **5.10** was unachievable due to time constraints. However it is anticipated, that reduction via use of sodium / naphthalene in THF or Birch reduction[26] would likely offer

thiocyclotricatechylene via reduction of the isopropyl protecting groups as these conditions have been used previously in the of synthesis of $L_{5\text{-}2}$.[22b]

5.2.2 Attempted Synthesis of 2,3,6,7-tetrathiol-9,10-dimethyl-9,10-dihydro-9,10-ethanoanthracene (thio-thea)

In order to provide the thiolated homologue to H_4thea (**4.9**), synthesis of 2,3,6,7-tetrathio-9,10-dimethyl-9,10-dihydro-9,10-ethanoanthracene (thio-thea) was anticipated to proceed *via* the Newman-Kwart rearrangement of 2,3,6,7-tetrakis(dimethylcarbamothioate)-9,10-dimethyl-9,10-dihydro-9,10-ethanoanthracene, as outlined in **Scheme 5.8** below.

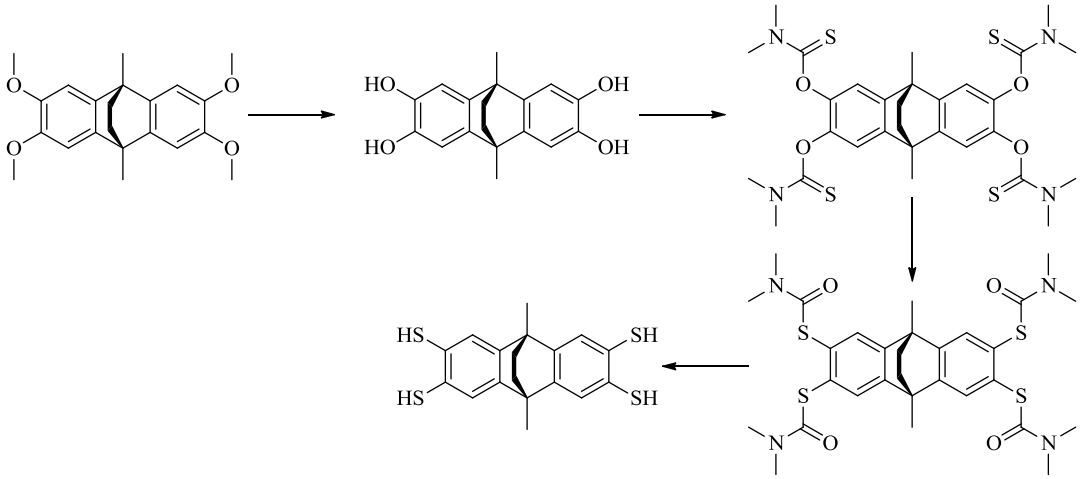

Scheme 5.8. Proposed reaction route towards thio-thea.

5.2.3 Synthesis and Characterisation of *O*,*O*',*O*'',*O*'''-2,3,6,7-Tetrakis(dimethylcarbamothioate)-9,10-dimethyl-9,10-dihydro-9,10-ethanoanthracene (5.11).

In order to provide an accessible pathway to 2,3,6,7-tetrathio-9,10-dimethyl-9,10-dihydro-9,10-ethanoanthracene without using the unpleasant and odorous thiol precursors, the decision to use the Newman-Kwart rearrangement was made. In order to provide a molecule with functional group capable of this rearrangement, **4.9** was reacted with dimethylthiocarbamoyl chloride in the presence of a large excess of DABCO in dry DMF, as shown in **Scheme 5.9** . The reaction proceeded with few side-products which could be extracted by trituation from ethanol giving **5.11** cleanly and in good yield (82%). Analysis by ^{1}H NMR confirmed the tetra-substituted nature of **5.11**, displaying a spectrum corresponding to only one environment for each proton as observed with one CH_{Ar} at δ = 7.08 ppm and a pair of resonances corresponding to the two CH_3 groups of the *N,N'*-dimethylcarbamothioate arms at 3.42 and 3.27 ppm whilst the core ethanoanthracene CH_3

and CH_2 resonances were observed at 1.92 and 1.66 ppm. Similary, the $^{13}C\{^1H\}$ NMR displayed characteristic resonances with one belonging to the thiocarbonyl carbon at 186.9 ppm and two from the *N,N*-dimethylthiocarbamate carbons at 35.7 and 38.8 ppm. All other resonances within the spectrum corresponded to the 9,10-dimethyl-9,10-dihydroethanoanthracene core. Aromatic proton resonances were observed at 144.1, 142.8 and 116.7 ppm, whilst those at 43.3, 41.8 and 18.2 ppm belong to the two CH_2 carbons of the ethano-bridge and methyl carbons respectively. Additionally, IR analysis (solid state) of the product confirmed the presence of the thiocarbonyl with a broad absorption at 1121 cm^{-1} corresponding to ν(C=S).

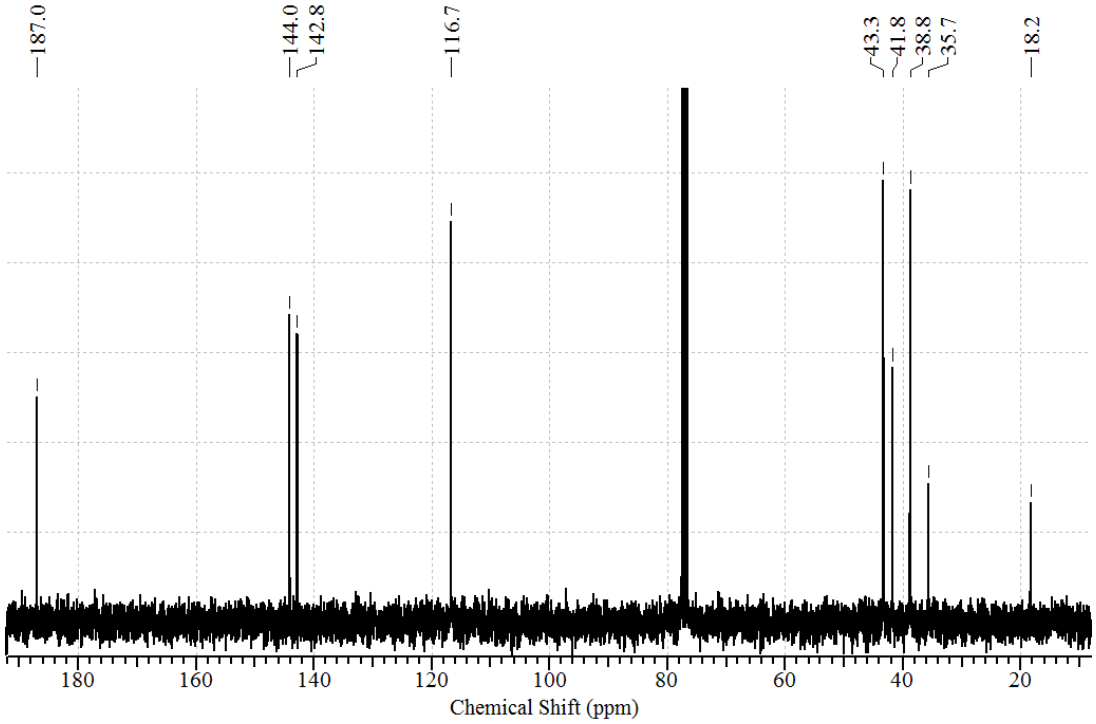

Figure 5.9. $^{13}C\{^1H\}$ (121 MHz, $CDCl_3$) of compound **5.11**.

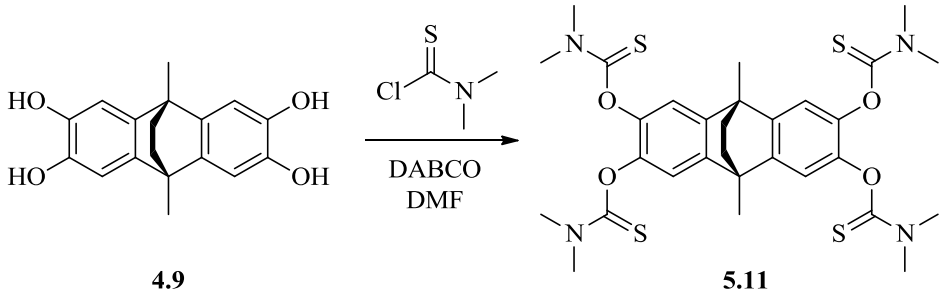

Scheme 5.9. Schematic representation of the synthesis of **5.11** from **4.9**.

Single crystals suitable for X-ray diffraction were grown from the slow diffusion of pentane into a dichloromethane solution of **5.11**. Structural characterisation confirmed the tetra-substituted product as assigned above. The asymmetric unit was shown to contain one

formula unit only, showing no obvious disorder of any atoms. All crystallographically ordered non-H atoms in the structure were refined anisotropically and there were no restraints applied. All hydrogen atoms were placed in calculated positions and refined using a riding model. The highest residual Fourier peak of 0.93 $e.A^{-3}$ is found approximately 1.88 Å from O(31) of one dimethylcarbamothioate arm, this could not be modelled however.

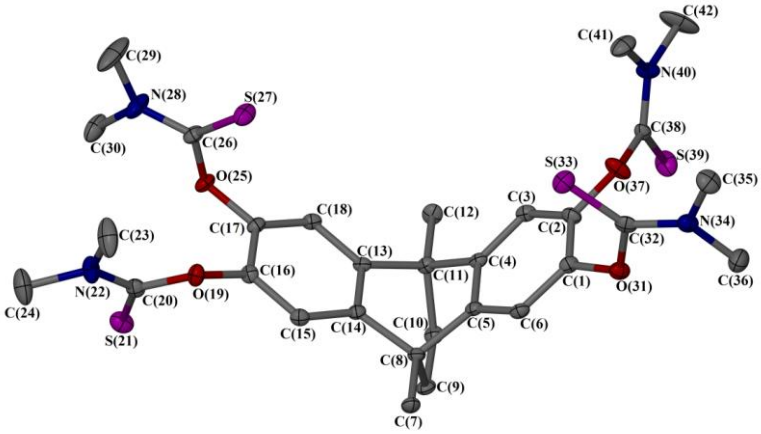

Figure 5.10. View and atom numbering scheme of **5.11.** Thermal displacement ellipsoids are set at 50% and all hydrogen atoms have been removed for clarity. Colour code: S, purple; O, red; N, blue; C, grey; H, white

Importantly, after substitution at the $[thea]^{4-}$ upper-rim, the angled nature of the molecule was retained, with dihedral angle between least squares planes of the two aromic rings equal to approximately 121°. This corresponds to a contraction of approximately 9°, when compared to the only previously reported structure of **4.9**.[27] Within the lattice, the molecules pack closely together in rows with no solvent voids (<2% as calculated by a *SQUEEZE*[23] analysis).

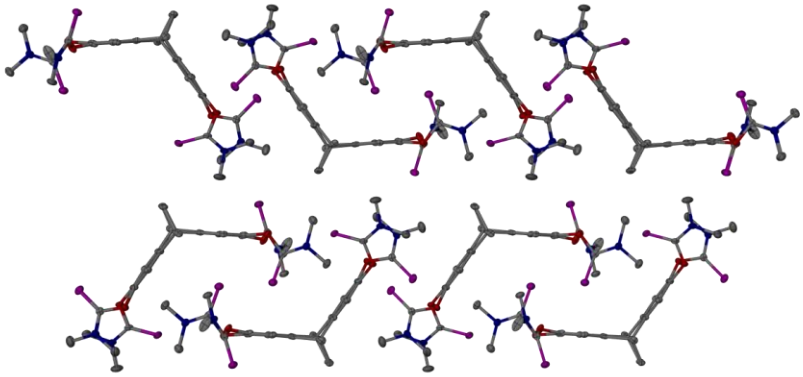

Figure 5.11. Packing diagram of **5.11** viewed along crystallographic plane [100]. Thermal displacement ellipsoids are set at 50% and all hydrogen atoms have been removed for clarity. Colour code: S, purple; O, red; N, blue; C, grey; H, white

Two of the molecules within these layers pack together, forming a simple dimeric close-packed arrangement, where one dimethylthiocarbonyl arm points into the 'cavity' of opposing molecule as shown in **Figure 5.12**.

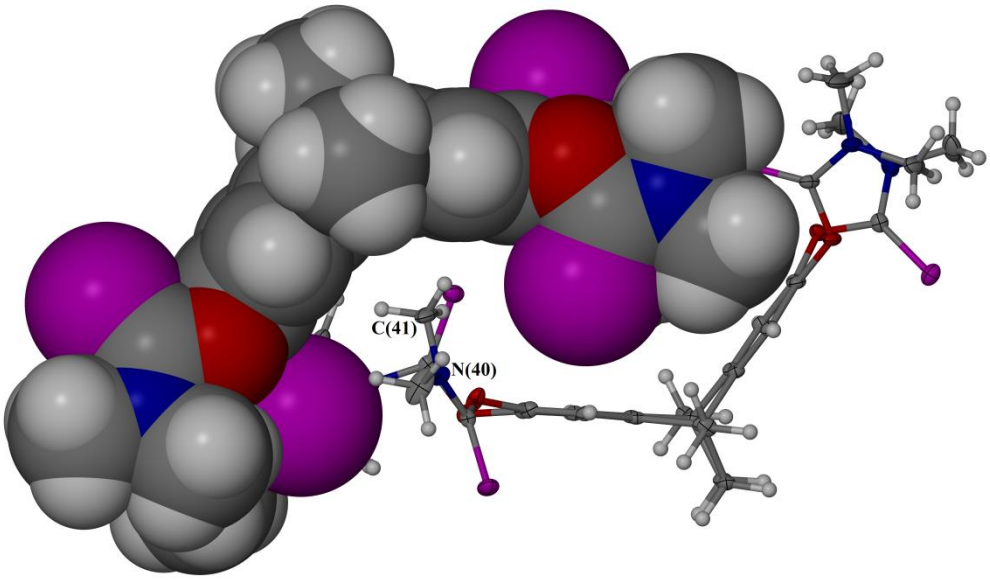

Figure 5.12. Association between two formula units of **5.11** within the crystal structure. The top formula unit is shown according to its Van Der Waal's radii whilst the bottom molecule is shown with thermal displacement ellipsoids are set at 50%. Colour code: S, purple; O, red; N, blue; C, grey; H, white.

Table 5.2. Selected bond distances and angle between least squares planes (θ) of *bis*(dimethylcarbamothioate) rings extracted from the crystal structure of **5.11.**

	C-O [Å]	C=S [Å]	θ
5.11	1.368(2) - 1.398(2)	1.657(2) - 1.665(2)	121.32(6)

5.2.4 Synthesis and Characterisation of *S*,*S*',*S*'',*S*'''-2,3,6,7-Tetrakis(dimethylcarbamothioate)-9,10-dimethyl-9,10-dihydro-9,10-ethanoanthracene (5.12).

Starting from **5.11,** *S*,*S*',*S*'',*S*'''-2,3,6,7-tetrakis(dimethylcarbamothioate)-9,10-dimethyl-9,10-dihydro-9,10-ethanoanthracene (**5.12**) was formed in almost quantative yield (98%) using conditions appropriate for a Newman-Kwart rearrangement, by heating the **5.12** to 240 ^{o}C in diphenyl ether for 30 minutes, as in the synthesis of **5.4** above. During the investigation, a variety of temperatures and reaction times were attempted until a high yield (94%) of the product was obtained. The product may be isolated from the crude reaction in two ways, the first by precipitation using *n*-hexane and recrystallisation from 2.5% diethyl ether in *n*-hexane or, by column chromatography (silica, dichloromethane → 10% ethyl acetate in dichloromethane). The best yields were achieved by column chromatography.

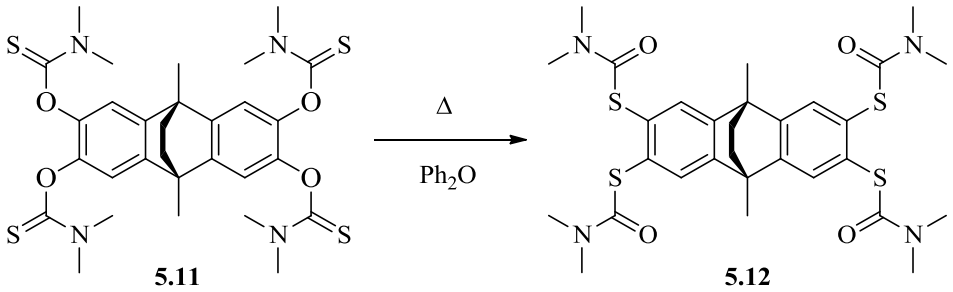

Figure 5.13. Schematic representation of the conversion of **5.11** to **5.12** via Newman-Kwart rearrangement.

Analysis showed the rearrangement had proceeded differently to that of **5.4** whereby O → S migration was demonstrated, instead of the formation of an analagous benzo(1,3)dithiol-2-one. This migration has been observed once before in the synthesis of benzobisthietes, but was not characterised in detail.[28] The structure of **5.12** was confirmed by symmetric ^{1}H and ^{13}C{^{1}H} NMR spectra showing retention of the carbamoyl N(CH_3)$_2$ resonances (although reduced into one broad resonance with downfield shift) along with loss of the thio-carbonyl resonance at δ = 186.9 ppm, and growth of carbonyl resonance at δ = 166.7 ppm which was not present in the DEPT-135 spectrum. Additional evidence came *via* IR spectroscopy (solid state) which displayed a distinctive ν(C=O) at 1653 cm^{-1}. Mass spectroscopic (ES+)

evidence showed the presence of a peak at m/z 669.2 corresponding to the sodium adducted target compound whilst single crystals suitable for X-ray diffraction were grown from the slow evaporation of a dichloromethane / *n*-hexane solution.

The asymmetric unit of the obtained structure was shown to contain one formula unit and one Fourier peak, which was not bonded to any other atoms, that refined reasonably as one fully occupied molecule of water, residing in hydrogen bonded pocket. One dimethylcarbamothioate arm shows disorder over two sites, centred on C(41A) and N(40), which refined well as half-occupancied with C(38) and N(40) as common atoms. All crystallographically ordered non-H atoms in the molecule were refined anisotropically and there was no further disorder modelled or restraints applied. The highest residual Fourier peak of 0.53 $e.A^{-3}$ was found close to S(39) of the disordered dimethylcarbamothioate arm, but could not be modelled. All hydrogen atoms were placed in calculated positions and refined using a riding model, with the exception of H(43A) and H(43B) of the water molecule which were found in the Fourier map and their bond distances and angles restrained.

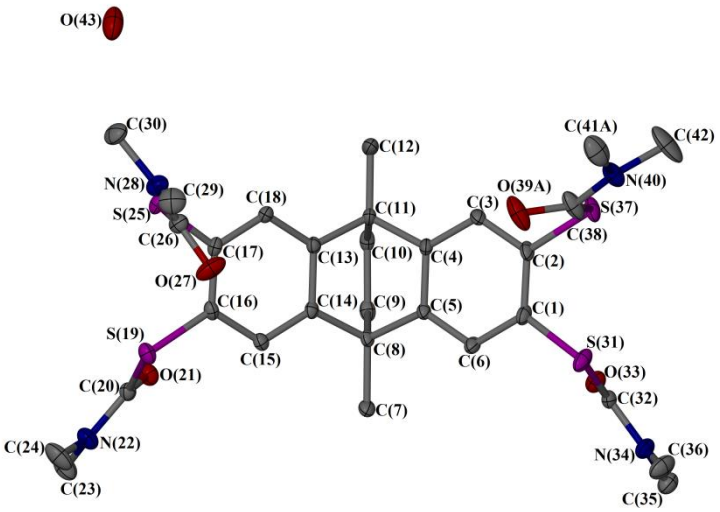

Figure 5.14. View and atom numbering scheme of **[5.12]**•H_2O. Thermal displacement ellipsoids are set at 50% and all hydrogen atoms have been removed for clarity. Only one orientation of the disordered N,N'-dimethylcarbamoylthiol arm is displayed. Colour code: S, purple; O, red; N, blue; C, grey; H, white.

Importantly, as can be seen from **Figure 5.14**, the bent shape of the molecule is retained, implying excellent stability of the 9,10-dimethyl-9,10-dihydroethanoanthracene core at elevated temperatures. There was also an increase in the dihedral angle least squares planes of each substituted dithiocarbamoyl ring of approximately 7°, which translates to a small

increase of approximately 0.1 Å between *ipso* carbon atoms C(4)...C(13) and C(5)...C(14) of the 9,10-dimethyl-9,10-dihydroethanoanthracene core, when compared to structure **5.11**.

Table 5.3. Selected bond distances and angle between least squares planes (θ) of *bis*(dimethylcarbamothioate) rings extracted from the crystal structure of **5.11.**

	C-S [Å]	C=O [Å]	θ
5.12•H_2O	1.7941(18) - 1.7982(17)	1.231(2) - 1.296(5)[a]	128.10(2)

[a] The large variation between values is consequent of the disorder centred on O(39A).

For the synthesis of novel complexes containing the core 2,3,6,7-tetrathiol-9,10-dimethyl-9,10-dihydroethanoanthracene core, **5.12** may be used as a precursor in the presence of a strong base, potassium *tert*-butoxide, for example and appropriate metal salt. For the purposes of characterisation of the neutral ligand though, cleavage of the dimethylcabomyl was attempted *via* hydrolysis using sodium hydroxide (2 equivalents per dimethylthiocarbamothioate moiety) in degassed water at 70 °C, followed by an acid-workup. This failed to offer any conversion however, with the characteristic broad N(CH_3) resonance and carbonyl peak still evident in the ^{1}H and ^{13}C{^{1}H} NMR. Unfortunately, as with the attempted synthesis of thio-ctc, no further work was conducted on the deprotection of **5.13** due to time constraints. Despite this, it is anticipated that cleavage of each dimethylcarbamoyl- moiety would be achievable using either potassium hydroxide in methanol (due to increased solubility of **5.13**) followed by acid workup,[19] or $LiAlH_4$ reduction in THF.[28]

5.3 Summary and Future Work

The synthesis of both thio-ctc and thio-thea could not be completed due to time constraints although it is anticipated that deprotection of both compounds is achievable via previously reported reaction routes.[19] **[22b]** The synthesis of a novel thiolated member of the cyclotriveratrylene family has been completed. Of which, it is the first that has been crystallographically analysed. Additionally, the synthesis of a novel thiolated compound of the 9,10-dihydro-9,10dimethylethanoanthracene core has been completed which may be deprotected in situ, in reactions requiring a *bis*-dithiol ligand. It is anticipated that this ligand will display more intense optical spectra in addition to the interesting redox chemistry seen in complexes of the [thea]$^{n-}$ core seen in chapter 4.

5.4 References

[1] K. Ray, S. G. DeBeer, E. I. Solomon, K. Wieghardt, F. Neese, *Chem. Eur. J.* **2007**, *13*, 2783-2797.

[2] a) B. S. Lim, K.-M. Sung, R. H. Holm, *J. Am. Chem. Soc.* **2000**, *122*, 7410-7411; b) B. S. Lim, R. H. Holm, *J. Am. Chem. Soc.* **2001**, *123*, 1920-1930.

[3] R. Kato, *Chem. Rev.* **2004**, *104*, 5319-5346.

[4] S. Archer, J. A. Weinstein, *Coord. Chem. Rev*, **2012**, *256*, 2530-2561.

[5] T. Lazarides, T. M. McCormick, K. C. Wilson, S. Lee, D. W. McCamant, R. Eisenberg, *J. Am. Chem. Soc.* **2011**, *133*, 350-364.

[6] J. Zhang, P. Du, J. Schneider, P. Jarosz, R. Eisenberg, *J. Am. Chem. Soc.* **2007**, *129*, 7726-7727.

[7] T. Kreickmann, F. E. Hahn, *Chem. Commun.* **2007**, 1111-1120.

[8] a) H. Nishihara, M. Okuno, N. Akimoto, N. Kogawa, K. Aramaki, *J. Chem. Soc.*, *Dalton Trans.* **1998**, 2651-2656; b) R. Sakamoto, T. Kambe, S. Tsukada, K. Takada, K. Hoshiko, Y. Kitagawa, M. Okumura, H. Nishihara, *Inorg. Chem.* **2013**, *52*, 7411-7416.

[9] S. Sproules, F. L. Benedito, E. Bill, T. Weyhermueller, S. DeBeer George, K. Wieghardt, *Inorg. Chem.* **2009**, *48*, 10926.

[10] a) C. Milsmann, E. Bothe, E. Bill, T. Weyhermueller, K. Wieghardt, *Inorg. Chem.* **2009**, *48*, 6211-6221; b) R. Eisenberg, H. B. Gray, *Inorg. Chem.* **2011**, *50*, 9741-9751.

[11] M. A. Little, University of Leeds Thesis **2012.**

[12] a) H. Kwart, E. R. Evans, *J. Org. Chem.* **1966**, *31*, 410-413; b) M. S. Newman, H. A. Karnes, *J. Org. Chem.* **1966**, *31*, 3980-3984.

[13] C. Zonta, O. De Lucchi, R. Volpicelli, L. Cotarca, in *Sulfur-Mediated Rearrangements II, Vol. 275* (Ed.: E. Schaumann), Springer Berlin Heidelberg, **2007**, pp. 131-161.

[14] a) S. Otto, R. L. E. Furlan, J. K. M. Sanders, *Science* **2002**, *297*, 590-593; b) R. Zieba, C. Desroches, F. Chaput, C. Sigala, E. Jeanneau, S. Parola, *Tetrahedron Lett.* **2007**, *48*, 5401-5405.

[15] F. Teplý, I. G. Stará, I. Starý, A. Kollárovič, D. Šaman, Š. Vyskočil, P. Fiedler, *J. Org. Chem.* **2003**, *68*, 5193-5197.

[16] I. Llarena, A. C. Benniston, G. Izzet, D. B. Rewinska, R. W. Harrington, W. Clegg, *Tetrahedron Lett.* **2006**, *47*, 9135-9138.

[17] G. C. Lloyd-Jones, J. D. Moseley, J. S. Renny, *Synthesis* **2008**, *5*, 661-689.

[18] a) M. A. Little, J. Donkin, J. Fisher, M. A. Halcrow, J. Loder, M. J. Hardie, *Angew. Chem., Int. Ed.* **2012**, *51*, 764-766; b) J. Sanseverino, J.-C. Chambron, E. Aubert, E. Espinosa, *J. Org. Chem.* **2011**, *76*, 1914-1917.

[19] M. A. Little, M. A. Halcrow, M. J. Hardie, *Chem. Commun.* **2013**, *49*, 1512-1514.

[20] a) B. M. R. Liénard, N. Selevsek, N. J. Oldham, C. J. Schofield, *ChemMedChem* **2007**, *2*, 175-179; b) A. Mahendran, A. Vuong, D. Aebisher, Y. Gong, R. Bittman, G. Arthur, A. Kawamura, A. Greer, *J. Org. Chem.* **2010**, *75*, 5549-5557.

[21] T. Brotin, V. Roy, J.-P. Dutasta, *J. Org. Chem.* **2005**, *70*, 6187-6195.

[22] a) Z. Duan, Z. Wei, W. Xu, D. Zhu, *Tetrahedron Lett.* **2009**, *50*, 2597-2600; b) H. V. Huynh, C. Schulze-Isfort, W. W. Seidel, T. Lugger, R. Frohlich, O. Kataeva, F. E. Hahn, *Chem. Eur. J.* **2002**, *8*, 1327-1335.

[23] A. Spek, *Acta Cryst., Sect. D* **2009**, *65*, 148-155.

[24] H. Zhang, J. Atwood, *J. Crystallogr. Spectrosc. Res.* **1990**, *20*, 465-470.

[25] M. J. Hardie, *Chem. Soc. Rev.* **2010**, *39*, 516.

[26] a) A. J. Birch, *J. Chem. Soc. Res.* **1944**, 430-436; b) A. J. Birch, *J. Chem. Soc. Res.* **1945**, 809-813; c) A. J. Birch, *J. Chem. Soc. Res.* **1946**, 593-597; d) A. J. Birch, *J. Chem. Soc. Res.* **1947**, 102-105; e) A. J. Birch, *J. Chem. Soc. Res.* **1947**, 1642-1648; f) A. J. Birch, S. M. Mukherji, *J. Chem. Soc. Res.* **1949**, 2531-2536.

[27] B. Masci, M. Nierlich, P. Thuery, *Acta Cryst., Sect. C* **2002**, *58*, o86-o87.

[28] H. Meier, N. Rumpf, *Tetrahedron Lett.* **1998**, *39*, 9639-9642.

Chapter 6

Experimental

6.1 Methods and Instrumentation

6.1.1 NMR Spectroscopy

NMR spectra were recorded on a DPX 300 MHz or Avance 500 MHz (Bruker Corp.) spectrometer using automated procedures. All deuterated solvents were purchased from Euriso-Top and used as received.

6.1.2 Mass Spectrometry

High resolution electrospray (ES) mass spectra were recorded on a MicroTOF mass spectrometer (Bruker Corp.) in either positive or negative ion mode by the University of Leeds mass spectrometry service. Samples were injected directly from feed solutions diluted to 10 μg / cm^3 and acquired over the *m/z* range 50 – 4000. Low resolution electrospray mass spectra were recorded on an open access Micromass LCT (Bruker Corp.) after passing through a short HPLC column. All spectra were recorded using an acetonitrile / water mix as an eluent and sodium formate calibrant.

6.1.3 Elemental Analysis

Elemental composition of samples were determined by Mr. Ian Blakely of the University of Leeds Microanalytical Service.

6.1.4 X-ray Crystallography

Crystals were mounted under Fomblin or Paratone onto a glass fibre, Mitegen tip or nylon loop. In-house diffraction data collected was using a Bruker Nonius X8 Apex diffractometer with ApexII detector, using graphite monochromated Mo-K_α radiation (λ = 0.71073 Å) by FR59 rotating anode generator. Data collected using synchrotron radiation was acquired at Diamond Light Source (λ = 0.6889 Å) using a Rigaku Saturn 724 CCD diffractometer. Crystals were held at 150(1) K or 120(1) K throughout the data capture using an Oxford Cryostream (Oxford Cryosystems) low temperature device. Reflections were measured from a hemisphere of data collected of frames, each covering ω = 0.5° as standard. Datasets were corrected for absorption, Lorentz and polarisation effects by semiempirical methods based upon symmetry-equivalent and multi-scan methods. Structures were solved by direct methods using *SHELXS-97*[1] and refined by full-matrix least squares on F^2 using *SHELXL-97*[1] though *X-Seed*.[2] All hydrogen atoms were refined anisotropically and hydrogen atoms included as invariants at geometrically estimated positions unless otherwise stated. The *ADSYMM* algorithm within *PLATON*[3] was utilised to analyse symmetry of the asymmetric unit and transform where appropriate. Editing and viewing of the crystallographic

information file for experimental and physical parameter data table construction of the crystal structures was performed using *PLATON* and *ENCIFER*. Graphics of the crystal structures outlined in this report were generated using *POV-RAY* and *via X-Seed*.

6.1.5 Infrared Spectroscopy

FTIR spectra were recorded using a Spectrum One spectrophotometer (PerkinElmer) fitted with diffuse reflectance probe with zinc-selenide window. IR Spectra were recorded using a globular light source through KBr beamsplitter for the range 4000-400 cm^{-1} using DLATGS detector with KBr window. Eight scans were recorded for each averaged spectrum with a new background recorded after each sample. IR spectra were analysed using the spectroscopy software package *OPUS* (v 6.5, Bruker Optiks GmbH).

6.1.6 Electrochemical Analysis

Electrochemical analysis was carried out using a PGstat 30 (Metrohm Autolab B.V.) controlled by a PC running software *GPES* (v 4.9, Metrohm Autolab B.V.). The working electrode was a platinum disk, the counter electrode a piece of platinum wire and the reference $Ag^{+}/AgCl$. In all cases, solutions containg 0.1 M $[^{n}Bu_4N]PF_6$ was used as a supporting electrolyte and all peaks referenced to ferrocene as an internal standard.

6.1.7 Electronic Absorbance (UV/vis-NIR) Spectroscopy

UV/vis/NIR spectra were recorded using a Lambda900 spectrophotometer (PerkinElmer) in 1 cm quartz cuvettes. Spectra were recorded over the range 40,000-3,333 cm^{-1} using tungsten-halogen and deuterium lamps where appropriate and R6872 photomultiplier detector for UV/vis radiation and cooled PbS detector for NIR radiation. All data was normalized and tabulated using Origin Pro 8 (OriginLab).

6.1.8 Spectroelectrochemical Analysis

UV/vis/NIR spectroelectrochemical spectra were recorded in collaboration with Dr. Nathan Patmore of The University of Sheffield, using an optically transparent thin layer electrode (OTTLE) cell and Cary 5000 spectrophotometer controlled by a PC running *WinUV Scan 3.0* (Aglient Technologies). The working electrode was a piece of platinum gauze in the path of the beam, and silver wire used as the reference electrode. All data was normalized and tabulated using Origin Pro 8 (OriginLab).

6.1.9 Electron Paramagnetic Resonance

Continuous wave (CW) X-band (9.4 GHz) EPR spectra were recorded either in-house on a Bruker EMX spectrometer (Bruker Biospin GmbH) fitted with a frequency counter or at the EPSRC EPR service centre (Manchester, UK) were recorded in collaboration with Dr. Stephen Sproules and Professor Eric McInnes for X- (9.4 GHz), S- (3.8 GHz) and Q- (34.1

GHz) band spectra. All spectra were recorded and viewed using the WINEPR software package (Bruker Analytische Messtechnik GmbH). Experimental *g* values calculated using the relationship outlined in **Equation 6.1.**

$$g = {}^{h\nu}/_{\beta B} \qquad \textbf{(Equation 6.1)}$$

Where, *g* = Landé *g* factor, *h* = Planck's constant, *v* = frequency of the instrument, β = Bohr magneton and *B* = the experimental position of the absorbance peak.

6.1.10 DFT Computational Procedures

All calculations were performed using a standalone version of *Gaussian03W*[4] with *GaussView* 3.0 graphical interface. All calculations were performed using the B3LYP functional method and SDD basis set (Dresden / Stuttgart pseudopotential on platinum and D95 basis set on all other atoms).[5]

6.2 Experimental Details for Chapter 2

6.2.1 Preparation of Cyclotriveratrylene (ctv, 2.1)

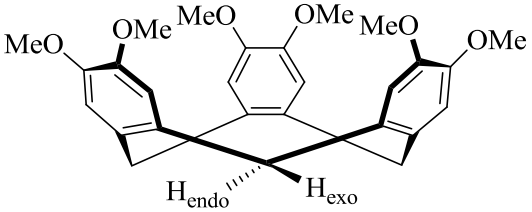

3,4-dimethoxybenzyl alcohol (5.87 g, 34.9 mmol) and a catalytic quantity of phosphoric acid were heated to 70 °C for 16 hours, during which time the mixture solidified. The reaction was then cooled to room temperature and trituated with 100 cm^3 of methanol yielding a white precipitate which was isolated, washed several times with diethyl ether and dried *in vauco* to give cyclotriveratrylene as a white solid. 4.66 g (89%).

^{1}H NMR ($CDCl_3$, 300 MHz): δ = 3.58 (d, 3H, $^2J_{HH}$ = 13.8 Hz, CH_{exo}), 3.82 (s, 18H, OCH_3), 4.80 (d, 3H, $^2J_{HH}$ = 13.8 Hz, CH_{endo},), 6.89 (s, 6H, CH_{Ar}). ^{13}C{^{1}H} NMR ($CDCl_3$, 121 MHz): δ = 148.2, 132.2, 113.6, 56.5, 36.9 ppm. Mass spectrum ES(+) (*m/z*) : 257 (100%, $\{[C_{27}H_{30}O_6].[Na]_2.[H_2O]\}^{2+}$).

Consistent with data previously reported.[6]

6.2.2 Preparation of Cyclotricatechylene[7] (ctc, 2.2)

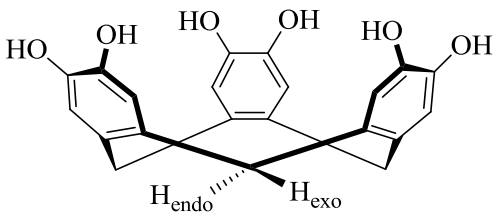

Cyclotriveratrylene (10 g, 22.2 mmol) was dissolved in dry dichloromethane (150 cm^3) and cooled to 0 ^{o}C, prior to the cautious addition of boron tribromide (15.1 cm^3, 157 mmol) over 30 minutes. The reaction mixture was stirred at 0 ^{o}C for 2 hours then slowly heated to reflux for 18 hours. Once cooled, the reaction was poured quickly onto ice and filtered. The crude purple/off white precipitate was recrystallised from ethanol / water to give cyclotricatechylene as a light purple/off white solid. Yield 6.50 g (80%).

^{1}H NMR (Acetone-*d*, 500 MHz): δ = 7.39 (s, br, 6H, O*H*). 6.66 (s, 6H, CH_{Ar}), 4.49 (d, 3H, $^2J_{HH}$ = 15.0 Hz, CH_{endo}), 3.21 ppm (d, 3H, $^2J_{HH}$ = 15.0 Hz, CH_{exo}). ^{13}C{^{1}H} NMR (Acetone-*d*, 121 MHz): δ 144.2, 132.5, 117.4, 36.2 ppm. Mass spectrum (ES+) (*m/z*): 384.1 (100% $\{[C_{21}H_{18}O_6].[H_2O]\}^+$, 750.3 (64% $\{[C_{21}H_{18}O_6]_2[H_2O]\}^+$. Mass spectrum (ES-) (*m/z*): 365.1 (42% $[C_{21}H_{17}O_6]^-$), 411.1 (100% $\{[C_{21}H_{18}O_6][O_2CH]\}^-$).

Consistent with data reported in the literature.[7-8]

6.2.3 Preparation of Cyclotricatechylene (ctc) : Tetracyanoethylene (tcne) Donor : Acceptor Complex (2.3)

Cyclotricatechylene (0.02 g, 0.05 mmol) was dissolved in tetrahydrofuran (3 cm^3) and tetracyanoethylene (0.007 g, 0.05mmol) added. The solution was filtered to remove any undissolved material and pentane slowly diffused into the solution yielding large blue crystals of the donor : acceptor complex $[ctc]_2.[tcne].[THF]_6$.

Mass spectrum (ES+) (*m/z*): 611.3 (13% $\{[C_{21}H_{19}O_6]^+.[Na].[C_4H_8O]_2.[H_2O]_2.[C_2H_3N]\}^+$), 407.2 (19% $\{[C_{21}H_{19}O_6][Na].[H_2O]\}^+$), 317.2 (69% $\{[C_{21}H_{18}O_6][Na]_3[C_4H_8O]_2[H_2O]_3[H]\}^{2+}$), 285.1 (34% $\{[C_{21}H_{18}O_6][Na][C_4H_8O]_2[H_2O]_2[H]\}^{2+}$), 230.8 (16% $\{[C_{21}H_{19}O_6][Na]_2[C_4H_8O]\}^{2+}$), 215.1 (100% $\{[C_{21}H_{18}O_6][Na]_2[H_2O]_2\}^{2+}$), 175.1 (11% $\{[C_{21}H_{18}O_6][Na]_3.[H_2O]_5\}^{3+}$). Mass spectrum (ES-) (*m/z*): 249.0 (39% $\{[C_{21}H_{18}O_6].[Na].[O_2CH]_2.[H_2O]\}^{2-}$, 311.1 (18% $\{[C_{21}H_{18}O_6].[Na]_2[C_6N_4][H_2O][H]\}^-$), 365.1 (13% $\{[C_{21}H_{17}O_6]\}^-$), 411.1 (51% $\{[C_{21}H_{18}O_6][CO_2H]\}^-$), 469.2 (100% $\{[C_{21}H_{18}O_6][Na][O_2CH][H_2O][OH]\}^-$), 495.1 (24% $\{[C_{21}H_{18}O_6][C_6N_4][H]\}^-$), 731.2 (12% $\{[C_{21}H_{18}O_6].[C_{21}H_{17}O_6]\}^-$). Found C 65.45 H 5.50 N 5.05. Calculated for $[C_{21}H_{18}O_6]_2[C_6N_4][C_4H_8O]_3.[H_2O]$; C 65.80, H 5.71, N 5.12. IR (solid state, cm^{-1}) 3335 (s), 2989 (w), 2924 (w), 2879 (w), 2249 (w) TCNE $\nu_{(CN)}$, 2238 (w) tcne $\nu_{(CN)}$, 2220 {tcne}, 1614 (s), 1515 (s), 1480 (m), 1447 (m), 1361 (m), 1235 (s) ctc $\nu_{(CO)Ar}$,

1185 (m), 1130 (m), 1071 (m), 1024 (m), 857 (s), 748 (m). UV/vis selected absorbances ν_{max} [cm^{-1}] (ε_{max} [10^3 $M^{-1}cm^{-1}$]); 15,200 (0.2), 33,000 (4.4), 33,900 (12.47), 38,500 (41.01).

6.2.4 Preparation of Cyclotricatcehylene (ctc) : Tetracyanoquinodimethane (tcnq) Donor : Acceptor Complex (2.4)

Cyclotricatechylene (0.02 g, 0.05 mmol) was dissolved in tetrahydrofuran (3 cm^3) and tetracyanoquinodimethane (0.010 g, 0.05 mmol) added. The solution was filtered to remove any undissolved material and pentane was slowly diffused into the solution at room temperature yielding large green crystals of the donor : acceptor complex $[ctc]_2.[tcnq].[THF]_4$.

Mass spectrum (ES+) (*m/z*): 175.1 (6% $\{[C_{21}H_{18}O_6].[Na]_3.[H_2O]_5\}^{3+}$), 215.1 (100% $\{[C_{21}H_{19}O_6].[Na]_2.[H_2O]\}^{2+}$), 230.8 (14% $\{[C_{21}H_{19}O_6].[Na]_2.[C_4H_8O]\}^{2+}$), 285.2 (10% $\{[C_{21}H_{18}O_6].[Na].[THF]_2.\ [H_2O]_2.[H]\}^{2+}$), 317.2 (69% $\{[C_{21}H_{18}O_6].\ [Na]_3.[C_4H_8O]_2.[H_2O]_3.[H]\}^{2+}$), 407.2 (19% $\{[C_{21}H_{19}O_6].\ [Na].[H_2O]\}^{+}$), 611.3(13% $\{[C_{21}H_{19}O_6].[Na].\ [THF]_2.[H_2O]_2.[MeCN]\}^{+}$). Mass spectrum (ES-) (*m/z*): 195.0 (96% $\{[C_{11}H_4N_3].[OH]\}^{-}$), 204.0 (100% $\{[C_{12}H_4N_4]\}^{-}$). Found: C 67.60, H 5.85, N 4.80. Calculated for $(C_{21}\ H_{18}\ O_6)_2(C_{12}\ H_4\ N_4)(C_4H_8O)_3.(H_2O)$; C 67.70, H 5.68, N 4.26. IR (solid state, cm^{-1}) : 3413 (vs), 3047 (w), 2219 (m) TCNQ ν(CN), 1605 (m), 1544 (w), 1518 (s), 1478 (w), 1445 (s), 1357 (m), 1282 (vs) $\nu(CO)_{Ar}$, 1173 (m), 1132 (m), 1070 (w), 1044 (w), 858 (m), 746 (m). UV/vis selected absorbances : ν_{max} [cm^{-1}] (ε_{max} [10^3 $M^{-1}cm^{-1}$]); 13,800 (0.007); 20,400 (5.2), 25,000 (31.4), 34,500 (26.75).

6.2.5 Preparation of Cyclotricatcehylene (ctc): Dimethylsulfoxide (dmso) Crystalline Clathrate (2.5)

Cyclotricatechylene (0.02 g, 0.05 mmol) was dissolved in dimethylsulfoxide (3 cm^3) and tetracyanoethylene added (0.010 g, 0.05 mmol) added. The solution was filtered to remove any undissolved material and ethyl acetate slowly diffused into the solution at room temperature yielding large orange crystals of the solvated clathrate $[ctc].[dmso]_5$ only.

6.2.6 Preparation of Cyclotricatcehylene (ctc): Dimethylacetamide (dmac) Crystalline Clathrate (2.6)

Cyclotricatechylene (0.02 g, 0.05 mmol) was dissolved in dimethylacetamide (3 cm^3) and tetracyanoethylene (0.010 g, 0.05 mmol) added. The solution was filtered to remove any undissolved material and diethylether slowly diffused into the solution at room temperature yielding large yellow crystals of the solvated clathrate $[ctc].[dmac]_3$ only.

6.2.7 Preparation of Cyclotricatcehylene (ctc) : Tetrahydrofuran (THF) Crystalline Clathrate (2.7)

Cyclotricatechylene (0.02 g, 0.05 mmol) was dissolved in tetrahydrofuran (3 cm^3) and tetracyanoethylene (0.010 g, 0.05 mmol) added. The solution was filtered to remove any undissolved material and pentane slowly diffused into the solution at room temperature yielding yellow crystals of the solvated clathrate [ctc].$[THF]_{3.5}$.$[H_2O]_{0.5}$ mixed with large blue crystals of the donor : acceptor complex $[ctc]_2$.[tcne].$[THF]_6$.

6.2.8 Preparation of Cyclotriveratrylene (ctv) : Tetracyanoethylene (tcne) Donor : Acceptor Complex (2.8)

Cyclotriveratrylene (0.02 g, 0.04 mmol) was dissolved in THF (3 cm^3) and tetracyanoethylene (0.01 g, 0.08 mmol) added. The solution was filtered to remove any undissolved material and pentane slowly diffused into the solution yielding very small blue needles of the donor : acceptor complex $[ctv]_2$.$[tcne]_3$.

Mass spectrum (ES+) (*m/z*): 809.5 (31% $\{[C_{27}H_{30}O_6][H][C_4H_8O]_3[C_2H_3N]_3\}^+$), 667.4 (21% $\{[C_{27}H_{30}O_6][H][C_4H_8O]_3\}^+$), 551.2 (5% $\{[C_{27}H_{30}O_6][H][C_2H_3N]_2[H_2O]\}^+$), 487.3 (100% $\{[C_{27}H_{30}O_6][H_2O]_2[H]\}^+$), 345.2 (91% $\{[C_6N_4][H][C_4H_8O]_3\}^+$), 201.1 ($\{[C_6N_4][H][C_4H_8O]\}^+$), 165.1 ($\{[C_6N_4][H][H_2O]_2\}^+$). Mass spectrum (ES-) (*m/z*): 420.1 (20% $\{[C_6N_4]_3[H_2O]\}^-$), 289.2 (15% $\{[C_{27}H_{30}O_6].C_6N_4\}^{2-}$). Found C 67.40, H 4.75, N 12.85%. Calculated for $[C_{27}H_{30}O_6]_2[C_6N_4]_3$ (1285.35); C 67.28, H 4.71, N 13.08%. IR (solid state, cm^{-1}): 2994 (m), 2956 (s), 2923 (s), 2835 (m), 2247 (m) TCNE $\nu_{(CN)}$, 2219 (w) TCNE, 1602 (m), 1574 (m), 1514 (s), 1489 (m), 1467 (s), 1445 (s), 1393 (m), 1341 (m), 1333 (m), 1259 (s), 1223 (s), 1190 (s), 1149 (s), 1083 (s), 1031 (m), 987 (m), 954 (m), 943 (w), 847 (m), 814 (w), 801 (w), 773 (w), 732 (s), 663 (m), 617 (s), 570 (s), 532 (m). UV/vis selected absorbances ν_{max} [cm^{-1}] (ε_{max} [10^3 $M^{-1}cm^{-1}$]); 15,200 (0.2), 33,000 (4.4), 33,900 (12.47), 38,500 (41.01).

6.3 Experimental Details for Chapter 3

6.3.1 Preparation of [(dppb)$PtCl_2$] (3.A)

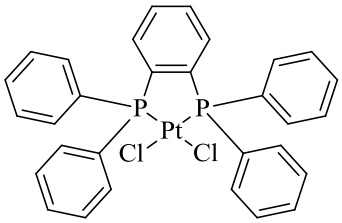

Diphenylphosphinobenzene (0.25 g, 0.61 mmol) was dissolved in chloroform (20 cm^3) and added dropwise to a solution of [$(dmso)_2PtCl_2$] (0.194 g, 0.46 mmol) in chloroform (15 cm^3), and the mixture stirred overnight. The resulting white precipitate was isolated under vacuum, washed with chloroform and dried *in vacuo* to give the product as a bright white solid. Yield 0.291 g (89%).

^{1}H NMR (DMSO-d_6, 300 MHz) : δ = 7.75 (m, 8H, dppb phenyl C$H^{2,6}$), 7.63 (m, 4H, dppb benzyl CH_{Ar}), 7.58 ppm (m, 12H, dppb phenyl C$H^{3,4,5}$). ^{31}P{^{1}H} NMR (DMSO-d_6, 121 MHz) : δ = 40.8 (Pt-P satellites δ = 55.6, 26.0 $J_{Pt\text{-}P}$ = 3577 Hz). Mass spectrum (ES-) (*m/z*): 735.0 (10% {[$C_{30}H_{24}Cl_2P_2Pt$].[Na]}$^+$), 677.1 (100% {[$C_{30}H_{24}ClP_2Pt$]}$^+$). Found C 50.55, H 3.30, Cl 10.15%. Calculated for $C_{30}H_{24}Cl_2P_2Pt$, C 50.57, H 3.40, Cl 9.95%. IR (solid state, cm^{-1}): 3075 (m) ν(C-H_{Ar}), 3059 (m) ν(C-H_{Ar}), 1585 (m), 1562 (m), 1483 (s), 1453 (s), 1434 (s), 1395 (w), 1332 (w), 1309 (s), 1256 (m), 1187 (s), 1161 (m), 1151 (s), 1102 (s), 1069 (w), 1029 (m), 993 (s), 973 (w), 773 (m), 780 (s), 746 (s), 736 (s), 717 (s), 697 (s), 674 (s), 625 (m), 575 (s), 546 (s), 509 (s), 496 (s) 470 (s).
Consistent with data previously reported.[9]

6.3.2 Preparation of [{(dppb)Pt}$_3$(ctc)] (3.2)

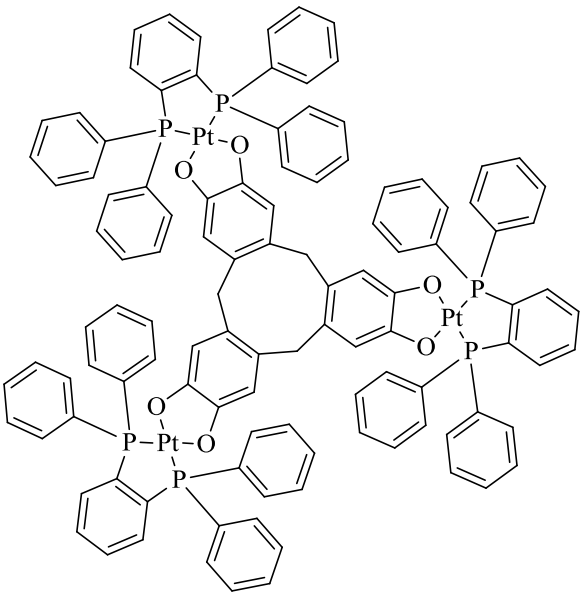

Cyclotricatechylene (0.040 g, 0.110 mmol) and [(dppb)$PtCl_2$] (0.250 g, 0.351 mmol) were added to deoxygenated dimethylacetamide (25 cm^3) and stirred for 30 minutes prior to the addition of potassium carbonate (0.096 g, 0.702 mmol) suspended in dry, deoxygenated methanol (10 cm^3) This mixture was heated to 50 ^{o}C for 18 hours during which time a colour change to deep orange was noted. Once cooled, an excess of dry, deoxygenated diethyl ether was added to precipitate the crude, orange product. The precipitate was isolated under an inert atmosphere of nitrogen and recrystallised from dry, deoxygenated dichloromethane / acetone yielding the product as an orange solid. Yield 0.141 g (56%).

^{1}H NMR (5 : 1 $CDCl_3$: MeOD, 300 MHz): δ = 7.66 - 7.31 (m, 72H, dppb CH_{Ar}), 6.59 (s, 6H, CH_{Ar}), 4.50 (d, $^{2}J_{HH}$ = 13.2 Hz, 3H, CH_{endo}), 3.22 ppm (partially obscured by solvent resonance, CH_{exo}). ^{31}P{^{1}H} NMR (5 : 1 $CDCl_3$: MeOD, 121 MHz): δ = 31.2, Pt satellites δ = 45.4, 17.1 ppm (J_{Pt-P} = 3492 Hz). Mass spectrum (ES+) (*m/z*): 2284.4 (9% $\{[C_{111}H_{84}O_6P_6Pt_3][H]\}^+$), 1645.3 (22% $\{[C_{81}H_{62}O_6P_4Pt_2][H]\}^+$), 1143.2 (17% $\{[C_{51}H_{40}O_6P_2Pt]_2[H]_2\}^{2+}$, 1006.2 (7% $\{[C_{51}H_{40}O_6P_2Pt][H]\}^+$), 677.1 (100% $\{[C_{30}H_{24}P_2PtCl][H]\}^+$). Found C 59.20, H 5.00%. Calculated for $C_{111}H_{84}O_6P_6Pt_3$ (2284.97): C 58.35, H 3.71%. IR (solid state, cm^{-1}) 3061 (w), 3049 (m), 2994 (m), 2961 (m), 2924 (m), 2907 (m), 2853 (m), 1653 (s), 1617 (s), 1587 (m), 1559 (m), 1480 (s), 1452 (m), 1435 (s), 1378 (w), 1334 (w), 1264 (s) *ν*(C-O), 1167 (m), 1100 (s), 1052 (m), 1026 (m), 999 (m), 933 (w), 859 (m), 802 (m), 746 (m), 692 (s), 643 (s), 618 (w), 573 (vs), 538 (vs), 508 (vs), 459 (s).

Consistent with data previously reported.[10]

6.3.3 Preparation of [{(dppb)Pt}$_3$(ctc)]PF_6 (3.2[PF_6])

Under an inert atmosphere, ferrocenium hexafluorophosphate (1.4 mg, 4.4 μmol) was added to [{(dppb)Pt}$_3$(CTC)] (10 mg, 4.4 μmol) dissolved in dry, deoxygenated dichloromethane at -78 ^{o}C. The mixture was stirred for 30 minutes and used without further purification.

6.3.4 Preparation of [(^{t}Bu$_2$Bipy)$PdCl_2$][11] (3.B)

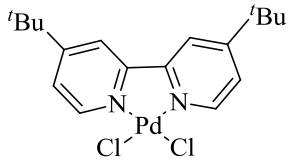

[$(PhCN)_2PdCl_2$] (0.500 g, 1.30 mmol) was dissolved in acetone (25 cm^3) and 4,4'-di-*tert*-butyl-2,2'-bipyridine (0.350 g, 1.30 mmol), also dissolved in acetone (20 cm^3) added dropwise . The mixture was stirred for 18 hours and filtered yielding the product as a golden microcrystalline solid. The product may be further purified by recrystallisation in chloroform if required. Yield : 0.525 g (91%).

^{1}H NMR ($CDCl_3$, 500 MHz): δ = 9.09 (d, 2H, $^{3}J_{HH}$ = 6.0 Hz, C$H^{6,6'}$), 7.86 (s, 2H, C$H^{3,3'}$), 7.64 (d, 2H, $^{3}J_{HH}$ = 6.0 Hz, C$H^{5,5'}$), 1.39 ppm (s, 18H, CH_3). ^{13}C{^{1}H} NMR ($CDCl_3$, 75 MHz) :δ = 156.5, 150.9, 134.0, 124.3, 119.6, 36.2. 30.7 ppm. Mass spectrum (ES+) (*m/z*): 855.1 (100% $\{[C_{18}H_{24}N_2PdCl_2].[C_{18}H_{23}N_2PdCl]\}^+$). IR (solid state, cm^{-1}) 3109 (m), 3053 (m), 1602 (s), 1563 (s), 1500 (s), 1467 (s), 1446 (s), 1425 (s), 1163 (s), 1109 (w), 1038 (m), 1024 (m), 758 (vs), 659 (m), 648 (m), 410 (s).

Consistent with data previously reported.[12]

6.3.5 Preparation of [{(^{t}Bu$_2$Bipy)Pd}$_3$(ctc)] (3.3)

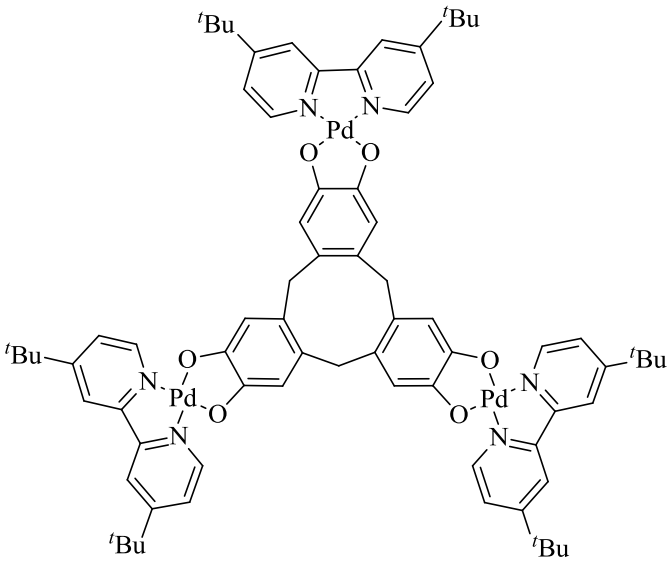

Cyclotricatechylene (0.052 g, 0.141 mmol) and [(^{t}Bu$_2$Bipy)PdCl$_2$] (0.105 g, 0.448 mmol) were added to deoxygenated dimethylacetamide (25 cm^3) and stirred for 30 minutes prior to the addition of potassium carbonate (0.090 g, 0.65 mmol) suspended in dry, deoxygenated methanol (10 cm^3). This mixture was stirred at room temperature for 18 hours during which time a colour change to deep purple was noted. Excess dry, deoxygenated diethyl ether / hexane (1 : 1) was added to precipitate the crude, purple product. The precipitate was isolated under an inert atmosphere of nitrogen and recrystallised from deoxygenated chloroform at -20 °C yielding the product as a deep purple solid. Yield: 0.072 g (73%)

^{1}H NMR (5 : 1 $CDCl_3$: MeOD, 500 MHz): δ = 8.53 (d, 6H, ^3J = 5.0 Hz, bipy H$^{6,6'}$) , 7.86 (s, 6H, bipy H$^{3,3'}$), 7.51 (d, 6H, ^{3}J = 5.0 Hz, bipy H$^{5,5'}$) , 6.61 (s, 6H, CH_{Ar}), 4.52 (d, 3H, ^2J = 15.0 Hz, CH_{endo}), 3.35 (partially obscured by solvent resonance, CH_{exo}) 1.36 ppm (s, 54H, CH_3). Mass spectrum (ES+) (*m/z*): 1485.4 (15% $\{[C_{75}H_{84}N_6O_6Pd_3]_2[H]_2\}^{2+}$), (4% 1298.3 $\{[C_{75}H_{84}N_6O_6Pd_3].[C_{57}H_{62}N_4O_6Pd_2].[H]\}^{2+}$), 1112.3 (9% $\{[C_{57}H_{62}N_4O_6Pd_2].[H]\}^{+}$), 930.2 (50% $\{[C_{75}H_{84}N_6O_6Pd_3].[C_{18}H_{24}N_2Pd].[H]\}^{+}$, 743.2 (13% $\{[C_{39}H_{40}N_2O_6Pd]_2.[H_2O]\}^{2+}$), 269.2 (100% $\{[C_{18}H_{24}N_2][H]\}^{+}$). Found C 54.00 H 5.50, N 4.95%. Calculated for $[C_{75}\ H_{84}\ N_6\ O_6\ Pd_3].[CHCl_3]_2$: C 53.66, H 5.03, N 4.88%. IR (solid state, cm^{-1}): 3120 (w), 2984 (m), 2961 (m), 2904 (m), 2852 (m), 1615 (vs), 1482 (vs), 1416 (m), 1263 (vs) *ν*(C-O), 1169 (s), 1133 (m), 1076 (w), 1055 (m), 852 (s), 648 (m), 614 (m), 428 (w).

6.3.6 Preparation of [(dppe)PtCl$_2$][13] (3.C)

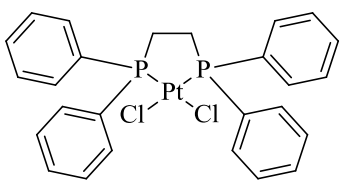

Diphenylphosphinoethane (0.396 g, 0.995 mmol) dissolved in dichloromethane (10 cm^3), was added dropwise to [(dmso)PtCl$_2$] (0.400 g, 0.947 mmol), also dissolved in dichloromethane (10 cm^3). The mixture was heated to 40 ^{o}C for 18 hours and the precipitate which had formed was isolated, washed with cold chloroform (2 × 15 cm^3) and dried *in vacuo*. Yield 0.410 (73%).

^{1}H NMR (DMSO-d_6, 121 MHz) : 7.95-7.77 (m 8H, C$H^{2,6}$), 7.66-7.49 (m, 12H, C$H^{3,4,5}$), 2.68-2.56 ppm (m, 2H, CH_2). ^{31}P{^{1}H} NMR (DMSO-d_6, 121 MHz) : δ = 42.5 (Pt-P satellites δ = 57.4, 27.7 J_{Pt-P} = 3593 Hz). Mass spectrum (ES+) *m/z*: 495.6 {10% {$[(C_{24}H_{26}P_2)_2Pt]\}^{2+}$}. IR (solid state) 3054 (m), 3044 (m), 2987 (m), 2961 (m), 1652 (s), 1617 (s), 1588 (m), 1552 (m), 1480 (s), 1452 (m), 1435 (s), 1378 (w), 1334 (w), 1264 (s) ν(C-O), 1167 (m), 1100 (s), 1052 (m), 1026 (m), 999 (m), 933 (w), 859 (m), 802 (m), 746 (m), 692 (s), 643 (s), 618 (w), 573 (vs), 538 (vs), 508 (vs), 459 (s).

Consistent with data previously reported.[13]

6.3.7 Preparation of [{(dppe)Pt}$_3$(ctc)] (3.4)

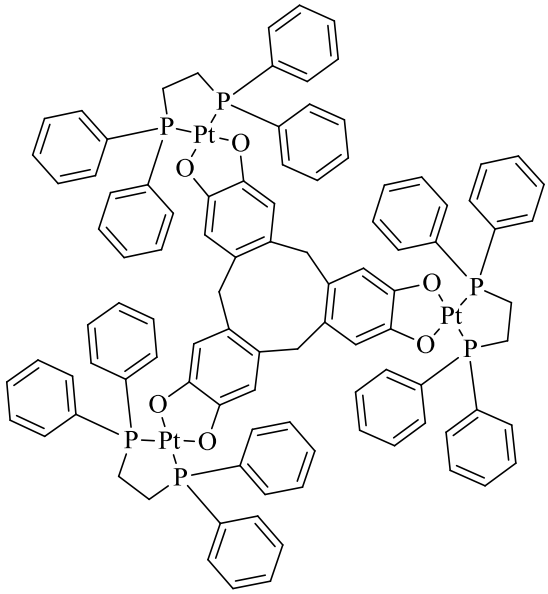

Cyclotricatechylene (0.037 g, 0.101 mmol) and [(dppe)$PtCl_2$] (0.243 g, 0.366 mmol) were dissolved in deoxygenated dimethylacetamide (25 cm^3) and stirred for 30 minutes prior to the addition of potassium carbonate (0.102 g, 0.732 mmol) suspended in dry, deoxygenated methanol (10 cm^3). This mixture was left to stir at 70 ^{o}C for 18 hours during which time a colour change to deep yellow was noted. Once cooled, excess dry, deoxygenated diethyl ether was added to precipitate the crude, yellow product. The precipitate was isolated under an inert atmosphere of nitrogen and recrystallised from dry, deoxygenated dichloromethane / acetone yielding the product as a deep yellow powder. Yield 0.035 g (16%).

^{1}H NMR (DMSO-d_6, 500MHz): δ = 8.16-7.99 (m, 24 H), 7.58-7.40 (m, 36 H), 6.53 (s, 6H, CH_{Ar}), 4.54 ppm (d, $^{2}J_{HH}$ = 12.6 Hz, 1H, CH_{endo}). ^{31}P{^{1}H} NMR (DMSO-d_6 ,121 MHz) δ = 30.8, Pt satellites δ = 44.6, 16.9 ppm (J_{Pt-P} = 3344 Hz). Mass spectrum ES(+) *m/z*: 2179.4 (100% $\{[C_{99}H_{84}O_6P_6Pt_3][K]\}^{+}$, 2163.4 (22% $\{[C_{99}H_{84}O_6P_6Pt_3][Na]\}^{+}$), 1148.2 (27% $\{[C_{99}H_{84}O_6P_6Pt_3]_2.[C_2H_6SO]_2\}^{2+}$), 1140.2 (33% $\{[C_{99}H_{84}O_6P_6Pt_3]_2.[Na][K][C_2H_6SO]\}^{2+}$), 1109.1 (38% $\{[C_{99}H_{84}O_6P_6Pt_3]_2.[C_2H_6SO]\}^{2+}$), 1101.2 (28% $\{[C_{99}H_{84}O_6P_6Pt_3]_2.[Na][K]\}^{2+}$), 1093.2 (13% $\{[C_{99}H_{84}O_6P_6Pt_3]_2.[Na]_2\}^{2+}$), 706.1 (31% $\{[C_{26}H_{24}P_2PtCl][C_2H_6SO]\}^{+}$), 629.1 (56% $\{[C_{26}H_{24}P_2PtCl]\}^{+}$). Found C 53.20 H 4.00%. Calculated for $[C_{99}H_{84}O_6P_6Pt_3]\bullet[H_2O]_2\bullet[CH_2Cl_2]$ (2261.80): C 53.10, H 4.01%. IR (solid state, cm^{-1}) 3450 (br. s) ν(O-H), 3061 (m), 3049 (m), 2994 (m), 2961 (m), 2924 (m), 2907 (m), 2853 (m), 1653 (s), 1617 (s), 1587 (m), 1559 (m), 1480 (s), 1452 (s), 1435 (m), 1378 (w), 1334 (w),

1306 (w), 1264 (s) ν(C-O), 1167 (m), 1100 (m), 1052 (m), 1026 (m), 999 (m), 933 (w), 859 (m), 802 (m), 746 (s), 692 (s), 643 (m), 618 (w), 605 (w), 573 (s), 538 (s), 508 (s), 459 (s).

6.3.8 Preparation of [{(dppe)Pt}$_3$(ctc)]PF_6 ([3.4]PF_6)

Under an inert atmosphere, ferrocenium hexafluorophosphate (1.5 mg, 4.6 μmol) was added to [{(dppe)Pt}$_3$(ctc)] (10 mg, 4.7 μmol) dissolved in dry, deoxygenated dichloromethane at -78 ^oC. The mixture was stirred for 30 minutes and used without further purification.

6.3.9 Preparation of [(^{t}Bu$_2$Bipy)$PtCl_2$] (3D)

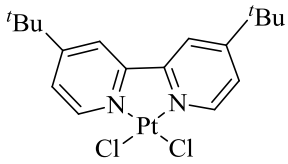

Platinum(II) dichloride (1.00 g, 3.76 mmol) was dissolved in hot methanol (250 cm3) and filtered to remove any insoluble impurities. To the hot filtrate, *bis*-4,4'-di-tert-butyl-2,2'-bipyridine (1.01 g, 3.76 mmol) was added and the reaction stirred for 18 hours at 70 °C. The resulting golden precipitate was isolated under vacuum, washed with cold methanol (3 × 10 cm^3) and recrystallised from chloroform. Yield : 1.81 g (91%). ^{1}H NMR ($CDCl_3$, 500 MHz): δ = 9.49 (d, $^3J_{HH}$ = 6.2 Hz, 2H, $H^{6,6'}$), 7.90 (d, $^4J_{HH}$ = 2.0 Hz, 2H, $H^{3,3'}$), 7.50 ppm (dd, $^3J_{HH}$ = 6.2, $^4J_{HH}$ = 2.0 Hz, 2 H, $H^{5,5'}$),1.47 ppm (s, 18H, CH_3). Mass spectrum (ES+) (*m/z*): 552.1 (100% {[$C_{18}H_{24}Cl_2N_2Pt$][H_2O]}$^+$). Found C 39.65; H 4.45; N 5.05; Cl 13.65%. Calculated for [$C_{18}H_{24}Cl_2N_2Pt$] (534.39); C 40.46; H 4.53; N 5.24, Cl 13.27%. IR (solid state, cm^{-1}): 3125 (w) 3046 (w), 2976 (s), 2873 (m), 1614 (s), 1540 (m), 1485 (s), 1471 (s), 1419 (s), 1250 (m), 1158 (m), 1121 (m), 1045 (s), 851, (s), 737 (m), 599 (s), 472 (s), 418 (s).

6.3.10 Preparation of [{(^{t}Bu$_2$Bipy)Pt}$_3$(ctc)] (3.5)

Cyclotricatechylene (0.023 g, 0.063 mmol)) and [(^{t}Bu$_2$Bipy)$PtCl_2$] (0.12 g, 0.22 mmol) were added to deoxygenated dimethylacetamide (15 cm^3) and stirred for 30 minutes prior to the addition of potassium carbonate (0.090 g, 0.65 mmol) suspended in dry, deoxygenated methanol (10 cm^3) This mixture was heated to 40 ^oC for 18 hours during which time a colour change to blue was noted. Once cooled, the solution was diluted with dry,

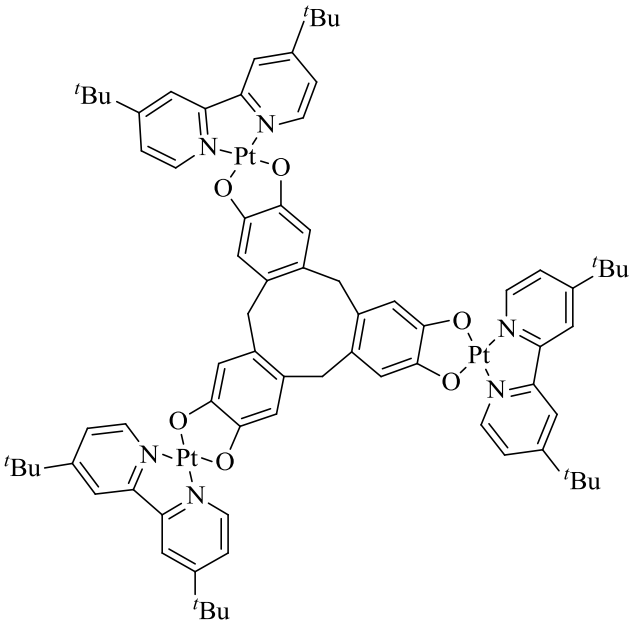

deoxygenated diethyl ether / pentane (1 : 1) and the deep blue precipitate isolated. The product may be purified by either recrystallisaion from dichloromethane / acetone at -20°C or column chromatography (silica, 98.5% CH_2Cl_2 : 1.5% MeOH) to yield the product as a deep blue powder. Yield 0.011g, 28%.

^{1}H NMR (5 : 1 $CDCl_3$: CD_3OD, 500 MHz) δ = 8.92 (d, $^3J_{HH}$ = 6.4 Hz, 6H, C$H^{6,6'}$), 7.99 (d, $^4J_{HH}$ = 1.9 Hz, 6H, C$H^{3,3'}$), 7.50 (dd, $3J_{HH}$ = 6.4, $^4J_{HH}$ = 1.9 Hz, 6H, C$H^{5,5'}$), 6.82 (s, 6H, CH_{Ar}), 4.66 (d, $^2J_{HH}$ =14.0 Hz, 3H, CH_{endo}), 3.45 (d, $^2J_{HH}$ = 14.0 Hz, 3H, CH_{exo}), 1.43 ppm (s, 54 H, CH_3). ^{13}C{^{1}H} NMR (5 : 1 $CDCl_3$: CD_3OD, 500 MHz): δ = 163.5, 156.1, 148.9, 124.2, 119.9, 38.0, 35.9, 35.1, 20.4. Mass spectrum ES+ (*m/z*): 1789.5 (29% $\{[C_{75}H_{84}N_6O_6Pt_3]_2[K]_2\}^{2+}$), 1772.5 (29% $\{[C_{75}H_{84}N_6O_6Pt_3]_2[Na]_2\}^{2+}$), 1762.5 (18% $\{[C_{75}H_{84}N_6O_6Pt_3]_2[H][Na]\}^{2+}$) 1751.5 (33% $\{[C_{75}H_{84}N_6O_6Pt_3]_2[H]_2\}^{2+}$), 1541.5 (11% $\{[C_{57}H_{62}N_4O_6Pt_2][C_{75}H_{84}N_6O_6Pt_3][C_2H_3N][H]_2\}^{2+}$) 1288.4 (10% $\{[C_{57}H_{62}N_4O_6Pt_2]\}^{+}$), 1167.4 (45% $\{[C_{75}H_{84}N_6O_6Pt_3]_3[H]_3\}^{3+}$), 875.8 (48% $\{[C_{75}H_{84}N_6O_6Pt_3]\}^{2+}$), 584.2 (100% $\{[C_{75}H_{84}N_6O_6Pt_3]_3[H]_3\}^{3+}$), 269.2 (52% $\{[C_{18}H_{24}N_2][H]\}^{+}$). Found C 50.05 H 5.15, N 4.30%. Calculated for $[C_{75}H_{84}O_6N_6Pt_3]\bullet[H_2O]\bullet[CH_2Cl_2]\bullet[C_3H_6O]$ (1893.79) : C 50.10, H 4.90, N 4.44%. IR (solid state, cm^{-1}): 2960 (m), 2906 (m), 2853 (s), 1621 (vs), 1484 (s), 1416 (m), 1266 (vs) *ν*(C-O), 1171 (s), 1132 (m), 1078 (w), 831 (s), 664 (m), 629 (m), 457 (w).

6.3.11 Preparation of [{(^{t}Bu$_2$Bipy)Pt}$_3$(ctc)]PF$_6$ ([3.5]PF$_6$)

Ferrocenium hexafluorophosphate (1.9 mg, 5.7 μmol) was added to [{(^{t}Bu$_2$Bipy)Pt}$_3$(ctc)] (10 mg, 5.7 μmol) dissolved in dry, deoxygenated dichloromethane (2 cm^3) at -78 °C, under an inert atmosphere. The mixture was stirred for 30 minutes and used immediately.

6.3.11 Preparation of [(^{t}Bu$_2$bipy)CuCl$_2$][14] (3E)

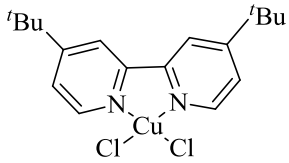

Copper(II) dichloride dihydrate (0.32 g, 1.86 mmol) was dissolved in warm ethanol (100 cm^3). To this solution, *bis*-4,4'-di-tert-butyl-2,2'-bipyridine (0.50 g, 1.86 mmol) was added and the reaction stirred for 60 mins at 40 °C. The resulting green/blue precipitate was isolated, washed with ethanol (3 × 10 cm^3) and dried *in vacuo*. Yield: 0.69 g (92%).

Mass spectrum (ES+) (*m/z*): 443.9 (100% $\{[C_{18}H_{24}N_2Cl_2Cu].[H_2O].[Na]\}^{+}$). Found C 53.55, H 6.00, N 6.90%. Calculated for $C_{18}H_{24}Cl_2N_2Cu$; C 53.67, H 6.00, N 6.95. IR (solid state, cm^{-1}) 3120 (w), 3057 (w), 2973 (s), 2912 (m), 2873 (w), 1615 (s), 1546 (m), 1484 (s), 1466 (s), 1410 (m), 1250 (w), 1201 (m), 1121 (w), 1029 (s), 852 (vs), 744 (m), 603 (vs), 428 (Cu-Cl).

Consistent with data previously reported.[14]

6.3.12 Preparation of [{(^{t}Bu$_2$Bipy)Cu}$_3$(ctc)] (3.6)

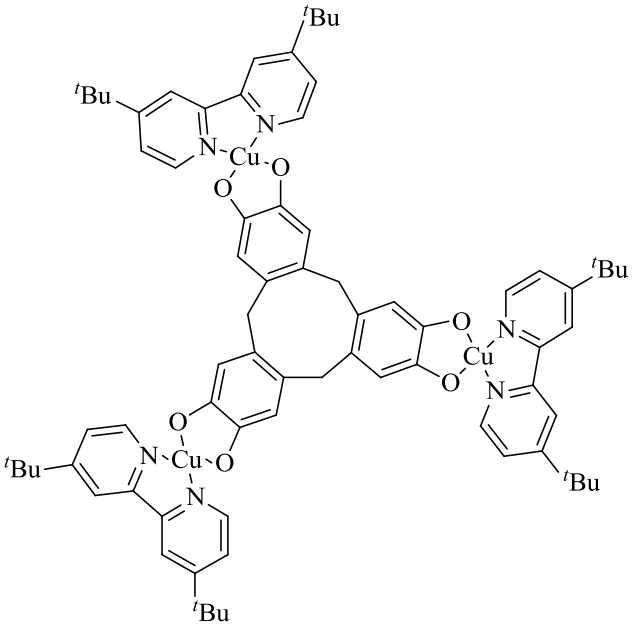

Cyclotricatechylene (0.054 g, 0.14 mmol and [(^{t}Bu$_2$Bipy)CuCl$_2$] (0.17 g, 0.44 mmol) were added to deoxygenated dimethylacetamide (10 cm^3) and stirred for 30 minutes prior to the addition potassium carbonate (0.12 g, 0.87 mmol) suspended in deoxygeneated methanol (10 cm^3), prompting an immediate colour change to deep green. The mixture was stirred at room temperature for a further 6 hours, then diluted with dry, deoxygenated diethyl ether / hexane (1 : 1) and the deep green precipitate isolated. The product was recrystallised in chloroform / diethyl ether at 5 °C yielding the product as a deep green powder. Yield 0.160 g (85%)

Mass Spectrum (ES+) (*m/z*): 868.1 (5% {[($C_{18}H_{24}N_2$)$_2$Cu][CuCN]$_4$}$^+$), 779.2 (21% {[($C_{18}H_{24}N_2$)$_2$Cu][CuCN]$_3$}$^+$), 688.2 (50% {[($C_{18}H_{24}N_2$)$_2$Cu][CuCN]}$^+$) 599.3 (86% {[($C_{18}H_{24}N_2$)$_2$Cu]}$^+$), 521.2 (7% {[$C_{21}H_{16}O_6$Cu][CN]$_2$[H][C_2H_3N]}$^+$), 390.1 (64% {[$C_{21}H_{18}O_6$].[Na]}$^+$, 366.1 (21% {[$C_{21}H_{18}O_6$]}$^+$), 359.1 (100% {[$C_{18}H_{24}N_2$Cu][H][HCN]}$^+$, 269.2 (33% {[$C_{18}H_{24}N_2$].H}$^+$). Found C 52.10, H 5.00, N 4.30%. Calculated for $C_{75}H_{84}N_6O_6Cu_3$ [CH_2Cl_2]$_5$: C 52.14, H 5.19 N 4.50%. IR (solid state, cm^{-1}) : 3069 (s), 2965 (w), 2926 (w), 2906 (w), 2872 (w) 1615 (m), 1481 (s), 1411 (w), 1251 (s), 1077 (w), 1032 (m), 849 (s), 605 (m), 511 (m). EPR (X-band, 150 K, CH_2Cl_2 frozen glass): $g_\parallel$ = 2.29, $g_\perp$ = 2.08 (ΔM_s = 2, $g_\perp$ = 4.16). $A_\parallel$ = 14.5 x 10^{-4} cm^{-1}.

6.3.13 Preparation of [{(dppe)Pt(DBCat)}][15] (3.7)

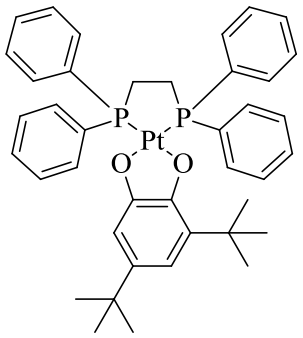

3,5-Di-*tert*-butyl catechol (0.049 g, 0.221 mmol) and potassium-*tert*-butoxide (0.051 g, 0.455 mmol) were dissolved in dry, deoxygenated methanol (15 cm^3) until complete dissolution of the reagents. To this, [(dppe) $PtCl_2$] (0.153 g, 0.230 mmol) was added and the mixture heated to 50 ^oC for 2 hours during which time the solution had darkened to deep orange with a yellow crystalline precipitate. The reaction was cooled, diluted with pentane (25 cm^3) and the crude precipitate recrystallised from dichloromethane at -20 ^oC yielding the product as a yellow crystalline solid. Yield 0.074. g, 41%.

^1H NMR ($CDCl_3$, 300 MHz): δ = 8.08 (m, 8H, dppe CH_{Ar}), 7.31 (m, 12H, dppe CH_{Ar}), 6.93 (s, 1H, DBCat CH_{Ar}), 6.61 (s, 1H, DBCat CH_{Ar}), 2.42 (m, 2H, dppe CH_2), 1.39 (s, 9H, DBCat CH_3), 1.32 ppm (s, 9H, DBCat CH_3). $^{31}P\{^1H\}$ NMR ($CDCl_3$, 121 MHz): δ = 30.30, 30.40, 31.95 and 32.05 ppm. Pt satellites ; 16.42, 16.52, 17.95, 18.05, 44.18, 44.28, 45.95 and 46.05 ppm. $J_{P\text{-}Pt}$ = 3585 Hz. Mass spectrum ES(+) (*m*/*z*): 814.3 (100%, [{(dppe)Pt}(DBCat)][H]$^+$), 928.3 (42%, [{(dppe)Pt}(DBCat)][H]$^+$(dmso)$(H_2O)_2]^+$). Found C 59.03, H 5.45%. Calculated for $C_{40}H_{44}O_2P_2Pt$: C 58.90, H 5.45%. IR (solid state, cm^{-1}) 3075 (w), 3055 (w), 3023 (m), 3008 (m), 2959 (m), 2939 (m), 2906 (m), 2887 (m), 2868 (m), 1589 (w), 1552 (m), 1459 (s), 1437 (s), 1411 (s), 1386 (m), 1354 (m), 1320 (s), 1281 (s) ν(C-O), 1241 (s), 1197 (w), 1106 (m), 1028 (w), 976 (s), 914 (w), 878 (m), 853 (m), 827 (s), 810 (s), 747 (s), 715 (s), 692 (s), 652 (m), 617 (s), 574 (w), 537 (s), 498 (s).

Consistent with data reported in the literature.[15]

6.3.14 Preparation of [{(^{t}Bu$_2$Bipy)Pt(DBCat)}][15-16] (3.8)

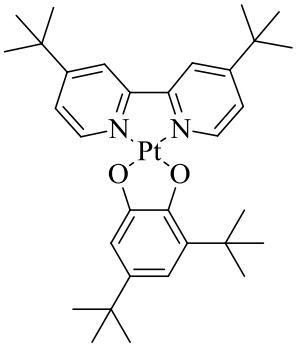

3,5-Di-*tert*-butyl catechol (0.085 g, 0.383 mmol) and potassium-*tert*-butoxide (0.088 g, 0.784 mmol) were dissolved in dry, deoxygenated methanol (15 cm^3) until complete dissolution of the reagents. To this, [(^{t}Bu$_2$Bipy)$PtCl_2$] (0.153 g, 0.585 mmol) was added and the mixture heated to 70 ^oC for 18 hours during which time the solution had darkened to deep purple. The reaction was cooled, the solvent evaporated and the crude material purified by column chromatography (silica, 0.5% MeOH in CH_2Cl_2). Yield 0.202 g, (77%).

^1H NMR (300 MHz, $CDCl_3$): δ = 9.35 (m, 2H, Bipy C$H_{Ar}^{6,6'}$), 7.77 (d, 2H, Bipy C$H_{Ar}^{3/3'}$ $^4J_{HH}$ = 1.9 Hz), 7.55 (dd, 1H, Bipy C$H_{Ar}^{5,5'}$, $^3J_{HH}$ = 6, $^4J_{HH}$ = 1.9 Hz), 7.43 (dd, 1H, Bipy C$H_{Ar}^{5/5'}$, $^4J_{HH}$ = 6, 1.9 Hz), 6.80 (br s, 1H, DBCat CH_{Ar}), 1.56 (s, 9H, DBCat CH_3), 1.44 (s,

18H, Bipy CH_3), 1.32 ppm (br s, 9H, DBCat CH_3). Mass Spectrum ES(+) (*m/z*): 684.3 (100%, $[(C_{18}H_{24}N_2Pt)C_{14}H_{22}O_2][H]^+$). Found C 53.95, H 6.40, N 3.60%. Calculated for $C_{32}H_{44}N_2O_2Pt$ $(CH_2Cl_2)_{0.5}$: C 53.75, H 6.25 N 3.86%. IR (solid state, cm^{-1}) 3081 (w), 3028 (w), 2950 (s), 2906 (s), 2869 (s), 1619 (m), 1562 (m), 1469 (s), 1439 (s), 1415 (s), 1385 (w), 1367 (m), 1316 (m), 1287 (s) ν(C-O), 1240 (s), 1202 (m), 1177 (m), 1157 (w), 1120 (w), 1073 (w), 1051 (w), 1025 (w), 980 (s), 927 (w), 902 (w), 884 (w), 842 (s), 826 (m), 809 (m), 755 (m), 723 (w), 694 (w), 639 (s), 597 (s), 547 (w), 516 (w), 501 (w).

Consistent with data reported in the literature. [**14**,16]

6.4 Experimental Details for Chapter 4

6.4.1 Preparation of *N*-(3,4-dimethoxybenzyl)sulfamide[17] (4.3)

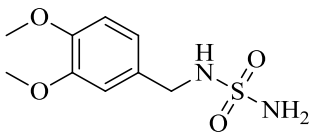

3,4-dimethoxybenzylamine (1.67 g, 10 mmol) and sulfamide (0.96 g, 10 mmol) were dissolved in water (10 cm^3) and heated to reflux overnight. The next day the solution was cooled to room temperature and acidified to pH 2 with 1 M hydrochloric acid and left to stand overnight at 4 ^oC. The precipitate formed was isolated, washed with water until the filtrate was neutral and dried in vacuo, yielding the product as a white microcrystalline powder. Yield: 3.81 g, 89.3%.

^1H NMR (300 MHz, d_6-DMSO): δ = 6.90 (m, 4H, CH_{Ar}, N*H*). 6.58 (s, 2H,[17]), 4.00 (d, 2H, ^2J = 6.4 Hz, CH_2), 3.75 (s, 3H, CH_3), 3.73 (s, 3H, CH_3) ppm. $^{13}C\{^1H\}$ NMR (d_6-DMSO, 75 MHz): δ = 148.5, 147.8, 130.9, 119.8, 111.7, 11.5, 55.5, 55.4, 45.9 ppm. Mass spectrum ES(+) (*m/z*): 659.3 (41% $[C_8H_{12}N_2O_4S]_2[K][C_2H_6SO]\}^+$), 515.1 (27% $[C_8H_{12}N_2O_4S]_2[H][CH_3OH]\}^+$), 413 (25% $\{[C_8H_{12}N_2O_4S][K][CH_3OH]_2[C_2H_6SO]\}^+$), 269.1 (100% $\{[C_8H_{12}N_2O_4S][H][H_2O]_2\}^+$), 255.0 (22% $\{[C_8H_{12}N_2O_4S][Na]\}^+$), 234.9 (10% $\{[C_9H_{14}N_2O_4S][H^+]\}^+$).

Consistent with data reported in the literature.[17]

6.4.2 Preparation of Cyclotetraveratrylene[17] (cttv, 4.4)

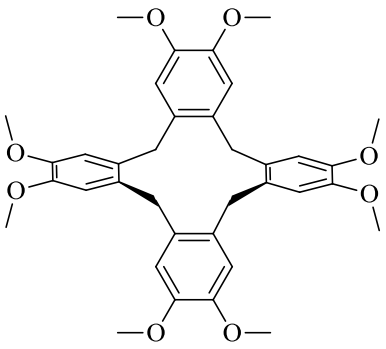

N-(3,4-dimethxoybenzyl)sulfamide (0.75 g, 3.52 mmol) was dissolved in trifluoroacetic acid (12 cm3) and stirred at room temperature for 3 hours during which time a white solid had formed. This solid was filtered, washed with trifluoroacetic acid and dried under vacuum overnight. The filtrate was concentrated (c.a. 5 cm^3) and sulfamide trituated by the addition of chloroform. CTTV was purified from the isolated white solid by column chromatography (2% acetone in chloroform) to unexpectedly give CTTV (70%) and CTV (18%) as white microcrystalline powders. Yield 0.139 g (66%).

^{1}H NMR ($CDCl_3$, 500 MHz): δ = 6.59 (s, br, 8H, CH_{Ar}), 3.79 ppm (s, br, 32H, CH_2, OCH_3). $^{13}C\{^1H\}$ NMR ($CDCl_3$, 125 MHz): δ = 147.2 (br.), 34.8 ppm. Mass spectrum ES+ (*m/z*): 623.1 (100% $\{[C_{36}H_{40}O_8].[Na]\}^+$). High resolution mass spectrum ES(+) (*m/z*): 623.2594 (calculated for $\{[C_{36}H_{40}O_8][Na]\}^+$ 623.2615). Found; C 65.25, H 5.95%. Calculated for $[C_{36}H_{40}O_8]\bullet[CH_2Cl_2]$ (685.64) C 64.82, H 6.17%.

Consistent with data reported in the literature.[18]

6.4.3 Preparation of Cyclotetracatechylene[19] (cttc, 4.A)

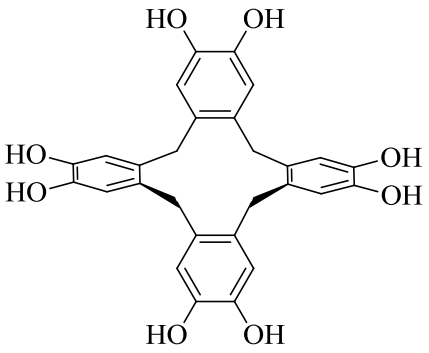

Cyclotetraveraveratrylene (2.1 g, 3.50 mmol) was dissolved in dry dichloromethane (150 cm^3) under an inert atmosphere, cooled to 0 ^oC in an ice bath and stirred for 15 minutes prior to the dropwise addition of boron tribromide (4 cm^3, 42 mmol). The mixture was slowly heated to reflux overnight during which time a white suspension had formed. The reaction was then again cooled to 0 ^oC in an ice bath and water (50 cm^3) added slowly. Once the fuming had stopped, the white precipitate was filtered, dried and recrystallised from ethanol-water to give cyclotetracetechylene as an off-white/brown precipitate. Yield: 1.21 g (71%).

^{1}H NMR (DMSO-d_6, 300 MHz): δ = 8.52 (s, br, 8H, O*H*), 6.44 (s, br, 8H, {H_3}), 3.42 ppm (s, br, overlapping with solvent resonance, CH_2). $^{13}C\{^1H\}$ NMR (DMSO-d_6, 75 MHz): δ = 143.0, 123.0. Mass spectrum ES(+) (*m/z*) : 511.1 (100% $\{[C_{28}H_{24}O_8].[Na]\}^+$). Found; C 67.15, H 4.85%. Calculated for $[C_{28}H_{24}O_8]_3\bullet[H_2O]_2$; C 67.19, H 5.10%.

Consistent with data reported in the literature.[19]

6.4.4 Preparation of 2,3,6,7-Tetramethoxy-9,10-dimethylanthracene[20] (4.5)

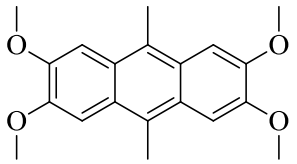

Veratrole (10.00 g, 72.38 mmol) was dissolved in 70% sulfuric acid (20 cm^3), cooled to 0 ^oC on an ice bath and stirred for 15 minutes prior to the dropwise addition of paraldehyde (5.50 cm^3, 41.37 mmol) with virogous stirring. The mixture immediately changed colour to red and solidified to a deep purple oil over the course of one hour. This was left to stand overnight at room temperature and the next day 100% ethanol (300 cm^3) was added and the mixture stirred for 3 hours. The off-white precipitate was collected, dried and extracted from chloroform using a Soxhlet to give 2,3,6,7-tetramethoxy-9,10-dimethylanthracene as a beige microcrystalline powder. Yield 12.01 g (89%).

^1H NMR ($CDCl_3$, 300 MHz) : δ = 7.42 (s, 4H, {C*H*}), 4.10 (s, 12H, {OCH_3}), 2.96 (s, 6H, {CH_3}). $^{13}C\{^1H\}$ NMR ($CDCl_3$, 121 MHz) : δ = 148.73, 125.81, 102.63, 55.68, 14.76 ppm. Mass spectrum ES(+) (*m/z*) : 349.1 $\{[C_{20}H_{22}O_4].[Na]\}^+$. Found; 73.20, H 6.75%. Calculated for $[C_{20}H_{22}O_4]$ (326.39) C 73.60, H 73.60%.

Consistent with previously reported.[20]

6.4.5 Preparation of 2,3,6,7-Tetrahydroxy-9,10-dimethylanthracene[20b] (4.B)

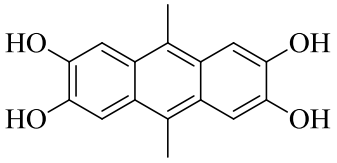

2,3,6,7-Tetramethoxy-9,10-dimethylanthracene (3.06 g, 9.38 mmol) was suspended in dry dichloromethane (200 cm^3) under an inert atmosphere and cooled to 0 °C prior to the dropwise addition of boron tribromide (8.0 cm^3, 56.25 mmol). This was stirred at 0 °C for 10 minutes then warmed to room temperature and stirred overnight. The mixture was again cooled to 0 °C prior to the slow addition of water (30 cm^3) and the crude yellow product collected, washed with water, recrystallised from ethanol and dried in a dessicator over phosphorus pentoxide to give 2,3,6,7-tetrahydroxy-9,10-dimethylanthracene as a yellow/green crystalline solid. Yield: 2.24 g (88%).

^1H NMR (DMSO-d_6, 300 MHz) : δ = 9.41 (s, br, 1H, {O*H*}), 7.34 (s, 4H, {C*H*}), 2.70 ppm (s, 3H, CH_3), 2.50 ppm (s, 3H, CH_3). $^{13}C\{^1H\}$ NMR (DMSO-d_6, 75 MHz) : δ = 145.8, 125.2, 120.9, 105.5, 14.1 ppm. Mass spectrum ES(+) (*m/z*) : 270.1 (100% $\{[C_{16}H_{14}O_4]\}^+$). 307.1 (73% $\{[C_{16}H_{14}O_4][H][H_2O]_2\}^+$), 387.1 (20% $\{[C_{16}H_{14}O_4][K][C_2H_6SO]\}^+$). Mass Spectrum ES(-) (*m/z*) : 269.1 (100% $\{[C_{16}H_{13}O_4]\}^-$). High resolution mass spectrum ES(+) : 270.0878 (calculated for $C_{16}H_{14}O_4$ 270.0878).
Consistent with data previously reported.[20b]

6.4.6 Preparation of 2,3,6,7-Tetramethoxyanthracene-9,10-dione[20] (4.6)

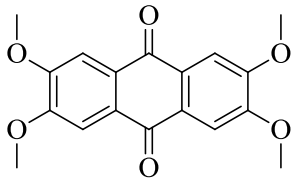

2,3,6,7-Tetramethoxy-9,10-dimethylanthracene (10 g, 30.6 mmol) and sodium dichromate dehydrate (56.9 g, 19.1 mmol) were heated to reflux in acetic acid (500 cm3) for 1 hour. The solution was cooled and left to stand at room temperature for 1 hour, filtered and the precipitate washed with water and methanol and dried overnight yielding 2,3,6,7-tetramethoxyanthracene-9,10-dione as a bright yellow powder. Yield: 7.85 g (86%).

^{1}H NMR ($CDCl_3$, 500 MHz) : δ = 7.69 (s, 4H, {CH_{Ar}}), 4.07 ppm (s, 12H, {CH_3}). ^{13}C{^{1}H} NMR (121 MHz, $CDCl_3$) : δ = 108.4, 56.5 ppm. High resolution mass spectrum ES(+) *m/z* : 328.0959 (calculated for $C_{18}H_{16}O_6$: 328.0941). Found; C 65.80, H 4.85%. Calculated for [$C_{18}H_{16}O_6$]; C 65.85, H 4.91%.

Consistent with data previously reported.[20]

6.4.7 Preparation of 2,3,6,7-Tetrahydroxyanthracene-9,10-dione[20] (4.C)

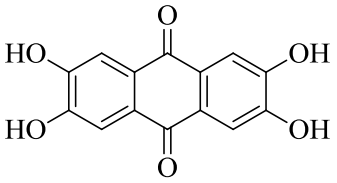

2,3,6,7-Tetramethoxy-9,10-dione (2.40 g, 7.31 mmol) was heated to reflux in 48% HBr solution (75 cm^3) for three days during which time the solution darkened to yellow/green. After 48 hours, more 48% HBr solution (15 cm^3) was added to wash the collected product off the condenser and the side of the flask. After a further 24 hours, the solution had stopped foaming and an orange/brown precipitate had formed which was collected and washed with water until the filtrate was of neutral pH. This crude product was then dried and recrystallised from hot pyridine/2 M HCl to give 2,3,6,7-tetrahydroxyanthracene-9,10-dione as a yellow/orange crystalline powder. Yield: 1.75 g (88%).

^{1}H NMR (DMSO-d_6, 300 MHz): δ = 10.80 (s, 4H, O*H*), 7.86 ppm (s, 4H, CH_{Ar}). ^{13}C{^{1}H} NMR (DMSO-d_6, 75 MHz): δ = 151.7, 127.9, 113.8 ppm. High resolution mass spectrum ES(-) (*m*/*z*) : 271.0237 (calculated for $C_{14}H_7O_6$: 271.0428).

Consistent with data previously reported.[20]

6.4.8 Preparation of 2,3,6,7-Tetramethoxyanthracene[21] (4.7)

Activation of zinc powder : Zinc powder (50 g, 0.76 mols) was added to a flask containing 2% aqueous hydrochloric acid (250 cm^3) and stirred until the surface of the zinc appears bright. The aqueous solution was then decanted and the active zinc washed with water (4 × 100 cm^3). The zinc powder was then collected by Buchner filtration under water (200 cm^3)and washed successively with ethanol (100 cm^3), acetone (150 cm3) and diethyl ether

(100 cm^3). The powder was then placed in 500 cm^3 round-bottomed flask, dried under vacuum for 30 minutes and used immediately.

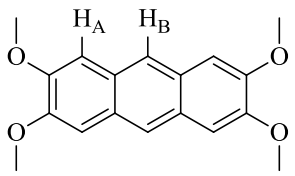

Active zinc power (42 g, 0.64 mols) and 2,3,6,7-tetramethoxyanthracene-9,10-dione (3.35 g, 10.2 mmol) were added to a stirred solution of sodium hydroxide (12.5 g, 0.31 mols) in water (290 cm^3) under an inert atmosphere. The mixture was heated to reflux for 24 hours and allowed to cool to room temperature prior to the slow addition of conc. hydrochloric acid (150 cm3) with vigorous stirring over one hour. The precipitate formed was isolated, washed with water, dried overnight and recrystallised from toluene to give 2,3,6,7-tetramethoxyanthracene as a bright white crystalline solid. Yield: 1.67 g (55%).

^{1}H NMR ($CDCl_3$, 300 MHz): δ = 8.04 (s, 2H, H_B), 7.16 (s, 4H, H_A), 4.04 (s, 12H, CH_3). $^{13}C\{^1H\}$ NMR ($CDCl_3$, 75 MHz) : δ = 149.41, 127.40, 122.03, 104.76, 55.83. Mass spectrum ES(+) (*m/z*) : 317.1 $\{[C_{18}H_{18}O_4].[H_2O].[H^+]\}^+$. Found C 72.15, H 6.15%. Calculated for $C_{18}H_{18}O_4$; C 72.17, H 6.08.

Consistent with data previously reported.[21]

6.4.9 Preparation of 2,3,6,7-tetramethoxy-9,10-dihydro-anthracene[21] (4.1).

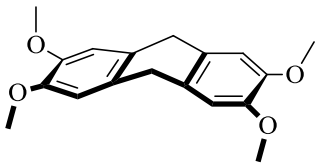

Lithium metal (0.500 g, 7.63 mmol) was slowly added to a suspension of 2,3,6,7-tetramethoxyanthracene (2.00 g, 6.70 mmol) in dry, degassed diethyl ether at -78°C. Ammonia was condensed into the mixture, and the reaction refluxed (at -78°C) for four hours. Excess lithium was quenched by the addition of ethanol and the reaction opened to the air to release the remaining ammonia. The product was extracted into diethyl ether, and washed with water (3 × 25 cm^3), brine, dried over magnesium sulfate and the solvent removed yielding the product as a white powder. (22%)

^{1}H NMR ($CDCl_3$, 300 MHz) : δ = 6.63 (s, 4H, CH_{Ar}), 3.86 (s, 12H, OCH_3), 3.23 ppm (s, 4H, CH_2). $^{13}C\{^1H\}$ NMR ($CDCl_3$, 75 MHz): δ = 135.1, 122.4, 110.6, 57.2 (CH_2), 35.0, 32.5 ppm. Mass spectrum (ES-) (*m/z*) : 301.2 (100% $\{[C_{18}H_{20}O_4][H]\}^+$). High resolution mass spectrum (ES-) (*m/z*): 301.2367 (calculated for $[C_{18}H_{20}O_4][H]\}^-$ 301.1434). Found C 71.00, H 7.90%. Calculated for $[C_{18}H_{20}O_4]_3[C_4H_9O]_2$ (1049.31); C 70.97, H 7.69%.

Consistent with data previously reported. [21]

6.4.10 Preparation of 2,3,6,7-tetramethoxy-9,10-dimethyl-9,10-dihydro-ethanoanthracene[22] (Me_4thea, 4.8)

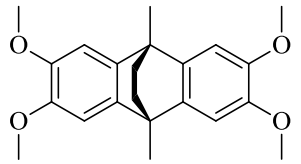

Hexane-2,5-dione (4.6 g, 40.30 mmol) was added dropwise to veratrole (11.00 g, 79.62 mmol) dissolved in 70% sulfuric acid (100 cm^3) at 0 ^oC. The mixture was stirred for 72 hours at room temperature, poured into cold water (1000 cm^3) and left to stand at 4 °C overnight during which time a light brown precipitate began to form. This was isolated, washer with water until the filtrate was neutral and recrystallised from ethanol giving 2,3,6,7-tetramethoxy-9,10-dimethyl-9,10-dihydro-ethanoanthracene as a bright white crystalline powder. Yield: 8.28 g (58%).

^1H NMR ($CDCl_3$, 300 MHz) δ = 6.89 (s, 2H, H_{Ar}), 3.89 (s, 6H, OCH_3), 1.96 (s, 6H, CH_3), 1.61 ppm (s, 4H, CH_2). $^{13}C\{1H\}$ NMR ($CDCl_3$, 75 MHz,) : δ = 146.5, 139.3, 105.6, 104.8, 56.4, 41.3, 36.4, 18.7 ppm. Mass spectrum (ES+) (*m/z*): 455.2 (79% $\{[C_{22}H_{26}O_4][Na][C_2H_6SO]\}^+$), 418.2 (13% $\{[C_{22}H_{26}O_4][Na][C_2H_3N]\}^+$), 377.2 (100% $\{[C_{22}H_{26}O_4][Na]^+$). High resolution mass spectrum (ES+) (*m/z*) : 377.1725 (calculated for $\{[C_{22}H_{26}O_4].[Na]\}^+$ 377.17232). Found; C 74.50, H 7.40%. Calculated for $C_{22}H_{26}O_4$; C 74.55, H 7.40%.

Consistent with data previously reported.[22]

6.4.11 Preparation of 2,3,6,7-Tetrahydroxy-9,10-dimethyl-9,10-dihydro-ethanoanthracene (H_4thea, 4.9)

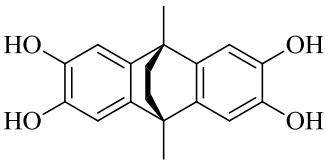

2,3,6,7-Tetramethoxy-9,10-dimethyl-9,10-dihydro-ethanoanthracene (2.10 g, 5.92 mmol) was dissolved in dry dichloromethane (100 cm^3) under an inert atmosphere. This solution was cooled to 0 ^oC and boron tribromide (2.8 cm^3 30 mmol) added cautiously over 30 minutes. The reaction mixture was stirred at 0 ^oC for 10 minutes and allowed to warm to room temperature. Once at room temperature, the reaction was heated to reflux for 4 hours during which time the reaction had turned brown. The reaction was again cooled to 0 ^oC and water (20 cm^3) added cautiously. This was stirred at 0 ^oC for 10 minutes and the brown/off white precipitate isolated under vacuum. The product was recrystallised from acetone/water and dried in a dessicator over phosphorus pentoxide to give 2,3,6,7-tetrahydroxy-9,10-dimethyl-9,10-dihydro-ethanoanthracene as a brown/off white solid. Yield 1.77 g (91%)

^1H NMR (DMSO-d_6, 300 MHz): δ = 7.40 (s, 4H, OH), 6.74 (s, 4H, CH_{Ar}), 1.76 (s, 6H, CH_3), 1.48 ppm (s, 4H, CH_2). $^{13}C\{^1H\}$ NMR (DMSO-d_6, 75 MHz): δ = 141.7, 137.6, 108.7, 36.2, 18.5 ppm. Mass spectrum ES(-) (*m/z*): 893.3 (37% $\{[C_{18}H_{18}O_4]_2[C_{18}H_{17}O_4]\}^-$), 595.2

(98% $\{[C_{18}H_{18}O_4][C_{18}H_{17}O_4]\}^-$), 393.1 (16% $\{[C_{18}H_{17}O_4][H_2O][C_2H_6SO]\}^-$), 343.1 (32% $\{[C_{18}H_{17}O_4][CO_2H]\}^-$), 297.1 (100% $\{[C_{18}H_{17}O_4]\}^-$). High resolution mass spectrum (ES+) (*m/z*): 297.1131 (calculated for $C_{18}H_{17}O_4$: 297.1132). Found C 70.15, H 6.10%. Calculated for $[C_{18}H_{17}O_4]_2$•$[H_2O]$ (614.69), C 70.34, H 6.23%. IR (solid state, cm^{-1}): 3323 (br s) O-H, 3054 (w), 3038 (w), 2963 (m), 2948 (m), 2900 (w), 2878 (m), 2860 (m), 1598 (s), 1506 (w), 1483 (m), 1444 (s), 1381 (m), 1347 (w), 1290 (s), 1211 (m), 1174 (w), 1146 (m), 1132 (s), 1073 (w), 1048 (w), 1018 (w), 991 (s), 878 (s), 849 (w), 811 (s), 797 (s), 748 (s), 712 (w), 668 (m), 639 (m), 589 (m), 573 (s), 541 (m), 516 (m).

Consistent with data previously reported.[23]

6.4.12 Preparation of $[\{(dppb)Pt\}_2(thea)]$ (4.10)

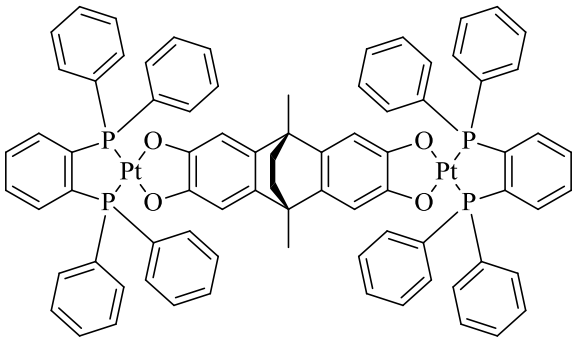

H_4thea (0.075 g, 0.251 mmol) and $[PtCl_2(dppb)]$ (0.356 g, 0.500 mmol) were dissolved in deoxygenated dimethylacetamide (25 cm^3) and stirred for 30 minutes prior to the addition of potassium carbonate (0.173 g, 1.26 mmol) suspended in dry, deoxygenated methanol (10 cm^3) This mixture was left to stir at 60 ^oC for 18 hours during which time a colour change to deep orange was noted. Once cooled, excess dry, deoxygenated diethyl ether was added to precipitate the crude, orange product. The precipitate was isolated under an inert atmosphere of nitrogen and recrystallised from dry, deoxygenated dichloromethane / acetone yielding the product as an orange powder. Yield 0.222 g, 56%. Crystals suitable for single crystal X-ray diffraction were grown from the slow diffusion of dry pentane into a solution of $[\{(dppb)Pt\}_2(thea)]$ in dry dichloromethane, inside a glovebox.

^1H NMR (10:1 $CDCl_3$:CD_3OD, 300 MHz): δ = 7.78-7.37 (m, 48H, dppb CH_{Ar}), 6.66 (s, 4H, thea CH_{Ar}), 1.71 (s, 6H, thea CH_3), 1.46 ppm (s, 4H, thea CH_2). ^{31}P NMR (10:1 $CDCl_3$:CD_3OD, 121 MHz): δ = 35.4 ppm. Pt satellites; 49.6 and 21.4 ppm. $J_{P\text{-}Pt}$ = 3441 Hz. Found C 56.8, H 3.95%. Calculated for $[C_{78}H_{62}O_4P_4Pt_2][CH_2Cl_2]$ (1662.34): C 57.1, H 3.88%. MS (ES+) (*m/z*): 686.1 (40%, $\{[C_{30}H_{24}P_2Pt][O_2CH]\}^+$), 754.1 (36%, $\{[C_{30}H_{24}P_2Pt][Na][O_2CH]_2\}^+$), 832.1 (30%, $\{[C_{30}H_{24}P_2Pt][Na][O_2CH]_2[C_2H_6SO]\}^+$), 937.2 (21%, $\{[(C_{30}H_{24}P_2Pt)C_{18}H_{16}O_4)]\}^+$), 1417.5 (18%, $\{[C_{30}H_{24}P_2Pt]_2[Na]_2[O_2CH]_2\}^+$), 1474.1 (18%, $\{[C_{30}H_{24}P_2Pt]_2[Na]_2[O_2CH]_2[C_2H_7SO]\}^+$), 1485.2 (100%, $[[C_{30}H_{24}P_2Pt]_2[Na][O_2CH]_2[H_2O]_5\}^+$), 1577.3 (16%, $\{[C_{78}H_{62}O_4P_4Pt_2]\}^+$). IR (solid state, cm^{-1}) 3055 (m), 3015 m, 2953 m, 2928 (m), 2874 m, 2849 (w), 1628 (m), 1556 (m), 1467 (s), 1454 (s), 1435 (s), 1370 (w), 1334 (w), 1291 (s) ν(C-O), 1233 (m), 1185 (w), 1161 (w), 1119 (m), 1101 (s),

1028 (w), 998 (w), 874 (m), 825 (m), 747 (m), 692 (s), 621 (m), 573 (s), 539 (s), 508 (s), 461 (s).

6.4.13 Preparation of [{(dppb)Pt}$_2$(thea)].[PF_6] (4.10[PF_6])

Under an inert atmosphere, ferrocenium hexafluorophosphate (4.2 mg, 12.7 μmol) was added to [{(dppb)Pt}$_2$(thea)] (20 mg, 12.7 μmol) dissolved in dry, deoxygenated dichloromethane at -78 ^oC. The mixture was stirred for 30 minutes and the solvent removed. The powder was washed repeatedly with diethyl ether and hexane until the filtrate was colourless. This powder was redissolved in dry, deoxygenated dichloromethane for EPR measurements. Yield 0.021 g, (96%). Crystals suitable for single crystal X-ray diffraction were grown from the slow diffusion of dry pentane into a solution of [{(dppb)Pt}$_2$(thea)].[PF_6] in dry dichloromethane, inside a glovebox.

Found C 52.75, H 3.60 P 8.40%. Calculated for [$C_{78}H_{62}O_4P_4Pt_2$][PF_6]•[CH_2Cl_2] (1807.30) (C 52.50, H 3.57, P 8.57%. IR (solid state, cm^{-1}) 3055 (w), 2957 (w), 2934 (w), 2899 (w), 2884 (w), 2859 (w), 1670 (m), 1481 (m) ν(C=C), 1435 (s) ν(C=C), 1423 (s) ν(C=C), 1374 (m) ν(C=O), 1335 (w), 1307 (w), 1290 (w), 1256 (m), 1167 (m), 1132 (s), 1092 (s), 838 (s) ν(P-F), 747 (m), 714 (w), 692 (m), 598 (m), 557 (s), 540 (s), 508 (m).

6.4.14 Preparation of [{(dppb)Pt}$_2$(thea)][PF_6]$_2$ (4.10[PF_6]$_2$)

Under an inert atmosphere, ferrocenium hexafluorophosphate (8.4 mg, 25.4 μmol) was added to [{(dppb)Pt}$_2$(thea)] (20 mg, 12.7 μmol) dissolved in dry, deoxygenated dichloromethane at -78 ^oC. The mixture was stirred for 30 minutes and the solvent removed. The powder was washed repeatedly with diethyl ether and hexane until the filtrate was colourless.

Found C 48.25, H 3.30%. Calculated for [$C_{78}H_{62}O_4P_4Pt_2$][PF_6]$_2$•[CH_2Cl_2] (1952.27) (C 48.60, H 3.04%. IR (solid state, cm^{-1}) 3061 (w), 3023 (w), 2959 (w), 2936 (m), 1635 (w), 1619 (w), 1586 (w), 1574 (w), 1533 (m), 1507 (m), 1479 (s) ν(C=C), 1455 (s) ν(C=C), 1408 (s) ν(C=C), 1373 (s) ν(C=O), 1336 (w), 1309 (s), 1253 (w), 1187 (w), 1162 (w), 1123 (s), 1104 (s), 1070 (w), 1053 (m), 1026 (w), 998 (m), 929 (w), 836 (s) ν(P-F), 748 (s), 717 (m), 693 (s), 601 (m), 576 (s), 557 (s), 542 (s), 505 (s), 470 (m), 455 (m).

6.4.15 Preparation of [{(dppe)Pt}$_2$(thea)] (4.11)

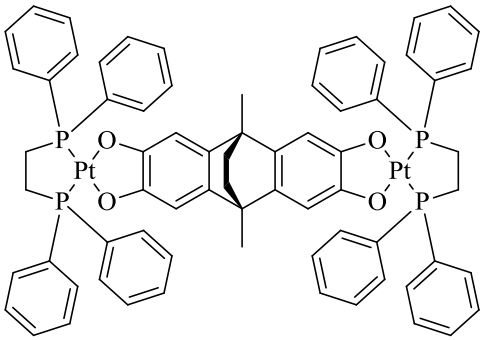

H_4thea (0.106 g, 0.355 mmol) and potassium-*tert*-butoxide (0.200 g, 1.78 mmol) were dissolved in dry, deoxygenated methanol (25 cm^3) until complete dissolution of the reagents. To this, [PtCl$_2$(dppe)] (0.476 g, 0.716 mmol) was added and the mixture heated to 50 ^{o}C for 18 hours during which time the solution had darkened to deep orange with a yellow precipitate. The solvent was removed and the crude deep yellow solid recrystallised from dichloromethane at -20 ^{o}C yielding the product as a yellow powder. Yield 0.231 g, 44%. Crystals suitable for single crystal X-ray diffraction were grown from the slow diffusion of dry pentane into a solution of [{(dppe)Pt}$_2$(thea)] in dry dichloromethane, inside a glovebox.

^{1}H NMR (10:1 $CDCl_3$:CD_3OD, 300 MHz): δ = 8.08 (m, 16H, dppe $H^{2,6}$) 7.42 (m, 24H, dppe Ph $H^{3,4,5}$), 6.90 (s, 4H, thea C*H*), 2.34 (d, $^2J_{HH}$ = 16.5 Hz, 8H, dppe CH_2), 1.88 (s, 6H, thea CH_3), 1.64 ppm (s, 4H, thea CH_2). ^{31}P{^{1}H} NMR (121 MHz, 10:1 $CDCl_3$:CD_3OD); δ = 29.8 ppm. Pt satellites; 43.8 and 15.8 ppm. $J_{P\text{-}Pt}$ = 3406 Hz. Mass spectrum (ES+) (*m*/*z*): 1503.2 (12%,{[$(C_{26}H_{24}P_2Pt)_2$(thea)][Na]$^+$}), 1480.2 (100%, {[$(C_{26}H_{24}P_2Pt)_2(C_{18}H_{14}O_4)$]$^+$}, 1220.4 (10%, {[Pt($C_{26}H_{24}P_2Pt$)$C_{18}H_{15}O_4$][Na][$C_2H_6SO$][$H_2O]_2$]}$^+$), 1020.1 (10%, {[($C_{26}H_{24}P_2Pt$)$C_{18}H_{15}O_4$][$C_2H_6SO$][$H_2O]_3$]}$^+$), 940.2 (56%, {[$(C_{26}H_{24}P_2Pt)_2C_{18}H_{15}O_4$][Na][$O_2CH$][$C_2H_6SO]_3(H_2O)$]}$^{2+}$), 911.1 (31%, {[($C_{26}H_{24}P_2Pt$)$C_{18}H_{15}O_4$][Na]}$^+$). Found C 54.8, H 4.20%. Calculated for [$C_{70}H_{62}O_4P_4Pt_2$]•[CH_2Cl_2] (1566.25): C 54.4, H 4.12%. IR (solid state, cm^{-1}) 3050 (m), 3031 (m), 3015 (m), 2957 (m), 2921 (m), 2845 (m), 1697 (w), 1675 (w), 1635 (w), 1570 (m), 1557 (m), 1486 (m), 1467 (m), 1436 (s), 1405 (m), 1368 (w), 1336 (w), 1290 (s) ν(C-O), 1233 (w), 1188 (m), 1161 (w), 1129 (m), 1105 (s), 1028 (w), 998 (w), 929 (w), 873 (s), 827 (s), 749 (m), 693 (s), 658 (m), 621 (m), 597 (w), 582 (m), 533 (s), 500 (m).

6.4.16 Preparation of [{(dppe)Pt}$_2$(thea)]PF_6 (4.11[PF_6])

Under an inert atmosphere, ferrocenium hexafluorophosphate (4.5 mg, 13.5 μmol) was added to [{(dppe)Pt}$_2$(thea)] (20 mg, 13.5 μmol) dissolved in dry, deoxygenated dichloromethane at -78 ^{o}C. The mixture was stirred for 30 minutes and the solvent removed. The powder was washed repeatedly with diethyl ether and hexane until the filtrate was colourless. 0.020 g (94%). This powder was redissolved for EPR measurements. Crystals suitable for single crystal X-ray diffraction were grown from the slow diffusion of dry pentane into a solution of [{(dppe)Pt}$_2$(thea)].[PF_6] in dry dichloromethane, inside a glovebox.

Found C 50.05, H 3.85. Calculated for $[C_{70}H_{62}O_4P_4Pt_2][PF_6]\bullet[CH_2Cl_2]$ (1711.22) (C 49.83, H 3.77%. IR (solid state, cm^{-1}) 3077 (w), 3056 (w), 3018 (w), 2959 (w), 2924 (w), 1669 (w), 1635 (w), 1480 (m) ν(C=C), 1416 (s) ν(C=C), 1372 (m) ν(C=O), 1336 (w), 1311 (w), 1254 (m), 1049 (br, s), 836 (s) ν(P-F), 749 (m), 708 (s), 690 (s), 582 (w), 567 (s), 534 (s), 497 (m).

6.4.17 Preparation of $[\{(dppe)Pt\}_2(thea)][PF_6]_2$ (4.11$[PF_6]_2$)

Under an inert atmosphere, ferrocenium hexafluorophosphate (9.0 mg, 13.5 μmol) was added to $[\{(dppe)Pt\}_2(thea)]$ (20 mg, 13.5 μmol) dissolved in dry, deoxygenated dichloromethane at -78 °C. The mixture was stirred for 30 minutes and the solvent removed. The powder was washed repeatedly with diethyl ether and hexane until the filtrate was colourless. Yield 0.023 g (92%).

Found C 47.55, H 3.35%. Calculated for $[C_{70}H_{62}O_4P_4Pt_2][PF_6]_2$ (1856.18) (C 47.47, H 3.53%. IR (solid state, cm^{-1}) 3057 (m), 3029 (w), 2959 (m), 2934 (w), 2857 (m), 1669 (m), 1632 (w), 1587 (w), 1574 (w), 1537 (m), 1506 (s), 1481 (m) ν(C=C), 1452 (s) ν(C=C), 1436 (s) ν(C=C), 1417 (m) ν(C=C), 1372 (s) ν(C=O), 1336 (w), 1307 (s), 1252 (w), 1189 (m), 1142 (m), 1108 (s), 1067 (m), 1027 (w), 836 (s) ν(P-F), 749 (m), 710 (s), 692 (s), 661 (w), 598 (m), 557 (s), 535 (s), 495 (m).

6.4.18 Preparation of $[\{(^tBu_2Bipy)Pt\}_2(thea)]$ (4.12)

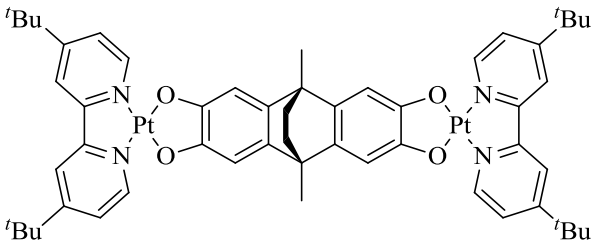

H_4thea (0.100 g, 0.335 mmol) and potassium-*tert*-butoxide (0.188 g, 1.68 mmol) were dissolved in dry, deoxygenated methanol (25 cm^3) until complete dissolution of the reagents. To this, $[(^tBu_2Bipy)PtCl_2]$ (0.358 g, 0.670 mmol) was added and the mixture heated to 70 °C for 18 hours during which time the solution had darkened to deep purple. The solvent was removed and the resulting solid purified by column chromatography (silica, 98.5 : 1.5% dichloromethane : methanol) and the deep blue fraction retained. Yield 0.323 g (79%).

^{1}H NMR ($CDCl_3$, 300 MHz); δ, ppm 1.38 (s, 36H, bipy CH_3), 1.71 (s, 4H, thea CH_2), 2.10 (s, 6H, thea CH_3), 6.63 (s, 4H, thea CH_{Ar}), 7.42 (dd, $^3J_{HH}$ = 6.0, $^4J_{HH}$ = 1.8 Hz, 4H, bipy $H^{5,5'}$), 7.74 (d, $^4J_{HH}$ = 1.8 Hz, 4H, bipy $H^{3,3'}$), 9.15 (d, $^3J_{HH}$ = 6.0 Hz, 4H, bipy $H^{6,6'}$). Mass spectrum (ES+) (*m*/*z*): 530.2 (39%, $[C_{18}H_{24}N_2Pt][O_2CH][Na]_2^+$), 541.2 (33%, $\{[(C_{18}H_{24}N_2Pt)(C_2H_6SO)]\}^+$), 610.2 (100%, $[Pt_2(C_{18}H_{24}N_2)_2(C_{18}H_{14}O_4)]^{2+}$, [**3**]$^{2+}$), 758.2 (37%, $\{[(C_{18}H_{24}N_2Pt)C_{18}H_{16}O_4][H]\}^+$), 1220.4 (13%, $\{[(C_{18}H_{24}N_2Pt)_2(C_{18}H_{14}O_4)]\}^+$). Found C 50.6, H 5.15, N 4.30%. Calculated for $[C_{54}H_{62}N_4O_4Pt_2]\bullet[CH_2Cl_2]$ (1306.21): C 50.6, H

4.94, N 4.29%. IR (solid state, cm^{-1}) 3053 (w), 3007 (w), 2957 (s), 2925 (s), 2870 (m), 2855 (m), 1669 (w), 1620 (m), 1583 (w), 1558 (w), 1487 (s), 1471 (s), 1456 (s), 1422 (s), 1369 (w), 1338 (w), 1292 (s) ν(C-O), 1263 (m), 1233 (w), 1203 (w), 1129 (s), 1102 (s), 1082 (s), 1024 (s), 929 (w), 873 (s), 839 (m), 821 (s), 751 (w), 735 (w), 694 (w), 642 (s), 598 (s), 534 (s), 492 (w), 478 (w).

6.4.19 Preparation of [{(^{t}Bu$_2$Bipy)Pt}$_2$(thea)]PF_6 (4.12[PF_6])

Under an inert atmosphere, ferrocenium hexafluorophosphate (1.1 mg, 3.3 μmol) was added to [{(^{t}Bu$_2$Bipy)Pt}$_2$(thea)] (4 mg, 3.3 μmol) dissolved in dry, deoxygenated dichloromethane at -78 °C. The mixture was stirred for 30 minutes and used without further purification. This compound could not be isolated in the solid state due to decomposition at ambient temperatures.

6.5 Experimental Details for Chapter 5

6.5.1 Synthesis of methyl 3,4-dihydroxybenzoate[24] (5.1)

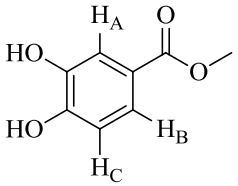

3,4-dihydroxybenzoic acid (10.02 g, 65.01 mmol) and a catalytic quantity of concentrated hydrochloric acid (37%, 1 cm^3) were heated to reflux in methanol for 14 hours. The solvent was then removed and the precipitate suspended in water (100 cm^3), the product was collected by filtration and washed repeatedly with water until the filtrate obtained was neutral. The product was dried *in vacuo* giving a white powder in high purity. Yield: 10.09 g (92%).

^{1}H NMR (DMSO-d_6, 300 MHz): δ = 10.35-9.02 (br. s, 2H, OH), 7.41 (d, $^4J_{HH}$ = 2.1 Hz, 1H, H_A), 7.37 (dd, $^3J_{HH}$ = 8.3, $^4J_{HH}$ = 1.9 Hz, 1H, H_B), 6.86 (d, $^3J_{HH}$ = 8.3 Hz, 1H, H_C), 3.82 ppm (s, 3H, CH_3). ^{13}C{^{1}H} NMR (DMSO-d_6, 75 MHz) : 116.1, 105.4, 145.0, 121.7, 124.5, 116.2, 115.3, 51.5. High resolution mass spectrum: (ES+) (*m/z*): 365.0611 (calc. for {[$C_8H_8O_4$]][Na][$C_2H_6SO]_2$[H_2O]}$^+$: 365.0699). Found C 56.90, H 4.80%. Calculated for $C_8H_8O_4$ (168.15) C 57.14, H 4.94%. Melting point: 165.2-166.8 °C.

Consistent with data previously reported.[24]

6.5.2 Synthesis of 3,4-dimethylthiocarbomyl methyl benzoate[24b, 24c] (5.2)

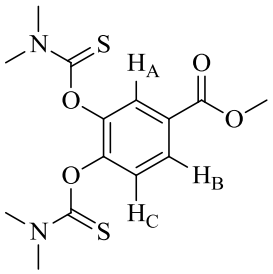

3,4-dihydroxy methyl benzoate (6.00 g, 35.83 mmol) and 1,4-diazabicyclo[2.2.2]octane (12.07 g, 107.48 mmol) were stirred under an inert atmosphere at 50 °C in dry dimethylformamide (30 cm^3) unil complete dissolution of the reagents prior to the dropwise addition of dimethylthiocarbomyl chloride (13.28 g, 107.57 mmol). This mixture was stirred at 50 °C for 16 hours, cooled, poured into cold water (250 cm^3) and the product extracted into ethyl acetate (3 × 50 cm^3). The combined organic layers were washed with water (3 × 15 cm^3), brine and dried over magnesium sulfate. The product was triturated from the resulting oil by addition of ethanol (50 cm^3) and cooling on ice yielding a white microcrystalline solid in high purity. Yield: 11.17 g (91%).

^{1}H NMR ($CDCl_3$, 300 MHz); δ = 7.99 (dd, $^3J_{HH}$ = 8.5, $^4J_{HH}$ = 2.1 Hz, 1H, H_B), 7.85 (d, $^4J_{HH}$ = 1.9 Hz, 1H, H_A), 7.24 (d, J=8.3 Hz, 1H, H_C), 3.90 (s, 3H, OCH_3), 3.42 (s, 3H, NCH_3), 3.42 (s, 3H, NCH_3), 3.29 (s, 3H, NCH_3), 3.29 ppm (s, 2H, NCH_3). ^{13}C{^{1}H} NMR ($CDCl_3$, 75 MHz): 186.5, 186.0, 165.62, 149.3, 145.5, 128.7, 128.1, 125.9, 124.4, 52.3, 43.4, 43.3, 38.9, 38.8 ppm. Found C 48.90, H 5.30, N 8.05, S 19.00%. Calculated for $C_{14}H_{18}O_4N_2S_2$ (342.07): C 49.10, H 5.30, N 8.18, S 18.73%. High resolution mass spectrum: (ES+) (*m/z*): 365.0611 (calculated for $[C_{12}H_{22}O_7S_2]^+$: 365.0600). Melting point: 109.9-112.0 °C.

Consistent with data previously reported.[24b, 24c]

6.5.3 Synthesis of Methyl 2-oxo-1,3-benzodithiole-5-carboxylate[24] (5.3)

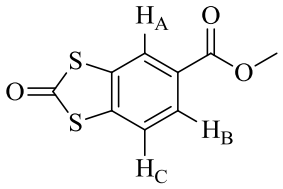

3,4-dimethylthiocarbomyl methyl benzoate (1.751 g, 5.11 mmol) was dissolved in diphenyl ether (25 cm^3) and heated to 240 °C under an inert atmosphere for 1 hour. The product was purified by column chromatography (PET 40-60 : dichloromethane, 1 : 1) to afford the product as a white microcrystalline solid. Yield: 0.624g (54%).

^{1}H NMR ($CDCl_3$, 300MHz): δ = 7.84 (d, J=1.5 Hz, 1H, H_A), 7.80 (dd, $^3J_{HH}$ = 7.9, $^4J_{HH}$ = 1.5 Hz, 1H, H_B), 7.22 (d, $^3J_{HH}$ = 8.3 Hz, 1H, H_C), 3.90 ppm (s, 3H, CH_3). ^{13}C{^{1}H} NMR ($CDCl_3$, 75 MHz) ;165.7, 137.9, 133.0, 129.1, 127.8, 124.1, 122.9, 52.5 ppm. Mass spectrum (ES+) (*m/z*): 285.2 (100% $\{[C_9H_6O_3S_2][Na][H_2O]_2\}^+$) Found C 48.05, H 2.85, S 28.05%. Calculated for $C_9H_6O_3S_2$ (225.98): C 47.77, H 2.85, S 28.34%. Melting point 141.0-143.1 °C.

Consistent with data previously reported.[24]

6.5.4 Synthesis of 3,4-dimercaptobenzoic acid[24] (5.4)

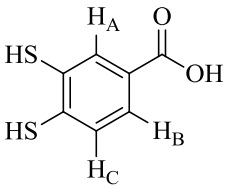

Methyl 2-oxo-1,3-benzodithiole-5-carboxylate (0.546 g, 2.41 mmol) and sodium hydroxide (1.306 g, 34.51 mmol) were added to deoxygenated water (30 cm^3) and heated to 70 °C for 6 hours under an inert atmosphere. The solution was cooled to room temperature and poured directly into excess 1 M HCl. The white solid was collected by filtration, washed with water until the filtrate was neutral and dried *in vacuo*. Yield 0.440 g: 98%.

^{1}H NMR (CD_3OD, 300 MHz): δ = 7.99 (d, $^4J_{HH}$ = 1.5 Hz, 1H, H_A), 7.65 (dd, $^3J_{HH}$ = 8.3, $^4J_{HH}$ = 1.9 Hz, 1H, H_B), 7.42 ppm (d, $^3J_{HH}$ = 8.3 Hz, 1H, H_C). $^{13}C\{^1H\}$ NMR (CD_3OD, 75 MHz): δ = 168.9, 140.4, 132.9, 131.4, 130.5, 129.5, 128.5 ppm. High resolution mass spectrum (ES-) (*m/z*): 184.9736 (calc. for $[C_7H_5O_2S_2]^-$ 184.9725). Melting point: 218.4-219.6 °C

Consistent with data reported in the literature.[24]

6.5.5 Synthesis of 3,4-dimercaptobenzyl alcohol (5.5)

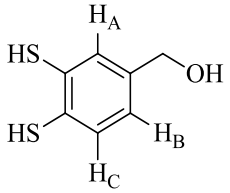

3,4-dimercaptobenzoic acid (0.450 g, 2.42 mmol) was dissolved in dry tetrahydrofuran (15 cm^3) and added dropwise to lithium aluminum hydride (0.458 g, 12.08 mmol) suspended in dry tetrahydrofuran (25 cm^3). The reaction was stirred at 0 °C for 1 hour, then slowly warmed to room temperature and stirred for 18 hours. The reaction was then cooled in an ice bath and the excess lithium aluminum hydride was quenched by the cautious addition of water. The solvent was removed under reduced pressure and the crude product was extracted into diethyl ether (3 × 25 cm^3). The oily residue was purified by extraction into hot hexane, affording the product as an air-sensitive white solid. Yield 0.317 g (76%).

^{1}H NMR ($CDCl_3$, 300 MHz): δ = 7.39 (d, $^4J_{HH}$ = 1.9 Hz, 1H, H_A), 7.36 (d, $^3J_{HH}$ = 7.9 Hz, 1H, H_C), 7.06 (dd, $^3J_{HH}$ =7.9, $^4J_{HH}$ = 1.9 Hz, 1H, H_B), 4.62 (s, 2H,CH_2), 3.75 - 3.78 (s, 1 H, *para*-S*H*), 3.70 ppm (s, 1H, *meta*-S*H*). $^{13}C\{^1H\}$ NMR ($CDCl_3$, 75 MHz): δ = 138.8, 130.4, 128.3, 124.3, 63.4 ppm. High resolution Mass Spectrum (EI+) (*m/z*): 172.0012 (calculated for $\{[C_7H_8OS_2]\}^+$ 172.0017). Melting point 56.1-58.3 °C. Decomposition in air prevented the acquisition of representative elemental analytical data.

6.5.6 Synthesis of 3,4-dibenzylthiobenzoic acid[22] (5.6)

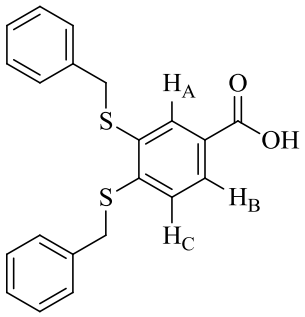

3,4-dimercaptobenzoic acid (0.530 g, 2.85 mmol) and sodium hydroxide (0.342 g, 8.55 mmol) were dissolved in methanol (30 cm^3) under an inert atmosphere. The methanol was removed *in vacuo* and acetone (30 cm^3) added prior to the addition of benzyl bromide (0.68 cm^3, 5.70 mmol). The mixture was heated to reflux for four hours and cooled to -20 °C. The white precipitate formed was isolated and washed with acetone. The precipitate was suspended in water, filtered to remove any insoluble impurities and the filtrate acidified using conc. hydrochloric acid (37%). The precipitate formed was isolated, washed with water (3 × 15 cm^3) and dried *in vacuo*. Yield 0.731 g (70%).

^{1}H NMR (DMSO-d_6, 300 MHz): δ = 12.99 (br s, 1H, O*H*), 7.85 (d, $^4J_{HH}$ =1.5 Hz, 1H, H_A), 7.75 (dd, $^3J_{HH}$ = 8.3, $^4J_{HH}$ = 1.9 Hz, 1H, H_B), 7.53 (s, 1H, H_C), 7.46 - 7.49 (m, 2H, CH_{Ar}), 7.42-7.25 (m, 8 H, CH_{Ar}), 4.38 (s, 2H, SCH_2), 4.29 ppm (s, 2H, SCH_2). ^{13}C{^{1}H} NMR (DMSO-d_6, 75 MHz): δ = 166.6, 136.6, 136.3, 133.8, 129.7, 129.0, 128.9, 128.5, 128.3, 127.6, 127.4, 127.1, 126.0, 36.6, 35.7 ppm. Mass spectrum (ES+) (*m/z*): 343.2 (100% $\{[C_{14}H_{10}O_2S_2][Na]_3\}^+$), 411.0 (26% $\{[C_{21}H_{17}O_2S_2][Na]_2\}^+$), 489.1 (29% $\{[C_{21}H_{17}O_2S_2][Na]_2[C_2H_6SO]\}^+$). High resolution mass spectrum ES(+) (*m/z*): 367.0812 (calculated for $\{[C_{21}H_{18}O_2S_2][H]\}^+$ 367.08209). IR (solid state, cm^{-1}) 3091 (m), 3033 (m), 1696 (vs) ν(C=O), 1581 (s), 1546 (m), 1499 (m), 1462 (s), 1410 (s), 1378 (m), 1277 (m, 1258 (s), 1234 (s), 1177 (w), 1139 (m), 1095 (m), 1069 (w), 1039 (m), 922 (m), 862 (w), 779 (w), 766 (m), 719 (m), 697 (s), 667 (w), 568 (m), 543 (w). Melting point: 157.0-159.3°C.

Consistent with data previously reported.[22]

6.5.7 Synthesis of 3,4-dibenzylthiobenzyl alcohol[22] (5.7)

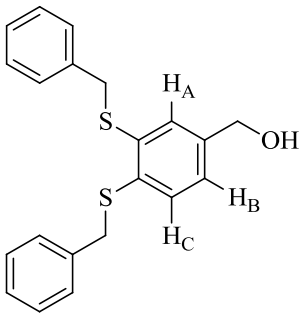

3,4-dibenzylthiobenzoic acid (0.344 g, 0.939 mmol) was dissolved in dry THF (25 cm^3) and added drop-wise to lithium aluminium hydride (0.410 g, 10.80 mmol), suspended in dry THF (25 cm^3) at 0 °C. The reaction was stirred at 0 °C for 30 minutes, then slowly warmed to room temperature and stirred for 18 hours. The reaction was then cooled in an ice bath and the excess lithium aluminum hydride was quenched by the cautious addition of excess water. The solvent was removed under reduced pressure, and the product extracted in ethyl acetate (3 × 25 cm^3). The organic layer was washed with H_2O (3 x 25 cm^3), dried over magnesium sulfate and the solvent removed. The oily residue was purified

by gradient column chromatography (silica, CH_2Cl_2 → 5% MeOH in CH_2Cl_2) yielding the product as an off-white solid. Yield: 0.212 g: 64%.

^{1}H NMR ($CDCl_3$, 300 MHz): δ = 7.35 - 7.15 (m, 12H, CH_{Ar}), 7.04 (dd, $^3J_{HH}$ = 7.9, $^4J_{HH}$ = 1.9 Hz, 1 H, H_B), 4.54 (d, J = 5.7 Hz, 2H, CH_2OH), 4.11 (s, 2H, SCH_2), 4.10 ppm (s, 2H, SCH_2). ^{13}C{^{1}H} NMR ($CDCl_3$, 75 MHz): δ = 139.6, 137.5, 137.0, 136.9, 136.1, 130.26, 129.1, 128.98, 128.5, 128.4, 127.2, 125.2, 64.7, 38.3, 38.2 ppm. Mass spectrum (ES+) (*m/z*): 375.1 (100% $[C_{21}H_{20}OS_2][Na]\}^+$), 285.2 (100% $[C_{14}H_{14}OS_2][Na]\}^+$) High resolution mass spectrum (ES+) (*m/z*): 375.0844 (calculated for $\{[C_{21}H_{20}OS_2][Na]\}^+$ 375.0848). Found C 68.50, H 5.65, S 17.30%. Calculated for $[C_{21}H_{20}OS_2]\bullet[H_2O]$ (370.53) C 69.07, H 5.80, S 17.31. IR (solid state, cm^{-1}) 3271 (s) (O-H), 2945 (s), 1601 (s), 1585 (s) ν(C-S), 1556 (s), 1499 (s), 1457 (s), 1388 (m),1321 (s), 1264 (m), 1233 (s), 1215 (m), 1199 (m), 1156 (w), 1112 (s), 1067 (s), 1040 (s), 1011 (s), 916 (m), 879 (s), 858 (s), 820 (m), 768(s), 691 (s), 674 (s), 621(m), 597 (w), 577 (s), 567 (m), 473 (s), 488 (s). Melting point: 71.0-72.9°C.

Consistent with data previously reported.[22]

6.5.8 Synthesis of 3,4-diisopropylthiobenzoic acid (5.8)

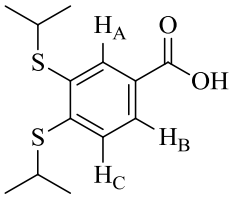

3,4-dimercaptobenzoic acid (0.670 g, 3.62 mmol) and sodium hydroxide (0.433 g, 10.86 mmol) were stirred in methanol until complete dissolution of the reagents. The methanol was removed *in vacuo* and acetone (30 cm^3) added prior to the addition of isopropyliodide (0.73 cm^3, 7.25 mmol). The mixture was heated to reflux reflux for four hours, cooled and the solvent removed. The resulting residue was suspended in water, acidified using 1 M HCl and the product extracted into diethyl ether (3 × 15 cm). The combined organic layers were washed with water (3 × 15 cm^3), brine and dried over magnesium sulphate to give the product as a mixture of disubstituted and monosubstituted product. Attempts were made to purify the products although were unsuccessful therefore the product was carried onto the next step, after which purification could be achieved. Crude yield 0.479 g.

^{1}H NMR ($CDCl_3$, 300 MHz) : δ = 7.97 (d, $^4J_{HH}$ = 1.9 Hz, 1 H CH_A), 7.78 (dd, $^3J_{HH}$ = 8.3, $^4J_{HH}$ = 1.9 Hz, 1 H, CH_B), 7.24 (d, $^3J_{HH}$ = 8.3 Hz, 1 H H_C), 3.39 - 3.57 (m, 2H (CH_3)$_2$), 1.31 ppm (dd, $^2J_{HH}$ = 19.6, $^3J_{HH}$ = 6.8 Hz, 12 H, CH(CH_3)$_2$). ^{13}C{^{1}H} NMR ($CDCl_3$, 75 MHz): δ = 171.2, 132.9, 128.3, 126.4, 125.7, 53.4, 37.7, 36.1, 22.9, 22.7 ppm. High resolution mass spectrum (EI+) (*m/z*): 270.0759 (calculated for $[C_{13}H_{18}O_2S_2]^+$ 270.0748).

6.5.9 Synthesis of 3,4-diisopropylthiobenzyl alcohol (5.9)

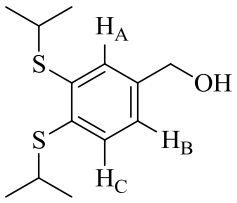

3,4-diisopropylthiobenzoic acid (0.500 g, 1.85 mmol) was dissolved in dry tetrahydrofuran (25 cm^3) and added drop-wise to lithium aluminium hydride (0.280 g, 7.40 mmol), suspended in dry tetrahydrofuran (25 cm^3) at 0 °C. The reaction was stirred at 0 °C for 30 minutes, then slowly warmed to room temperature and stirred for 18 hours. The reaction was then cooled in an ice bath and the excess lithium aluminum hydride was quenched by the cautious addition of water. The solvent was removed under reduced pressure, and the product extracted in ethyl acetate (3 × 25 cm^3). The organic layer was washed with H_2O (3 × 25 cm^3), dried over magnesium sulfate and the solvent removed. The oily residue was purified by gradient column chromatography (silica, CH_2Cl_2 → 2.5% MeOH in CH_2Cl_2) yielding the product as a low melting point and hygroscopic white solid. Yield: 0.395 g (82%).

^{1}H NMR ($CDCl_3$, 300 MHz): δ = 7.35 (s, 1 H, H_A), 7.32 (s, 1 H, H_B), 7.14 (dd, $^3J_{HH}$ = 7.9, $^4J_{HH}$ = 1.9 Hz, 1 H, H_c), 4.66 (CH_2OH s, 2 H), 3.50 (CH(CH_3)$_2$ dspt, $^2J_{HH}$ = 16.6, $^3J_{HH}$ = 6.7 Hz, 2 H), 1.34 ppm (CH_3)$_2$ dd, $^3J_{HH}$ = 6.6, $^4J_{HH}$ = 4.3 Hz, 12 H). ^{13}C{^{1}H} NMR ($CDCl_3$, 75 MHz): δ = 139.3, 138.2, 136.6, 131.1, 128.9, 124.9, 64.8, 37.1, 36.9, 22.9 ppm. High resolution mass spectrum (EI+) (*m/z*): 256.0955 (calc. for $[C_{13}H_{20}OS_2]^{+\cdot}$: 256.0950). IR (solid state, cm^{-1}): 3371 (s, OH), 3075 (w), 3040 (w), 2962 (s), 2925 (s), 2865 (s), 1588 (m), 1551 (w), 1452 (s), 1384 (s), 1366 (m), 1314 (w), 1237 (s), 1204 (w), 1154 (m), 1111 (m), 1051 (s), 1038 (s), 879 (m), 816 (m), 739 (w), 699 (w). Melting point: 64.1-65.0°C.

6.5.10 Synthesis of 2,3,7,8,12,13-hexakis-isopropylthio-10,15-dihydro-5*H*-tribenzo[*a*,*d*,*g*]cyclononene (5.10)

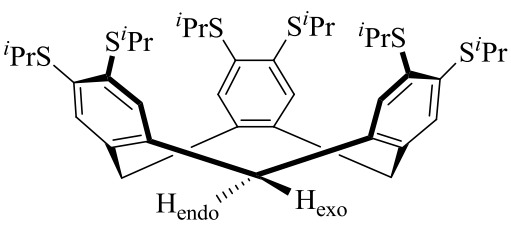

3,4-diisopropylbenzyl alcohol (0.402 g 1.568 mmol) was dissolved in formic acid (30 cm^3) and heated to 70 ^{o}C for 48 hours. The mixture was then cooled and the solvent removed. The product was extracted into dichloromethane and washed with water (3 × 25 cm^3), brine, dried over magnesium sulfate and the solvent removed. The product may be purified by two ways; i) trituratation from the resulting residue in 5% methanol in diethyl ether or ii) column chromatography (silica, CH_2Cl_2 :Hexane (1 : 3) → CH_2Cl_2). Yield 0.153 g (41%).

^{1}H NMR ($CDCl_3$, 300 MHz): δ = 7.33 (s, 6 H), 4.72 (d, $^2J_{HH}$ = 13.6 Hz, 3 H), 3.66 (d, $^2J_{HH}$ = 13.6 Hz, 3 H), 3.44 (spt, $^3J_{HH}$ = 6.7 Hz, 6 H), 1.31 ppm (dd, $^3J_{HH}$ = 6.7, 8.4 Hz, 36 H, (CH_3)$_2$). ^{13}C{^{1}H} NMR ($CDCl_3$, 75 MHz): δ = 137.7, 136.2, 132.8, 37.2, 36.4, 23.1 ppm.

High resolution mass spectrum: (ES+): 815.2581 (calc. for $\{[C_{39}H_{54}S_6][Na][C_2H_6SO]\}^+$: 815.2581). IR (solid state, cm^{-1}): 3075 (s), 3037 (s), 2962 (s), 2922 (s) 2863 (s), 1729 (w), 1581 (m), 1548 (vw), 1485 (m), 1456 (s), 1382 (m), 1365 (m), 1312 (w), 1281(w), 1237 (s), 1153 (s), 1131 (m), 1108 (m), 1051 (s), 943 (m), 902 (m), 880 (m), 815 (w), 762 (s), 738 (w), 718 (w), 697 (w), 649 (w), 628 (w) 599, (w), 571 (s), 498 (w), 462 (w). Melting point: 188.1-192.0 (with decomposition).

6.5.11 Synthesis of *O*,*O*',*O*'',*O*'''-2,3,6,7-Tetrakis(dimethylcarbamothioate)-9,10-dimethyl-9,10-dihydro-9,10-ethanoanthracene (5.11).

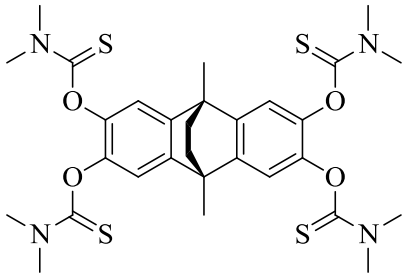

2,3,6,7-tetrahydroxy-9,10-dihydro-9,10-dimethylethanoanthracene (2.00 g, 6.70 mmol) and 1,4-diazabicyclo[2.2.2]octane (4.51 g, 40.22 mmol) were stirred under an inert atmosphere at 50 °C in dry dimethylformamide (40 cm^3) for 30 minutes. To this mixture, dimethylthiocarbomyl chloride (4.97 g, 40.22 mmol) dissolved in dry dimethylformamide (15 cm^3) was added dropwise and stirred at 50 °C for 48 hours. Once cooled, the mixture was poured into cold water (500 cm^3) and the product extracted into ethyl acetate (3 × 50 cm^3). The combined organic layers were washed with water (3 × 50 cm^3), brine, dried over magnesium sulfate and the solvent removed. The product was triturated from the resulting yellow residue by sonication in ethanol (50 cm^3) yielding a white solid in high purity. If required, the product may be further purified by column chromatography (silica, 10% ethyl acetate in dichloromethane). Single crystals suitable for X-ray diffraction were grown from the slow diffusion of pentane into a dichloromethane solution of **5.11**. Yield 3.21 g (74%).

^{1}H NMR ($CDCl_3$, 300 MHz): δ = 7.08 (s, 4H, CH_{Ar}), 3.42 (s, 12H, NCH_3), 3.27 (s, 12H, NCH_3), 1.92 (s, 6H, CH_3), 1.66 ppm (s, 4H, CH_2). ^{13}C{^{1}H} NMR ($CDCl_3$, 75 MHz): δ = 187.0, 144.0, 142.8, 116.7, 43.3, 41.8, 38.8, 35.7, 18.2 ppm. Mass spectrum (ES+) (*m/z*): 685.3 (100% $\{[C_{30}H_{38}N_4O_4S_4]K\}^+$), 669.3 (22% $\{[C_{30}H_{38}N_4O_4S_4]Na\}^+$). Found C 55.50, H 5.90, N 8.35, S 19.45%. Calculated for $C_{30}H_{38}N_4O_4S_4$ (646.92): C 55.70, H 5.92, N 8.66, S 19.83%. IR (solid state, cm^{-1}): 2930 (s), 2863 (s), 1738 (m), 1718 (m), 1528 (s), 1501 (s), 1475 (s), 1459 (s), 1415 (w), 1389 (s), 1339 (w), 1320 (w), 1286 (s), 1262 (s), 1234 (m), 1149 (vs), 1121 (vs) ν(C=S), 1058 (w), 1005 (w), 951 (w), 928(w), 896 (w), 883 (w), 866 (w), 825 (m), 723 (w), 693 (w), 667 (w), 568 (w), 479 (w), 458 (w). Melting point: 264.1-266.2 °C (with decomposition).

6.5.12 Synthesis of *S*,*S*',*S*'',*S*'''-2,3,6,7-Tetrakis(dimethylcarbamothioate)-9,10-dimethyl-9,10-dihydro-9,10-ethanoanthracene (5.12).

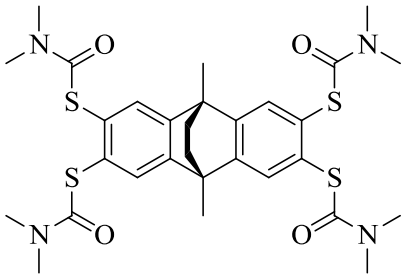

O,*O*',*O*'',*O*'''-2,3,6,7-Tetrakis(dimethylcarbamothioate)-9,10-dimethyl-9,10-dihydro-9,10-ethanoanthracene (0.988 g, 1.53 mmol) was dissolved in deoxygenated diphenyl ether (25 cm^3) and heated to 240 ^oC under an inert atmosphere for 30 minutes. The crude product was extracted by the addition of excess *n*-hexane and purified by either; i) recrystallisation from 2.5% diethyl ether in *n*-hexane or by gradient column chromatography (silica, dichloromethane → 10% ethyl acetate in dichloromethane) to give the product as an orange crystalline solid. Single crystals suitable for X-ray analysis were grown from the slow evaporation of a dichloromethane / *n*-hexane solution. Yield 0.929 g (94%).

^{1}H NMR ($CDCl_3$, 300 MHz,): δ = 7.55 (s, 4H, CH_{Ar}), 3.06 (br. s., 24 H, NCH_3), 1.94 (s, 6H, CH_3), 1.65 ppm (s, 4H, CH_2). ^{13}C{1H} NMR ($CDCl_3$, 75 MHz): δ = 166.7 (*C*=O), 147.4, 131.6, 129.7, 43.3, 41.9, 37.0, 35.1 (*C*H_2), 17.9 ppm. Mass spectrum (ES+) (*m/z*): 685.1 (17% $\{[C_{30}H_{38}N_4O_4S_4]K\}^+$), 669.2 (100% $\{[C_{30}H_{38}N_4O_4S_4][Na]\}^+$), 664.2 (83% $\{[C_{30}H_{38}N_4O_4S_4]H_2O\}^+$). Found C 52.25, H 5.85, N 8.70, S 18.20%. Calculated for $[C_{30}H_{38}N_4O_4S_4]_2$•$CH_2Cl_2$•$H_2O$. (1410.81): C 52.45, H 5.77, N 8.02, S 18.36%. IR (solid state, cm^{-1}): 3558 (s), 3505 (s), 3387 (w), 3289 (w), 3254 (vw), 3070 (s), 3008 (s) 2959 (vs), 2926 (vs), 2884 (vs), 1714 (m), 1653 (s) *ν*(C=O, 1472 (m), 1444 (m), 1410 (w), 1361 (s), 1259 (s), 1161 (w), 1099 (s), 1065 (m), 1009 (w), 905 (s), 867 (m), 841 (m), 803 (w), 779 (w), 734 (m), 691 (s), 656 (m), 568 (m), 542 (m), 509 (m), 482 (w). Melting point: 219.9-223.1 °C.

6.6 Crystallographic Data Tables

6.6.1 Crystallographic l Data Tables for Chapter 2

	2.3	**2.4**	**2.5**	**2.6**
Empirical Formula	$C_{72}H_{84}N_4O_{18}$	$C_{70}H_{72}N_4O_{16}$	$C_{31}H_{48}O_{11}S_5$	$C_{33}H_{45}N_3O_9$
Formula Weight	1293.48	1225.32	756.99	627.72
Crystal System	Triclinic	Monoclinic	Triclinic	Monoclinic
Space group	$P\bar{1}$	$C2/c$	$P\bar{1}$	$P2_1/n$
a (Å)	8.4993(8)	36.991(4)	10.7307(15)	10.6929(11)
b (Å)	19.5382(18)	8.4427(7)	13.8053(19)	29.946(3)
c (Å)	20.2820(19)	21.661(3)	13.9949(18)	10.8181(11)
α (^{o})	90.463(4)	90	73.045(6)	90
β (^{o})	92.464(5)	118.233(7)	75.117(6)	103.744(4)
γ (^{o})	95.706(4)	90	81.243(6)	90
V (Å^3)	3348.0(5)	5960.0(12)	1909.9(4)	3364.9(6)
D_{calc} (g/cm^3)	1.2829	1.366	1.316	1.239
Z	2	4	2	4
T (K)	150(1)	150(1)	150(1)	150(1)
μ (mm^{-1})	0.092	0.097	0.356	0.090
No. of reflections	105133	89496	80977	45901
Unique reflections	17469	8914	11108	8582
R_{int}	0.069	0.067	0.056	0.141
R_1[1] [$I \geq 2\sigma(I)$]	0.091	0.089	0.059	0.059
wR_2[2] (full set)	0.2519	0.280	0.184	0.174
Goodness-of-fit on F^2	1.043	1.038	1.02	1.03
Largest peak (e Å^{-3})	1.26	1.48	2.00	0.33
Deepest hole (e Å^{-3})	-0.82	-1.31	-0.90	-0.42

[1] $R_1 = [\sum^{\|}|F_o| - |F_c|^{\|} / \sum |F_o|]$.
[2] $wR_2 = [\sum w(F_o^2 - F_c^2)^2 / \sum wF_o^4]^{1/2}$.

	2.7	**2.8**
Empirical Formula	$C_{35}H_{47}O_{10}$	$C_{72}H_{60}N_{12}O_{12}$
Formula Weight	627.73	1285.32
Crystal System	Monoclinic	Orthorhombic
Space Group	$P2_1/c$	$Pc2_1b$
a (Å)	17.0327(18)	7.9905(8)
b (Å)	17.7830(19)	26.990(3)
c (Å)	11.0070(10)	30.169(3)
α (^{o})	90	90
β (^{o})	91.971(4)	90
γ (^{o})	90	90
V (Å^3)	3333.0(6)	6506.4(11)
D_{calc} (g/cm^3)	1.251	1.312
Z	4	4
T (K)	150(1)	150(2)
μ (mm^{-1})	0.091	0.092
No. of reflections	37625	76918
Unique reflections	8021	19628
R_{int}	0.066	0.0498
R_1[3] [$I \geq 2\sigma(I)$]	0.081	0.0545
wR_2[4] (full set)	0.270	0.1102
Goodness-of-fit on F^2	1.025	1.030
Highest Peak (e Å^{-3})	0.73	0.33
Largest Hole (e Å^{-3})	-0.33	-0.21

[3] $R_1 = [\sum^{\|}|F_o| - |F_c|^{\|} / \sum |F_o|]$.
[4] $wR_2 = [\sum w(F_o^2 - F_c^2)^2 / \sum wF_o^4]^{1/2}$.

6.6.2 Crystallographic Data Table for Chapter 3

	3.4•2H_2O•1.3dma•0.5MeOH	**3.4**•H_2O•8dma
Empirical Formula	$C_{104.70}H_{101.78}N_{1.30}O_{9.84}P_6Pt_3$	$C_{123}H_{140}N_6O_{13}P_6Pt_3$
Formula Weight	2306.78	2681.50
Crystal System / Space Group	Monoclinic	Hexagonal
Space group	$P2_1$	$P6_3/m$
a (Å)	14.860(3)	23.8013(6)
b (Å)	23.898(5)	23.8013(6)
c (Å)	15.103(3)	13.6022(5)
α (^{o})	90	90.00
β (^{o})	98.87(3)	90.00
γ (^{o})	90	120.00
V (Å^3)	5299.1(18)	6673.3(3)
D_{calc} (mg/M^3)	1.446	1.334
Z	2	2
T (K)	150	150
μ (mm^{-1})	4.094	3.264
No. of reflections	51623	66096
Unique reflections ($I > 2\sigma(I)$)	20525 (17240)	5310 (5134)
R_{int}	0.0389	0.0827
R_1[5] [$I \geq 2\sigma(I)$]	0.0474	0.0815
wR_2[6] (full set)	0.1373	0.1941
Goodness-of-fit on F^2	1.041	1.212
Largest peak (e Å^{-3})	1.735	1.418
Deepest hole (e Å^{-3})	-1.561	-1.340

[5] $R_1 = [\sum^{\|}F_o| - |F_c^{\|} / \sum |F_o]$.
[6] $wR_2 = [\sum w(F_o^2 - F_c^2)^2 / \sum wF_o^4]^{1/2}$.

6.6.3 Crystallographic Data Tables for Chapter 4

	4.3	[**4.4**].[CH_2Cl_2]	**4.10**•$x C_5H_{12}$•$(4-x)CH_2Cl_2$
Empirical Formula	$C_9H_{14}N_2O_4S$	$C_{19}H_{22}Cl_2O_4$	$C_{82.52}H_{72.62}O_4P_4Pt_2$
Formula Weight	246.28	385.28	1642.33
Crystal System / Space Group	Monoclinic	Monoclinic	Monoclinic
Space group	$P2_1$ / n	$P2_1$ / n	$P2_1/c$
a (Å)	9.4337(10)	14.2516(19)	14.8499(7)
b (Å)	7.7634(8)	7.3564(11)	22.2206(13)
c (Å)	15.6480(17)	19.158(3)	26.3410(17)
α (^{o})	90	90	90
β (^{o})	98.687(4)	105.860(6)	90.007(2)
γ (^{o})	90	90	90
V (Å^3)	1132.9(2)	1932.1(5)	8691.8(9)
D_{calc} (g/cm^3)	1.444	1.324	1.255
Z	4	4	4
T (K)	150(2)	150(2)	150(2)
μ (mm^{-1})	0.287	0.356	3.330
No. of reflections	26838	44252	25228
Unique reflections	3433	5582	10268
R_{int}	0.0321	0.0323	0.019
R_1[7] [$I \geq 2\sigma(I)$]	0.0361	0.0853	0.0982
wR_2[8] (full set)	0.0894	0.2507	0.2496
Goodness-of-fit on F^2	1.020	1.089	1.121
Highest Peak (*e* Å^{-3})	0.47	0.56	1.828
Deepest Hole (*e* Å^{-3})	-0.28	-0.81	-0.225

[7] $R_1 = [\sum^{\|}|F_o| - |F_c|^{\|} / \sum |F_o|]$.
[8] $wR_2 = [\sum w(F_o^2 - F_c^2)^2 / \sum wF_o^4]^{1/2}$.

	4.11•0.67H_2O•2.07CH_2Cl_2	[**4.10**]PF_6•*x*$C_4H_{10}O$•(5-*x*)CH_2Cl_2
Empirical Formula	$C_{72.07}H_{67.48}Cl_{4.13}O_{4.67}P_4Pt_2$	$C_{78}H_{62}F_6O_4P_5Pt_2$
Formula Weight	1668.79	1722.31
Crystal System	Orthorhombic	Orthorhombic
Space group	*P*212121	Pnma
a (Å)	17.404(4)	22.346(3)
b (Å)	32.011(7)	23.976(2)
c (Å)	41.109(9)	30.992(4)
α (^{o})	90	90
β (^{o})	90	90
γ (^{o})	90	90
V (Å^3)	22902(9)	16605(3)
D_{calc} (g/cm^3)	1.452	1.378
Z	12	8
T (K)	150(2)	150(2)
μ (mm^{-1})	3.933	3.518
No. of reflections	479509	36540
Unique reflections	50247	11253
R_{int}	0.079	0.0806
R_1[9] [$I \geq 2\sigma$ (*I*)]	0.091	0.1080
wR_2[10] (full set)	0.261	0.2789
Goodness-of-fit on F^2	1.024	1.063
Highest Peak (*e* Å^{-3})	8.10	2.92
Deepest Hole (*e* Å^{-3})	–21.20	-2.58

[9] $R_1 = [\sum^{\|}F_o| - |F_c^{\|} / \sum |F_o|]$.
[10] $wR_2 = [\sum w(F_o^2 - F_c^2)^2 / \sum wF_o^4]^{1/2}$.

	[**4.11**]PF_6•2.4CH_2Cl_2
Empirical Formula	$C_{72.80}H_{67.60}Cl_{4.60}F_{4.20}O_4P_{5.10}Pt_{22}$
Formula Weight	1797.47
Crystal System	Tetragonal
Space group	P4/nnc
a (Å)	25.5395(7)
b (Å)	25.5395(7)
c (Å)	24.7276(8)
α (°)	90
β (°)	90
γ (°)	90
V (Å^3)	16129.0(8)
D_{calc} (g/cm^3)	1.480
Z	8
T (K)	120(2)
μ (mm^{-1})	3.771
No. of reflections	12344
Unique reflections	9368
R_{int}	0.0424
R_1[11] [$I \geq 2\sigma(I)$]	0.0664
wR_2[12] (full set)	0.1938
Goodness-of-fit on F^2	1.120
Highest Peak (e Å^{-3})	3.838
Deepest Hole (e Å^{-3})	-1.246

[11] $R_1 = [\sum^{\|}F_o| - |F_c^{\|} / \sum |F_o|]$.
[12] $wR_2 = [\sum w(F_o^2 - F_c^2)^2 / \sum wF_o^4]^{1/2}$.

6.6.4 Crystallographic Data Tables for Chapter 5

	5.10	**5.11**	**5.12**
Empirical Formula	$C_{39}H_{54}S_6$	$C_{30}H_{38}N_4O_4S_4$	$C_{30}H_{40}N_4O_5S_4$
Formula Weight	715.26	646.88	664.93
Crystal System / Space Group	Triclinic	Monoclinic	Triclinic
Space group	$P\bar{1}$	$P2_1$ / c	$P\ \bar{1}$
a (Å)	8.9234(5)	9.2176(2)	11.6731(16)
b (Å)	15.1248(7)	20.8884(4)	12.0490(16)
c (Å)	15.6978(6)	19.2078(4)	12.9734(16)
α (^{o})	64.609(4)	90	94.152(7)
β (^{o})	83.062(4)	118.060(2)	92.051(7)
γ (^{o})	82.948(4)	90	115.118(7)
V (Å^3)	1894.02(17)	3263.57(12)	1643.3(4)
D_{calc} (g/cm^3)	1.2541	1.317	1.344
Z	2	4	2
T (K)	120(2)	100(1)	150(1)
μ (mm^{-1})	3.524	3.004	0.333
No. of reflections	12657	18623	42125
Unique reflections	6920	6468	9940
R_{int}	0.0827	0.0413	0.0431
R_1[13] [$I \geq 2\sigma$ (*I*)]	0.0598	0.0419	0.0483
wR_2[14] (full set)	0.1551	0.1096	0.1273
Goodness-of-fit on F^2	0.985	1.06	1.03
Highest Peak (*e* Å^{-3})	0.78	0.93	0.53
Deepest Hole (*e* Å^{-3})	-1.05	-0.42	-0.52

[13] $R_1 = [\sum^{\|}F_o| - |F_c^{\|} / \sum |F_o|]$.
[14] $wR_2 = [\sum w(F_o^2 - F_c^2)^2 / \sum wF_o^4]^{1/2}$.

6.7 References

[1] G. M. Sheldrick, *Acta Cryst., Sect. A* **2008**, *64*, 112.

[2] L. J. Barbour, *J. Supramol. Chem.* **2001**, *1*, 189.

[3] A. Spek, *Acta Cryst., Sect. D* **2009**, *65*, 148-155.

[4] M. J. Frisch, G. W. T, H. B. Schlegel, G. E. Scuseria, M. A. Robb, J. R. Cheeseman, J. A. Montgomery, T. Vreven, K. N. Kudin, J. C. Burant, J. M. Millam, S. S. Iyengar, J. Tomasi, V. Barone, B. Mennucci, M. Cossi, G. Scalmani, N. Rega, G. A. Petersson, H. Nakatsuji, M. Hada, M. Ehara, K. Toyota, R. Fukuda, J. Hasegawa, M. Ishida, T. Nakajima, Y. Honda, O. Kitao, H. Nakai, M. Klene, X. Li, J. E. Knox, H. P. Hratchian, J. B. Cross, V. Bakken, C. Adamo, J. Jaramillo, R. Gomperts, R. E. Stratmann, O. Yazyev, A. J. Austin, R. Cammi, C. Pomelli, J. W. Ochterski, P. Y. Ayala, K. Morokuma, G. A. Voth, P. Salvador, J. J. Dannenberg, V. G. Zakrzewski, S. Dapprich, A. D. Daniels, M. C. Strain, O. Farkas, D. K. Malick, A. D. Rabuck, K. Raghavachari, J. B. Foresman, J. V. Ortiz, Q. Cui, A. G. Baboul, S. Clifford, J. Cioslowski, B. B. Stefanov, G. Liu, A. Liashenko, P. Piskorz, I. Komaromi, R. L. Martin, D. J. Fox, T. Keith, M. A. Al-Laham, C. Y. Peng, A. Nanayakkara, M. Challacombe, P. M. W. Gill, B. Johnson, W. Chen, M. W. Wong, C. Gonzalez, J. A. Pople, *Gaussian 03*, **2004**.

[5] T. H. Dunning Jr., P. J. Hay in *Modern Theoretical Chemistry Vol. 3*, Plenum,, New York, **1977**.

[6] J. L. Scott, D. R. MacFarlane, C. L. Raston, C. M. Teoh, *Green Chem.* **2000**, *2*, 123-126.

[7] J. A. Hyatt, *J. Org. Chem.* **1978**, *43*, 1808.

[8] B. F. Abrahams, B. A. Boughton, N. J. FitzGerald, J. L. Holmes, R. Robson, *Chem. Commun.*, *47*, 7404-7406.

[9] a) D. A. Slack, M. C. Baird, *Inorg. Chim. Acta.* **1977**, *24*, 277-280; b) G. W. Watt, J. E. Cuddeback, *J. Inorg. Nucl. Chem.* **1971**, *33*, 259-263.

[10] D. Scott Bohle, D. Stasko, *Chem. Commun.* **1998**, 567-569.

[11] Z. Qin, M. C. Jennings, R. J. Puddephatt, *Inorg. Chem.* **2002**, *41*, 3967-3974.

[12] B. Butschke, H. Schwarz, *Organometallics* **2010**, *29*, 6002-6011.

[13] G. Annibale, M. Bortoluzzi, G. Marangoni, B. Pitteri, *Transition Met. Chem. (Dordrecht, Neth.)* **2005**, *30*, 748-750.

[14] D. J. Awad, U. Schilde, P. Strauch, *Inorg. Chim. Acta* **2011**, *365*, 127-132.

[15] J. Best, I. V. Sazanovich, H. Adams, R. D. Bennett, E. S. Davies, A. J. H. M. Meijer, M. Towrie, S. A. Tikhomirov, O. V. Bouganov, M. D. Ward, J. A. Weinstein, *Inorg. Chem.* **2010**, *49*, 10041-10056.

[16] N. M. Shavaleev, E. S. Davies, H. Adams, J. Best, J. A. Weinstein, *Inorg. Chem.* **2008**, *47*, 1532-1547.

[17] C. H. Lee, H. Kohn, *J. Org. Chem.* **1990**, *55*, 6098-6104.

[18] L. J. Barbour, J. W. Steed, J. L. Atwood, *J. Chem. Soc., Perkin Trans. 2* **1995**, 857-860.

[19] G. M. Martinez, O. P. Arroyo, O. F. Lara, P. G. Espinosa, O. S. Hernandez, U. M. I. Chavez, M. Salmon, R. Cruz-Almanza, *Tetrahedron* **1997**, *53*, 17633-17642.

[20] a) P. Boldt, *Chem. Ber.* **1967**, *100*, 1270-1280; b) T. S. Balaban, A. Eichhoefer, M. J. Krische, J.-M. Lehn, *Helv. Chim. Acta* **2006**, *89*, 333-351.

[21] P. W. Rabideau, *J. Org. Chem.* **1971**, *36*, 2723-2724.

[22] I. M. Davidson, O. C. Musgrave, *J. Chem. Soc.* **1963**, 3154-3155.

[23] B. F. Abrahams, N. J. FitzGerald, R. Robson, *Inorg. Chem.* **2010**, *49*, 5953-5956.

[24] a) A. Mahendran, A. Vuong, D. Aebisher, Y. Gong, R. Bittman, G. Arthur, A. Kawamura, A. Greer, *J. Org. Chem.* **2010**, *75*, 5549-5557; b) B. M. R. Liénard, N. Selevsek, N. J. Oldham, C. J. Schofield, *ChemMedChem* **2007**, *2*, 175-179; c) M. A. Little, University of Leeds **2012**.